CRANFIELD UNIVERSITY

S. BLANEY

GAMMA RADIATION METHODS FOR CLAMP-ON MULTIPHASE FLOW METERING

SCHOOL OF ENGINEERING

PHD THESIS

CRANFIELD UNIVERSITY

School of Engineering
Department of Process and Systems Engineering

PHD THESIS

Academic Year 2007 – 2008

S. BLANEY

Gamma Radiation Methods for Clamp-On Multiphase Flow Metering

Supervisor: Dr. H. Yeung

February 2008

This thesis is submitted in partial fulfilment of the requirements for the degree of Doctor of Philosophy

Abstract

The development of a cost-effective multiphase flow meter to determine the individual phase flow rates of oil, water and gas was investigated through the exploitation of a single clamp-on gamma densitometer and signal processing techniques. A fast-sampling (250 Hz) gamma densitometer was installed at the top of the 10.5 m high, 108.2 mm internal diameter, stainless steel catenary riser in the Cranfield University multiphase flow test facility. Gamma radiation attenuation data was collected for two photon energy ranges of the caesium-137 radioisotope based densitometer for a range of air, water and oil flow mixtures, spanning the facility's delivery range.

Signal analysis of the gamma densitometer data revealed the presence of quasi-periodic waveforms in the time-varying multiphase flow densities and discriminatory correlations between statistical features of the gamma count data and key multiphase flow parameters.

The development of a mechanistic approach to infer the multiphase flow rates from the gamma attenuation information was investigated. A model for the determination of the individual phase flow rates was proposed based on the gamma attenuation levels; while quasi-periodic waveforms identified in the multiphase fluid density were observed to exhibit a strong correlation with the gas and liquid superficial phase velocity parameters at fixed water cuts.

Analysis of the use of pattern recognition techniques to correlate the gamma densitometer data with the individual phase superficial velocities and the water cut was undertaken. Two neural network models were developed for comparison: a single multilayer-perceptron and a multilayer hierarchical flow regime dependent model. The pattern recognition systems were trained to map the temporal fluctuations in the multiphase mixture density with the individual phase flow rates using statistical features extracted from the gamma count signals as their inputs. Initial results yielded individual phase flow rate predictions to within ±10% based on flow regime specific correlations.

Keywords: gamma densitometry, multiphase flow, signal analysis, flow measurement, pattern recognition.

Acknowledgements

Completion of this research work has only been made possible through the valuable contributions of a number of people over the past three years. The following list is by no means exhaustive.

I would like to thank my supervisor Dr Hoi Yeung who has been a constant source of guidance, support and ideas throughout the duration of this work.

I would also like to express my sincere gratitude to Mr David Whittingham, Mr Andrew Jamieson, Dr Vladimir Kratirov, Mr. Ivan Endovovitski and all the staff and associates of the Neftemer Ltd family who have offered a considerable amount of assistance and encouragement.

A big thank you to all those in the PASE group with a special mention to Dr Yi Cao, Dr Salem Al-lababbidi and Mr Flemming Nielsen for their technical assistance in a number of capacities; and to Mrs Linda Whitfield and Mrs Sam Skears for their patience and assistance in unravelling the mysteries of university administration.

This work was undertaken with the financial assistance of EPSRC and De Flow Ltd and the author is eternally grateful for their support.

Finally, I would like to thank all my family and friends for their endless encouragement and support. Je tiens à remercier tout particulièrement ma petite Nadia qui m'a beaucoup soutenu et m'a conseillé pendant ce travail de thèse et qui a dû subir mes interminable plaintes, surtout pendant la période de rédaction!

Table of Contents

List of Figures

List of Tables

Notation

Symbols		**Units**
a_k	k^{th} Linear predictor filter coefficient	-
A	Wavelet packet approximation coefficient matrix	-
A_g	Cross-sectional area occupied by gas	m^2
A_l	Cross-sectional area occupied by liquid	m^2
A_o	Cross-sectional area occupied by oil	m^2
A_p	Pipe cross-sectional area	m^2
A_w	Cross-sectional area occupied by water	m^2
b	Neuron bias	-
b_l	l^{th} Linear predictor filter coefficient	-
b_0	Initial term of linear predictor transfer function	-
B	Build-up factor	-
B_s	Bandwidth	Hz
c	Speed of light in a vacuum or intercept	ms^{-1}, -
C	Wavelet transform coefficient matrix or Chisholm constant	-
C_e	Measured capacitance	F
C_m	Multiphase fluid mixture capacitance	F
C_p	Electrode-pipe wall capacitance	F
d	Euclidean distance or bubble diameter	- , m
D	Internal pipe diameter or wavelet packet detail coefficient matrix	m, -
e_n	Residual error of linear prediction	-
E	Photon energy	eV
E_b	Electron binding energy	eV
E_d	Objective function for neural network error minimisation	-
E_e	Electron energy	eV
E_o	Original photon energy	eV
E_{pe}	Photoelectric energy	eV
E_q	Average quantisation error	-
E_r	Neural network output associated relative error	%
E_R	Residual error of linear prediction coefficients	-
E_t	Topographic error	-
E_T	Total signal energy	s^{-2}
E_W	Sum of squares of network weights	-
f	Neural network activation function	-
f_s	Sampling frequency	Hz
F	Modified objective function or input vector scale factor	-
F_a	Wavelet centre frequency	Hz
F_c	Signal pseudo-frequency	Hz
G	Conductivity, gain factor or mass flux	$S.m^{-1}$, -, $kg/s.m^2$
G_g	Gas mass flow rate	kg/s
G_o	Oil mass flow rate	kg/s

G_t	Total mass flow rate	kg/s
G_w	Water mass flow rate	kg/s
h	Planck constant, thickness of absorber, or number of hidden nodes	$m^2 \cdot kg.s^{-1}$, m, -
h_a	Gamma beam path length through air	m
h_l	Gamma beam path length through liquid	m
h_o	Gamma beam path length through oil	m
h_w	Gamma beam path length through water	m
H	Hessian matrix	-
I	Current or measured gamma radiation intensity	s^{-1}
I_0	Initial gamma radiation intensity	s^{-1}
I_a	Gamma radiation intensity of air filled conduit	s^{-1}
I_l	Gamma radiation intensity of liquid filled conduit	s^{-1}
I_o	Gamma radiation intensity of oil filled conduit	s^{-1}
I_w	Gamma radiation intensity of water filled conduit	s^{-1}
K	Smith slip ratio correlation entrainment factor	-
l	Bubble axial length	m
L	Length; distance between sensors; or wavelet packet decomposition level	m, m, -
L_b	Axial length of separated flow element	m
L_s	Axial length of dispersed flow element	m
m	Gradient	-
M_i	i^{th} Moment of discrete wavelet transform	-
m_c	Best matching unit vector	-
m_o	Rest mass of an object	kg
n	Number of layers in neural network	-
N	Total number of points in a sampled record or number of radioactive nuclei	-
p	Linear predictor filter order or neural network input	-
P	Pressure	bara
P(x)	Probability density function	-
P(z)	Symmetric polynomial	-
Q_g	Gas volumetric flow rate	m^3/s
Q_l	Liquid volumetric flow rate	m^3/s
Q_o	Oil volumetric flow rate	m^3/s
Q_t	Total volumetric flow rate	m^3/s
Q_w	Water volumetric flow rate	m^3/s
Q(z)	Anti-symmetrical polynomial	-
r_o	Classical electron radius	m
R	Covariance coefficient or input vector range	-
R_e	Effective resistance	Ω
R_m	Multiphase fluid mixture resistance	Ω
R_{xx}	Autocorrelation function	-
R_{xy}	Cross-correlation function	-
s	Wavelet scale	-
S	Slip ratio or generic signal	-
t	Time or neural network target output	s, -
u	Topographic error constant	-

u_b	Gas bubble velocity	ms^{-1}
V_{drift}	Drift velocity	ms^{-1}
V_g	Gas phase velocity	ms^{-1}
V_l	Liquid phase velocity	ms^{-1}
V_m	Multiphase mixture velocity	ms^{-1}
V_o	Oil phase velocity	ms^{-1}
V_{sg}	Superficial gas velocity	ms^{-1}
V_{sl}	Superficial liquid velocity	ms^{-1}
V_{slip}	Slip velocity	ms^{-1}
V_w	Water phase velocity	ms^{-1}
W	Neural network weight	-
x	Vapour quality	-
$\overline{x}$	Mean	-
x(t)	Sample time history	-
X	Lockhart-Martinelli number	-
y	Neural network output	-
Z	Atomic number	-
Z_e	Electrical impedance	Ω
α	Gas volume fraction or control parameter in Bayesian regularisation	-
α_g	Gas volume fraction	-
α_l	Liquid volume fraction	-
β	Water volume fraction or control parameter in Bayesian regularisation	-
γ	Oil volume fraction; linear attenuation coefficient; or number of effective parameters	-
γ_a	Air linear attenuation coefficient	m^{-1}
γ_l	Liquid linear attenuation coefficient	m^{-1}
γ_o	Oil linear attenuation coefficient	m^{-1}
γ_w	Water linear attenuation coefficient	m^{-1}
δ	Outer layer error	-
Δ	Sampling period	s
Δt	Bubble transit time	s
ε_a	Air chordal hold-up	-
ε_o	Oil chordal hold-up	-
ε_w	Water chordal hold-up	-
η	Step size	-
θ	Photon deflection angle	rad
λ	Mean free path or radioactive decay constant	m, s^{-1}
λ_g	Liquid hold-up	-
λ_l	Gas void fraction	-
μ_l	Liquid viscosity	Pa.s
ρ_g	Gas density	kg/m^3
ρ_l	Liquid density	kg/m^3
ρ_m	Mixture density	kg/m^3
ρ_o	Oil density	kg/m^3
ρ_w	Water density	kg/m^3

σ	Surface tension, standard deviation or photon interaction probability	N/m, -, barnes/atom
τ	Lag or wavelet translation	s,
υ	Frequency of electromagnetic radiation	Hz
ψ	Mother wavelet function	-
ω	Excitation frequency of electronic circuitry	Hz
Ω	Solid angle	sr

Acronyms

ACF	Autocorrelation function
BMU	Best matching unit
CK	Coefficient of kurtosis
CS	Coefficient of skewness
CV	Coefficient of variance
FFT	Fast Fourier transform
GOR	Gas oil ratio
GVF	Gas volume fraction
KSOFM	Kohenon self-organising feature map
LGR	Liquid to-gas ratio
LM	Levenberg-Marquardt
LPC	Linear prediction coefficient
LSF	Line spectral frequency
MLP	Multi-layer perceptron
MPFM	Multiphase flow meter
PCA	Principal component analysis
PDF	Probability density function
PMF	Probability mass function
PSD	Power spectral density
RMS	Root mean square
SCG	Scaled conjugate gradient
SD	Standard deviation
SFFT	Short-time Fourier transform
SG	Specific gravity
SSE	Sum of square errors
WC	Water cut
ZMUV	Zero-mean and unit variance

Chapter 1: Introduction

1.1 Background

Within the power and process industries, there are many instances of multiphase flow. The term 'multiphase flow' is used to define two or more phases flowing simultaneously in a conduit. However, this term can be misleading as it also encompasses multi-component systems, **Table 1.1**.

<table>
<tr><th>Multiphase Flow</th><th>Examples</th></tr>
<tr><td rowspan="4">Flow in an conduit where more than one fluid is present.</td><td>3-Phase: Liquid – Liquid – Gas
e.g. Water – Oil – Gas</td></tr>
<tr><td>2-Phase: Liquid – Liquid
e.g. Water – Oil</td></tr>
<tr><td>2-Phase: Liquid – Solid
e.g. Water – Sand</td></tr>
<tr><td>2-Phase: Liquid – Gas
e.g. Water – Air</td></tr>
</table>

Table 1.1 – Nature of Multiphase Flows in Process Industries

This document focuses on multiphase flows comprising oil, water and natural gas found in upstream oil and gas production operations. Knowledge of the individual fluid flow rates of each producing oil well is required to facilitate reservoir management, field development, operational control, flow assurance, and production allocation [**1**].

Conventional solutions concerning two- and three-phase metering systems require expensive and cumbersome test separators, high maintenance, field personnel intervention, and do not lend themselves to continuous monitoring or metering. Moreover, with diminishing oil resources, oil companies are now frequently confronted with the prospect of recovering hydrocarbons from marginally economic reservoirs [**2**].

In order to ensure economic viability of these accumulations, the wells may have to be completed subsea or crude oil from several wells sent to a common production facility. The economic constraints on such developments do not favour the deployment of three-phase separators as the primary measurement device. Consequently, viable alternatives to three-phase separators are essential. Industry's response is the multiphase flow meter (MPFM).

The oil and gas industry began to generate a serious interest in developing MPFMs in the early 1980s. Beforehand, single-phase measurements were sufficient to meet the industry's needs. However, depleting oil reserves, along with smaller, deeper wells with higher water contents, saw the advent of increasingly frequent occurrences of multiphase flow where the single-phase meters were unable to cope.

After a lengthy gestation period, MPFMs with an adequate performance for selected applications became commercially available. Since 1994, MPFM installation numbers have steadily increased as technology in the field has advanced, with substantial growth witnessed from 1999 onwards, **Figure 1.1** [3].

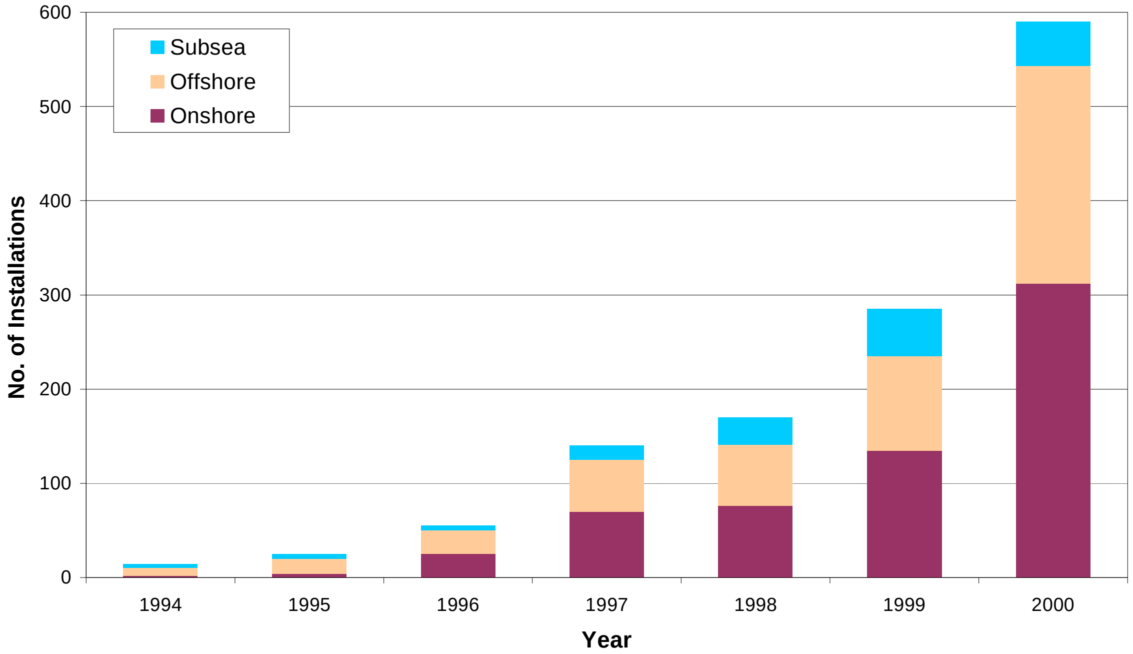

Figure 1.1 – Multiphase Meter Survey 1994 – 2000

Also apparent is the change in the MPFM applications. Initially, interest in multiphase metering technology was confined to offshore and subsea applications where weight and space are at a premium and MPFMs offered an attractive alternative to bulky three-phase separators. However, more than half of the installations in 2000 were in onshore operations.

A recent study estimated that there were approximately 2,700 MPFM applications including field allocation, production optimisation and mobile well testing in 2006 suggesting that the MPFM market is still growing [**4**].

A number of factors have instigated the recent rapid uptake of multiphase measurement technology: improved meter performances, decreases in meter costs, more compact meters enabling deployment of mobile systems, increases in oil prices and a wider assortment of operators.

As the initial interest in multiphase flow metering came from the offshore industry, most of the multiphase metering activity was concentrated in the North Sea. However, the present distribution of multiphase flow meters is much more diverse. **Figure 1.2** shows the global distribution of MPFM installations in 2000.

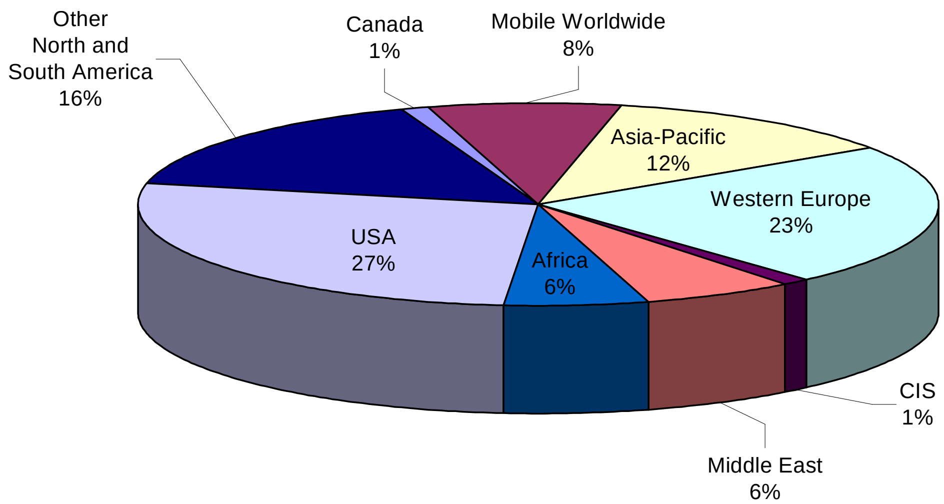

Figure 1.2 – Multiphase Meter Distribution in 2000

Multiphase metering is a nascent sector in the oil and gas industry and continues to expand as technology develops and installation prices decrease, facilitating economic deployment. Nevertheless, after ten years of market growth, the number of actual installations is still less then 3,000, a mere fraction of the potential market: there were 890,000 producing wells worldwide in 2000, **Table 1.2** [**5**]. It has been suggested that, with the current market climate, a modest target for the oil industry would be to have MPFMs installed on 1% of the world's wells by 2010 [**6**].

Location	**Wells**	**Average Daily Production (Mbbls)**
North America	590,000	11
South America	49,000	7
Western Europe	5,000	7
Eastern Europe	124,000	8
Africa	8,000	8
Middle East	11,000	22
Far East	95,000	7
South Pacific	1,000	1
Total	**885,000**	**69**

Table 1.2 – Summary of Oil Well Production in 2000

Industry experts have forecast that MPFMs will become feasible on an installation per well basis when their capital cost falls to around US$40,000 – US$60,000. The cost of

MPFMs today remains in the range of US$100,000 – US$500,000 (varying with onshore/offshore, topside/subsea, the physical dimensions of the meter and the number of units ordered). Installation of these MPFMs can cost up to 25% of the hardware cost and associated operating costs are estimated at between US$20,000 and $40,000 per year [**7**].

A number of novel multiphase metering techniques, employing a variety of technologies, have been developed which eliminate the need for three-phase separator deployment. These MPFMs offer substantial economic and operating advantages over their phase separating predecessor. Nevertheless, it is still widely recognised that no single MPFM on the market can meet all multiphase metering requirements. Despite the advances in multiphase flow metering, industrial deployment of this technology remains expensive for meters that offer an acceptable performance. Thus, there is a clear need for further development of multiphase flow monitoring devices within the petroleum industry.

Clamp-on gamma-densitometry is a suitable technique to facilitate non-intrusive multiphase flow metering as it does not require breaking into the pipeline for installation. As a result, meter units could be retrofitted without having to stop the production process. The reduced hardware and installation costs associated with deploying such units as MPFMs, in conjunction with increasing oil prices, would facilitate economic justification of a per well installation basis.

Low intensity gamma radiation sources, such as those employed in gamma densitometer units, do not present significant technical problems for installation and use in onshore oilfield environments. However, in some countries, administrative and logistical issues in deploying radioactive sources in the field are virtually insuperable. Consequently, gamma densitometer units cannot be readily deployed in such countries as MPFMs; nevertheless, a sizeable market remains in the countries where radiation based instrumentation can be installed. Indeed, many commercially available multiphase flow meters employ gamma-densitometry techniques as part of their measurement systems [**8**].

1.2 Objectives

This research work reports on the author's application of a single gamma-densitometer unit to determine both the phase volume fractions and velocities to yield the individual phase flow rates of a multiphase flow as part of the development programme of a commercial clamp-on gamma radiation based multiphase flow meter [**9**]. The objectives of the research were to:

- Conduct a literature review of multiphase flow and its measurement, gamma radiation in multiphase metering and the application of pattern recognition techniques in multiphase measurement.
- Undertake experimental data collection of a gamma-densitometer's response to a variety of vertical multiphase flow conditions.
- Analyse the gamma densitometer signal characteristics in relation to key multiphase flow parameters.

- Investigate a mechanistic approach to determining the individual phase flow fractions and phase velocities from the gamma densitometer output data.
- Investigate the suitability of the gamma densitometer data for exploitation in a pattern recognition based multiphase flow measurement system.

Figure 1.3 displays the thesis roadmap which illustrates the concepts, methodology and links in the research work carried out to fulfil these objectives.

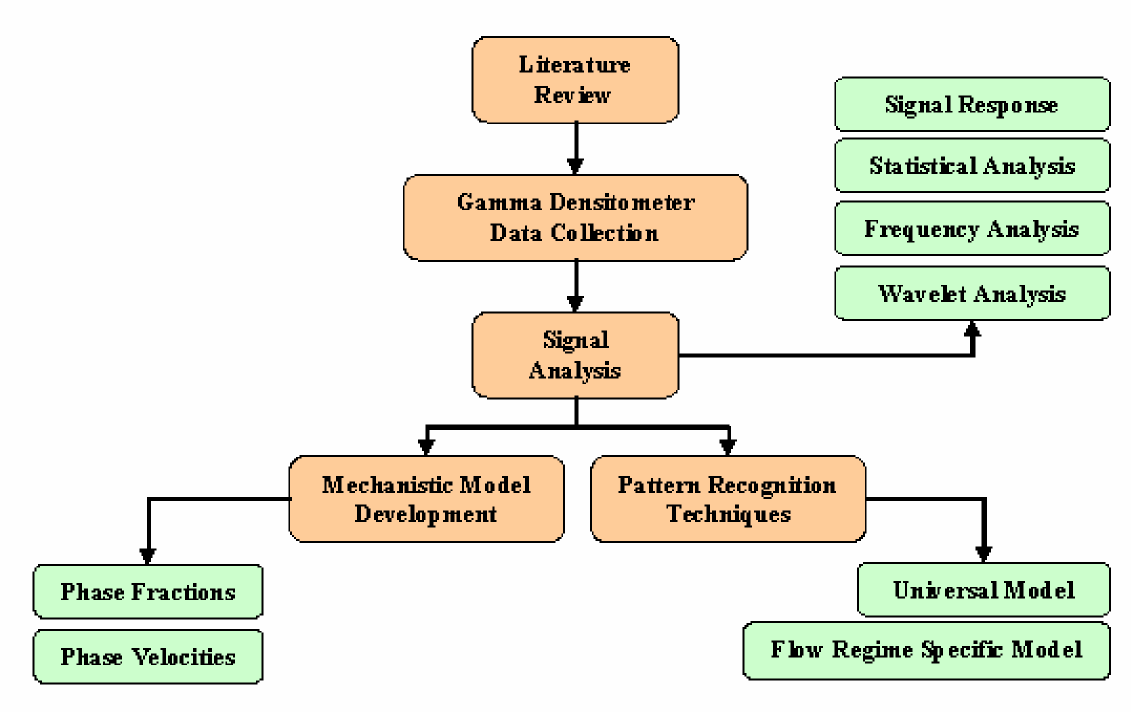

Figure 1.3 – Thesis Roadmap

1.3 Thesis Structure

The thesis is divided into 7 chapters. An overview of the remaining chapters' content is given below:

<u>Chapter 2</u>: A literature review of the subject area is presented encompassing multiphase flow and its measurement, gamma radiation in multiphase metering and pattern recognition based measurement approaches.

<u>Chapter 3</u>: The experimental set up used to study gamma radiation methods for multiphase flow measurement is described. An outline of the Cranfield University multiphase flow loop is provided as well as descriptions of the gamma densitometer instrument's installation, calibration, operation, data acquisition and processing, signal characteristics and details of experimental campaign undertaken are documented.

Chapter 4: The response of the gamma-densitometer unit to different multiphase flow conditions was examined. Various statistical parameters were then extracted from the time-varying gamma count signals and were investigated to establish their correlation with characteristic parameters of the multiphase flows which produced them. Analysis of the signals was also conducted in the frequency domain. Furthermore, wavelet analysis was employed to facilitate simultaneous analysis of the signals' time and frequency domain characteristics.

Chapter 5: A mechanistic approach to extracting flow measurement information in dynamic conditions was then examined. Determination of the individual phase fractions of the dynamic multiphase flow gamma count data collected was investigated through the exploitation of the gamma attenuation information. Quasi-periodic waveforms identified in the multiphase fluid density were analysed for their dependence on the gas and liquid superficial phase velocity parameters.

Chapter 6: An investigation of pattern recognition techniques as a vehicle to obtain the individual phase flow rates of vertical multiphase flows from the variations they induce in the gamma densitometer count signals was conducted. Two neural network models were developed for comparison: a single multilayer-perceptron and a multilayer hierarchical flow regime dependant model. The pattern recognition systems were trained to map the temporal fluctuations in the multiphase mixture density with the individual phase flow rates using statistical features extracted from the gamma count signals as their inputs. The use of wavelet transform features as input vectors to the pattern recognition systems was also examined.

Chapter 7: The main conclusions drawn from the research work, and proposals for future work, are presented.

Chapter 2: Literature Review

The following chapter presents an overview of the basic concepts of multiphase flow and its measurement. A review of the current state of multiphase flow measurement is presented looking at the various approaches and techniques employed in commercially available meters. Finally, the use of gamma-radiation in multiphase flow metering, and the application of pattern recognition in this domain, are considered.

2.1 Principles of Multiphase Flow

2.1.1 Multiphase Flow

Multiphase flow is the simultaneous flow of oil, water and gas in a pipeline. It is a complex phenomenon, making it difficult to understand, predict and model. Well-established single-phase flow characteristics, including boundary layer, velocity profile and turbulence, are rendered ineffective in describing their nature. A useful tool to illustrate multiphase flows, and their associated intricacies, is the multiphase composition triangle diagram championed by Jamieson [**10**], **Figure 2.1**.

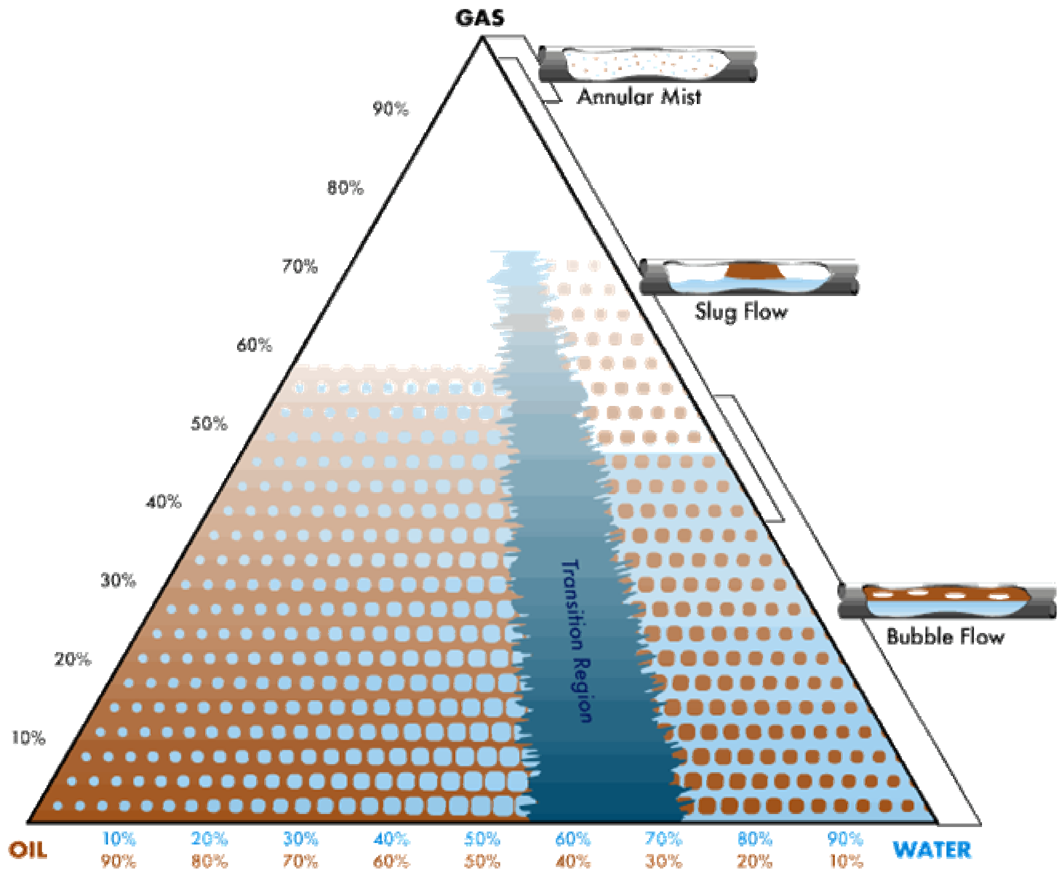

Figure 2.1 – Multiphase Composition Triangle

Pure oil, water and gas are located at the vertices of the triangle, with their corresponding two-phase mixtures (oil/gas, water/gas and oil/water) found along the triangle's sides. The area enclosed by the triangle represents multiphase mixtures of the three components. It can be observed that changing the fluid composition can induce different geometrical distributions of the fluid (annular mist, slug and bubble). Furthermore, a transition region has been designated to indicate the evolution of the liquid phase from oil continuous to water continuous. Considering that such a diagrammatic representation is only valid for a single fluid system at constant temperature, pressure, pipe diameter and flow orientation, one can appreciate the complexity implicated in dealing with multiphase flows.

A simplified representation of a multiphase flow is depicted in **Figure 2.2**.

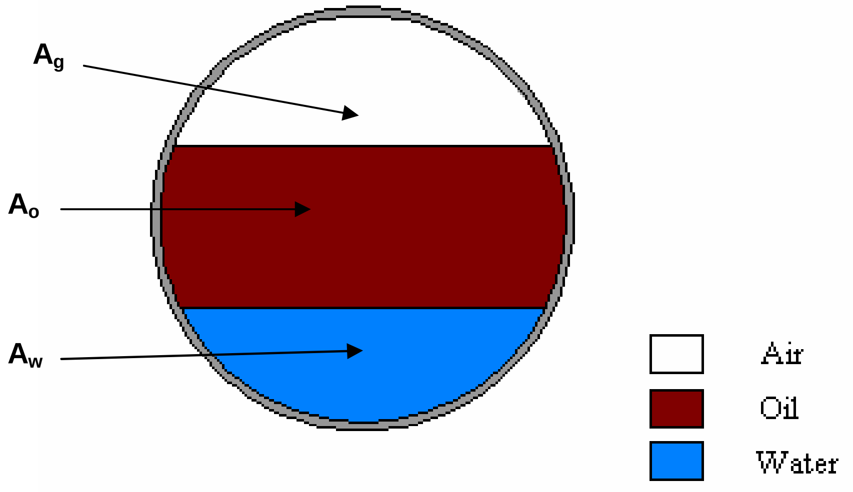

Figure 2.2 – Multiphase Pipe Flow Cross-Section

Each phase occupies a fraction of the total cross-sectional area of the conduit through which the fluid is flowing. The total volumetric flow rate through the pipe (Q_t) is the sum of its component volumetric flow rates of gas, water and oil (Q_g, Q_w, and Q_o respectively).

$$Q_t = Q_g + Q_w + Q_o \qquad \text{(Eq. 2.1)}$$

Mass flow rate (G_t) is determined by multiplying each component's volumetric flow rate by its corresponding density (ρ). The densities of oil, water and gas are calculated using well-established pressure, volume and temperature (PVT) data.

$$G_t = G_g + G_w + G_o = Q_t \rho_m \qquad \text{(Eq. 2.2)}$$

$$G_t = Q_g \rho_g + Q_w \rho_w + Q_o \rho_o \qquad \text{(Eq. 2.3)}$$

The phase volume fractions of the gas, water and oil (α, β, γ respectively) are given by the ratios of their individual cross-sectional areas to the pipe cross-sectional area (A_p).

$$\alpha = \frac{A_g}{A_p}; \beta = \frac{A_w}{A_p}; \gamma = \frac{A_o}{A_p} \qquad \text{(Eq. 2.4)}$$

In the mass flow expression derived (Eq. 2.3), the volumetric flow rate of each component can be replaced by the product of its cross-sectional area and velocity. Hence, where V_i denotes the velocity of component i, the total mass flux of the multiphase flow mixture can be expressed.

$$\frac{G_t}{A_p} = \alpha V_g \rho_g + \beta V_w \rho_w + \gamma V_o \rho_o \qquad \text{(Eq. 2.5)}$$

The liquid phase water cut (WC) is defined as the ratio of the water mass flow to the total liquid mass flow and is normally expressed as a percentage.

$$WC = \left(\frac{\beta \rho_w}{\beta \rho_w + \gamma \rho_o} \right) \times 100\% \qquad \text{(Eq. 2.6)}$$

2.1.2 Slip and Drift

In a multiphase flow, the gas phase velocity is typically higher than that of the liquid components. In vertical pipe lines, the density difference between the gas and liquid phases results in the gas phase being driven by a strong buoyancy force; meanwhile, in off-vertical flows, the liquid phase has a tendency to accumulate in horizontal and inclined pipe sections while the gas phase can easily traverse these sections unimpeded. This phenomenon is known as slip and the difference between the gas and liquid phase velocities is called the slip velocity.

$$V_{slip} = V_g - V_l \qquad \text{(Eq. 2.7)}$$

The deviation of the gas velocity from a homogenised flow velocity is the drift velocity.

$$V_{drift} = V_g - V_m \qquad \text{(Eq. 2.8)}$$

Homogeneity is achieved when the slip ratio (S), is equal to 1, i.e. the gas and liquid phase velocities have the same magnitude.

$$S = \frac{V_g}{V_l} \qquad \text{(Eq. 2.9)}$$

Liquid hold-up (λ_l) and gas void fraction (λ_g) are the liquid and gas volume fractions (α_l and α_g) as measured under flow conditions. In flow conditions conducive to phase slip, the liquid hold-up will be larger than the liquid volume fraction and the gas void fraction smaller than the gas volume fraction. The liquid hold-up and gas void fraction are only equal to their respective phase volume fractions under non-slip conditions, **Figure 2.3.**

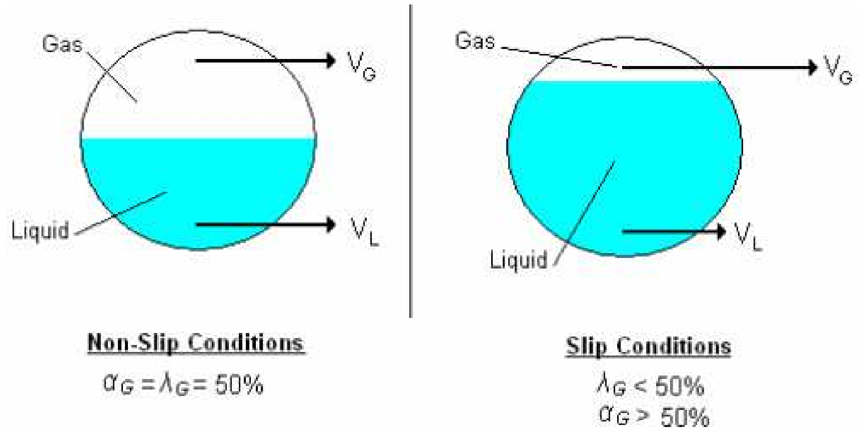

Figure 2.3 – Slip Effect on Phase Fractions

2.1.3 Slip Correction Correlations

In perfectly homogeneous flows, the slip ratio is unity (S = 1) and the measured void fractions are equal to the actual phase volume fraction. However, in practical measurement situations, the phase fraction composition of a multiphase flow will be determined by a senor in non-homogenised dynamic flow conditions. Phase slippage between the gas and liquid phases will result in underestimated gas fractions and overestimated liquid fractions owing to the larger gas phase velocity.

A number of researchers have investigated the influence of phase slip on the measured phase void fractions and its relationship to the actual phase volume fractions: a comprehensive review is given by Woldesemayat and Ghajar [**11**]. Four of the most commonly applied slip correlations are described in the following sections in order of increasing complexity and perceived accuracy.

2.3.2.1 Armand

Armand [**12**] proposed a slip ratio of S = 1.2 which acknowledges that the gas phase was travelling at a velocity in excess of that of the liquid phase. This function proposes a direct linear relationship between the measured void fraction (λ_g) and the actual volume fraction (α_g) under non-slip conditions.

$$\alpha_g = 1.2\lambda_g \qquad \text{(Eq. 2.10)}$$

2.3.2.2 Chisholm

Unlike the Armand correction which employs a single constant for the slip correlation, Chisholm [**13**] derived an expression for the slip ratio as a function of the vapour quality (x) and the ratio of the liquid and gas phase densities.

$$\alpha_g = \left[1 + \sqrt{1 - x\left(1 - \frac{\rho_l}{\rho_g}\right)} \cdot \left(\frac{1-x}{x}\right) \cdot \left(\frac{\rho_g}{\rho_l}\right)\right]^{-1} \qquad \text{(Eq. 2.11)}$$

2.3.2.3 Smith

Smith [**14**] developed a slip correlation on a model assuming equal velocity heads of a homogeneous multiphase mixture core and an annular liquid phase. The slip correction factor is a function of the phase density ratio, vapour mass quality and an entrainment ratio (K).

$$\alpha_g = \frac{1}{1 + \left(\frac{1-x}{x}\right)\left(\frac{\rho_g}{\rho_l}\right) \cdot S_{SM}} \qquad \text{(Eq. 2.12)}$$

$$S_{SM} = K + (1-K) \cdot \left(\frac{\left(\frac{\rho_l}{\rho_g}\right) + K\left(\frac{1-x}{x}\right)}{1 + K\left(\frac{1-x}{x}\right)} \right)^{1/2} \qquad \text{(Eq. 2.13)}$$

An entrainment ratio of K = 0.4 was found to correlate well with the three sets of experimental data considered.

2.3.2.4 Premoli et al

Premoli *et al* [**15**] have published an empirically derived mass flux based slip ratio corrrelation model. The slip correction factor is much more complicated than the other correlations detailed and is based on a complex function of the total mass flux (G), liquid phase surface tension (σ), liquid phase viscosity (μ_l), and the internal pipe diameter (d).

$$\alpha_g = \frac{1}{1 + \left(\frac{1-x}{x}\right)\left(\frac{\rho_g}{\rho_l}\right) \cdot S_{PRM}} \qquad \text{(Eq. 2.14)}$$

$$S_{PRM} = 1 + E_1 \cdot \sqrt{\frac{y}{1 + y \cdot E_2} - y \cdot E_2} \qquad \text{(Eq. 2.15)}$$

$$y = \left(\frac{\rho_l}{\rho_g}\right)\left(\frac{x}{1-x}\right) \qquad \text{(Eq. 2.16)}$$

$$E_1 = 1.578 \cdot \left(\frac{G \cdot d}{\mu_l}\right)^{-0.19} \cdot \left(\frac{\rho_l}{\rho_g}\right)^{0.22} \qquad \text{(Eq. 2.17)}$$

$$E_2 = 0.0273 \cdot \left(\frac{G^2 \cdot d}{\sigma \cdot \rho_l}\right) \cdot \left(\frac{G \cdot d}{\mu_l}\right)^{-0.51} \cdot \left(\frac{\rho_l}{\rho_g}\right)^{0.08} \qquad \text{(Eq. 2.18)}$$

The Premoli *et al* correlation was optimised to minimise liquid density prediction errors. This approach is well suited for exploitation in multiphase flows where the liquid phase density will vary according to the water cut.

2.1.4 Superficial Phase Velocities

Superficial phase velocities are commonly employed to describe multiphase flows. The superficial gas velocity (V_{sg}) is the gas velocity that would be obtained if the gas occupied the whole cross-section of the pipe. Mathematically, this is determined by dividing the total gas volumetric throughput by the total cross-sectional area of the pipe.

$$V_{sg} = \frac{Q_g}{A_p} \qquad \text{(Eq. 2.19)}$$

The superficial liquid velocity is derived in an analogous manner.

$$V_{sl} = \frac{Q_l}{A_p} \qquad \text{(Eq. 2.20)}$$

The sum of the liquid and gas superficial velocities yields the corresponding multiphase mixture velocity.

$$V_m = V_{sg} + V_{sl} \qquad \text{(Eq. 2.21)}$$

However, the multiphase mixture velocity is a derived velocity and only has a meaningful value if the multiphase flow is homogeneous and slip free. In most instances, the liquid hold-up will be larger than the liquid volume fraction and the gas void fraction will be smaller than the gas volume fraction because of phase slip. The superficial gas and liquid velocities can be calculated from the phase hold-ups and actual velocities.

$$V_{sg} = \frac{Q_g}{A_p} = \frac{Q_g}{A_g} \cdot \frac{A_g}{A_p} = V_g \lambda_g \qquad \text{(Eq. 2.22)}$$

$$V_{sl} = \frac{Q_l}{A_p} = \frac{Q_l}{A_l} \cdot \frac{A_l}{A_p} = V_l \lambda_l \qquad \text{(Eq. 2.23)}$$

2.1.5 Flow Regimes

Multiphase flows can distribute themselves in an infinite number of ways. Flow regimes are classifications that have been developed to describe, in general terms, the multiphase flow geometry. The flow regime adopted by a multiphase flow is dictated by a number of parameters including the operating conditions, fluid properties, flow rates, pipe geometry, and pipe orientation.

Although many flow regimes classifications exist, they can all be broadly classified into dispersed flow, separated flow, intermittent flow or a combination of these, **Figure 2.4**.

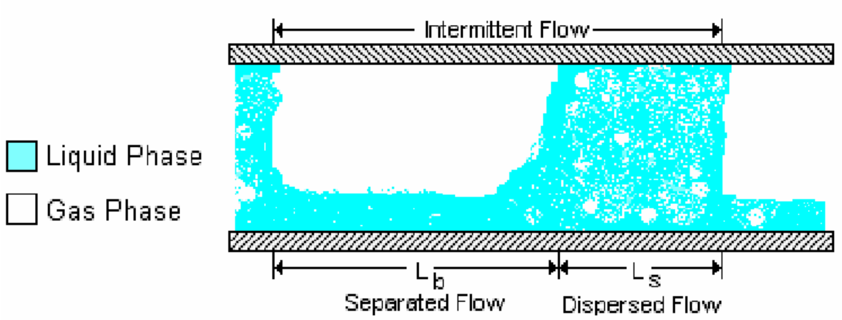

Figure 2.4 – Multiphase Flow Regime Classes

A dispersed flow regime (L_b=0) is defined by a uniform phase distribution across both the radial and axial directions. The separated flow regimes (L_s=0) are distinguished by the fact that they comprise a non-continuous phase distribution in the radial direction but a continuous phase in the axial direction. The final group of multiphase flow regimes are the intermittent flows which tend to display localised unsteady behaviour due to a non-continuous phase in the axial direction.

Liquid-liquid interactions in a multiphase system usually exhibit less significant influence, when compared to the gas-liquid interactions, on the flow regime adopted. In such cases, the liquid-liquid portion can be modelled as a dispersed flow although it should be noted that the liquid mixture properties can be highly dependent on the volumetric ratio of the two components present.

Researchers have reported a number of experimental based methods to rationalise flow regime identification. Data from sensors have been analysed using techniques such as statistical analysis of signal responses [**16, 17**], fractal analysis [**18**], template matching [**19**], and neural networks [**20, 21**]. While these techniques enable general classification of flows operating within particular regimes, describing the boundaries between flow regimes remains somewhat subjective as these are sensitive transitional areas rather than clear-cut boundaries. Accordingly, multiphase flows that lie close to regime boundaries still cannot be definitively established.

Flow regimes maps are graphical charts that are used to predict the different types of flow patterns that will occur for a particular system. Baker [**22**] was amongst the first to publish horizontal flow regime map that enabled the flow pattern to be predicted upon knowing the mass velocities of the liquid and gas phases and the fluid properties. Many other researchers have studied flow patterns employing their own modified parameters to describe the gas and liquid flows [**23-26**]. Mandhane *et al* [**27**] published a set of multiphase flow maps that were able to predict the flow regime present in a pipe based on the superficial phase velocity parameters. Taitel *et al* [**28**] exploited superficial phase velocities to produce a model describing the flow regime transitions in vertical flow. Following its publication, the Taitel-Dukler map was found to define the transition between different flow regimes more accurately than other models. Flow regime maps plotted using the superficial phase velocity parameters are widely used in the oil and gas industry owing to their comparative simplicity.

A few detailed studies of oil, water and gas systems have been undertaken. These have reported the existence of similar flow regimes as those witnessed in standard two-phase flow systems but a particular emphasis is placed on identification of the dispersed and continuous components in the liquid phase [**29, 30**].

Nevertheless, certain key discrepancies have been reported between two and three phase flow patterns. At low flow velocities, the liquid density difference may be sufficient to induce separation of the oil and water phases. In vertical flow this can result in the production of alternating oil and water slugs while in the liquid phase substantial slip between the liquid phases has been reported [**31**]. Furthermore, at low gas flow rates, near vertical multiphase flows have been shown to have significant differences when compared to flows contained in a purely vertical conduit [**32**].

2.1.5.1 Vertical Pipe Flow Regimes

Multiphase flow is fairly common in oil well pipelines despite the fact that the well pressure at the bottom can exceed the bubble point of the oil. The pressure drop experienced by the oil as it is transported from the seabed to the surface can result in gas liberation from the liquid oil phase. The flow regimes witnessed in vertical risers are usually fully developed and essentially axial-symmetrical. Generally, the multiphase flow features present vary with well age with older wells exhibiting a larger gas vapour fraction. **Figure 2.5** illustrates a generic multiphase flow map, based on gas and liquid superficial velocities, for vertically upward multiphase flow in a vertically orientated pipeline [**33**].

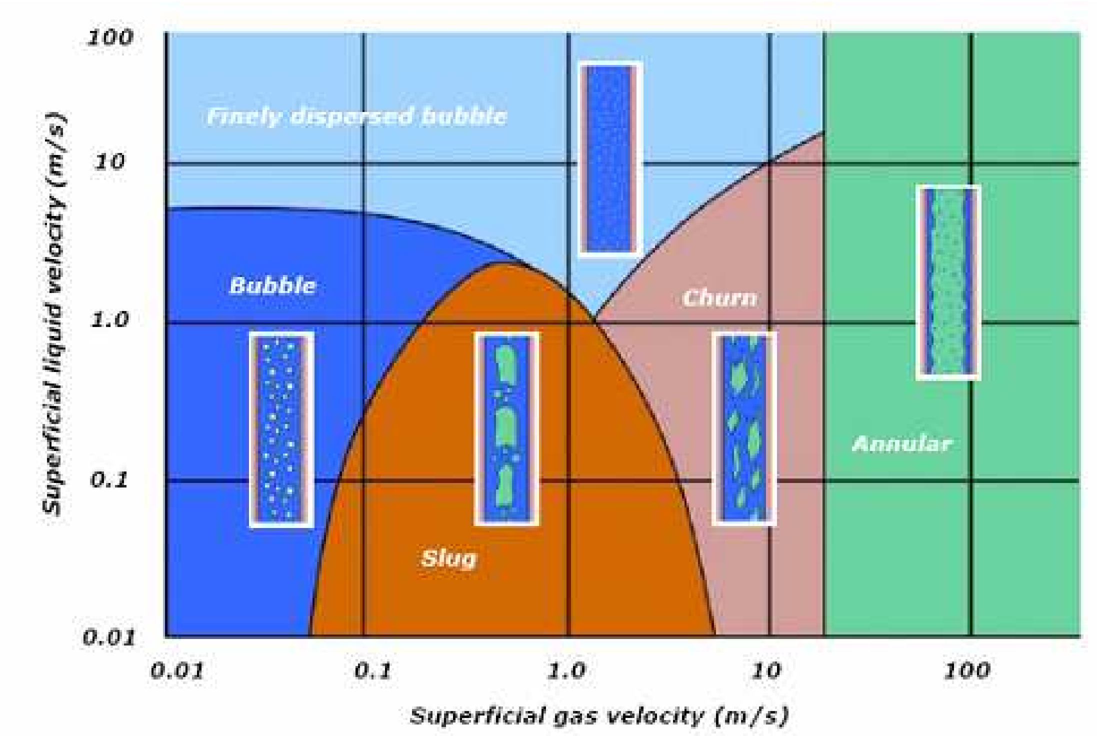

Figure 2.5 – Multiphase Flow Map for Vertical Flow

The vertical flow regimes are commonly categorised into four main classifications:

> Bubble (including finely dispersed bubble): At low gas flow rates, a continuous liquid phase is formed with the gas phase producing discrete bubbles within the continuum. The gas bubbles may coalesce to form larger bubbles or slugs.
>
> Slug: Increased gas flow rates increase bubble coalescence until the bubble diameter eventually approaches that of the pipe diameter. The resulting flow alternates between high-liquid and high-gas composition.
>
> Churn: Somewhat similar to slug flow, but more chaotic in nature owing to the larger gas flow rates. The slug bubbles have become distorted to form longer, narrow structures and the flow adopts a random oscillatory nature. The liquid flow occurs mainly at the pipe wall but a significant proportion is vigorously mixed with the gaseous core.
>
> Annular: At very high gas flow rates, the liquid phase is forced to flow up the pipe wall as a liquid film while the gas flow in the centre. The interface between the phases is typically wavy. The wavy interface enables liquid entrainment in the gaseous core. When the quantity of entrained liquid becomes significant, the flow is described as having an annular mist regime.

2.1.5.2 Horizontal Pipe Flow Regimes

As with vertical flow, flow regime transitions in horizontal pipes are functions of parameters such as pipe diameter, interfacial tension, and phase densities. However, the flow patterns exhibited in horizontal regimes are not axially symmetrical and a pipe length equivalent to at least 100 pipe diameters is required to establish fully developed flow. Multiphase flow maps based on superficial phase velocities are also readily available for horizontal flows **Figure 2.6** [**33**]. However, a multiphase map like this will only supply valid flow regime predictions for a specific pipe, pressure and fluid system.

The flow regimes observed for horizontal flows will tend to be more complex than their vertical counterparts due to gravity induced asymmetries. The heavier phase will be inclined to accumulate at the bottom of the pipe. The horizontal flow regimes are commonly categorised into six main classifications:

> Bubble: The gas phase exists as discrete bubbles within a liquid continuum. The gas bubbles will tend to flow in the upper section of the pipe. However, with larger gas flow rates, a uniform bubble distribution across the pipe cross-sectional area may be witnessed.
>
> Plug: Reducing the liquid flow rate will enable the gas bubbles to coalesce into larger bubbles or plugs which will occupy the upper section of the conduit.
>
> Stratified: Further reductions to both the gas and liquid flow rates will result in phase stratification whereby the two phases flow separately with a relatively smooth interface. The liquid phase will occupy the lower section of the pipe due to gravity.

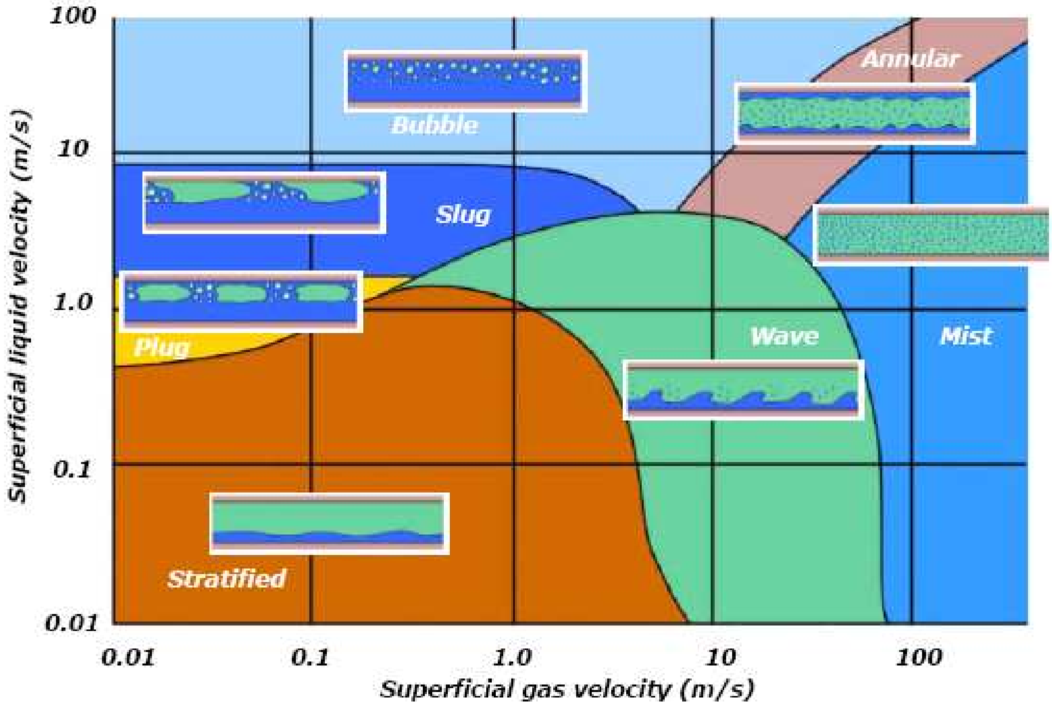

Figure 2.6 – Multiphase Flow Map for Horizontal Flow

Wave: Increasing the gas flow rate of a stratified system will produce a less stable phase interface as a result of the increased turbulence. The interface between the liquid and gas phases will be irregular and wavy in nature although good separation between phases will be maintained.

Slug: Increasing the liquid flow will produce waves of a much larger magnitude until the liquid is increased to such a point where the wave occupies the whole of the pipe cross-section. This facilitates the propagation of a high velocity fluid slug down the pipe.

Annular/Mist: At very high gas flow rates, the liquid phase is forced to flow up the pipe wall as a liquid film while the gas flow in the centre. The liquid film will be thicker at the bottom of the pipe owing to gravitational effects.

2.2 Multiphase Flow Measurement

2.2.1 Inferential Multiphase Flow Measurement

Multiphase flow measurement has become an increasingly important concept in recent years [**34**]. The fundamental function of a multiphase flow meter in the petroleum industry is to supply the user with information on the mass flow rate of oil, water and gas components in a flow. In an ideal situation, a flow meter would simply make direct measurements of each of these three quantities. Unfortunately, direct mass flow meters for multiphase flows do not exist yet.

As the mass flow rates are unable to be measured directly in a multiphase flow, an inferential mass method is used instead [**8**]. There are two categories of variable type in inferential multiphase metering systems: primary and secondary, **Table 2.1**.

Multiphase Flow Metering System Variables	
Primary Variables	**Secondary Variables**
Phase Fractions Phase Velocities Phase Density	Flow Regime Phase Viscosity Phase Salinity Phase Permittivity/Conductivity

Table 2.1 – Classification of Multiphase Metering System Variables

Determination of the primary variables is a prerequisite in applying the inferential method for multiphase flow measurement. Quantification of the secondary variables is not strictly required, but could facilitate more accurate measurements if they are taken into consideration. The flow regime parameter may be considered a primary variable if a flow regime dependent sensing technique is to be employed in the determination of the core primary variables.

The inferential method requires the resolution of the instantaneous velocity, cross-sectional fraction, and density of each component in order to be able to calculate the individual flow rates and the total mixture flow rate, **Figure 2.7**.

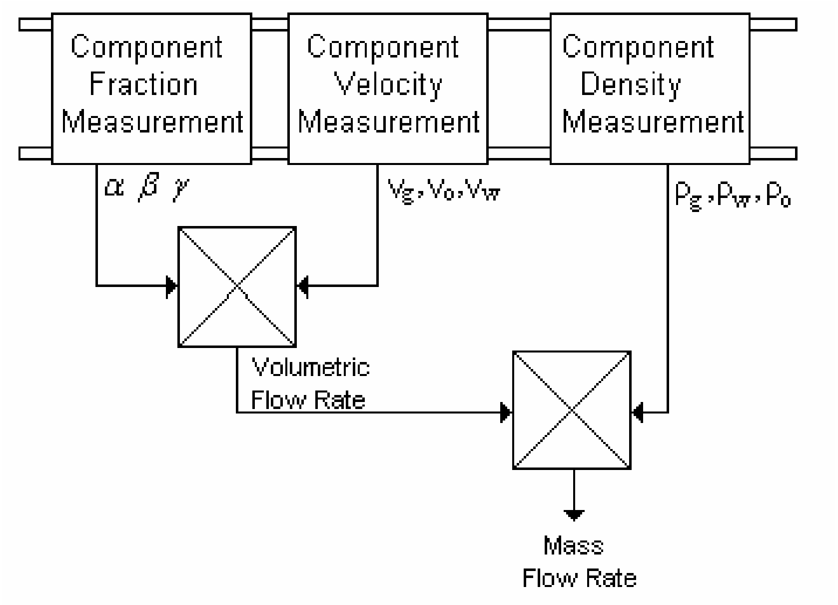

Figure 2.7 – Inferential Method of Multiphase Flow Measurement

Density data for all three components is readily available from other parts of the production process or can be estimated using PVT diagrams. Thus, the problem is to measure the component velocities and two of the three component volume fractions, usually the gas phase fraction and the liquid phase water fraction, in order to calculate the total mass flow.

$$G_t = \alpha V_g \rho_g + \beta V_w \rho_w + [1 - (\alpha + \beta)] V_o \rho_o \qquad \text{(Eq. 2.24)}$$

Where it is assumed that:

$$\alpha + \beta + \gamma = 1 \qquad \text{(Eq. 2.25)}$$

It is common practice to simplify the problem by assuming that the liquid phase velocity parameters are equal, reducing the number of unknown variables to five. Homogenisation of the multiphase mixture may be employed to reduce the velocity parameters to a single uniform mixture velocity [**35**].

Current state of the art multiphase flow meters employ a variety of technologies to determine the multiphase component volume fractions and velocities. These methods are detailed in the following sections along with an overview of some important computational techniques that could have a significant role in the future development of multiphase flow meters. A comprehensive review is given by Sanderson [**36**].

2.2.2 Operating Principles of Multiphase Meters

2.2.2.1 Phase Volume Fraction Measurement

2.2.2.1.1 Electrical Impedance Methods (Capacitance and Conductance)

Impedance methods have attracted a great deal of interest due to both their non-invasive instrumentation and almost instantaneous dynamic response. Electrical impendence methods operate by characterising the multiphase fluid flowing through a pipe section as an electrical conductor, **Figure 2.8**.

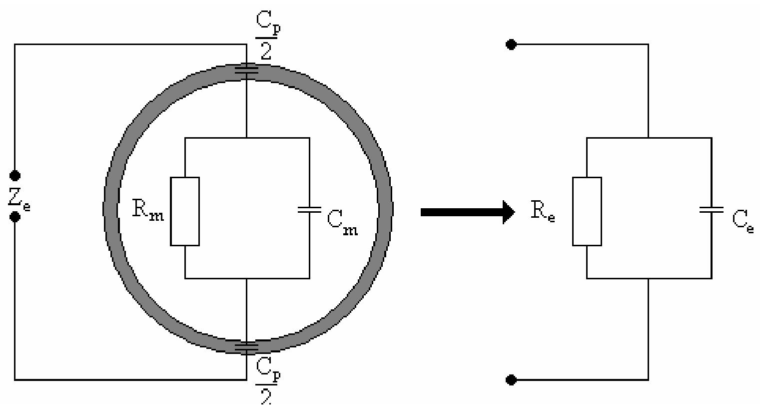

Figure 2.8 – Capacitance Method for Component Fraction Measurement

Either contacting or non-contacting electrodes are employed to quantify the electrical impedance across the pipe diameter of the multiphase flow line thus enabling determination of the capacitance or conductance of the fluid mixture. The frequency of the input signal determines whether the measurement is in the impedance or the capacitance mode. By measuring the electrical impedance (Z_e) across two electrodes, the measured resistance (R_e) and capacitance (C_e) can be calculated from the expressions:

$$R_e = \frac{1+\omega^2 R_m{}^2 (C_m + C_p)^2}{\omega^2 R_m C_p{}^2} \quad \text{(Eq. 2.26)}$$

$$C_e = \frac{[1+\omega^2 R_m{}^2 C_m (C_m + C_p)]C_p}{1+\omega^2 R_m{}^2 (C_m + C_p)^2} \quad \text{(Eq. 2.27)}$$

The resistance (R_m) and capacitance (C_m) of the multiphase fluid mixture in the pipe are functions of the conductivity and permittivity of the multiphase flow constituents, the void fraction, water fraction and prevailing flow regime. Consequently, the measured resistance and capacitance will be related to the intrinsic R_m and C_m values of the multiphase mixture as well as the excitation frequency of the electronics (ω), electrode geometry and material. The capacitance of the electrode-pipe coupling (C_p) is fixed for a particular geometric configuration. For a fixed electrode geometry and flow regime, the measured electrical impedance is a direct function of the flow's component ratio.

The system depicted in **Figure 2.8** is based on two electrodes installed opposite each other on the inner walls within the measurement section, thus facilitating the determination of the dielectric constant of the mixture. The difference in the dielectric coefficient between water and oil allows determination of the water cut. However, capacitance composition measurement technologies can only be used in a continuous oil or gas continuous flow regimes as in the presence of continuous water phases the multiphase mixture will 'short-circuit' the capacitance circuit.

When the liquid phase water cut is above 60 – 70%, capacitance measurements must be replaced by conductivity measurements as the fluid transforms from oil to water continuous. Typically, the conductivity will be measured by injecting a controlled electrical current into the flow and measuring the voltage drop between the electrodes along an insulated section of the pipe, **Figure 2.9**.

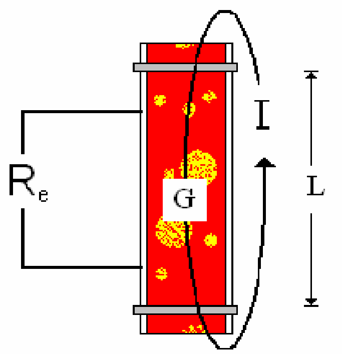

Figure 2.9 – Conductance Method for Component Fraction Measurement

Electrical current can be injected using contact electrodes or non-contact electrodes (inductive mode). Applying Ohm's law, the effective resistance (R_e) offered by the multiphase flow can be determined by dividing the measured voltage drop by the current injected (I). Since the distance between the electrodes is also known (L), this resistance measurement can be expressed in terms of conductivity (G).

Electrical impedance methods have two limitations that have to be considered: flow regime dependence and measurement discontinuity over the full component fraction range. Switching between capacitance and conductivity measurements is used to overcome the latter although measurement difficulties can occur around the inversion point if the fluid oscillates between oil and water continuous.

Furthermore, to remove the uncertainty obtained in electrical impendence owing to their flow regime bias, two techniques are commonly exploited:

1. Homogenisation of the multiphase mixture prior to measurement.
2. Modification of electrode design to reduce bias.

Several modified electrode designs have been reported such as helical [**37**] and rotating fields [**38**]. These sensor designs ameliorate the metering performance within identified flow regimes. Nevertheless, impedance sensors are still not suitable for use in applications where the flow regime is unknown or unstable.

2.2.2.1.2 Gamma Radiation Attenuation

Gamma radiation attenuation techniques can be used to resolve two-component mixture phase fractions based using a single-energy gamma source or three-component mixtures using a dual-energy gamma source [**39**].

A collimated gamma ray beam is directed at the pipe with a sensor placed diametrically opposite the source on the other side of the pipe, **Figure 2.10**.

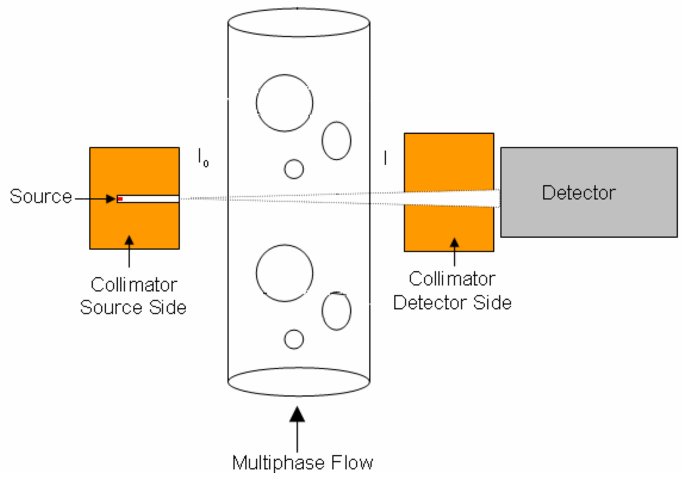

Figure 2.10 – Gamma Attenuation Measurement

The intensity of the gamma beam decays approximately exponentially as it passes through matter flowing in through the pipe measurement section. A gamma ray beam will be attenuated to different degrees by materials according to their density: a more dense material will attenuate the electromagnetic radiation to a greater extent than a less dense material. If the gamma source employed has two distinct energy levels, this can be exploited to determine the volumetric fractions of oil, water and gas in a three-phase mixture as the atomic attenuation coefficients depend not only on the density of a material but also the energy of the gamma beam itself.

A more detailed discussion of the application of gamma-ray attenuation in multiphase flow metering is given in **Chapter 2.3**.

2.2.2.1.3 Microwave Sensor

Microwave sensors are used to distinguish between water and oil in the liquid phase of a multiphase flow. Water and oil have distinctly different dielectric constants and conductivities and it is this difference that allows a microwave sensor to determine the water content of a water-oil mixture, **Table 2.2**.

Property	Gas	Oil	Water
Density (kg/m^3)	10	840	998
Dielectric Constant (dimensionless)	0	2	75
Conductivity (μScm^{-1})	1	10^{-6}	10

Table 2.2 – Typical Properties of Gas, Oil and Water Components

There are three main different microwave sensor operation principles [**40**].

1. <u>Transmission sensor and measurement on a single frequency</u>:
A probe is use to transmitted microwave radiation through the multiphase medium to a receiving probe. Caution must be exercised to prevent reflections in the pipe/sensor and a guided wave sensor may be deployed to prevent against this. The microwave-receiving sensor may be configured to output the attenuation of or the phase change in the transmitted microwave radiation.

2. <u>Transmission sensor and measurement on a varying frequency</u>:
Owing to the large attenuation of water continuous liquid phases on high frequency microwaves, it may be beneficial to employ a varying frequency method where the frequency of microwave radiation transmitted is a function of the dielectric properties of the fluid. This can be implemented by monitoring the change of phase such that the meter can determine the frequency where the phase change is constant.

3. <u>Resonator sensor</u>:
The meter measures the dielectric properties of the mixture using the resonant cavity method. A resonant cavity comprises a metal structure which confines an electric field, causing it to reflect back and forth within the cavity. By matching one of the dimensions of the cavity to the wavelength of the electromagnetic

radiation, a standing wave is produced. When this cavity is filled with a specific fluid, the resonant frequency of the cavity will shift in direct proportion to the dielectric constant of the fluid present. As a result, measuring the resonant frequency and peak width, the dielectric properties of fluid can be determined. The system can be calibrated to give the water cut.

In practise, microwave sensors use a combination of techniques, using the resonating cavity principle for oil continuous flows and the varying transmission frequency for in water continuous. A microwave sensor would be used in tandem with either electrical impendence or gamma attenuation technique to obtain the gas volume fraction of the multiphase flow.

2.2.2.2 Phase Velocity Measurement

2.2.2.2.1 Positive Displacement Meter

The positive displacement meter is used in partial separation type meters on the liquid phase. It operates by dividing up the flow into distinct volume ‘packets’ and then summing these to give the total volume flow by counting the unit volumes passing through the meter. The meter comprises of a number of chambers which are continuously charged and discharged with the fluid. For each ‘cycle’ of fluid charging-discharging, the rotation is transmitted to a mechanical or electrical counter which reads the total volumetric flow [**41**]. Owing to the nature of a positive displacement meter, downstream of the instrument there is no phase slip

These meters have moving parts and are driven by the pressure drop across the meter. Adequate sealing is required to ensure segregation of the fluid volume packets. Nevertheless, the performance of the positive displacement meters is affected to some extent by the presence of entrained gas. In addition, the mechanical nature of the equipment renders it liable to jamming, leakage, rotor imbalance and wear.

2.2.2.2.2 Differential Pressure Measurements

In instances where a multiphase flow is sufficiently mixed, differential pressure based flow measurement techniques such as Venturi and orifice sections can be utilised to determine the flow velocity and also measure the mixture flow rate [**42**]. The pressure drop measured across these sections can be expressed as a function of the fluid flow rate and vice-versa. The Venturi and orifice meter operating principles are well-established and well-understood single-phase flow measurement methods. Full descriptions of their technical designs are detailed in ISO 5167:2003.

Figure 2.11 illustrates the geometry of the Venturi and orifice inserts and their characteristic flow profiles. In the Venturi section, the reduction in the flow area results in increased fluid velocity and, consequently, reduced fluid pressure. The small angle of the downstream cone facilitates large pressure recovery by minimising frictional losses. In contrast, the abrupt reduction in flow diameter in the orifice plate results in creation of regions of fluid recirculation and the downstream pressure recovery is hindered by the disturbed flow pattern induced by the restriction.

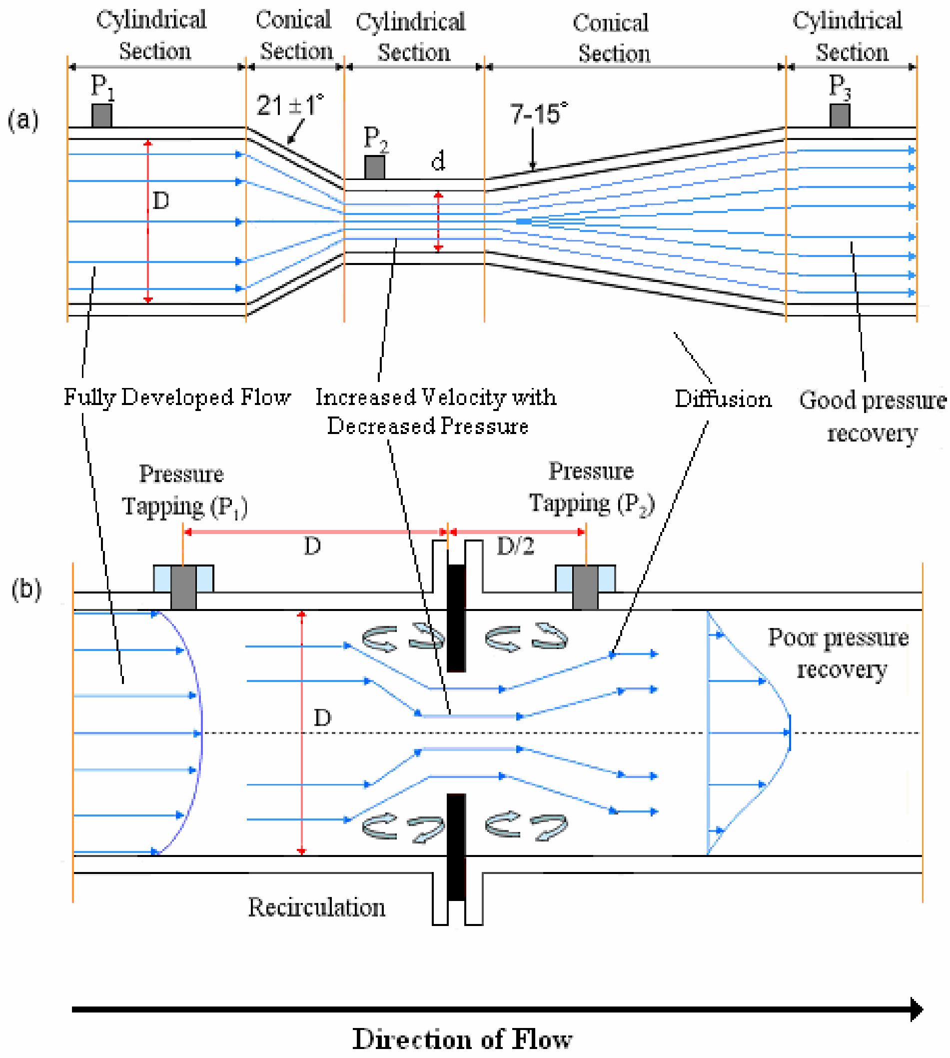

Figure 2.11 – Differential Pressure Measurement Systems (a) Venturi (b) Orifice

The use of orifice plates tends to be restricted to wet gas measurements owing to their poor pressure recovery properties. The gas phase flow rate can be determined from the two phase mixture pressure drop through the application of either the Murdock [**43**] or Chisholm [**44**] correlation.

Murdock: $$Q_g = \frac{Q}{1+1.26X} \qquad \text{(Eq. 2.28)}$$

Chisholm: $$Q_g = \frac{Q}{\sqrt{1+CX+CX^2}} \qquad \text{(Eq. 2.29)}$$

Where, Q denotes the wet gas flow rate derived from the orifice plate pressure drop and C is the Chisholm constant and X is the Lockhart-Martinelli parameter:

$$C = \left(\frac{\rho_l}{\rho_g}\right)^{0.25} + \left(\frac{\rho_g}{\rho_l}\right)^{0.25} \qquad (X < 1) \qquad \text{(Eq. 2.30)}$$

$$X = \frac{Q_l}{Q_g} \cdot \sqrt{\frac{\rho_l}{\rho_g}} \qquad \text{(Eq. 2.31)}$$

In order to determine the flow rate of the homogeneous gas-liquid mixture using a Venturi, an experimentally determined corrected differential pressure formula must be applied, such as that proposed by Hammer and Nordvedt [**45**]: the volumetric liquid flow rate can be obtained from a measured pressure drop (ΔP) for a known gas volume fraction and liquid density.

$$Q_l = \sqrt{\frac{(1-\alpha)\Delta P}{\rho_l}} \qquad \text{(Eq. 2.32)}$$

The Venturi method has many advantages including low cost, good pressure recovery, familiarity, and simple operation. Furthermore, high accuracy velocity measurements (relative error <1%) can be obtained as long as the multiphase flow mixture maintains homogeneity. On the other hand, the multiphase flow will require pre-conditioning in order to induce a state of homogeneity. In addition, the differential pressure lines of the Venturi meter require regular purging and scale formation can yield excessively high-pressure drops

2.2.2.2.3 Cross-Correlation

The cross-correlation method is a commonly used technique for determination of phase velocities in multiphase flow measurement systems. Two sensors are mounted on the conduit to monitor the fluid flow, one at a known distance (L) downstream of the other, **Figure 2.12**.

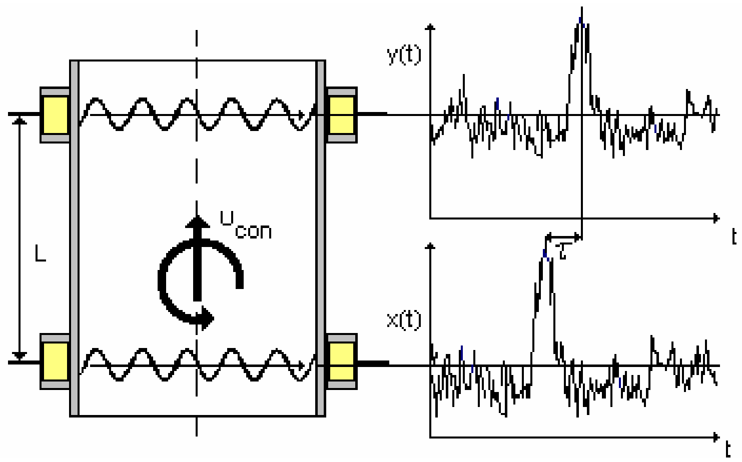

Figure 2.12 – Principle of Cross-Correlation

The upstream and downstream sensors will record disturbances in a specified fluid property (e.g. density, permittivity or conductivity) and produce time-varying output signals *x(t)* and *y(t)* respectively. The cross-correlation function is defined as:

$$R_{xy}(\tau) = \frac{1}{T}\int_0^T x(t)\,y(t-\tau)\,dt \qquad \text{(Eq. 2.33)}$$

Where, $R_{xy}(\tau)$ describes the value of the cross-correlation function when the upstream signal output $y(t)$ has been delayed with a time lag τ, while T denotes the duration of the sensor data. The transit time of the flow between the two sensors is found by observing the time lag at which the cross-correlation function exhibits its maximum value, **Figure 2.13**.

Knowing the distance between the sensors (L) and the time lag (τ_{max}), the velocity (V) of the tracer signal, and thus the flow velocity, can be determined.

$$\upsilon = \frac{L}{\tau_{\max}} \qquad \text{(Eq. 2.34)}$$

The cross-correlation method has been successfully implemented utilising a variety of sensors, from microwave to capacitance. The uncertainty implicated in the velocity values obtained is highly dependent on the validity of the relationship applied to connect the inferred velocities from the mean velocity of the flow. However, in oil-water-gas multiphase systems the presence of slip can result in the occurrence of significant measurement errors.

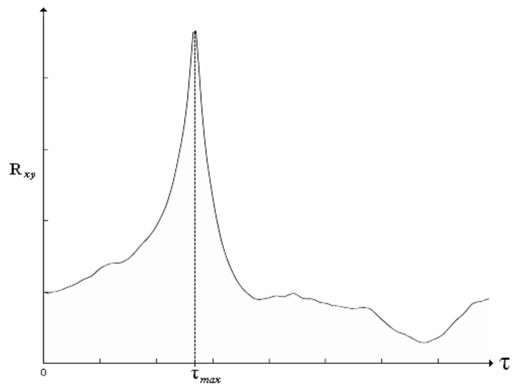

Figure 2.13 – Cross-Correlation Function

Methods to overcome these errors induced by the presence of slip have been developed. The simplest solution involves homogenisation of the flow upstream of the sensors. This process attempts to ensure that there is a uniform velocity profile across the pipe. Twin-cell rotational type mixers are employed as conventional in-line mixers offer an insufficient mixing performance over the phase fraction ranges encountered in multiphase flow measurement applications [**46**].

Alternatively, two sets of capacitance sensors can be utilised to determine the velocity of the gas and liquid phases individually [**47**]. One set of sensors monitors the velocity of the large gas bubbles which are assumed to be representative of the velocity of the dispersed phase. The remaining set of sensors is used to measure the velocity of the small gas bubbles. These small gas bubbles are assumed to be representative of the non-dispersed liquid phase.

Beck *et al* [**48**] published some general procedures that should be applied to obtain good accuracy with a cross-correlation system:

1. To maximise correlation response to flow noise turbulence, the sensor bandwidth (B_s) should be as large as possible. White noise produces a perfectly narrow correlation spectrum which could dominate the cross-correlation function output if the sensor bandwidth is itself too narrow.

2. The distance between the sensors L should be minimised to reduce the possibility of flow evolution between the sensors. On the other hand, if this length is too small relative spacing uncertainty, signal quantisation errors and signal crosstalk error will be produced. For a homogeneous flow, Ong and Beck [**49**] suggest a sensor separation of 3 – 4 pipe diameters.

2.2.2.3 Artificial Neural Networks

Application of artificial neural networks (ANNs) to multiphase flow measurement is a recent development in the field. A neural network is a data processing paradigm that was inspired by the way biological nervous systems process data. The real strength in the application of neural networks to multiphase flow measurement problems lies in their ability to represent both linear and non-linear relationships and their capability to learn these relationships directly from the data being modelled [**50**]. A more detailed discussion of ANNs, and other pattern recognition methods, as applied to multiphase flow measurement is given in **Chapter 2.4**.

2.2.2.4 Tomography Systems

Electrical capacitance tomography (ECT) is a non-intrusive technique for obtaining distribution data of the contents of closed conduits by measurement of the variations in the dielectric properties of the fluid inside the conduit [**51**]. Typical information yielded includes cross-sectional images of the conduit contents and the measurement of the phase fraction and velocities of the contents of pipes for multiphase flows. A basic ECT system comprises a capacitance sensor, a capacitance-measuring unit and a control computer. The pipe cross-section to be imaged is surrounded by one or more circumferential sets of capacitance electrodes and the electrical capacitances between all combinations of the electrodes within each set are recorded. This data can then be used to build an image of the pipe contents enclosed by the sensors, based on variations in the permittivity of the material inside the measurement area.

2.2.3 Current Commercially Available Multiphase Flow Meters

There are a number of commercially available multiphase flow meters that have been deployed in the field. These meters employ a diverse range of measurement principles and solutions. Certain types of meters perform better in certain applications than others. Thus, a detailed comparison and selection process is needed to determine the MPFM best suited to a particular application. A review of current commercially available multiphase meters was undertaken as part of this research work, **Appendix A**. The information presented was compiled from published papers, sales documentation, third-party test reports, and author correspondence with the vendors. However, access to details of research undertaken pertaining to the development of the measurement technologies was severely limited owing to its commercial sensitivity.

2.2.4 Multiphase Flow Meter Performance

Given that multiphase flow metering in field applications is still in its early stages of development, there are few generally accepted standards to quantify performance of meters. At present, industry employs a mixture of manufacture sponsored testing, third party testing, and end-user field-testing in an attempt to verify the performance of a multiphase flow meter.

Slijkerman *et al* [**52**] specified their desired targets for multiphase flow meter performance in order to apply them to a number of applications for potential benefits in their respective operating companies: monitoring of large well stream throughputs of up to 5,000 m^3 of liquids and 60,000 m^3 of gas per day; metering of even higher flow rates in total satellite allocation; handling high gas-vapour fractions (>70% is common); handling variable water cuts that can range from 0 – 90 % over the well life; harsh meter operating conditions (high pressure and high temperature environments). Although it was acknowledged that specific requirements would vary from case to case, the target accuracy levels called for by the oil companies were set at ±5 – 10% relative accuracy in the total liquid flow rate; ±5 – 10% relative accuracy in the gas flow rate and ±2% absolute error in the water cut measurement.

In reality, modern MPFMs fail to live up to the requirements for such an instrument. Babelli [**53**] argues that an ideal MPFM would fulfil the following criteria:

- Accurate determine of void fractions and flow rates;
- Independent of fluid type, flow regime, pipe size, pressure and temperature;
- Non-intrusive measurements;
- Robust and low maintenance;
- Consistent in measurements over long period of time;
- Simple and inexpensive.

To date, there is no one meter on the market that fulfils all the above criteria.

2.3 Gamma Radiation in Multiphase Metering

2.3.1 Gamma Radiation

Unstable isotope nuclei undergo radioactive decay. This is a set of processes by which unstable atomic nuclei emit subatomic particles. After an alpha or beta radioactive decay, the nucleus is still often in an ‘excited’ state. Rather than emitting another beta or alpha particle, this energy can be dissipated by emitting a pulse of electromagnetic radiation called a gamma ray, **Figure 2.14**.

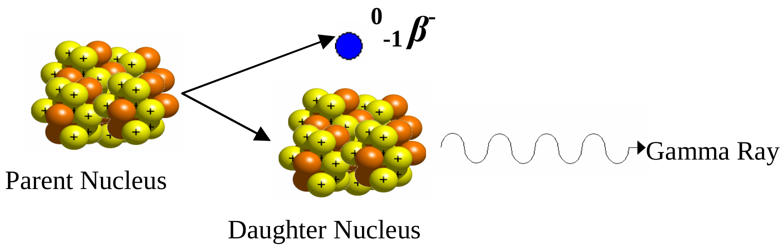

Figure 2.14 – Gamma Decay of Radioactive Isotope

Like all forms of electromagnetic radiation, gamma radiation has no mass and no charge. It is emphasised that most alpha and beta emitters emit gamma rays as part of their decay process and that pure gamma-only emitters do not exist.

2.3.2 Photon Interactions

Gamma radiation photons can interact with material in a variety of manners, the probabilities of which are strong functions of the photon energy and the atomic number of the absorbing material. **Figure 2.15** illustrates the different interaction probabilities (σ) plotted as a function of photon energy for hydrogen, carbon, krypton and lead [**54**].

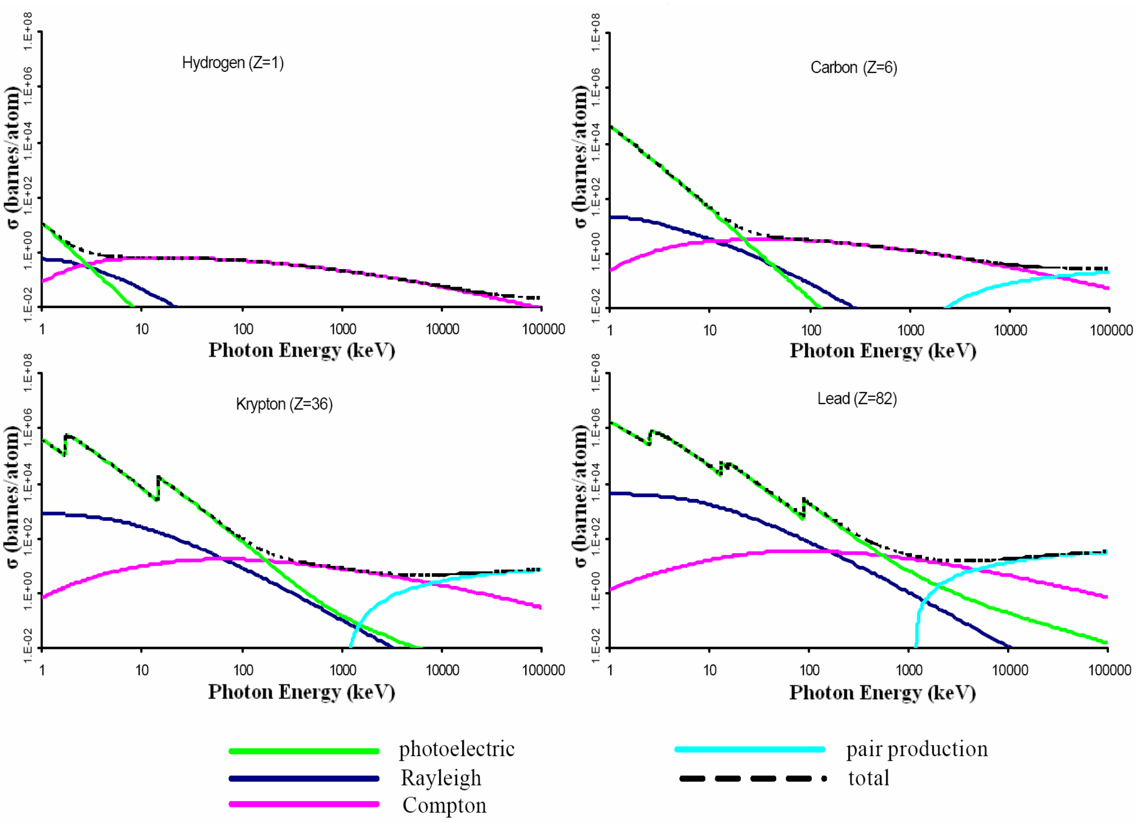

Figure 2.15 – Photon Interaction Probability Cross-Sections

The interaction probabilities are expressed as cross-sections in units of area. Conventionally, the area is expressed in barns, where 1 barn is equivalent to 10^{-28} m^2. The interactions of interest, over the photon energies examined, are Raleigh (elastic/coherent) scattering, Compton (inelastic/incoherent) scattering, photoelectric interaction and pair production.

The magnitudes of the interaction cross-section probabilities increase as a function of atomic number. At the lowest photon energies, the photoelectric effect dominates the total cross-section. For higher photon energies, Compton scattering dominates. The energy at which Compton scattering begins to dominate is a function of an element's atomic number. Heavier elements' photon interaction cross-sections are dominated by pair production at photon energies greater than 10,000 keV. A heavy nucleus is required for pair production which is why there is no pair production probability cross-section shown in the hydrogen plot.

2.3.2.1 Photoelectric Effect

In photoelectric effect interactions, the photon is entirely absorbed and its energy used to ionise the absorbing atom and impart kinetic energy to an ejected electron, **Figure 2.16 (a)**. A photoelectron will be released with an energy (E_{pe}) equal to that of the incoming photon minus the electron binding energy (E_b).

$$E_{pe} = h\upsilon - E_b \qquad \text{(Eq. 2.35)}$$

Where, h and υ denote the Planck constant and photon frequency respectively.

The most probable source of the photoelectron depends on the energy of the absorbed photon. The most highly bound electrons have the largest absorption cross-section, provided that the photon energy is in excess of the binding energy of that shell. For example, photons with an energy above that of the K-shell binding energy have a K-shell interaction cross-section approximately four to five times larger than that of the L-shell cross-section. The ejected electron leaves a vacancy in the shell, inducing the atom to emit a characteristic X-ray or Auger electrons as it returns to its normal state. The cross-section for photoelectric interactions can be expressed as a function of the absorbing material atomic number (Z) and incident photon energy (E).

$$\sigma_{photoelectric} \propto \frac{Z^x}{E^y} \qquad \text{(Eq. 2.36)}$$

Where x and y are slowly varying functions of Z and E respectively (x = 4 and y = 3 can be used as a rule of thumb). Discontinuities, or absorption edges, occur in the photoelectric interaction cross-section at photon energies corresponding to the electron shell binding energies of the absorbing material.

2.3.2.2 Compton Scattering

A Compton scattering interaction is an inelastic scattering process. The gamma photon collides with a loosely bound electron, imparting part of its energy before being deflected through an angle θ itself, **Figure 2.16 (b)**. The energy of the scattered photon can be quantified by the following expression.

$$E = \frac{E_o}{1+\alpha(1-\cos\theta)} \quad \text{(Eq. 2.37)}$$

Where, E_o is the original photon energy and α represents the term $h\upsilon/m_oc^2$, where m_o is the rest mass and c is the velocity of light.

The Klein-Nishina formula for differential scattering cross-section can predict the angular distribution of the scattered photons. The differential cross-section for a photon scattered into the solid angle $d\Omega$ is obtained from the expression:

$$\frac{d\sigma_{Compton}}{d\Omega} = Z \cdot r_o^2 \left(\frac{1}{1+\alpha(1-\cos\theta)}\right)^2 \left(\frac{1+\cos^2\theta}{2}\right)\left(\frac{\alpha^2(1-\cos\theta)^2}{(1+\cos^2\theta)[1+\alpha(1-\cos\theta)]}\right) \quad \text{(Eq. 2.38)}$$

Where, r_o denotes the classical electron radius.

An increasing tendency towards forward peaked scattering is exhibited by the angular distribution as the incident photon energy increases, and this tendency is independent of scattering medium. At lower energies, the differential cross-section is inclined to produce a more symmetrical angular distribution.

The probability of Compton scattering interactions is dependent on the number of electrons available as targets. Thus, the probability is directly proportional to the atomic number.

$$\sigma_{Compton} \propto Z \quad \text{(Eq. 2.39)}$$

As photons can be scattered over all angles in the 4π steradians, the energies transferred to the recoil electron can range from almost zero, when the photon is barely deflected, to a maximum value obtained when the photon is deflected 180^o, where the energy of the scattered photon is approximately equal to 256 keV ($m_oc^2/2$) and $E_o >> m_oc^2/2$.

2.3.2.3 Pair Production

Gamma-ray photons with energies in excess of 1.02 MeV can interact with an atomic nucleus to form an electron-positron pair, **Figure 2.16 (c)**. This amount of energy is the minimum required to provide the rest masses of the electron and positron (0.51 MeV each). Photons above this energy threshold can spontaneously convert into an electron-positron pair in the coulomb field of an atomic nucleus.

Excess energy is carried away equally by these two particles which produce ionisation as they travel in the material. The positron is eventually captured by an electron and annihilation of the two particles occurs. This results in the release of two photons each of 0.51 MeV known as annihilation radiation. These photons then lose energy by Compton scattering or photoelectric interactions.

The magnitude of the pair production interaction probability, above the energy threshold, varies approximately with the square of the atomic number of the absorber and linearly with photon energy (up to 100 MeV).

$$\sigma_{pp} \propto Z^2 E \quad \text{(Eq. 2.40)}$$

Although pair production is an important photon interaction at high energies; the 1.022 MeV threshold means that pair production is of no practical importance at the gamma ray energies considered in this study.

2.3.2.4 Rayleigh Scattering

Rayleigh scattering is an elastic scattering process between an atomic electron and an incident photon, where the energies of the incident and scattered photons are identical. The oscillating transverse electric field of the incident photon induces oscillations at the same frequency in the atomic electrons and the accelerating electric charge emits electromagnetic radiation. This radiation will be of the same frequency and in phase of the original incident photon. Therefore, the electron appears to scatter the incident radiation. The Rayleigh scattering probability cross-section is a function of photon energy and atomic number of the scattering material.

$$\sigma_{Rayleigh} \propto \frac{Z^{8/3}}{E^2} \quad \text{(Eq. 2.41)}$$

The Rayleigh scattering interactions never dominate the total interaction cross-section.

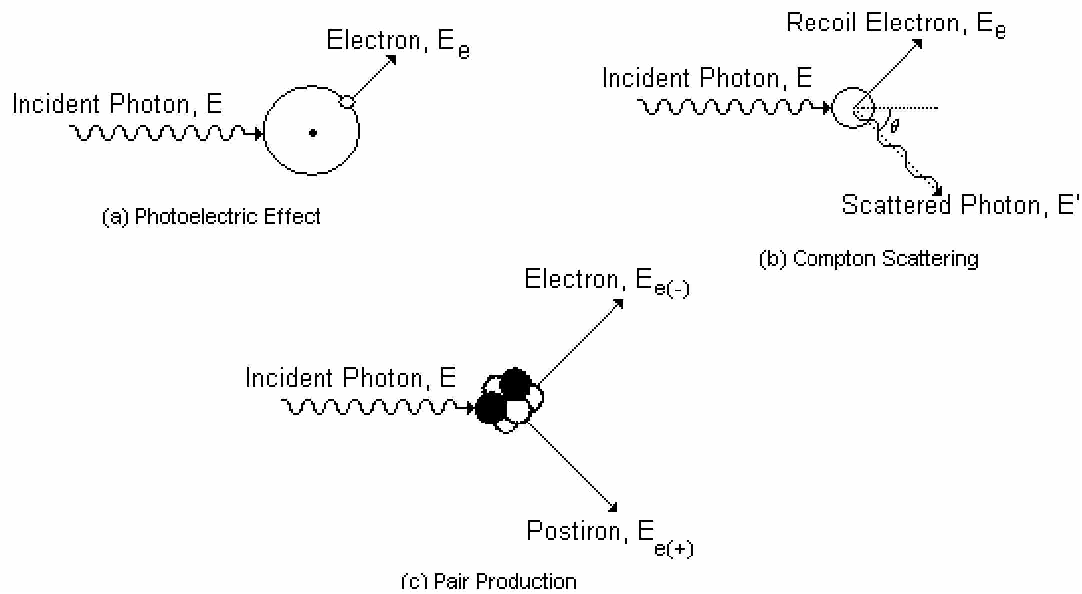

Figure 2.16 – Photon Interactions

2.3.3 Interaction Phenomena Cross-Sectional Probabilities

The relative contributions of the different mechanisms to the total interaction cross-sections of water and oil (assumed to be 86% carbon and 14% hydrogen by mass) for photon energies up to 100 keV are shown in **Figure 2.17** [**55**].

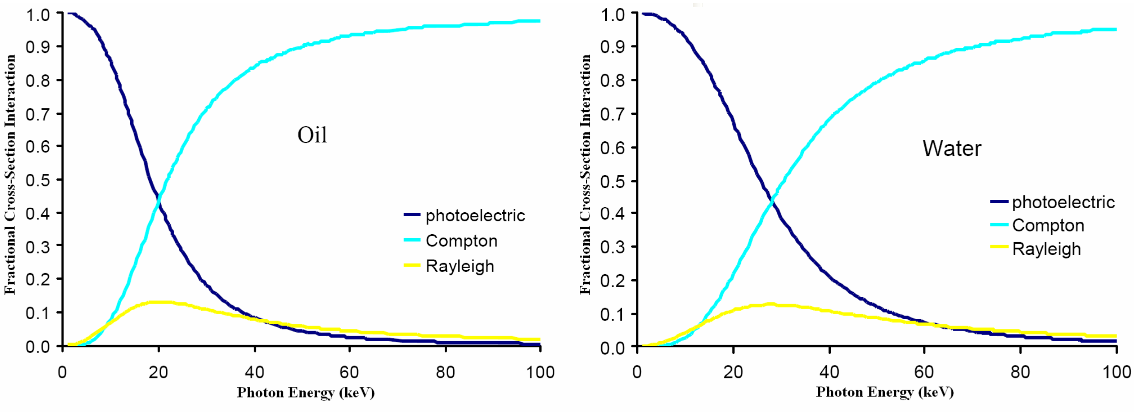

Figure 2.17 – Relative Interaction Cross-Sections for (a) Oil and (b) Water

It can be seen that the relative dominance of each of the interaction phenomena is broadly similar in both the oil and water; however, for a given photon energy, the photoelectric effect exhibits a higher fractional cross-section interaction in water. Above approximately 30 keV, both the oil and water cross-sections are dominated by the Compton scattering effect.

Plotting the linear attenuation coefficients of water and kerosene over the same energy range indicates how the differences in the photon absorption can be used to distinguish the two materials, **Figure 2.18.**

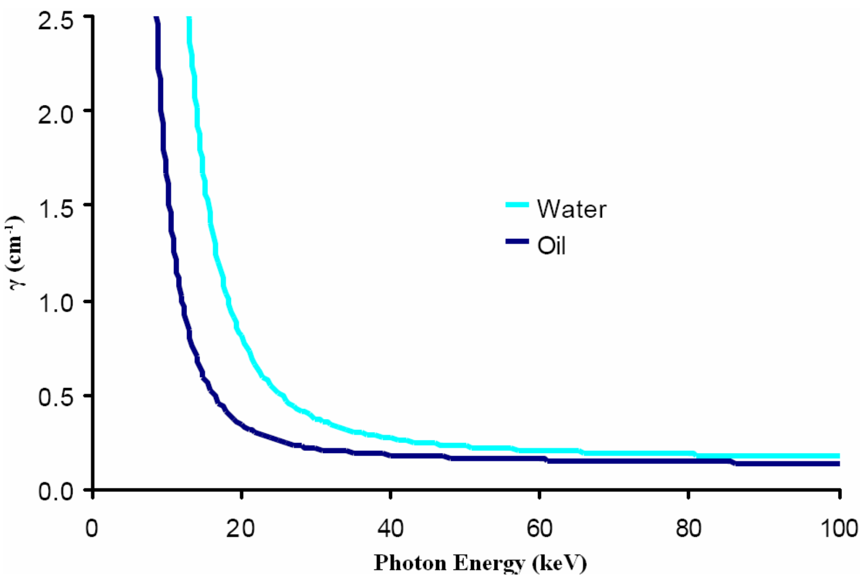

Figure 2.18 – Linear Attenuation Coefficients of Oil and Water

Attenuation is greater in water than in oil. This is because oxygen, the dominant constituent of water, has a higher atomic mass than carbon, the main constituent of oil. The higher density of water (~1000 kg/m^3), compared to that of most oils (typically 800 – 900 kg/m^3), is also a contributing factor.

As the photoelectric interaction is a stronger function of atomic number and photon energy than the Compton interaction, there is clearly a greater contrast in the linear attenuation coefficients of the water and oil in the region where the photoelectric effect dominates the interaction cross-sections.

Figure 2.19 illustrates the relative difference in the linear attenuation coefficients as a function of photon energy for the same energy interval. A measurement system relying on the difference between oil and water attenuations to distinguish the two materials would obtain maximum discrimination employing photon energies below 40 keV. Nevertheless, a reasonable contrast extends well into the Compton scattering region.

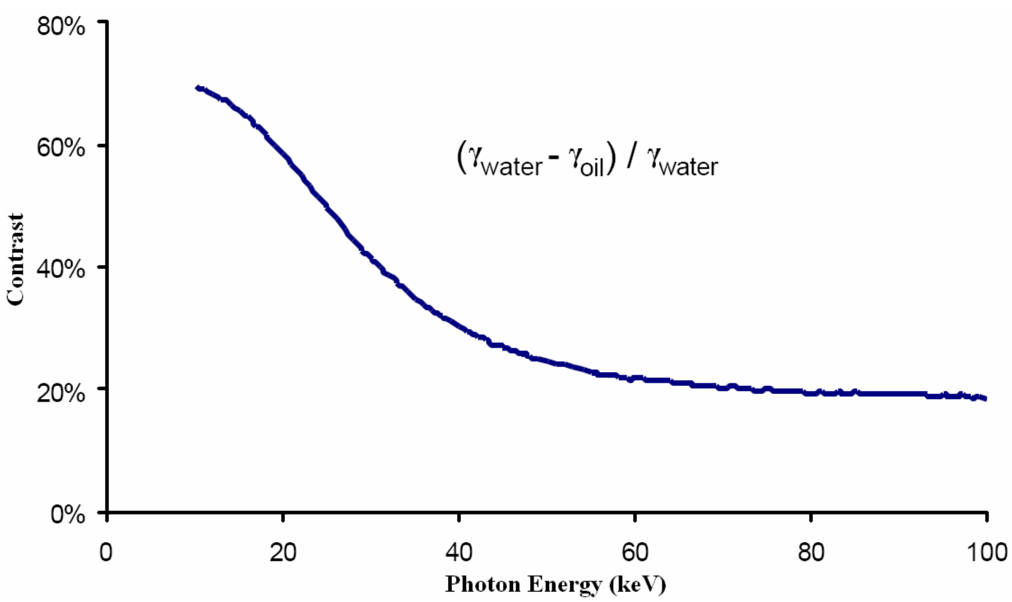

Figure 2.19 – Contrast between Oil and Water Linear Attenuation Coefficients

2.3.4 Gamma Radiation Attenuation

The photon interactions, described above, all contribute with varying probabilities to the removal of photons from the original beam path and the total interaction probability is the sum of the individual probability processes.

$$\sigma_{Total} = \sigma_{Photoelectric} + \sigma_{Compton} + \sigma_{Pair\ production} + \sigma_{Rayleigh} \qquad \text{(Eq. 2.42)}$$

The loss of incident photons from the original beam through interactions is known as attenuation. Important concepts in gamma radiation attenuation are those of the mean free path (λ) and the linear attenuation coefficient (γ).

The mean free path is defined as the average distance a photon can traverse in a medium before an interaction takes place. The magnitude of the mean free path depends on the photon energy and the density of the matter: the higher the energy of the photon the longer the free mean path of the photon; whereas, the higher the density of the matter the shorter the free mean path. Linear attenuation is defined as the inverse of the mean free path and is the sum of the attenuations for each of the photon interactions involved.

$$\gamma(E,\rho) = \frac{1}{\lambda(E,\rho)} \qquad \text{(Eq. 2.43)}$$

$$\gamma(E,\rho) = \gamma(absortion) + \gamma(Compton) \qquad \text{(Eq. 2.44)}$$

When a mono-energetic gamma radiation beam is collimated to a thin beam and directed at a gamma-detector unit obstructed by an absorber of thickness *h*, the intensity *I* (number of photons per second) of the gamma ray beam detected can be calculated as an exponential decay of the original beam intensity I_0 [**56**].

$$I = I_0 e^{-\gamma h} \qquad \text{(Eq. 2.45)}$$

Rewriting the attenuation expression in the form below, one can observe that the logarithm of the number of photons striking the detector decreases in a linear fashion with respect to the thickness of absorber present.

$$\ln\left(\frac{I}{I_0}\right) = -\gamma h \qquad \text{(Eq. 2.46)}$$

2.3.4.1 Two-Phase Flow (Gas – Liquid Systems)

In a two-phase measurement system, the gamma radiation absorber comprises the pipe wall and the working fluids. The gamma source is located on one side of the pipe with the detector installed diametrically opposite. The collimator of the source side forces the gamma rays into a narrow beam that is directed diametrically across the pipe, **Figure 2.20**.

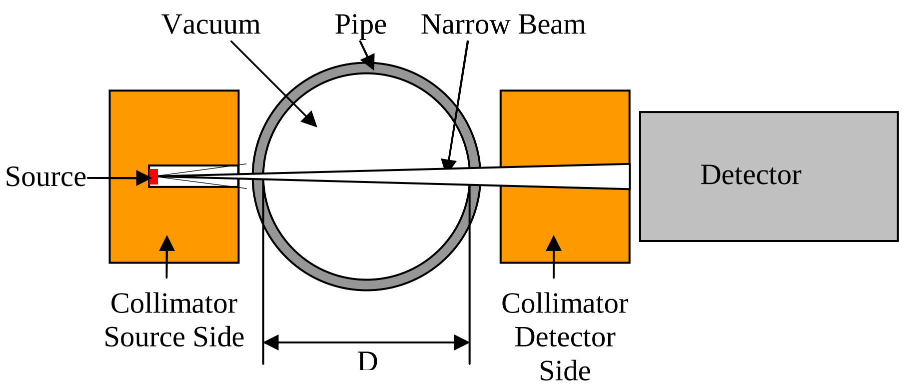

Figure 2.20 – Arrangement of Source, Pipe, Collimators and Detector

In the first instance, the gamma radiation has to negotiate the pipe wall, leading to photon-matter interactions, diminishing the number of photons that will reach the detector unit. In practice, this rate of photon loss will remain approximately constant as the pipe wall thickness will not vary with time. Low-energy photons are more susceptible to absorption or scattering interactions by the pipe wall than their higher-energy counterparts.

Assuming the presence of a vacuum within the pipe, the intensity gamma radiation measured at by the detector unit is defined to be I_o. Filling the pipe with air, the intensity measured for a given photon energy can be expressed by:

$$I_a = I_0 e^{-\gamma_a D} \quad \text{(Eq. 2.47)}$$

In this case, the number of transmitted photons detected *(I_a)* is the calibration value of the pipe (internal diameter D) full of air. Owing to the relatively low density of air, very little attenuation will be experienced by the gamma radiation and I_a should be very close to I_0. Accordingly, the linear attenuation coefficient for air (γ_a) is almost zero, regardless of the photon energy. Thus, I_a can be taken to represent the maximum photon count that will be recorded by the detector during two-phase flows.

The detected intensity of a mono-energetic photon beam across the same pipe filled by a liquid (I_l) is calculated in a similar fashion:

$$I_l = I_0 e^{-\gamma_l D} = I_a e^{-(\gamma_l - \gamma_a) D} \quad \text{(Eq. 2.48)}$$

The magnitude of I_l defines the lower count range limit for two-phase flow that will be obtained when the pipe full of liquid. Owing to the liquid phase's larger density, and thus higher degree of attenuation, I_l will be much smaller than I_a.

Having obtained the upper and lower limit calibration values I_a and I_l, it is possible to deduce the difference between the linear attenuation coefficients of the liquid and air.

$$\gamma_l - \gamma_a = \frac{1}{D} \ln\left(\frac{I_a}{I_l}\right) \quad \text{(Eq. 2.49)}$$

For a two-phase flow system, if the absorbance thickness of the liquid in the measurement section is taken to be h_l, the corresponding air thickness will be given by $D - h_l$. Consequently, the detected photon intensity will obey:

$$I = I_0 e^{-\gamma_a (D - h_l)} e^{-\gamma_l h_l} \quad \text{(Eq. 2.50)}$$

$$I = I_0 e^{-\gamma_a D} e^{-(\gamma_l - \gamma_a) h_l} \quad \text{(Eq. 2.51)}$$

$$I = I_a e^{-(\gamma_l - \gamma_a) h_l} \quad \text{(Eq. 2.52)}$$

Having determined the values I_a and I_l through calibration measurements, the thickness of liquid along the measurement path of the gamma ray beam (h_l) can be calculated from the measured intensity I.

$$\ln\left(\frac{I}{I_a}\right) = -(\gamma_l - \gamma_a)h_l = \frac{h_l}{D}\ln\left(\frac{I_l}{I_a}\right) \qquad \text{(Eq. 2.53)}$$

Therefore, the liquid hold-up (ε_l) can be found.

$$\varepsilon_l = \frac{h_l}{D} = \frac{\ln\left(\frac{I}{I_a}\right)}{\ln\left(\frac{I_l}{I_a}\right)} \qquad \text{(Eq. 2.54)}$$

The magnitude of the measured intensity I will lie between the calibration values I_a and I_l; thus, generating a liquid hold-up value lying between 0 (I=I_a) and 1 (I=I_l).

2.3.4.2 Three-Phase Flow (Air-Water-Oil Systems)

As the magnitude of radiation attenuation is a function of the photon energy, the component ratios of a three-component mixture can be resolved through the exploitation of a gamma source comprising two distinct photon energies [**39**].

In an air, water and oil measurement system, the intensity presence of the multiphase fluid in the pipeline will result in the measured of the gamma beam diminishing according to the attenuation law:

$$I = I_0 e^{-\gamma_a h_a} e^{-\gamma_w h_w} e^{-\gamma_o h_o} \qquad \text{(Eq. 2.55)}$$

Where, $\gamma_x h_x$ denotes the logarithmic decay constant for the attenuation experienced by the radiation beam due to component x. To resolve the individual phase fractions, the two energy levels from the dual-energy source are used to measure two of the three chordal hold-ups in the multiphase mixture. The third chordal hold-up is derived from the fact that the sum of the gamma rays' paths through the individual components is equal to the internal pipe diameter.

$$h_a + h_w + h_o = D \qquad \text{(Eq. 2.56)}$$

Employing a dual-energy gamma source, let I_{01} be the measured intensity of photons with energy level 1 and I_{02} the measured intensity of photons with energy level 2. The calibration values when the pipe is full of air, water and oil respectively for each photon energy level, are given by:

$$I_{a1} = I_{01} e^{-\gamma_{a1} D} \qquad \text{(Eq. 2.57)}$$

$$I_{a2} = I_{02} e^{-\gamma_{a2} D} \qquad \text{(Eq. 2.58)}$$

$$I_{w1} = I_{01} e^{-\gamma_{w1} D} \qquad \text{(Eq. 2.59)}$$

$$I_{w2} = I_{02} e^{-\gamma_{w2} D} \qquad \text{(Eq. 2.60)}$$

$$I_{o1} = I_{01} e^{-\gamma_{o1} D} \qquad \text{(Eq. 2.61)}$$

$$I_{o2} = I_{02} e^{-\gamma_{o2} D} \qquad \text{(Eq. 2.62)}$$

Where, γ_{x1} and γ_{x2} are the linear attenuation coefficients of component x for photon energy levels 1 and 2 respectively.

From the above equations (**Eq. 2.57 – 62**), the calibration values for the liquid phases can be expressed in terms of the air calibration value.

$$I_{w1} = I_{a1} e^{-(\gamma_{w1} - \gamma_{a1}) D} \qquad \text{(Eq. 2.63)}$$

$$I_{o1} = I_{a1} e^{-(\gamma_{o1} - \gamma_{a1}) D} \qquad \text{(Eq. 2.64)}$$

$$I_{w2} = I_{a2} e^{-(\gamma_{w2} - \gamma_{a2}) D} \qquad \text{(Eq. 2.65)}$$

$$I_{o2} = I_{a2} e^{-(\gamma_{o2} - \gamma_{a2}) D} \qquad \text{(Eq. 2.66)}$$

The differences between the linear attenuation coefficients can be determined for the components at each photon energy level.

$$\gamma_{w1} - \gamma_{a1} = \frac{1}{D} \ln\left(\frac{I_{a1}}{I_{w1}}\right) \qquad \text{(Eq. 2.67)}$$

$$\gamma_{o1} - \gamma_{a1} = \frac{1}{D} \ln\left(\frac{I_{a1}}{I_{o1}}\right) \qquad \text{(Eq. 2.68)}$$

$$\gamma_{w2} - \gamma_{a2} = \frac{1}{D} \ln\left(\frac{I_{a2}}{I_{w2}}\right) \qquad \text{(Eq. 2.69)}$$

$$\gamma_{o2} - \gamma_{a2} = \frac{1}{D} \ln\left(\frac{I_{a2}}{I_{o2}}\right) \qquad \text{(Eq. 2.70)}$$

For an air, oil and water multiphase mixture in a pipe of diameter D, the detected photon intensity for photons of energy 1 (I_1) can be expressed by:

$$I_1 = I_{01} e^{-\gamma_{a1}(D - h_w - h_o)} e^{-\gamma_{w1} h_w} e^{-\gamma_{o1} h_o} \qquad \text{(Eq. 2.71)}$$

Substituting in equation **Eq. 2.57**:

$$I_1 = I_{a1} e^{-(\gamma_{w1} - \gamma_{a1}) h_w} e^{-(\gamma_{o1} - \gamma_{a1}) h_o} \qquad \text{(Eq. 2.72)}$$

Rearranging the equation to express attenuation as a linear logarithmic decay:

$$\ln\left(\frac{I_1}{I_{a1}}\right) = -(\gamma_{w1} - \gamma_{a1}) h_w - (\gamma_{o1} - \gamma_{a1}) h_o \qquad \text{(Eq. 2.73)}$$

Substituting in **Eq. 2.67** and **Eq. 2.68** expresses the attenuation of photons of energy level 1 in terms of water and oil hold-ups:

$$\ln\left(\frac{I_1}{I_{a1}}\right)=\frac{h_w}{D}\ln\left(\frac{I_{w1}}{I_{a1}}\right)+\frac{h_o}{D}\ln\left(\frac{I_{o1}}{I_{a1}}\right) \quad \text{(Eq. 2.74)}$$

Similarly, the measured photon intensity for the second energy level (I_2) is given by:

$$I_2 = I_{02}e^{-\gamma_{a2}(D-h_w-h_o)}e^{-\gamma_{w2}h_w}e^{-\gamma_{o2}h_o} \quad \text{(Eq. 2.75)}$$

Substituting in equations **Eq. 2.58**:

$$I_2 = I_{a2}e^{-(\gamma_{w2}-\gamma_{a2})h_w}e^{-(\gamma_{o2}-\gamma_{a2})h_o} \quad \text{(Eq. 2.76)}$$

Rearranging the equation to express attenuation as a linear logarithmic decay:

$$\ln\left(\frac{I_2}{I_{a2}}\right)=-(\gamma_{w2}-\gamma_{a2})h_w-(\gamma_{o2}-\gamma_{a2})h_o \quad \text{(Eq. 2.77)}$$

Substituting in **Eq. 2.69** and **Eq. 2.70** expresses the attenuation of photons of energy level 1 in terms of water and oil hold-ups:

$$\ln\left(\frac{I_2}{I_{a2}}\right)=\frac{h_w}{D}\ln\left(\frac{I_{w2}}{I_{a2}}\right)+\frac{h_o}{D}\ln\left(\frac{I_{o2}}{I_{a2}}\right) \quad \text{(Eq. 2.78)}$$

Therefore, the system of two equations expressing the gamma radiation attenuation at the two distinct photon energy levels, **Eq. 2.70** and **Eq. 2.74**, can to be solved to yield values for the water and oil component hold-ups, ε_w and ε_o respectively.

$$\varepsilon_w=\frac{h_w}{D}=\frac{\left(\dfrac{\ln\frac{I_2}{I_{a2}}}{\ln\frac{I_{a2}}{I_{o2}}}\right)-\left(\dfrac{\ln\frac{I_1}{I_{a1}}}{\ln\frac{I_{a1}}{I_{o1}}}\right)}{\left(\dfrac{\ln\frac{I_{w2}}{I_{a2}}}{\ln\frac{I_{a2}}{I_{o2}}}\right)-\left(\dfrac{\ln\frac{I_{w1}}{I_{a1}}}{\ln\frac{I_{a1}}{I_{o1}}}\right)} \quad \text{(Eq. 2.79)}$$

$$\varepsilon_o=\frac{h_o}{D}=\frac{\left(\dfrac{\ln\frac{I_2}{I_{a2}}}{\ln\frac{I_{w2}}{I_{a2}}}\right)-\left(\dfrac{\ln\frac{I_1}{I_{a1}}}{\ln\frac{I_{w1}}{I_{a1}}}\right)}{\left(\dfrac{\ln\frac{I_{o2}}{I_{a2}}}{\ln\frac{I_{w2}}{I_{a2}}}\right)-\left(\dfrac{\ln\frac{I_{o1}}{I_{a1}}}{\ln\frac{I_{w1}}{I_{a1}}}\right)} \quad \text{(Eq. 2.80)}$$

Having obtained h_w and h_o, one can determine h_a, and, thus, the air void fraction ε_a.

$$\varepsilon_a = \frac{h_a}{D} = 1 - \varepsilon_w - \varepsilon_o \qquad \text{(Eq. 2.81)}$$

In the three-component multiphase system, the solution is less direct than in the two-phase case. The measured gamma radiation intensity at energy level 1 I_1 should have a value between I_{a1} and I_{w1}; while I_2 should fall between I_{a2} and I_{w2}. The linear combination of the logarithms of the photon intensities I_1 and I_2 should give a value for h_x/D in the range of 0 – 1 for component x (air, water or oil). The system of equations for the resolution of a three-component mixture using two energy levels can be represented in a graphical form, **Figure 2.21**.

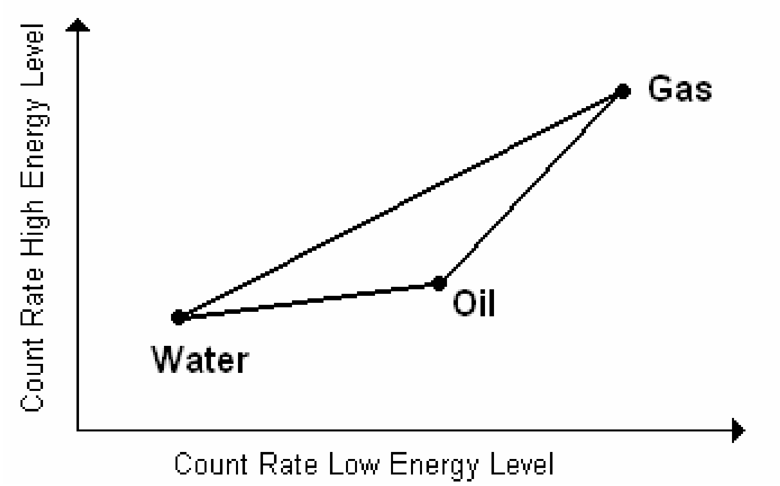

Figure 2.21 – Composition Triangle on a Log-Log Scale

To construct the graph, the logarithms of the detected gamma count for each of the pure components are plotted for each of the photon energy levels. The vertices of the resulting triangle are the pure water, oil and gas calibration detected gamma intensities, and any point inside the triangle represents a particular multiphase composition of water, oil and gas defined by the measured high and low energy photon intensities.

The contrast between the different phases needs be high if such a measurement system is to be of practical use. The geometric form of the triangle depicts the phase discrimination, as experienced by the gamma radiation, and is a function of the energy levels employed and the fluid properties. If the energy levels exploited are too close, or the oil and water densities too similar, the triangle will transform into a straight line: such a system is not suitable for multiphase composition measurement.

2.3.5 Detection of Gamma Radiation

A variety of methods are available to detect gamma radiation including gas-filled counters, solid-state detectors and scintillation detectors. All multiphase flow meters on the market that exploit gamma radiation attenuation as part of their measurement system employ scintillation type detectors.

In scintillation detectors, the gamma radiation strikes an organic or inorganic crystal and interacts with the crystal atoms through the photoelectric and/or Compton effects. These interactions produce a mixture of scattered photons and charged particles. The scattered photons will travel a finite distance through the crystal and, depending on their energies, may participate in further interactions. Meanwhile, the charged particles travel a relatively short distance across the crystal, leaving behind a trail of excited atoms. As these excited atoms return back to their ground state, some of them may emit radiation with a wavelength in the ultra-violet or visible spectrum. These 'scintillations' are detected by a photomultiplier attached to the crystal. Consequently, materials used as scintillators need to be transparent to their own light so it can be detected. Sodium iodide (NaI) crystals are commonly used in scintillator detectors.

The reader is directed to Prepost [**57**] for a more complete discussion on gamma radiation detection systems.

2.3.6 Gamma Radiation in Multiphase Flow Measurements

Early research work in the application of gamma radiation techniques to multiphase flow measurement focussed on exploitation of gamma attenuation for component ratio determination in two-phase systems [**58**] and the development of the radiation detector units [**59**]. A comprehensive review of gamma attenuation measurement system design and implementation for multiphase flow hold-up measurement are given by Mareuge [**60**] and Chan and Banarjee [**61**].

Jiang and Rezkallah [**62**] extended work undertaken in two-phase flow void fraction determination by analysis of the sensitivity of the gamma attenuation measurement method to the pipe diameter. Experimentation on upward and downward co-current gas-liquid flows in a 9.525 mm diameter pipe was carried out using a single beam gamma densitometer system comprising a caesium-137 (662 keV) source and a sodium iodide (NaI) detector crystal. Void fraction measurements were obtained to within ±5% relative agreement with the reference values yielded from a quick closing valve system. The data was then compared to data obtained for larger diameter pipes and it was noted that pipe diameter had no significant effect on the accuracy of the gamma attenuation based void fraction measurement.

Abouelwafa and Kendall [**39**] were the first to propose a multi-energy gamma attenuation technique to resolve three-phase mixture component ratios. Various static mixtures of oil, water and gas were examined in a 0.1 m diameter pipe section using cobalt-57 (122 keV) and barium-133 (365 keV) radioisotopes and a lithium-drifted germanium based detector. Gas fraction measurements were detected to within ±1%; oil fractions to within ±10% and the water fraction within ±10%.

More recently, Li *et al* [**63**] also analysed static oil, water and gas mixtures using a gamma densitometer system comprising two radioactive isotopes, americium-241 (59.5 keV) and caesium-137 (662 keV), a sodium iodide detector crystal, and a 600 mm long square (100 mm × 100 mm) Plexiglas conduit. They employed a modification algorithm to adjust readings for error, reporting that small errors in the intensity measurements can be transferred to large errors in liquid phase component resolution owing to the similarities in the magnitude of the water and oil attenuation coefficients. After application of the modification algorithm, all phase fraction readings were calculated to be within ±6% of their true values.

Scheers and Slijkerman [**64**] have reported on a triple-energy gamma ray multiphase composition measurement that facilitates the determination of the oil, water and gas phase fractions and the water salinity. However, in this case the gamma measurement system was intrusive with an americium-241 gamma source occupying the centre of the pipe in a concentric installation. Operating the meter in a standard dual energy mode (and 59.5 keV) to determine the individual phase compositions yielded measurements with associated absolute errors of ±2%. Utilising a third energy level (26.3 keV) facilitated simultaneous water salinity measurement provided that the dynamics of the salinity variation could be assumed to have a time span of hours. The corresponding phase fractions measurements were defined to be ‘acceptable’ but were not quantified.

Åbro and Johansen [**65**] proposed a multi-beam configuration for void fraction measurement using gamma attenuation and compared the results of their system against those obtained from a single-beam gamma densitometer. The measurement apparatus comprised an americium-241 (59.5 keV) gamma source, a single CdZnTe semiconductor detector and a pipe with an inner diameter of 80 mm and an outer diameter of 90 mm. A series of static multiphase combinations were presented to the gamma measurement system. For each test, a complete measurement consisted of determine the gamma attenuation at 17 different positions around the pipe, from 180° (diametrical position) to 52°. It was reported that the multi-beam arrangement yielded results to within ±10% when measurements from four of the detector positions were combined and that the system was less sensitive to flow regime than the conventional single beam technique.

In 2003, Tjugum *et al* [**66**] followed up the work undertaken by Åbro and Johansen and produced a multi-beam instrument with an americium-241 (59.5 keV) source and three detectors all of which were collimated and embedded in the pipe wall. Two of the detectors measured the gamma ray attenuation across the pipe flow while one detector was installed at a 90° angle for the purpose of monitoring the scattered radiation. Tjugum *et al* recorded that the multi-beam design with 3 detectors gave more accurate results than the conventional single beam and that the multi-beam geometry and dual modality of the gamma system enabled data on the flow regime water fraction salinity to be obtained.

Tjugum *et al* [**17**] proposed a multi-beam gamma-ray densitometry system to facilitate void fraction measurement. A 9-beam fan collimated measurement geometry was employed using an americium-241 (59.5 keV) source and a row of 9 CdZnTe semiconductor radiation detectors on the other side of a 2-inch pipe. A number of oil, water and gas flow combinations were tested for pipe section tilt angles of 0°, 45° and 90° (with respect to the horizontal). Improved GVF measurements on non-homogeneous flows flow, with respect to those obtained using a conventional single beam configuration, were reported, typically to within ±10%. Significant errors were obtained for test points at high GVFs and at separated flows, typically deviations greater than 25%. The source of these errors was attributed to possible backflow (for vertical tests), slip and unstable flow regimes.

Stahl and von Rohr [**67**] investigated the accuracy of void fractions measurements in a horizontal pipe using a single-beam gamma densitometer. A theoretical model to determine the measurement accuracy for a number of idealised flow regimes was presented. The model described the measurement accuracy as dimensionless function of the pipe radius and liquid absorption coefficient. Experimental verification of the model was conducted using air and water in a 21 mm pipe. A single beam gamma-densitometer comprising an iodine-125 (35.5 keV) source and a NaI scintillator detector crystal was employed as the measuring device. It was found that a linear approximation correction was best suited to flow regimes where the phase interfaces are mainly orientated parallel to the radiation beam; while, logarithmic corrections gave better results for flow profiles with a perpendicular orientation or dispersed flow pattern. The maximum absolute deviation owing to inaccuracy in the two-phase mixture void fraction, as determined by the application of the correction models was defined to be one tenth of the product of the pipe internal diameter and the liquid attenuation coefficient.

Frøystein *et al* [**68**] published results on a dual-gamma tomography system for high-pressure multiphase flows. A barium-133 (31 keV and 81 keV) source was coupled with a CdZnTe detector and a digital spectrum analyser was employed to monitor gamma attenuation for different chordal positions of the pipe cross-section. Results indicated that the tomography system was able to reconstruct different fluid zones for different flow regimes. However, difficulties were also reported in discerning between fluid regions for some configurations where different fluid mixtures with similar attenuation coefficient values were located next to each other.

Gamma attenuation has also been exploited in multiphase flow pattern recognition systems [**69-73**]. Pattern recognition techniques in multiphase flow measurement are discussed in **Chapter 2.4**.

2.4 Pattern Recognition Techniques in Multiphase Flow Measurement

2.4.1 Signal Processing

Signal processing involves the design, analysis and implementation of systems that extract information of interest from existing data signals. The continued progress of digital technology and information theory has stimulated the development of sophisticated signal processing techniques that are exploited in many different fields, including speech recognition, audio signal processing, digital communications and analysis and control of industrial processes.

Most sensor outputs comprise a continuously varying analogue voltage waveform. In order to use the signal in further mathematical signal processing techniques on a computer system, it must first be digitised with an analog-to-digital converter. Analogue signals are digitised employing a technique known as sampling. Sampling is executed in two stages: discretisation and quantisation. In discretisation, the space of a signal is partitioned into a series of equivalence classes. The quantisiation process then allocates approximated representative signal values to the each of the partitions from a set of finite values.

The Nyquist-Shannon sampling theorem is a fundamental theorem in the field of information theory which stipulates the constraints for accurately constructing a signal from a sampled version of itself. It states that the sampling frequency f_s must be strictly greater than twice the signal's bandwidth B_s, the difference between the maximum and minimum frequencies of its sinusoidal components [**74**].

$$f_s > 2B_s \qquad \text{(Eq. 2.82)}$$

Failure to satisfy the criterion set out in the Nyquist-Shannon theorem results in overlapping frequencies; whereby, frequencies above half the sampling rate will appear as frequencies below half the sampling rate. This phenomenon is known as aliasing as the high frequencies are said to be “under an alias”.

2.4.2 Feature Extraction

Having obtained a digital form of a signal of interest, various parametric representations can be derived. In applications with time-varying signals, in order to exploit all the available data, it may be possible to use all the sampled data points in the pattern recognition analysis. However, this may not be practical with systems with long measurement times and/or high sampling frequencies where the number of data points is too large to be efficiently manipulated by a pattern recognition system. In these instances, a set of features that are capable of describing the signal’s characteristics may be employed.

Selection of an appropriate feature set to represent raw data signals is crucial if feature extraction is to be employed successfully. Effective feature selection can be difficult as it necessitates the selection of a feature set that will distinguish between different data class volumes and there are an infinite number of features and feature combinations from which to select. If too many features are included in the feature set, there is a tendency for the pattern recognition model to become over-complex and this will result in a reduced generalisation capability. In practice, a pattern recognition or data visualisation analysis will be conducted on the training data using the selected feature set in order to analyse its effectiveness.

The features employed to represent a signal can come from a variety of information domains, e.g. time, frequency, cepstrum or wavelet. The most effective domain depends on the problem being modelled. The goal of feature extraction is to reduce a large complex signal into a small number of manageable parameters that conserve the key features of the original signal. **Appendix B** details features that were exploited as part of this research work.

2.4.3 Pattern Recognition Models

The purpose of a pattern recognition system is to classify input data (patterns) based on *a priori* knowledge or statistical information extracted from the patterns. A pattern recognition system can be thought of comprising three major parts: gathering the observations to be classified; computation of the numeric or symbolic information from the observations; classifying or describing observations based on the extracted features presented.

Thus, a pattern recognition model has to be able to map the relationship between input features and the target outputs. There are several pattern recognitions techniques available to implement the mapping process including: artificial neural networks; statistical models; fuzzy logic; and expert systems.

Although these models are distinguished from each other, there is a certain amount of overlap between them: artificial neural networks can be thought of as an extension of conventional statistical pattern recognition techniques and fuzzy logic employs similar types of logical rules that can be found in expert systems.

2.4.4 Artificial Neural Networks

An artificial neural network (or neural network) is a mathematical computing paradigm that is based on the operation of a biological neural system: functions are executed collectively and in parallel by the nodes, instead of there being a specific delineation of sub-tasks to which various nodes are assigned. The advent of neural networks facilitated the development of advanced pattern recognition systems with non-linear decision boundaries, through the implementation of simple training algorithms, to model complex multivariate relationships.

A neural network system will learn to classify inputs through a training process in which the network is presented with a series of inputs and target outputs. Based on this training data, the neural network will generate a map between the inputs and outputs. Subsequent input data will then be processed using the relationship derived using the training process to produce corresponding output variable values.

There are many classes and sub-classes of neural networks that are widely used in engineering applications. These have been described extensively in published literature [**75, 76**]. The most widely used neural network classes and subclasses are summarised in **Table 2.3**.

Three major learning paradigms can be applied in neural network modelling depending on learning task: supervised learning; unsupervised learning; and reinforcement learning. Pattern recognition and regression problems employ a supervised learning paradigm whereby a set of example inputs and targets are presented to the network and the aim of the learning process is to determine a function that describes the relationship between the variables. In unsupervised learning, the network training is entirely data-driven and no target results for the input data vectors are provided. A neural network which exploits unsupervised learning type, such as Kohonen self-organizing maps, can be used to cluster the input data and extract features inherent to the problem.

Neural Network Class	Sub-Class
Feedforward	Multi-Layer Perceptron
	Radial Basis Functions
	Kohonen Self-Organising Feature Map (KSOFM)
Recurrent	Simple Recurrent Network
	Hopfield Network
Stochastic	Boltzmann Machine
Modular	Committee of Machines
	Associative Neural Network

Table 2.3 – Neural Network Classes and Subclasses

In the research work undertaken, feedforward multi-layer perceptron and Kohonen self-organising feature map neural networks were examined.

2.4.4.1 The Multilayer Perceptron (MLP)

All types of neural network stem from McCulloch and Pitts' [**77**] description of a processing model comprising a building block known as a neuron and a networked interconnection. Rosenblatt [**78**] expanded on this concept to investigate the computation of the eye and developed the first type of neural network which was known as a perceptron. However, Minksky and Papert [**79**] showed that a single-layer perceptron neural network was limited to modelling linearly separable patterns and was unable to describe exclusive disjunction (XOR) functions and conjectured (incorrectly) that the same would be true of multilayer perceptrons. Grossberg [**80**] later demonstrated that multilayer perceptron models could indeed resolve XOR problems.

Figure 2.22 depicts the multilayer perceptron type neural network architecture.

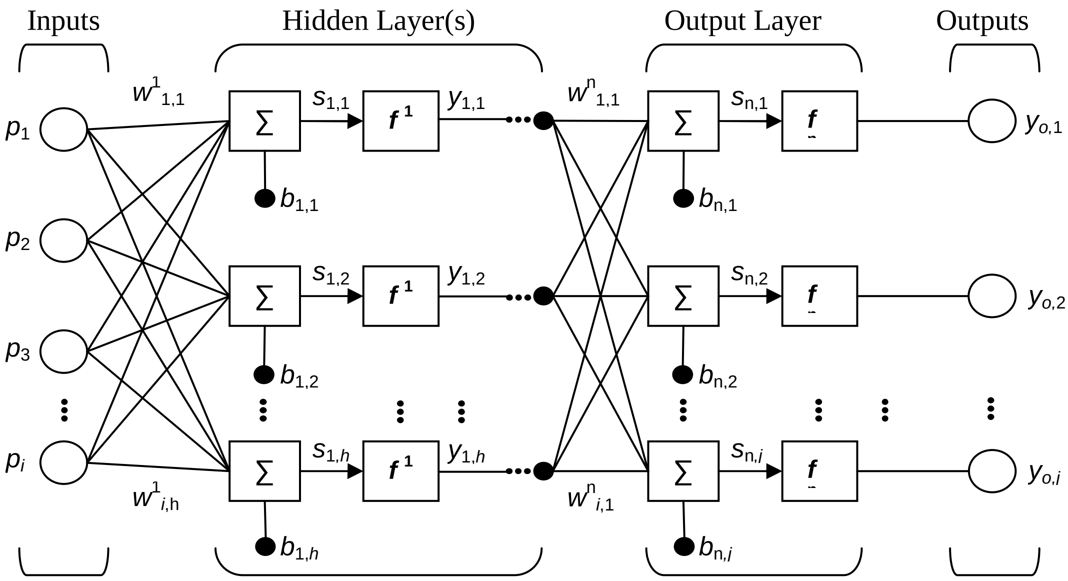

Figure 2.22 – Multilayer Perceptron Network

Each input (p_i) is connected to all nodes in the first hidden layer. If successive hidden layers are employed, all outputs from the preceding layer are input to each node in the successive layer. For all nodes in the MLP, the inputs are summed (*s*), after having been multiplied by their respective weights (*w*), a bias (*b*) is added to this total. The resulting value is used as the input to an activation function (*f*). Hence, the first hidden layer output ($y_{1,h}$) from each processing nodes in the for an MLP system with *I* inputs can be expressed by:

$$y_{1,h} = f^1\left(\sum_{i=1}^{I}\left(w^1{}_{i,h}\,p_i + b_{1,h}\right)\right) \qquad \text{(Eq. 2.83)}$$

Accordingly, the outputs ($y_{o,j}$) from a two layer system (n=2) can be determined from the expression:

$$y_{o,j} = f^2\left(\sum_{h=1}^{H}\left(w^2{}_{h,j}\left(f^1\left(\sum_{i=1}^{I}\left(w^1{}_{i,h}\,p_i + b_{1,h}\right)\right)\right) + b_{2,j}\right)\right) \qquad \text{(Eq. 2.84)}$$

Defining the network architecture is a key stage in neural network analysis. In most applications, the number of input and output neurons is fixed; thus, the problem of network architecture specification is reduced to selection of layer function types, the number of hidden layers and the number of neurons therein.

It has been demonstrated that a two layer MLP with sigmoid non-linearity can approximate any function with arbitrary accuracy [**81**]. Consequently, the only remaining parameter to be defined is the number of nodes to deploy in the hidden layer. There are no rules for the selection of the number of hidden nodes but, generally, the more complex the function one is attempting to model, the greater the number of hidden nodes required.

However, specifying the number of hidden nodes is a delicate balancing act: if too many nodes are used the network training data will simply be memorised and the system will exhibit poor generalisation; nevertheless, too few hidden nodes will result in a system with insufficient parameters to model the underlying function and severe underfitting will be experienced [**82**].

2.4.4.2 MLP Neural Network Training Techniques

The purpose of MLP training algorithms is the iterative adjustment of the network weights and biases in order to minimise the network performance function. All training algorithms use the derivative of the performance function to determine the weight values that will minimise the performance function. Several different types of algorithm have been reported and exploited, **Table 2.4**.

Algorithm	Optimisation Technique
Gradient Descent with Momentum	Modified Back-propagation
Variable Learning Rate	Modified Back-propagation
Resilient Back-propagation	Modified Back-propagation
Scaled Conjugate Gradient	Numerical Optimisation Techniques
Fletcher-Powell Conjugate Gradient	Numerical Optimisation Techniques
Polak-Ribiere Conjugate Gradient	Numerical Optimisation Techniques
One-Step Secant	Numerical Optimisation Techniques
Levenberg-Marquardt	Numerical Optimisation Techniques
Quasi-Newton	Numerical Optimisation Techniques

Table 2.4 – MLP Training Algorithms

2.4.4.2.1 Back-propagation

Back-propagation is the core supervised learning technique employed in feed-forward neural networks. The errors propagate backwards from the output nodes to the inner nodes. The error for an output variable is calculated as the difference between the network output (y_o) and the target value presented to the network (t). Thus, back-propagation is used to calculate the gradient of the error of the network with respect to the network's modifiable weights. An error function is chosen which will have to be minimised using gradient descent such as the sum of squares error (*SSE*) function.

$$SSE = \frac{1}{2}\sum_{j=1}^{N}\left(y_o - t\right)^2 \qquad \text{(Eq. 2.85)}$$

The first step is the initialisation of the input layer. Employing matrix notation, this can be described as shown in equation **Eq. 2.82**. In this notation, the biases, weights, net inputs, activations, and error signals for all units in a layer are combined into vectors, while all the non-bias weights from one layer to the next are held in a matrix *W*.

$$\vec{y}_o = \vec{p} \qquad \text{(Eq. 2.86)}$$

For an N-layer system, the activity propagates forward for n=1 to N.

$$\vec{y}_n = f^n\left(W_n \vec{y}_{n-1} + \vec{b}_n\right) \qquad \text{(Eq. 2.87)}$$

The error obtained in the output layer is the difference between target and actual output values.

$$\vec{\delta}_L = \vec{t} - \vec{y}_L \qquad \text{(Eq. 2.88)}$$

The error is back-propagated from layer L–1 to the first hidden layer.

$$\vec{\delta}_l = \left(W_{l+1}^T \vec{\delta}_{l+1}\right)\cdot f_l^{'}\left(n\vec{e}t_l\right) \qquad \text{(Eq. 2.89)}$$

The MLP neural network weights and biases are then updated accordingly.

$$\Delta W_l = \vec{\delta}_l \vec{y}_{l-1}^T \qquad \text{(Eq. 2.90)}$$

$$\Delta \vec{b}_l = \vec{\delta}_l \qquad \text{(Eq. 2.91)}$$

This process of updating the network weights and biases is repeated iteratively until the sum of squares error function is minimised.

2.4.4.2.2 Conjugate Gradient

The basic back-propagation algorithm adjusts the weights in the steepest descent direction. However, this does not necessarily always produce the fastest convergence. In conjugate gradient based algorithms a search is performed along conjugate directions, which produces generally faster convergence than steepest descent directions.

An example of a conjugate gradient technique is the scaled conjugate gradient (SCG) method. A single iteration of the SCG algorithm involves the computation of two gradients (second-order technique) and one call to the error function in contrast to one of each for the standard back-propagation. It has been determined that a single iteration of SCG is as complex as approximately 10 – 16 iterations of standard back-propagation. Nevertheless, although SCG is computation intensive it yields quicker convergences and has been reported to produce better results than the standard back-propagation in some applications [**83**].

SCG does not incorporate learning parameters such as the step width of the gradient descent which are used in back-propagation based techniques and need to be fine-tuned to achieve optimum performance of the network. The SCG algorithm’s parameters are non-critical and only influence the speed of convergence, not the outcome.

2.4.4.3 Avoiding Over-fitting

Bad generalisation by a neural network can stem from over exposure of the network to the training data set. This problem is known as over-fitting. Deciding when to end the training algorithm can have a major influence on the ability of the trained network to generalise new data sets. Training algorithms are nominally terminated when a local minimum has been attained or when the convergence rate is insignificantly low, i.e. improvement between successive iterations is zero or negligible after exposure to the training set for a certain number of epochs (cycles). There are two main routines employed to avoid over-fitting and improve neural network generalisation: cross validation and regularisation.

2.4.4.3.1 Cross-Validation

Cross-validation (also know as ‘early-stopping’) involves dividing the available data into three groups instead of two. In addition to the conventional training and test data sets, a validation set is produced. During the training process, the training data set is used to compute the network weights and biases. Simultaneously, the validation set is used to produce a validation error for the network configuration. The validation error is monitored and when the validation error continuously increases for a specified number of iterations, the training process will be terminated and the weights and biases present at the minimum validation error will be implemented for testing with test data set.

Although good results can be obtained using cross-validation, it is not particularly suited for applications with limited data. As not all of the data is used to train the model, and the training is terminated before attaining the minimum training error, the information contained in the selected data is not optimal and the network may suffer from under-constrained training.

2.4.4.3.2 Bayesian Regularisation

Bayesian techniques exploit probability to quantify errors in inferences and produce a distribution presenting the beliefs of how likely different predictions are. The Bayesian approach offers a tool for control of neural network model complexity as it can be exploited to select the optimal number of neurons in the hidden layer, thus avoiding over-fitting, and offers an alternative approach to error minimisation techniques [**84**].

Bayesian regularisation involves modifying the objective function, normally the mean sum of the squared errors. The aim of the modification is to improve the model's generalisation capacity. As seen below, the objective function (E_d) is expanded with the addition of a term E_w which is the sum of squares of the network weights.

$$F(w) = \alpha E_d + \beta E_w \qquad \text{(Eq. 2.92)}$$

Where, α and β denote control parameters which are to be optimised within the Bayesian framework of MacKay [**85**] which has been successfully applied to a number of practical engineering problems.

Employing the modified performance function, described in **Eq. 2.92**, will yield a network with smaller weights and biases, thus forcing a smoother network response that is less likely to over-fit. It is assumed that the weights and biases are random variables with a Gaussian distribution. The regularisation parameters are related to the unknown variances associated with these disturbances. Analysis has shown that the optimal regularisation technique requires the determination of the Hessian matrix which necessitates intensive computation.

Alternative approximation techniques which are less calculation intensive have been developed such as Bayesian regularisation with the use of Levenberg-Marquardt (LM) algorithm [**86**]. The key steps in this algorithm are:

1. Initialisation of the α and β control parameters, network weights, and biases.

2. Execute a single iteration of the LM algorithm to minimise the objective function described in **Eq.2.92**.

3. Determine the effective number of parameters (γ) using the Gauss-Newton approximation to the Hessian matrix available in the LM algorithm.

$$\gamma = N - 2\alpha \mathrm{Tr}(H)^{-1} \qquad \text{(Eq. 2.93)}$$

Where, N denotes the number of parameters and *H* denotes the Hessian matrix.

4. Calculate new estimates for the objective function control parameters α and β.

$$\alpha = \frac{\gamma}{2E_d(w)} \qquad \text{(Eq. 2.94)}$$

$$\beta = \frac{N-\gamma}{2E_d(w)} \qquad \text{(Eq. 2.95)}$$

5. Repeat steps 2 – 4 until convergence is attained.

Examining the number of effective parameters for different numbers of hidden layer neurons will optimise the neural network architecture. If the effective number of parameters is very close to the total number then additional hidden layer neurons may be required. However, if the expanded network yields an identical number of effective parameters, the previous smaller configuration was large enough.

2.5.4.4 Kohonen Self-Organising Feature Maps (KSOFMs)

In 1982, Kohonen [**87**] described an unsupervised learning technique that involved the use of self-organising feature maps to classify data. The objective of a KSOFM network is to map the natural structures inherent in the input data vectors, of an arbitrary dimension *N*, onto a discrete map with just 1 or 2 dimensions, **Figure 2.23**.

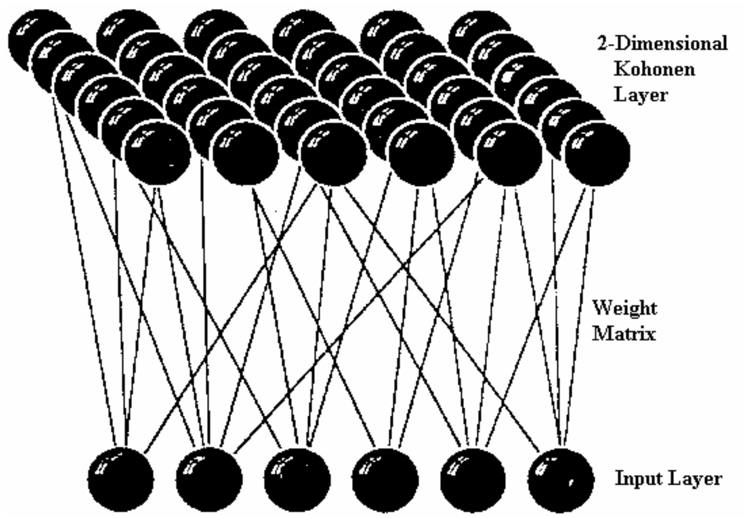

Figure 2.23 – Kohonen Self-Organising Feature Map

Patterns exhibiting similarities in the input space should be topographically arranged close to one another in the output map. These networks are particularly useful where complex high dimensional data needs to be presented in an understandable format.

KSOFMs have been successfully applied to a number of practical engineering applications [**88**].

The KSOFM learning process comprises the following stages:

1. Initialisation of output node weights.
2. Looping of the following stages until node weights converge:
    - 2.1 For each data point:
        - 2.1.1 Present the input feature vector
        - 2.1.2 Calculate the similarity
        - 2.1.3 Determine the winning output node
        - 2.1.4 Locate all nodes in the neighbourhood of the winner
        - 2.1.5 Update the weight vectors of neighbourhood nodes
    - 2.2 Reduce the size of the neighbourhood (if required)
3. End learning process.

Similarity of a data point is normally determined by calculating the Euclidian distance between the input pattern and the weight vector. The network weights are exploited in a different manner to that experienced in MLP neural networks: the weights are not multiplied with the input vector.

Thus, the Euclidean distance (d_i) is calculated for an input vector $\overline{p}$ and each i^{th} output node which has a corresponding weight vector $\overline{w}_i$.

$$d_i = \sqrt{(\overline{p} - \overline{w}_i)^T \cdot (\overline{p} - \overline{w}_i)} \quad \text{(Eq. 2.96)}$$

The winning output unit, or best matching unit (BMU), is simply the unit with the weight vector that has the smallest Euclidean distance to the input pattern, i.e. the most similar.

The neighbourhood of a node is defined as all nodes within a specified distance of the node on the grid. For example, in a square geometry grid, if the size of the neighbourhood is 1 then all units no more than 1 either horizontally or vertically from any unit fall within its neighbourhood. The weights of every node in the neighbourhood of the winning node, including the winning node, are updated according to **Eq. 2.97**; thus, moving each node in the neighbourhood closer to the input data point.

$$\overline{w}_i \rightarrow \overline{w}_i + \eta(\overline{p} - \overline{w}_i) \quad \text{(Eq. 2.97)}$$

Where, η denotes the step size.

As time progresses, the learning rate and the neighbourhood size are reduced. If the parameters are well chosen the final network should capture the natural clusters in the input data.

2.4.5 Pattern Recognition in Multiphase Flow Measurement

Pattern recognition techniques have previously been employed for multiphase flow measurement and analysis. The most prominent work in this field documented in published literature is the pioneering research work by Imperial College researchers in developing the ESMER multiphase measurement system (**Appendix A.12)**.

Darwich [**89**] proposed that time-varying characteristics of multiphase flow are reproducible and this fact could be exploited to determine the individual phase flow rates of a multiphase flow. A 2-inch horizontal measurement spool piece comprising radially mounted pressure transducers and axially mounted capacitance and conductance sensors was constructed to perform two-phase tests with air and water. It was determined that 8 features were effective in characterising the multiphase flow: 3 amplitude features (standard deviation, skewness and kurtosis) and 5 linear prediction coefficients. All 8 features were extracted form pressure transducer signals but only the amplitude features were found to be discriminatory for the conductance/capacitance sensors. Template matching was employed as the pattern recognition method whereby the individual phase flow rates were identified by matching measured vectors to those in a reference database. A measurement accuracy of ±10% was reported for each of the individual phase flow rates with a confidence level of 90%.

Toral *et al* [**90**] introduced an orifice plate to the horizontal spool piece set up by Darwich, described above, to study its ability to produce effective features for multiphase flow classification. It was reported that the presence of the orifice plate led to the production of enhanced discriminability for the extracted features.

Beg *et al* [**69**] incorporated a gamma densitometer device into the measurement spool piece for the resolution of oil, water and gas flow rates in a multiphase flow. However, the gamma densitometer was just one of an array of sensors employed with their system: pressure, conductance and capacitance sensors were also exploited to predict flow regimes and individual phase flow rates in 3” and 16” diameter multiphase pipes. From each sensor, 24 feature vectors were extracted. However, these were limited to the mean, variance, minimum, maximum and a 20-bin amplitude histogram of each sensor. Accuracies of ±10% were reported employing the gamma densitometer and ±18% from the pressure sensor for horizontal gas and liquid flows.

Arkartuna [**91**] undertook an experimental campaign with a 2-inch horizontal measurement spool piece with strip type capacitance sensors and pressure transducers in the slug flow regime for both two and three-phase flows. Two additional features were employed to those originally studied by Darwich: slug frequency and slug length. The template matching classification technique was compared and contrasted with an MLP neural network employing the SCG training algorithm. Akartuna reported that the MLP neural network system yielded superior classification properties when pressure and capacitance sensor fusion was employed: 97% of water cut, 90% of air velocity, and 90% of liquid velocity measurements were predicted to within ±10% relative error.

Cai [**92**] proposed the development of a flow regime specific pattern recognition model using a Kohonen self-organising feature map to classify data point flow regimes and then employing a separate MLP neural network for flow rate determination for each flow regime. An F-ratio feature saliency technique was applied to facilitate the selection of an effective feature set. Phase flow rate measurement accuracies for the multi-level hierarchical system were reported to be ±5% for 100% of oil continuous data points and 95.2% of water continuous samples. In terms of superficial velocity determination, 99.3% of gas and 100% of liquid phase superficial velocities were calculated to within ±9%.

Beg [**93**] built upon previous work undertaken by Darwich using radially and axially mounted absolute and differential pressure transducers in 2, 3, and 4-inch horizontal multiphase flows. A new feature set was employed comprising the mean and variance from the amplitude domain, and 5 features from the Cepstrum domain. Template matching was the pattern recognition technique applied and it was reported that 100% of liquid phase and 93% of gas phase measurements could be obtained to within ±10 % through feature combinations. Comparisons made between the feature maps for the different pipe sizes revealed that different turbulence signatures were obtained for the same flow conditions. Accordingly, a method of scaling was proposed based on the hydrodynamic coordinates and feature vectors. Measurement accuracy with the scaling technique was reported to be poorer than that obtained through *in-situ* calibration.

Toral *et al* [**94**] and Wood [**95**] have described the commercial version of the ESMER multiphase flow meter developed through the aforementioned studies. Stochastic features are extracted from three differential pressure sensors (one top axial, one bottom axial and another radially mounted), impedance sensors (axially mounted on top) and a temperature sensor and input to an MLP neural network. The neural network system is trained and then validated, using the cross-validation technique to avoid over-fitting, before being subjected to tests. The individual phase flow measurements made by the ESMER meter were reported to match those yielded by the test separators to within ±10%.

A number of pattern recognition studies in multiphase flow measurement have been conducted outside of the ESMER development programme.

Goudinakis [**96**] investigated the feasibility of using an MLP neural network for flow regime identification in a horizontal pipeline and an S-shaped riser for air-water flow using capacitance sensors and pressure transducers respectively. Stratified smooth, stratified wavy, bubble and slug flow regime classifications were identified using raw time-series data (fixed length window) as the input to the system. The S-shaped system was determined to accommodate long sever slugging flow cycles up to 230 seconds; while the horizontal system cycles did not take more than 10 seconds. It was reported that a delay window of 200 inputs (20 seconds of data at 10 Hz) was required for horizontal pipe regime classification; while 100 inputs (100 seconds of data at 1 Hz) was adequate for identification of the S-shaped riser's flow pattern. Nevertheless, it was identified that the excessive training time required to enable classification would prevent this technique from being suitable for practical applications

Jama [**97**] reported on the use of pattern recognition techniques using absolute and differential pressure signals from a Venturi meter to measure wet gas flow rates. A Bayesian MLP network was implemented using feature extraction from the pressure sensor signals. It was reported that, employing cross-sensor data fusion of amplitude features, all test data points predicted the gas and liquid superficial velocities to within ±5% relative error.

Ibrahim [**98**] studied the application of a single back-propagation MLP neural network to multiphase slug flow measurement in a horizontal pipeline. A horizontal spool piece with capacitance and pressure sensors was employed. Various amplitude and frequency domain features were extracted from these sensors and used as inputs to the neural network. Slug length and slug frequency features were also included as part of the study. Feature fusion from both the pressure and capacitance sensors were reported to give the best classification results. In two-phase tests, 100% of liquid superficial velocities and 93% of gas superficial velocities were classified to within ±10%. In multiphase flow tests, 90% of both liquid and gas superficial velocities and 97% of the water cuts were predicted to within ±10% relative error.

Wylie *et al* [**99**] proposed the use of an electromagnetic cavity resonator based sensor to determine multiphase flow rates. Low power radio frequencies were transmitted across a pipeline carrying a multiphase flow and the phase fractions calculated by monitoring the shift in the resonant frequencies with different fluid properties. Neural networks were exploited to overcome the modelling complications induced through the application of the system to different flow velocities, temperatures, pressures, installations etc. Measurement accuracies of ±10% for phase fractions were reported and a measurement repeatability of 4% was claimed based on the experimental data presented.

Several publications have reported the use of gamma ray attenuation measurements as part of part of their pattern recognition system including Beg *et al* [**69**] detailed earlier in this section.

Sheppard and Russell [**70**] investigated the ability of a neural network to classify horizontal gas and liquid flow rates from the response of a gamma densitometer. No information was provided on the gamma densitometer system employed but it is reported that standard statistical parameters were extracted from the raw signals for use as the system inputs. The neural network was trained on 12 time series covering a range of flow regimes. The pattern recognition model was firstly evaluated using unseen data from the 12 time series used to train the network and produced gas and liquid flow rates to within a root mean square error of 13%. A second phase of analysis was undertaken using data from previously unseen flow rates: the classification accuracy was reduced to a root mean square error of 15%.

Bishop and James [**71**], and Bishop [**72**], proposed a technique using gamma attenuation based on the use of three vertical and three horizontal dual-energy gamma densitometer beams installed in a parallel configuration across a pipe section. The input features to the neural network were the six path lengths measured by the gamma densitometers and the target outputs were the volume fractions of the oil and water phases. The Quasi-Newton training algorithm was employed in these studies. It was concluded that a neural network technique based on gamma attenuation could provide a practical solution in determining component phase fractions from the gamma densitometer data.

Åbro *et al* [**73**] documented their findings using an amercium-241 source and a multi-beam configuration with a neural network to identify the flow regime and the void fraction. A computer simulation model of the gamma emission and detection system was employed to create training data sets for the neural network. The input to the network was an energy spectrum for the photon range 30 to 68 keV (i.e. 38 bins of 1 keV) for single sensor investigations and an energy spectrum for the photon range 55 to 64 keV for the multi-detector experiments. Fourteen output neurons were used to represent the void fraction in10% increments and the three flow regimes (homogeneous stratified or annular) whereby an output of +1 was returned by the network for the identified regime and void fractions while all other outputs returned a value of 0. Test data was collected on an 8 cm aluminium pipe using a 14 mCi americium-241 source and a CZD detector from eV Products Inc. Using a single detector position at 180° to the source an average error of 15.8% was obtained for the void fraction measurements with a standard error deviation of 8%. Using a multi-detector setup, the inputs were parts of spectra at detector positions of 180°, 156°, and 140°. The multi-detector configurations yielded average void fraction errors of just 3% and a reduced standard error deviation of 4.2%.

Chapter 3: Experimental Set Up and Data Acquisition

This chapter describes the experimental set up used to study the exploitation of gamma radiation for multiphase flow measurement. An outline of the multiphase flow loop facility at Cranfield University is provided as well as descriptions of the gamma densitometer instrument's operation, data acquisition and processing, installation and calibration, and signal characteristics. Finally, details of the experimental campaign undertaken are documented.

3.1 Cranfield University Multiphase Flow Test Facility

The Cranfield University multiphase flow test facility comprises an air, water, and oil delivery section, a test section, and a fluid separating section, **Figure 3.1**. The test facility is used for flow assurance, multiphase metering and control systems research. It is designed to process continuous flow of air, oil and water. The facility has a maximum operating pressure of 25 barg and the test fluids comprise air, tap water (doped with biocide) and BP-7269 lubricating oil (ρ = 815 kg/m^3 and μ = 0.004 Pa.s at 20 ºC). The reader is referred to Loh [**100**] for a detailed description of the multiphase test facility and its full operating procedures.

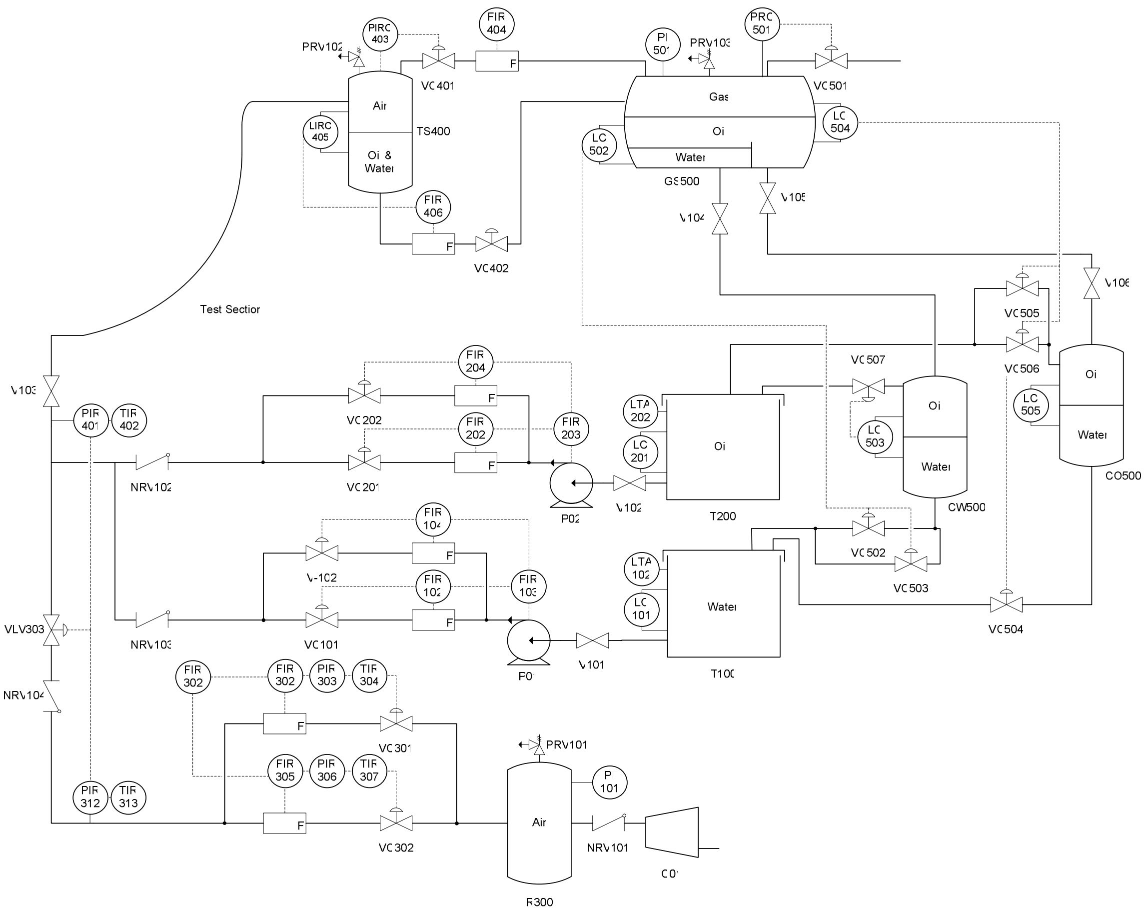

Figure 3.1 – Cranfield University Multiphase Flow Test Facility

3.1.1 Fluid Delivery

Air is supplied from an Atlas Copco Electonikon GA75 compressor (C01), capable of supplying a maximum flow rate of 1275 m^3/hr free air delivery at up to 7 barg. Air from the compressor is passed to a 2.54 m^3 receiver (R300) to dampen the compressor loading and unloading cycle pulsations. The air is then available to enter the metering section where it passes through either the ½-inch (0 – 100 Sm^3/h) or 1-inch (95 – 1275 Sm^3/h) pipeline, controlled by valves VC302 and VC301 respectively.

Oil from a 8 m^3 oil reservoir tank (T200) is pumped to the test section by a Grundfos CRN 90-5 multistage inline centrifugal pump (P02) which has a maximum delivery of 90 m^3/h. An inverter is employed to control the pump speed to prevent overworking and overheating of the equipment. There are two oil delivery lines: low flow rates (0 – 1 kg/s) are controlled using control valve VC202 on a 1-inch line; whereas, higher flow rates (>1 kg/s) are controlled by VC201 in a 2-inch line.

Water from a 10 m^3 water reservoir tank (T100) is pumped to the test section by a second Grundfos CRN 90-5 multistage inline centrifugal pump (P01). Similar to the oil delivery system, there are two water supply pipelines: low flow rates (0 – 1 kg/s) are controlled using control valve VC102 on a 1-inch line; whereas, higher flow rates (>1 kg/s) are controlled by VC101 in a 2-inch line.

3.1.2 Test Section

The test section comprises a 55 m long, 2° downward inclined, 4-inch NB schedule 10 (internal diameter = 108.2 mm) steel pipeline joined to 10.5 m high catenary riser with a vertical topside separator where the gas and liquid phases are separated. The gamma densitometer instrument is installed at the top of the riser's vertical section, **Figure 3.2**[1].

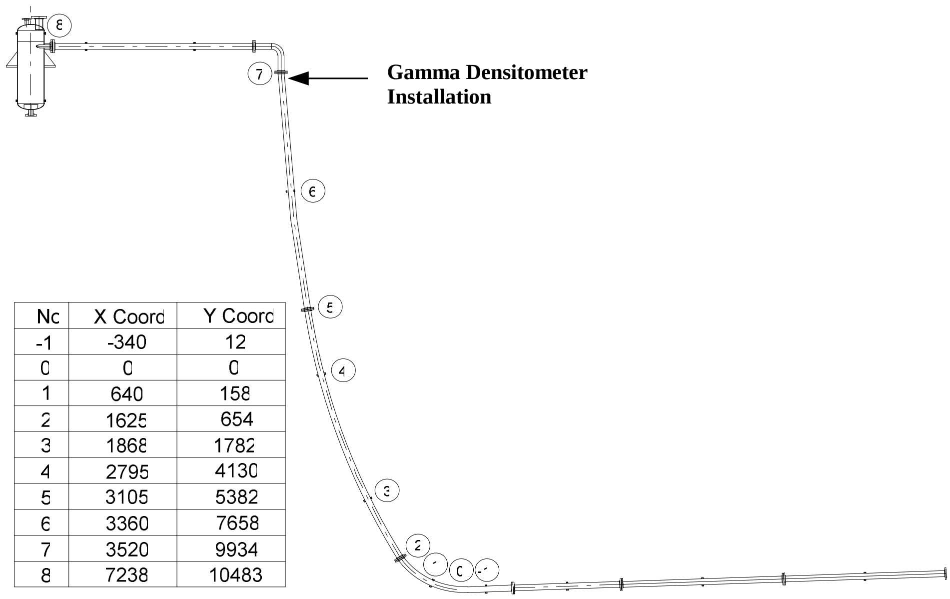

No	X Coord	Y Coord
-1	-340	12
0	0	0
1	640	158
2	1625	654
3	1868	1782
4	2795	4130
5	3105	5382
6	3360	7658
7	3520	9934
8	7238	10483

Figure 3.2 – Multiphase Flow Loop Test Section Riser and Separator

[1] Riser co-ordinates are in millimetres with (0,0) denoting the riser base.

Although the gamma densitometer is installed on the vertical section of the catenary riser, it is recognised that the upstream pipeline geometry will affect the fluid flow characteristics with the gas phase having a tendency to favour the side of the riser. However, the gamma densitometer was installed with its measurement path in parallel with the topside separator inlet pipe work to minimise the instrument's exposure to biases in the fluid distribution from riser induced asymmetries.

3.1.3 Fluid Separation

Air, water and oil are separated by gravity in a three-phase separator vessel (GS500). The air is vented to atmosphere while the oil and water phases are passed to their respective coalescers (CW500 and CO500) to undergo fine separation before being returning to their respective reservoir vessels. Each fluid return comprises two lines (1-inch and 3-inch) enabling split range flow control to maintain stable fluid interfaces in the three-phase separator.

3.1.4 Reference Instrumentation

The multiphase flow facility is equipped with a state-of-the-art process control and management system, the Emerson Process Management DeltaV automation system. All instrumentation in the multiphase flow test facility is interfaced with the DeltaV system which was configured to record instrument output values at a rate of 1 Hz. Historical data could be downloaded from the DeltaV cache after experimental work for reference purposes. The multiphase flow test facility fluid delivery and test section instrumentation is detailed in **Table 3.1**.

Tag	Description	Details	Range	Accuracy
FIR102	Inlet Water Flow Meter (high flow rate)	Coriolis – 2" Foxboro CFS 20	0.12 – 11.6 kg/s	±0.15%
FIR104	Inlet Water Flow Meter(low flow rate)	Electromagnetic – 1" Rosemount 8742	0.005 – 5.0 kg/s	±0.20%
FIR202	Inlet Oil Flow Meter (high flow rate)	Coriolis – 2" Foxboro CFS 20	0.12 – 11.6 kg/s	±0.15%
FIR204	Inlet Oil Flow Meter (low flow rate)	Coriolis – 1" Micro Motion CF3M	0.02 – 3 kg/s	±0.50%
FIR302	Inlet Air Flow Meter (high flow rate)	Differential Pressure – 1" Rosemount Mass Probar	90 – 4250 sm^3/h	±0.90%
FIR305	Inlet Air Flow Meter (low flow rate)	Differential Pressure –0.5" Rosemount Mass Probar	0 – 100 sm^3/h	±0.90%
FIR404	Topside Separator Gas Outlet Flow Meter	Vortex – 1" Rosemount 8800D	13 – 134 sm^3/h	±0.65%
FIR406	Topside Separator Liquid Outlet Flow Meter	Coriolis – 2" Micro Motion CF3M	0.12 – 11.6 kg/s	±0.15%
PIRC403	Topside Separator Pressure Transducer	Rosemount 3051	0 – 7 barg	±0.15%
PIR401	Riser Base Pressure Transducer	Rosemount 3051	0 – 7 barg	±0.15%
PIR312	Air Flow Line Pressure Transducer	Rosemount 3051	0 – 7 barg	±0.15%

Table 3.1 – Multiphase Flow Test Facility Instrumentation

3.2 Gamma Densitometer

A clamp-on fast sampling gamma densitometer unit was supplied by Complex Resource Ltd (Russia) for use in the experimental campaign. The instrument comprises three parts: a gamma source block, a detector block and a mounting bracket for installation on a vertical length of pipe, **Figure 3.3**.

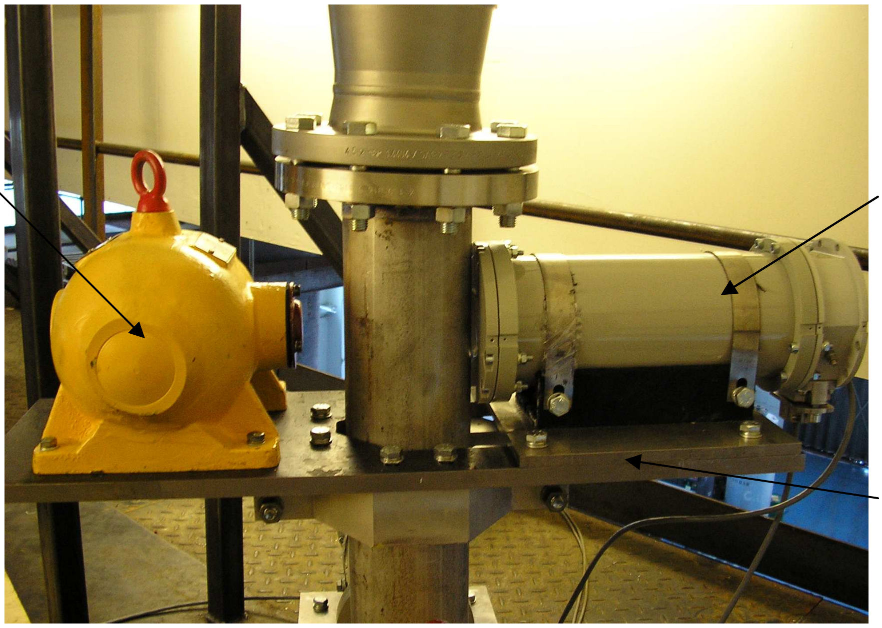

Figure 3.3 – Gamma Densitometer Installation at the Top of the Riser

The unit was enclosed in a area clearly identified as containing radioactive material with restricted access. Operation of a mechanical 'sliding rod' type lock at the side of the source block (not visible in **Figure 3.3**) enabled the gamma source to be moved between its safe 'dormant' and 'active' positions. At all times, a large colour coded panel located in the enclosed area indicated whether the gamma source was in its 'active' open (red) or closed (green) position. During the test campaign, the source was retained in its active position to ensure source positioning was identical for all tests.

3.2.1 Gamma-Source Block

The gamma-source block consists of a gamma radionuclide source capsule surrounded by a lead body to shield the surrounding environment from the gamma radiation emitted by the source. The outer casing of the source block is fabricated from stainless steel to add mechanical strength and rigidity to the lead lining. A collimating passage has been machined to provide an outlet that produces an isotropic conic beam of gamma radiation with an angle of 7º to be directed across the pipe diameter. The intensity of the gamma radiation beam is controlled through the insertion of brass discs of various thicknesses in the collimated beam's outlet path. The combination of brass discs employed varies according to the size and thickness of the installation pipe and the activity of the source.

A 6.6×10^9 Bq caesium-137 source was employed as the radionuclide in the source block in the form of a VZ-1508 type capsule. The nucleus of the caesium-137 undergoes a radioactive decay mechanism which yields gamma radiation, **Figure 3.4**.

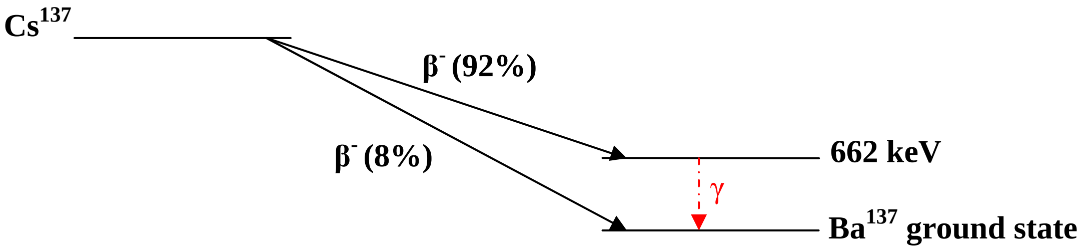

Figure 3.4 – Caesium-137 Decay

The caesium-137 emits an electron (β) and an antineutrino. This increases its nuclear charge from 55 to 56 by changing a neutron into a proton. As shown, 92% of the decays result in only 514 keV being transferred to the electron and neutrino, leaving the barium-137 in a metastable, excited state. This will further decay by either emitting a 662 keV gamma (90% of cases result in this outcome) or by ‘internally converting’ the gamma before it leaves the barium atom and ejecting a K-shell electron instead.

Figure 3.5 illustrates the measured caesium-137 spectrum obtained for an empty pipe using the gamma densitometer instrument.

The x-axis of the spectrum plot represents the channels from the multiple channel analyser used to classify the gamma photon energy distribution, where the channel number is directly proportional to the gamma photon energy. The y-axis represents the number of counts per second. The main features of the caesium pulse height spectrum have been labelled:

A. This is the complete absorption of 662 keV gammas. This energy usually is derived from a Compton scatter followed by a secondary scatter and/or photoelectric absorption. The detector side collimator directs all the incoming gammas to the centre of the scintillator crystal so that they are unlikely to be able to escape the crystal without further interaction.

B. This is the ‘Compton Edge’ of the spectra. Here the gammas which have been scattered once and then escape can transfer a maximum of 478 keV if they are scattered backwards ($\theta = \pi$).

C. This plateau corresponds to the Compton scatters with $0 < \theta < \pi$. The region extends from the ‘Compton Edge’ all the way to zero energy.

D. This peak arises from scatterings at $0 < \theta < \pi$ which originated outside of the crystal. This can occur when a 662 keV gamma photon from the source strikes the lead at the cavity at the back of the source holder. A 662 keV photon can be scattered forward with 182 keV and pass into the detector where it will be detected.

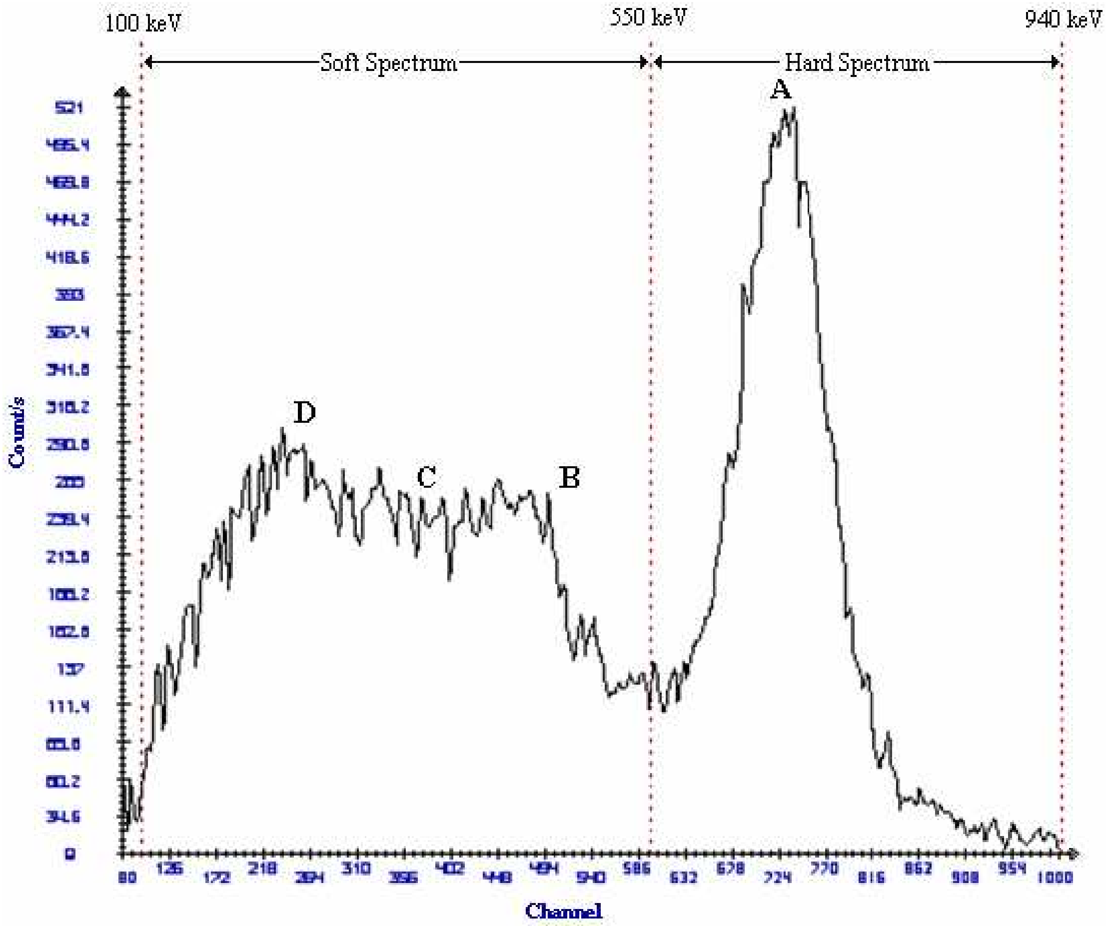

Figure 3.5 – Measured Caesium-137 Spectrum

There are a number of interactions at the lower photon energies including the return of excited electrons to their K-shells in the lead shielded can yield X-rays of 75 keV and 32 keV X-rays from Ba-139 after internal conversion. However, these are not shown in **Figure 3.5** as the lower limit of detection is set to ignore these.

The gamma densitometer unit employed in the experimental work exploited both the direct high-energy photons in the range 550 – 940 keV and the lower energy Compton scattered photons in the 100 – 550 keV range. Throughout this study, the high and low energy photons ranges are also referred to by the terms ‘hard’ and ‘soft’ spectrum respectively.

3.2.2 Gamma-Detection Block

The gamma-detection block comprises four key components: scintillation crystal, photomultiplier tube, amplifier electronics and two single-channel analysers (SCA), **Figure 3.6**. The detection block also contains a temperature regulating circuit to ensure that the internal detector temperature does not fall below 20 ºC; thus, minimising the influence of temperature on the detection electronics.

A 30 mm × 60 mm sodium iodide (NaI) scintillation crystal doped with thallium was employed in the gamma-detector system. This crystal produces a pulse of visible light with an energy proportional to that of the incident gamma photon.

The light pulses are detected by a FEU-115M photomultiplier which converts the light pulses into voltage pulses of proportional amplitudes. Propriety electronic circuits are employed to amplify and condition the voltage pulses which are then passed on to channel analysers for classification.

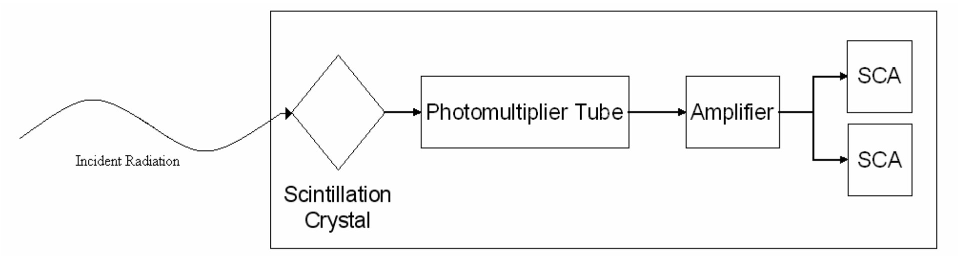

Figure 3.6– Gamma Detection Block Components

The single-channel analysers effectively act as counters of the voltage pulses produced that originate from gamma-photons with an energy of interest. The SCAs were configured to measure the gamma count of the 550 – 940 keV hard energy spectrum and the gamma count for all photon energies of interest: 100 – 940 keV. The soft energy spectrum count (100 – 550 keV) was determined by calculating the difference between the two measured ranges. The accuracy of the gamma densitometer count measurements is quoted as ±0.5% by the manufacturer Complex Resource Ltd (Russia).

3.2.3 Data Acquisition and Processing

The gamma densitometer detection unit was connected via a RS-485 serial interface to an ICP I-7188D PLC where the raw densitometer signal was processed into a gamma count signal and passed to a local PC workstation through an RS-232 serial connection.

During data collection, gamma count measurements were made at a rate of 250 Hz and passed from the PLC to the local PC through the RS-232 serial connection and stored in a text file for offline data processing. For each measurement, two text files were created: one to record the hard-energy count and the other to record that of the soft-energy gamma count. Raw data text files were imported into MATLAB and transformed into workspaces for further processing.

All data and signal processing operations were undertaken on a 1700 MHz Intel Pentium 4 desktop system with 1024 MB RAM. MathWorks Inc MATLAB version 7.1.0.246 (R14) was the platform used for all digital signal processing and neural network simulations performed as part of this research work.

3.2.4 Installation and Calibration

The gamma-source and detection blocks are mounted diametrically opposite each other on a vertical pipe section using a clamp-on mounting bracket, **Figure 3.7**. Caution was exercised to align the source and detection units with the centre of the pipe. The unit distance from pipe wall should be approximately 0.01 m and 0.07 m for the detector and source blocks respectively. Once physical installation of the unit has been completed, the caesium-137 pulse height spectrum detected must be analysed to ensure installation has been successful. A bespoke program supplied with the instrument was used to produce a pulse height spectrum for gamma densitometer installation.

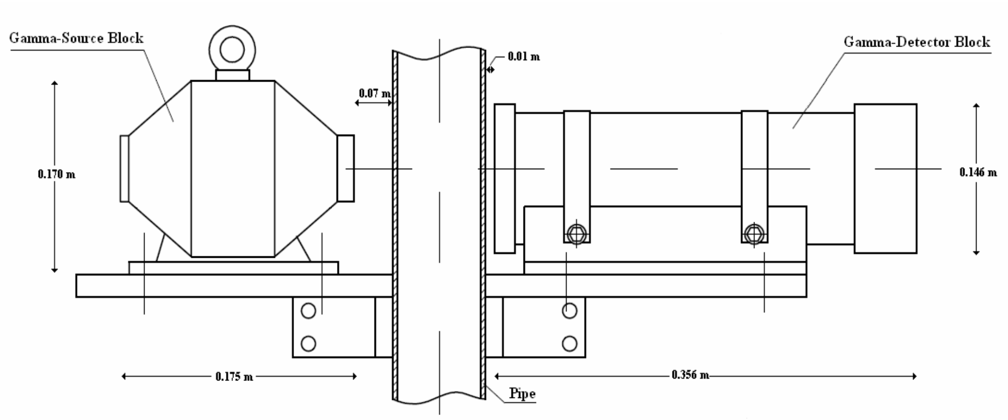

Figure 3.7 – Gamma Densitometer Instrument Installation

The pulse height spectrum obtained is shown in **Figure 3.5**. The spectrum produce is examined to ensure that the characteristic features associated with a caesium-137 spectrum are present in the detected spectrum. It may be required to adjust the physical installation of the unit if distinct features are not produced in the detected spectrum.

Prior to undertaking experimental data collection for multiphase flow mixtures, reference gamma count values for the individual test fluids were determined in static conditions in the multiphase flow facility. For each fluid (air, water and oil) the catenary riser section (internal diameter of 0.1082 m) was flooded and the flow stopped so that the test fluid formed a continuum in the gamma densitometer measurement section. Gamma densitometry data was collected for a period of 1 hour and the mean count for each of the two energy levels determined. This experiment was repeated three times for each fluid and the average value calculated. The mean gamma count and corresponding mass attenuation coefficients, based on the assumption that the attenuation air at 1 atm is negligible, are summarised in **Table 3.2**.

Spectrum	Mean Gamma Count			Linear Attenuation Coefficients (m^{-1})		
	Air	Water	Oil	Air	Water	Oil
Hard	179.7	78.7	90.1	0	7.63	6.38
Soft	490.3	262.5	291.2	0	5.77	4.81

Table 3.2 – Mean Gamma Count and Attenuation Coefficients for Test Fluids

The linear attenuation coefficients illustrate that the water attenuates the gamma radiation to a greater degree than the oil phase for both energy levels owing to its higher density. However, the ratio of attenuation imposed by the water and oil phases differ for the two energy ranges analysed: 1.196 and 1.199 for the hard and soft ranges respectively.

The mean gamma count values for the calibration experiments were correlated with the attenuating material densities, **Figure 3.8**.

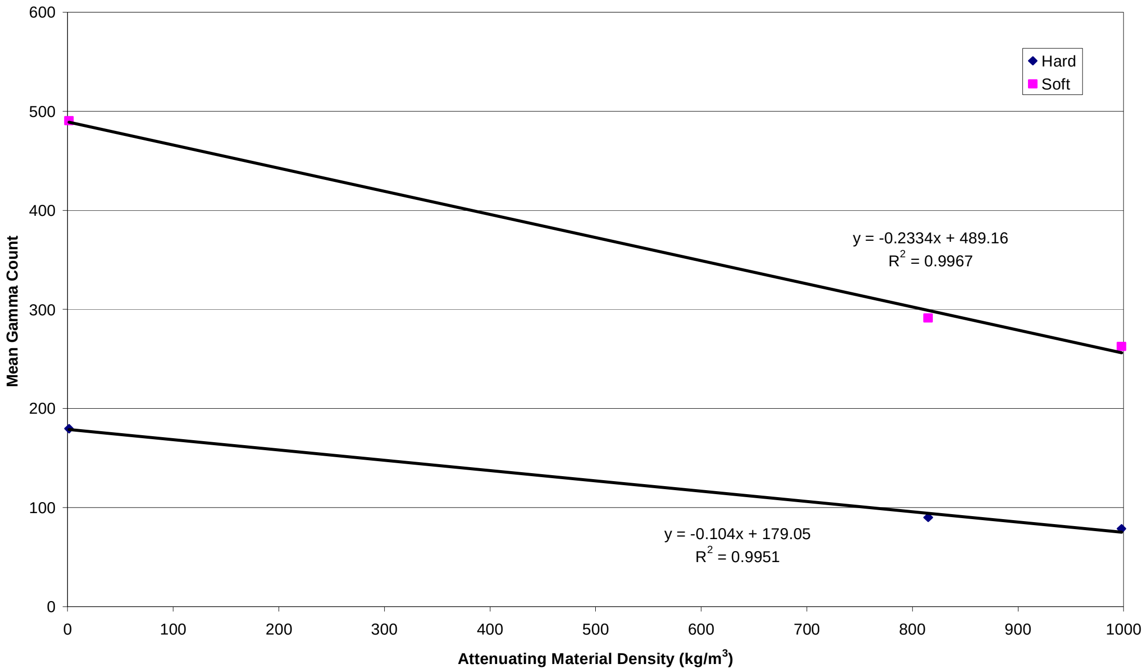

Figure 3.8 – Gamma Attenuation as a Function of Material Density

The gamma densitometer exhibited an approximately linear decrease in gamma count with increasing attenuating material density for both the hard and soft signals. The hard and soft energy gamma counts experienced differing rates of attenuation with increasing density. Consequently, the installed dual-energy caesium-137 gamma densitometer demonstrated that it was functioning correctly and exhibited the expected discriminatory response to materials of differing densities to instil confidence in the reliability of the instrument for data analysis purposes.

3.2.5 Radiation Safety

In order to comply with Heath and Safety legislation, it was necessary to measure the radioactivity levels around the installation each month. **Figure 3.9** illustrates the gamma count measurements taken around the source.

Position 1 is 90º to the right of the 4-inch nominal bore pipe, position 2 is diametrically opposite the source and position 3 is 1 metre away from the pipe. The working area is approximately 2 m away southeast of the pipe.

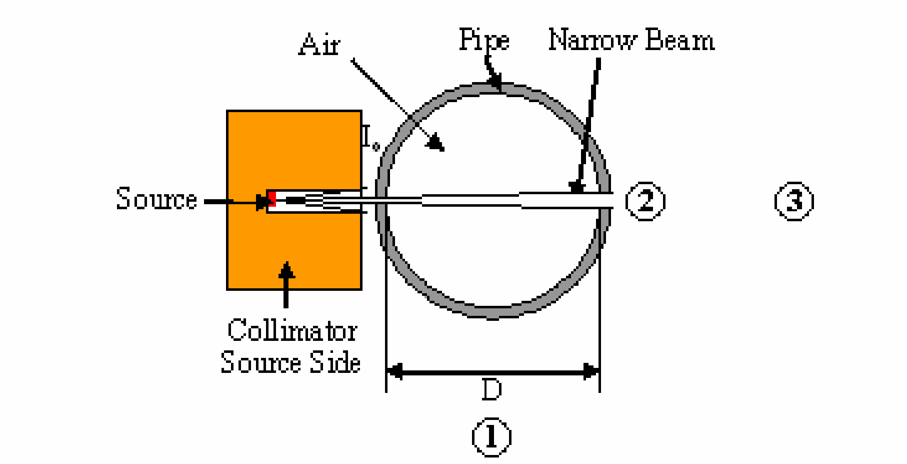

Figure 3.9– Radiation Level Measurement Points

Gamma count readings were taken when the source was exposed. The results are summarised in **Table 3.3**.

Position	Average Dose Rate
1	50 µSv/hr
2	500 µSv/hr
3	1 µSv/hr

Table 3.3 – Radiation Level Measurements

Additional readings were taken near the working area and below the platform:

1	1.5 meter away in the working area	0.2 µSv/hr
2	Mid way between working area and source	0.3 µSv/hr
3	Under the platform at ground level	0.07 µSv/hr

The unit of effective dose is the Sievert (Sv). The maximum effective dose for radiological workers is set at 20 mSv per year (whole body dose). This figure is averaged over a 5-year period and no single year can exceed 50 mSv. The installation radiation levels and control measures met the Environment Agency and Health Protection Agency criteria. Nevertheless, personal thermoluminescent dosimetry (TLD) radiation detectors were worn at all time in the laboratory to record exposure during experimentation with instrument; thus, ensuring that personnel exposure did not breach the specified limits.

3.2.6 Signal Characteristics

Radioactive phenomena are random and discrete in their nature. Accordingly, measurements made with a gamma detection instrument are subject to statistical fluctuations. This variation cannot be eliminated, but its significance can be diminished by increasing the number of measurements (i.e. longer data collection periods). An analysis of the gamma densitometer's signal characteristics was performed to ensure that the proposed data gathering procedure employed the optimal data collection period.

The mean gamma count for both the hard and soft energy photons was monitored with respect to time in order to ascertain the optimal measurement period. The mean count value was calculated after each cumulative minute of data collection and its percentage variation plotted to track the stabilisation of the mean value with time. Analysis of gamma count measurements in static air, water and oil configurations revealed that the high-energy hard spectrum was less affected by statistical fluctuations. The percentage change in the mean gamma count for both the hard and soft energy levels for static oil are shown in **Figure 3.10**.

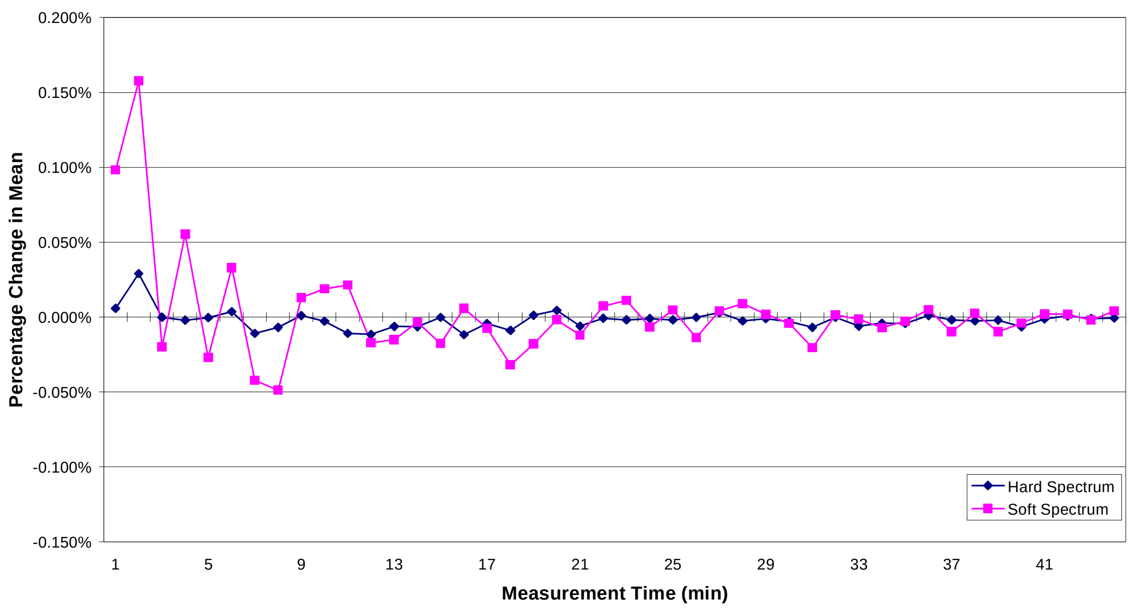

Figure 3.10 – Count Stability for Static Oil

The hard spectrum demonstrates very low fluctuations in the static oil: after 19 minutes of data collection the variation in the mean value fell to ±0.01%. The soft energy level's mean value stabilises to within reasonable limits after the same measurement time as the hard energy level but it is prone to larger variations: up to ±0.02%. Similar trends were observed for tests undertaken with static air and static water.

The high-energy hard gamma photon count will be subjected to less severe statistical fluctuation owing to its narrower window range and larger transmission rate. The increased detection frequency results in a lower standard statistical error as it is known that the standard error is inversely proportional to the square root of the number of samples. Consequently, the hard spectrum was exploited in subsequent statistical analyses of the output signals to attain the maximum data collection period required.

Figure 3.11 illustrates the effect of the fluid on the soft spectrum mean gamma count stabilisation.

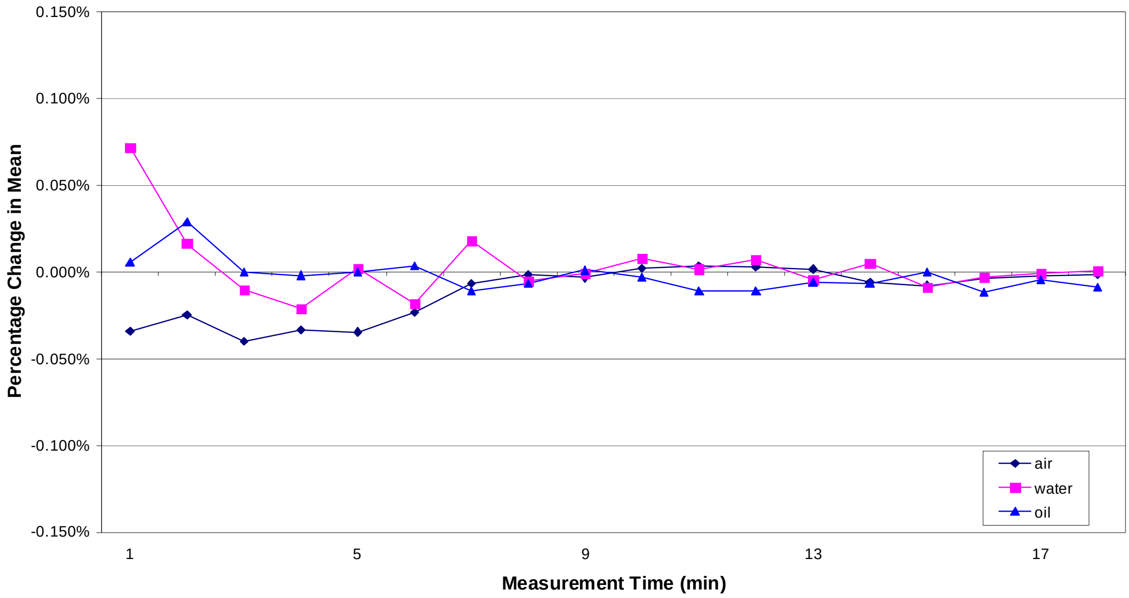

Figure 3.11 – Hard Energy Count Stability for Static Fluids

Initially, the gamma count on the static water experiences the largest variation in its mean value but stabilisation to within ±0.01% was achieved after only 8 minutes of data collection. For static air, the hard spectrum mean value converged to stability of ±0.01% within 7 minutes. Thus, it can be stated with confidence that taking a measurement time of 20 minutes for static fluid test will enable sufficient stabilisation of the gamma count to give a stable count value representative of the fluid.

The stability of the hard spectrum mean value was subsequently investigated for dynamic multiphase flows. **Figure 3.12** exemplifies the range of results obtained from analysis of the statistical stability of the gamma count for a range of different GVFs. From the results obtained, it was concluded that initial level of variation in the mean measurement could not be correlated to any of the multiphase flow properties as large and small variations were witnessed for all flow compositions and types. However, the time taken to attain an acceptably stable value (±0.015%) is relatively low for low GVF data points (16 minutes for a GVF of 23%); whereas, high GVF data points required a longer time to establish the prescribed level of stability (35 minutes for GVF of 89%).

As a result, a measurement time of 40 minutes was employed for all data points to ensure that the gamma counts of both energy levels attained stable mean values regardless of the test fluid mixture GVF. Test facility flows were monitored to ensure steady flow conditions were maintained throughout the gamma densitometer data collection period.

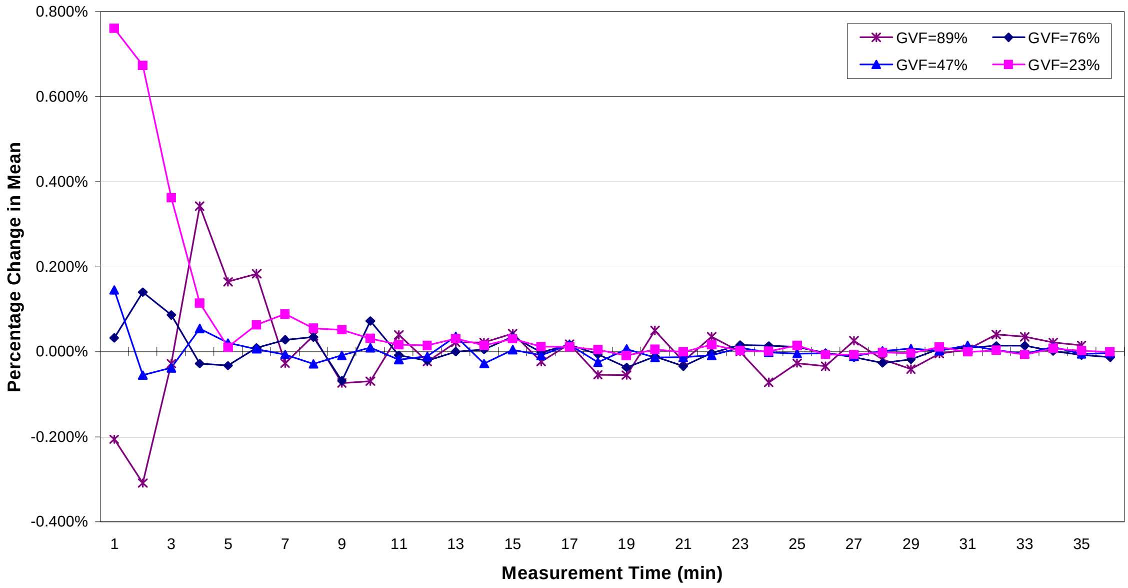

Figure 3.12 –Hard Energy Count Stability for Multiphase Flow Tests

3.3 Experimental Campaign

Gamma count data for 126 different multiphase fluid conditions was collected across the full operating range of the Cranfield University multiphase flow test facility to expose the gamma densitometer instrument to a wide range of different flow regimes, **Figure 3.13**.

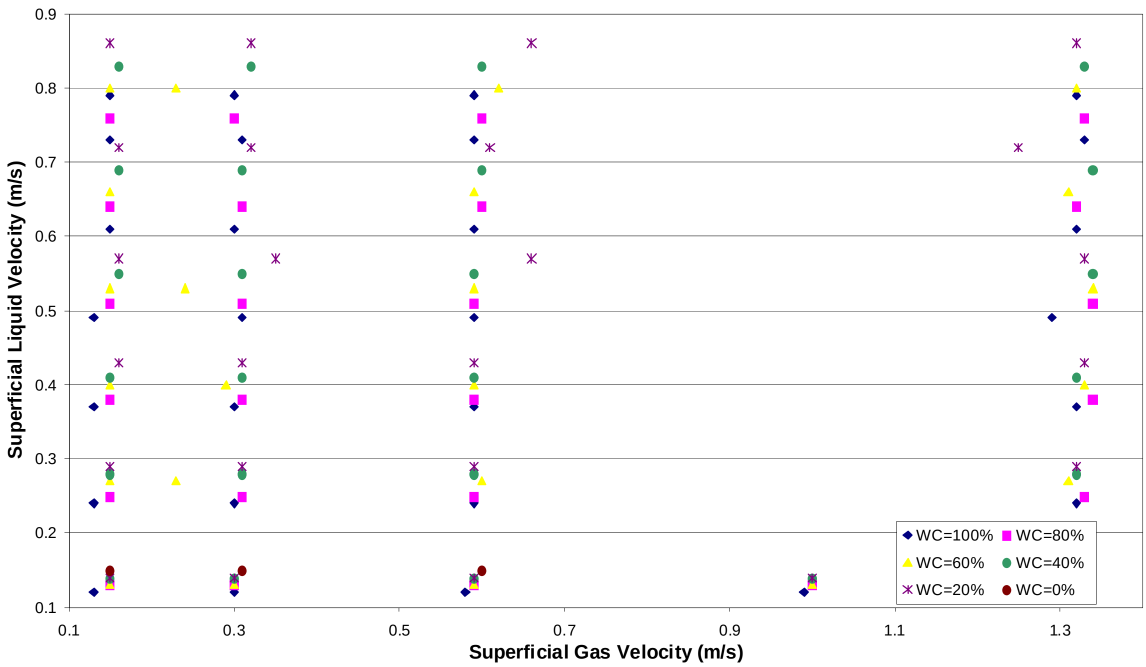

Figure 3.13 – Test Matrix

Technical difficulties with the gamma densitometer unit necessitated its removal for repair at the beginning of the collection of data for gas superficial velocities of 1 ms^{-1} resulting in a reduced data set than originally anticipated. However, all data points at gas superficial velocities of 0.12, 0.3, 0.6 and 1.3 ms^{-1} had been collected before the densitometer failure and this was considered sufficient for analysis. The multiphase flow conditions are expressed in terms of the superficial phase velocities and the liquid phase water cut. The superficial gas velocity values have been corrected for pressure and temperature to account for conditions at the point of measurement. For the purposes of this research work, it was assumed that the difference between the water and oil phase velocity were negligible and that their velocities could be represented by a common value for the total liquid phase.

Each test point involved the setting and the monitoring of the flow parameters in the test facility on the DeltaV system. Gamma count recording was initiated when steady-state conditions had been attained over a period of 20 minutes. For each data point, gamma densitometer data collection was undertaken for a period of 40 minutes so as to obtain statistically stable count information.

Chapter 4: Signal Analysis

This chapter summarises the signal analysis work conducted on the gamma count data collected from the gamma densitometer as described in **Chapter 3**. The response of the gamma-densitometer unit to different multiphase flow conditions was examined. Various statistical parameters were extracted from the time-varying signals and were investigated to establish their correlation with characteristic parameters of the multiphase flows which produced them. Analysis of the signals was also conducted in the frequency domain. Furthermore, wavelet analysis was employed to facilitate simultaneous analysis of the signals' time and frequency domain characteristics.

4.1. Sensor Response

The response of the gamma densitometer's output signals as a function of time when subjected to different multiphase flow conditions was examined, **Figure 4.1**. In each of the test points illustrated, the water cut of the liquid phase was 100%; thus, the responses observed are functions of the gas and liquid interphase interactions with no dependency on intraphase phenomena.

(a) V_{sg} = 0.15 ms^{-1}, V_{sl} = 0.79 ms^{-1} and WC = 100%

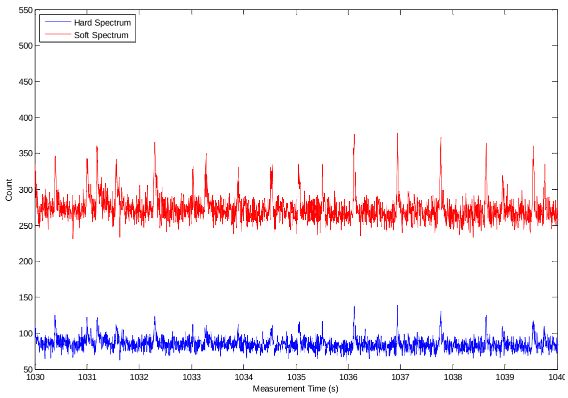

(b) V_{sg} = 0.13 ms^{-1}, V_{sl} = 0.12 ms^{-1} and WC = 100%

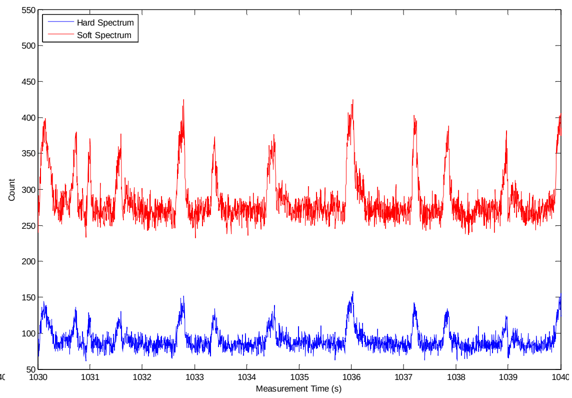

(c) V_{sg} = 1.32 ms^{-1}, V_{sl} = 0.79 ms^{-1} and WC = 100%

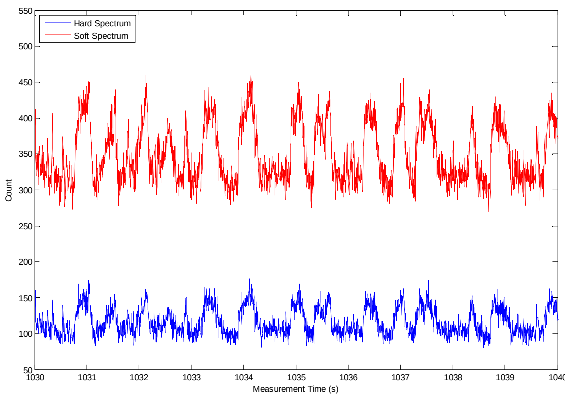

(d) V_{sg} = 0.99 ms^{-1}, V_{sl} = 0.12 ms^{-1} and WC = 100%

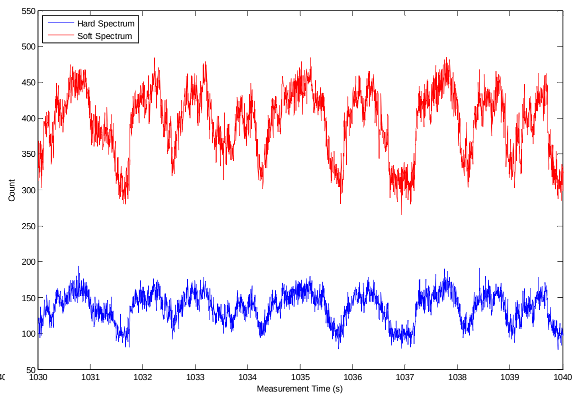

Figure 4.1 – Gamma Count Data Signals

The gamma photon count variations for the hard and soft energy gamma photons exhibited complementary time-varying responses. Identification of density fluctuations in the multiphase flows is obvious from the series of peaks and troughs in the amplitude of the output signals. For high-density, liquid-rich, fluid segments, the number of gamma photons absorbed by the fluid increases. Accordingly, the magnitude of the detector unit's output signal decreases. Conversely, the signal magnitude will increase for low-density, gas-rich, fluid segments where the number of photons absorbed by the multiphase mixture decreases.

When analysed over a short period (e.g. 10 – 30 seconds), the raw signal traces provide a useful visual indication of the flow features present in the multiphase flow pipeline. As the gas loading increases, the peaks produced by the passing gas elements increase first in amplitude and then in width. The peaks present in the signals' amplitude represent the passage of gas structures through the measurement section: the greater the amplitude of the signal peak, the larger the magnitude of the gas structure's length in the radial direction, with large peaks inferring a high local gas void fraction. Peak width provides an indication of the gas structure length in the axial direction: longer structures will induce wider peaks. However, the width of a peak will also be dependant on the structure's velocity and a wide peak could represent the passage of more than one gaseous structure in close proximity to each other.

For data points with identical gas and liquid phase mass flows, visual examination of the sensor response to changes in the liquid phase water cuts was not possible owing to the much smaller scale variations they induced in the signals compared to the gas phase induced variations: the component density ratio of gas:oil:water for the test fluids was 1:679:831 at 20 ^{o}C.

Figure 4.1 (a) – (d) exhibit flows with increasing GVF values: 16%, 51%, 63% and 89% respectively. **Figure 4.2** illustrates the location of the data points on a superficial phase velocity flow regime map composed employing the Taitel-Dukler bubble-slug flow regime boundary **[28]**.

The flow regime map classification compliments the observations made on the raw signal traces. **Figures 4.1 (a)** and **(b)** have sharp, narrow peaks characteristic of the passage of small, discrete gas structures and were classified as bubble type flows. Similarly, **Figures 4.1 (c)** and **(d)** comprise higher and wider peaks suggesting the passage of larger gas structures that could be the slug type features predicted to dominate by the flow regime map.

Examination of the full data set revealed that each test point's gamma count signal differed from its counterparts in terms of amplitude, time and frequency features and correlated well with the Taitel-Dukler flow regime classifications. Flow regime classification of data points located near to the flow regime boundary was not possible as traits of both regimes were evident and any classification would have been subjective.

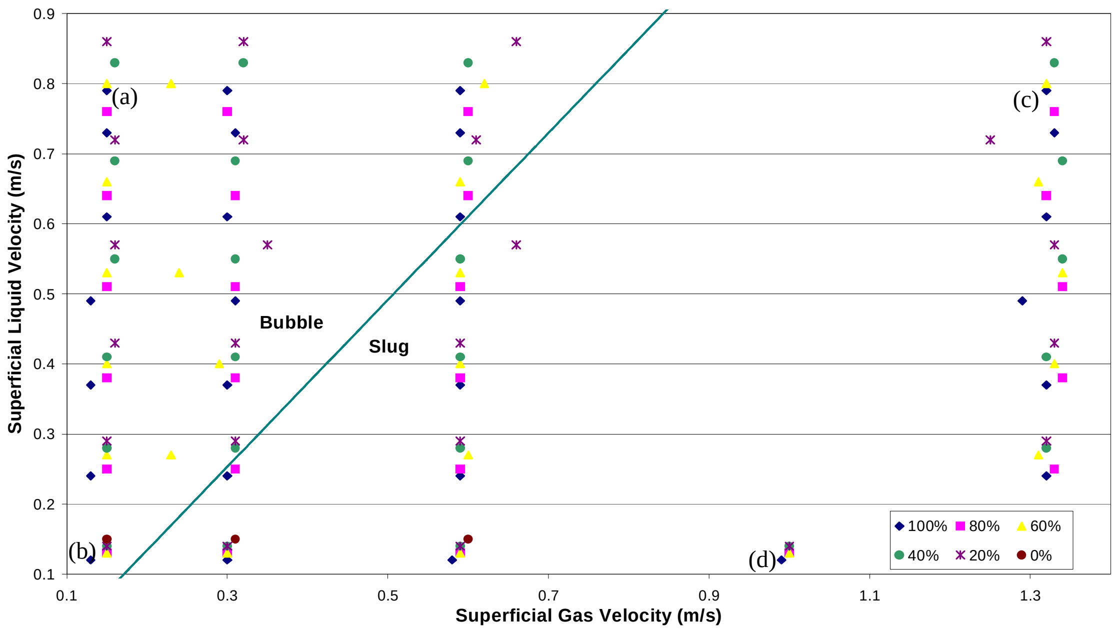

Figure 4.2 – Taitel-Dukler Flow Regime Classification of Test Points

Nevertheless, the sensor response analysis revealed that clear indications as to the characteristics of the multiphase flow present in a pipeline could be obtained through the extraction of appropriate features from the gamma count output signals

4.2. Statistical Analysis

4.2.1 Statistical Parameter Dependence on Flow Characteristics

A number of statistical parameters were calculated from the hard energy output signals to analyse their relationship with key multiphase flow characteristics. The central moments, linear prediction coefficients (LPCs), and linear spectral frequencies (LSFs) were plotted against the multiphase flow gas void fraction (GVF), **Figures 4.3 – 4.17**, and the gas-oil ratio (GOR), **Figures 4.18 – 4.32**. Definition of the statistical parameters employed in the investigation is provided, **Appendix B**.

The mean gamma count was observed to increase with increasing GVF due to the decreasing average mixture density, **Figure 4.3**. At low GVFs the water cut influences the mean count in a manner one would expect: the lowest water cuts yielding higher mean values. However, at GVFs in excess of 60% the influence of the water cut on the mean value diminishes as high and low water cut data points intermingle.

The standard deviation also increases with GVF as the measurement range increases for test points, **Figure 4.4**. In general, increasing the water cut led to increases in the standard deviation. However, the largest standard deviations were obtained for test points with a water cut of 40%. It is hypothesised that phase inversion in the liquid phase may induce this increased variation in the measurements.

The skewness and kurtosis exhibited a linear decrease with GVF until GVFs of 75% or greater were attained, at which point further increases in GVF had led to an increase in both the skewness and kurtosis as the probability distributions become dominated by a high count peak structures and start to narrow, **Figure 4.5** and **4.6**. In general, both the skewness and kurtosis increased with increasing water cuts. However, test points with a water cut of 40% did not follow this tend and exhibited lower values of skewness and kurtosis than expected. Again, liquid phase-inversion at water cuts of 40% was hypothesised as the source of these discrepancies.

Increasing the GVF had little effect on the magnitude of the LPC2 and LPC3 values but the variation between different data points with the same GVF but different water cuts diminished, **Figure 4.7** and **4.8**. The magnitudes of the LPC2 and LPC3 values are a function of water cut. The data points produced increasing LPC2 and LPC3 magnitude values for water cuts in the following order: 0%, 20%, 100%, 80%, 60% and 40%. From the data, it was hypothesised that liquid phases with significant water/oil content were susceptible to phase inversion that produce a characteristic response to the gamma signal depending on the water cut.

LPC4, LPC5, and LPC6 yielded similar reactions to the different multiphase flows, **Figure 4.9 – 4.11**. As observed for LPC2 and LPC3, the magnitudes of the LPC4, LPC5, and LPC6 values displayed no significant dependence on the GVF value but the variation between the data points for different water cut decreased with increasing GVF. The water cut was the major influence on the LPC magnitudes, with phase inversion effects again prominent. However, the response was the inverse of that seen with the LPC2 and LPC3 parameters, decreasing magnitudes for water cuts in the following order: 0%, 20%, 100%, 80%, 60% and 40%.

The linear prediction coefficient error (E_R) demonstrated an approximately linear relationship with the GVF, increasing in magnitude with increasing GVF, **Figure 4.12**. The water cut influences the error yielded in the linear prediction operation. Large variability for water cuts was observed for GVFs in the range 24 – 80%. At GVFs <25% and >80%, a significant decrease in the influence of the water cut was observed. The LPC residual error magnitude increased with water cuts of 100%, 0%, 20%, 80%, 60% and 40% respectively for constant GVF values.

A decrease in magnitude of the LSF1 parameter was observed with increasing GVF; particularly for GVFs in excess of 40%, **Figure 4.13**. Water cut was observed to exhibit a significant influence on the LSF1 magnitude. LSF1 parameter exhibited successively increasing magnitudes for water cuts in the following order: 0%, 20%, 100%, 80%, 60% and 40%.

LSF2 and LSF4 yielded similar responses to the multiphase flows demonstrating no detectable reaction to variations in the GVF, **Figures 4.14** and **4.16**. The parameters' magnitudes showed sensitivity to the liquid phase water cut with increasing values for waters cuts of 40%, 60%, 80%, 100%, 20% and 0% respectively. The variation between parameter magnitudes with water cut for data points of equivalent GVFs decreased with increasing multiphase flow GVFs.

The LSF 3 and LSF 5 coefficients decreased in magnitude with increasing GVF, **Figures 4.15** and **4.17**. In this instance, the variation between data points of different water and equivalent GVF was observed to be at a minimum for GVF <25 % and GVF >75% and increase significantly for GVFs between 25% and 75%. Parameter magnitude was again a strong function of water cut with increasing parameter magnitudes obtained for data points with water cuts of 40%, 60%, 80%, 100 and 20% respectively.

GOR is defined as the volume of gas produced per volume of oil produced at for a given temperature and pressure. For the purpose of this study, GOR values were calculated at the measurement section pressure and temperature for each test point to enable comparison of data points taken at different flow conditions.

Figure 4.18 depicts the mean count's relationship with the GOR. At a fixed water cut, the mean value increases in a linear fashion for GORs up to 5, at which point the rate of change of the mean with GOR begins to decrease in magnitude with increasing GOR values. The data plot suggests that, for fixed liquid phase water cuts, operating above a critical GOR value yields no further influence on the mean gamma count as the liquid content decreases below the minimum threshold concentration required to produce a measurable attenuation effect on the gamma beam.

The standard deviation was found to increase in a similar fashion to the mean with increasing GOR values, **Figure 4.19**. However, the water cut exerted a different effect on the magnitude of the standard deviation parameter; increasing standard deviations were obtained from water cuts in the order: 0%, 20%, 80%, 60% and 40%. This agrees with the results obtained for the standard deviation variation with the GVF. The presence of a larger standard deviation at a water cut of 40% was attributed to phase inversion effects in the liquid phase.

Both the skewness and kurtosis were observed to decrease with increasing multiphase flow GOR, **Figures 4.20** and **4.21**. A sharp decrease in skewness and kurtosis was obtained for GOR of up to 4. Increasing the GOR above 5 had little effect on the magnitude of the kurtosis or skewness coefficients.

The linear prediction coefficient (LPC) and line spectral frequency (LSF) coefficients were analysed with respect to the GOR but no quantifiable response was observed.

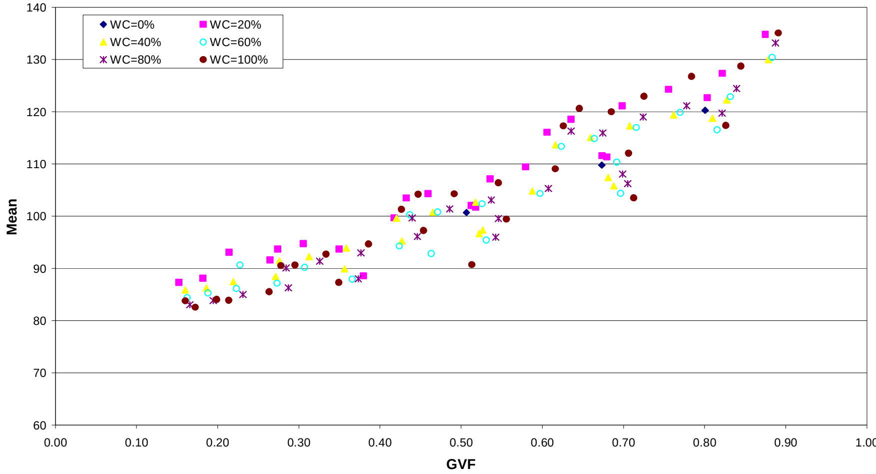

Figure 4.3 – Scatter Plot of Mean against GVF

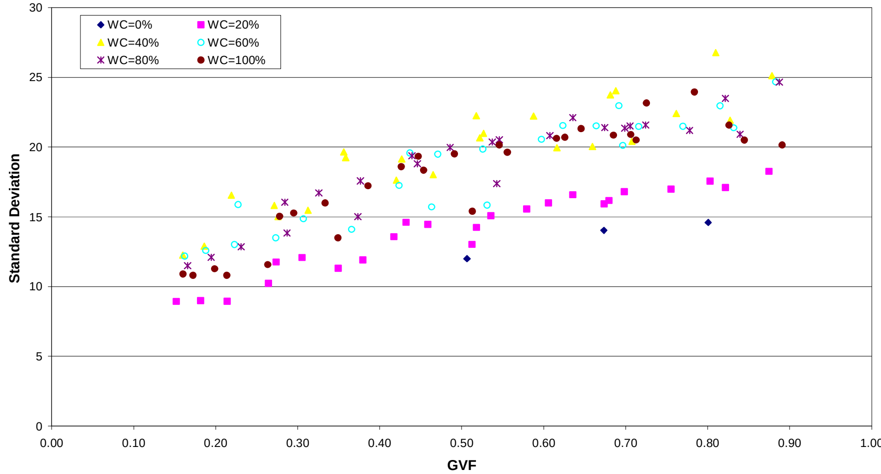

Figure 4.4 – Scatter Plot of Standard Deviation against GVF

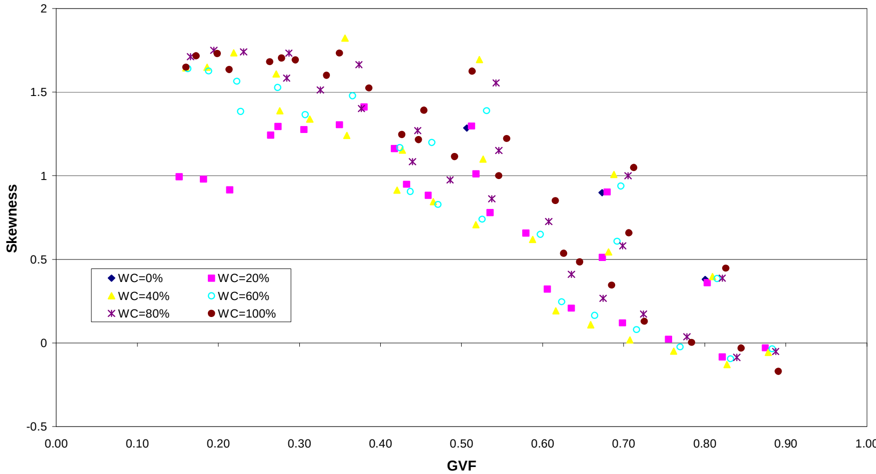

Figure 4.5 – Scatter Plot of Skewness against GVF

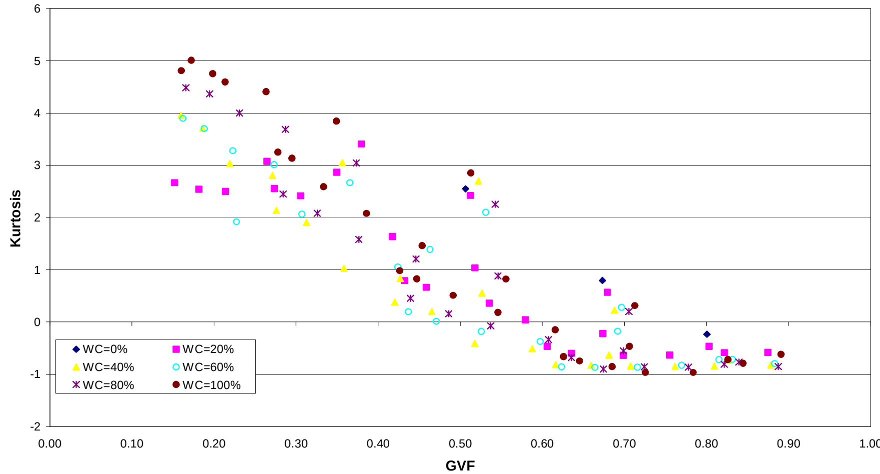

Figure 4.6 – Scatter Plot of Kurtosis against GVF

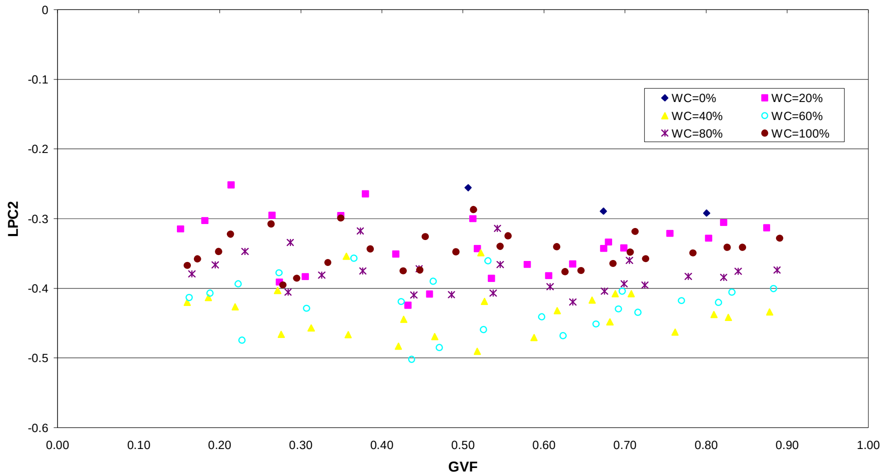

Figure 4.7 – Scatter Plot of LPC2 against GVF

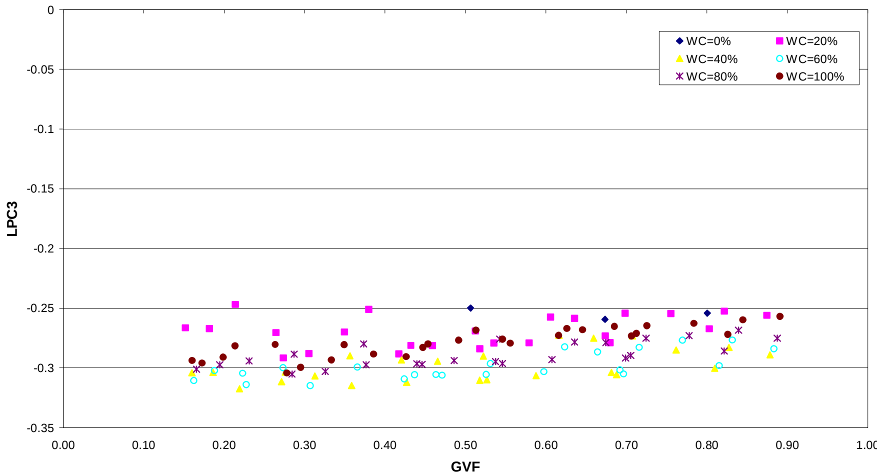

Figure 4.8 – Scatter Plot of LPC3 against GVF

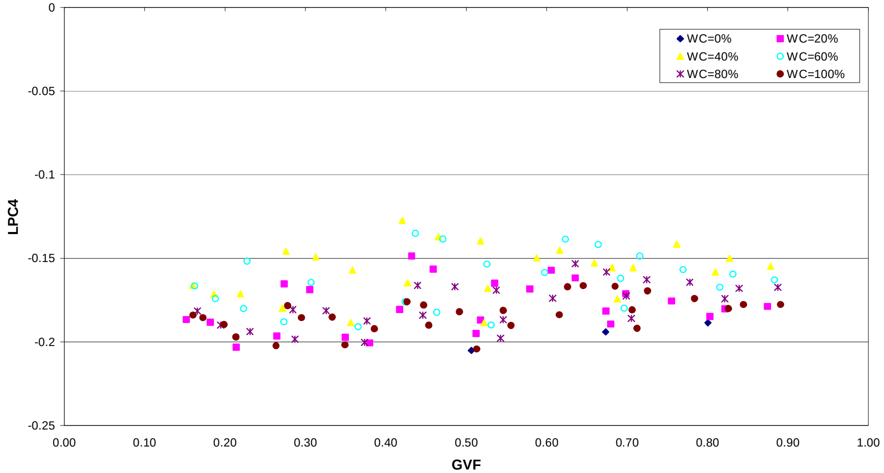

Figure 4.9 – Scatter Plot of LPC4 against GVF

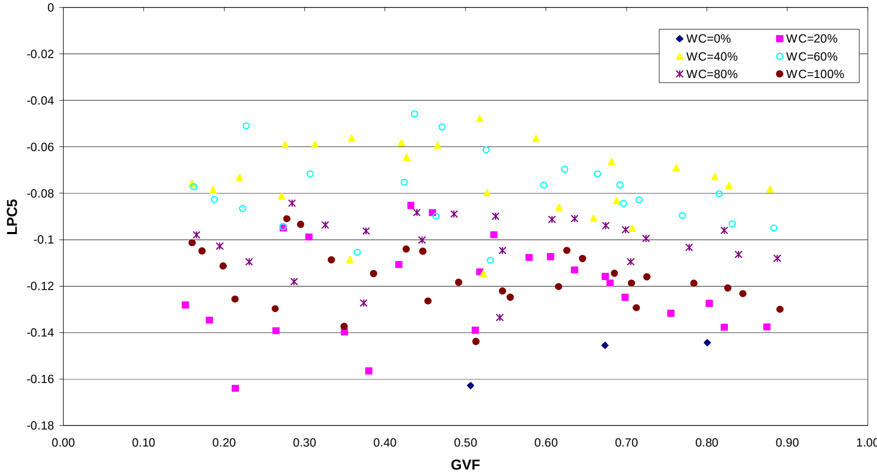

Figure 4.10 – Scatter Plot of LPC5 against GVF

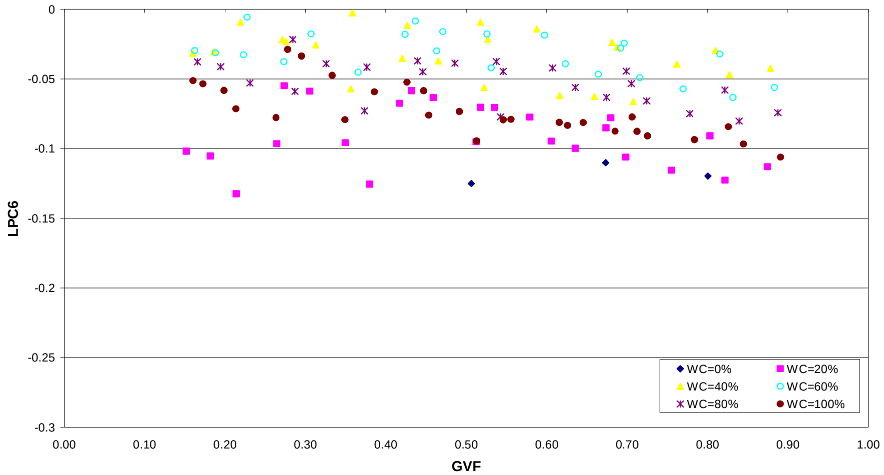

Figure 4.11 – Scatter Plot of LPC6 against GVF

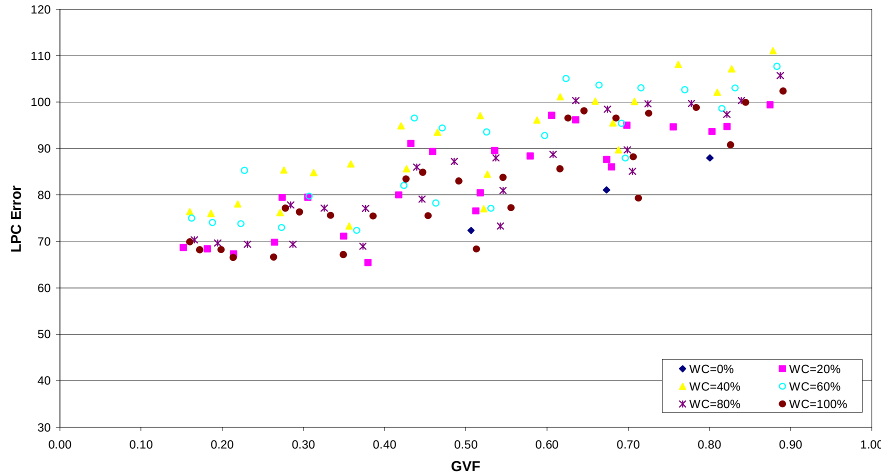

Figure 4.12 – Scatter Plot of LPC Residual Error against GVF

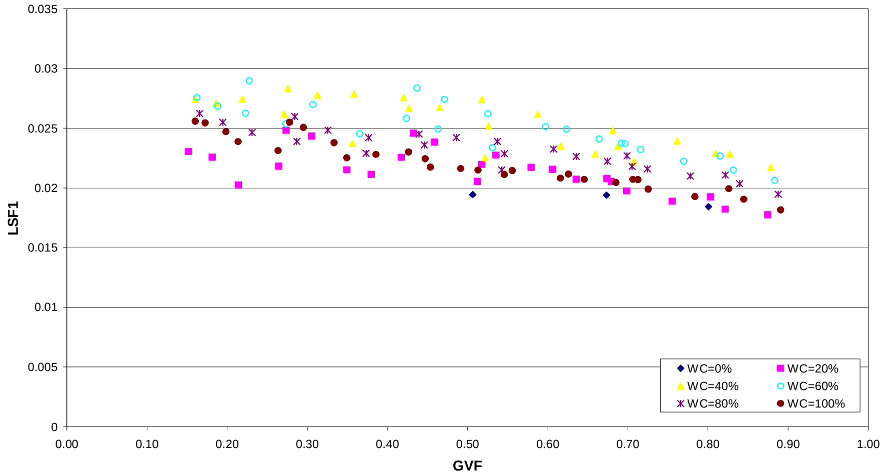

Figure 4.13 – Scatter Plot of LSF1 against GVF

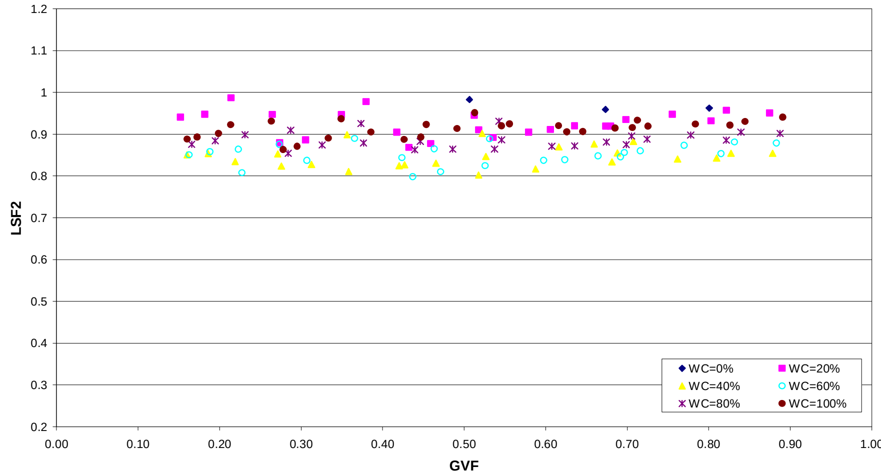

Figure 4.14– Scatter Plot of LSF2 against GVF

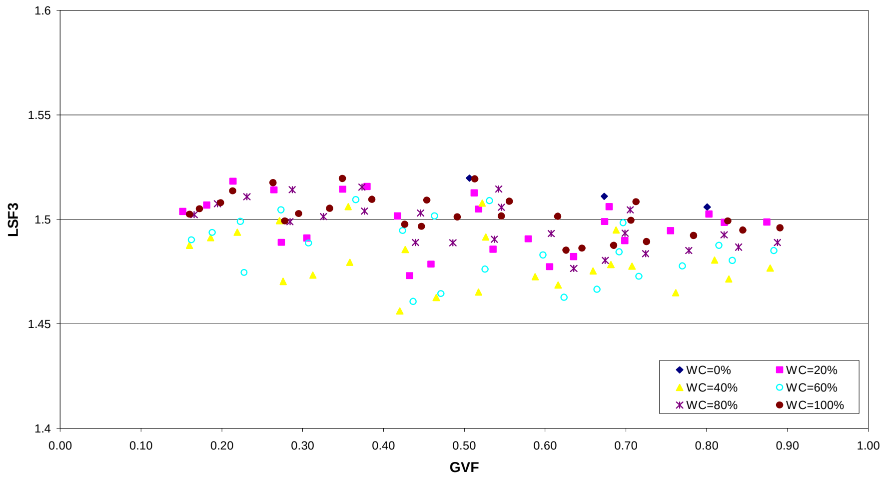

Figure 4.15 – Scatter Plot of LSF3 against GVF

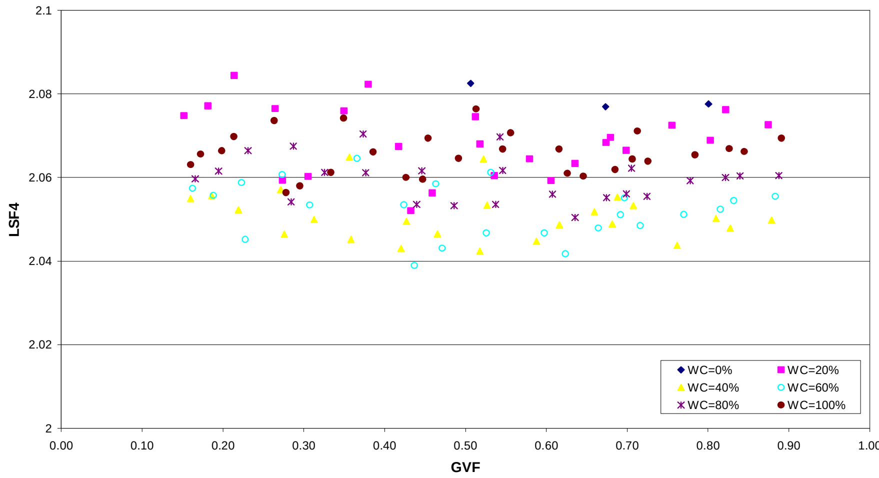

Figure 4.16 – Scatter Plot of LSF4 against GVF

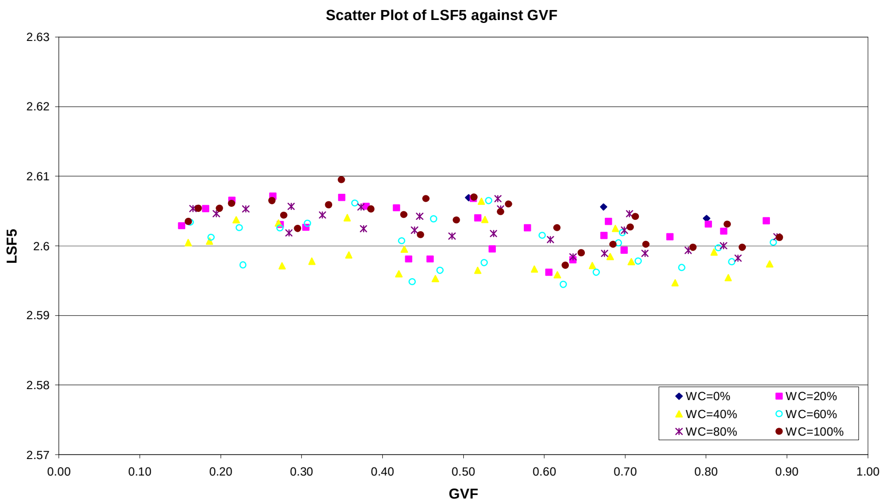

Figure 4.17 – Scatter Plot of LSF5 against GVF

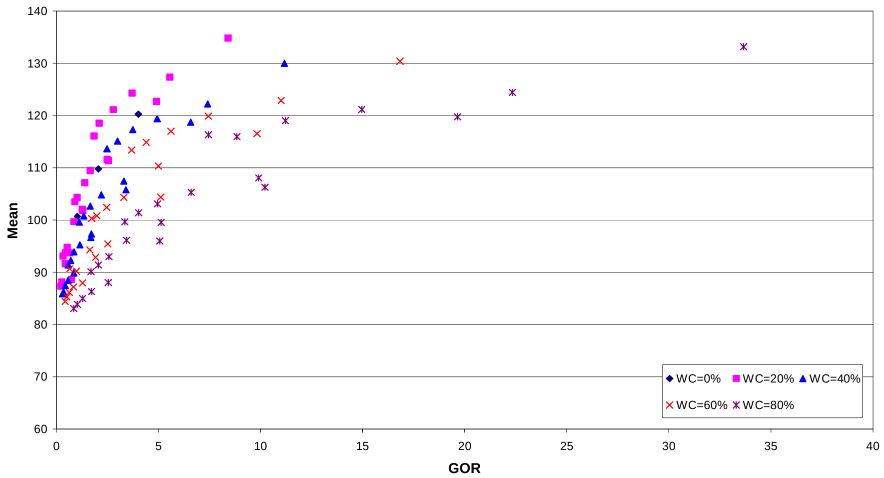

Figure 4.18 – Scatter Plot of Mean against GOR

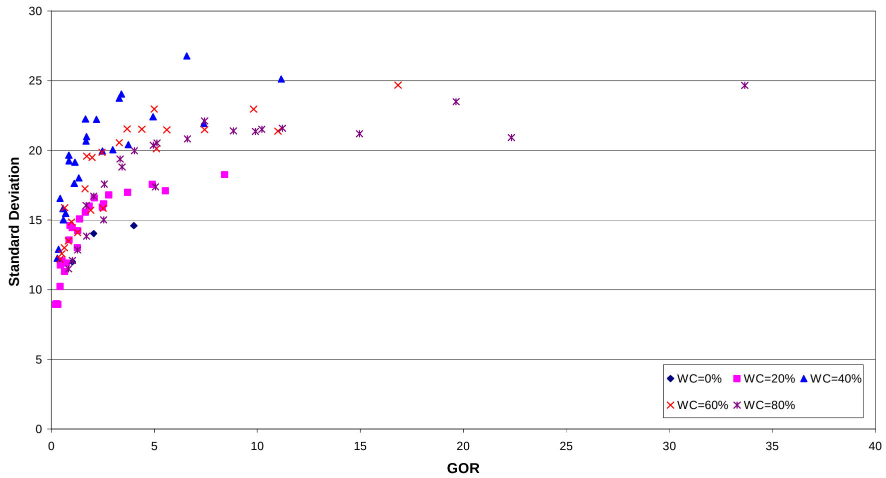

Figure 4.19 – Scatter Plot of Standard Deviation against GOR

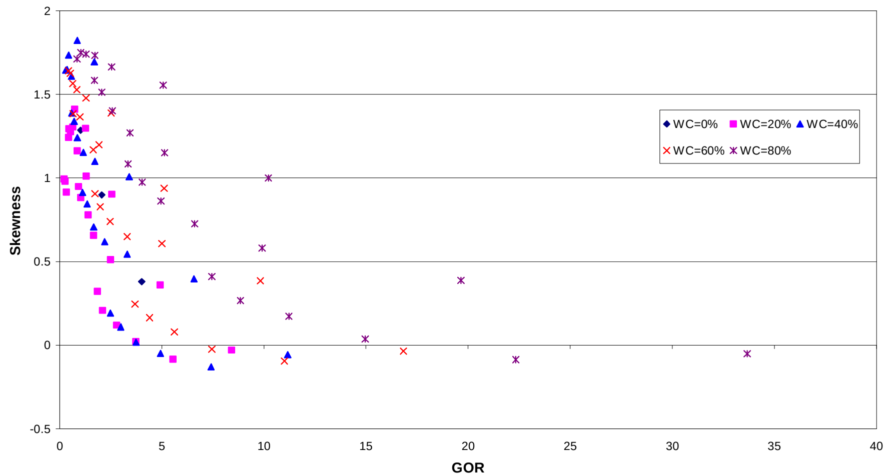

Figure 4.20 – Scatter Plot of Skewness against GOR

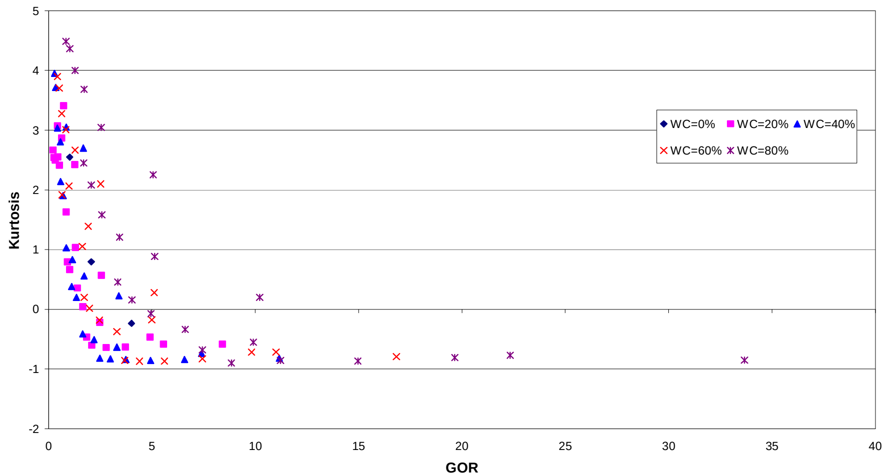

Figure 4.21 – Scatter Plot of Kurtosis against GOR

4.2.2 Probability Distribution Analysis

Analysing the probability mass function (PMF) of the signal output from a sensor subjected to multiphase flow conditions is an established technique for flow regime identification **[16]**. PMF plots were produced for the hard energy signals and analysed with respect to the raw data plots and the statistical properties of this data, in an attempt to rationalise the variations in the PMF distribution geometry with respect to the flow conditions and statistical property variations.

A number of different PMF shapes were witnessed, with a number of test points sharing a common geometry. the differences between the raw signals for different flow conditions are conserved in the PMF representation through the PMFs' geometries. **Figure 4.22 (a) – (d)** depicts the corresponding probability mass functions (PMFs) of the hard spectra raw signals featured in **Figure 4.1**.

(a) V_{sg} = 0.15 ms^{-1}, V_{sl} = 0.79 ms^{-1} and *WC* = 100%

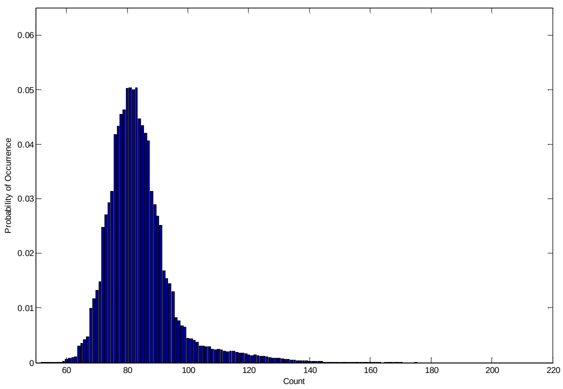

(b) V_{sg} = 0.13 ms^{-1}, V_{sl} = 0.12 ms^{-1} and *WC* = 100%

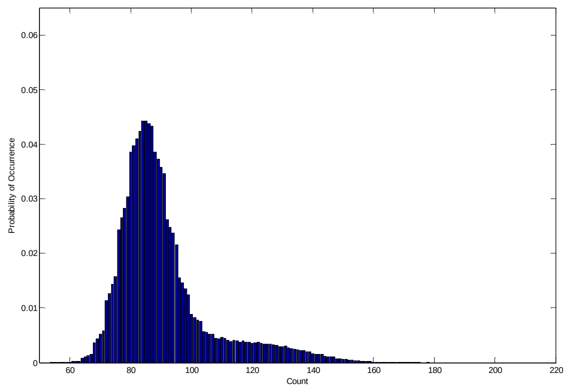

(c) V_{sg} = 1.32 ms^{-1}, V_{sl} = 0.79 ms^{-1} and *WC* = 100%

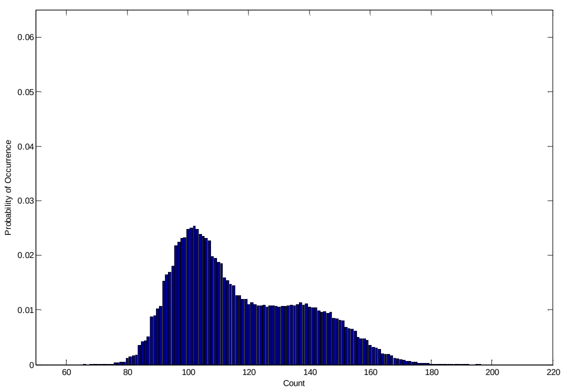

(d) V_{sg} = 0.99 ms^{-1}, V_{sl} = 0.12 ms^{-1} and *WC* = 100%

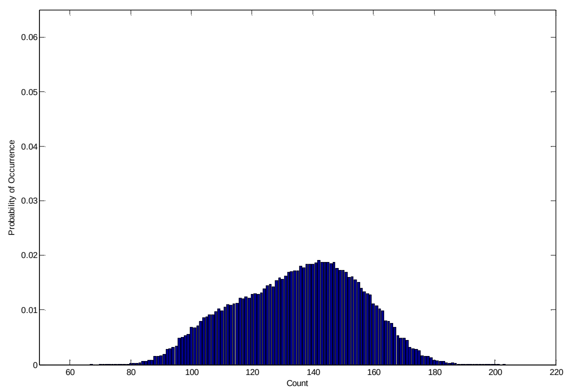

Figure 4.22 – PMF of Output Signals

Figure 4.22 (a) is typical of a low GVF test point: there is a high proportion of low counts in the signal, owing to the high fluid density, but a narrow band is observed for counts between 110 and 190 induced by the passage of relatively small quantities of gas. The Cranfield University test facility does not facilitate visual identification of flow regimes during testing. As a result, the flow regimes were inferred from raw signal analysis and published flow regime maps. Examining features in the raw output signal, and plotting the test conditions on a Taitel-Dukler flow regime map, indicated a bubble type regime was present (**Figure 4.1 (a)** and **4.2**).

Figure 4.22 (b) illustrates that as the liquid load is reduced, the basic bubble flow PMF shape is conserved. The main differences observed with respect to (a) is that the main peak has moved slightly to the right to accommodate a higher mean value and the count variation is larger, giving rise to a wider peak of reduced amplitude. The proportion of high counts increases with the increased gas presence and the narrow band in the 110 to 190 count range is more prominent. Analysis of the raw output signal, in conjunction with the plotting of the test point conditions on a Taitel-Dukler flow regime map, indicate a bubble type regime (**Figure 4.1 (b)** and **4.2**).

Figure 4.22 (c) shows the PMF for a data point with the same liquid loading as seen in **Figure 4.22 (a)** but for a higher gas content. In this case, the PMF geometry is distinctly different to that observed in **(a)** and **(b)**. The proportion of low counts that formed the dominant peak structure in **(a)** and **(b)** has been significantly reduced. The increased gas content enables a higher proportion of counts in the range 110 to 190 and the formation of a second peak structure in this range is evident. Two-peaked PMF have been shown to be characteristic of slug type flows with one peak representative of the passage of liquid slugs and the other of the gas dominated legs. Furthermore, both raw signal analysis and plotting the test point conditions on the Taitel-Dukler flow regime map, indicated a slug type regime (**Figure 4.1 (c)** and **4.2**).

Figure 4.22 (d) depicts the PMF for a gas dominated multiphase flow. The PMF geometry is somewhat different to the other test points as the major peak is migrating towards the high-count range. The liquid loading is still sufficient to produce a significant proportion of lower counts. As a result, a wider, flatter distribution than observed in **Figure 4.33 (c)** is obtained. Analysis of the raw output signal, in conjunction with the plotting of the test point conditions on the Taitel-Dukler flow regime map, indicates that the multiphase flow exhibits slug type structures , albeit larger than those observed in **Figure 4.22 (c)** (**Figure 4.1 (b)** and **4.2**).

PMF analysis of the full data set yielded results consistent with the above analysis: PMF geometries were found to give a reliable indication of the test point flow regime, with reference to raw signal and published flow regime maps. Using the PMF, raw data plots and the test points were classified into their flow regime: bubble or slug. Scatter plots for a host of statistical parameters were produced and their suitability for flow regime identification purposes was analysed.

It is known that the first four statistical moments describe certain features of a probability distribution. Consequently, scatter charts of the first four moments were produced to examine their potential for flow regime classification, **Figures 4.23 – 4.28**. The multiphase flow data points illustrated in **Figures 4.1** and **4.22** have been identified on each plot for reference purposes.

All of the plots generated yielded data point clusters with similar PMF geometries and displayed a clear boundary between bubble and slug flow regime points. **Figure 4.26** and **4.27** did not exhibit clear trends in PMF geometry transitions and produced widely scattered data points not suitable for classification. These diagrams showed the relationships between the PMF asymmetry and spread, and peakedness and spread respectively. Thus, it can be concluded that the combination of these parameters alone are insufficient to describe the PMF geometry effectively.

Figures 4.23, **4.24**, **4.25** and **4.28** all illustrated a clear trend in the PMF geometry transition. Furthermore, the data points in **Figures 4.24**, **4.25** and **4.28** can be described effectively using regression trend functions with reasonable accuracy. Approximating the scatter plots as a function enables flow regime classification to be carried out through the calculation of two key statistical parameters.

Consequently, it was concluded that scatter plots of skewness and mean; kurtosis and mean; and skewness and kurtosis provide useful information about the expected PMF geometry of a test point and thus, its likely flow regime. Nevertheless, flow regime boundary conditions still have to be specified in such a case and around these borders some data points exhibited features of both slug and bubble regimes. It was recognised that this technique has limitations in flow regime classification for flow conditions operating close to designated flow regime boundaries.

As visual identification of the flow regime was not possible during data collection, verification of the signal analysis findings was undertaken using a multiphase flow simulation code. There are three main commercial multiphase flow simulation codes: PLAC, TACITE and OLGA [**101**]. For the purposes of this study OLGA 2000, developed by Scandpower AS, was used owing to its license availability at Cranfield University.

Using the OLGA 2000 software, a model of the Cranfield University multiphase test facility was developed, **Appendix C**. A series of steady state simulations were undertaken to model some of the multiphase flows studied during the experimental campaign. The simulation output enables theoretical quantification of the fluid conditions in the test section that would have been obtained during experimental data collection. A host of different multiphase flow parameters were available for analysis including the dominating flow regime and the superficial phase velocities.

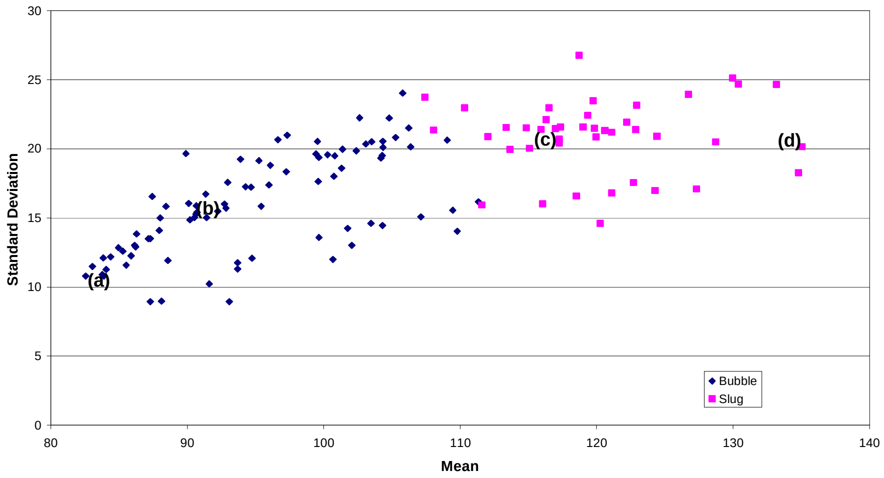

Figure 4.23 – Scatter Plot of Standard Deviation against Mean

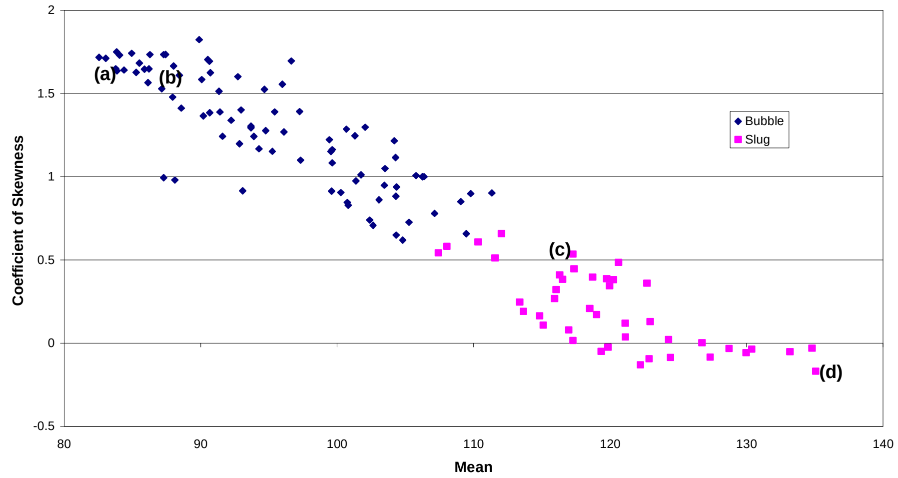

Figure 4.24 – Scatter Plot of Skewness against Mean

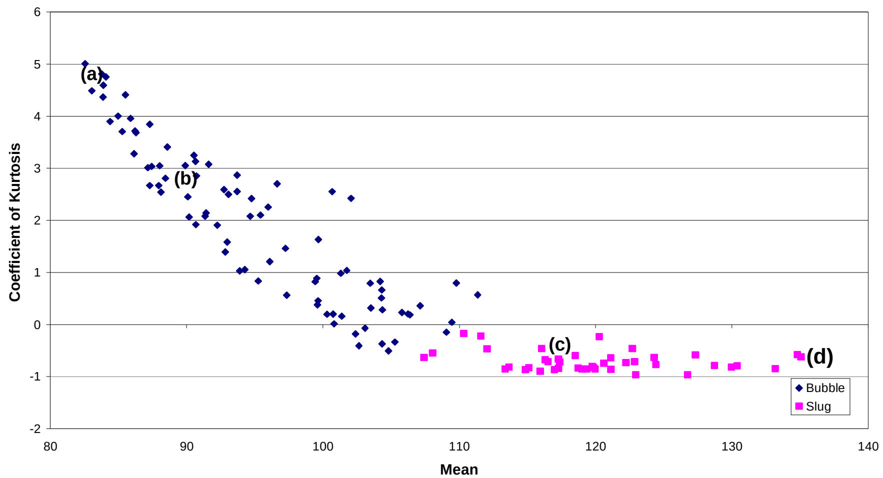

Figure 4.25 – Scatter Plot of Kurtosis against Mean

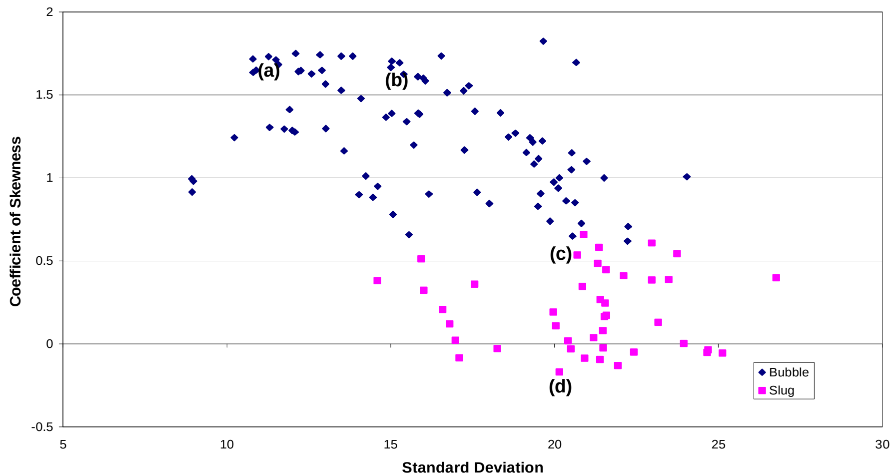

Figure 4.26 – Scatter Plot of Skewness against Standard Deviation

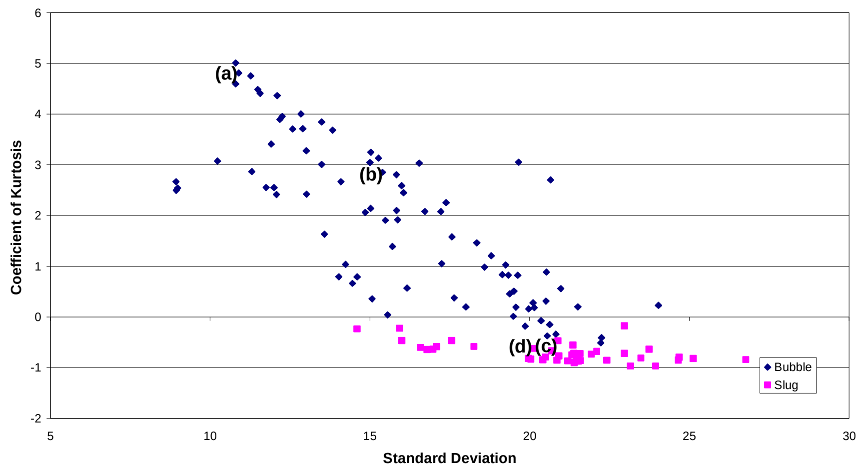

Figure 4.27 – Scatter Plot of Kurtosis against Standard Deviation

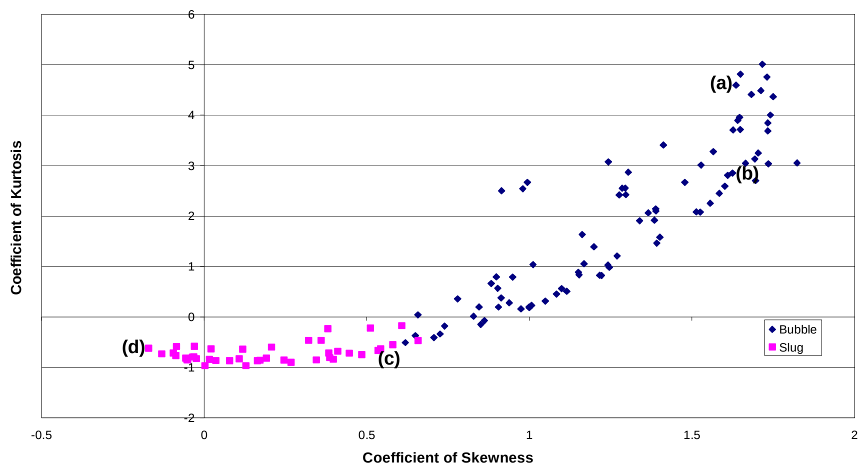

Figure 4.28 – Scatter Plot of Kurtosis against Skewness

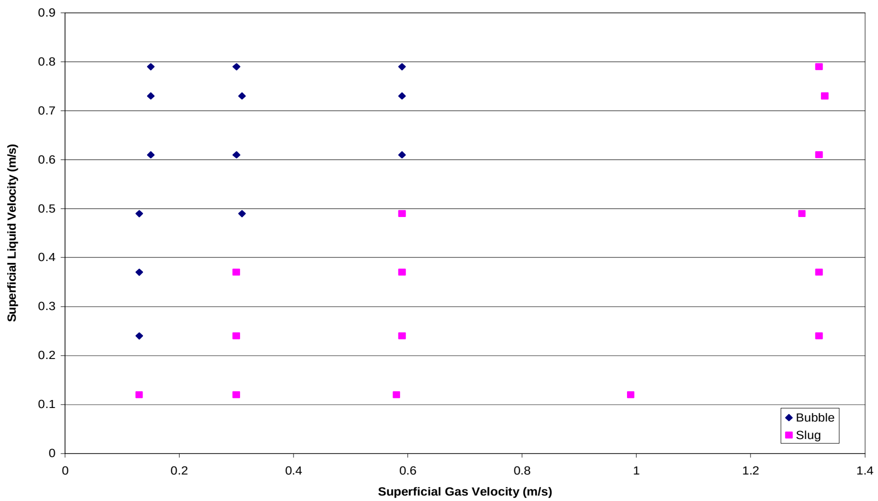

Figure 4.29 – Theoretical Flow Regime Classification

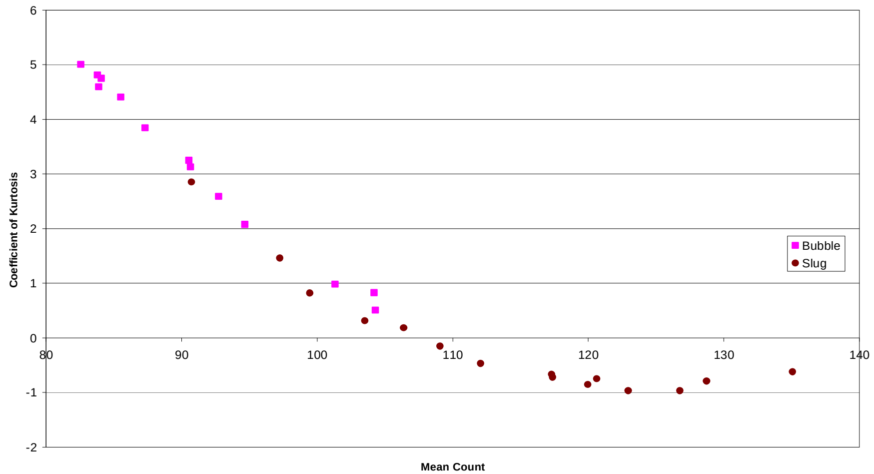

Figure 4.30 – Scatter Plot of Kurtosis against Mean: OLGA Classified Flow Regimes

Figure 4.29 illustrates the OLGA 2000 flow regime classification of the air –water data points on the test matrix. Discrepancies were observed between the Taitel-Dukler data point classification in the definition of the bubble-slug regime boundary. The OLGA simulations predicted that slug regimes would be dominant in the test phase facility at lower superficial gas velocities.

Figure 4.30 illustrates a scatter plot of the mean gamma count against the coefficient of kurtosis with the OLGA flow regime classifications indicated. In contrast to **Figure 4.25**, there is a discontinuity in the flow regime transition between the OLGA identified slug and bubble regimes employing the scatter plot of the mean gamma count and coefficient of kurtosis. Discrepancies arose for data points located near to the flow regime boundary. It was recognised that not one of the flow regime classification methods would yield a definitive answer. At flow conditions close to the flow regime boundaries, the bubble and slug description of test points breaks is merely for convenience as fluid will exhibits properties of both and none of these classifications. One possible explanation for these inconsistencies is that the OLGA model took into account the sight deviation from the vertical of the gamma densitometer installation point on the riser.

Nevertheless, the theoretical comparison of the experimental flow regime classifications did agree for test conditions where clear identification of a dominating regime was expected. Consequently, it was concluded that in the absence of visual verification, the statistical scatter plot method proposed for flow regime identification can be used as a tool as long as caution is exercised with points classified in the proximity of the imposed regime boundaries.

4.2.3 Interim Summary: Statistical Analysis

A host of statistical parameters were extracted from the time-varying gamma count signals and their correlation with characteristic parameters of the multiphase flow composition investigated. Parameters demonstrating discrimination for different flow conditions were observed to be complex functions of the gas and liquid phase loadings and the water cut. The probability mass function plots provided a good indication of the prevailing flow regime. A scatter plot of the mean hard gamma count against the coefficient of kurtosis produced a quantifiable quadratic relationship which enabled classification of the flow regimes. Nevertheless, classification was subjective when operating in the proximity of the defined flow regime boundary as traits of more than one regime were evident and discrepancies were obtained in classifications from experimental data with published flow maps and those from multiphase flow simulations.

4.3 Frequency Domain Analysis

4.3.1 Dependency of Signal Dominant Frequencies on Flow Parameters

Dynamic fluctuations are inherent in all multiphase flow systems. The time-varying gamma count signals were analysed in the frequency domain. Fourier analysis was conducted on the raw output signals using a fast-Fourier transform (FFT) algorithm based on Cooley and Turkey [**102**]. From preliminary investigations it was observed that the frequency response of the hard and soft signals were intrinsically complementary. Accordingly, the detailed frequency analysis work undertaken was restricted to the hard energy densitometer signals

Power spectral density (PSD) diagrams were compiled from the FFTs employing the Welch technique. The PSD describes how the power of a signal is distributed with frequency. Welch's technique calculates a signal's average FFT spectrum across a number of overlapping split sections to increase the accuracy of the frequency spectrum obtained.

For each gamma densitometer signal, a 15,000 data point Hamming window was employed to undertake a 15,000 data point FFT employing a fixed overlap between windowed sections of 50% of the window size. **Figure 4.31 (a) – (d)** depicts the corresponding PSD plots of the hard spectrum raw signals featured in **Figures 4.1** and **4.6**.

(a) V_{sg} = 0.15 ms^{-1}, V_{sl} = 0.79 ms^{-1} and WC = 100% (b) V_{sg} = 0.13 ms^{-1}, V_{sl} = 0.12 ms^{-1} and WC = 100%

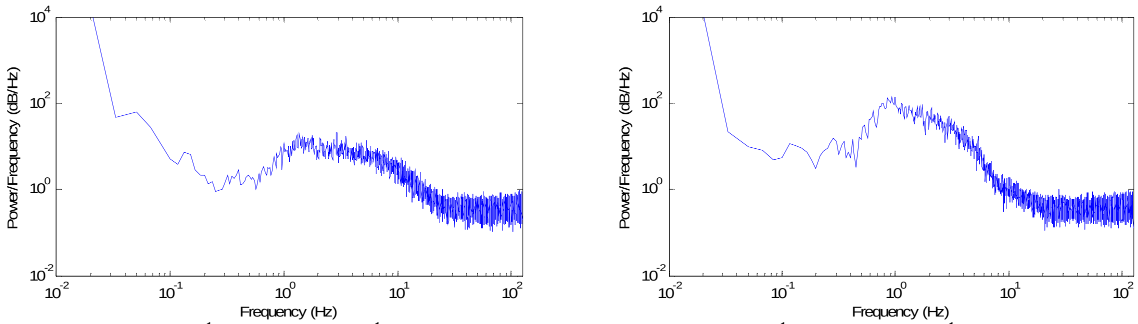

(c) V_{sg} = 1.32 ms^{-1}, V_{sl} = 0.79 ms^{-1} and WC = 100% (d) V_{sg} = 0.99 ms^{-1}, V_{sl} = 0.12 ms^{-1} and WC = 100%

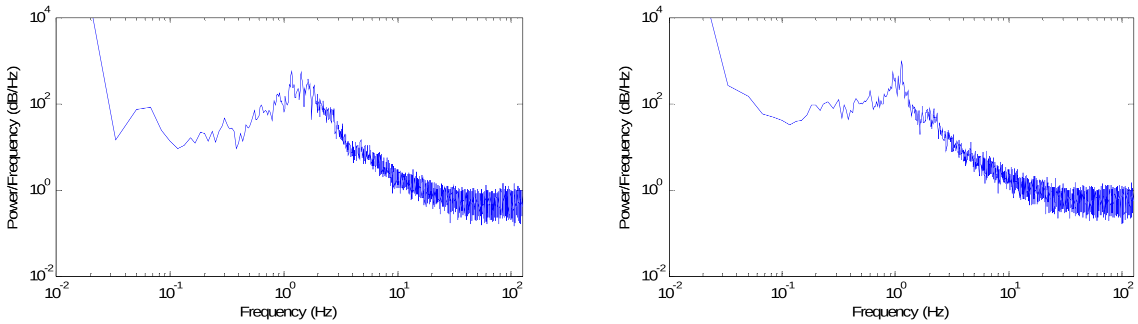

Figure 4.31 – PSDs of Output Signals for Various Flow Conditions

The region of interest was the signals' frequency content between 0.5 Hz and 2 Hz which was identified from the raw signals as being the dominating frequency range for the multiphase flow mixtures investigated. It can be seen that above approximately 10 Hz the spectra were identical irrespective of the flow conditions. The flat nature of the spectra in this region suggests that it stems from the white noise floor inherent in the gamma decay process; thus, it was deduced that little flow parameter information is likely to be obtained from it.

Between 0.5 Hz and 2 Hz, a discernable difference in the PSD geometries was identified for the different flow conditions. Exploiting the data yielded by the PSDs of the raw gamma data signals, the major frequency components of each signal were identified. The dominant signal frequency data was extracted and then plotted on a contour plot to exhibit the variation in the magnitude of the signal's dominating frequency with changes in the multiphase fluid's superficial phase velocities, **Figure 4.32**.

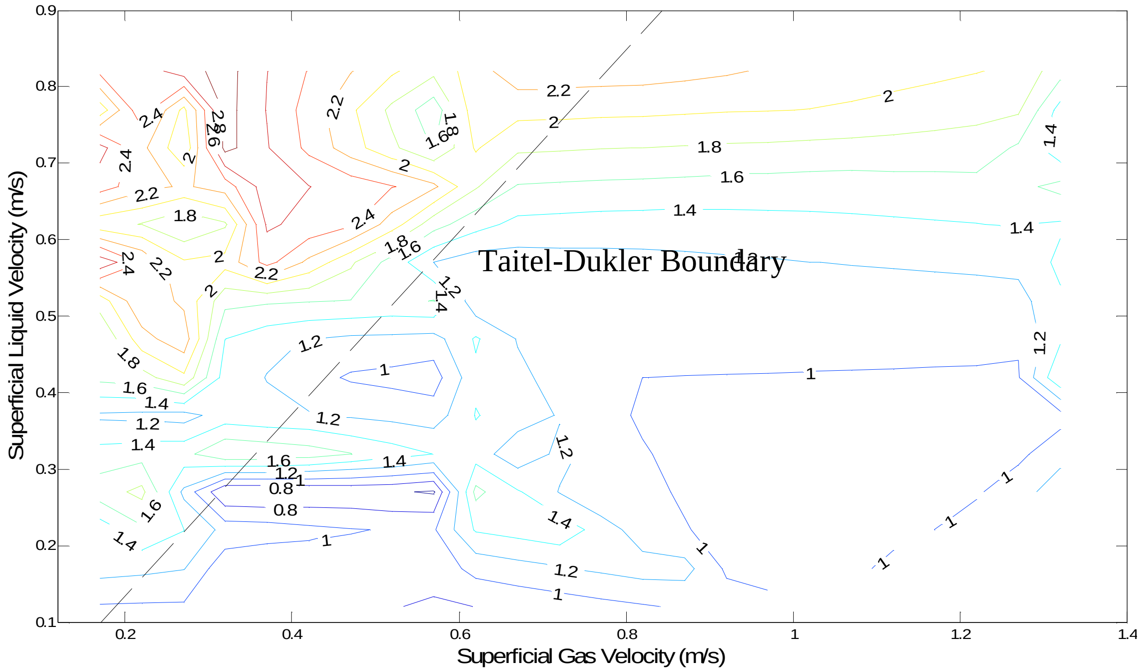

Figure 4.32 – FFT Dominant Frequency Contour Plot

Employing the superficial phase velocities as the basis for the contour plot axes facilitates the designation of the bubble-slug flow regime boundary; thus, enabling the flow regime sensitivity of the dominating signal frequency data generated to be ascertained. The Taitel-Dukler definition of the flow regime boundary was employed in all cases.

In general, the magnitude of the dominant frequency was observed to increase with decreasing gas superficial velocity and increasing liquid superficial velocity. The influence of the liquid phase loading decreases with increasing gas loads. The maximum dominant signal frequency values were obtained at maximum liquid phase loading for liquid superficial velocities of approximately 0.3 ms^{-1}. Nevertheless, the dominant signal frequencies provide insufficient discrimination to phase loading variations to facilitate classification on a global scale.

Examining the flow regime classified regions of the contour plot independently; it was observed that the dominating signal frequency in the bubble regime exhibited a complex response to variations in the flow's phase loadings. The magnitude of the dominant frequency did not demonstrate any evidence of a quantifiable underlying dependence on either of the phase loadings. In contrast, the slug regime region demonstrated a more uniform response with significantly less sensitivity to variations in the liquid phase loading. At gas loadings above 0.5 ms^{-1}, the magnitude of the dominant frequency exhibits a strong dependence on the gas superficial velocity. However, at lower superficial gas velocities, the liquid phase exerts an increasing influence and the resulting response is complex, although with less variation as observed with the bubble regime.

The influence of the liquid phase water cut on the magnitude of the dominant frequency yielded by the PSDs of the gamma densitometer signals was evaluated by compiling individual contour plots for data points with common water cuts, **Figures 4.33 (a) – (d)**.

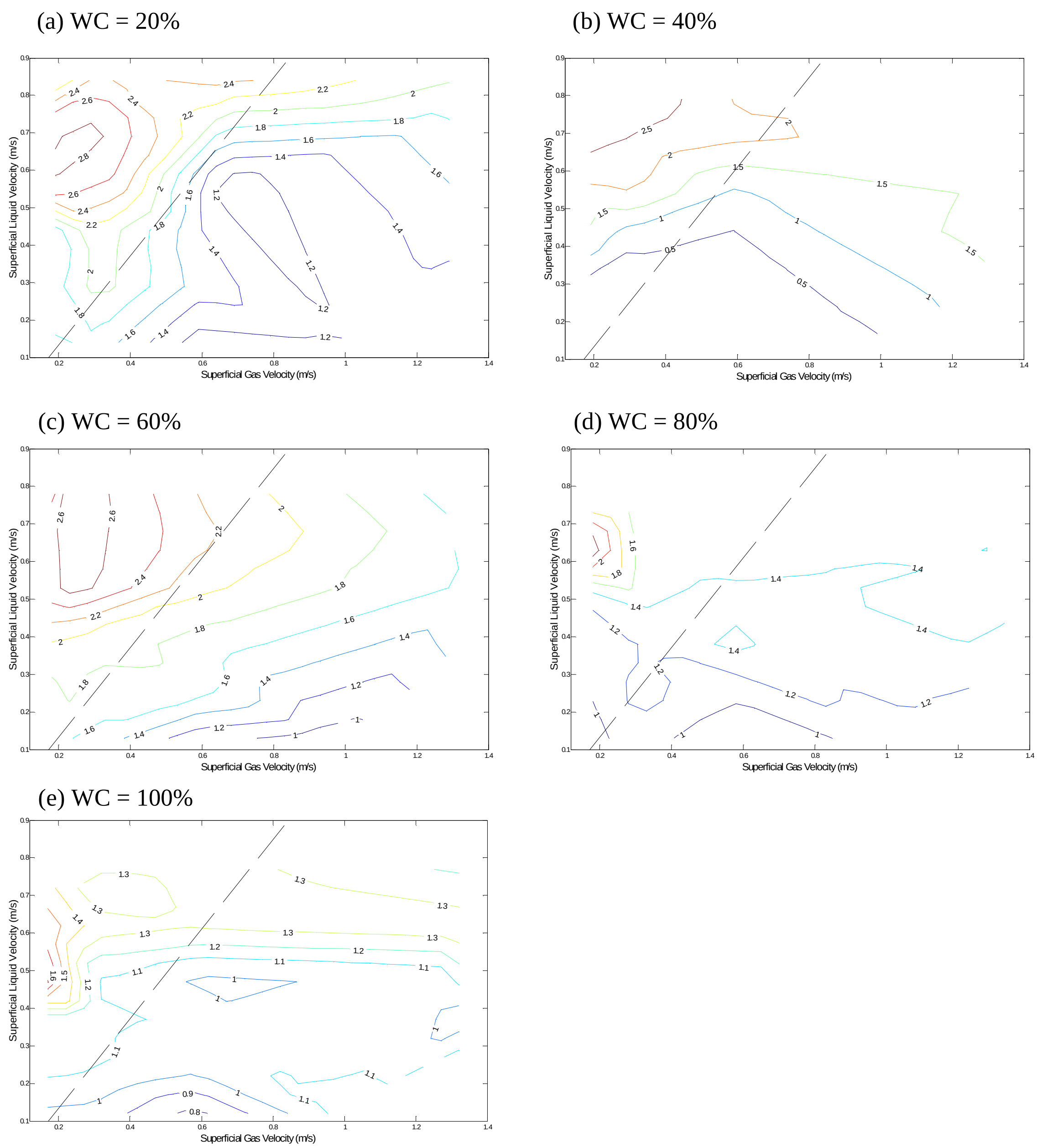

Figure 4.33 – Signal Dominant Frequency Contour Plots for Constant Water Cuts

Each of the individual liquid phase water cut values can be seen to exert a different dominant frequency feature response to the variations in the multiphase fluid phase loadings on both a global and flow regime specific basis. In general, the magnitude of the dominant signal frequency increased with decreasing water cut as the density of the liquid phase increases. Larger than might be expected frequency magnitudes were observed at water cuts of 60% where it was hypothesised that phase inversion phenomenon in the liquid phase could e contributing to the increased dominating signal frequency. However, based on the results, it was concluded that the liquid phase composition provides an additional layer of complexity to the relationship between the phase loadings. However, even when the water cut are isolated the relationships between the dominant frequency and superficial phase velocities do not lend themselves to quantification.

Analysis of the passage frequency of gas structures in the measurement section, as identified by the large temporal fluctuations in the gamma densitometer output signals, was also conducted and compared with the conventional FFT based frequency analysis technique.

4.3.2 Dependency of Gas Structure Frequencies on Flow Parameters

A MATLAB function was created to identify the number of maximum peaks, of a defined minimum amplitude, were induced by the passage of gas structures within each of the gamma count signals; thus, facilitating the determination of the gas structure frequency for each of the multiphase flow mixtures. A variety of different minimum amplitude criteria were set and the gas structure repeating frequencies determined were analysed to quantify their dependence on key multiphase flow parameters.

The gas structure frequency calculations were undertaken for minimum peak amplitude magnitude thresholds of 50, 30, 20 10, 5 and 1 count(s) of the hard-energy gamma photons. The results were plotted on a series of contour plots to exhibit the variation in the gas structure frequency magnitude with changes in the superficial phase velocities, **Figures 4.34 (a) – (f)**. The Taitel-Dukler flow regime boundary has been superimposed to facilitate determination of the flow regime sensitivity of the gas structure frequency data generated.

At the upper (50 counts) and lower (1 count) threshold limits examined, **Figures 4.34 (a)** and **(f)** respectively no quantifiable correlation was observed between the gas structure frequency and the superficial phase velocities. Nevertheless, the gas structure frequency magnitude did exhibit distinctly flow regime specific responses.

In the bubble regime, it was observed that the gas structure frequency of the large gas peaks (threshold = 50 counts) was dominated by the gas superficial velocity: the gas structure frequency increases with increasing gas superficial velocity and the liquid loading having a comparatively negligible influence. In contrast, the total gas structure frequency, determined through the application of an amplitude threshold of a single count, was found to increase with decreasing gas and/or decreasing liquid superficial velocities.

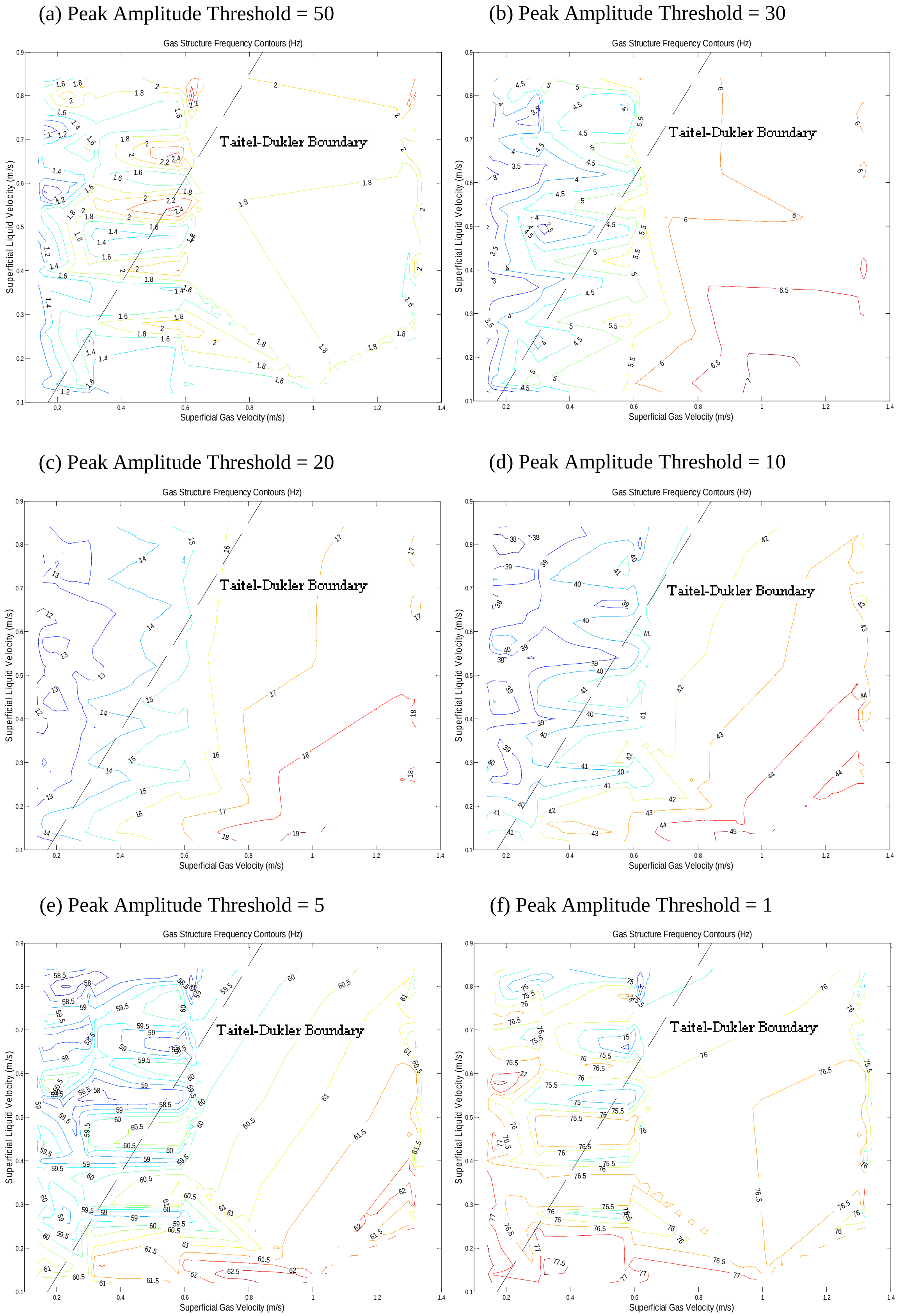

Figure 4.34 – Variation in Multiphase Flow Gas Structure Frequency

In the slug regime designated area of the plots, the large gas structure frequency was observed to increase with increasing gas superficial velocity and remain insensitive to the liquid loading; meanwhile, the unit count threshold gas structure frequency analysis showed an increasing sensitivity to the gas superficial velocity, and a decreasing dependence on the liquid superficial phase velocity was produced with increased gas loading.

Employing peak amplitude thresholds of 30, 20, 10 and 5 counts, **Figures 4.34 (b)**, **(c), (d)** and **(e)** respectively, it can be seen that strong flow regime dependent relationships were exhibited between the gas-structure frequencies measured and the superficial phase velocities. However, in these cases one can observe that the magnitudes of the gas structure frequency contours are largely segregated across the flow regime boundary. In general, the magnitude of the gas structure frequency was found to increase with increased gas loading and/or decreased liquid loading. The sensitivity of the gas structure frequency to the gas loading diminishes with increasing gas superficial velocities as the liquid phase velocity dominates the magnitude of the gas structure frequencies observed. Within the slug regime, to the right-hand side of the Taitel-Dukler boundary, the relationship between the gas structure frequency and the phase superficial velocities is more distinct than that observed within the bubble regime. In addition, the contours in these plots demonstrated a quasi-uniform distribution, especially in the slug flow regime, in contrast to those obtained at the extremes of the amplitude threshold range considered.

Consequently, although the discrimination of the gas structure frequency parameter is not sufficient to classify superficial phase velocities, it could be exploited to indicate the prevailing flow regime of a multiphase flow. Nevertheless, as with all methods of flow regime identification, designation of the geometric form of the dominating flow conditions in proximity to the defined classification boundaries remains nebulous.

In order to analyse the effect of the multiphase flow's liquid phase water cut on the gas structure frequency, contour plots were produced illustrating the influence of the liquid phase water cut at different liquid loadings and 'fixed' gas flow rates. **Figures 4.35 (a) – (d)** show the gas structure frequency variation with water cut and liquid phase superficial velocity for a minimum peak amplitude threshold of 10 counts.

It was observed that the influence of the water cut on the gas structure frequency was a complex function of the peak amplitude threshold, gas superficial velocity and liquid superficial velocity. All of the amplitude threshold values analysed yielded contour plot of comparable geometric forms. However, the contour geometries exhibited by the 5, 10 and 20 count thresholds were more clearly pronounced and exhibited superior contour distribution forms for analytical purposes. No data was available for the high gas superficial velocity – low liquid superficial velocity combination owing to the test data set examined; hence, the reduced contour plot in **Figure 4.35 (d)**.

At fixed gas loadings, the gas structure frequency is a function of both the liquid loading and the liquid phase water cut. At gas superficial velocities between 0.13 and 0.16 ms^{-1} it can be observed that the maximum gas structure frequency is obtained for low liquid loading-low water cut flow combinations, i.e. the lower liquid phase density the greater the gas structure frequency. It can be seen that the lower the liquid loading the more sensitive the gas structure frequency will be to variations on the water cut. As the gas loading is increased, the liquid loading begins to dominate.

(a) $0.13 \leq V_{sg} \leq 0.16$ ms^{-1} (b) $0.29 \leq V_{sg} \leq 0.32$ ms^{-1}

(c) $0.59 \leq V_{sg} \leq 0.62$ ms^{-1} (d) $1.29 \leq V_{sg} \leq 1.34$ ms^{-1}

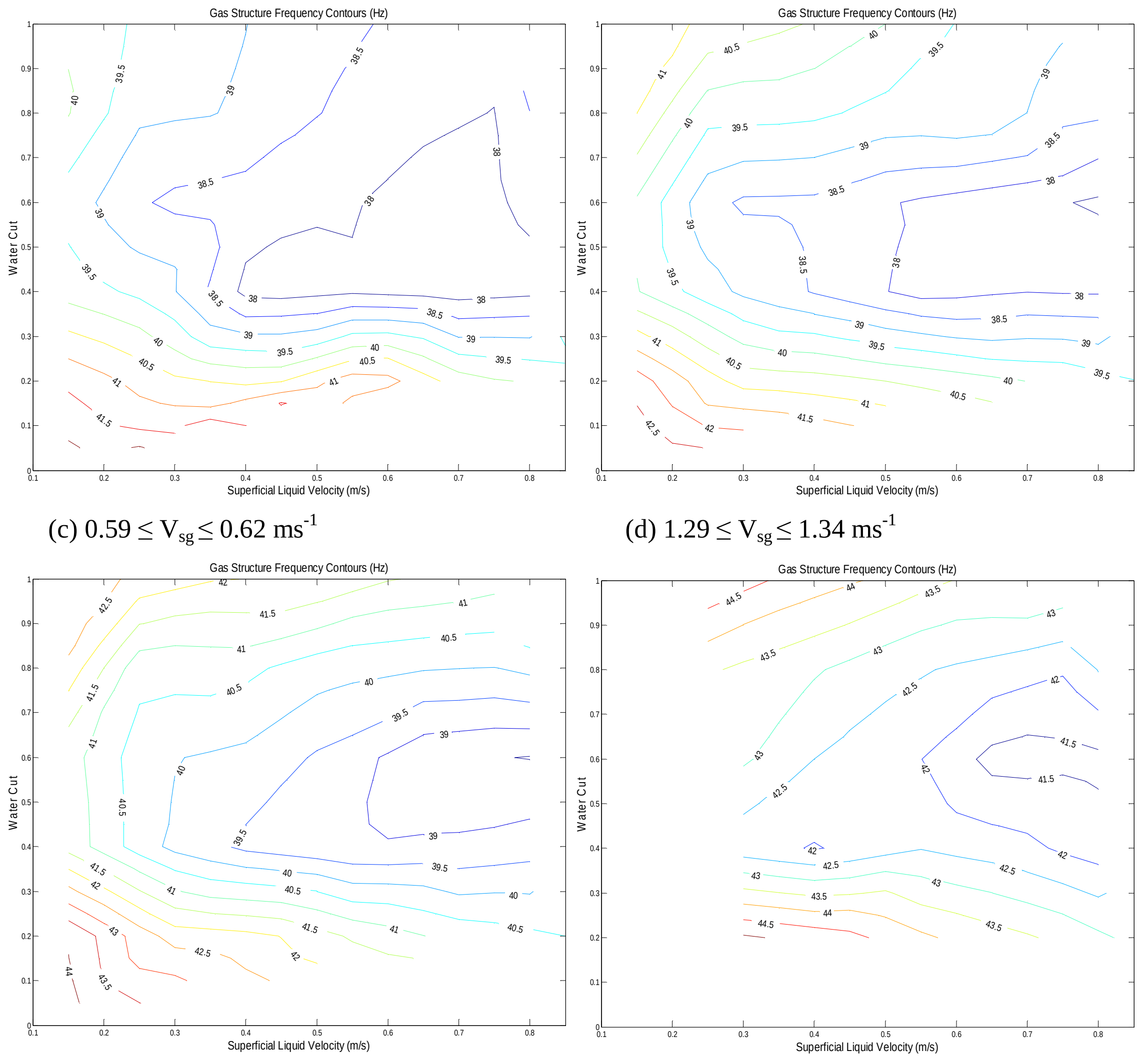

Figure 4.35 – Influence of Water Cut on Gas Structure Frequency

At gas superficial velocities in excess of 0.59 ms^{-1} it can be seen that the maximum gas structure frequencies are obtained for pure liquid phase mixtures with the minimum frequencies being observed for water cuts in the range of 40 – 60%. It is hypothesised that increased shear forces between the oil and water components due to phase inversion in these flows results in the prevention of a significant proportion of the larger gas structure formations.

4.3.3 Interim Summary: Frequency Domain Analysis

Frequency domain analysis of the signals using FFT proved unsuccessful in decrypting the relationship between the frequency spectra densities, and the dominating signal frequencies, with respect to the multiphase flow parameters on both a global and flow regime specific basis. Investigation of the gas-structure frequency relationship proved more fruitful with the passage frequency of gas structures demonstrating exhibiting a strong flow regime specific dependency on the gas phase loading. Correlation with the liquid phase was observed to increase with increased gas loading while the water cut exerts a significant influence on the gas structure frequency at low liquid loadings. It was hypothesised that analysis of the time-frequency using wavelet analysis may result in increased discriminability between data points.

4.4 Wavelet Analysis

The use of Fourier analysis for signal analysis has one major drawback: it loses all time domain information. Accordingly, it is impossible to tell when a particular event occurred. A modified version of the Fourier transform was developed to enable the determination of both signal time and frequency characteristics: the short-time Fourier transform (SFFT). However, the SFFT has its own limitations, namely information domain resolution trade-off. The SFFT employs a fixed window size to analyse the frequency content of small segments of the signal; thus, it provides a fixed resolution analysis. As a result, using a narrow SFFT window will yield high-resolution time domain information but poor frequency resolution. Conversely, employing a wide SFFT window, detailed frequency information is obtained at the expense of the temporal resolution.

Wavelet analysis is a technique that facilitates multi-resolution analysis of a signal's frequency and time domain characteristics. In the low frequency sections one obtains high-resolution time information; whereas, in the high frequency part one will get low-resolution time information, **Figure 4.36** [**103**].

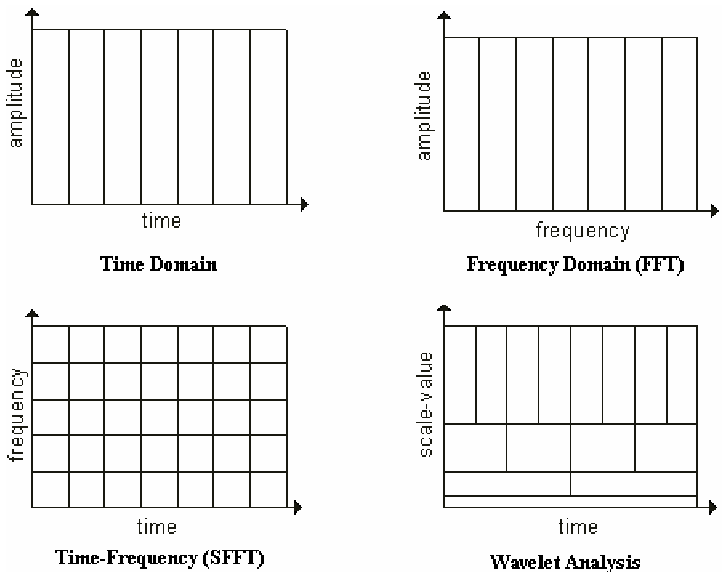

Figure 4.36 – Wavelet Analysis

A wavelet is defined as a waveform of finite duration that has an average value of zero. There are a number of different types of wavelets, each with their own specific strengths and weaknesses, some common examples are illustrated in **Figure 4.37**. A detailed review of wavelet family properties and selection criteria is available in the MATLAB Wavelet Toolbox User Guide [**104**].

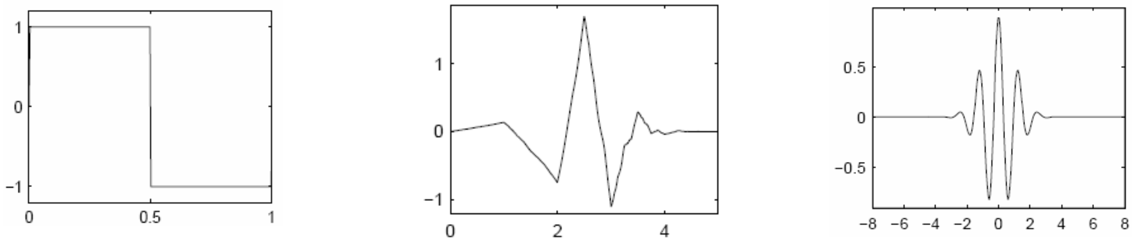

Figure 4.37 – Wavelet Functions

Wavelet transformation of a signal involves decomposing the signal into a number of coefficients (C) based on the correlation of the original signal $x(t)$ with a series of scaled and translated wavelets based on a single mother wavelet function φ.

$$C(\tau, s) = \int_{-\infty}^{+\infty} x(t) \frac{1}{\sqrt{|s|}} \overline{\varphi\left(\frac{t-\tau}{s}\right)} dt \qquad \text{(Eq. 4.1)}$$

Where, τ and s represent the translation and scale of the mother wavelet respectively, and $\bar{z}$ is the complex conjugate of z.

These coefficients can then be exploited to analyse the signal energy distribution in a time-scale plot: the x-axis displaying the position along the original signal (i.e. time), the y-axis showing the corresponding wavelet scale, and the colour allocated to the x-y intersections depict the magnitude of the associated wavelet coefficient.

It should be emphasised that the wavelet coefficient plots have time-scale and not time-frequency axes. The term frequency is term reserved explicitly for use with Fourier analysis procedures. In wavelet analysis, the wavelet functions correlated with the original signal are not purely periodic, so it is incorrect to directly interpret the results in terms of frequency. However, one can examine low frequency features present in a signal using high scaling factors on the mother wavelet function and vice versa. Abry [**105**] proposed a technique to link the scale s to signal frequency content based on the following expression.

$$F_a = \frac{F_c}{s \cdot \Delta} \qquad \text{(Eq. 4.2)}$$

Where, F_c and Δ denote the wavelet centre frequency and sampling period respectively. The frequencies determined are not true values but theoretical pseudo-frequency based on the approximation of scaled wavelet function's centre frequency. Caution should be exercised when comparing analyses undertaken employing purely period frequency with those employing pseudo-period frequency.

There are two categories of wavelet transform: continuous and discrete. Although both these procedure operate on discrete signals, the continuous transform is defined as such that wavelet coefficients are determined at all scales, from that of the original signal up to the defined maximum, and translation is undertaken across the full domain of the signal being analysed. On the other hand, discrete transformation calculates the coefficient terms at a chosen subset of scales and positions.

4.4.1 Wavelet Transform Coefficient Analysis

Investigation of continuous wavelet transform parameters revealed that the use of a special type of continuous transform called the dyadic wavelet transform facilitated accurate representation of the original signals' fractal properties with considerably less computer processing. Dyadic wavelet analysis is a special case of continuous wavelet analysis whereby discrete scale parameters based on the power of 2 series, and continuous parameters in the spatial domain, are employed with no appreciable loss of information [**106**]. Preliminary analysis exhibited that utilising the Daubechie db3 wavelet and a raw signal length of 2750 samples (11 seconds of collected data), the continuous wavelet transform enables good distinction between the frequency-time characteristics of the gamma densitometer signals, **Figure 4.38**.

Figures 4.38 (a) – (d) delineate the corresponding continuous wavelet coefficient plots for the hard spectrum densitometer signals featured in **Figures 4.1**, **4.22 and 4.31** (signal response, probability mass function and power spectral density plots respectively). The wavelet coefficients at each of the dyadic scale-sample intersections have been coloured according to their magnitude: white/light-pink regions represent large magnitude coefficients; while, black areas indicate points with small magnitude wavelet coefficients. Irregularities can be observed at the wavelet coefficient plot boundaries: data in these regions should not be used for analysis is it is produced from extrapolated data and it cannot be guaranteed to be characteristic of the signal. The wavelet coefficient plots gave a good visual indication of the fractal properties of the density fluctuations in the multiphase flows for different gas and liquid loadings. The liquid phase water cut was 100% in for each of the analysis illustrated.

It can be seen that as that the gas void fraction of the multiphase flow increases from **Figure 4.38 (a)** through to **(d)**, there is an increasing presence of high-scale wavelet coefficients indicating an increase in the low frequency content of the gamma signal (pseudo-frequency < 4 Hz). This corresponds to the raw signal trace indicating low frequency slug features. The high frequency content (pseudo-frequency >12 Hz) of the signals was largely similar for all gas-liquid combinations. The intermediate pseudo-frequencies showed larger prominence and time variability for data points lying close to flow regime boundaries.

(a) V_{sg} = 0.15 ms^{-1}, V_{sl} = 0.79 ms^{-1} and WC = 100%

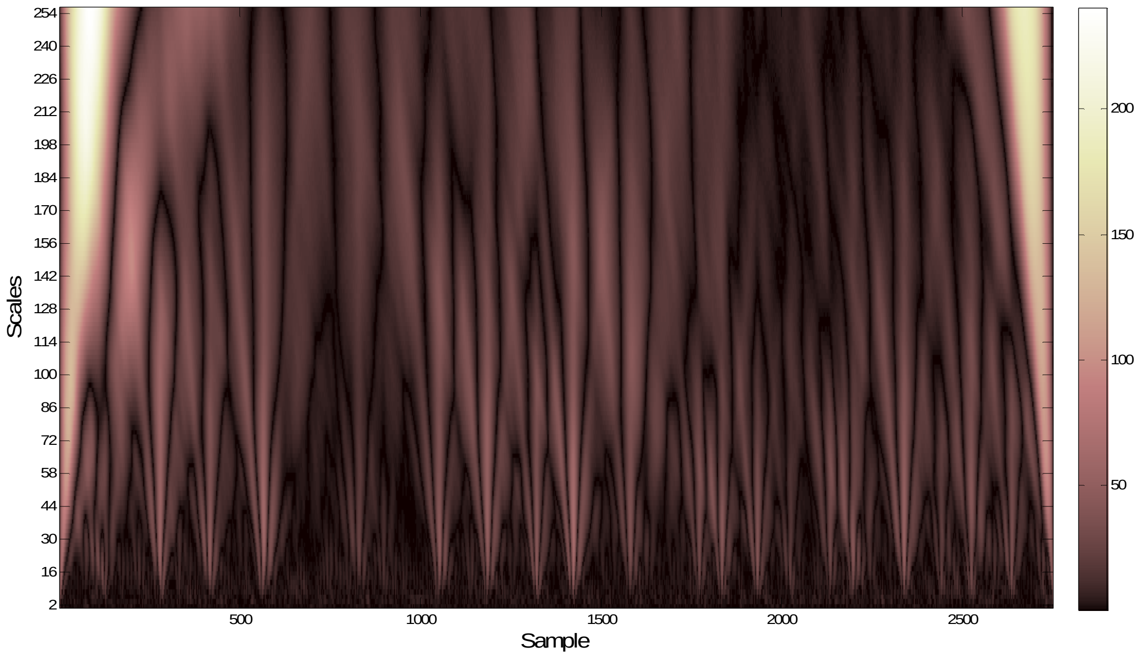

(b) V_{sg} = 0.13 ms^{-1}, V_{sl} = 0.12 ms^{-1} and WC = 100%

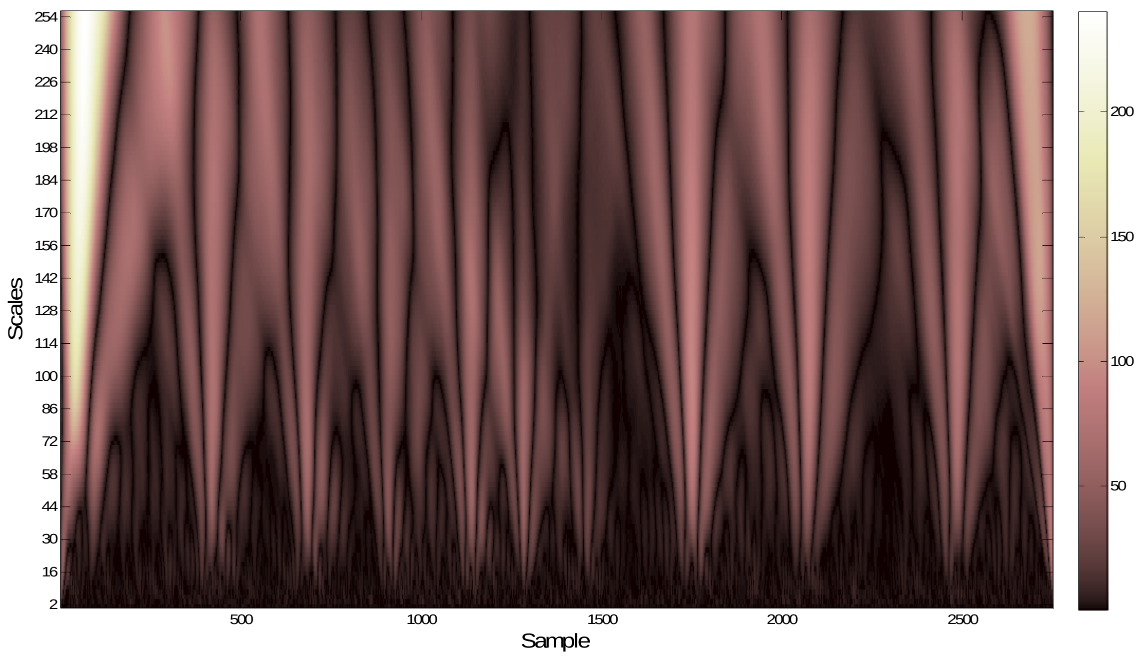

Figure 4.38 – Continuous Wavelet Transform Coefficient Plots

(c) V_{sg} = 1.32 ms^{-1}, V_{sl} = 0.79 ms^{-1} and WC = 100%

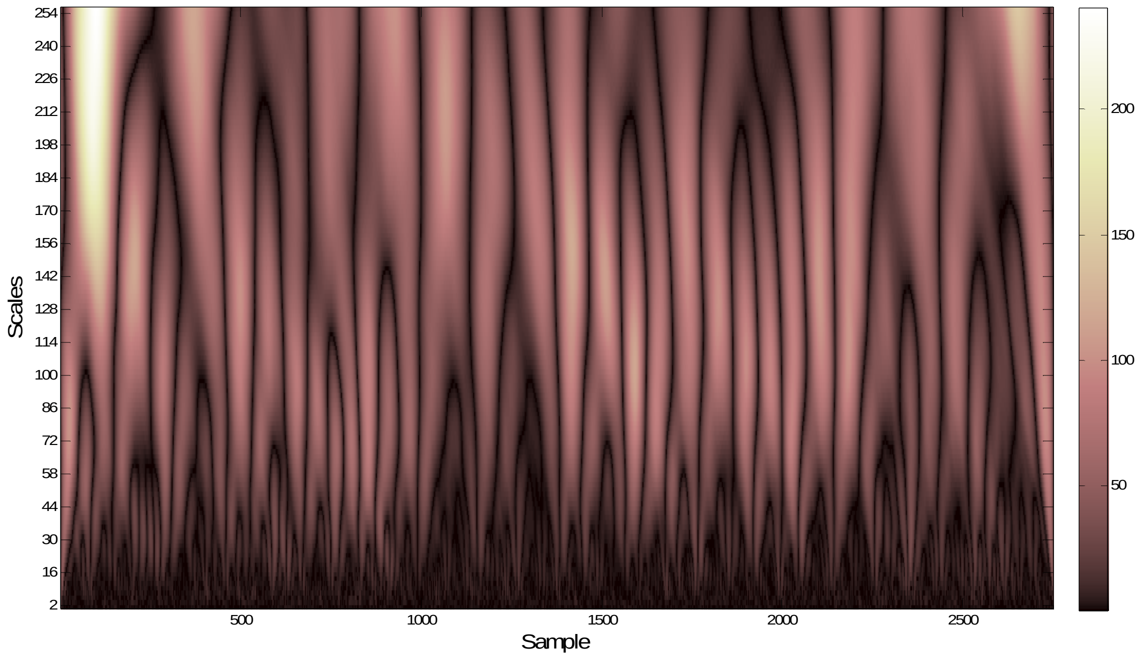

(d) V_{sg} = 0.99 ms^{-1}, V_{sl} = 0.12 ms^{-1} and WC = 100%

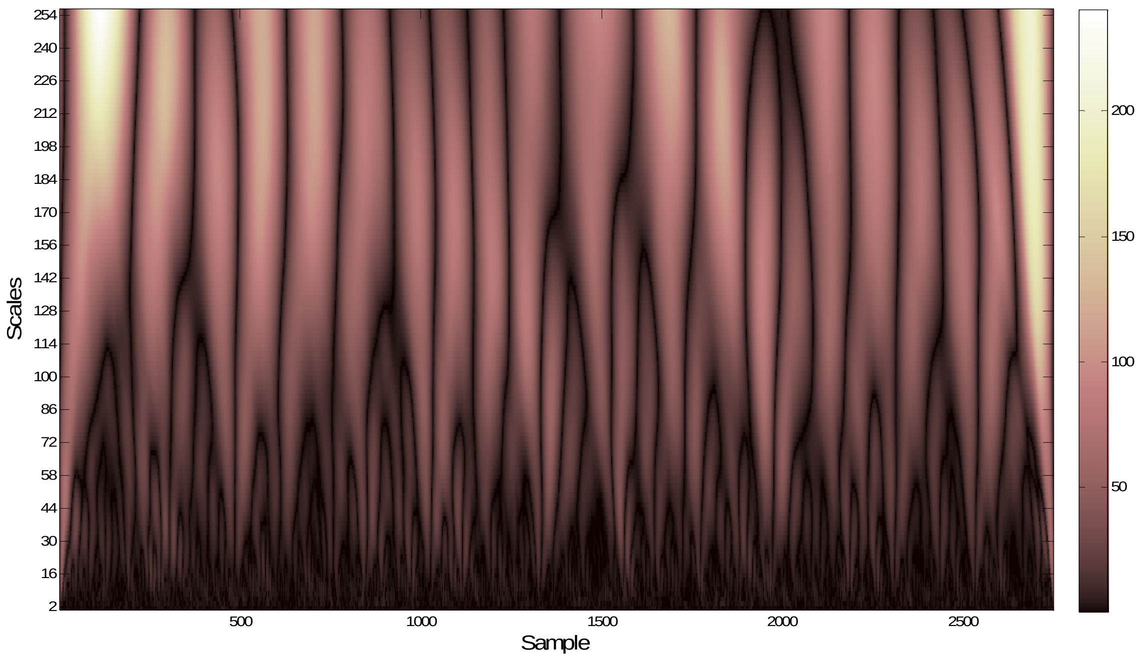

Figure 4.38 – Continuous Wavelet Transform Coefficient Plots

The influence of the GVF on the low frequency content of the signal was reinforced in extending the analysis to the full data set. In addition, the liquid phase water cut was observed to exert a significant influence on the wavelet coefficients. The fractal properties induced by the liquid phase water cut were most significant for water cuts of 40% and 60% where one would expect phase inversion phenomena in the liquid phase. The degree of variation introduced in the wavelet coefficient transform for different water cuts is a complex function of the gas and liquid phase loadings, coefficient scale and time. The relationship between the wavelet coefficients and fluid flow properties were examined in more detail using wavelet packet analysis.

The wavelet coefficient plot scale values can be quantified in terms of periodic pseudo-frequencies, as determined from **Eq. 4.2**, **Figure 4.39**.

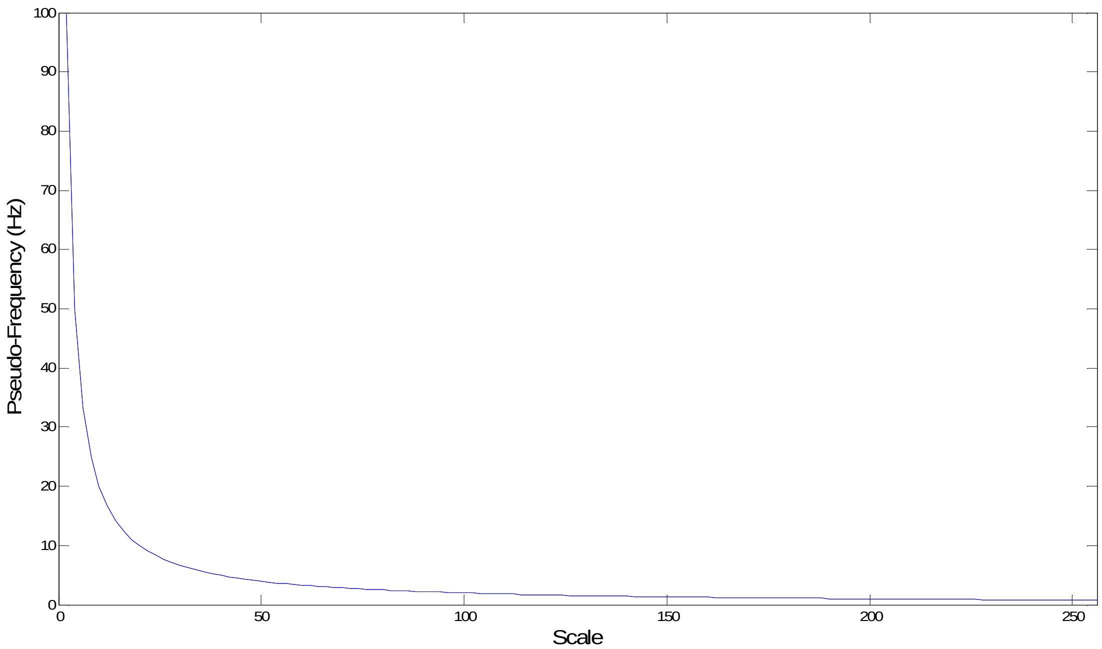

Figure 4.39 – Scale against Pseudo-Frequency for Wavelet Coefficient Plots

4.4.2 Wavelet Packet Analysis

Wavelet packet analysis is a generalised form of discrete wavelet decomposition that involves splitting the original signal *S* into a series of low-frequency approximations (*A*) and high-frequency details (*D*) coefficients through the employment of a series of band-pass filters, **Figure 4.40**. The reader is directed to Misiti *et al* [**104**] for information on wavelet packet analysis theory and applications.

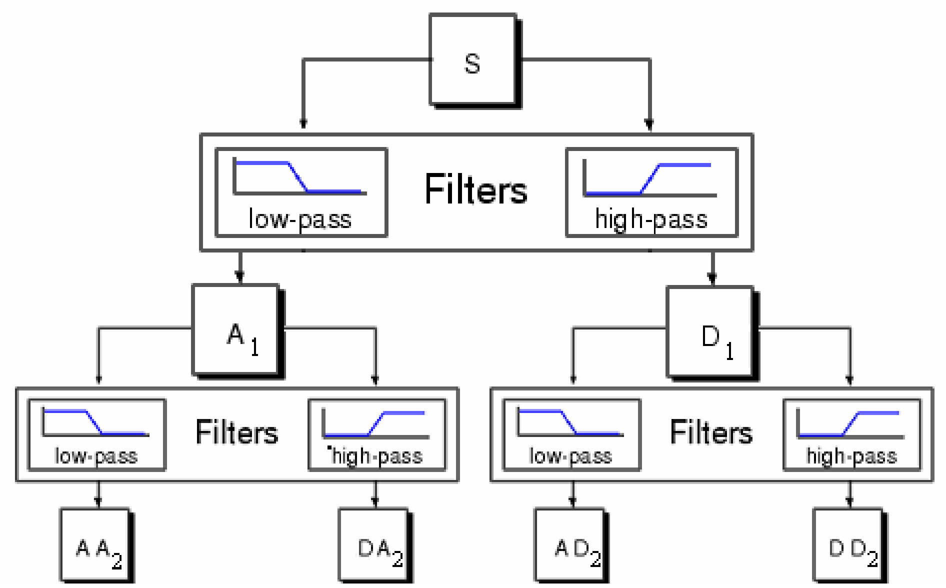

Figure 4.40 – Two Level Decomposition Wavelet Packet Analysis

A four-level decomposition was performed on the 2750 sample signals employing the db3 wavelet. The Shannon non-normalised entropy based criterion was exploited to determine the optimal level of signal decomposition [**107**].

Figures 4.41 (a) – (d) illustrates the resulting wavelet decomposition of the signals used in previous illustrations: exhibiting their fourth level approximation and each of the approximation levels' associated detail coefficients.

The fourth level approximation of the signals (a_4) yields a smooth noise-free signal enabling clear distinction of the low-frequency (0 – 7.8 Hz) fluctuations induced by the passage of large gas structures. Discrepancies can also be observed in the level 4 detail coefficients (d_4) for the different flow conditions. However, examination of any discrimination existing between the detail coefficients at each of the higher levels was not possible by visual means owing to their complexity. Consequently, analysis of the statistical properties of all wavelet packet coefficients was undertaken with respect to multiphase flow superficial phase velocities and liquid phase water cuts.

The statistical parameters from all wavelet packets were extracted after performing level 4 wavelet decompositions on the full length signals, **Appendix D**. The statistical properties of the wavelet packets in **Figure 4.41** are detailed in **Table 4.1**.

The relationships exhibited between the wavelet detail coefficient statistics and the flow parameters were complex and dependent on the individual packet involved. The gas phase parameters (superficial gas velocity and GVF) exhibited the strongest correlation with the standard deviation; however, their relationship was not sufficiently interdependent to derive a quantifiable relationship. The liquid superficial velocity displayed no obvious dependence on any of the statistical parameters analysed.

(a) $V_{sg} = 0.15\ \text{ms}^{-1}$, $V_{sl} = 0.79\ \text{ms}^{-1}$ and $WC = 100\%$

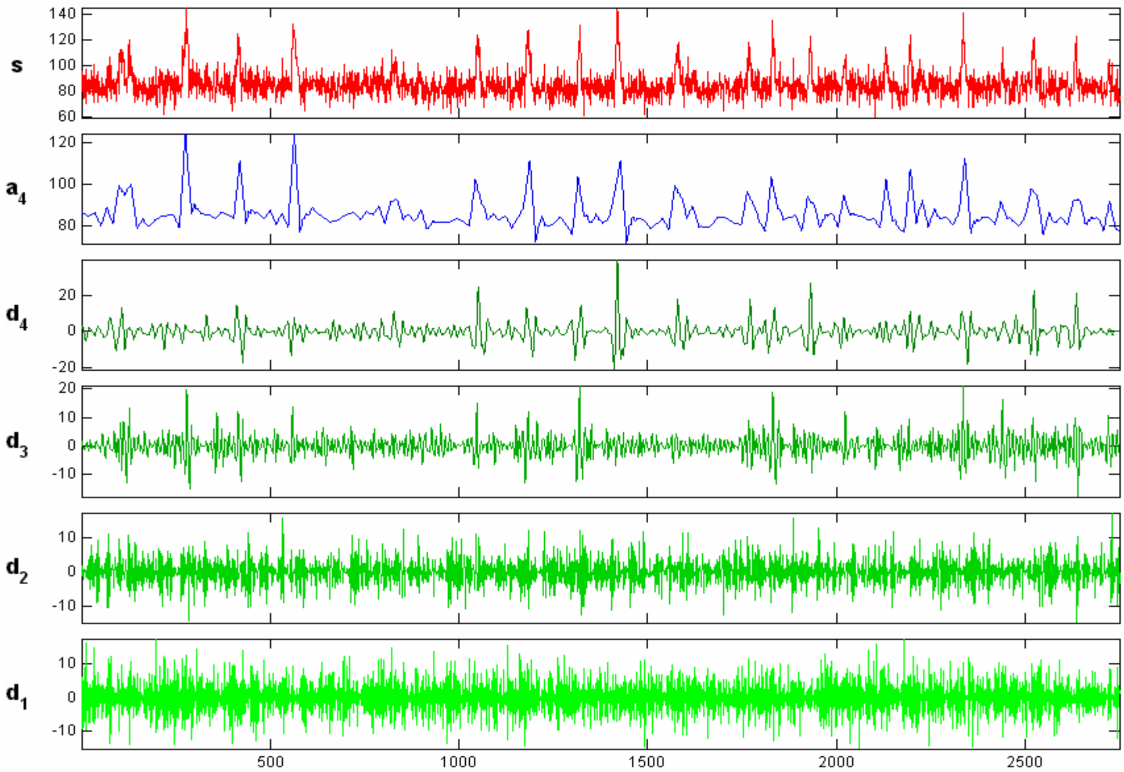

(b) $V_{sg} = 0.13\ \text{ms}^{-1}$, $V_{sl} = 0.12\ \text{ms}^{-1}$ and $WC = 100\%$

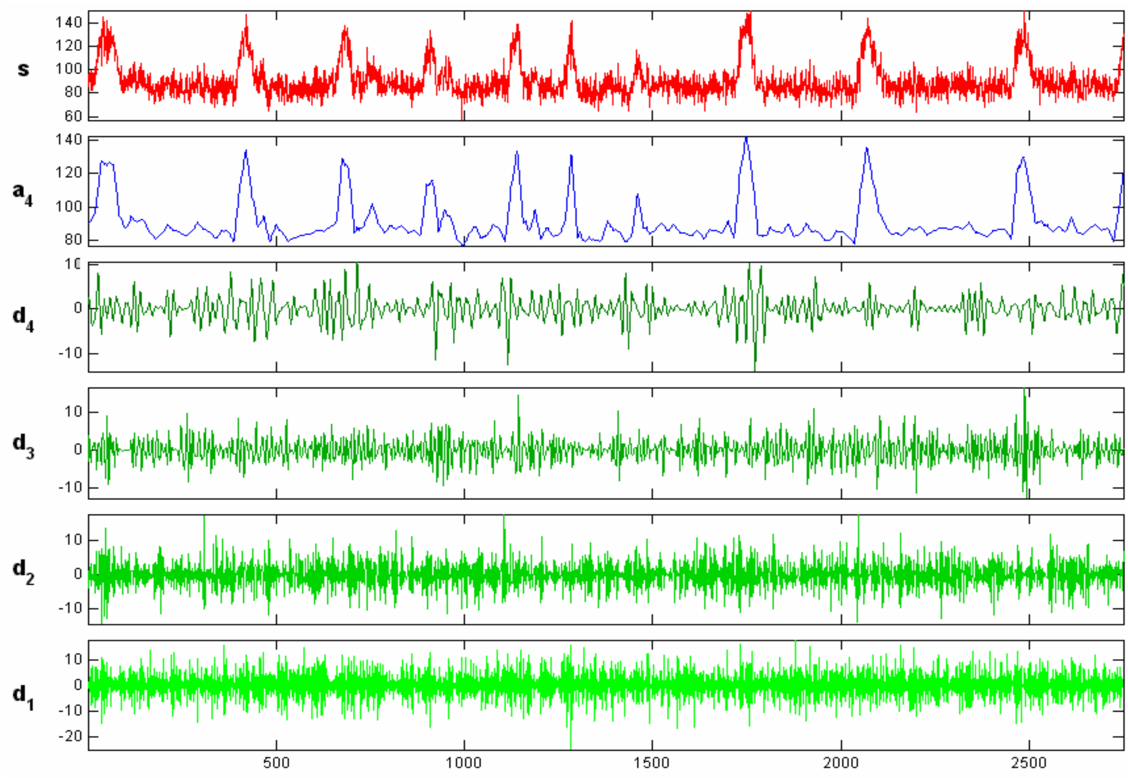

Figure 4.41 – Wavelet Packet Analysis

(c) V_{sg} = 1.32 ms^{-1}, V_{sl} = 0.79 ms^{-1} and WC = 100%

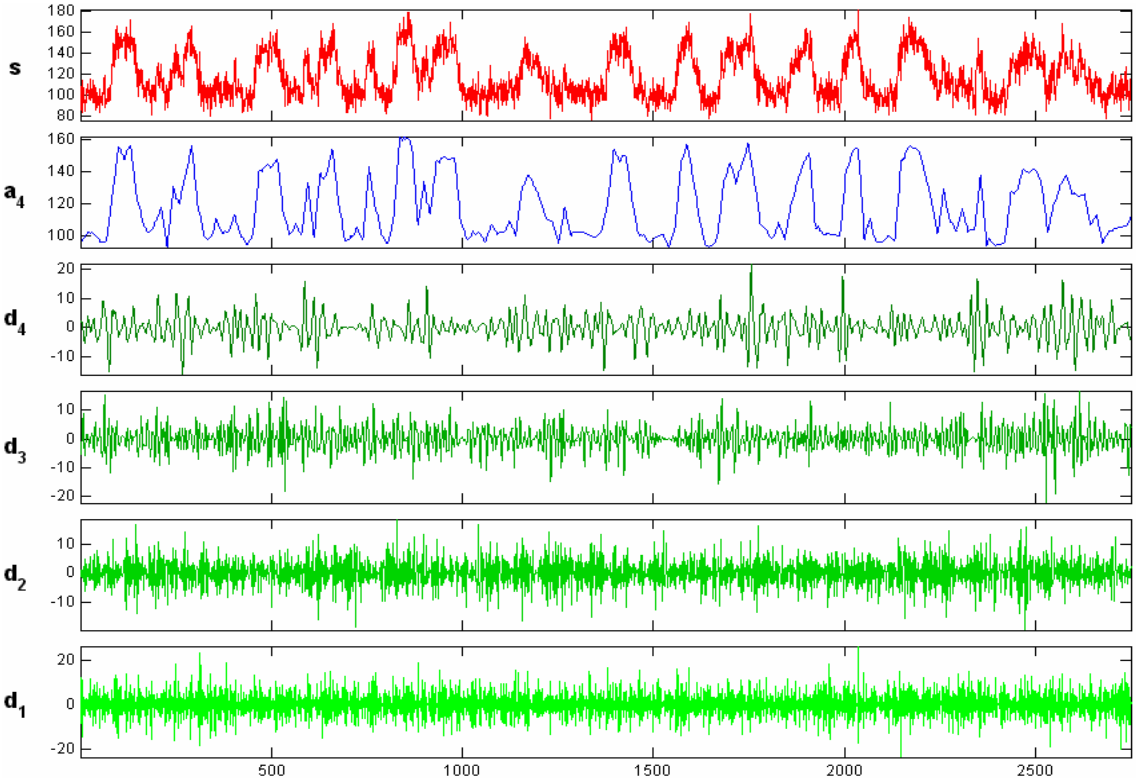

(d) V_{sg} = 0.99 ms^{-1}, V_{sl} = 0.12 ms^{-1} and WC = 100%

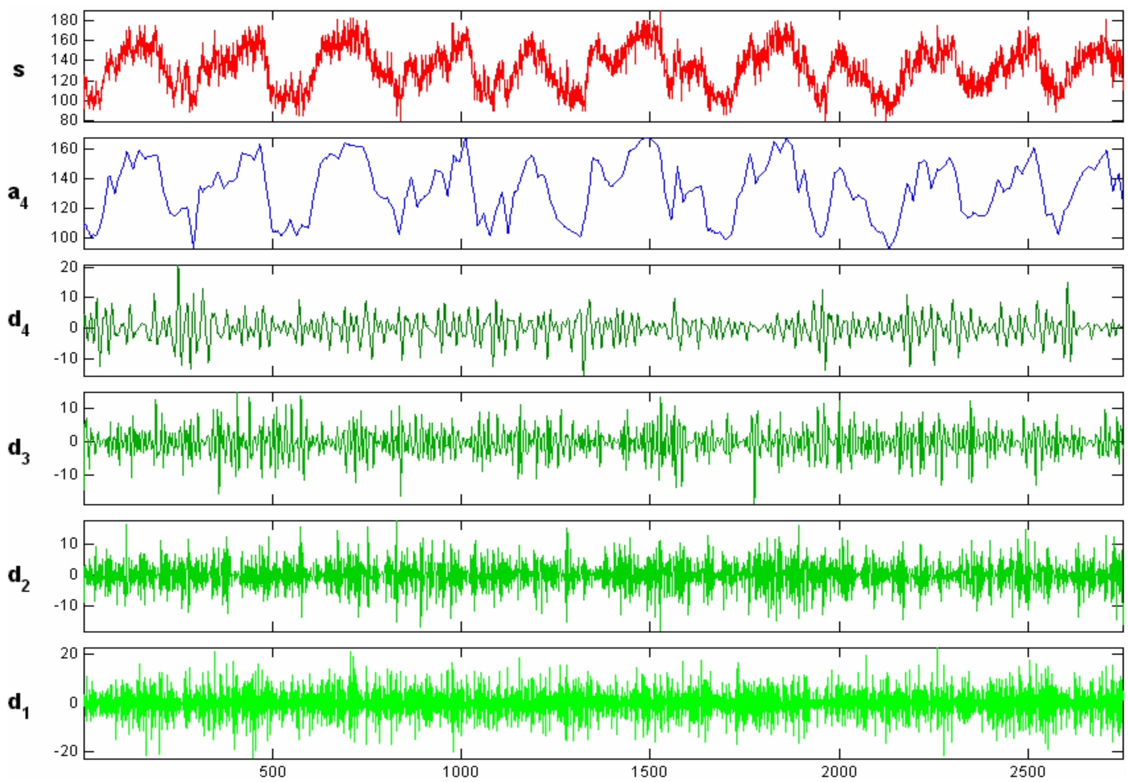

Figure 4.41 – Wavelet Packet Analysis

Extending the analysis to the full data set (**Appendix D**), it was observed that the fourth level approximation signals retain the discriminatory statistical characteristics of the original signals. Again, the strongest correlations were obtained between the gas phase parameters and the standard deviation of wavelet packet coefficients with all packets. However, these correlations offer no improvement on those that were obtained employing the original gamma count signals. Both the liquid phase superficial velocity and water cut exhibited poor correlations with the statistical parameters extracted from the wavelet packet coefficients.

The wavelet packet statistics were also subject to analysis on a flow regime specific basis employing the Taitel-Dukler definition of the bubble-slug regime boundary. Nevertheless, the individual flow regime data sets exhibited weaker correlations with the same statistical parameters as observed treating the data as a single data set.

		Mean	Standard Deviation	Coefficient of Variance	Coefficient of Skewness	Coefficient of Kurtosis
Original Signal	**(a)**	83.78	10.895	1.3E-01	1.6E+00	4.812
	(b)	90.71	15.395	1.7E-01	1.6E+00	2.854
	(c)	117.28	20.697	1.8E-01	5.4E-01	-0.665
	(d)	135.07	20.148	1.5E-01	-1.7E-01	-0.620
Level 4 (a_4)	**(a)**	84.19	7.606	1.1E+01	2.0E+00	5.094
	(b)	90.65	13.562	6.7E+00	2.1E+00	3.995
	(c)	117.43	18.860	6.2E+00	6.4E-01	-0.896
	(d)	135.01	18.061	5.5E+00	-2.7E-01	-0.883
Level 4 (d_4)	**(a)**	-	4.287	-1.4E-05	4.2E-02	2.554
	(b)	-	2.650	1.8E-06	-7.8E-03	1.568
	(c)	-	3.787	-5.4E-06	3.8E-03	0.584
	(d)	-	3.615	6.6E-06	2.4E-04	0.711
Level 3 (d_3)	**(a)**	-	3.020	-7.0E-07	-3.6E-03	1.323
	(b)	-	2.591	-8.8E-06	5.5E-04	0.381
	(c)	-	3.573	-1.1E-05	9.5E-04	0.397
	(d)	-	3.609	-1.8E-06	9.1E-04	0.329
Level 2 (d_2)	**(a)**	-	3.531	-6.8E-07	2.0E-06	0.017
	(b)	-	3.451	-8.0E-07	1.1E-03	0.327
	(c)	-	4.069	-1.1E-06	6.2E-06	0.048
	(d)	-	4.338	-7.1E-08	-1.1E-03	0.226
Level 1 (d_1)	**(a)**	-	4.952	-5.1E-07	1.2E-02	0.026
	(b)	-	5.098	1.0E-06	1.3E-02	0.051
	(c)	-	5.719	-1.1E-06	1.4E-02	0.096
	(d)	-	6.054	7.2E-07	1.2E-02	0.073

Table 4.1 – Statistical Analysis of Wavelet Packet Coefficients

4.4.3 Interim Summary: Wavelet Analysis

Wavelet analysis indicated the intricate relationship between the time-frequency content of the signals was a complex function of the gas and liquid phase flow rates, and the liquid phase water cut. Discriminatory fractal properties were observed in the continuous wavelet transforms but it was not possible to determine any quantitative relationship between these fractal properties and the multiphase flow parameters on either a global or flow regime specific basis. However, from the results obtained, it was determined that any potential discriminatory information observed in the fractal properties of the wavelet transform of the gamma signals is complex in its nature. However, it was hypothesised that the wavelet transform data would lend itself better to analysis using pattern recognition signal processing techniques (**Chapter 6.6**).

4.5 Summary

This chapter analysed the characteristics of the gamma densitometer's response to a number of multiphase flow conditions in a number of information domains.

The output signals exhibited fluid density fluctuations characteristic of the flow regimes predicted by published flow regime maps. A host of statistical parameters were extracted from the time-varying gamma count signals and their correlation with characteristic parameters of the multiphase flow composition investigated. Parameters demonstrating discrimination for different flow conditions were observed to be complex functions of the gas and liquid phase loadings and the water cut.

The probability mass function plots provided a good indication of the prevailing flow regime. A scatter plot of the mean hard gamma count against the coefficient of kurtosis produced a quantifiable quadratic relationship which enabled classification of the flow regimes. Nevertheless, classification was subjective when operating in the proximity of the defined flow regime boundary as traits of more than one regime were evident and discrepancies were obtained in classifications from experimental data with published flow maps and those from multiphase flow simulations.

Frequency domain analysis of the signals using FFT proved unsuccessful in decrypting the relationship between the frequency spectra densities, and the dominating signal frequencies, with respect to the multiphase flow parameters on both a global and flow regime specific basis. Investigation of the gas-structure frequency relationship proved more fruitful with the passage frequency of gas structures demonstrating exhibiting a strong flow regime specific dependency on the gas phase loading. Correlation with the liquid phase was observed to increase with increased gas loading while the water cut exerts a significant influence on the gas structure frequency at low liquid loadings.

Wavelet analysis indicated the intricate relationship between the time-frequency content of the signals was a complex function of the gas and liquid phase flow rates, and the liquid phase water cut. Discriminatory fractal properties were observed in the continuous wavelet transforms but it was not possible to determine any quantitative relationship between these fractal properties and the multiphase flow parameters.

Based on the signal analysis conducted, two approaches were investigated to infer the determination of key multiphase measurement parameters from the gamma densitometer signals.

A mechanistic approach (**Chapter 5**) was undertaken which aimed to utilise the degree of attenuation from the two gamma energies to extract phase fraction information. In addition, it was hypothesised that the fractal properties of the gamma densitometer signals could be exploited to infer phase velocity information.

Concurrently, the exploitation of pattern recognition techniques (**Chapter 6**) was considered the most suitable means to investigate underlying correlations in the complex relationships exhibited by a number of statistical parameters and key multiphase flow parameters.

Chapter 5: Mechanistic Determination of Flow Parameters

This chapter reports the investigative work undertaken to develop a mechanistic approach to establish multiphase flow parameters from the gamma densitometer data. Based on the inferential mass flow measurement model, it was attempted to infer the flow mixtures' individual phase volume fractions and velocities. Determination of the individual phase fractions of the dynamic multiphase flow gamma count data collected was investigated through the exploitation of the gamma attenuation information. Quasi-periodic waveforms identified in the multiphase fluid density were analysed for their dependence on the gas and liquid superficial phase velocity parameters.

5.1 Determination of Phase Fractions

The main limitations of directly applying gamma radiation attenuation based equations (**Chapter 2.3.4**) is that they do not take into account the circular geometry of the pipe, the prevailing flow regime or the presence of phase slip; thus, the calculated phase fractions could contain significant errors depending on the flow conditions. The fluid composition measured by a single sensor exposed to multiphase flow mixtures can vary significantly from the actual composition, **Figure 5.1**.

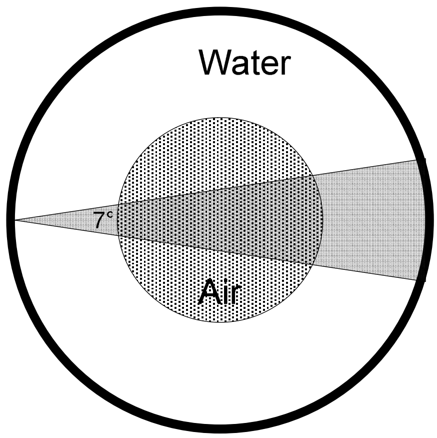

Figure 5.1 – Sensor's View of Multiphase Fluid Composition

In **Figure 5.1**, the actual air volume fraction of the mixture is 25%; whereas, owing to the annular flow regime and the limited measurement zone, the sensor will detect an air volume content of 48% in the pipe. If the air core was to be moved off-centre the sensor will observe yet another fluid composition.

Resolution of the individual phase fractions from the data generated by the gamma densitometer's response to a series of vertical multiphase flows in the multiphase test facility was investigated employing the gamma radiation attenuation principles described in **Chapter 2.3.4**.

5.1.1 Two-Phase (Air-Water) Model

A two-phase model was developed exploiting the air-water flow data collected in the multiphase flow test facility. To resolve the phase fractions of a two-component mixture, only one energy level of gamma photon count information was required. However, the two energy levels available from the caesium-137 were exploited as a means of verification. The gamma attenuation equations in **Chapter 2.3.4.1** were employed. The measured gas and liquid phase fractions as determined from the hard energy spectrum, and their deviations from the test facility reference values, are illustrated in **Figure 5.2**.

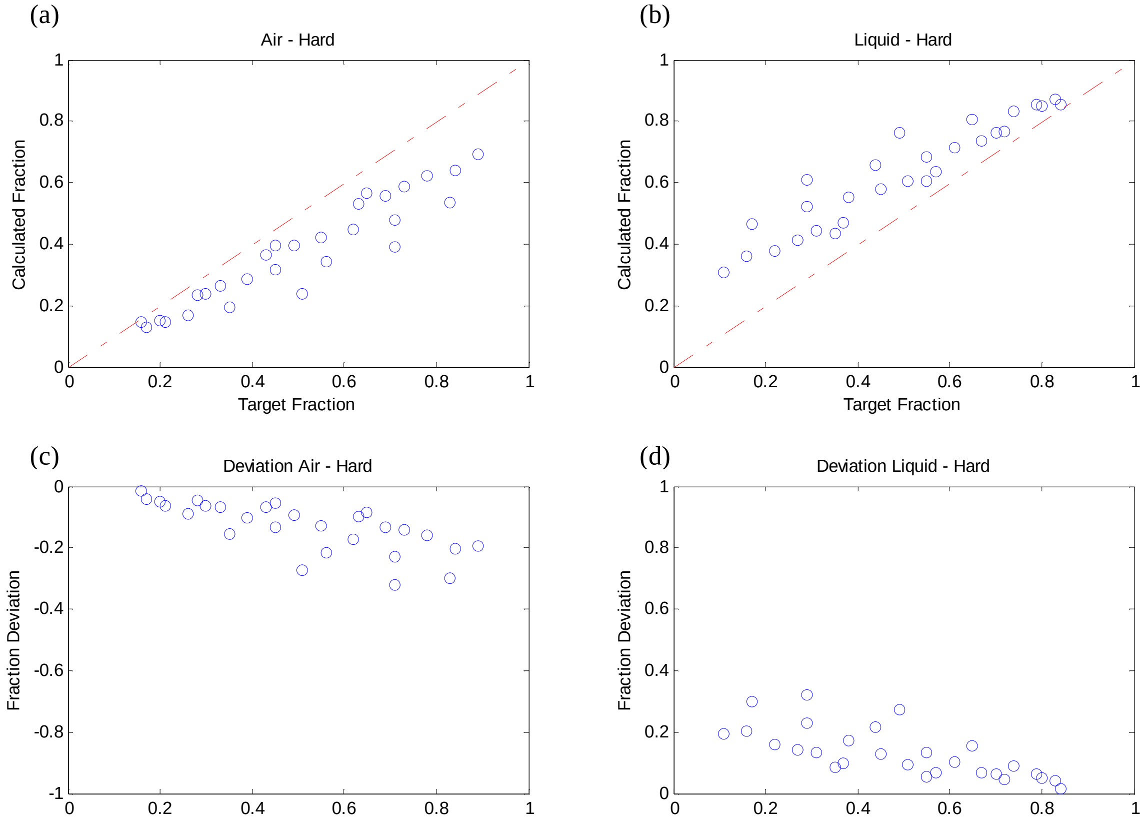

Figure 5.2 – Air-Water Component Fractions using Hard Energy

The reference phase fractions values employed in the analysis were the non-slip equivalent phase fractions at the gamma densitometer measurement point in the riser. These were calculated using the reference input flows and the riser base and top side separator pressure and temperature measurements. The temperature was assumed to constant throughout the test section and a linear pressure gradient from the riser base to the. Reference phase fractions were calculated at 1.5 m below the riser top.

Significant errors were yielded in the calculation of the component fractions in the air-water tests. These errors can be attributed to many sources. However, it is thought that the dynamic nature of the tests; thus, the presence of phase slip, the sensor's limited view of the pipe cross-section, and differing flow regimes were the most significant error sources. From the phase fraction deviation plots, it can be seen that the deviation in the air fraction's calculated value tends to increase from the reference GVF with increasing multiphase flow gas fraction. Conversely, the deviation present in liquid phase fraction measurement diminishes with increasing actual liquid content.

Repeating the calculations using the soft energy gamma count yielded almost identical results to those obtained employing the high-energy gamma count. However, the discrepancy between the calculated GVF values was observed to be a function of the multiphase fluid GVF, **Figure 5.3**.

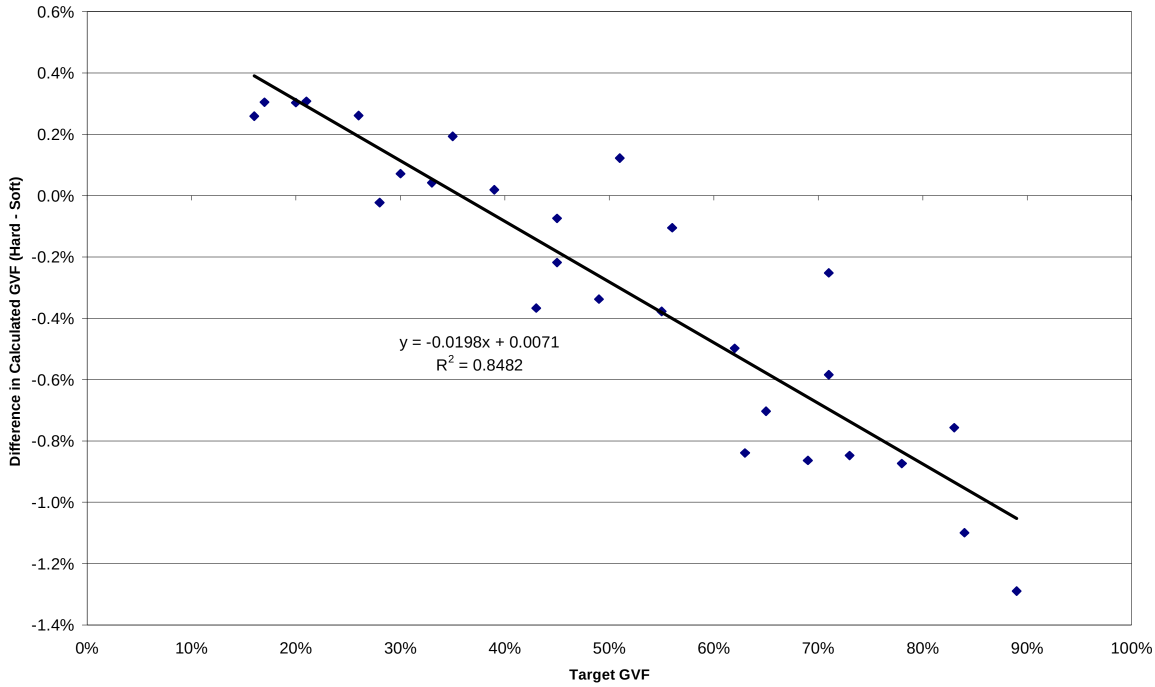

Figure 5.3 – Difference in Calculated GVF Values as a Function of Actual GVF

The deviation between the hard and soft energy calculated GVF values was observed to demonstrate an approximately linear relationship with the actual multiphase mixture GVF. At GVFs less than 35%, the hard-energy gamma count provides GVF values up to 0.4% greater than GVFs obtained from the soft-energy gamma count. At GVFs greater than 35%, the soft-energy calculated GVF values were less than GVFs determined exploiting the hard gamma count. At high GVFs (>85%), the difference between the calculated GVF values using the different spectra count data was as large as 1%.

The hard energy signal yielded GVF measurements up to 1.5% more accurate than those from the soft energy signal at actual multiphase flows GVFs between 0% and 25%. At GVFs in excess of 45%, the soft energy derived GVF measurements outperformed the hard energy measurements by up to 1%. Between GVFs of 25% and 45% the measurement performance from the two signals were similar, **Figure 5.4**.

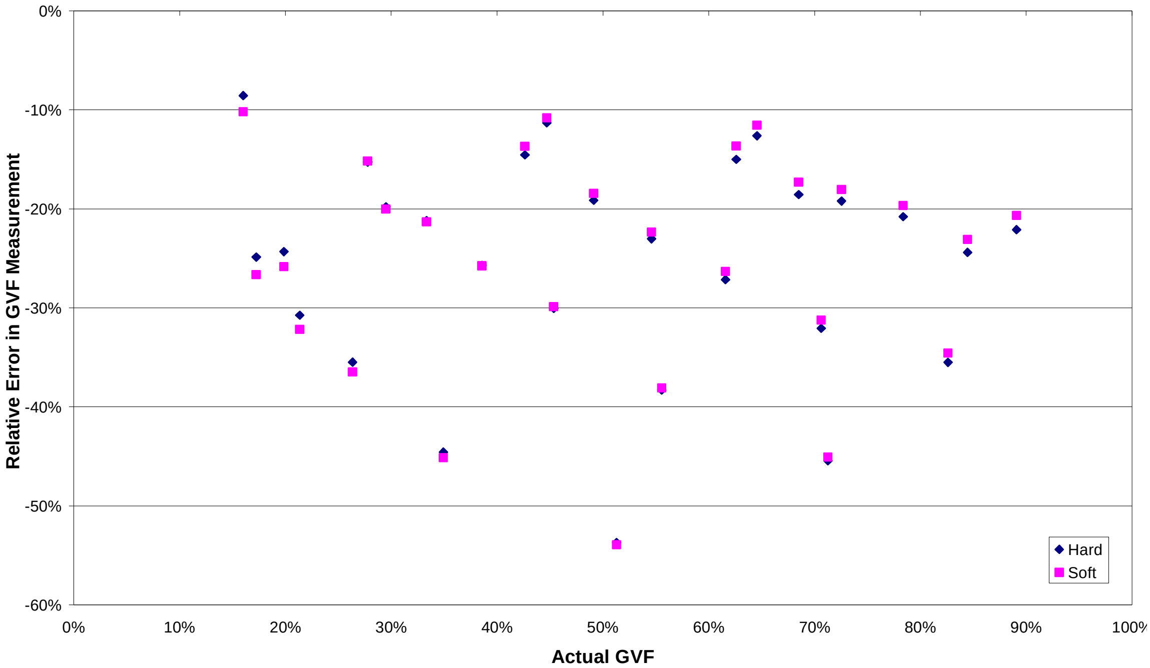

Figure 5.4 – Hard and Soft Energy GVF Measurement Errors against Actual Flow GVF

The hard energy photon attenuation is entirely dependent on photoelectric effect absorption of the direct 662 keV radiation beam and has been shown to be statistically the more stable of the two signals. In contrast, the soft energy signal monitors photons which have undergone Compton scattering across a larger cross-sectional area of the pipe. Accordingly, at low GVFs, where deviations in the fluid distribution are insignificant, the superior stability of the hard signal yields a more accurate phase fraction measurement. However, as the GVF increases the phase distribution becomes less uniform and the scattered soft energy photons will give a measurement marginally more representative of the flow structure. Nevertheless, the results from both signals contain large errors owing to the measurement system's inability to account for the dominating flow regime and phase slip effects.

The results of the statistically more stable hard energy signal determined GVFs were compared against published results of similar experiments by analysing their dependence on the superficial phase velocities of the test fluids, **Figure 5.5**.

The results obtained show that the void fraction increases with increases in the superficial gas velocity; whereas, it decreases with increasing superficial liquid velocity magnitude. This is consistent with published data for void fraction measurement in upward flows in pipes of various diameters [**108-111**]. The concurrence of the data collected using the current densitometer unit with published findings demonstrates that a high level of confidence can be instilled in the test facility and test procedures employed in this research work.

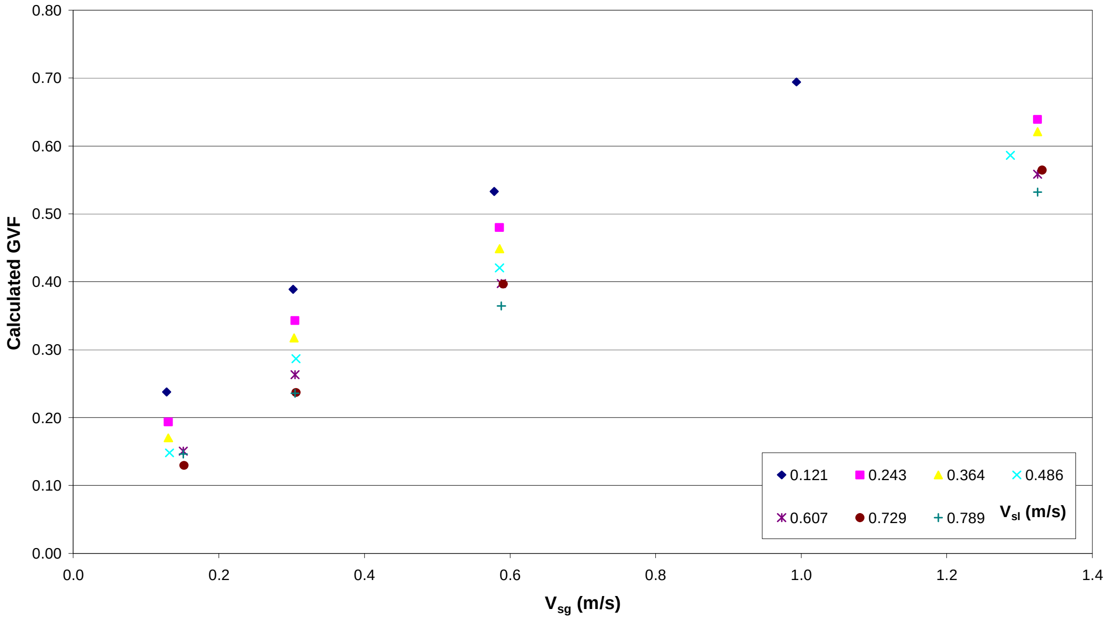

Figure 5.5 – GVF Measurement Dependence on Phase Velocities

Based on the observed gas superficial phase velocity dependency of the GVF measurement, the calculated air fractions can be expressed as a set of linear functions of the gas superficial velocity, **Figure 5.6**.

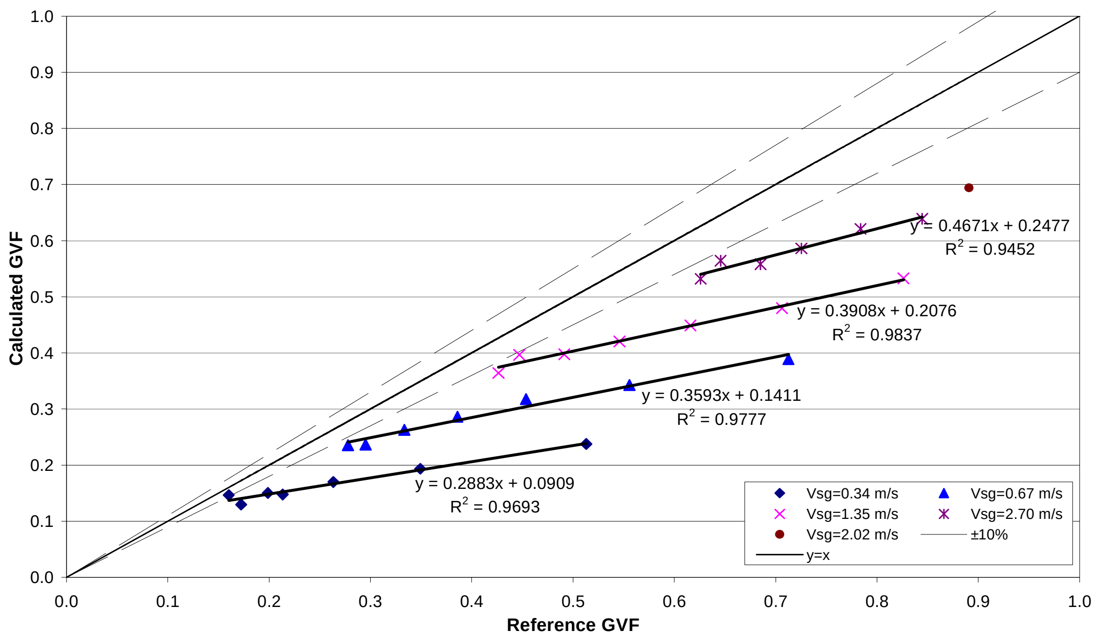

Figure 5.6 – GVF Measurement Dependence on Superficial Gas Velocity

For a fixed gas superficial phase velocity, an approximately linear response was exhibited between the calculated and reference GVF values. Accordingly, linear correction factors were developed for the GVF values determined from the gamma attenuation. The dependence of the gradient (*m*) and intercept (*c*) parameters of the linear correction factor on the reference superficial gas velocity was investigated, **Figure 5.7**.

The linear correction factors were then employed to recalculate the GVF using the expression:

$$GVF_{corrected} = \frac{GVF_{calculated} - c}{m} \qquad \text{(Eq. 5.1)}$$

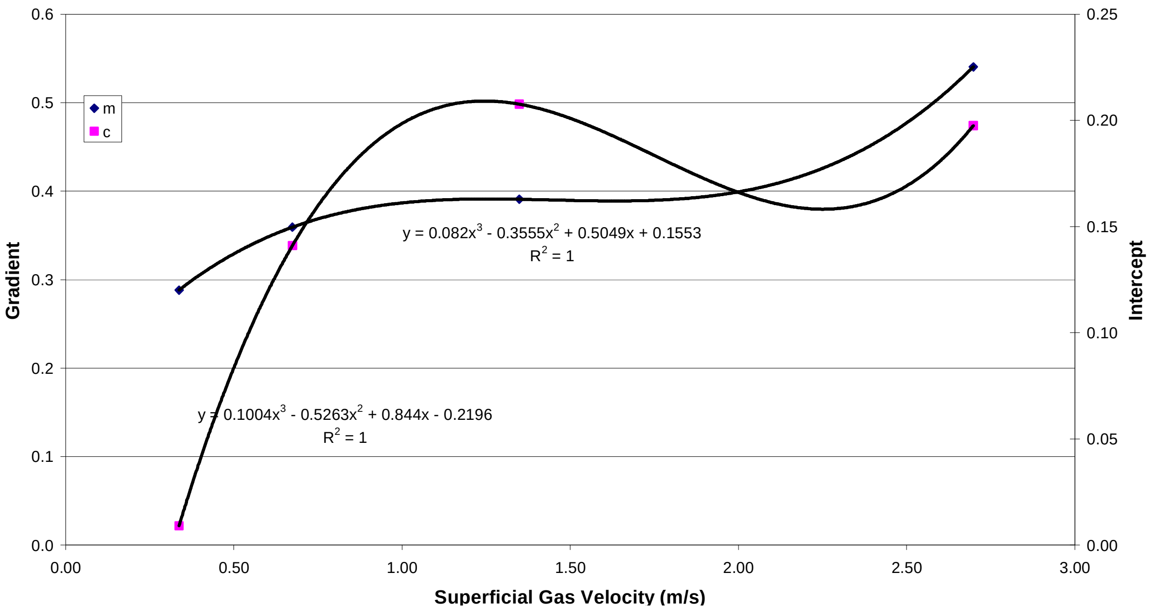

Figure 5.7 – GVF Linear Correction Factor Correlations

Employing a correction factor based on the gas superficial velocity, the gas volume fraction of the multiphase flow can be calculated from the gamma count attenuation data to within ±5% relative error of the test facility reference values with a confidence of 79%, **Figure 5.8**.

Therefore, it can be seen that the application of a slip correlation coefficient based on the gas phase superficial velocity yields a good approximation to the actual gas volume fraction. Nevertheless, this method of phase fraction correction assumes that accurate gas velocity data can be obtained and is only valid for air-water mixtures.

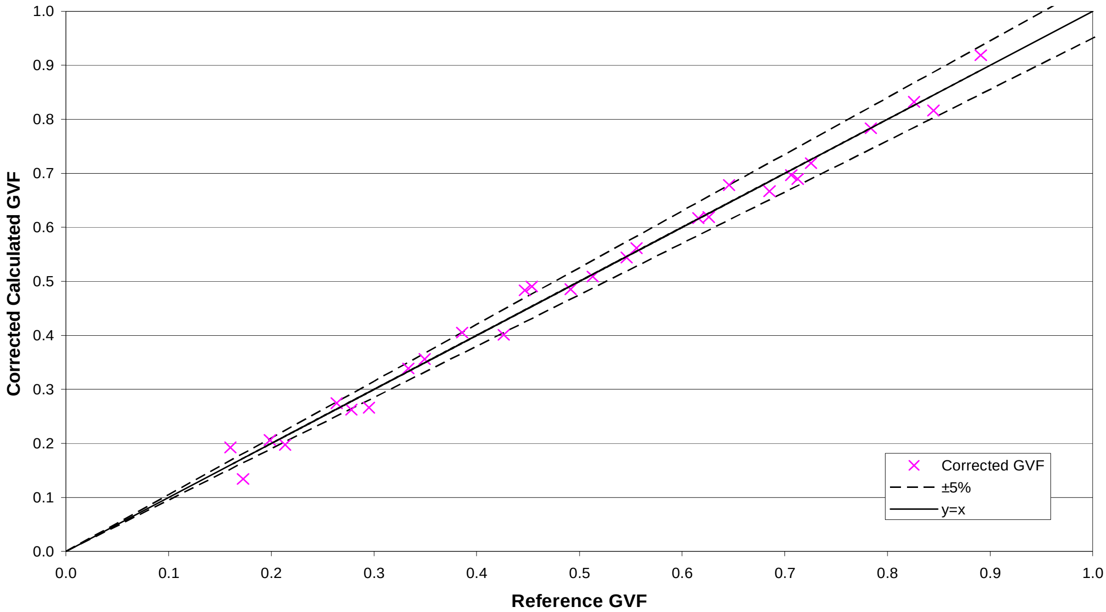

Figure 5.8 – GVF Values Corrected For Superficial Gas Velocities

5.1.2 Three-Phase (Air-Water-Oil) Model

Utilising the dual-energy gamma attenuation equations (see **Chapter 2.3.4.2**) to resolve three-component mixtures, the gamma count data for the hard and soft energy photons were exploited to determine the air, water and phase fractions, **Figure 5.9**.

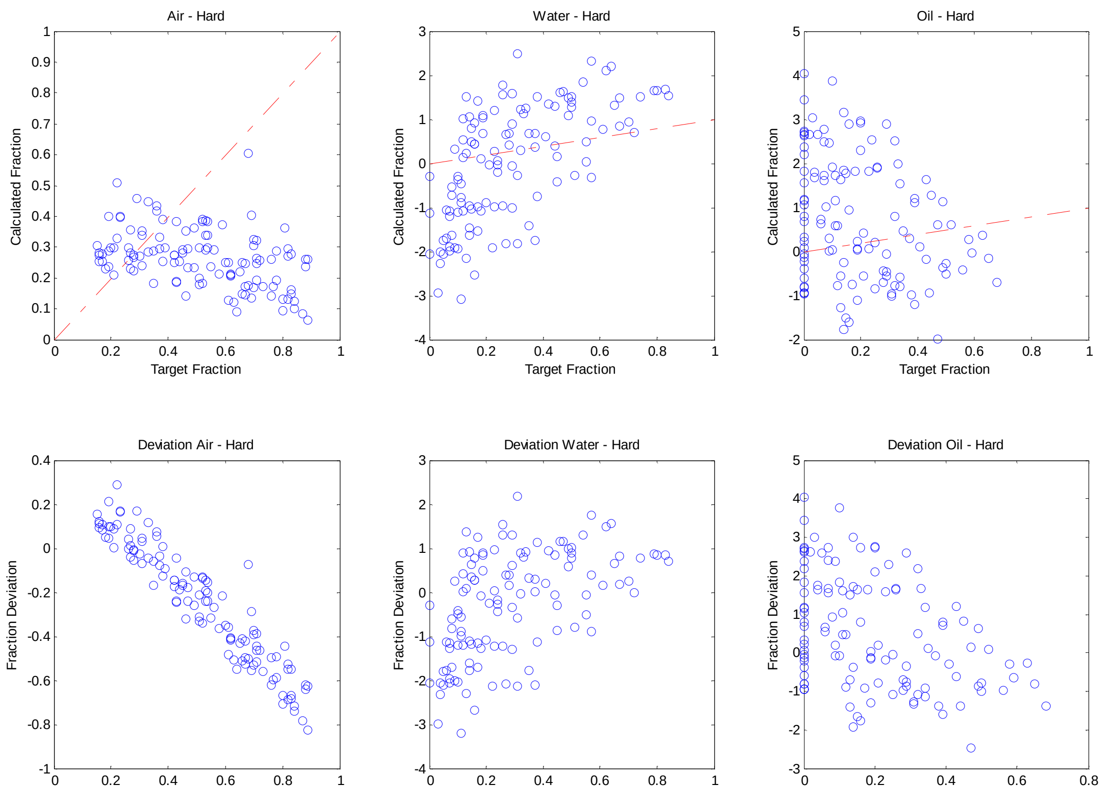

Figure 5.9 – Resolution of Multiphase Flow Individual Phase Volume Fractions

Results illustrate that attempting to resolve the three components using the two gamma energy levels yields large errors in each of the component's calculated fraction values, particularly the liquid phase parameters. The deviation between the calculated and reference GVF was observed to a strong function of the multiphase mixture GVF, as was seen with the two-phase tests. However, at fixed GVFs, the magnitude of deviation obtained with the three-phase data was significantly larger than the deviation witnessed with the two-phase data.

The largest errors were observed in the liquid phase determination. The caesium-137 radionuclide source employed exploits gamma photon energies which seem to be too high to distinguish clearly between the oil and water phases. Literature work revealed that photon energies less than 40 keV are required to facilitate clear distinction between the aqueous and organic phases [**55**]. The caesium-137 direct and scattered energy levels permit high-resolution detection of temporal flow features. However, this is achieved at the expensive of the oil-water discrimination due to the high photon energies required for high-resolution measurements. In addition, the organic phase employed in the Cranfield University is relatively light (815 kg/m^3); thus, the oil-water distinction will be even more problematic in heavy oil production situations where oil densities can range from 920 – 1000 kg/m^3.

Accordingly, it was attempted to resolve the gas and liquid phase fractions only from the three-component multiphase mixture systems by treating as a two-phase system. The output from the high-energy hard spectrum was used for calculations as this energy level makes the least distinction between the oil and water phases allowing them to be treated effectively as a single liquid phase, **Figure 5.10**.

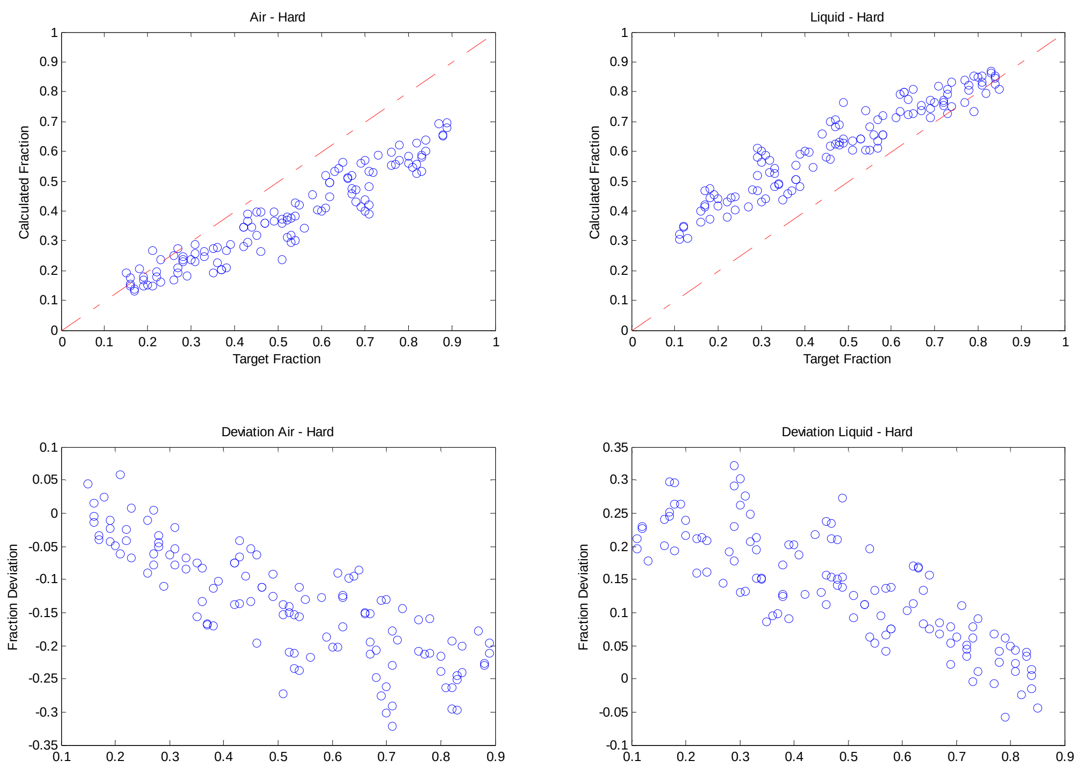

Figure 5.10 – Multiphase Tests Treated as Two-Phase System (Hard Spectrum)

The results indicate that modelling the three-component systems as a two-phase system yields phase fraction predictions in accordance with those obtained for the air-water tests. Although the deviation for the gas phase fraction calculated value decreased in an approximately linear fashion with the test facility GVF, as was observed for the two-phase air-water tests, a much wider range of deviation. The liquid phase water cut is increased deviation was induced by the varying data point liquid phase water cut values. **Figures 5.11 – 5.14** depict the effect of the liquid phase water cut on the gas superficial velocity correlations developed.

At V_{sg} = 0.15 ms^{-1}, increasing the water cut from 0% to 100% produced an increased deviation in the calculated GVF from the test facility reference GVF, **Figure 5.11**.

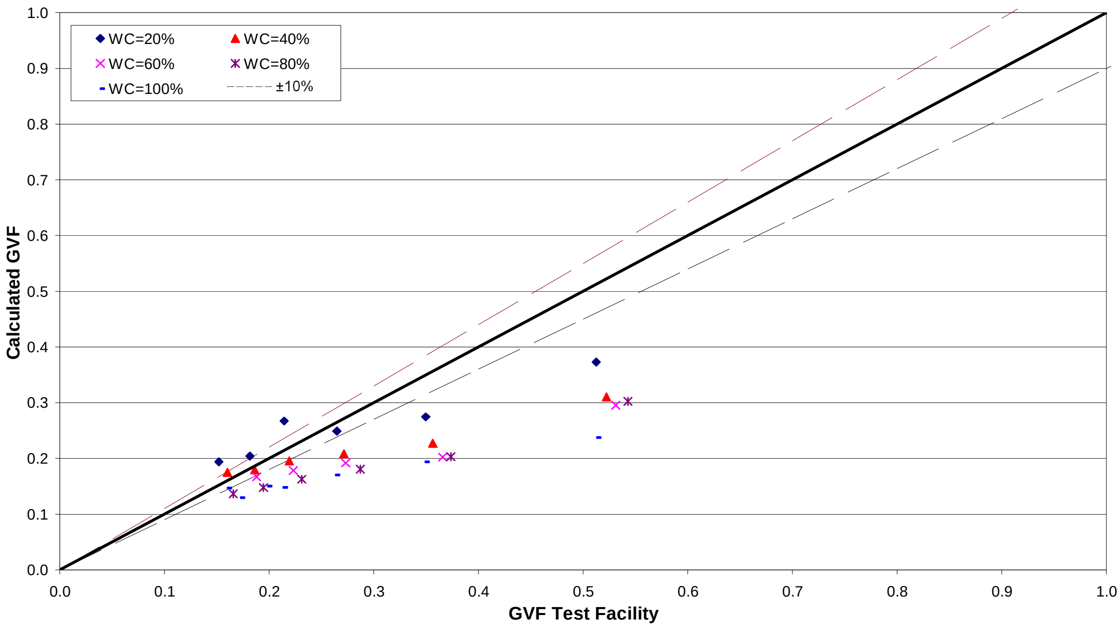

Figure 5.11 – Influence of Water Cut on GVF at V_{sg} = 0.15 ms^{-1}

Each of the water cut series can be trended using a linear function that runs approximately parallel alongside the base case of 100% water cut. This facilitates correction of the calculated GVF values if water cut data from a separate correlation can be derived or from physical sampling of the multiphase fluid.

Increasing the gas superficial velocity to 0.32 ms^{-1}, the influence of the water cut on the GVF value was much less marked, **Figure 5.12**.

Data points for water cuts between 40% and 100% fall approximately on the same plane and should be able to be corrected using the correction developed for the two-phase flow. Data points for water cut of 20% yielded more accurate calculated GVF values. Ignoring the outlying data point, a linear correction factor can be applied to the GVF results obtained for water cuts of 20%.

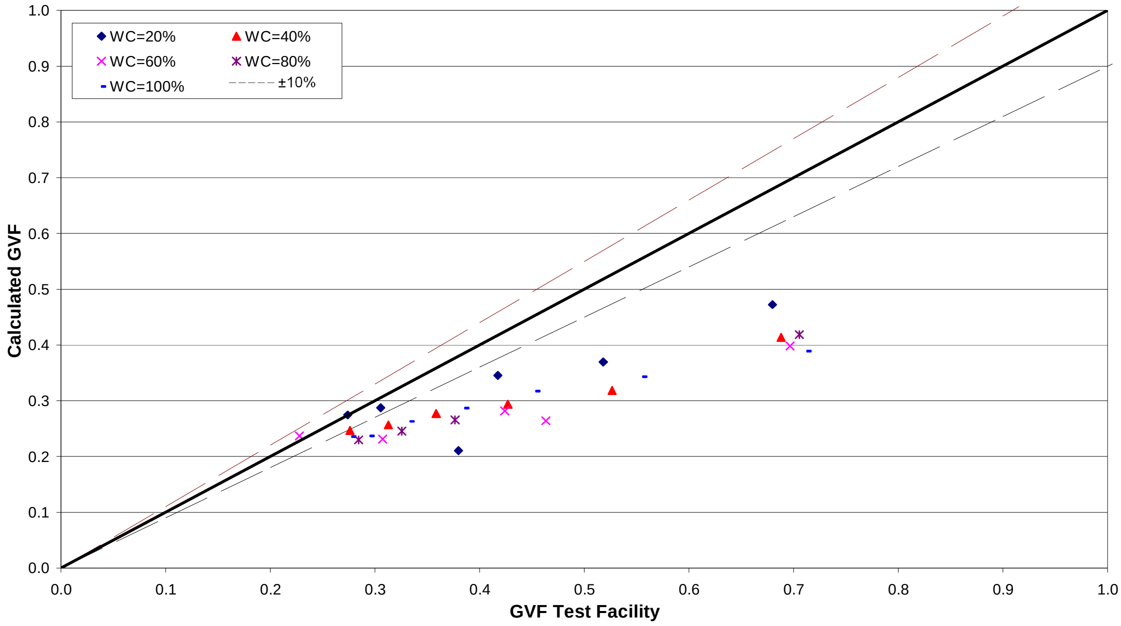

Figure 5.12 – Influence of Water Cut on GVF at V_{sg} = 0.32 ms^{-1}

At superficial gas velocities of greater than 0.62 ms^{-1}, it was observed that the data points formed two distinct groupings, **Figures 5.13** and **5.14**.

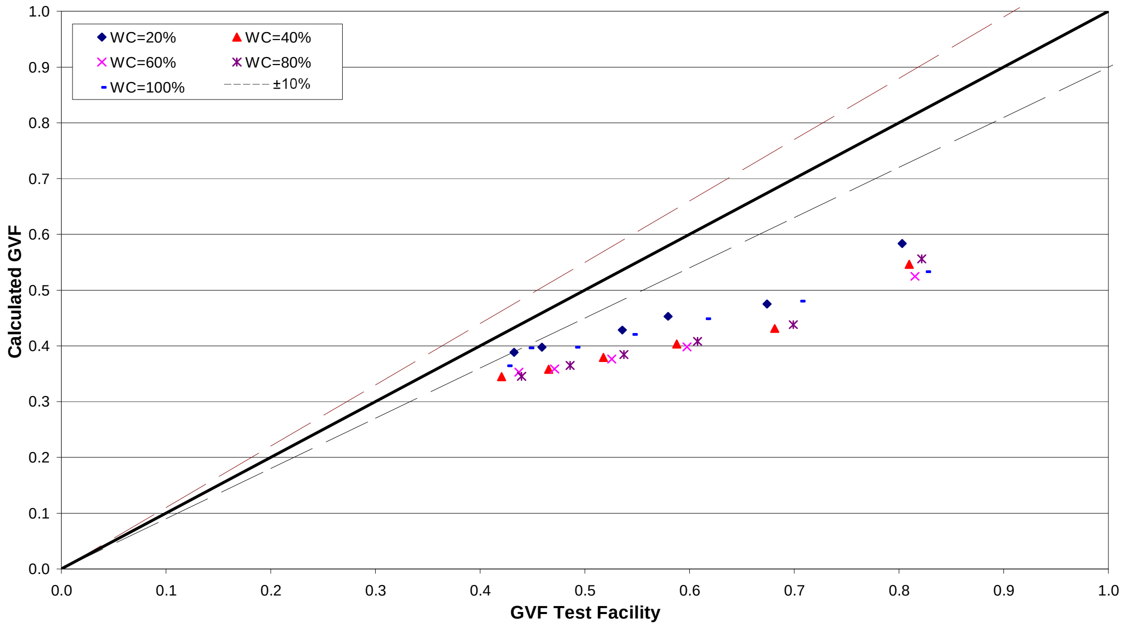

Figure 5.13 – Influence of Water Cut on GVF at V_{sg} = 0.62 ms^{-1}

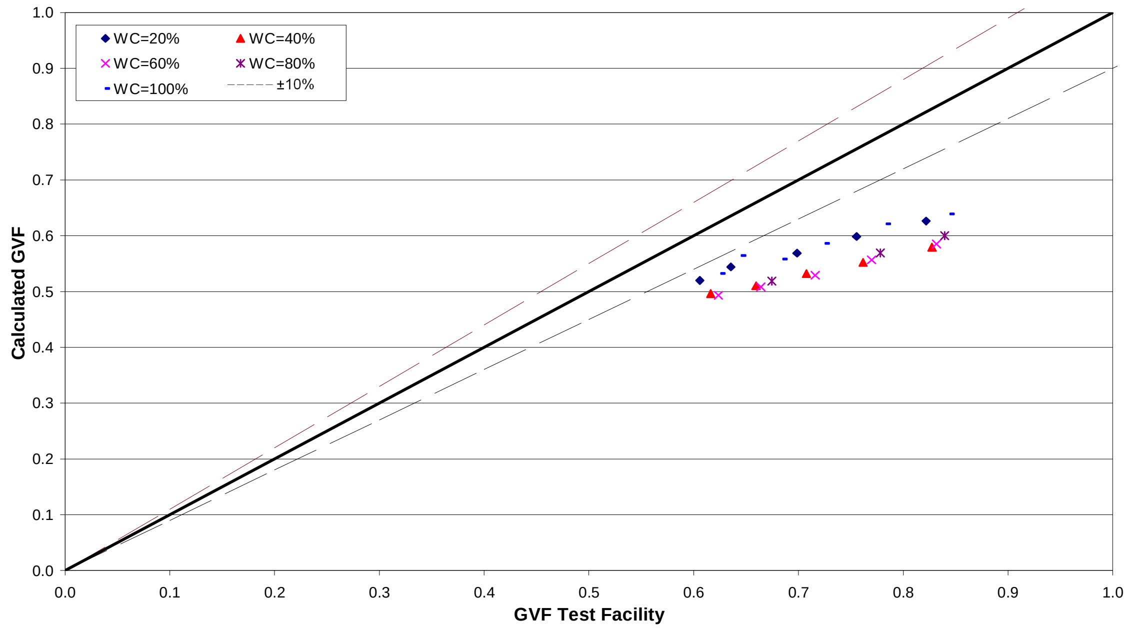

Figure 5.14 – Influence of Water Cut on GVF at V_{sg} = 1.32 ms^{-1}

Exploiting the responses obtained in **Figures 5.11 – 5.14**, a set of linear correction factors were developed for the multiphase data GVF values. The dependence of the gradient (*m*) and intercept (*c*) parameters of the linear correction factors on the reference superficial gas velocity and liquid phase water cut was determined, **Figures 5.15** and **5.16**. The measured GVF values for the multiphase data were then corrected employing the linear correction parameters determined in with **Eq. 5.1**.

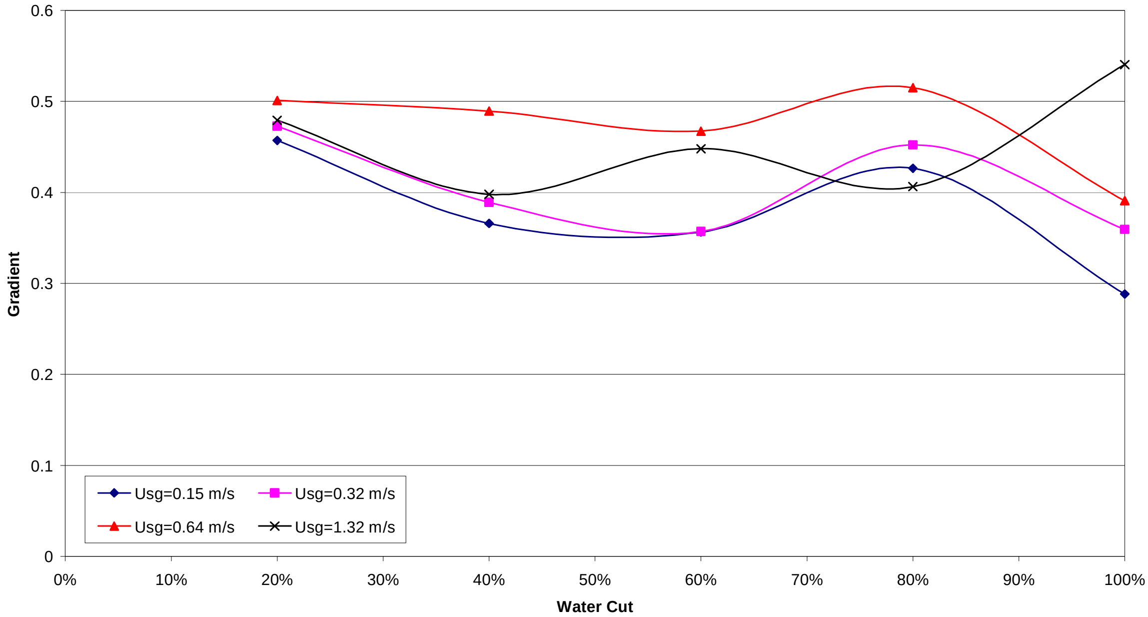

Figure 5.15 – Multiphase Data GVF Linear Correction Factor: Gradient

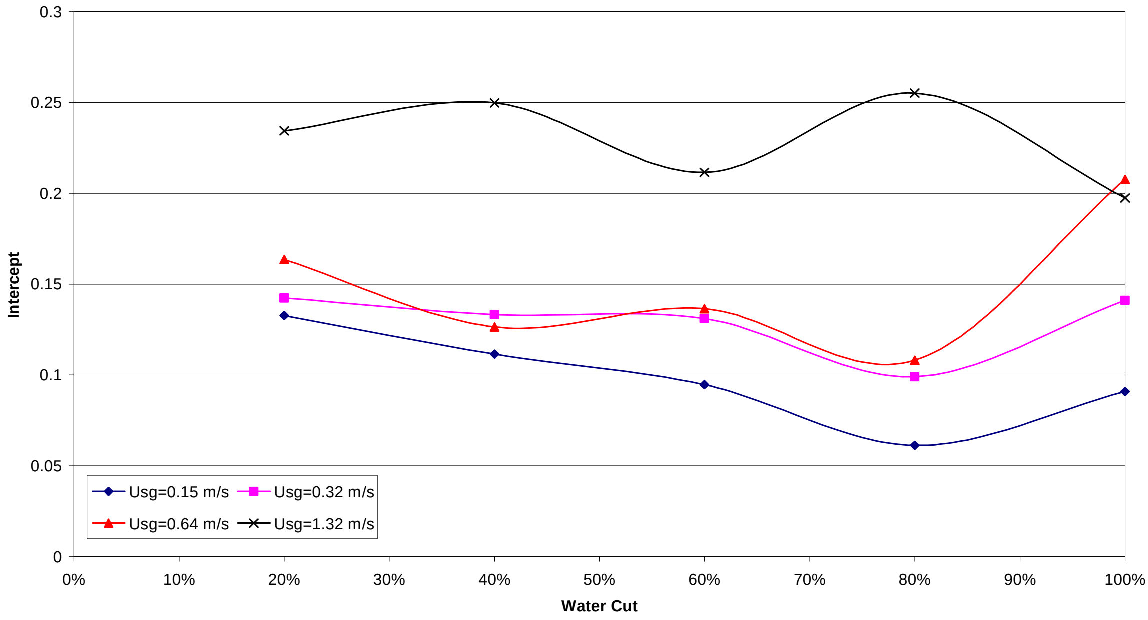

Figure 5.16 – Multiphase Data GVF Linear Correction Factor: Intercept

The performance of the GVF slip correction technique developed was compared against well-established published correlations by Armand [**12**], Chisholm [**13**], Smith [**14**] and Premoli *et al* [**15**], **Figure 5.17**.

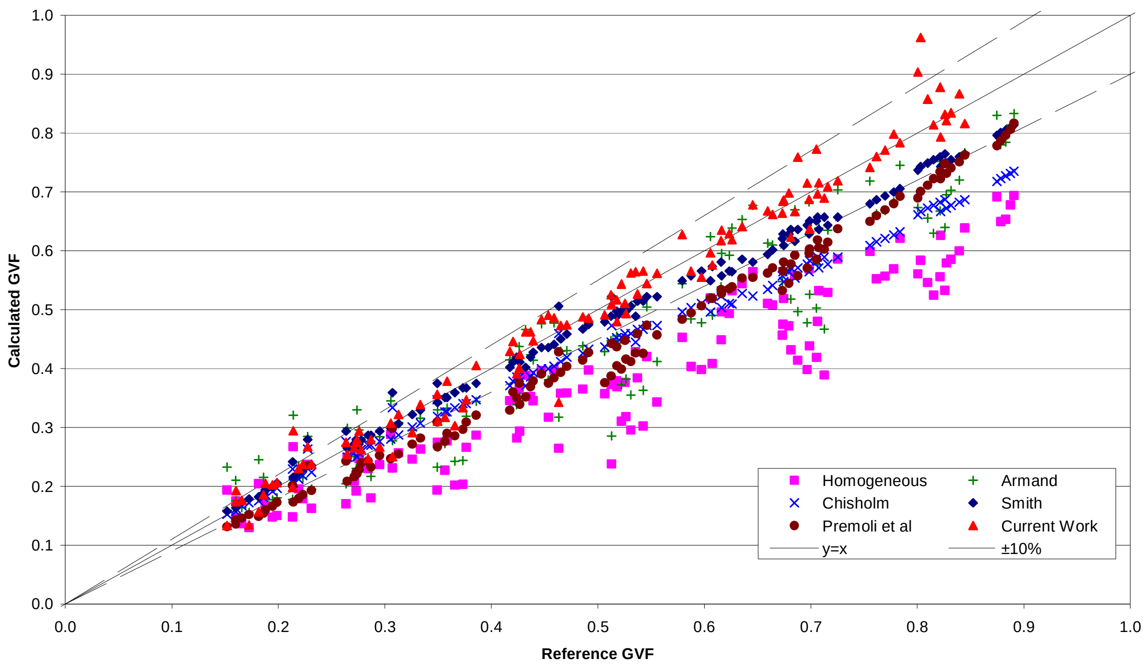

Figure 5.17 – Corrected GVF Values for Multiphase Data

Again, the reference GVFs employed were the non-slip equivalent at the gamma densitometer measurement point in the riser. These were calculated using the reference input flows and the riser base and top side separator pressure and temperature measurements. The temperature was assumed to constant throughout the test section and a linear pressure gradient from the riser base to the. Reference GVFs were calculated at 1.5 m below the riser top. The root mean square (RMS) error and standard deviation of each of the correlations are listed in **Table 5.1**.

Correlation	RMS Error	Standard Deviation
Homogeneous	25%	10%
Armand	14%	11%
Chisholm	12%	6%
Smith	6%	4%
Premoli *et al*	15%	5%
Current Work	7%	6%

Table 5.1 – Classification Accuracy of Phase Fraction Correction Correlations

All phase fraction correction methods examined were observed to improve upon the initial GVF measurement which assumed homogeneity of the multiphase flow mixture. The Armand correlation assumes a slip of 1.2 for all flow mixtures which yields a more accurate GVF measurement. Chisholm's method derives an improved approximation for the slip ratio (1.1 – 3.2) based on the measured GVF and the gas and liquid phase reference densities. The best overall performance was obtained applying the Smith correlation to obtain the slip ratios (1.1 – 1.8); however, this correlation necessitated the tuning of an entrainment factor (K = 0.685) which is data set dependent.

The relatively poor performance of the Premoli *et al* correlation can be attributed to its reliance on supplying accurate physical properties for the liquid phase. To apply the Premoli *et al* correction to the multiphase data, the oil and water were treated as a single pseudo-liquid phase with parameters extrapolated according to the water cut. Applying the correction technique proposed in the current work enabled multiphase GVFs to be determined to within without the need to tune an entrainment factor. However, successful exploitation of this technique requires prior information about the gas phase velocity and the liquid phase water cut.

5.1.2.3 Liquid Phase Water Cut

Water cut determination through the application of dual energy gamma attenuation equations was shown to be unfeasible, **Figure 5.9**. From the literature review, it was determined that gamma photon attenuation coefficients are a function of photon energy and attenuating material's atomic number. It was hypothesised that at a fixed GVF, the changes in the liquid phase water cut not only produce changes in both the hard and soft mean gamma counts, but the relative difference between the two energy levels should exhibit a quantifiable variation.

Figure 5.18 shows the difference between the mean gamma count values for the hard and soft spectra against the test point reference GVFs. Each multiphase data point has been annotated with its water cut so as the relationship between the differences in the spectra mean gamma values and associated multiphase flow water cut, at fixed GVFs, can be examined.

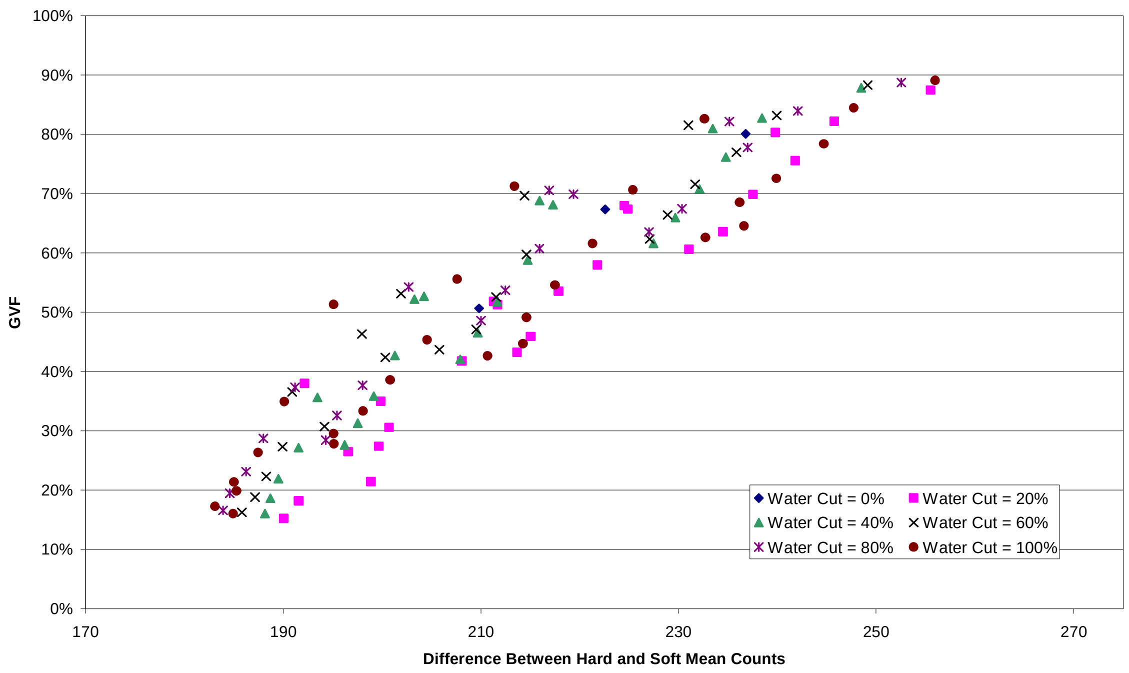

Figure 5.18 – Dependence of Water Cut on Energy Count Difference and GVF

At GVFs up to 40%, there is a definite trend for difference between the hard and soft energy mean gamma count of the data points, at approximately fixed GVFs, to increase with decreasing water cuts in a coherent manner. At GVFs greater than 40%, the predictability of the water cut distribution of the data points diminishes. However, it was observed that the 100% and 20% water data points tended to be located in close proximity to each other; while all other intermediate water cuts tended to be clustered too. Only a small number of air-oil data points were collected so no definitive conclusion was able to be formed on their response.

5.2 Determination of Phase Velocities

In multiphase flows the oil, water and gas components will travel at different velocities. Multiphase measurement usually assumes that the difference between the water and oil liquid phases is negligible compared to the relative difference between the liquid phase velocities and that of the gas phase. Thus, the problem in ascertaining the phase velocities is reduced to determining two variables: gas phase velocity and liquid phase velocity.

A well-established technique in multiphase metering is to determine the velocity of the gas phase based on the velocity of large diameter gas bubbles and the liquid phase velocity is derived from the velocity of small diameter, liquid entrained, gas bubbles which are assumed to be travelling at the same velocity as the liquid phase [**47**]. No published information was found in the public domain on the determination of multiphase flow phase velocities employing a single sensor.

5.2.1 Gas Structure Peak Analysis

The passage of a gas structure through the gamma densitometer measurement section induces a peak in the raw gamma count signal, **Figure 5.19**.

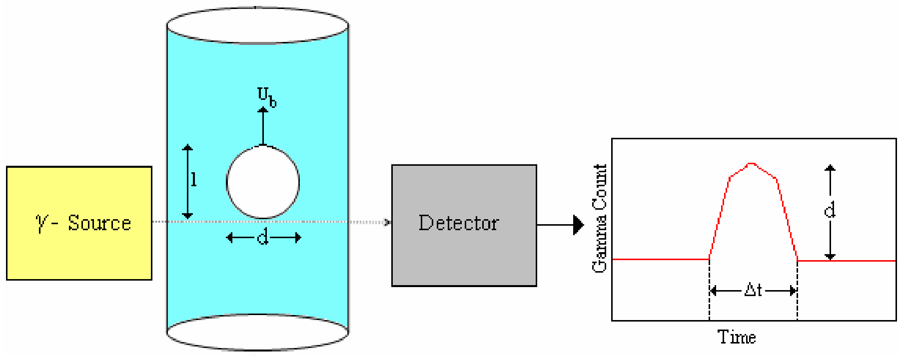

Figure 5.19 – Gas Structure Induced Gamma Count Peak

The gamma count peak's characteristics are inherently linked to those of the gas structure that induced it. The maximum count value from the bubble-induced peak (I_{max}) is representative of the gas structure's maximum radial length. If one assumes that the gas structures can be considered to be spherical, this radial length equates to the gas bubble diameter (d).

$$d = \frac{\ln\left(\frac{I_0}{I_{\max}}\right) - \gamma_l D}{\gamma_a - \gamma_l} \qquad \text{(Eq. 5.2)}$$

Where, D denotes the internal pipe diameter, I_0 is the empty pipe count, and γ_a and γ_l are the gas and liquid linear attenuation coefficients respectively. The internal pipe diameter of the Cranfield University multiphase flow facility test section is 0.1082 m.

The peak width represents the transit time (Δt) of the gas bubble through the measurement section and is a function of the gas structure's axial length (l) and velocity. Gamma count peak characteristics, induced by the passage of the principle gas structures in air-water flows, were investigated to quantify their dependence on the phase velocities. Peak information from the raw data plots were analysed over 2 minute periods and the mean gas structure properties determined for each of the flow configurations. The mean bubble diameter and mean bubble transit time information is detailed in **Figure 5.20** and **Figure 5.21** respectively.

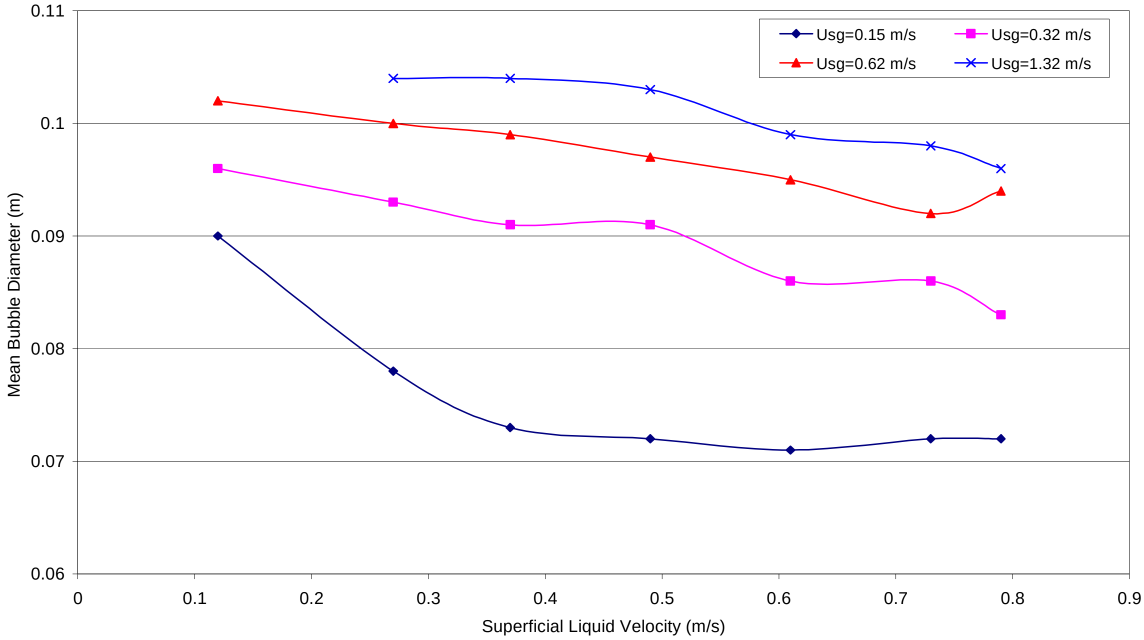

Figure 5.20 – Mean Diameter of Principal Gas Structures in Air-Water Flows

At constant gas loadings, the mean bubble diameter was observed to decrease with increasing liquid superficial velocities. Conversely, increasing the gas loading at fixed liquid superficial velocities resulted in increasing mean bubble diameters. The sensitivity of the mean bubble diameter to the liquid loading decreased with increased liquid loading. Gas superficial velocity influence on the magnitude of the mean bubble diameter increases with increased liquid loading.

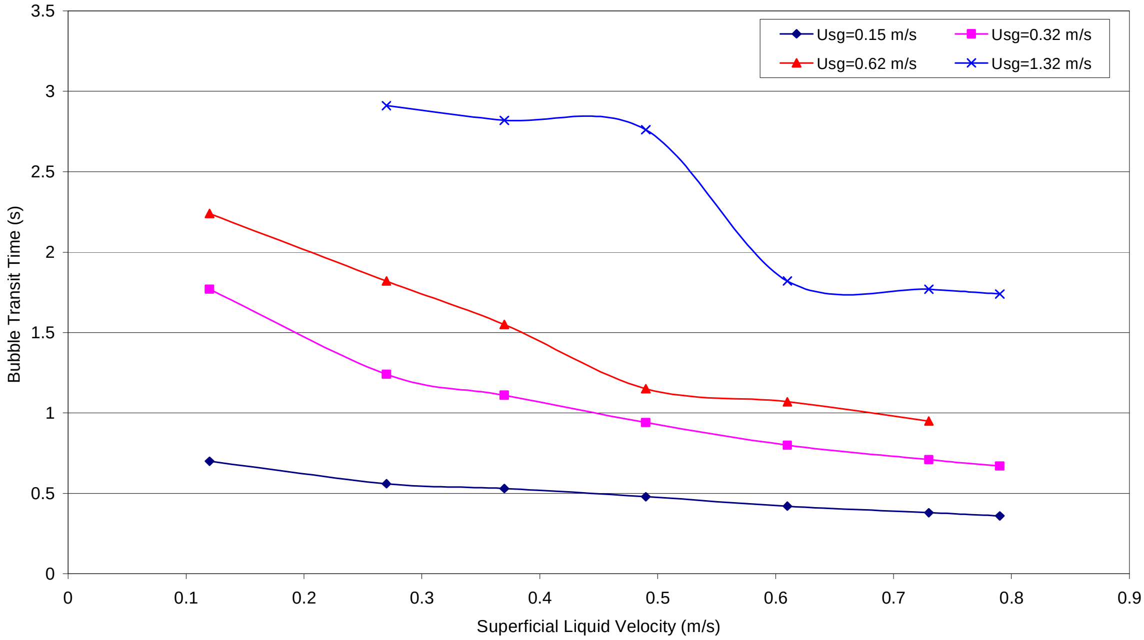

Figure 5.21 – Mean Transit Time of Principal Gas Structures in Air-Water Flows

The bubble transit time was found to decrease with decreasing gas superficial velocities and increasing liquid loading. Increasing the gas loading, increases the sensitivity of the mean bubble transit time to the liquid superficial phase velocity; while, increasing the liquid phase loading decreased the influence of the gas phase loading.

Determination of the gas bubble's velocity necessitates knowledge of the time it takes to travel a known distance. If one has knowledge of the geometric form of the gas bubbles, the length of the bubble (l) can be inferred from the bubble's axial diameter (d). Assuming that the bubble is spherical, the axial distance travelled by the bubble for the peak duration is equal to the bubble's diameter, i.e. $l = d$. Thus, the bubble's axial velocity component through the measurement section can be calculated.

$$u_b = \frac{l}{\Delta t} \qquad \text{(Eq. 5.3)}$$

The average bubble velocity was calculated for the air-water data points modelling the gas structures as spherical bubbles, **Figure 5.22**.

Treating the large gas structures as purely spherical objects, the bubble velocities were observed to increase with increasing liquid superficial velocities and decrease with increasing gas superficial velocities. The relationship between the calculated bubble velocities and the gas phase superficial velocities is somewhat counterintuitive but this relationship is obtained due to the fact that the gas structures were approximated as spherical objects.

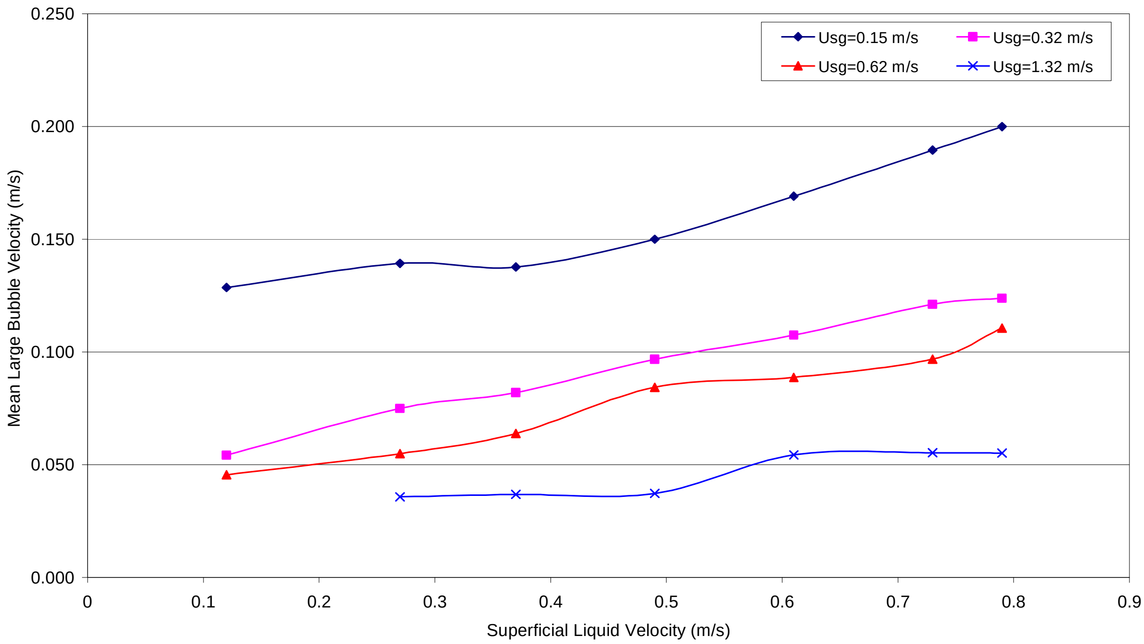

Figure 5.22 – Average Bubble Velocity of Principal Gas Structures in Air-Water Flows

However, as the gas bubble diameter approaches that of the internal pipe diameter, slug regime flow dominates and the gas structure's geometric form takes on that of a Taylor bubble [**112**] and the length of theses Taylor bubble is a function of the pressure, pipe diameter, superficial phase velocities and the degree of flow development [**113**].

Increasing Taylor bubble lengths are obtained with increasing gas superficial velocity and deceasing liquid superficial velocity. As the superficial gas velocity increases, the transit time of the gas structure increases, but its diameter is restricted to that of the internal pipe diameter. Consequently, modelling the Taylor bubbles as spherical structures will lead to an apparent decrease in the bubble velocity. Determination of Taylor bubble velocity necessitates knowledge of the Taylor bubble length. However, these lengths cannot be determined without prior knowledge of the phase velocities.

Thus, independent determination of the gas phase velocity by modelling the large gas structures as spherical bubbles is not a feasible approach as these characteristics were observed to be functions of the liquid phase loading too.

Previous work (**Chapter 4.3.2**) showed how the frequency of gas structure detected by the gamma densitometer was phase velocity dependent. Thus, it was proposed to analyse the periodic properties of the multiphase flow gas structures for their dependence on the phase velocities.

5.2.2 Investigation of Quasi-Periodic Waveforms

Fokin [**114**] reported the presence of distinct quasi-periodic wave features in hydrodynamic parameters that appeared to be strongly related to the spatial-temporal structure of two phase (air-water) flows. It was hypothesised that the observed appearance of regulated spatial-temporal structures from the chaotic disorder of the multiphase mixture was driven by the system's requirement to dissipate energy in self-organisation to attain its state of minimum potential energy with minimum entropy production.

Examining the gamma count output plots in **Figure 4.1**, the passage of gas structures are seen to induce characteristic peaks in the gamma count signals whose geometry reflect the magnitude and velocity of the passing bubble. Quasi-periodic waveforms can be observed for the appearance of the gas structure induced peaks in the gamma densitometer's response to the multiphase flow.

It was hypothesised that the quasi-periodic oscillations of the large gas structures could be correlated with the gas phase velocities; meanwhile, analysis of quasi-periodic waveforms for the smaller, liquid entrained gas structures were investigated with respect to the liquid phase velocities.

An eight-level wavelet packet decomposition with the db3 mother wavelet was employed to create an extensive bank of bandpass filters to facilitate the separation of the raw gamma signals into their high and low frequency components for analysis. The filtered signals were then autocorrelated and analysed to obtain a pseudo-period for the fluctuations induced by the gas structures in the gamma count signal. Cubic spline interpolations were employed to interpolate smoothly between the autocorrelation data points obtained from the filtered signals.

5.2.2.1 Gas Phase Velocity

The normalised autocorrelation response of the low frequency approximation signals for the first eight levels of wavelet packet decomposition was determined for each of the multiphase flow gamma count signals. Autocorrelated signal traces for the example signals employed throughout **Chapter 4** are illustrated in **Figure 5.24 (a) – (d)**. The filtered signal's frequency range at each decomposition level (L) is detailed in **Table 5.2**.

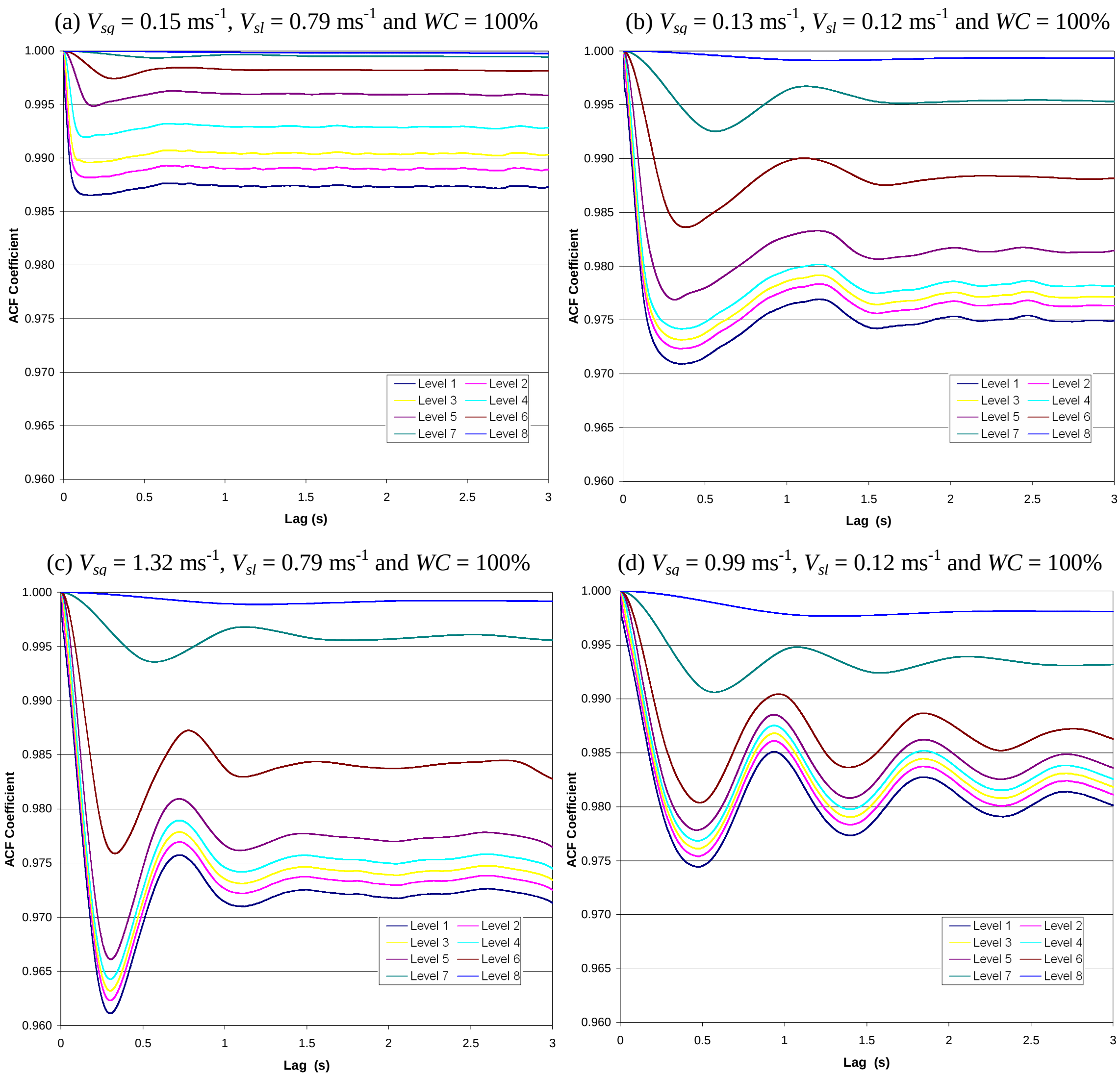

Figure 5.23 – Autocorrelation of Low Frequency Approximation Signals

The autocorrelation response of the filtered gamma signals exhibited a clear discriminability for the first seven decomposition levels based on the liquid and gas flow parameters of the multiphase flow. At the eighth level decomposition, the autocorrelation response becomes devoid of characteristic features to facilitate effective discrimination between data points.

Decomposition Level (L)	**Approximation Signal Frequency Range Wavelet Packet [L 0]**
1	0 – 62.5 Hz
2	0 – 31.2 Hz
3	0 – 15.6 Hz
4	0 – 7.8 Hz
5	0 – 3.9 Hz
6	0 – 2.0 Hz
7	0 – 1.0 Hz
8	0 – 0.5 Hz

Table 5.2 – Wavelet Packet Approximation Signal Frequency Ranges

The geometric form of the autocorrelated signals was observed to be intrinsically linked to the flow regime of the vertical multiphase flows that induced the gamma count signals. Data points identified as belonging to the bubble regime demonstrated a sharp reduction in the autocorrelation coefficient over the initial stages of the lag increase followed by gradual increasing of the coefficients to a local maximum and then stabilisation to an approximately constant value for the autocorrelation function coefficient with changes in the lag, **Figure 5.23 (a)**. Slug regime data points were characterised by exponentially decaying cosine waveforms. The distinctive oscillations formed in these signals as repeating slug units correlate to induce local maximums in the signal with changing lag-time, **Figure 5.23 (c)** and **(d)**. Data points lying close to the flow regime boundary exhibited characteristics of both the bubble and slug regime ACF forms, **Figure 5.23 (b)**.

The pseudo-period of the gas structures was defined as the lag time at the first local maximum in the ACF coefficients which is representative of the average repeating period of the gas structures in the whole signal for the frequency range analysed. In all cases, the lag time to the ACF minimum feature was also recorded for analysis.

Increasing the wavelet decomposition level was observed to result in increased autocorrelation coefficients for the signal as the filtered signals move increasingly towards uniformity. There was no difference between the pseudo-periods of the first four levels of wavelet decomposition which can be observed to increase with decreasing gas superficial velocity. The pseudo-periods calculated in the higher levels wavelet packets were observed to increase with the packet level but still exhibited increasing magnitudes with decreased gas loadings.

Accordingly, the relationship between the pseudo-periods determined by the autocorrelation functions of the fourth, fifth, sixth and seventh level wavelet packet decomposition signals and the gas phase superficial velocity were analysed. Investigation of the extracted pseudo-period data revealed that autocorrelation function features became indistinct for the seventh level decomposition signals for low GVF data points (<40%). The ACF pseudo-period data for the fourth, fifth and sixth levels are illustrated in contour plot **Figure 5.24 (a)**, **(b)** and **(c)** respectively with their corresponding ACF minimum feature time lag information shown in **Figure 5.24 (d)**, **(e)** and **(f)**.

The ACF pseudo-period was observed to be a complex function of both phase superficial velocities and the flow regime. No clear quantifiable relation was exhibited by the pseudo-period on the gas phase velocity. The maximum pseudo-period was obtained at minimum gas and liquid loading; while the minimum pseudo-period was obtained for a number of liquid loadings at the minimum gas loading. The bubble regime pseudo-period exhibited a distinctly more complex relationship with the phase superficial velocities with a number of local maxima and minima; while the slug regime pseudo-period contours exhibited a more stable response, with the pseudo-period increasing with decreasing liquid superficial velocity.

The fourth and fifth level plots exhibited almost identical contour responses for the pseudo-period, the only exception being the magnitude of the ACF pseudo-period were determined to be slightly greater employing the fifth level wavelet approximation signal. The sixth level approximation signal ACF pseudo periods exhibited a similar response; however, there was no maximum pseudo-period region in the high liquid – low gas loading region.

The ACF-minimum lag time exhibited a slightly more quantifiable response than that obtained with the pseudo-period. Maximum parameter magnitudes were obtained at medium range gas loadings and minimal liquid loadings, with an increased sensitivity to the liquid loading being exhibited with increasing gas superficial velocities. The magnitude of the ACF-minimum lag time variable was observed to increase with level of the wavelet approximation signal. However, the responses of both the pseudo-period and minimum lag time were determined to be insufficient to enable inference of the gas phase superficial velocity.

The effect of the liquid phase water cut on the pseudo-period was investigated. The ACF pseudo-period data from the fifth level wavelet packet approximation signals was utilised to compile contour plots on a water cut specific basis. **Figure 5.25 (a) – (e)** illustrate the water cut specific responses obtained for the fifth level decomposition signals.

It can be observed that the pseudo-period of the multiphase flow large gas structures is a strong function of the liquid phase water cut with each water cut specific contour plot yielding a different response. For fixed water cuts, it was observed that the pseudo-period of the large gas structure was still dependent of the on both the phase superficial velocities, although this relationship was not as irregular.

In general, the largest pseudo-periods were obtained for low water cuts with minimum gas superficial velocity and maximum liquid loading. The influence of the liquid loading on the magnitude of the pseudo-period can be observed to increase with increasing gas loading varies and is also a complex function of the liquid phase water

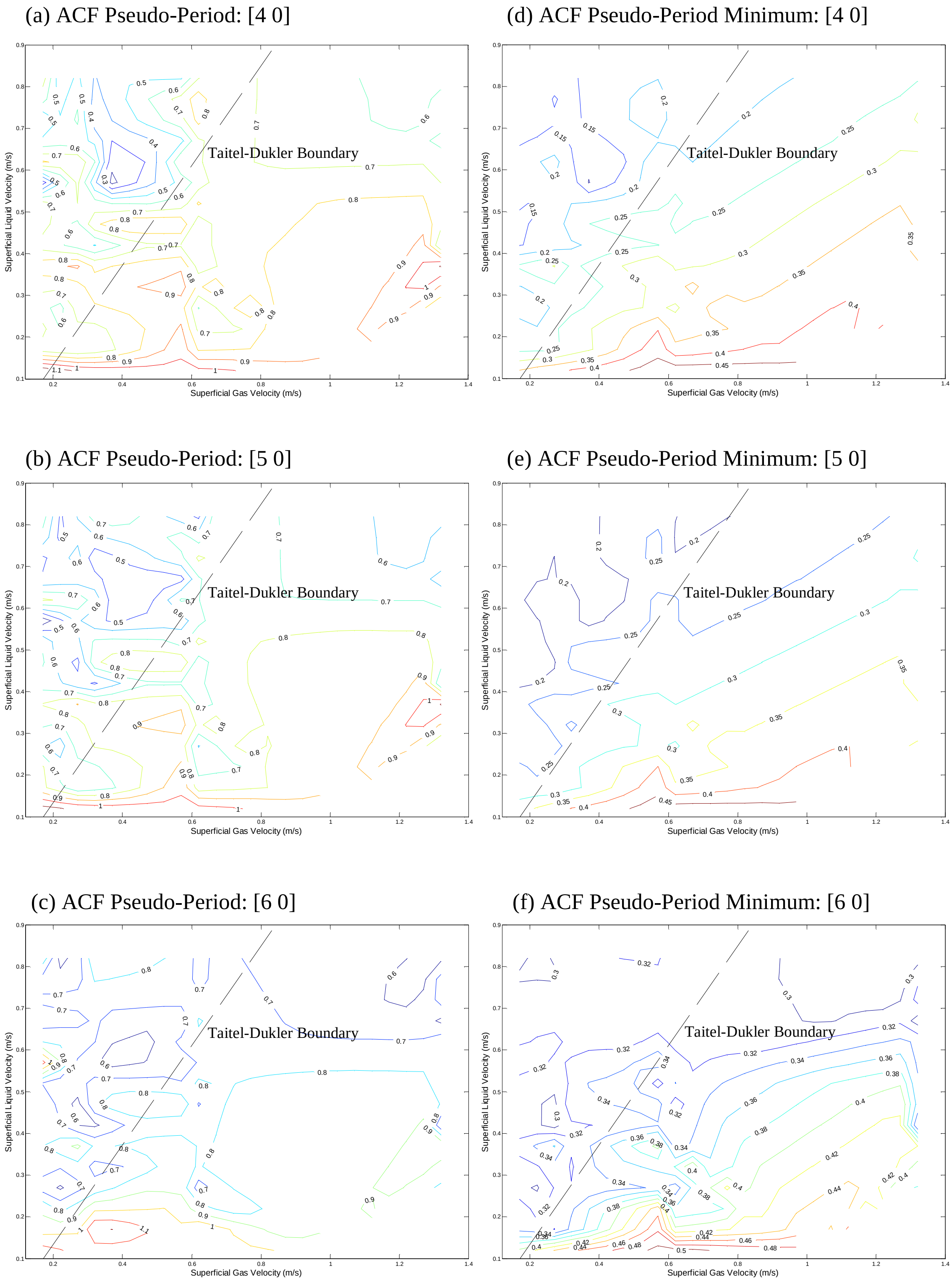

Figure 5.24 – Contour Plots of ACF Pseudo-Period Parameters

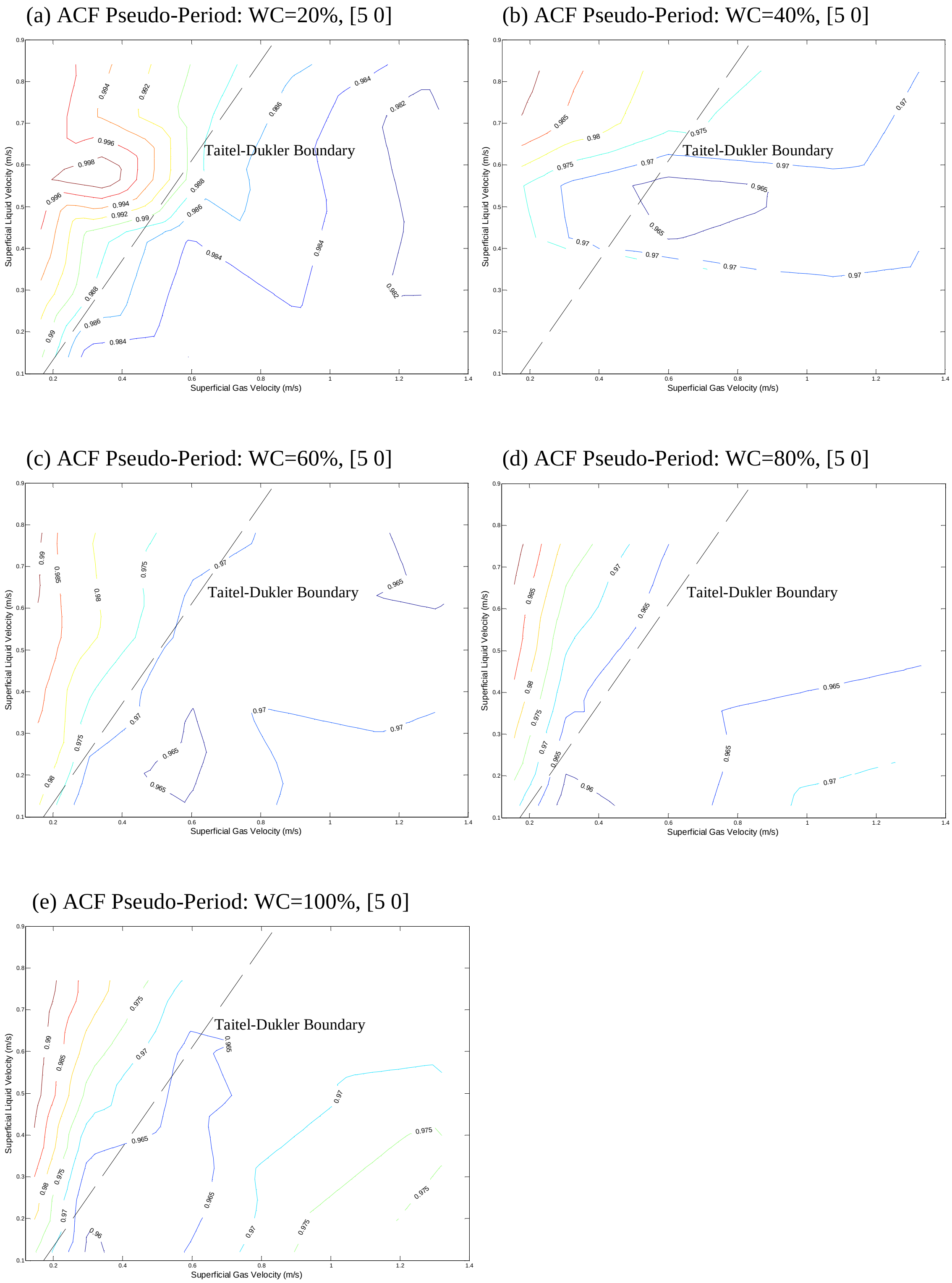

Figure 5.25 – Water Cut Influence on ACF Pseudo-Period

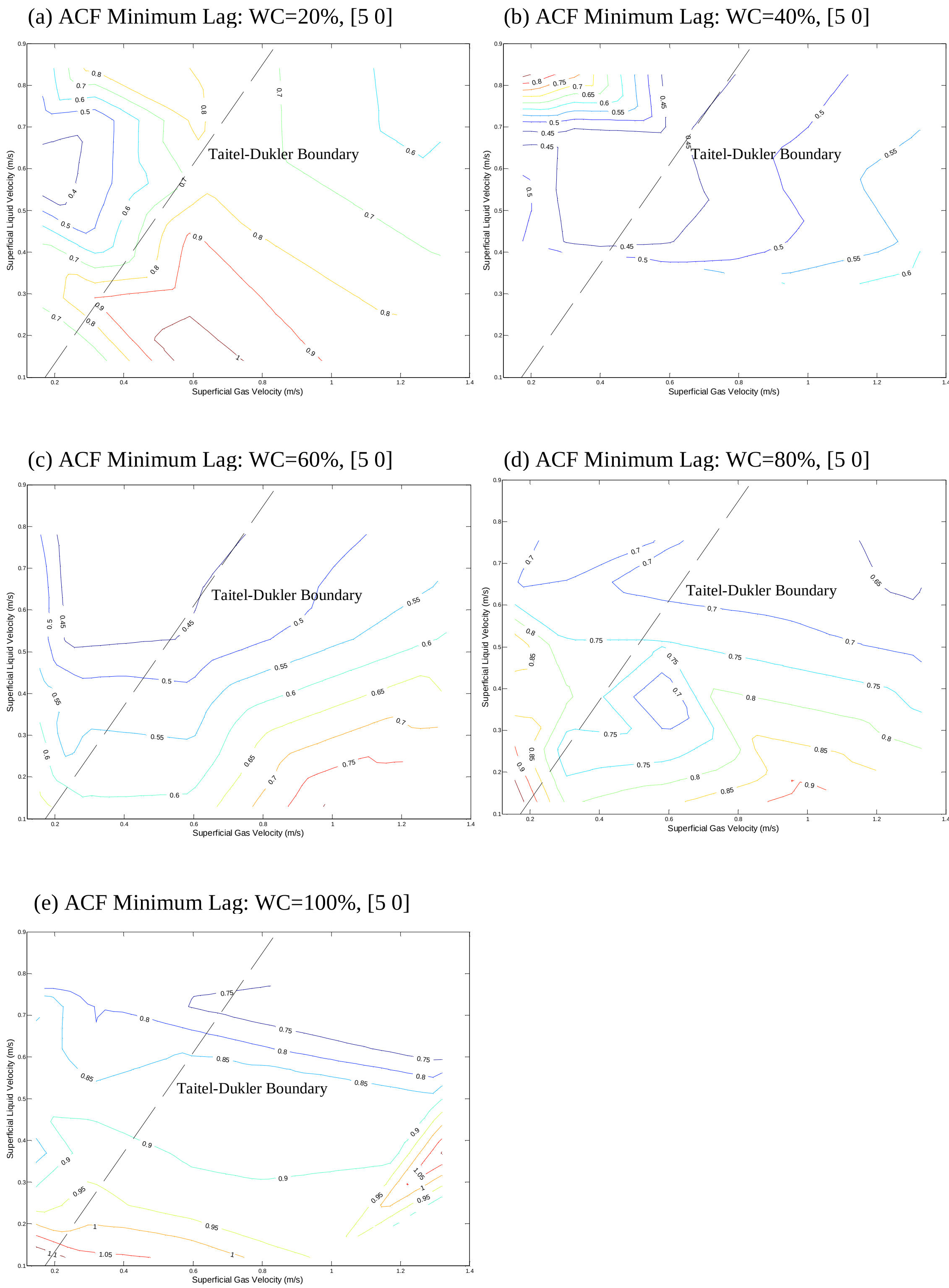

Figure 5.26 – Water Cut Influence on ACF Minimum Lag

cut. Accordingly, an independent, reliable inference of the gas superficial velocity from the large gas structure pseudo-period was deemed to be impractical.

The water cut specific study was extended to analyse the ACF-minimum time lag parameter, **Figure 5.26 (a) – (e)**. This parameter also exhibited irregular water cut specific relationships with both phase velocities; thus, it was not able to be exploited to facilitate independent determination of the gas superficial either.

5.2.2.2 Liquid Phase Velocity

The relationship between the pseudo-periodicity of the small, higher frequency gas structures and the liquid phase superficial velocity was investigated. The autocorrelation functions of the gamma signal detail wavelet packets were more complex than those obtained for the low frequency dominated approximation signals. A typical ACF output is shown for wavelet packet [4 1] (7.8 – 15.6 Hz content of original signal) illustrates that a number of smaller, equally dominant autocorrelation peaks are detected, **Figure 5.27**.

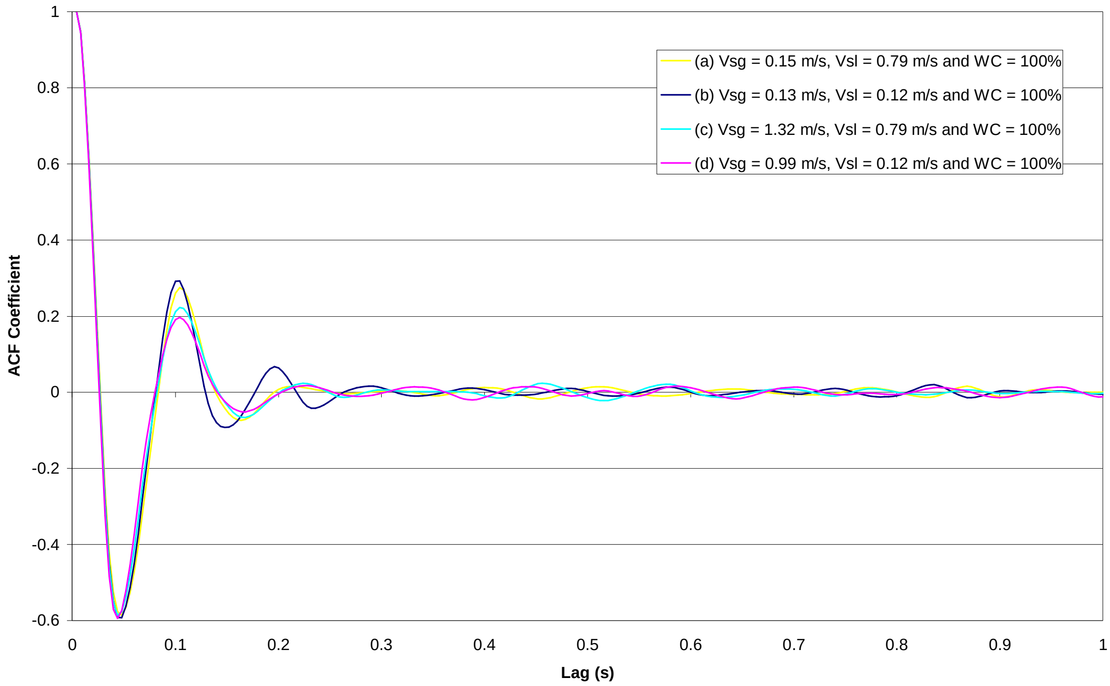

Figure 5.27 – Autocorrelation of Wavelet Detail Signals from Packet [4 1]

The ACF plots of the detail signal exhibited no variation with flow regime and the pseudo-periods obtained were typically one order of magnitude lower than those obtained in the low frequency signals. The autocorrelation coefficients attained at the pseudo-periods were also approximately 4 – 5 times lower than those exhibited by the large gas structure analysis.

Visual identification of the dominant pseudo-period from the all the ACF plots of the different test points was not feasible. Consequently, Fourier analysis of the ACF data was undertaken to facilitate the determination the dominant underlying pseudo-repeating frequency for each data point in each of the wavelet packets. A 256-window Fourier transform was employed to produce power spectral density plots to facilitate the resolution of the ACF peak information, **Figure 5.28**.

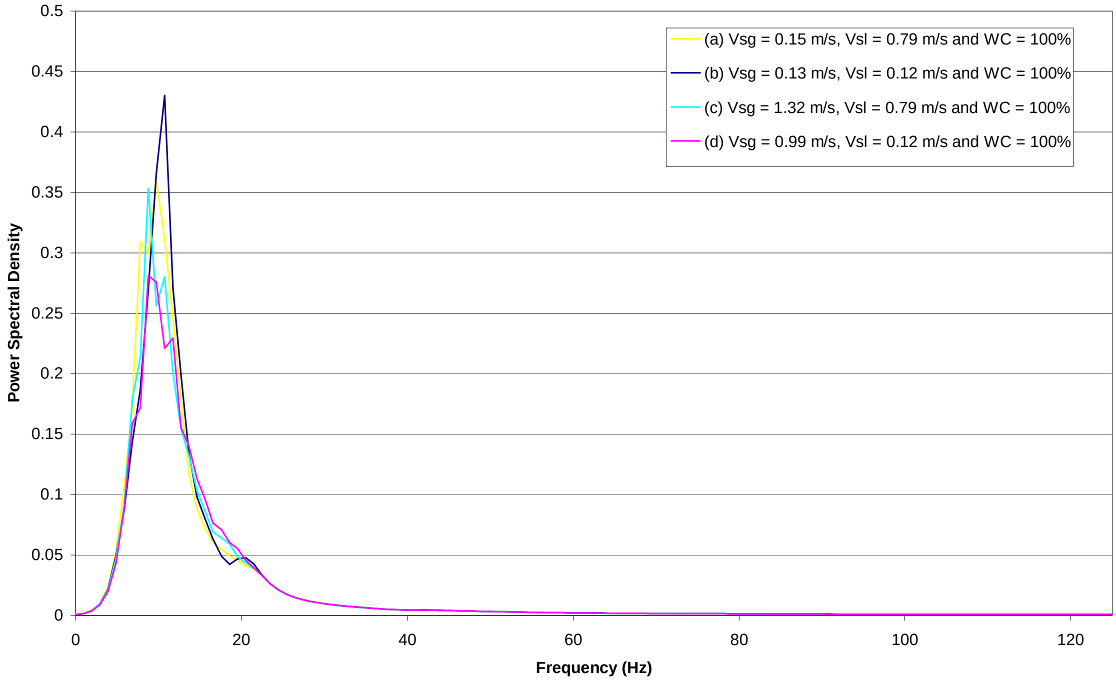

Figure 5.28 – PSD of Autocorrelated Wavelet Detail Signals from Packet [4 1]

The PSD analysis of the ACF data determined the dominating underlying pseudo-frequency in the signal. Discrimination between the data point pseudo-frequencies can be observed based on their flow parameters. The corresponding data point pseudo-periods were calculated by taking the reciprocals of their pseudo-frequency.

The pseudo-period determined from the autocorrelation function of the detail signal wavelet packets from the eight-level decomposition data were compiled into a series of contour plots to facilitate analysis of their dependence on the superficial phase velocities. Analysing the contour plots, it was observed that the greatest liquid phase discrimination exhibited for the pseudo-period data was obtained in the frequency range up to 62.5 Hz of the original signal.

The contour plots for the detail wavelet packets of the second, third and fourth decomposition level are illustrated in **Figure 5.29**. The wavelet packet detail signals' frequency ranges for the contour plots shown are detailed in **Table 5.3**. At higher decomposition levels the pseudo-period discrimination deteriorated owing to the narrowing frequency ranges of the packets.

The pseudo-period of the small gas structures in the multiphase flows were observed to be complex functions of both the liquid and gas superficial velocities in each of the wavelet packets. The maximum pseudo-period magnitude did not tend to be localised for specific flow conditions and were observed to be a function of the wavelet packets'

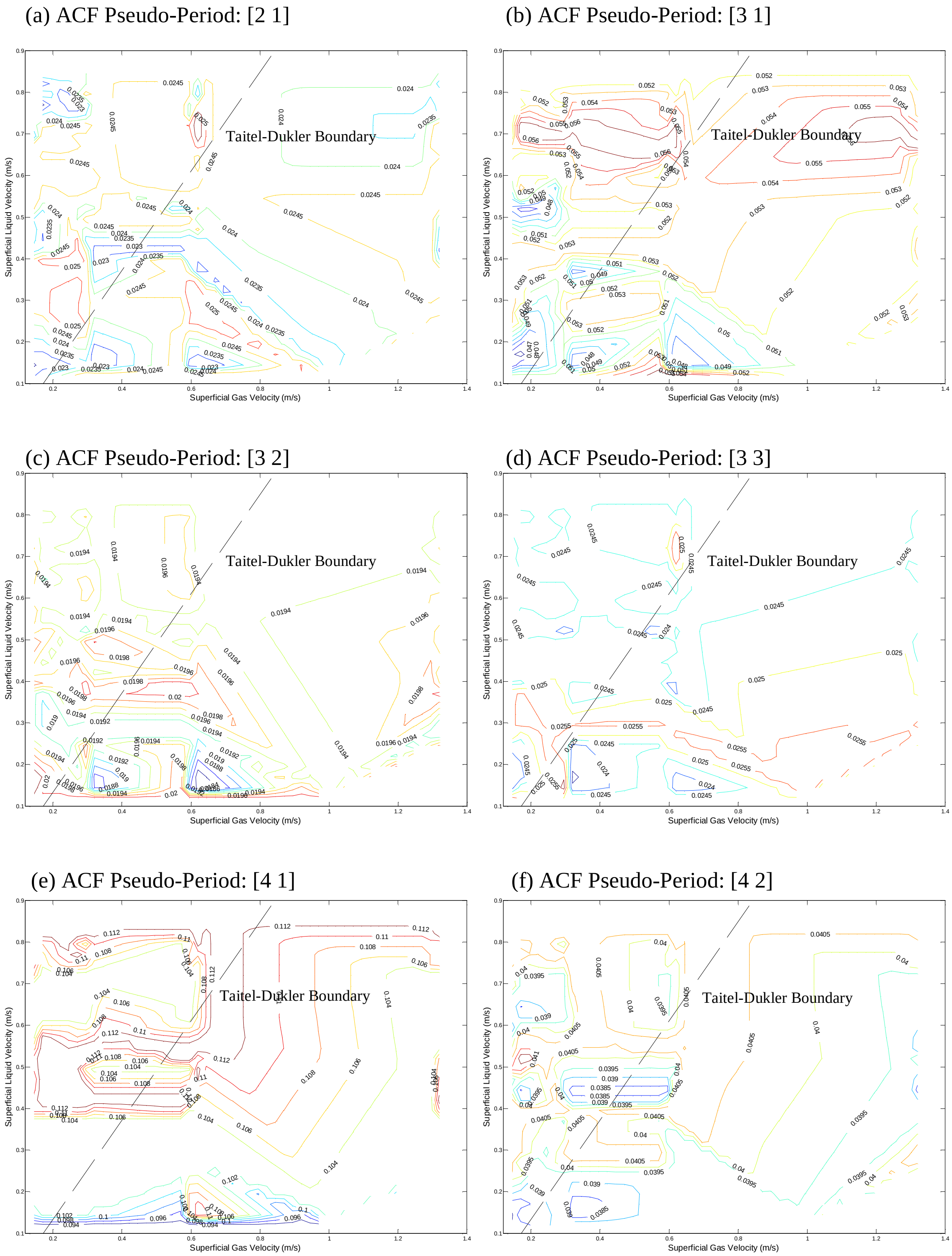

Figure 5.29 – Contour Plots of ACF Pseudo-Period Parameters

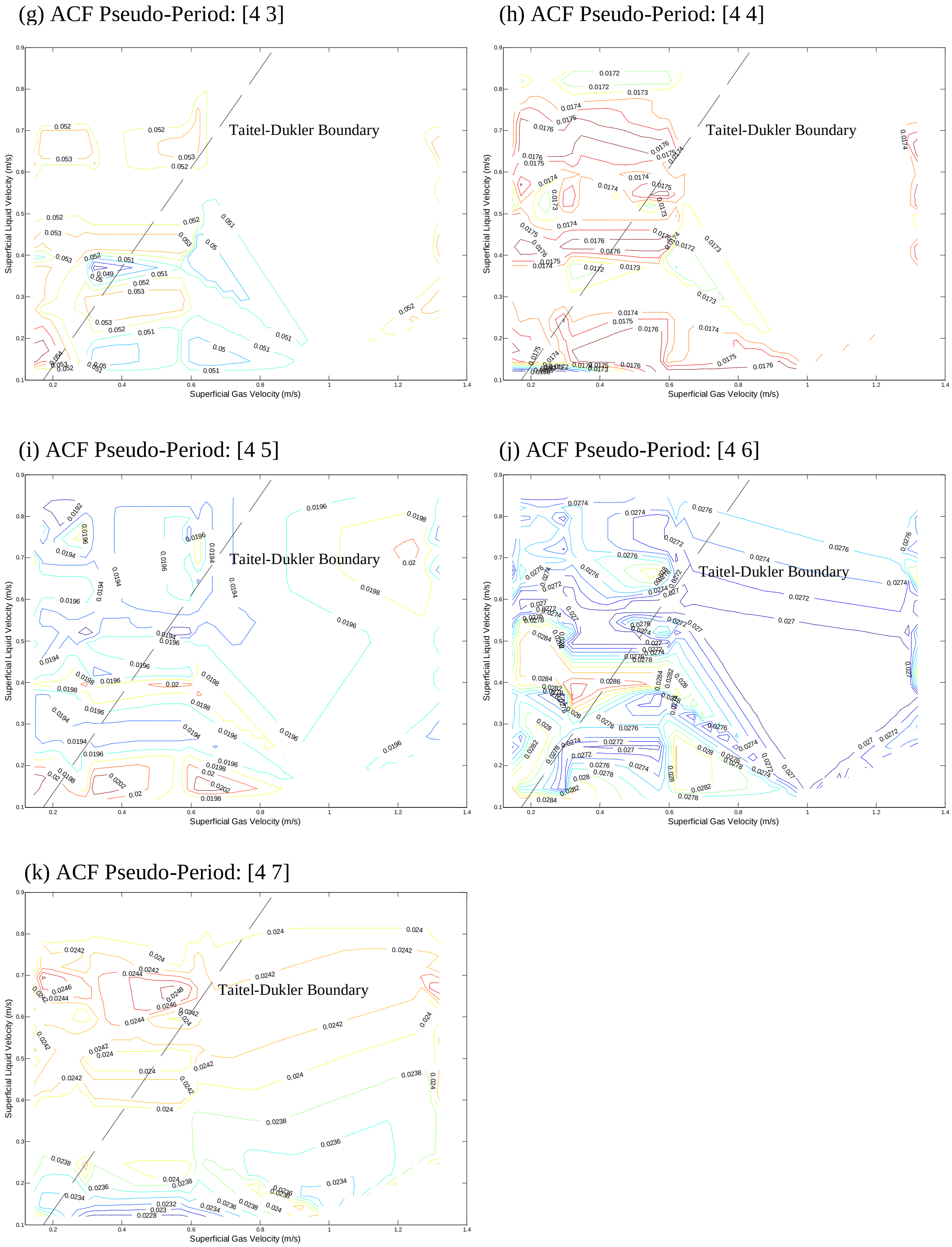

Figure 5.29 – Contour Plots of ACF Pseudo-Period Parameters

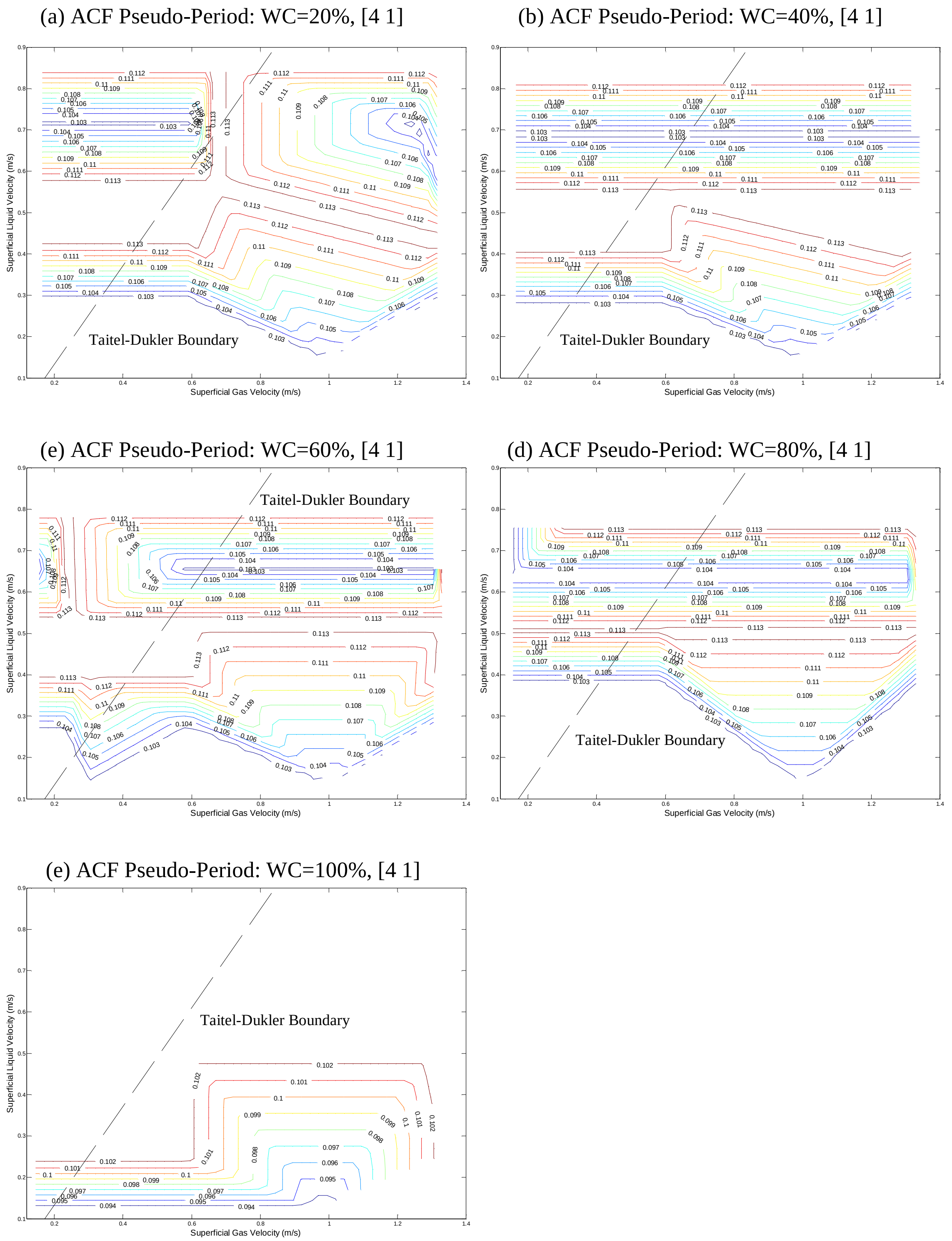

Figure 5.30 – Water Cut Influence on ACF Pseudo-Period for Wavelet Packet [4 1]

Wavelet Packet [L D]	Detail Signal Frequency Range
[2 1]	31.2 – 62.5 Hz
[3 1]	15.6 – 31.2 Hz
[3 2]	31.3 – 46.9 Hz
[3 3]	46.9 – 62.5 Hz
[4 1]	7.8 – 15.6 Hz
[4 2]	15.6 – 23.4 Hz
[4 3]	23.4 – 31.2 Hz
[4 4]	31.2 – 39.1 Hz
[4 5]	39.1 – 46.9 Hz
[4 6]	46.9 – 54.7 Hz
[4 7]	54.7 – 62.5 Hz

Table 5.3 – Wavelet Packet Detail Signal Frequency Ranges

frequency range. As with the large gas structure pseudo-period data, flow regime specific response were obtained with the contours in the bubble regime exhibiting complex unclassifiable geometric forms.

Good liquid superficial velocity discrimination was obtained in the slug regime regions for both the lower and higher frequency detail wavelet packets in the range studied: [2 1], [3 1], [3 3], [4 1], [4 2] and [4 7]. Intermediate frequency based wavelet packets offered poor discrimination properties based on the superficial phase velocities. The phase velocity parameter discrimination exhibited by lower and higher frequency detail wavelet packets was superior to that demonstrated by the large gas structures in the analysis of the low frequency approximation signals. Nevertheless, the relationship exhibited between the ACF pseudo-periods and the liquid phase superficial did not lend itself to quantification to facilitate independent determination of the multiphase flow liquid phase velocity parameters.

The influence of the liquid phase water cut on the small gas structure pseudo-period was investigated. The ACF pseudo-period data from the wavelet packet details exhibiting good liquid phase velocity discrimination signals was utilised to compile contour plots on a water cut specific basis. **Figure 5.30 (a) – (e)** illustrate the water cut specific responses obtained for [4 1] wavelet packet which was representative of the responses obtained from all the wavelet packets analysed on a water cut specific basis. In accordance with the analysis conducted on the large gas structure pseudo-period data, water cut specific responses were produced for the contour plots; however, in this instance the magnitude of the pseudo-period was observed to be dominated by the liquid phase superficial velocity as opposed to that of the gas phase in both flow regime regions. These relationships were complex and the same pseudo-period was obtained for a range of liquid velocity conditions with no apparent underlying trend that could be exploited to extract reliable liquid velocity information.

As with the large gas structure analysis, the ACF minimum feature also analysed for its correlation with the phase superficial velocities. However, the phase velocity discriminability of the data was poor and not suitable for exploitation to infer the liquid phase velocity of the multiphase flows.

5.3 Summary

The development of a mechanistic model for multiphase flow measurement based on the determination of the individual phase volume fractions and velocities from the gamma densitometer attenuation data collected from the dynamic flows in the multiphase riser was investigated.

Phase volume fraction information was interpreted from the degree of gamma attenuation induced by the multiphase flows. Direct application of gamma attenuation equation to determine the phase fractions of the two-phase (air-water) data yielded significant errors owing to the presence of phase slip and flow geometry considerations. A linear correction model based on the superficial gas velocity was derived for the two-phase data and yielded air volume fraction measurements to within ±5% at a confidence level of 79%.

Resolution of the multiphase data phase fractions exploiting dual-energy attenuation resulted in irreconcilable errors. It was concluded that the best strategy to establish the individual multiphase fractions was to firstly treat the system as a two-phase mixture and determine the gas and liquid phase fraction before attempting to resolve the liquid phase water cut.

Modification of the correction model developed for the air-water data for the multiphase flow data facilitated determination of the gas volume phase fraction of the multiphase data to within ±10% with a confidence level of 100%. However, the modified correction model required input of both superficial gas velocity and water cut information. Nevertheless, the correction model performance was favourable in comparison with published correction correlations.

Investigation of the liquid phase water cut was conducted examining the deviation between the two different gamma energy counts. It was proposed that, owing to the dependence of gamma attenuation coefficients on the gamma photon energy, at fixed gas volume fractions the deviation between the spectra counts should be representative of the liquid phase composition. Analysis of the experimental data showed that such a correlation yielded water cut data for multiphase flows with gas volume fractions up to 40%. At higher gas volume fractions, there was little distinction between data points of different water cuts.

Phase velocity was investigated through the exploitation of quasi-period waveforms in the gamma count signals induced by the presence of gas structures in the multiphase flow. It was hypothesised that gas phase data could be extracted from the quasi-period oscillations of the large gas structures; whereas, the high frequency quasi-periodic oscillations of small liquid entrained gas structures Wavelet packet decomposition was exploited to separate the gamma densitometer signals into their high and low frequency components.

The autocorrelation function of the wavelet approximation signals was employed to determine the pseudo-period of the large gas structures. The autocorrelation pseudo-period for the fourth, fifth and sixth level approximation signal demonstrated the flow regime specific geometry of the ACF signals. Phase velocity discrimination was exhibited by the pseudo-period information from fourth, fifth and sixth level approximation signals with flow regime specific responses. Analysing the data for constant liquid phase water cuts, a strong dependence of the pseudo-period magnitude on the gas superficial velocity was exhibited. However, the underlying relationship between the two parameters was too irregular to be quantified and did not lend itself to independent determination of the gas velocity parameters through it exploitation.

Liquid phase velocity dependence on the pseudo-period of the small, high frequency gas structures was investigated exploiting the ACF defined pseudo-period of the detail wavelet packets. Flow regime specific phase discrimination was obtained for wavelet packets with a frequency range of up to 62.5 Hz and good liquid superficial velocity discrimination was obtained in the slug regime regions for both the lower and higher frequency detail wavelet packets in the range studied. Analysing these wavelet packets on a constant water cut basis exhibited the dependence of the high frequency small gas structure pseudo-period on the liquid phase superficial velocity; however, the complexity of the underlying relationship prohibited the independent determination of liquid phase velocity data from the magnitude of the small gas structure pseudo-period.

A mechanistic approach to multiphase flow parameter determination employing a single gamma densitometer did yield a successful measurement model. A satisfactory performance was obtained for the phase fraction analysis but the model required gas phase velocity and liquid phase water cut data. Water cut data from period well sampling may be available, but the provision of the gas phase velocity data would still be required. An investigation of the quasi-periodic oscillations in the multiphase flow did not demonstrate a quantifiable relationship between the pseudo-period of the gas structures and the phase velocity parameters. However, deployment of a secondary sensor such as a pressure transducer, ultrasonic meter, or a hydrophone would facilitate cross-correlation with the gamma signal to facilitate phase velocity measurement. The utilisation of the aforementioned sensors types would not infringe the benefits yielded by the clamp-on installation nature of the measurement solution.

The next chapter considers an alternative approach to multiphase flow parameter determination from the gamma densitometer data by investigating the potential of pattern recognition techniques.

Chapter 6: Pattern Recognition Techniques

This chapter documents the investigation of pattern recognition techniques as a vehicle to infer the individual phase flow rates of vertical multiphase flows from the variations they induce in the gamma densitometer count signals. Two neural network models were developed for comparison: a single feedforward multilayer perceptron and a multilayer hierarchical flow regime dependent model. The pattern recognition systems were trained to map the temporal fluctuations in the multiphase mixture density with the gas and liquid phase superficial velocities and the liquid phase water cut using statistical features extracted from the gamma count signals as their inputs. The use of wavelet transform features as input vectors to these systems was also examined.

6.1 Feature Extraction and Analysis

Feature extraction is a dimensionality reduction technique employed to reduce the amount of resources required to represent a large quantity of data. It was employed to represent the gamma densitometer data for two reasons:

1. The statistical nature of gamma radiation analysis dictated a measurement period of 40 minutes. This generated a 600,000-dimensional input space (40 minutes × 60 seconds/minute × 250 Hz). The sheer volume of the data being processed could not be practically handled by a neural network system.

2. Previous studies on the application of pattern recognition to multiphase flow measurement reported that feature extraction is the most effective way to isolate discriminatory information related to the flow conditions [**89-95, 97-98**].

The hard and soft energy gamma signals were used to produce suitable input parameters. Features were also extracted from a third synthesised ‘difference’ signal that recorded the absolute difference between the soft and hard energy counts. The features extracted are described in **Appendix B**.

All features were subjected to a contour profile analysis to determine their discriminability with respect to key multiphase flow parameters. Features exhibiting poor discriminability were omitted from further investigation.

A number of different pre-processing routines were tested with the feature sets to identify suitable pre-processing techniques to apply in the pattern recognition systems. Details of the feature contouring and selection process, and the pre-processing routines examined, are supplied in **Appendix E**.

6.2 Data Classification

The gamma count data points collected were classified into training and test set, **Figure 6.1**. Preliminary investigations demonstrated that 91 training points and 35 test points provided an appropriate training to test data ratio.

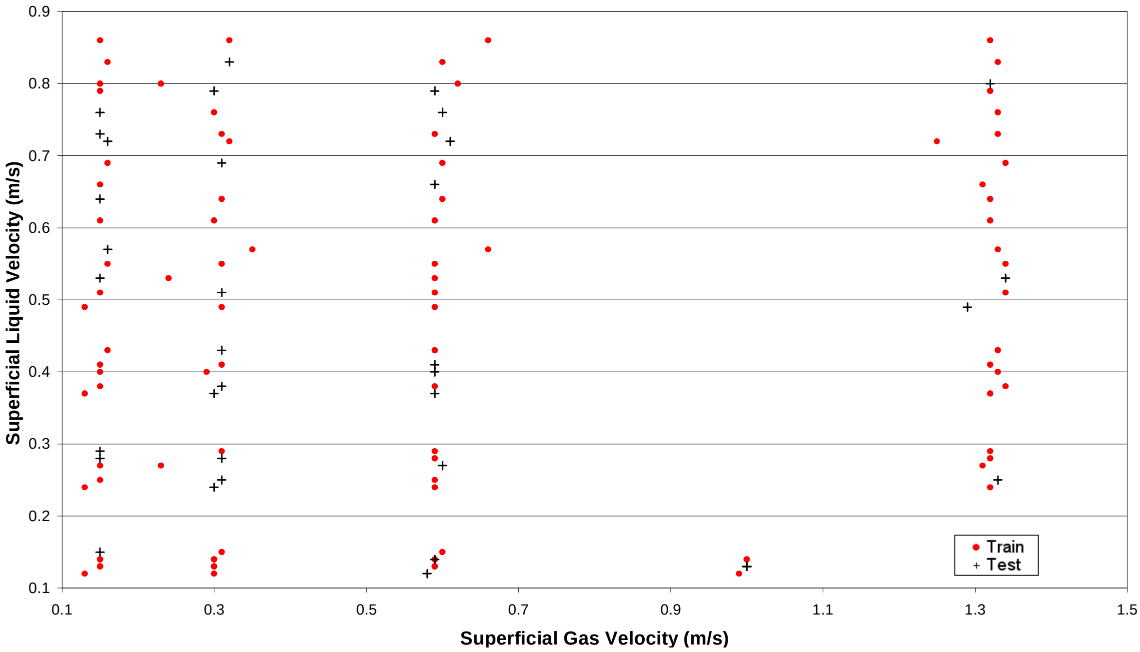

Figure 6.1 – Data Set Classification

6.3 Single Feedforward Multilayer Perceptron Model

A universal measurement model was developed employing a single feedforward multilayer perceptron (MLP) model, **Figure 6.2**.

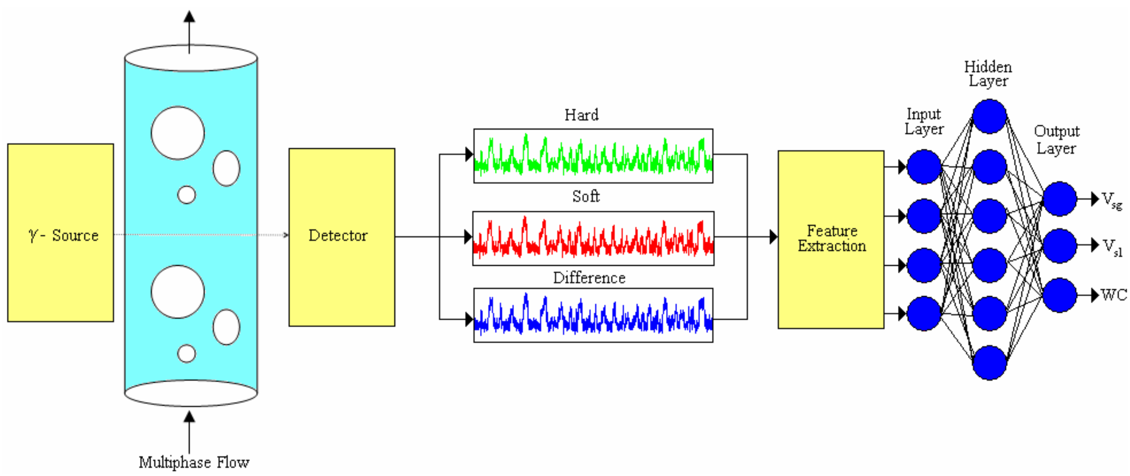

Figure 6.2 – Single Neural Network Model Concept

Three outputs were defined for the model: the superficial gas velocity (V_{sg}), the superficial liquid velocity (V_{sl}) and the water cut (WC).

6.3.1 Neural Network Design, Training, and Testing

Figure 6.3 illustrates the mechanism conceived and applied to design, train, and test MLP neural network systems in this research work.

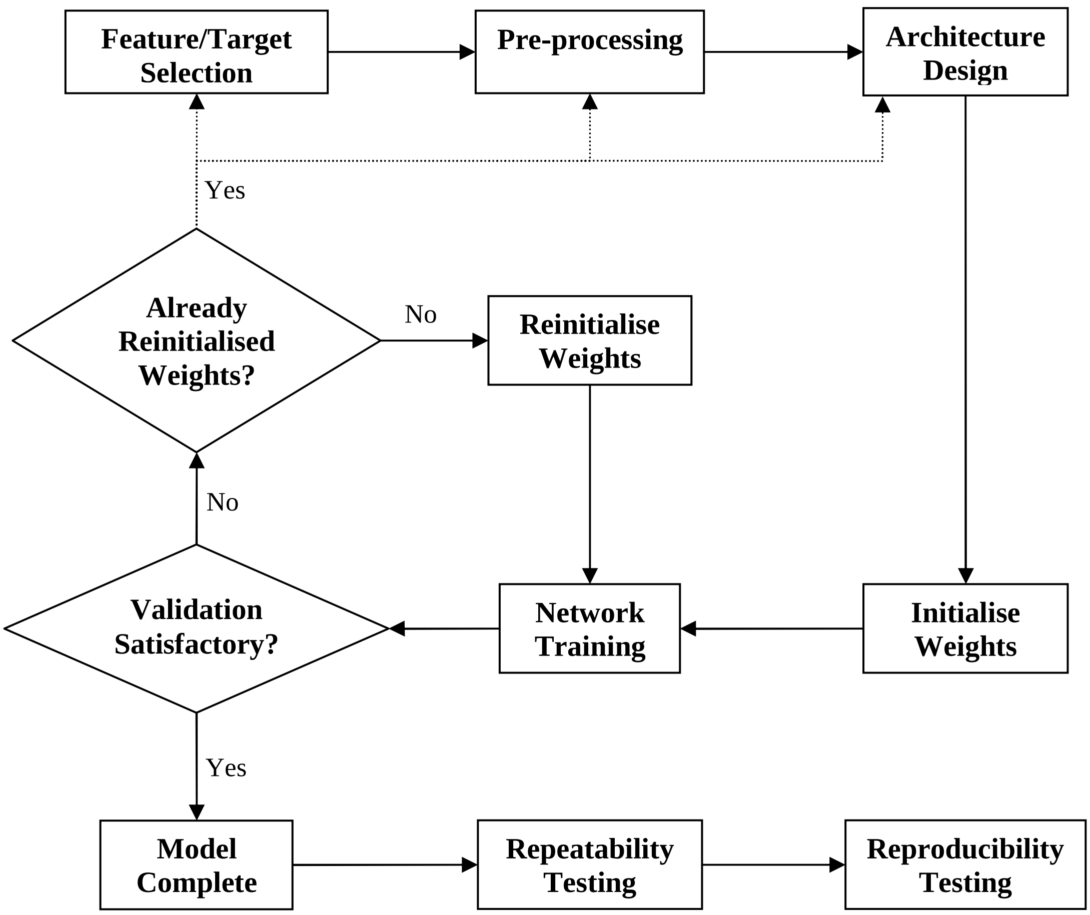

Figure 6.3 – Mechanism for Neural Network Design, Training, and Testing

Definition of the model inputs and outputs was the starting point for all investigations. Input selection involved identifying the feature set to be examined from each of the available signals. The outputs are the measurements one desires to obtain: the superficial phase velocities and the water cut.

A pre-processing routine is employed to remove bias and improve generalisation properties of the data set. As part of this study, two different pre-processing techniques were evaluated for their influence on the neural networks' performance: zero-mean and unit variance (ZMUV) and principal component analysis (PCA). Further details on the pre-processing routines are provided in **Appendix E**.

Neural network architecture is user defined and problem specific. Previous work has determined that a two-layer MLP network comprising a sigmoid transfer function in the hidden layer and a linear transfer in the output layer can be used to approximate any function with arbitrary accuracy [**81**]. However, some particularly complex non-linear processes cannot be sufficiently modelled with only one hidden layer and require additional layers to attain the desired level of performance. Preliminary investigations with the current data set illustrated that increasing the number of hidden layers merely increased the simulation's computational time with no appreciable benefit in terms of accuracy. Consequently, it was opted to implement two-layered MLP systems throughout the course of this study.

Selecting the number of nodes to deploy in the hidden layer is somewhat less straightforward than the input and output layer definitions: the number of nodes will vary in accordance with the complexity of the underlying function the network is attempting to model. A system in which the hidden layer contains an excessive quantity of nodes will tend to memorise the training data set and exhibit difficulty in accurately processing previously unseen input data. On the other hand, a system with too few nodes in the hidden layer will not provide an adequate quantity of mapping parameters to accurately express the underlying function between the input and output variables.

Bayesian regularisation was employed to optimise the number of nodes in the hidden layer through monitoring of the number of effective parameters in the system. **Figure 6.4** illustrates the effect of increasing the number of nodes in the hidden layer on the number of effective parameters for an input matrix comprising all features from the hard spectrum.

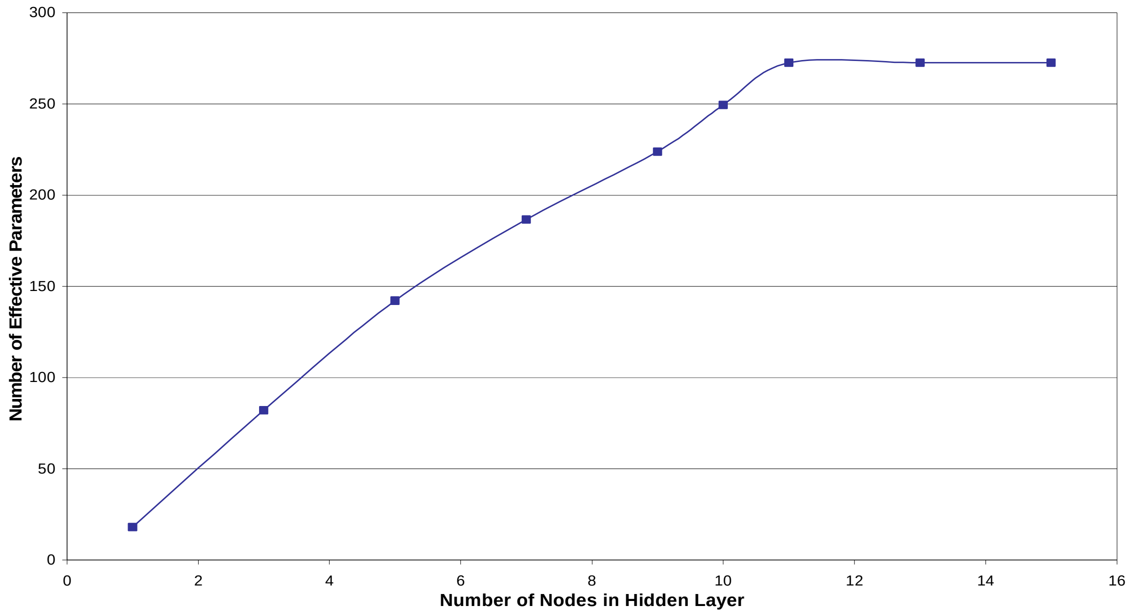

Figure 6.4 – Variation in Effective Parameters with Hidden Nodes

The number of effective parameters increases with the number of nodes until the optimum number of nodes is attained (i.e. 11 hidden layer nodes). At this point, increasing the number of nodes has no influence on the number of effective parameters. In this case, it was concluded that 11 nodes in the hidden layer would be an appropriate selection for a single feedforward two-layer perceptron model.

Prior to undertaking network training, initial values have to be assigned to the weight and bias parameters created through the architecture definition. The initial values assigned to these parameters has a strong influence in the learning speed and in the quality of the solution obtained after training process attains convergence. An inadequate initial choice of the weight values may cause the training process to get stuck in a poor local minimum or to face abnormal numerical problems.

The Nguyen-Widrow [**115**] method provides optimal weight initialisation for back-propagation based neural network systems. The methodology involves normalisation of the input vector within the scale of -1 to +1. A scale factor *F* for the input vector is then determined using the following equation.

$$F = \frac{0.7h^{\frac{1}{i}}}{R} \qquad \text{(Eq. 6.1)}$$

Where, *i* denotes the number of inputs, *h* is the number of hidden nodes, and *R* is the range of the input vector. Having determined the scale factor, the node biases are assigned a random value in the range -*F* and +*F*. The network initialisation weights are then designated by assigning random values between -0.5 and +0.5 to the weights and then multiplying these values by the scale factor *F*.

Neural network training implies the adjusting of the network's weight and bias parameters in an iterative fashion until the network output values eventually converge with the outputs' target values. A number of training algorithms encountered in the literature survey were tested to evaluate their performance in the current research application. The Levenberg-Marquardt (LM) routine was observed to yield superior data classification. However, a common problem with the LM algorithm is that of over-fitting: poor classification of unseen data.

Over-fitting was experienced in early stages of testing but was overcome by the implementation of Bayesian regularisation. The cross-validation technique was also considered and was observed to improve data classification but at the expense of test data points as the data has to be classified into three groups (training, validation and test) to facilitate this technique. Bayesian regularisation offered a significant improvement in the generalisation properties of the network at no cost to the number of test data points available for analysis. As a result, Bayesian regularisation was the preferred method for surmounting the over-fitting in this work.

Figure 6.5 depicts the training of a single feedforward neural network with 11 hidden nodes. In this example, the hard energy gamma signal features were used as the inputs. In training process the network's weight and bias values are updated according to Levenberg-Marquardt optimisation. The training algorithm minimises a combination of squared errors and weights to determine the best configuration for network generalisation.

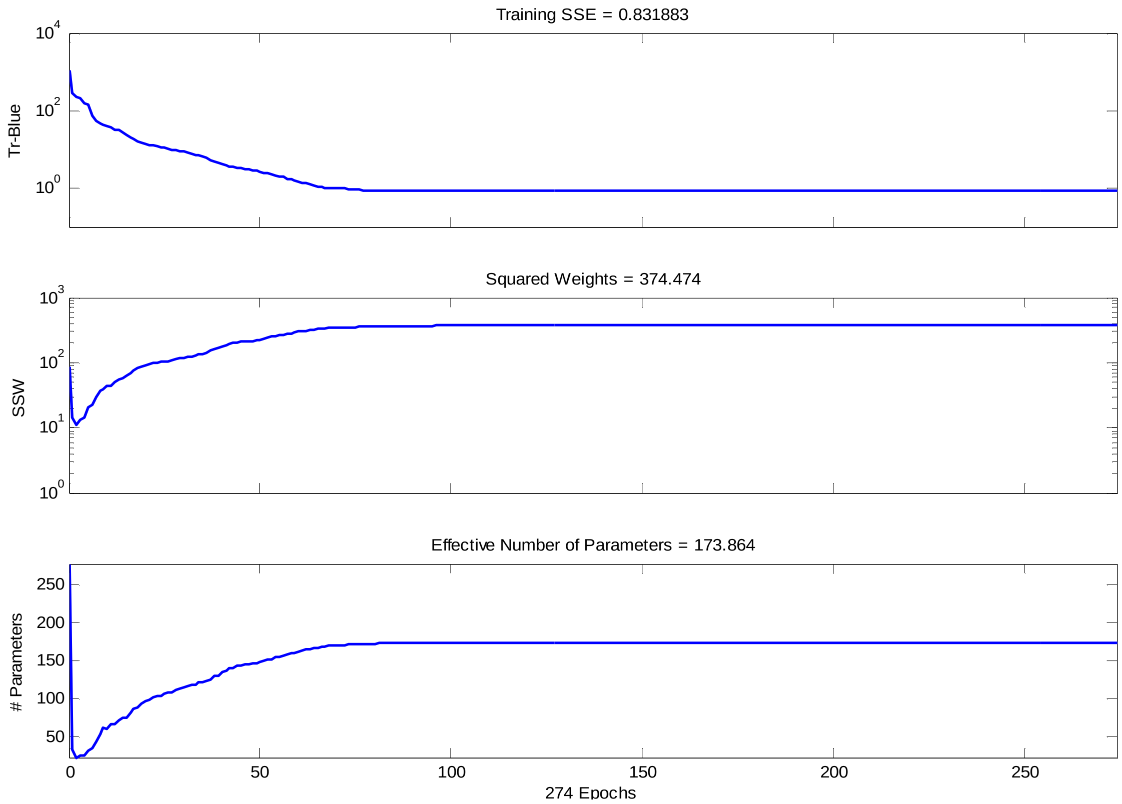

Figure 6.5 – MLP Network Training (a) Sum Square Errors (b) Sum Square Weights (c) Effective Number of parameters

Once trained, the neural network model was assessed to evaluate its repeatability capabilities. The training input data is presented to the trained neural network for testing. Satisfactory classification of the training data demonstrates good network repeatability and that the network is suitable for testing on previously unseen data points, i.e. the test data.

The repeatability results show the output variables determined by the neural network simulation plotted against the target outputs, **Figure 6.6**. Good linear approximation was obtained; therefore, indicating that the neural network model developed has good repeatability properties and is suitable for testing previously unobserved data.

After definition of the network architecture, the performance of the single feedforward MLP network in predicting the superficial phase velocities and the liquid phase water cut from the input features presented was examined. The input features were input in a variety of permutations enabling the relationships between the different spectrum, information domains and output variables to be investigated.

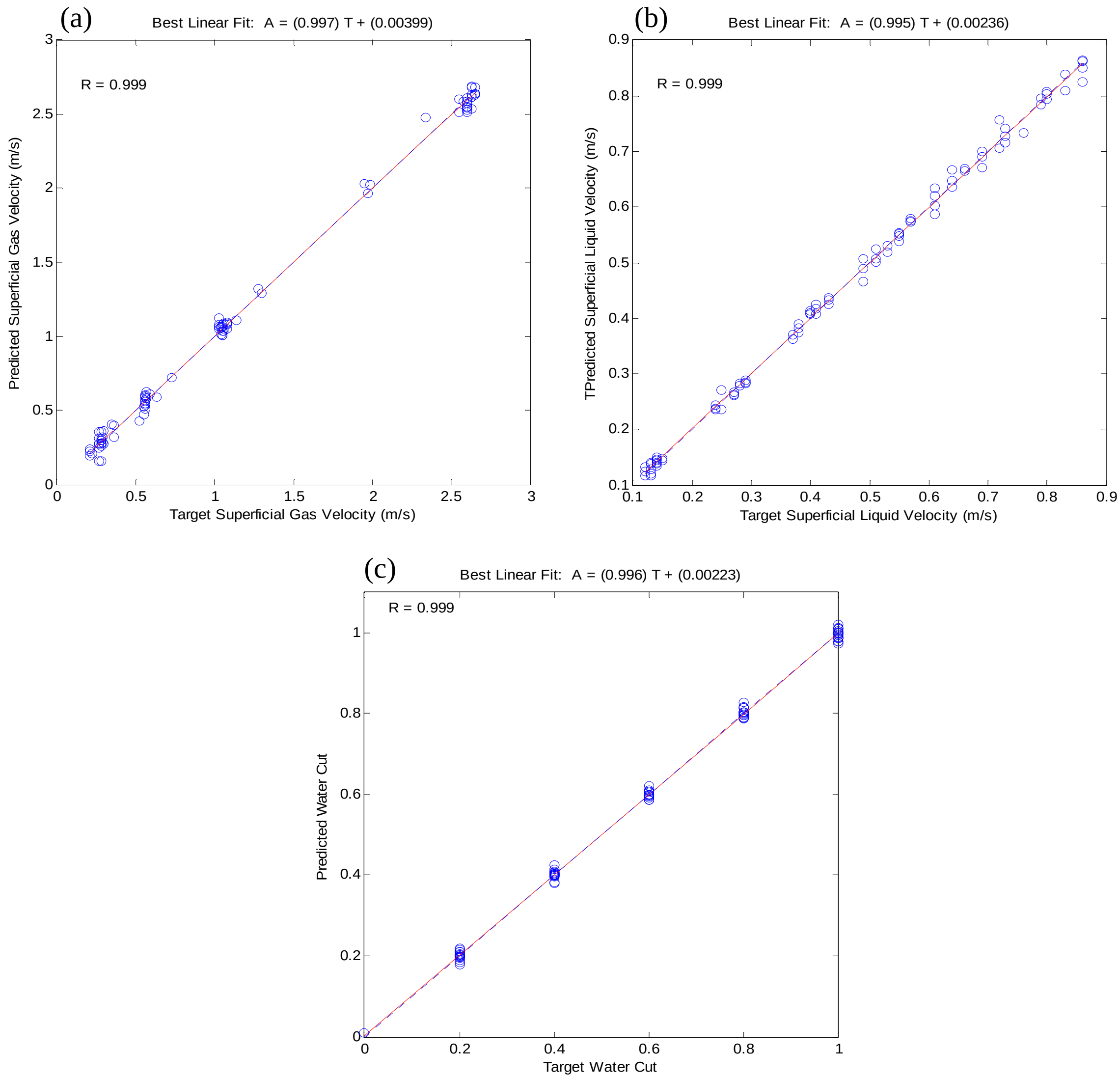

Figure 6.6 – Repeatability Performance (a) Superficial Gas Velocity (b) Superficial Liquid Velocity (c) Water Cut

6.3.2 Architecture Definition

The network architecture was defined as [n – 11 – 3]. This notation denotes the number of nodes in each of the layers:

- n – the number of input feature vectors (variable)
- 11 – the number of nodes in the hidden layer (fixed)
- 3 – the number of output nodes: one for each target (fixed)

6.3.3 Test Parameters

During preliminary testing, it was seen that the neural network performance varied as a function of the number of input features: the more input features presented the higher the quality of the network prediction in terms of accuracy. There are a vast number of input vector permutations possible with the 63 extracted features.

Previous work in the use of feature extraction with multiphase flow observed that an efficient method of feature vector construction was obtained through combining features of each of the information domains and this was verified through preliminary investigations [**92, 97**]. This method provides a systematic methodology for comparing the discriminatory abilities of the various information domains across the different spectra, **Table 6.1**.

Information Domain	Training Data	Test Data
Amplitude	6 × 91	6 × 35
Linear Prediction Coefficients (LPC)	6 × 91	6 × 35
Line Spectral Frequencies (LSF)	5 × 91	5 × 35
Autocorrelation Function (ACF)	4 × 91	4 × 35
All (Amplitude + LPC + LSF + ACF)	21 × 91	21 × 35

Table 6.1 – Input Feature Vector Sets for Analysis

The 126 gamma count data points collected were divided so that 91 for neural network training and the remaining 35 were exploited for testing purposes, **Figure 6.7**.

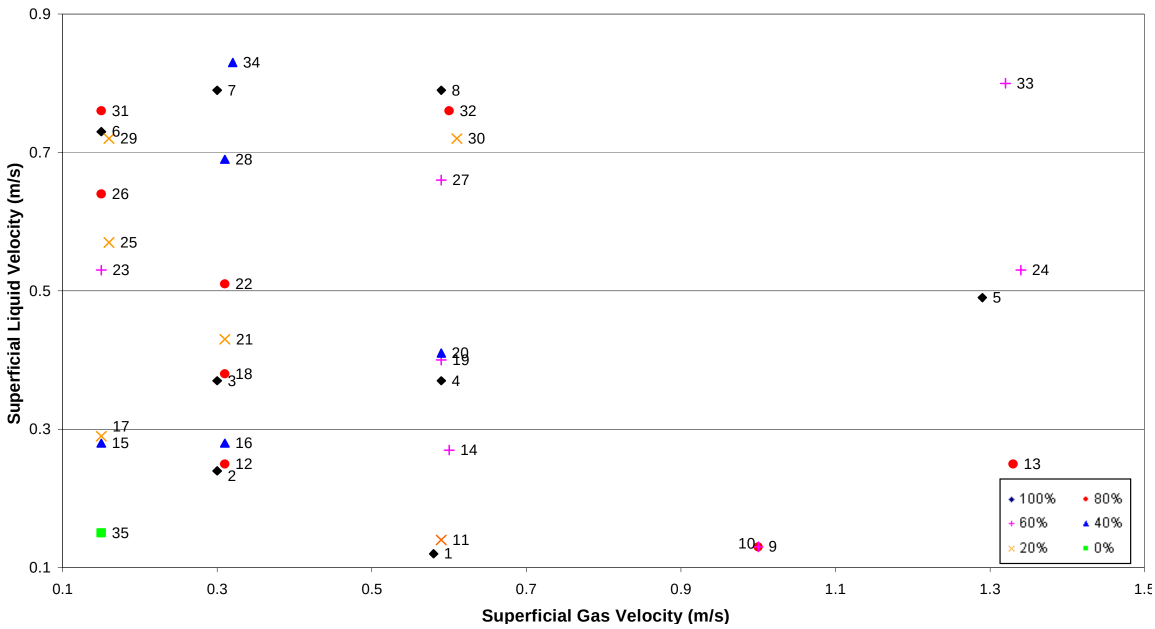

Figure 6.7 – Test Data Matrix

The target accuracy in this work was set at ±10% for each of the target outputs. The measurement error was calculated as a relative error over the range of measurement as defined by the expression:

$$E_r = \frac{y_{i(calculated)} - y_{i(measured)}}{y_{range}} \times 100\% \qquad \text{(Eq. 6.2)}$$

Where, y_i denotes the variable of interest and y_{range} denotes the measurable range, i.e. $y_{max} - y_{min}$. This modified version of the relative error expression has been widely used to express the classification performance of several pattern recognition based multiphase flow measurement systems [**97**].

6.3.4 Multiphase Flow Parameter Prediction

6.3.4.1 Gas Superficial Velocity

Figures 6.8 summarises the simulation results obtained within the target accuracy (±10%) for the gas superficial velocity measurements. It can be seen that the measurement variable's performance is described by two graphs: one for zero-mean and unit-variance normalisation (ZMUV), **Figure 6.8 (a)**; the other showing the results obtained performing feature set orthogonalisation and pruning (PCA), **Figure 6.8 (b)**. This enables direct comparison of the pre-processing routines' influence on the network performance. Results demonstrated that feature fusion input vectors provided the strongest discriminatory abilities for gas superficial velocity determination. The LPC features also showed strong gas velocity classification capabilities. In general, the ZMUV processed features produced better gas superficial velocity predictions than those subjected to the PCA technique.

Figure 6.9 (a) displays the error distribution plot as a function of gas void fraction for the feature fusion input vectors. The best overall performance was obtained using the ZMUV pre-processing routine and an input vector comprising feature fusion of the hard spectrum features: 97% of test data points were predicted within ±10% of their target values and 71% were within ±5%.

Figure 6.9 (b) illustrates the test conditions for the outlying data point, test point 9 with an error of +13.3%. The error is not significant in comparison to the results obtained for the other test points and cannot be attributed to any one particular systematic source and must be inherent in the network. It is anticipated that increasing the quantity of training data utilised during the training phase would lead to an increase in the gas velocity determination accuracy.

6.3.4.2 Liquid Superficial Velocity

Figures 6.10 presents the liquid superficial velocity measurements obtained from the neural network models. Liquid superficial velocity measurement accuracies were significantly poorer than those obtained for the gaseous phase. The reduction of the input vector dimensionality through the application of the PCA pre-processing routine resulted in a marginal improvement in the liquid velocity predictions.

In accordance with the gas velocity measurements, the linear prediction coefficients and feature fusion provided the best discriminatory properties for liquid velocity determination. Employing PCA, 69% of all liquid superficial phase velocities were resolved to within ±10% for the soft signal LPCs and feature fusion of the hard and soft signal features. However, the soft spectra LPCs exhibited a slightly superior classification prowess as 51% of liquid velocities, compared to 49% from the hard and soft signal feature fusion, were calculated to within ±5%.

Figure 6.11 (a) depicts the liquid superficial velocity error distribution as a function of GVF for the LPC input vectors. The best overall performance was obtained using the PCA pre-processing routine and an input vector comprising soft spectrum LPCs. The data points lying outside the target accuracy have been identified on the plot and can be seen to be homoscedastic with respect to the GVF.

Figure 6.11 (b) shows the location of the erroneous test points on the test matrix. As seen with the outlying gas velocity data points, there was no apparent systematic reason that could be attributed to their error source. Nevertheless, it was anticipated that the liquid results would not be as accurate as those obtained for the gas phase. The gamma count signal is dominated by the passage of gas structures. The underlying features of this data will be more relevant to gas phase correlations than for those of the liquid phase. It may be that signal conditioning, to remove the large gas induced fluctuations, would allow liquid phase sensitive parameters to be exploited to their full potential.

6.3.4.3 Water Cut

The water cut measurement performance obtained from the input feature and signal permutations examined are summarised in **Figure 6.12**. In this instance, the amplitude features and the feature fusion input vectors were found to provide the optimal output responses. The ZMUV pre-processing routine was more successful in water cut classification than its PCA counterpart. The amplitude feature fused from all three signals yielded the best water cut classification results with 83% of the test data points meeting the specified target accuracy and 49% within ±5%.

Figure 6.13 (a) displays the water cut error distribution plot as a function of gas void fraction for the amplitude feature input vectors and **Figure 6.13 (b)** illustrates the outlying test point locations on the test matrix. Errors were observed homoscedastic with respect to the GVF magnitude. Examining the test matrix map, the outlying data points were not observed to arise for specific flow conditions.

A variety of parameters were investigated in order to improve the output accuracies of the single neural network topology. Alternative network configurations were investigated, including:

- Altering the target outputs to the inlet delivery values.
- Simplifying the network architecture through removal of the water cut determining output node.
- Raw signal differentiation, before feature extraction, to reduce background noise.

Despite these modifications, the results yielded by the single feedforward MLP network were poorer than those obtained from the original simulations described above. It is hypothesised that the presence of more than one flow regime with different correlations between the input features and the outputs could be at fault. If these correlations are significantly different then a single neural network will not be able to model the relationships effectively.

As a result, the sensitivity of the input feature to output variable correlations to the dominating flow regime was investigated. This study was undertaken through the implementation of a multilayer hierarchical configuration neural network. Kohonen self-organising feature maps (KSOFM) were employed to divide data points into groups exhibiting common underlying properties in their defining features.

(a)

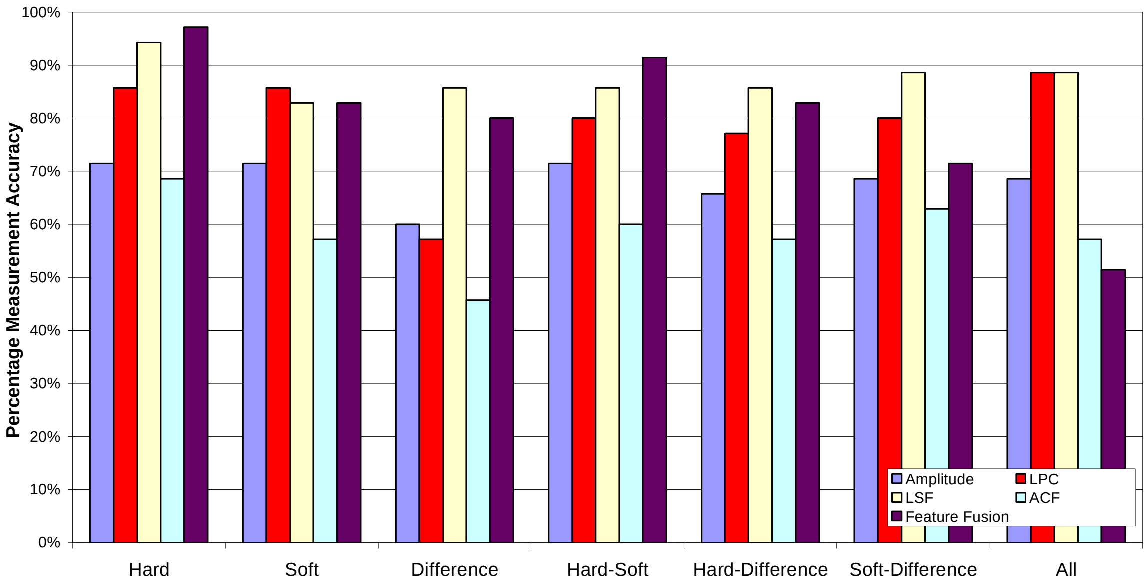

(b)

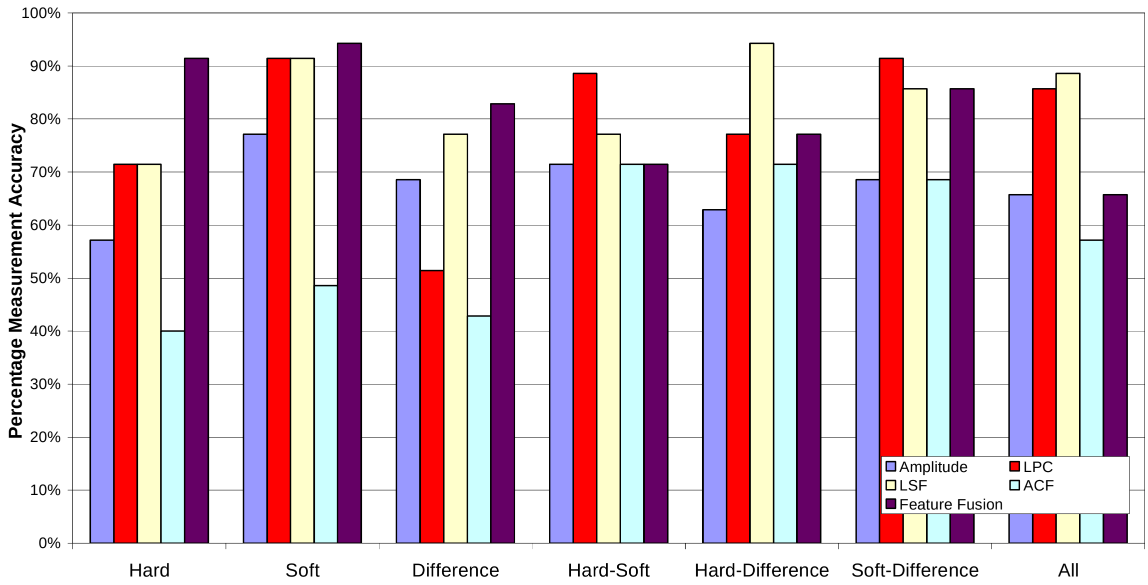

Figure 6.8 – Percentage Measurement Accuracy for the Superficial Gas Velocity (a) ZMUV (b) PCA

(a)

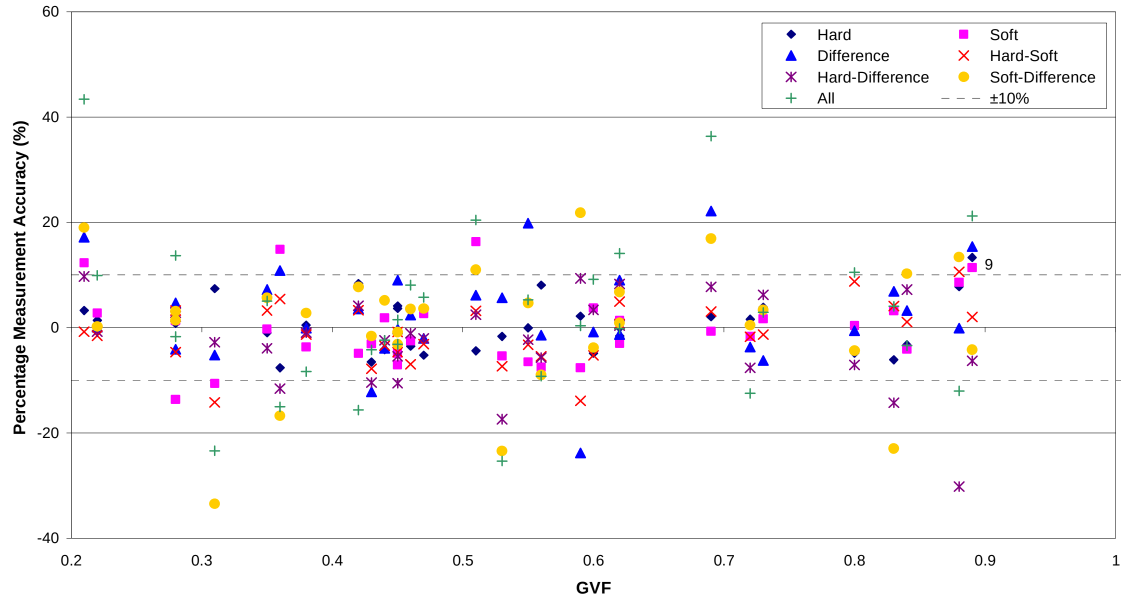

(b)

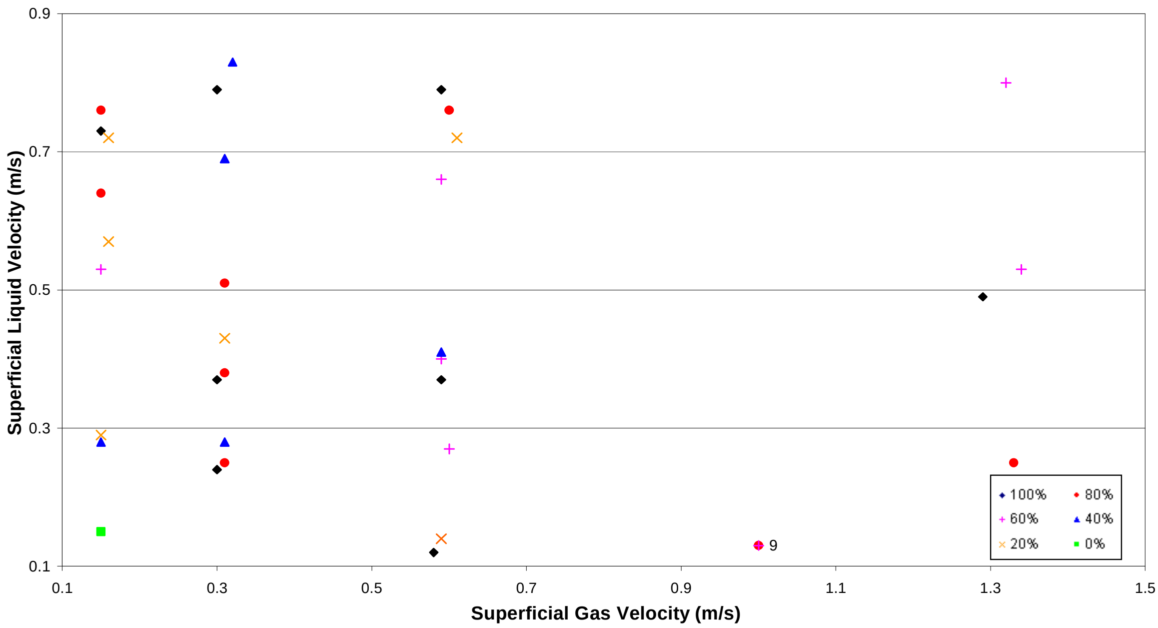

Figure 6.9 – Percentage Gas Error Distribution for Feature Fusion (PCA)
(a) GVF Plot (b) Outlying Test Point Matrix Location

(a)

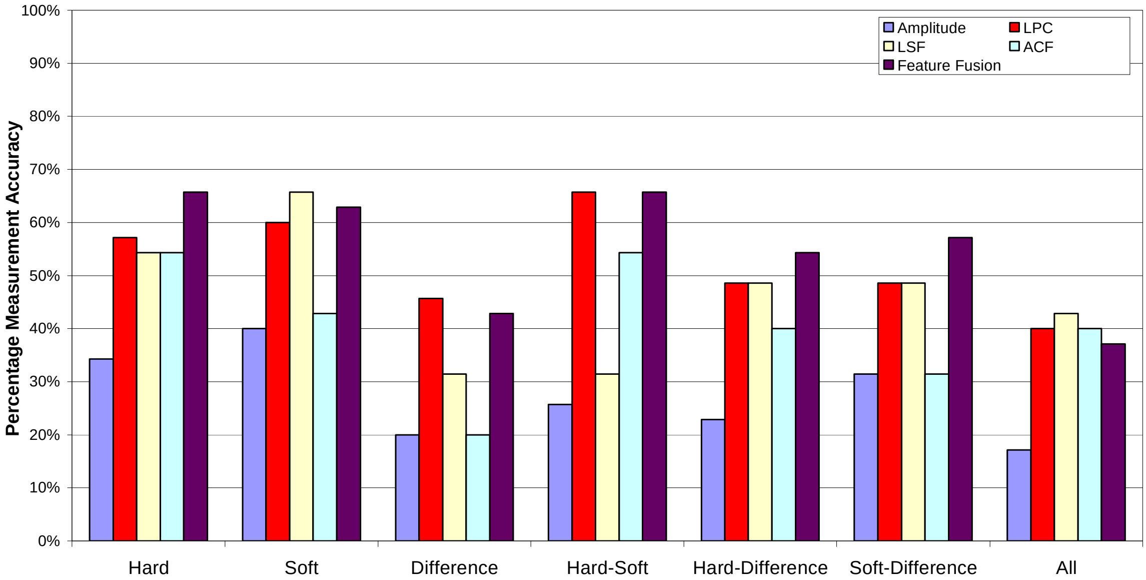

(b)

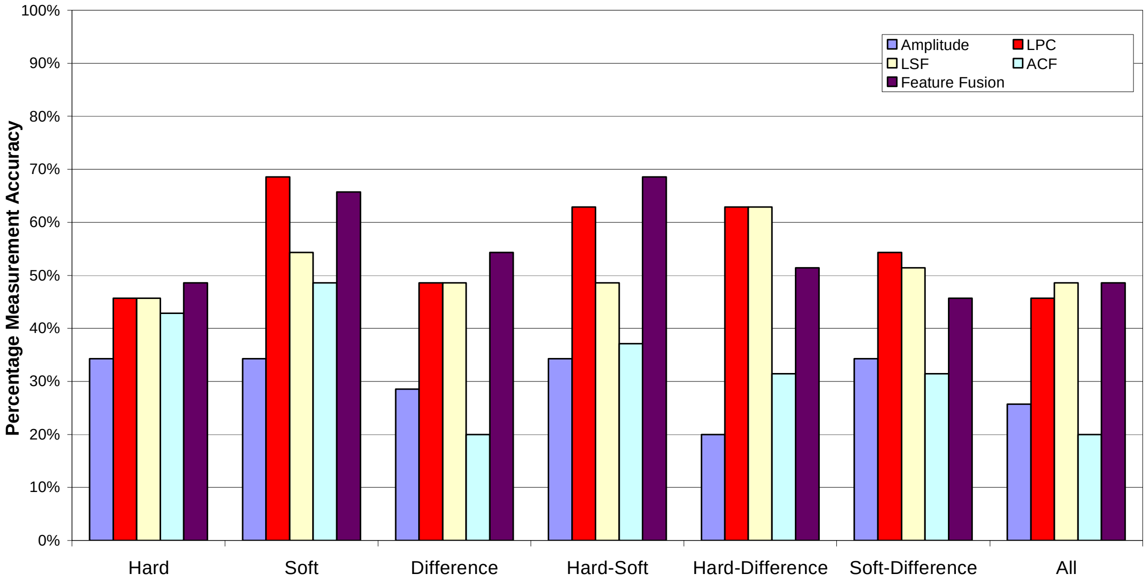

Figure 6.10 – Percentage Measurement Accuracy for the Superficial Liquid Velocity (a) ZMUV (b) PCA

(a)

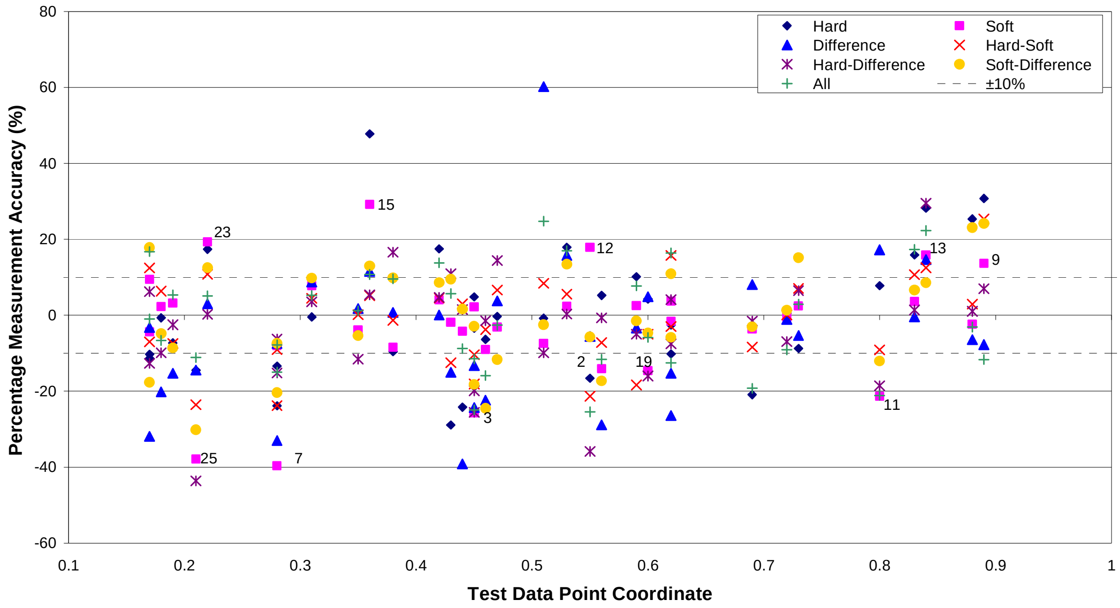

(b)

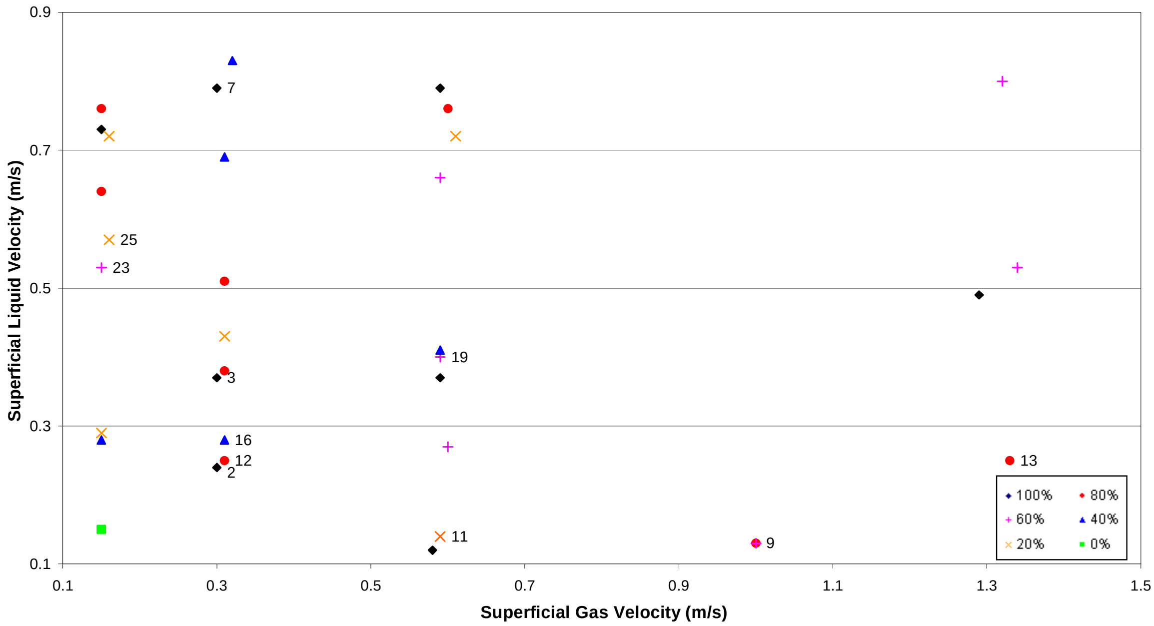

Figure 6.11 – Percentage Liquid Error Distribution for LPC Features (PCA)
(a) GVF Plot (b) Outlying Test Point Matrix Location

(a)

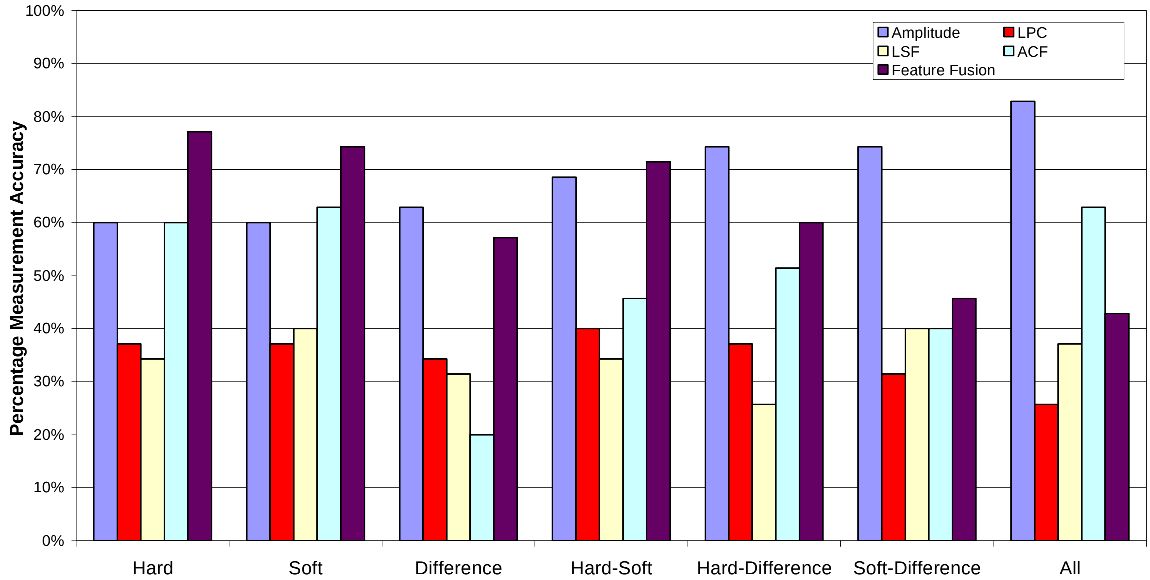

(b)

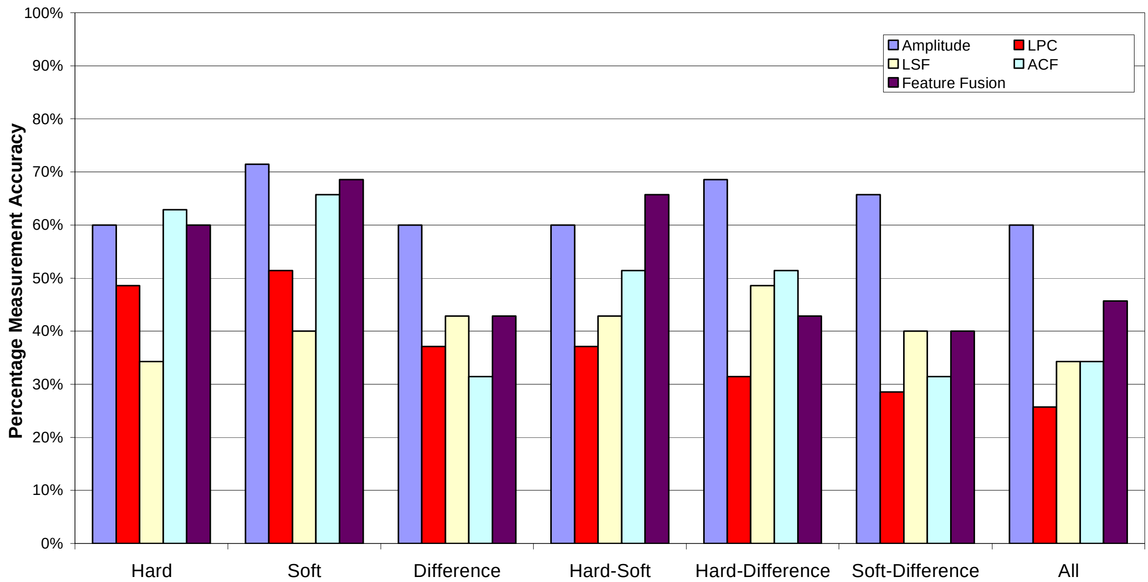

Figure 6.12 – Percentage Measurement Accuracy for the Water Cut (a) ZMUV (b) PCA

(a)

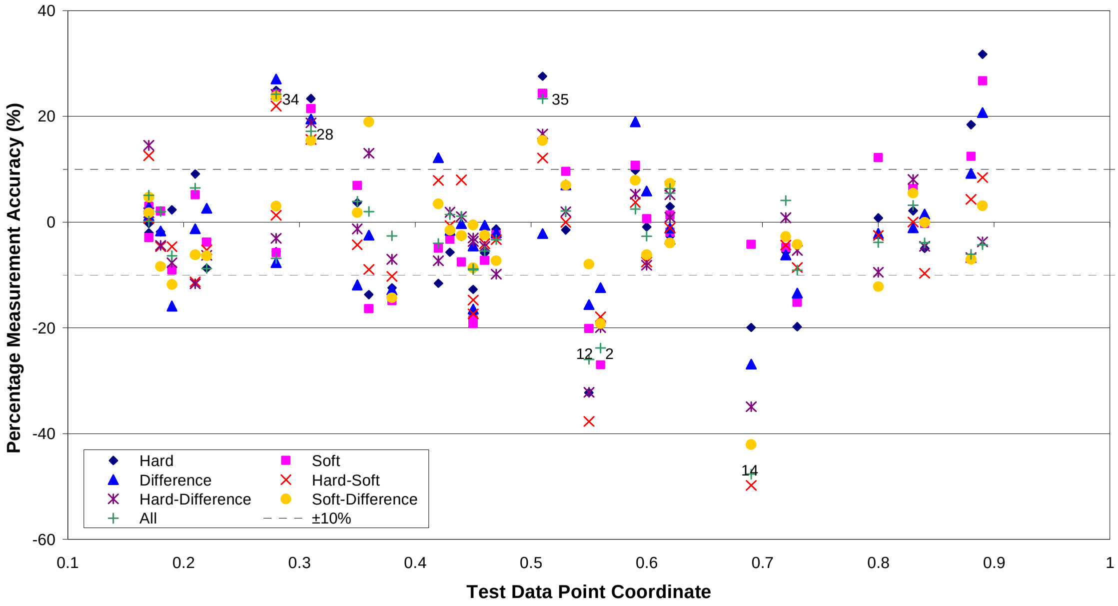

(b)

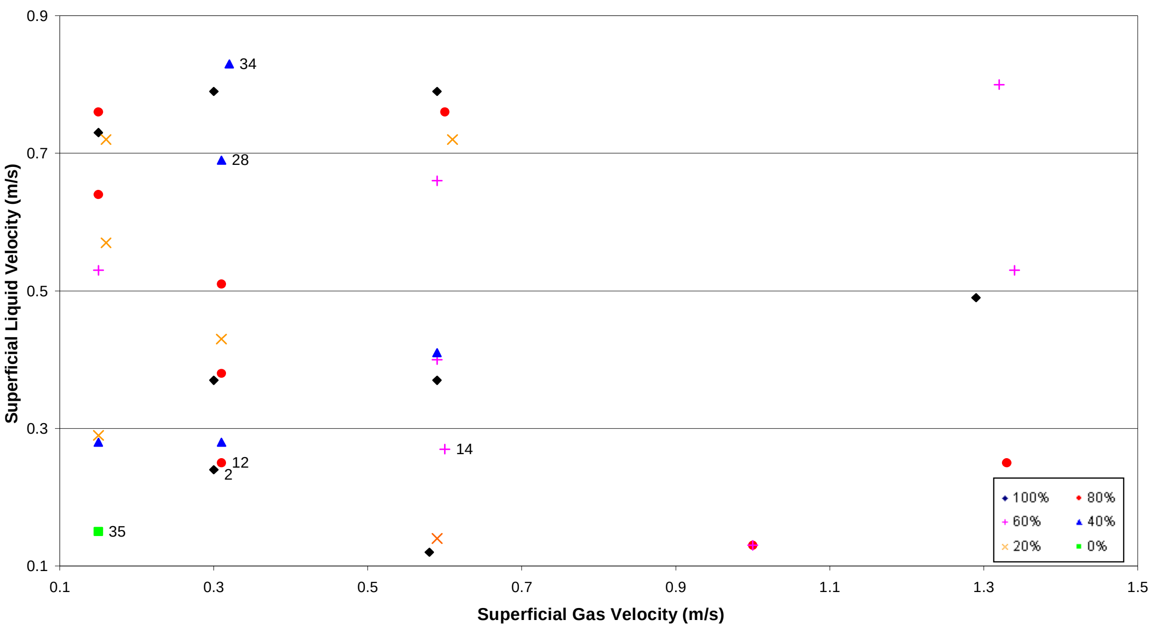

Figure 6.13 – Percentage Water Cut Error Distribution for Amplitude Features (ZMUV) (a) GVF Plot (b) Outlying Test Point Matrix Location

6.4 Flow Regime Dependent Multilayer Hierarchical Model

6.4.1 KSOFM Flow Regime Classification

Flow regime effects were analysed by constructing a multilevel hierarchical neural network, **Figure 6.14**. The data points are classified according to their flow regime using a Kohonen self-organising feature map (KSOFM) and the identification of the phase flow parameters is achieved through the employment of a second layer of MLP neural networks: one for each of the identified flow regimes.

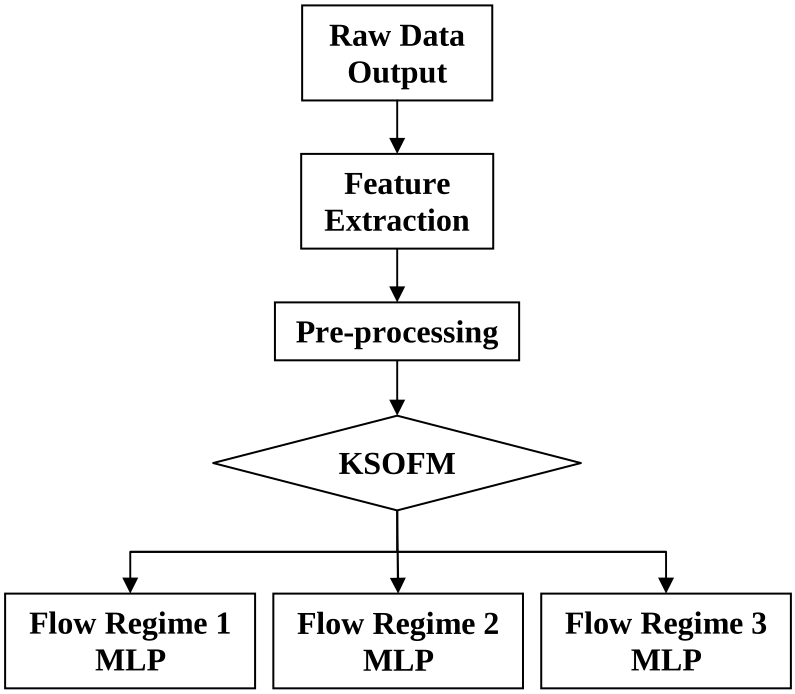

Figure 6.14 – Flow Regime Dependent Pattern Recognition Model

If the correlations between the extracted feature inputs and the target outputs are indeed flow regime dependent then reduced error magnitudes should be observed for the output parameters in comparison to those obtained using a single MLP.

Flow regime identification by visual means was not possible owing to restrictions imposed by the experimental facility. Nevertheless, an initial flow regime classification was undertaken thorough statistical analysis of the signals. Previous analysis revealed that a scatter plot of the hard signal mean value plotted against the coefficient of kurtosis provides a good indication of the likely prevailing flow regime (**Chapter 4.2.2**). However, although this correlation agrees well with the signal time traces, and published flow regime maps, there was no way of verifying the classification.

A useful application of neural networks is their ability to classify data. Self-organising maps can examine a series of data points and group them according to some underlying characteristic property. These networks are particularly useful in multiphase flow measuring where complex high dimensional data needs to be presented in an understandable format. An overview of KSOFMs is given is **Chapter 2.5.4.4**.

6.4.2 Two-Regime Classification Model

Each input data point to the KSOFM comprised a 16-dimensional vector comprising the hard signal amplitude, linear prediction, and line spectral frequency features. Each data point was also labelled with their associated flow regime as identified from statistical analysis and flow regime map predictions.

An empirical approach was adopted to determine the optimal magnitude for the output grid. Several grid configurations were analysed. It was found that too large a grid resulted in the creation of redundant nodes due to an insufficient quantity of training data; whereas, too small a grid yielded overlapping flow patterns. It was established that a 6 × 6 grid was best suited for the data set.

Applying the KSOFM learning algorithm to the data set produced the node topology shown in **Figure 6.15**.

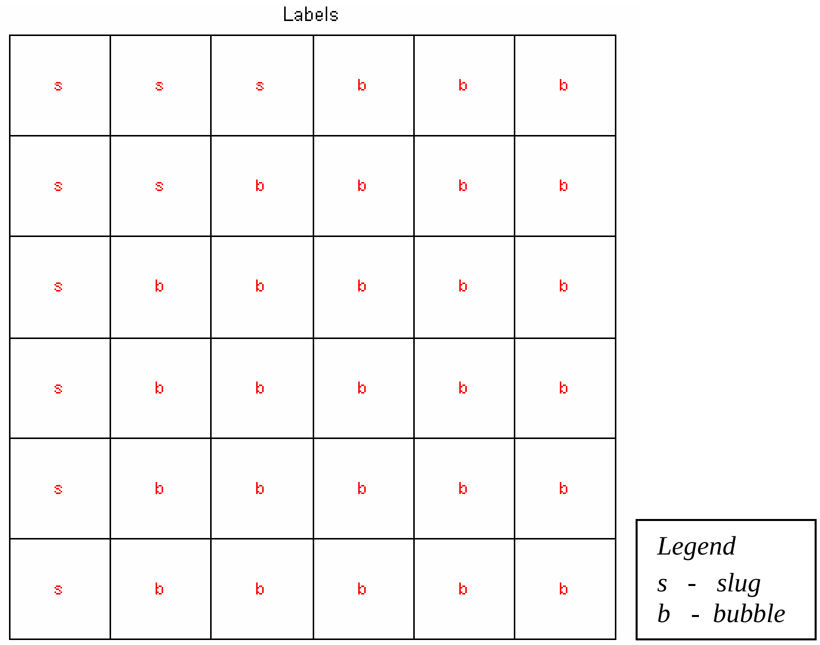

Figure 6.15 – Flow Regime Identification by KSOFM

The KSOFM was able to locate different underlying patterns in the input vectors and the topological arrangement of the output grid relates well to the initial flow pattern classification undertaken with the formation two distinct areas being formed in the output grid: one for bubble flow points and the other for slug flow. The relative distances between these nodes can be represented in a unified distance matrix, **Figure 6.16**.

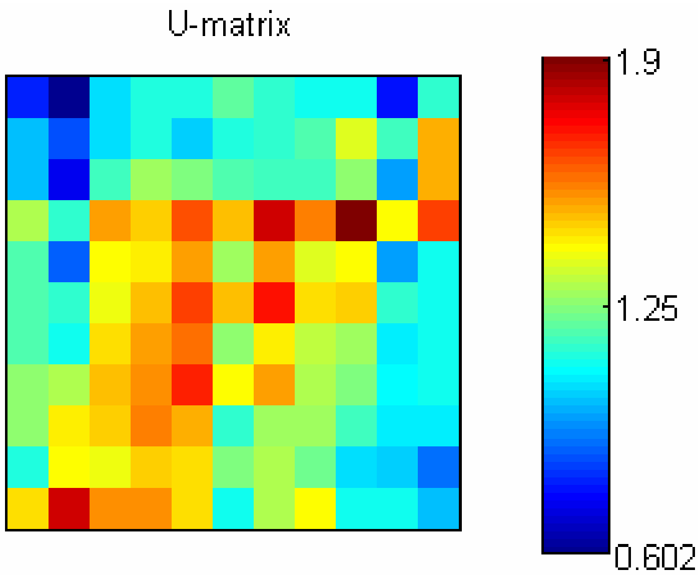

Figure 6.16 – Unified Distance Matrix for Test Data

The unified distance matrix (or U-matrix) visualises the distances between the nodes in the output grid. The distance between the adjacent nodes is calculated and presented with different colorings between the adjacent nodes. A red colouring between the neurons corresponds to a large distance and thus a gap between the codebook values in the input space. A blue colouring signifies that the data points contained within these nodes are close to each other in the input space. Thus, blue areas can be thought as clusters and red areas as cluster separators. From the U-matrix produced from the test data, one can observe two main clusters: one in the top left hand corner and the other running along the right-hand side of the grid.

Figure 6.17 shows the distribution of the data points in the output grid according to the best matching unit (BMU) classification. The BMU unit data enables the identification of each test point within the output grid. The green shading indicates data points previously identified as slug flow regimes; while the blue denotes those points thought to be in the bubble regime. The relative area of shading observed in each node is proportional to the number of data points residing within the node. It can be seen that at the boundary between the slug and bubble regimes previously identified there is some overlap in the nodes. In this case, the node classification is assigned depending on relative quantity of slug and bubble points. From the KSOFM analysis it is possible to obtain the location of each data point on the output grid. Thus, data points occupying the boundary between bubble and slug regime were able to be classified more appropriately by associating the data points with other that exhibited similar patterns in their input vectors.

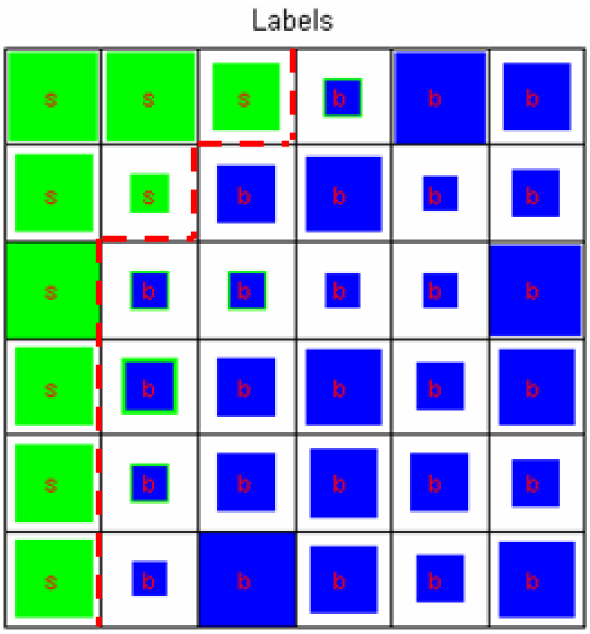

Figure 6.17 – KSOFM Labelled with Best Matching Units

Following analysis using a KSOFM, each data point was reclassified according to the arrangement proposed by the self-organising map, **Figure 6.18**.

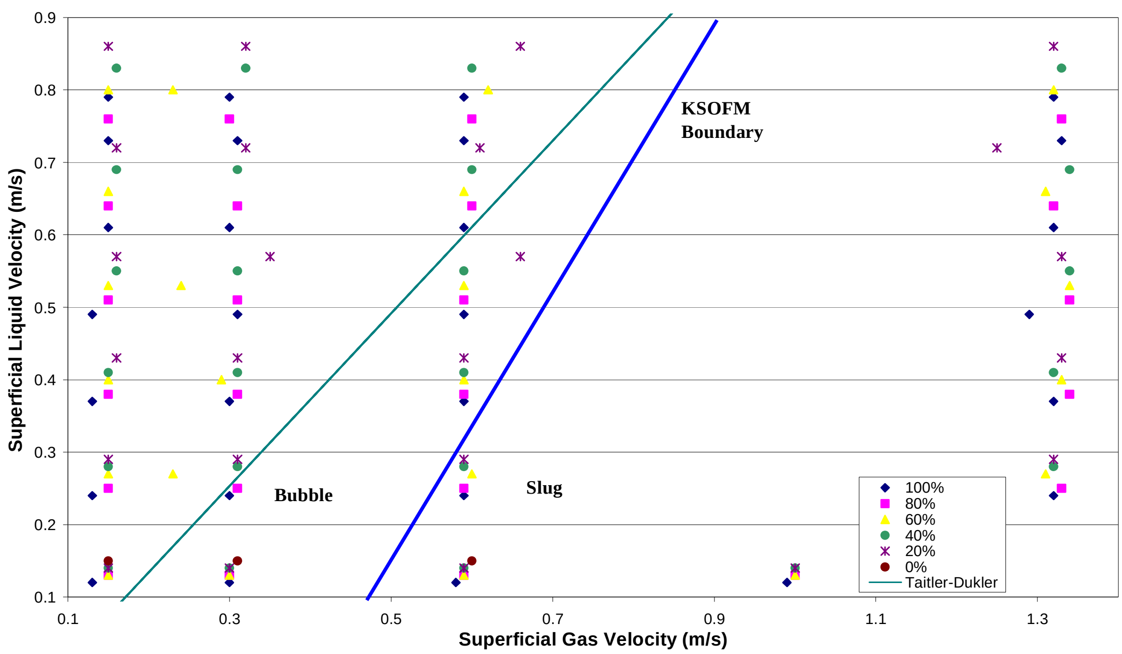

Figure 6.18 – KSOFM Flow Regime Classification of Data Points

The original Taitel-Dukler classification is illustrated on the flow regime map. It can be seen that the KSOFM classified a significant proportion of the original slug data points as have characteristic properties of bubble data points. The data set was subsequently split into three distinct groups: bubble regime training data, slug regime training data and test data. The test data set comprised a mixture of slug and bubble regime points.

After training the neural network on one set of training data, the classification of data points for both flow regimes could be compared and contrasted. It was hypothesised that if relationship between the input features and output variable is flow regime dependent, good classification would be seen for test points who shared a common flow regime with the training data, whilst poor performance would be witnessed for test points of the unseen flow regime.

6.4.2.1 Bubble Regime MLP Neural Network

The bubble regime MLP network was trained on the bubble regime training data. Based on the results obtained from extensive preliminary repeatability tests, the architecture of the bubble flow MLP network was defined to be [n – 8 – 3]. All other parameters were as per the original single feedforward MLP model.

6.4.2.1.1 Gas Superficial Velocity

Figures 6.19 and **6.20** display the gas superficial velocity measurement results obtained from the bubble regime Bayesian MLP neural network using a range of different input signal, feature and pre-processing routine combinations. **Figure 6.19** illustrates the network performance for the bubble test points; while **Figure 6.20** depicts the classification results for the slug regime test points.

In general, the ZMUV pre-processing algorithm yielded higher accuracy predictions than obtained employing PCA, **Figure 6.19**. 100% of the bubble test point gas superficial velocities were predicted within the specified target accuracy of ±10% using the following combinations:

- Soft signal – linear spectral frequencies
- Hard and soft signals – feature fusion
- Hard and difference signals – feature fusion
- Soft and difference signals – feature fusion
- All signals – linear spectral frequencies

Further analysis of the successful input feature combinations revealed that the feature fusion of the hard and difference signals yielded the best classification of the bubble superficial gas superficial velocity with 88% of bubble test points determined to within ±5%.

Figure 6.20 illustrates the comparatively poor classification exhibited for the slug regime test points. The network had been trained to classify input features according to the function derived in a learning process conducted entirely with bubble regime points and classified the slug points according to this function. This comparatively poor performance illustrates the flow regime dependence of the relationship between the extracted features and the target outputs.

Figure 6.21 (a) displays the errors associated with each of the test data points for neural network simulations conducted employing feature fusion as the input features and the ZMUV normalisation. The hard signal data points exhibiting errors in excess of ±10% are labelled. One can observe the heteroscedastic relationship between the measurement error and the GVF: as the test point GVF increases – the less bubble like the flow regime – the larger the probability and magnitude of the error in the gas superficial velocity classification. A significant majority of all gas velocity measurements at GVFs greater than 70% were under-predicted with respect to their target.

The location of the outlying test data points classified out with the target accuracy are shown on the test matrix, **Figure 6.21 (b)**. It can be seen that all of the bubble regime test points were accurately classified while only one slug test point was successfully predicted to within ±10%. Test point 14 can be seen to reside in close proximity to the KSOFM defined regime boundary. As the transition between flow regimes is not distinct, test point 14 could be exhibiting traits common to the bubble regime points, enabling classification by the bubble MLP network.

6.4.2.1.2 Liquid Superficial Velocity

Figures 6.22 and **6.23** depict the liquid superficial velocity measurement results obtained from the bubble regime Bayesian MLP neural network for the bubble and slug test data points respectively.

Figure 6.22 illustrates that liquid velocity bubble regime classification accuracies were significantly poorer than those obtain for the gas phase measurement. This observation agrees with what was witnessed for the single-MLP system, where liquid phase measurements were observed to be less accurate than the gas phase parameter determination. In this instance, the pre-processing routine employed did not exert a large influence on the simulation results. Nevertheless, the best classification results were obtained from the ZMUV pre-processing routine. Feature fusion proved to be the strongest input feature group. Optimal classification of the liquid superficial velocities was obtained exploiting feature fusion of the soft signal: 65% of bubble test points classified within ±10% and 54% to within ±5%.

Figure 6.23 shows the classification results for the slug regime data points. Again, slug point classification by the bubble-trained network was considerably poorer than the bubble test results reinforcing the hypothesis that input feature – output correlations are a strong function of flow regime. The liquid velocity classification for the slug test data points were more accurately mapped according to the bubble regime training regression than the gas phase velocities.

Figure 6.24 (a) presents the measurement errors obtained for each of the test data points using the feature fusion group as the input features and ZMUV pre-processing routine. The soft signal data points exhibiting errors in excess of ±10% have been labelled. Significant errors were obtained across the GVF range for both bubble and slug test points. There is a definite increase in error magnitude with increasing GVF but this increase was much less pronounced than that observed for the gas velocity measurements.

Figure 6.24 (b) illustrates the location of the outlying data points on the test matrix. In this instance, although the network was trained on bubble data, errors were yielded for both bubble and slug test data points. The fact that bubble test points exhibiting significant errors were not restricted to those lying close to the flow regime boundary suggests that the neural network was unable to sufficiently map the liquid superficial velocity within the target accuracy using the input features examined. As the raw gamma count signal is dominated by the passage of gas structures, features extracted from the signal will encode mainly data reflecting induced by the passage gas fluid elements. Features representative of the liquid phase properties are likely to exhibit smaller variations that are drowned out by the more dominant gas structure induced signal features.

6.4.2.1.3 Water Cut

Figures 6.25 and **6.26** display the water cut measurements observed employing the bubble MLP network for the bubble and slug test points respectively.

Figure 6.25 indicates that the hard signal autocorrelation function coefficients and the fused amplitude features provided the strongest performances. PCA pre-processing reduces the classification performance for all features in water cut classification, indicating that salient information resides within relatively small parameter variations. Employing the ACF features extracted from the hard signal and the ZMUV pre-processing algorithm, 77% of the bubble test data points were successfully resolved within the ±10% target accuracy and 46% to within ±5%.

Figure 6.26 illustrates that the slug test data points were not well classified using the function derived by the bubble point network training, demonstrating the flow regime dependent nature of the water cut parameter correlation. This trend was seen for all three output variables suggesting that the superficial phase velocities and the water cut have a strong flow regime specific relationship with the statistical features extracted from the raw signals.

Figure 6.27 (a) shows the errors obtained for all of the test data points. As expected, an increasing frequency and magnitude of error, outside of target specification, was seen with increasing test point GVF as the test point flow regime shifted from bubble to slug. The recurrence of this phenomenon reinforces the flow regime sensitivity of the non-linear regression modelled by the network. Nevertheless, significant errors in the bubble test data points were also attained across the whole GVF range of the bubble regime.

Figure 6.27 (b) illustrates that the vast majority of the slug regime test data points exhibited significant errors. The bubble test point water cut predictions did yield some results with errors in excess of ±10%. These erroneous bubble test points were seen scattered across the bubble region of the flow regime map. It is hypothesised that classification of all data points into just two regimes may be an over-simplification of the system and may not facilitate accurate representation of underlying relationships owing to the presence of more than two characteristic input feature – output interactions.

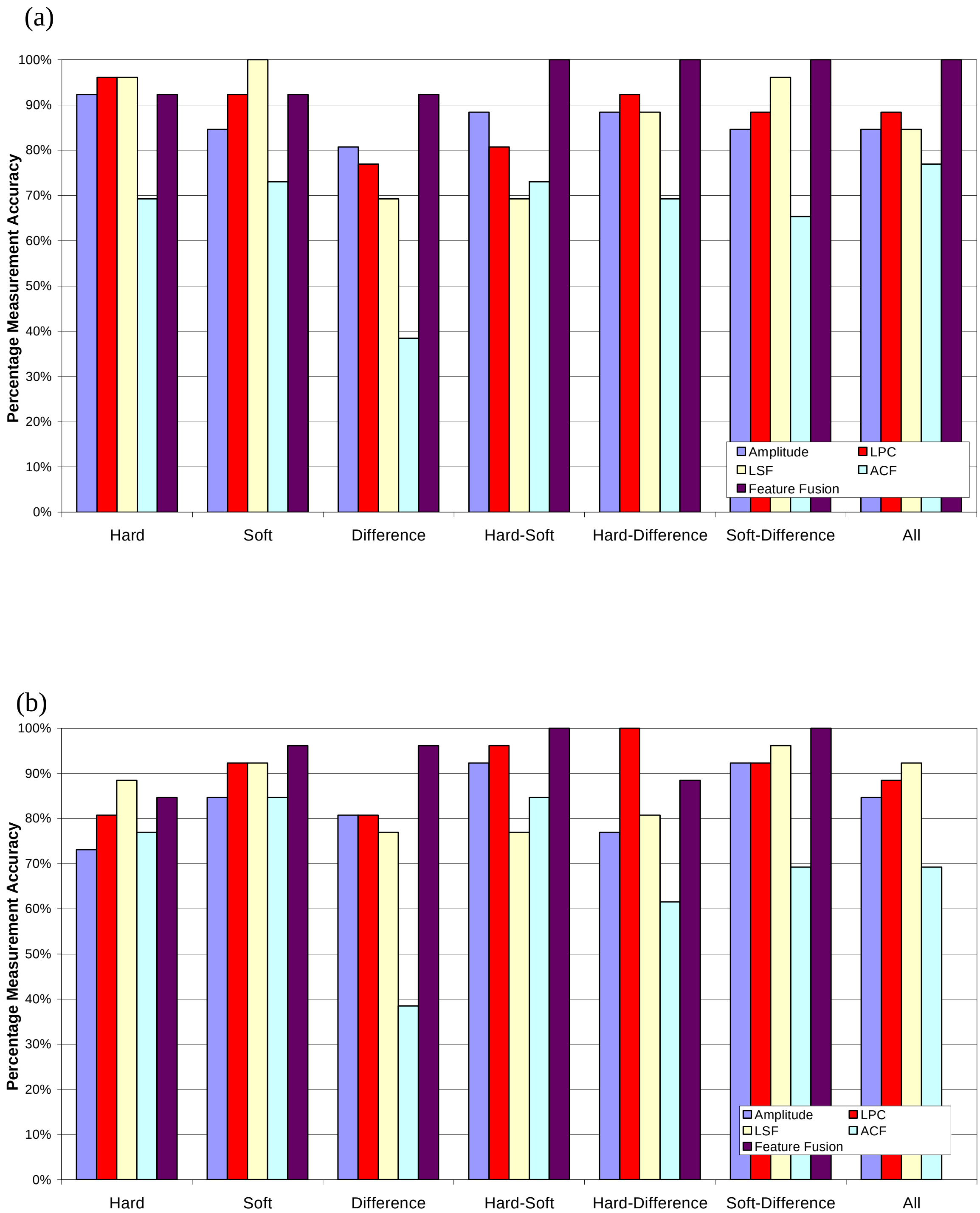

Figure 6.19 – Bubble MLP: Percentage Measurement Accuracy for the Superficial Gas Velocity of Bubble Test Points (a) ZMUV (b) PCA

(a)

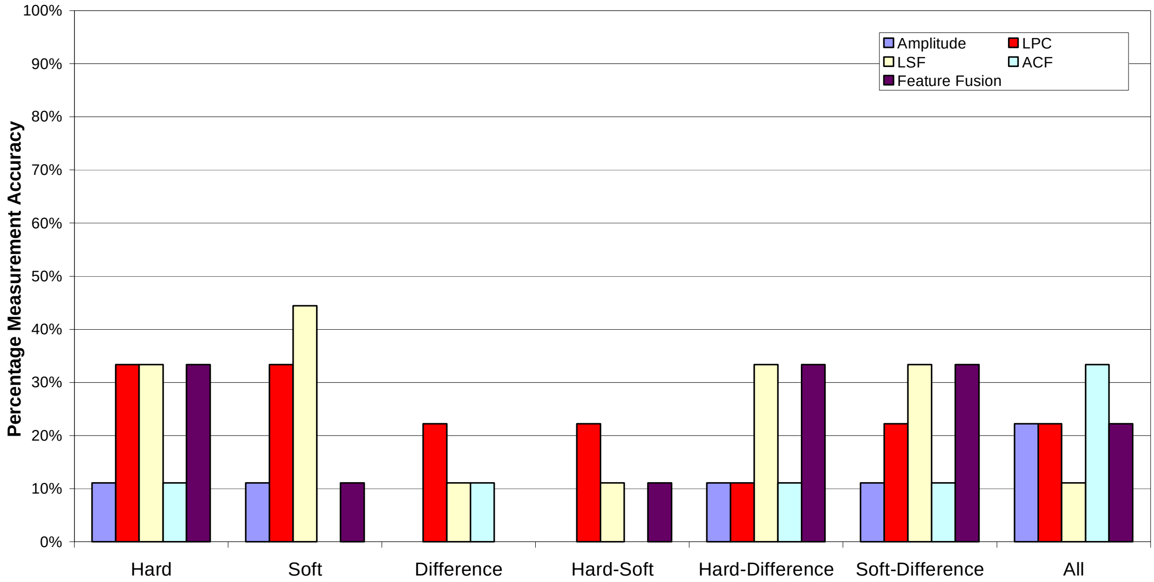

(b)

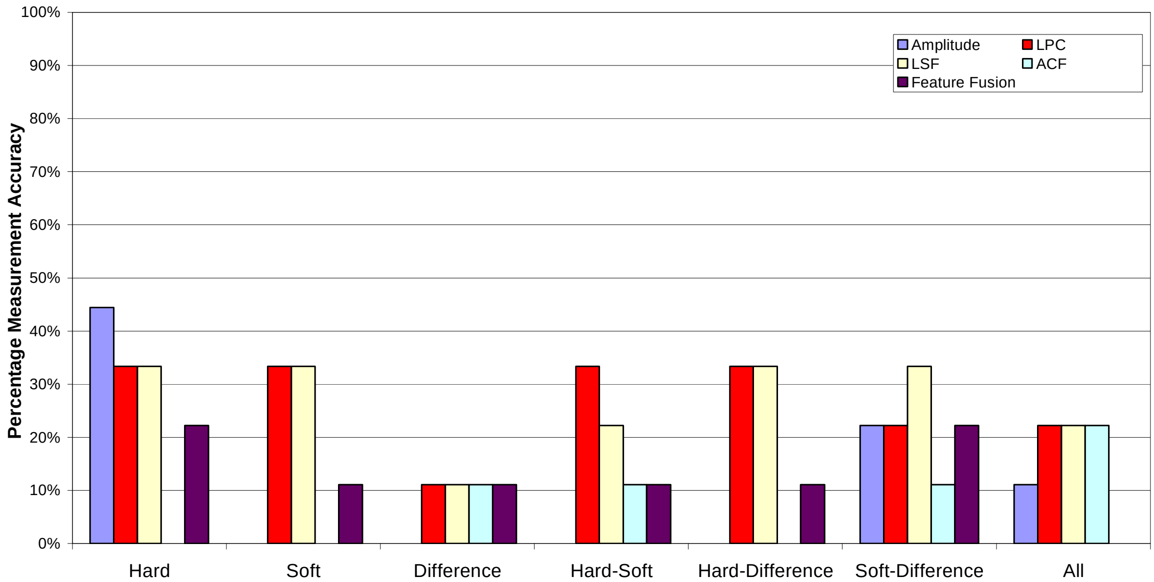

Figure 6.20 – Bubble MLP: Percentage Measurement Accuracy for the Superficial Gas Velocity of Slug Test Points (a) ZMUV (b) PCA

(a)

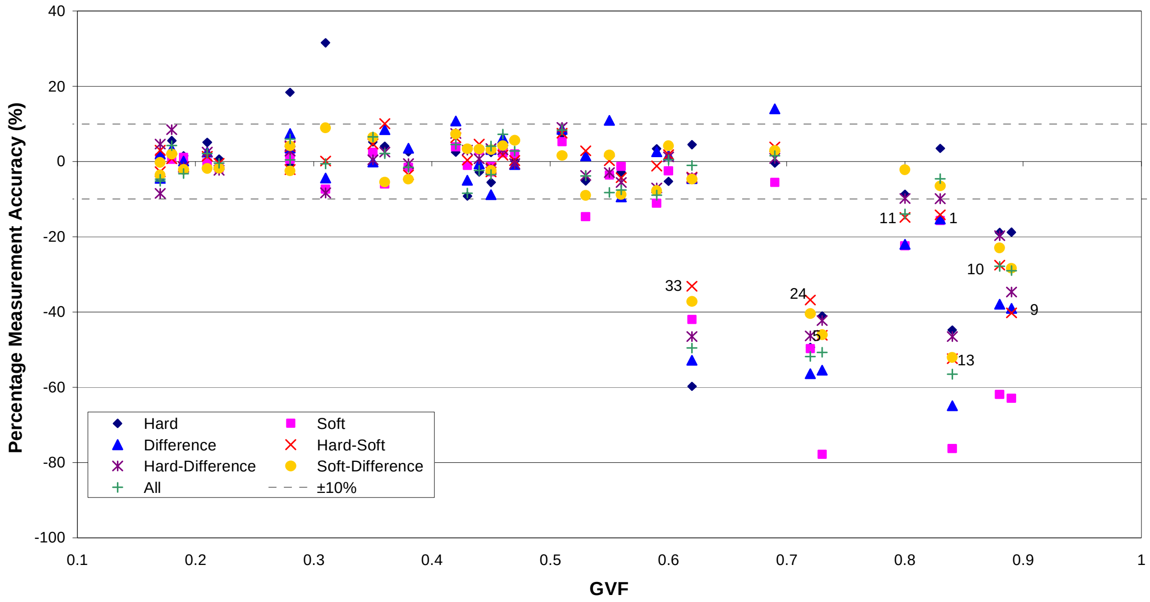

(b)

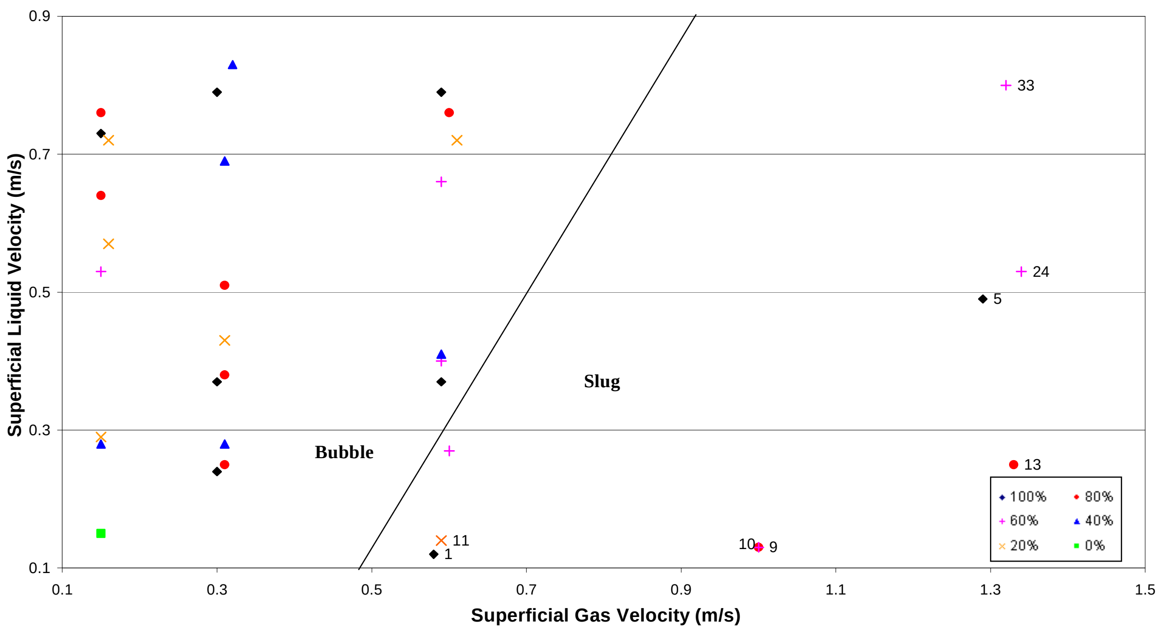

Figure 6.21 – Bubble MLP: Percentage Gas Error Distribution for Feature Fusion (ZMUV) (a) GVF Plot (b) Outlying Test Point Matrix Location

(a)

(b)

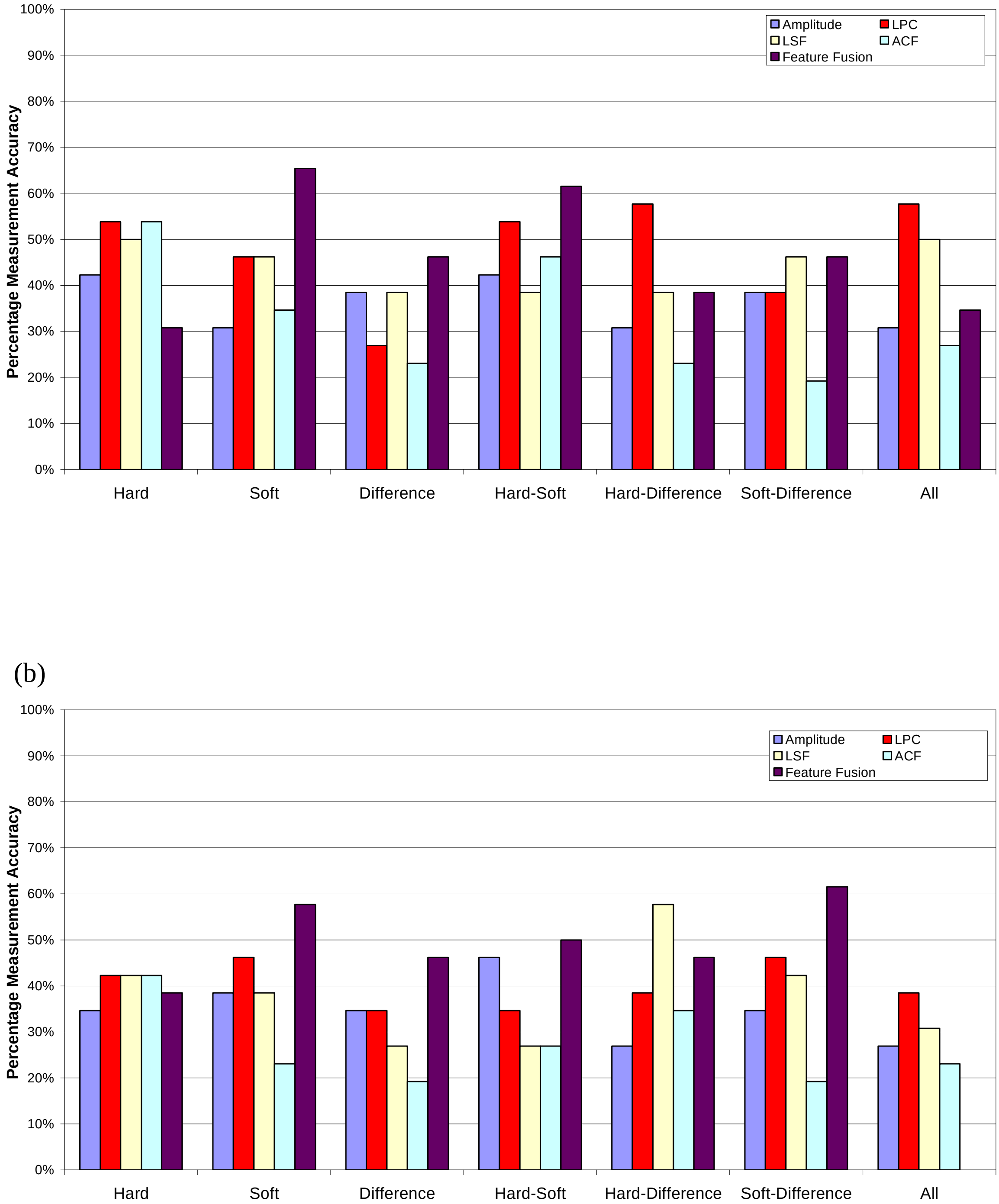

Figure 6.22 – Bubble MLP: Percentage Measurement Accuracy for the Superficial Liquid Velocity of Bubble Test Points (a) ZMUV (b) PCA

(a)

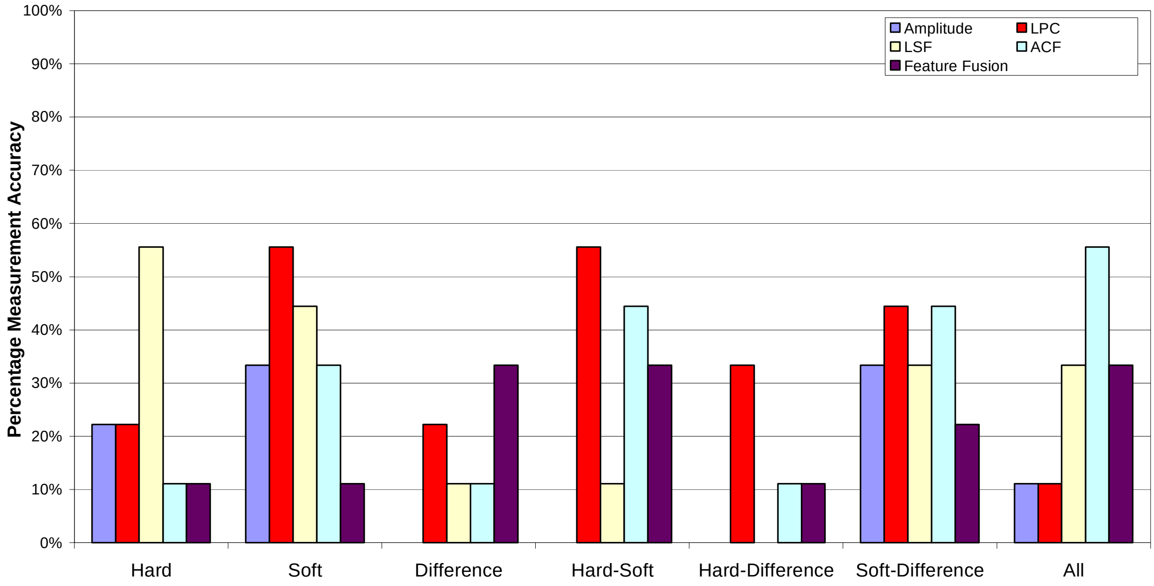

(b)

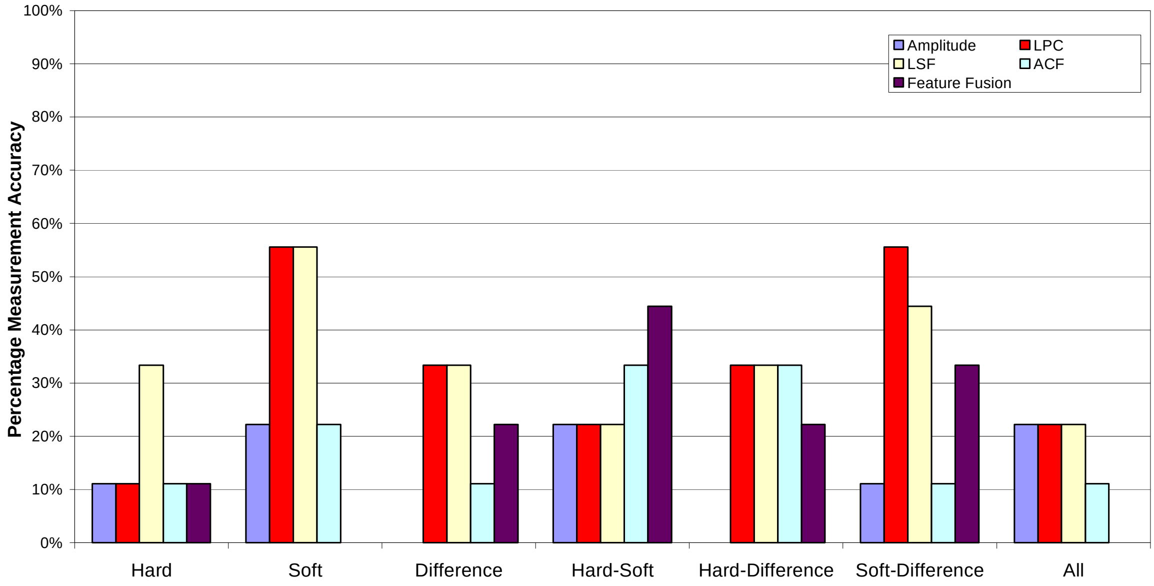

Figure 6.23 – Bubble MLP: Percentage Measurement Accuracy for the Superficial Liquid Velocity of Slug Test Points (a) ZMUV (b) PCA

(a)

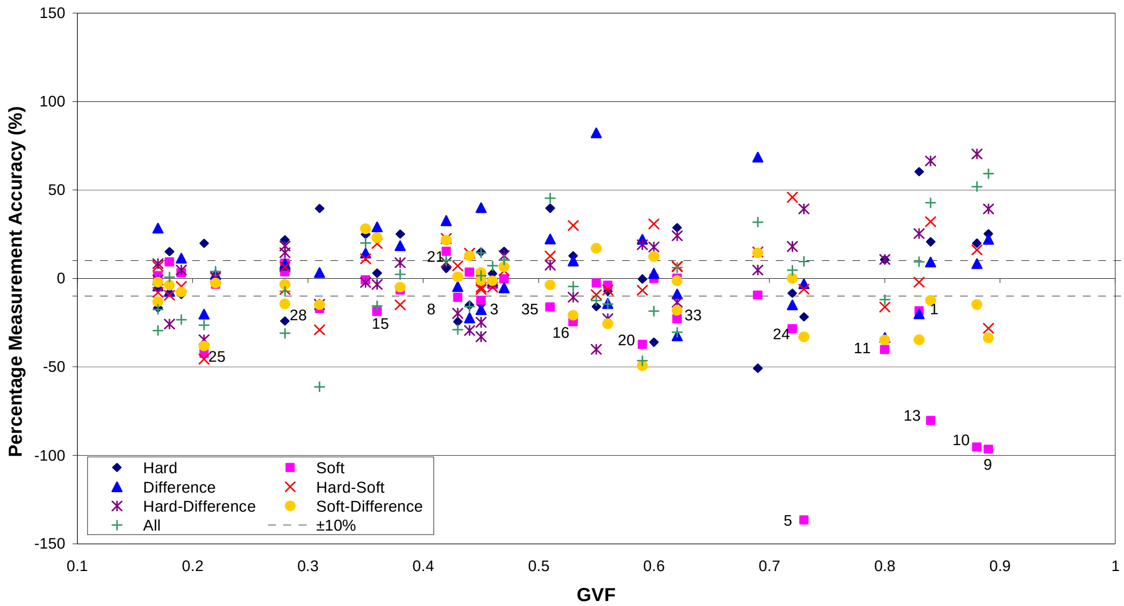

(b)

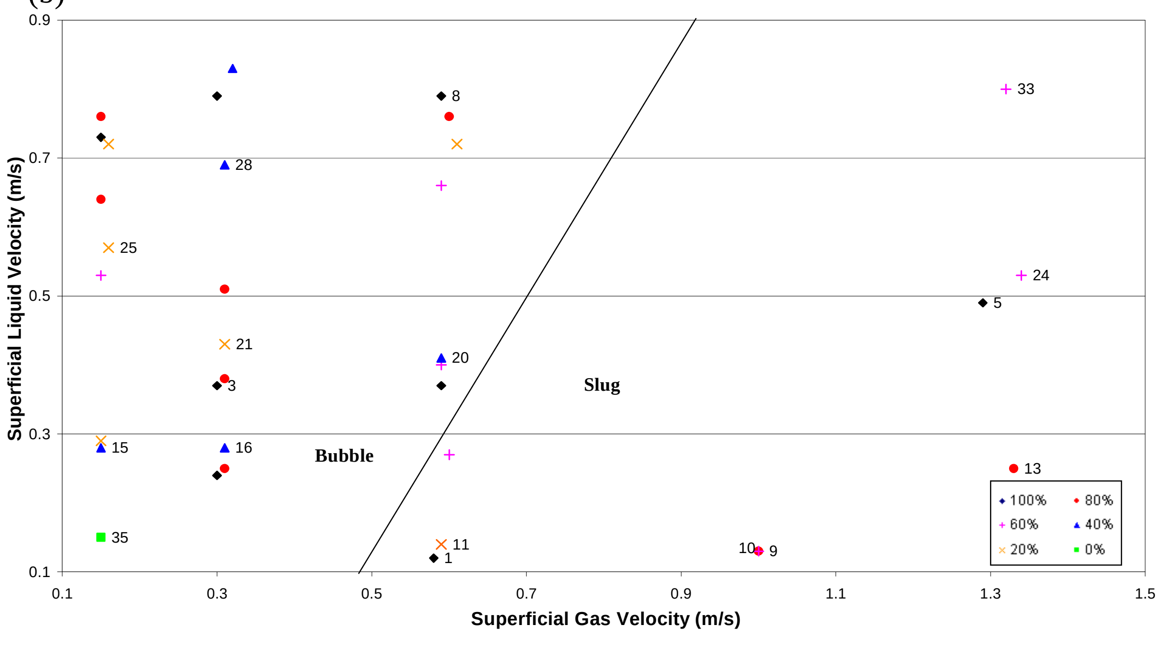

Figure 6.24 – Bubble MLP: Percentage Liquid Error Distribution for Feature Fusion (ZMUV) (a) GVF Plot (b) Outlying Test Point Matrix Location

(a)

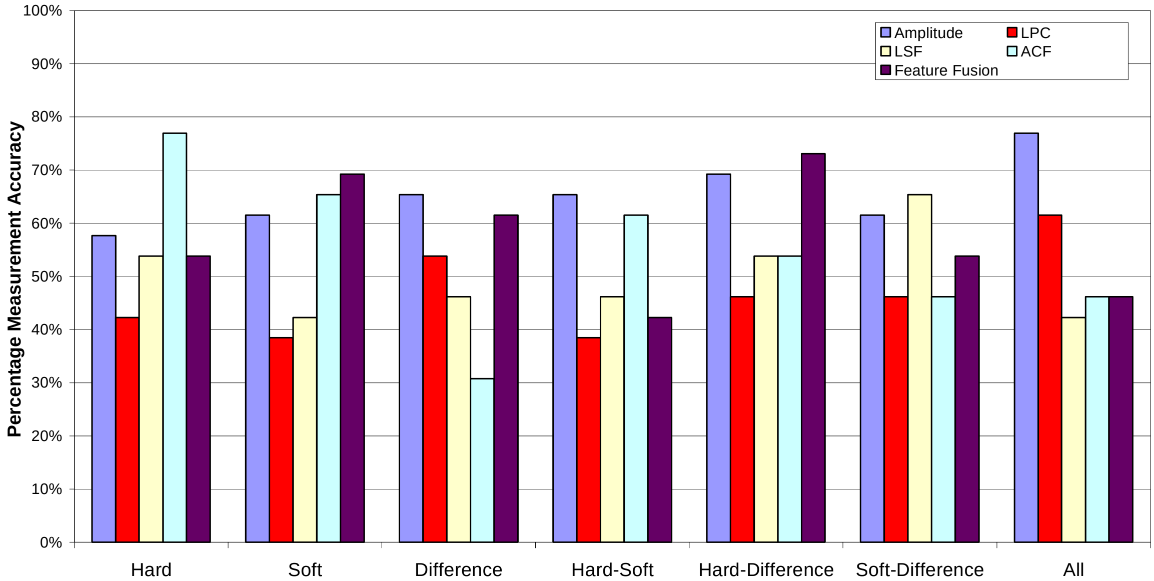

(b)

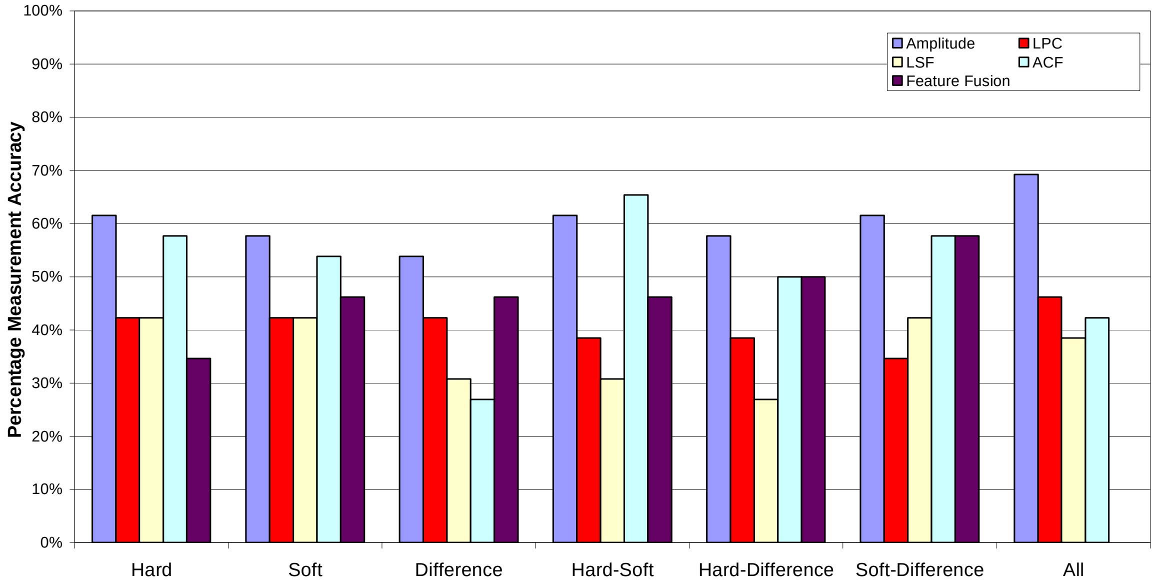

Figure 6.25 – Bubble MLP: Percentage Measurement Accuracy for the Water Cut of Bubble Test Points (a) ZMUV (b) PCA

(a)

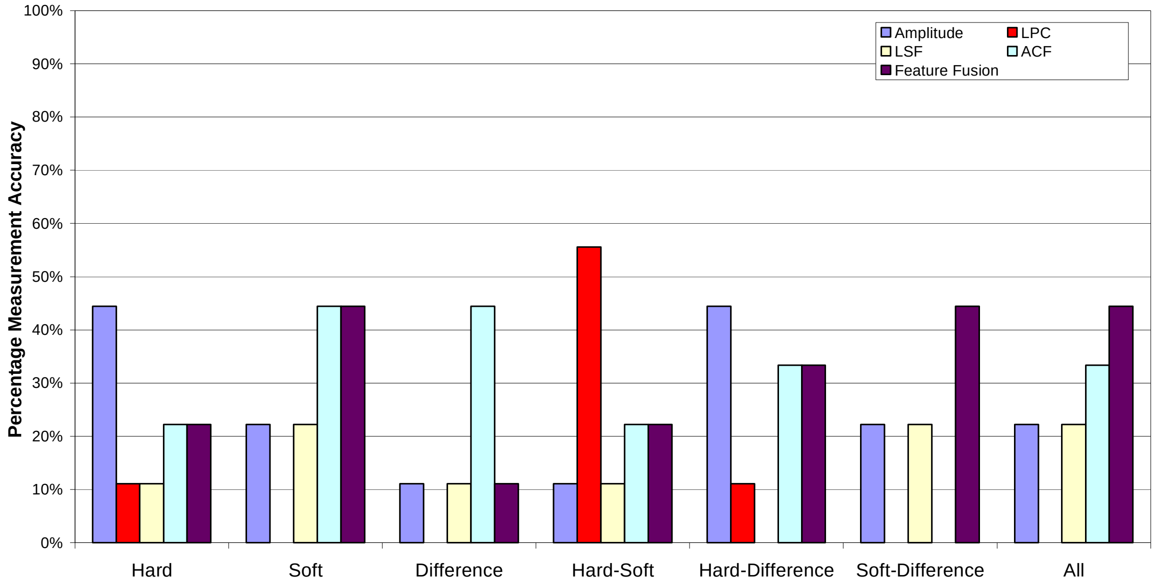

(b)

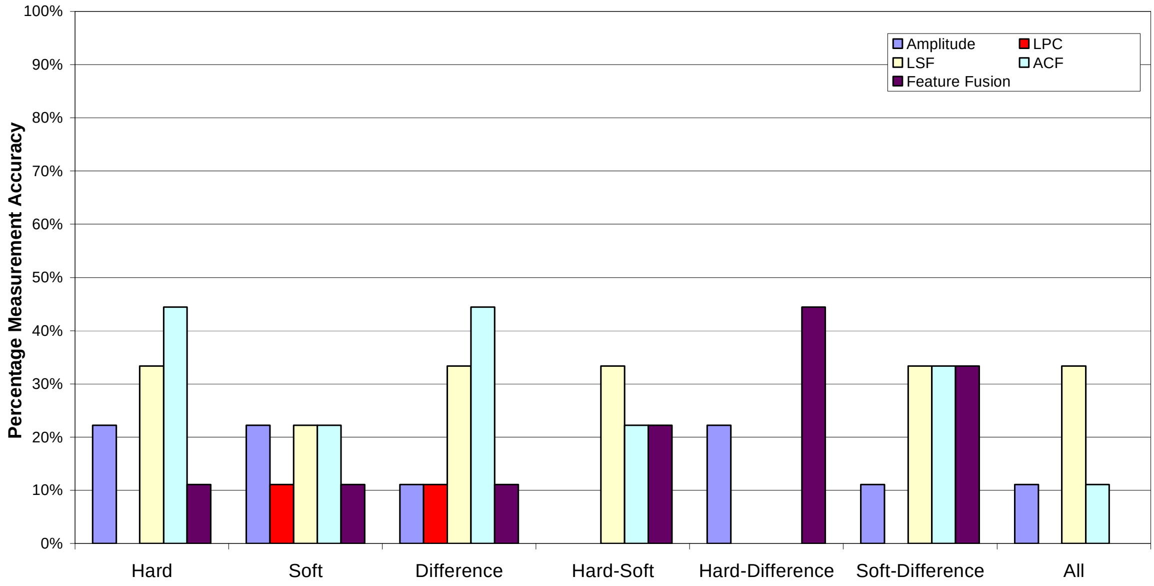

Figure 6.26 – Bubble MLP: Percentage Measurement Accuracy for the Water Cut of Slug Test Points (a) ZMUV (b) PCA

(a)

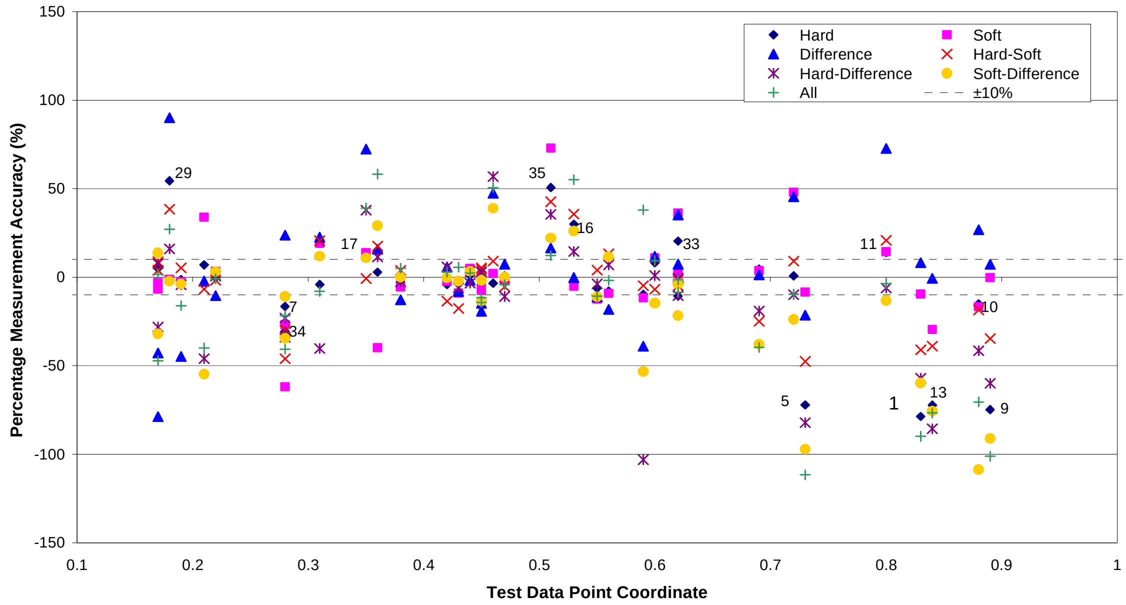

(b)

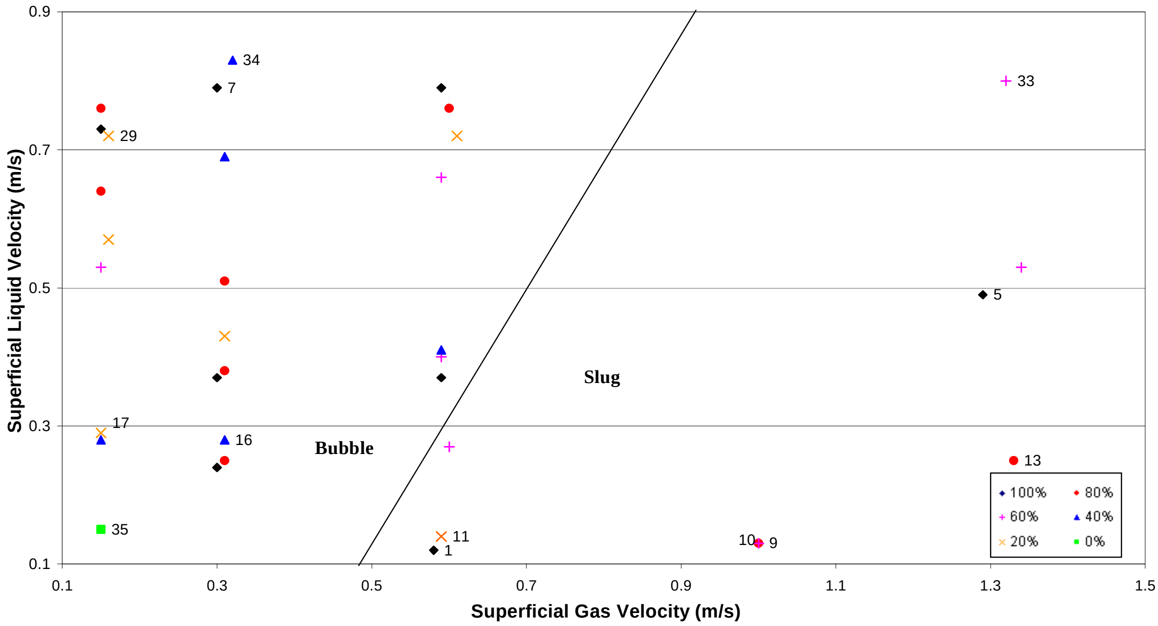

Figure 6.27 – Bubble MLP: Percentage Water Cut Error Distribution for ACF (ZMUV) (a) GVF Plot (b) Outlying Test Point Matrix Location

6.4.2.2 Slug Regime MLP Neural Network

Based on the repeatability results obtained from extensive preliminary repeatability test, the slug regime MLP neural network architecture was defined to be [n – 6 – 3]. All other parameters were as per the original Bayesian MLP. The trained network was presented with same test data set, a mixture of bubble and slug flow regime test points.

6.4.2.2.1 Gas Superficial Velocity

Figures 6.28 and **6.29** display the gas superficial velocity measurement results acquired from the slug regime MLP neural network using a variety of different input signal and feature combinations for the ZMUV and PCA pre-processing routines respectively. Feature fusion results employing PCA pre-processing were unobtainable when using two or more input signals owing to the sparse quantity of slug training data points available: the number of input features became greater than the number of slug training data points.

Figure 6.28 illustrates the network performance for the slug test points. Employing the PCA routine, the LSF features provided good gas superficial velocity predictions: 89% of data points achieved measurement predictions within ±10% for the hard signal, fused soft and difference signals, and all signals permutations. However, the best performance was yielded using the ZMUV pre-processing algorithm and exploiting the feature fusion features of the hard signal: 100% of slug data points were predicted within the target accuracy of ±10% and 89% of data points to within ±5%. Furthermore, 100% of slug point gas velocities were also obtained for fused LSF features of the soft and difference signals and the fused LPC from all signals. However, only 78% of slug points were classified to within ±5% using the LSF and LPC inputs described.

Figure 6.29 presents the bubble test point results for the slug regime trained network. As anticipated, the bubble point classification observed was relatively poor reinforcing the hypothesis that different underlying relationships exist between features and flow parameters for each of the flow regimes. In all cases, less than 47% of bubble test points were predicted within the specified target accuracy.

Figure 6.30 (a) displays the errors associated with each of the test data points for neural network simulations undertaken employing feature fusion as the input features and the ZMUV pre-processing routine. The hard signal data points exhibiting errors in excess of ±10% have been identified. One can observe that as the test point GVF increases, the more slug-like the flow regime, the number of measurement errors out with the target specification decreases.

The location of the test data points out with the target accuracy on the test matrix, and their flow regime classification are shown in **Figure 6.30 (b)**. It can be seen that all of the slug regime test points were accurately predicted. Bubble test points located near to the KSOFM defined regime boundary were classified within the target accuracy despite the network being trained on slug regime data only. This suggests that data points located close to the regime boundary exhibit regime duality that enables them to be classified according to their slug or bubble characteristics.

6.4.2.2.2 Liquid Superficial Velocity

Figures 6.31 and **6.32** show the liquid superficial velocity measurement results obtained from the slug regime MLP neural network for the slug and bubble test points respectively.

Figure 6.31 illustrates that the slug regime liquid superficial velocity classification was significantly better than that obtained for the bubble points in the bubble MLP: 100% of slug data points were predicted within ±10% their target outputs employing ZMUV and the feature fusion input vectors of the hard and soft signals (78% of calculations were within ±5%). Based on the results obtained, it would appear that the liquid phase exerts a larger influence on the signal in the slug flow regime than the bubble flow regime.

Figure 6.32 exhibits the liquid measurement results for the bubble regime test points. Although accurate predictions were obtained for the slug test points, this model obviously does not transfer well to bubble data points; typically, 75% of bubble test points produced errors outside the target threshold.

Figure 6.33 (a) presents the measurement errors obtained for each of the test data points using the feature fusion group as the input features and ZMUV pre-processing. The hard-soft signal data points exhibiting errors in excess of ±10% have been identified. One can see that at high GVFs (>62%) liquid superficial velocity classifications were within the desired ±10% target accuracy range. Decreasing the GVF of the test point, thus increasing its bubble regime type characteristics, results in increased error frequency and magnitude. **Figure 6.33 (b)** indicates the location of the erroneous test points on the test matrix and reinforces the flow regime sensitivity of the slug trained network: all off-specification measurements reside in the bubble flow regime sector. Bubble test points successfully classified were located near to the KSOFM boundary.

6.4.2.2.3 Water Cut

Figures 6.34 and **6.35** display the water cut measurements observed employing the slug data trained MLP for slug and bubble test points respectively.

Figure 6.34 illustrates the improvement in the performance yielded in the water cut determination through the employment of a flow regime dependent model. Exploiting the amplitude features of the hard signal and the PCA pre-processing routine, 100% of slug test points were measurement to within ±10% of their target output and 78% to within ±5%. Strong water cut classifications were witnessed for all input signals studied using the amplitude features.

Figure 6.35 demonstrates the poor water cut determination measurement yielded for bubble regime points from a slug regime trained network reiterating the flow regime specificity of the models developed in the multilevel hierarchical neural network system.

Figure 6.36 (a) reveals that water cut measurements tended to be more prone to error as the test point flow conditions deviated from those experienced during training, i.e. slug. One can see that points in the slug flow regime and some bubble points near to the boundary were less prone to exhibit errors outside the target threshold, **Figure 6.36 (b)**.

(a)

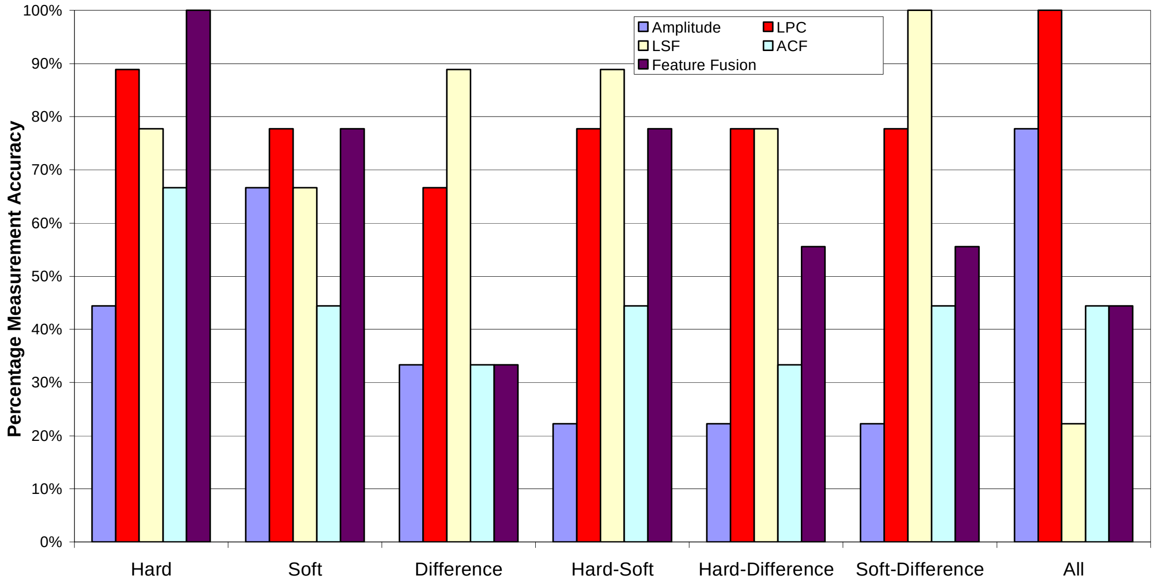

(b)

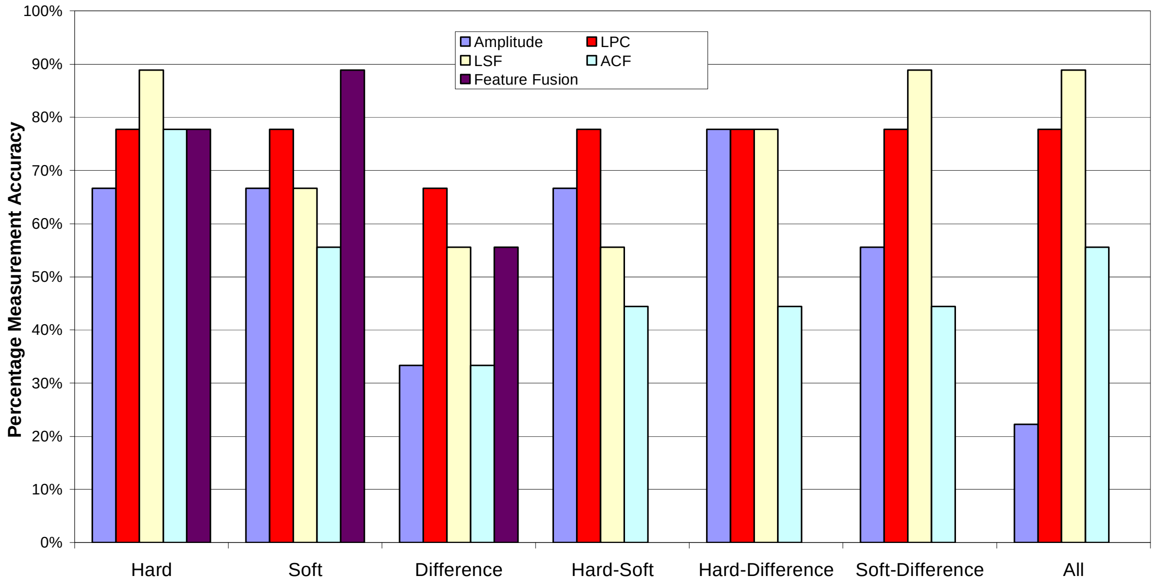

Figure 6.28 – Slug MLP: Percentage Measurement Accuracy for the Superficial Gas Velocity of Slug Test Points (a) ZMUV (b) PCA

(a)

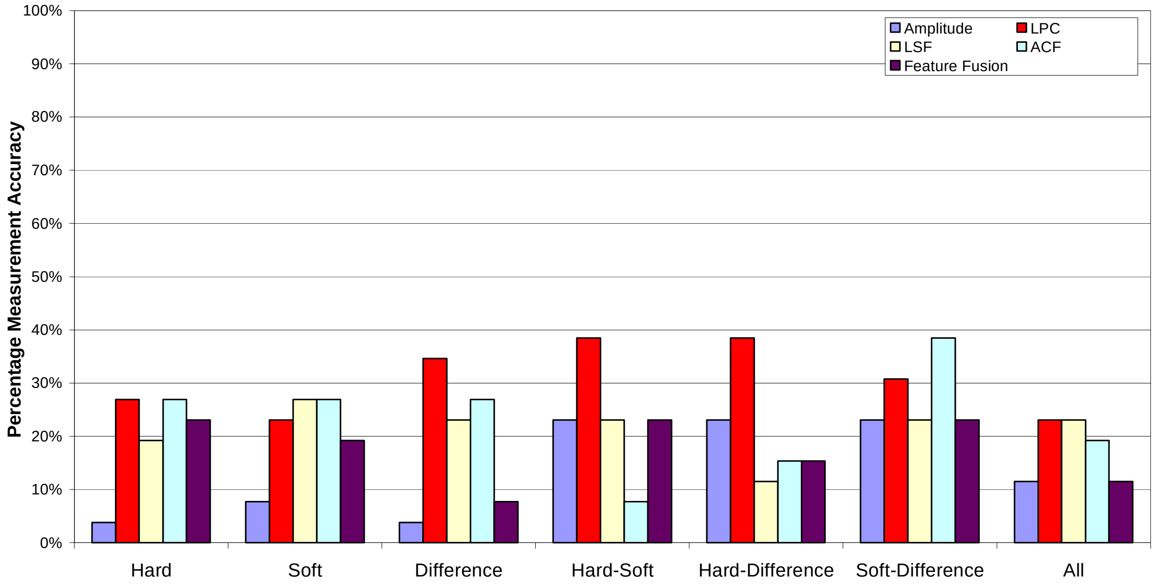

(b)

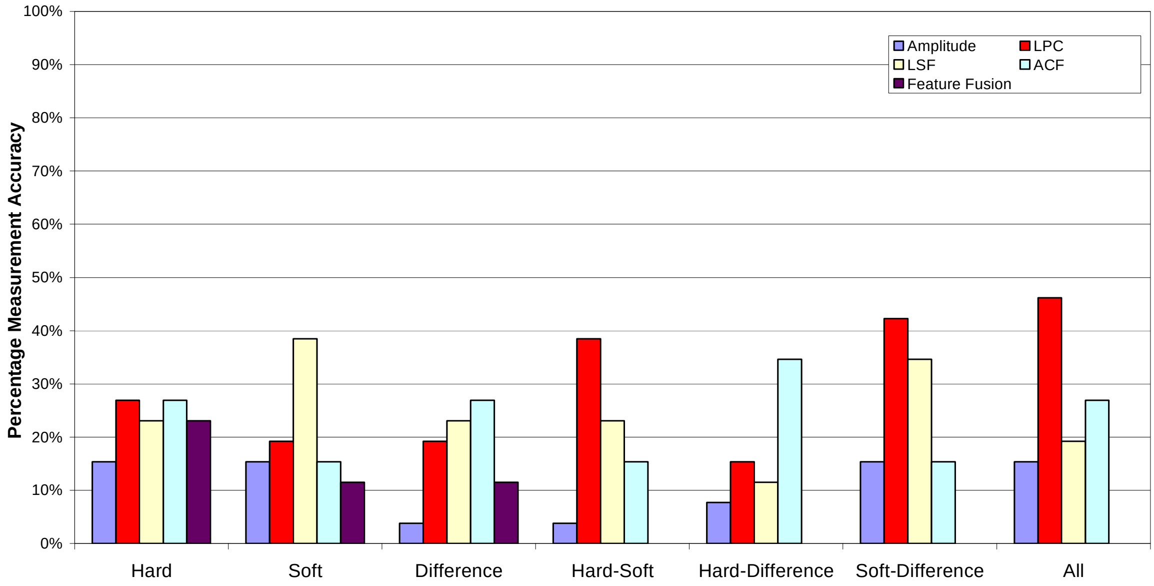

Figure 6.29 – Slug MLP: Percentage Measurement Accuracy for the Superficial Gas Velocity of Bubble Test Points (a) ZMUV (b) PCA

(a)

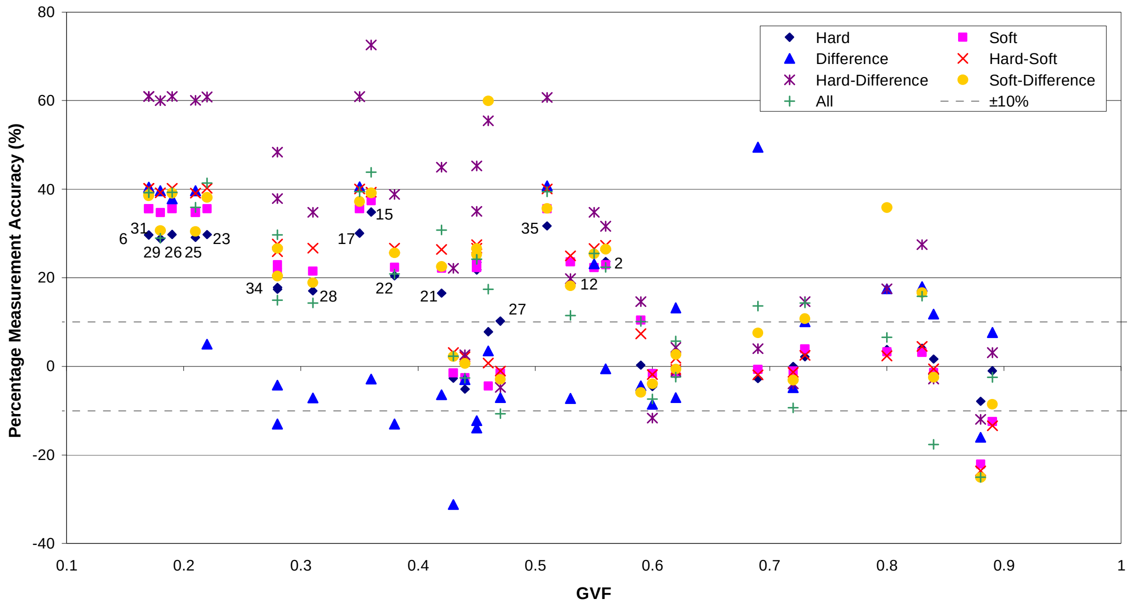

(b)

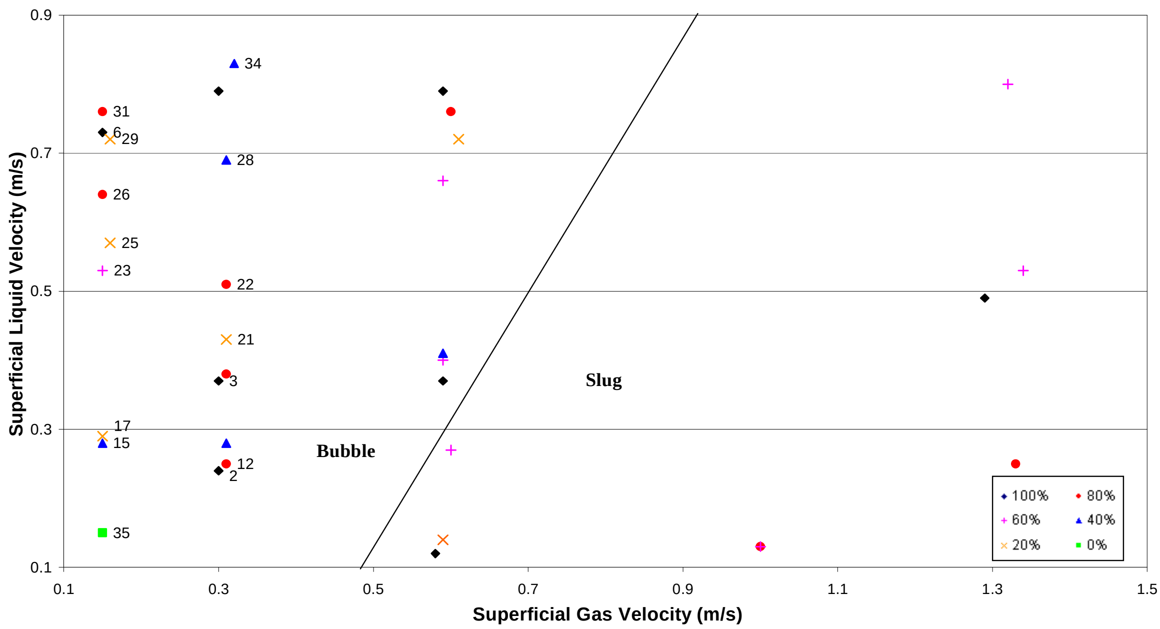

Figure 6.30 – Slug MLP: Percentage Gas Error Distribution for Feature Fusion (ZMUV) (a) GVF Plot (b) Outlying Test Point Matrix Location

(a)

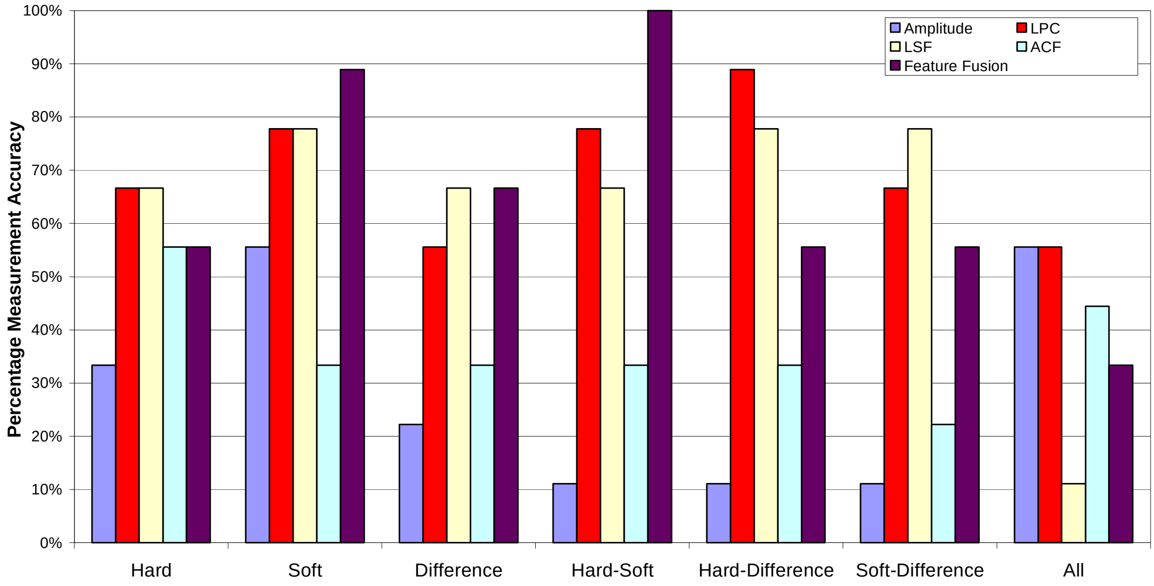

(b)

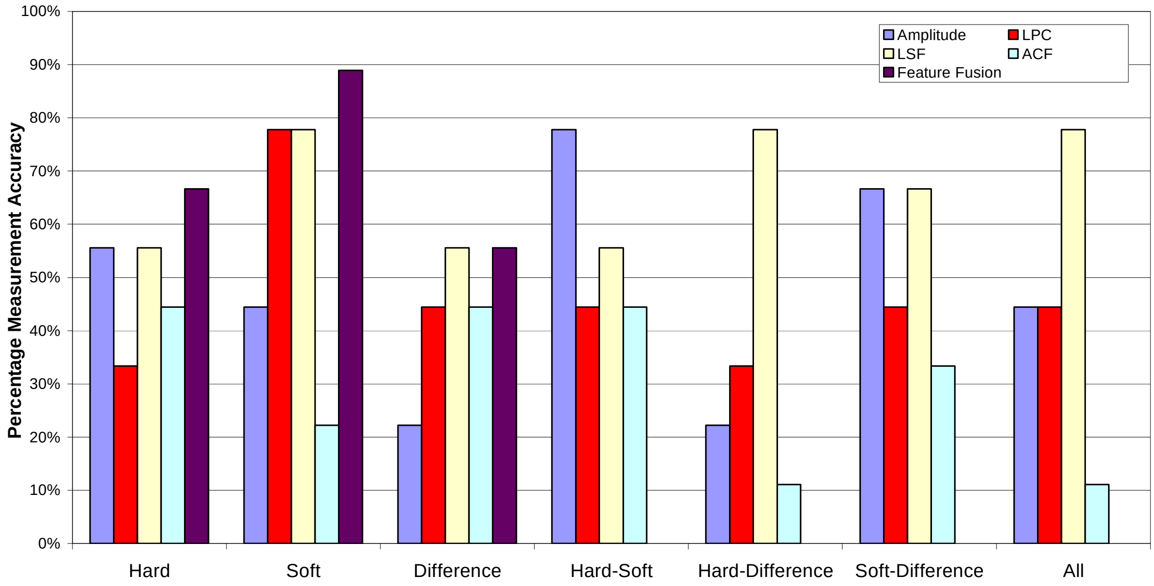

Figure 6.31 – Slug MLP: Percentage Measurement Accuracy for the Superficial Liquid Velocity of Slug Test Points (a) ZMUV (b) PCA

(a)

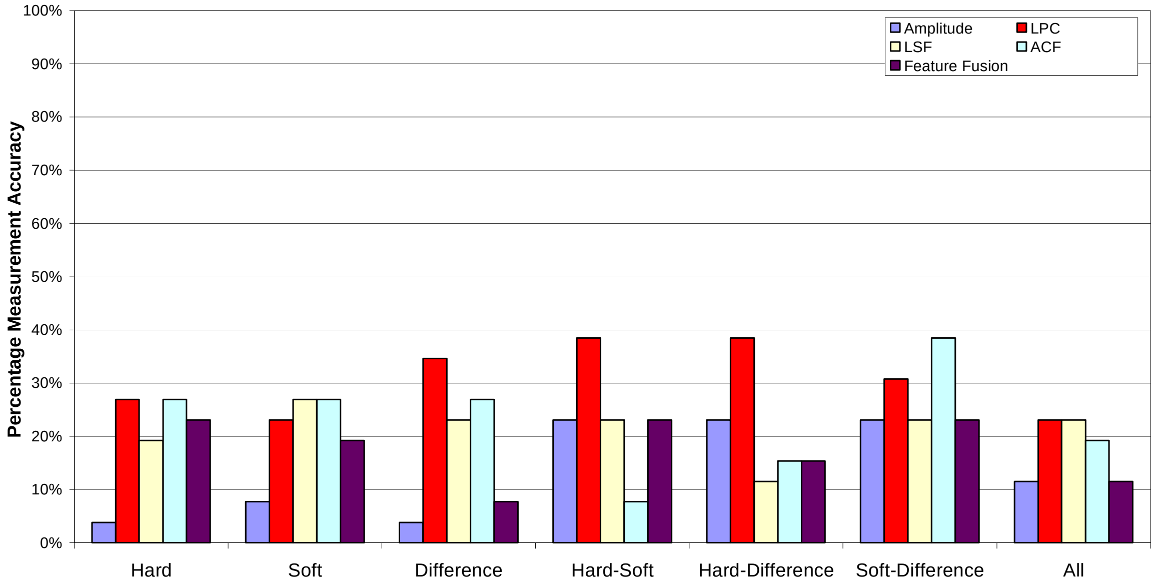

(b)

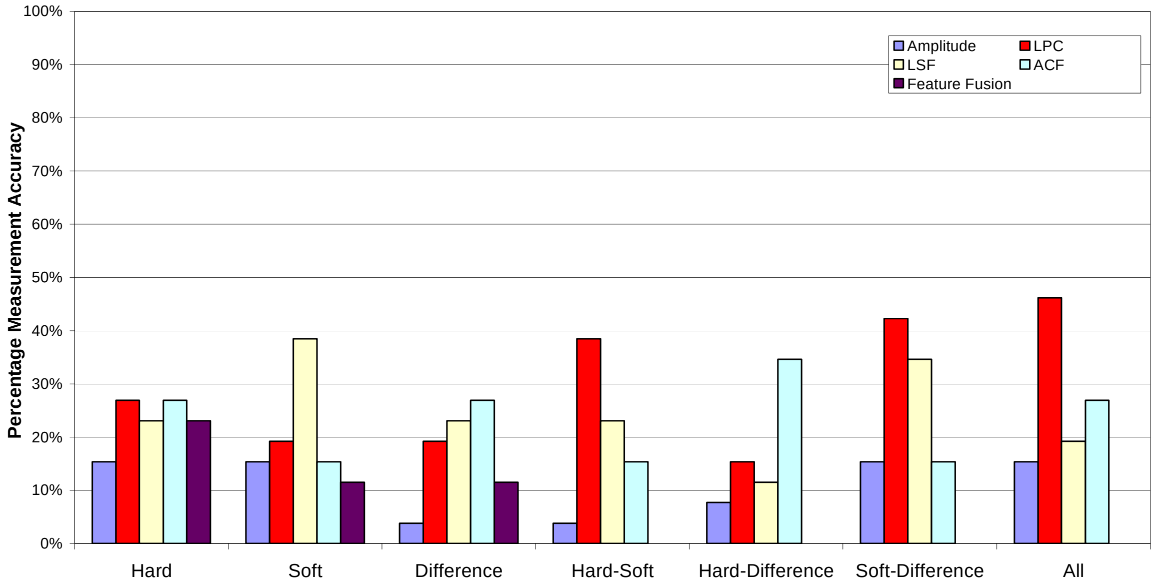

Figure 6.32 – Slug MLP: Percentage Measurement Accuracy for the Superficial Liquid Velocity of Bubble Test Points (a) ZMUV (b) PCA

(a)

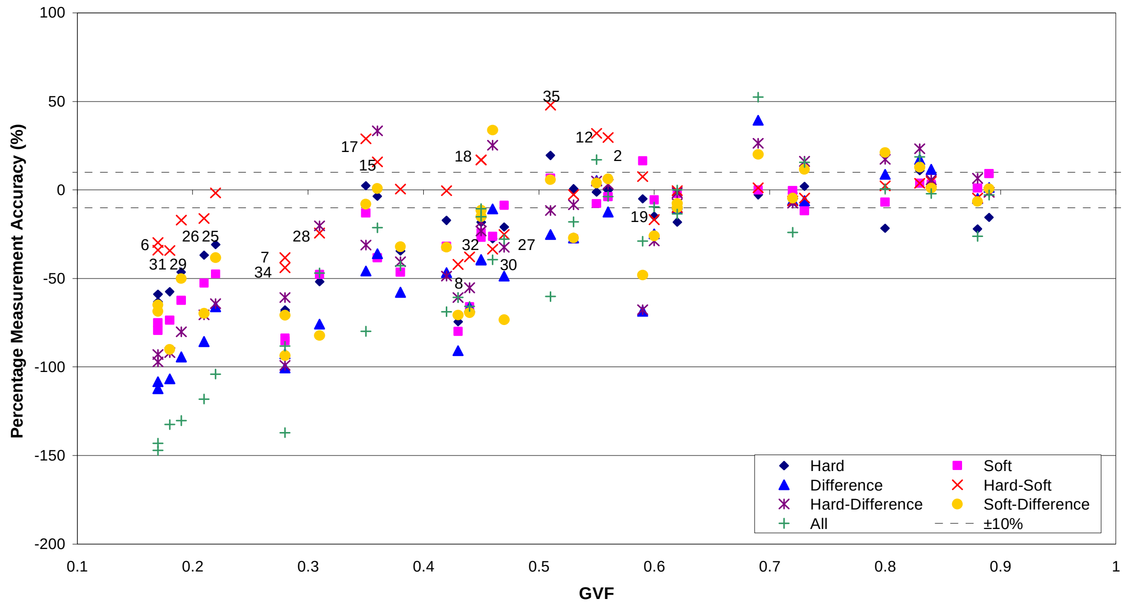

(b)

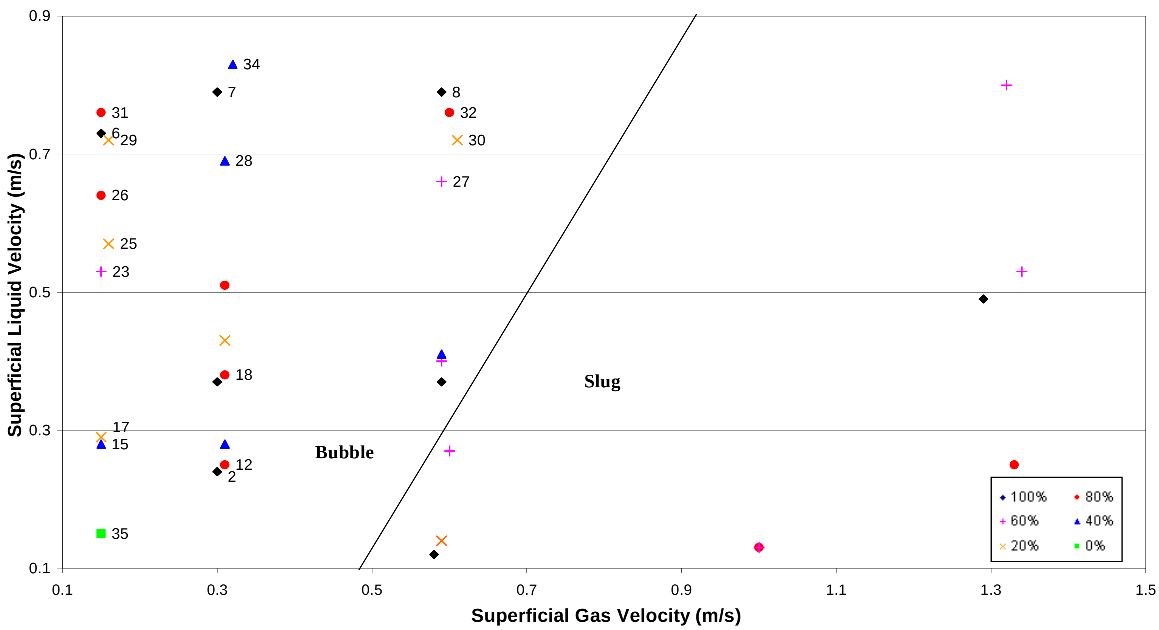

Figure 6.33 – Slug MLP: Percentage Liquid Error Distribution for Feature Fusion (ZMUV) (a) GVF Plot (b) Outlying Test Point Matrix Location

(a)

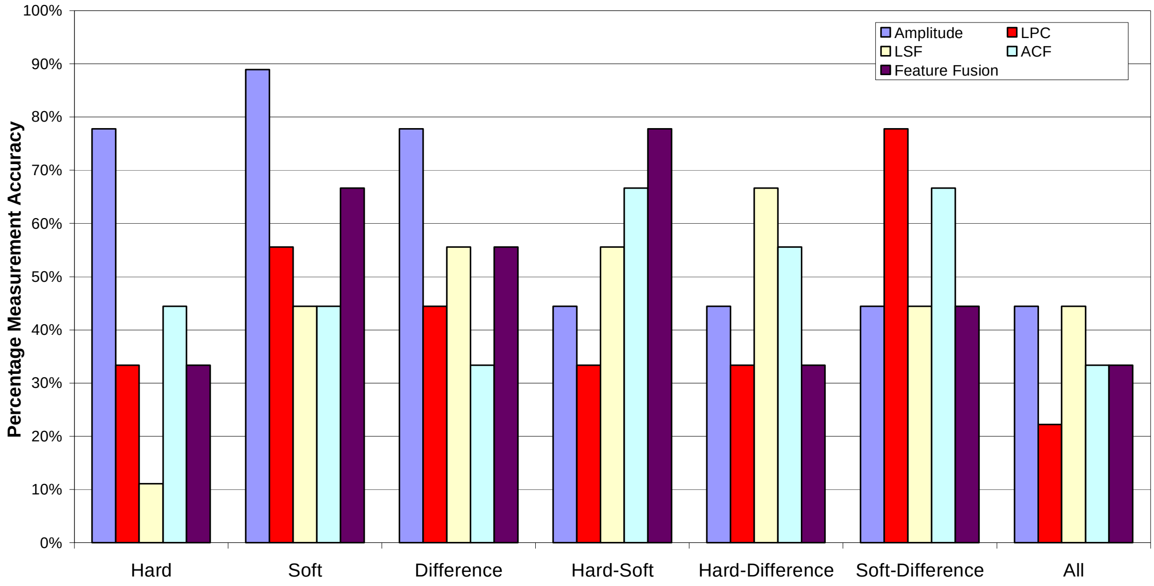

(b)

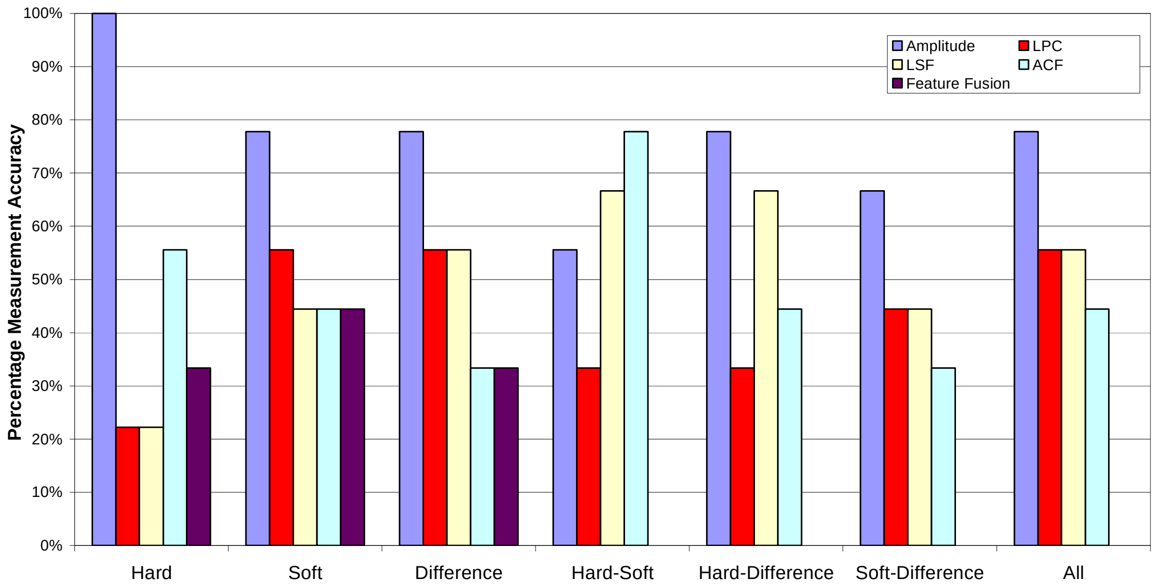

Figure 6.34 – Slug MLP: Percentage Measurement Accuracy for the Water Cut of Slug Test Points (a) ZMUV (b) PCA

(a)

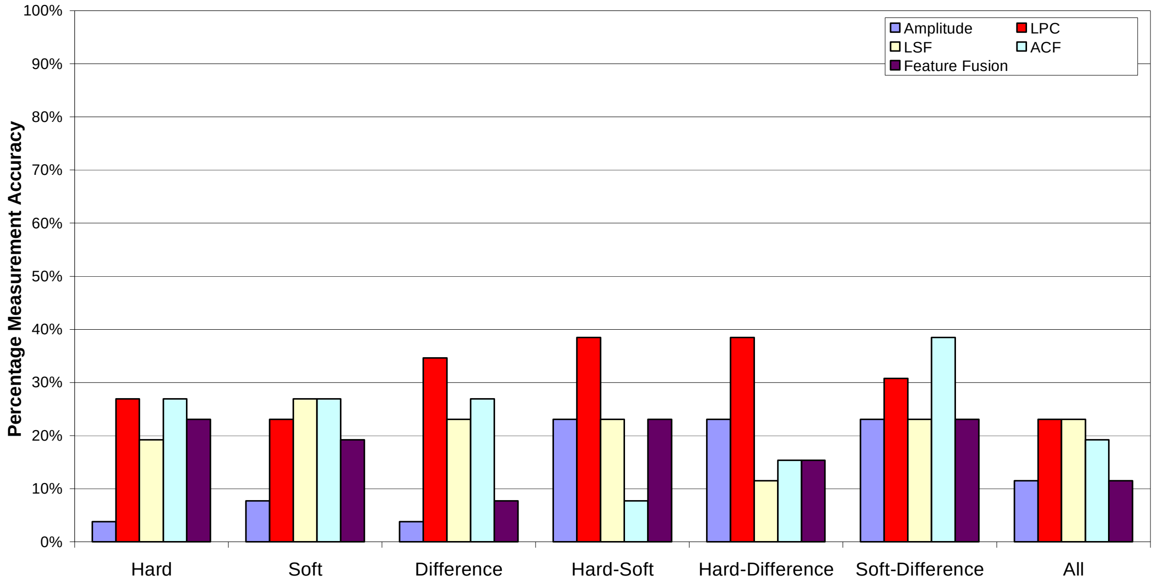

(b)

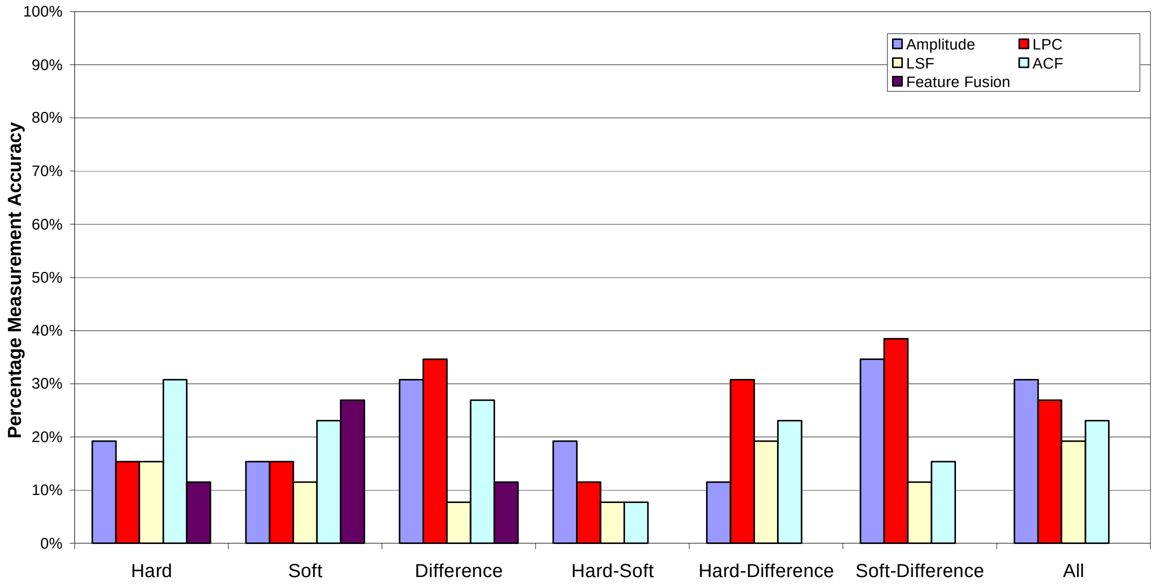

Figure 6.35 – Slug MLP: Percentage Measurement Accuracy for the Water Cut of Bubble Test Points (a) ZMUV (b) PCA

(a)

(b)

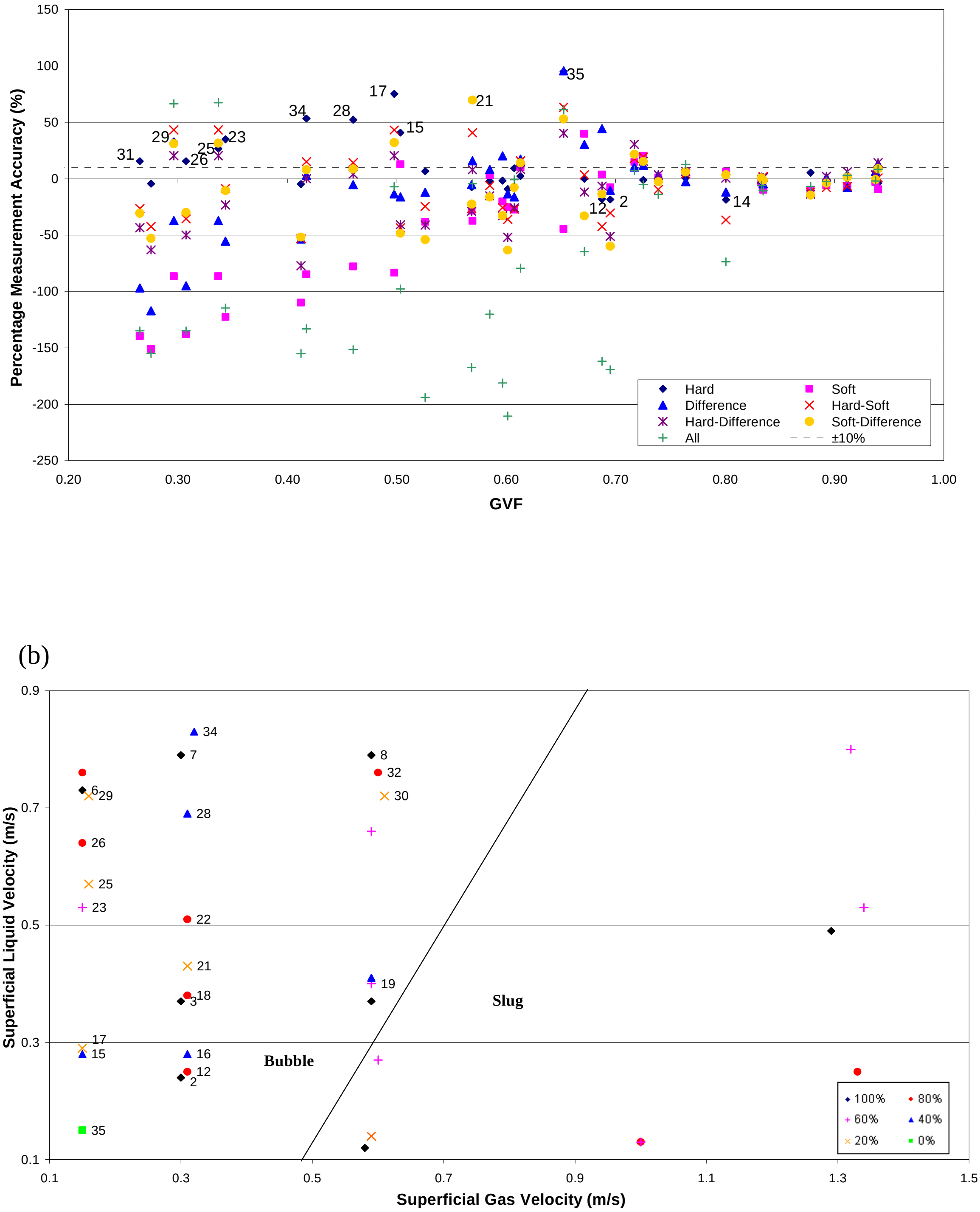

Figure 6.36 – Slug MLP: Percentage Water Cut Error Distribution for Amplitude Features (ZMUV) (a) GVF Plot (b) Outlying Test Point Matrix Location

6.5 Pattern Recognition Model Classification Results

Output variable classification accuracy for the single MLP and multilevel hierarchical pattern recognition models are summarised in **Table 6.2**.

Output	**Single MLP Model**		**Two-Regime Multilevel Hierarchical Model**					
			Bubble		**Slug**		**Overall**	
	±10%	**±5%**	**±10%**	**±5%**	**±10%**	**±5%**	**±10%**	**±5%**
Gas Velocity (Superficial)	97%	71%	100%	88%	100%	89%	100%	89%
Liquid Velocity (Superficial)	69%	51%	65%	54%	100%	78%	74%	60%
Water Cut	83%	49%	73%	54%	100%	78%	78%	60%

Table 6.2 – Summary of Pattern Recognition Flow Classification Accuracies

The single MLP neural network model classified 97% of all test point gas superficial velocities to within ±10% and 71% to ±5%; however, the liquid parameter predictions were not of the same standard. This suggests that the extracted features yielded good correlation with the multiphase flow gas phase properties across the measurement range studied and discrepancies in the correlations between flow regimes could be sufficiently modelled by a single neural network model. However, with the current feature set, it is not possible to obtain satisfactory liquid parameter predictions using only a single MLP neural network.

The multi-level hierarchical neural network model with flow regime dependent MLPs yielded an overall improvement in measurement accuracy. An increased proportion of test points' superficial phase velocities were classified within the target accuracy employing the multilevel hierarchical model. However, a reduction in the number of test point water cuts measured to within the ±10% target was observed but an increase was observed for those classified to within ±5%. Furthermore, the liquid phase parameter classification in the slug regime MLP was significantly better than that obtained in the bubble regime MLP suggesting that features in the raw count signal in slug flow regimes have stronger correlations with the liquid phase parameters than those present in bubble regime flows.

Table 6.3 summarises the feature input vector and signal(s) that gave the optimal response for each of the output targets. It was observed that each multiphase flow parameter offered a variety of responses based on the input features-signal combination presented. Each parameter exhibited a preference for a different input feature configuration.

The performance of the LPC and LSF parameters was not as. However, the author recognises that the LPC transforms (and by extension the LSF representations) were perhaps determined for too small an order to extract discriminatory data for the relatively high sampling rate. Accordingly, the LPC would be representative of the high frequency signal features whereas the majority of the discriminatory information was found to be in the low frequency range. For future studies, the author recommends the use of a higher-order LPC of the application of the low order LPC to a down-sampled version of the signal.

Examining the results of both models, it was observed that the ZMUV pre-processing routine outperformed that of the PCA. This indicates that trimming features from input set owing to their relatively small variability is not particularly helpful in multiphase flow studies. Indeed, it appears though salient data may be encoded within these small variations and that they can be exploited to yield significantly more accurate output predictions.

Output	**Single MLP Model**	**Two-Regime Multilevel Hierarchical Model**	
		Bubble	**Slug**
Superficial Gas Velocity	Amplitude *Hard Signal*	Fusion *Hard & Difference Signals*	Fusion *Hard Signal*
Superficial Liquid Velocity	LPC *Soft Signal*	Fusion *Soft Signal*	Fusion *Hard and Soft Signals*
Water Cut	Amplitude *All Signals*	ACF *Hard Signal*	Amplitude *Hard Signal*

Table 6.3 – Summary of Input Feature-Signal Combinations Yielding Optimal Classification

Table 6.4 summaries the response of the flow regime dependent MLPs when presented with input data from the alien flow regime.

Output	**Bubble**		**Slug**	
	±10%	**±5%**	**±10%**	**±5%**
Superficial Gas Velocity	44%	44%	31%	27%
Superficial Liquid Velocity	56%	44%	46%	46%
Water Cut	44%	33%	38%	38%

Table 6.4 – Flow Regime MLP Performance with Alien Flow Regime Data

Comparing the MLP results in **Tables 6.2** and **6.4** it can be seen that each individual MLP network yielded good results for test points of the same flow regime as the training data and poor prediction of those test points belonging to the alien flow regime.

These findings support the hypothesis that each flow regime exhibits its own characteristic correlations between statistical features of the generated gamma count signal and the multiphase flow parameters.

During testing of the two-regime multi-level hierarchical it was seen that test points located near to the boundary were classified within their target accuracy by both the slug and bubble MLPs. It was hypothesised that such data points must exhibit features of both regimes. If this is so, the presence of such points during the training sequence may hinder the MLP networks capability to develop an effective model for one specific regime. As a result, a separate classification MLP network for data points exhibiting this bubble-slug regime duality may lead to an overall improvement in the test points' prediction accuracies.

Accordingly, a three-regime multilevel hierarchical model was conceived and tested. The KSOFM was employed to generate three flow regime classifications: bubble, slug and intermediate. The intermediate flow regime was produced from the KSOFM nodes that housed both slug and bubble data points and were located along the flow regime boundary produced in the two-regime flow regime classification. **Figure 6.37** portrays the KSOFM node classification for three-regimes from which the data points were reclassified.

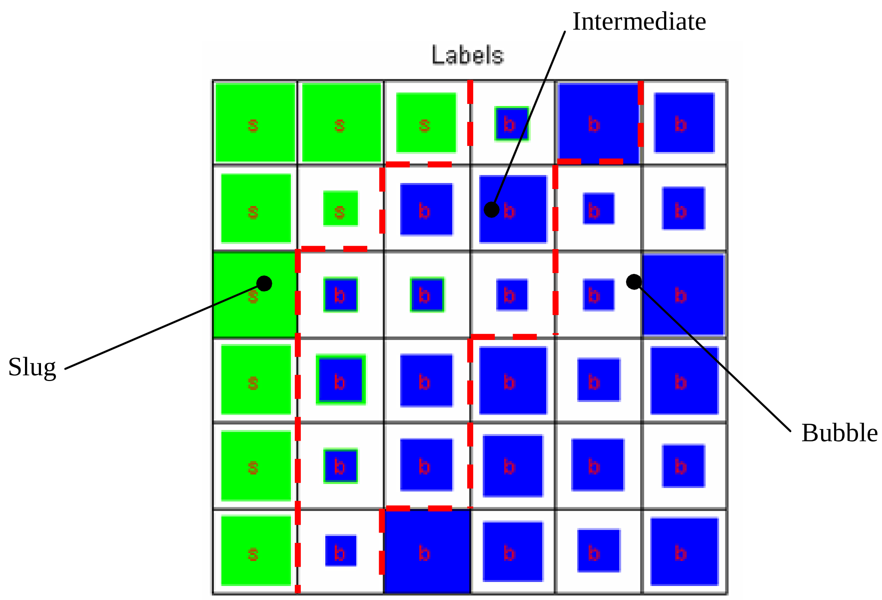

Figure 6.37 – Three-Regime KSOFM BMUs

Following reclassification using the KSOFM, the flow regime boundaries on the test matrix were redrawn to incorporate the intermediate regime, **Figure 6.38**. The training and test data points were altered to ensure an unbiased test point distribution. Consequently, the number of test points has been reduced in order to conserve the training to test point ratio in each of the flow regimes.

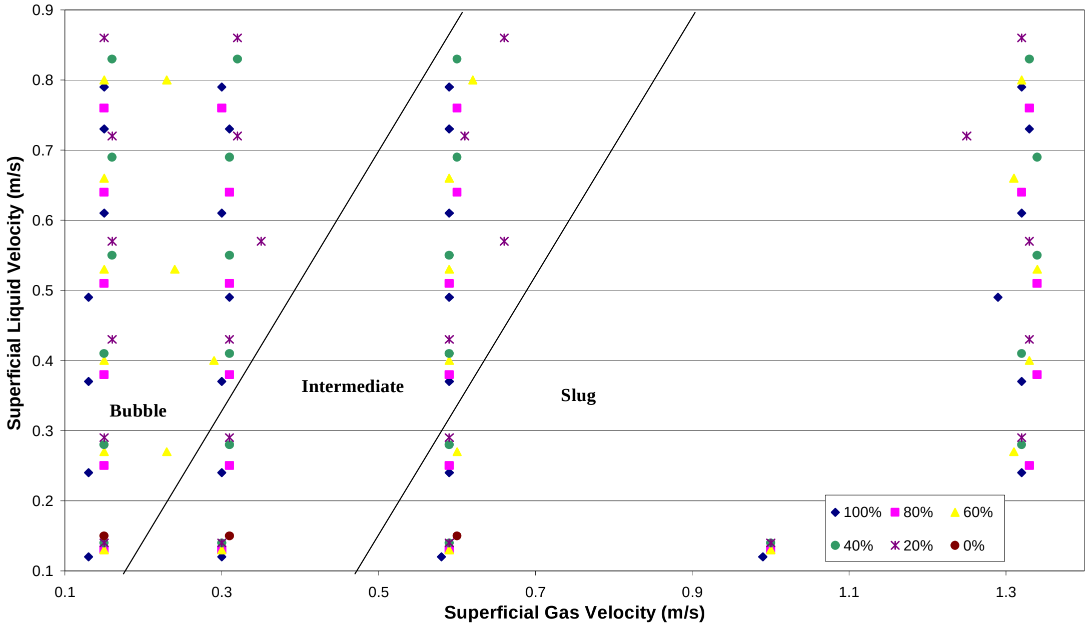

Figure 6.38 –Three-Regime Classification of Data Points

Network design yielded the following architectures for the systems: bubble MLP model [n – 7 – 3]; intermediate MLP [n – 8 – 3]; and slug MLP [n – 4 – 3]. The classification results of the 3-regime multi-level hierarchical model are summarised in **Table 6.5**.

Output	Bubble		Intermediate		Slug		Overall	
	±10%	±5%	±10%	±5%	±10%	±5%	±10%	±5%
Gas Velocity (Superficial)	100%	85%	100%	100%	71%	57%	90%	79%
Liquid Velocity (Superficial)	62%	62%	100%	71%	71%	71%	72%	66%
Water Cut	62%	23%	100%	71%	57%	43%	69%	41%

Table 6.5 – Classification Accuracies for Three-Regime Multilevel Hierarchical Model

Results obtained reinforced the flow regime specificity of the feature correlations with the multiphase flow properties. Good classification was obtained for test points sharing a common flow regime with the MLP training data; while, test points from a differing flow regime were poorly classified. The overall performance of the three-regime model was not as strong as that observed for the two-regime model. However, it should be noted that the capacity to analyse a three-regime model was hindered by the decreased training data available to each flow regime specific MLP.

6.6 Wavelet Transform Feature Inputs

Wavelet analysis of temporal signals exhibited discrimination between data points with differing flow conditions (**Chapter 4.4**). Wavelet packet decomposition of the signals facilitated separation of the high and low-frequency components. It was hypothesised that such decomposition may enable better liquid phase parameter classification.

A two level decomposition was performed on the gamma count signals yielding six coefficient packets. To reduce the dimensionality of the wavelet transform data, six moment features (*M*) were extracted from each of the sub-signals as this technique has been successfully applied in similar engineering studies [**116**].

$$M_m = \sum_{n=0}^{N_j - 1} \left(\frac{S[n]}{N_j} \right)^m S[n], m = 0,1,2,3,4,5 \qquad \text{(Eq. 6.3)}$$

Where *S[n]* denotes wavelet transform packet sequences A, D, AA, DD, DA and DD. Two pattern recognition models were constructed using the wavelet coefficient data: a single feedforward MLP network and a flow regime specific hierarchical model. Network design yielded the following architectures for the systems: signal MLP model [n – 15 – 3]; bubble MLP [n – 7 – 3]; and slug MLP [n – 5 – 3]. Designation of the point flow regime was undertaken employing a KSOFM which yielded the same classification as detailed in the statistical feature models. All other parameters were as per the previous pattern recognition models developed.

Results of the multiphase flow parameter classification accuracies of the wavelet transform feature models are summarised in **Table 6.6**.

	Single MLP Model		**Two-Regime Multilevel Hierarchical Model**					
			Bubble		**Slug**		**Overall**	
Output	**±10%**	**±5%**	**±10%**	**±5%**	**±10%**	**±5%**	**±10%**	**±5%**
Gas Velocity (Superficial)	71%	51%	96%	81%	89%	56%	94%	74%
Liquid Velocity (Superficial)	46%	11%	46%	23%	56%	44%	49%	29%
Water Cut	54%	20%	73%	50%	44%	44%	66%	49%

Table 6.6 – Summary of Wavelet Feature Based Flow Parameter Classifications

As observed with previous models, the flow regime specific network exhibited superior flow parameter classifications than a single feedforward MLP network. However, the data point classification from the wavelet features examined was less accurate than that obtained employing the statistical parameters of the original signal for both models. Gas superficial velocity predictions were still reasonable, but those of the liquid parameters were disappointing. Nevertheless, it is anticipated that these results could be ameliorated through further examination of wavelet functions and feature extraction techniques.

6.7 Summary

This chapter analysed the application of pattern recognition techniques to obtain the individual phase flow rates of a multiphase from the raw output signals of a single-source, dual-energy gamma densitometer.

Feature extraction was employed to represent the gamma count signals in a memory efficient and contour analysis studies observed that the features offered discrimination between different multiphase flow conditions. Examination of different pre-processing routines revealed that salient data may be encoded within small signal variations and , in the majority of instances, feature pruning through principal component analysis resulted in reduced classification accuracies.

A single MLP neural network system was outperformed in multiphase flow parameter classification by a multilayer flow regime specific model. The optimal input vectors were found to vary for each of the output parameters. It was shown that individual phase flow measurements to within ±10% are possible with an appropriate network set up.

Gas phase parameters exhibited higher prediction accuracies than their liquid counterparts, for all models, owing to the domination of the raw gamma count signal's properties by the passage of gas structures. However, liquid sensitivity to feature correlations was also found to be flow regime dependent. Good classification of slug regime liquid parameters was obtained in comparison to those exhibited in the bubble regime. It is anticipated that the application of the flow regime specific pattern recognition model in flow regimes unavailable during the study (annular flow) will yield measurement result accuracies similar to those presented.

Evidence of data point flow regime-duality was observed in the flow regime specific model as bubble test points lying close to the flow regime boundary were well classified by the slug MLP network and vice versa. Classification of the data points in the KSOFM also indicated that some data points exhibited characteristics associated with both slug and bubble regimes. Accordingly, caution should be exercised when developing flow regime specific models to build in boundary flexibility for flow regime specific correlations.

Application of wavelet transform based input vectors derived from the statistical moments of the first two levels packet decomposition were investigated. Reasonable classifications were obtained for the gas phase but liquid phase parameter classification was considerably poorer than conventional input approach. Nevertheless, wavelet packet decomposition was observed to be a powerful analysis tool and offers a multitude of new approaches to signal analysis. It is anticipated that further investigation of wavelet functions and feature extraction should enable improved liquid phase parameter determination.

Chapter 7: Conclusions and Future Work

This chapter summarises the original project objectives before documenting the conclusions that have been drawn from undertaking the research work. In addition, a number of recommendations are presented to the reader, each with the intention of extending the knowledge and understanding of the topic through future investigative work with a view to developing a robust, yet economic, clamp-on multiphase measurement device.

7.1 Conclusions

In the oil and gas industry, multiphase flow measurement is the determination of the individual flow rates of the oil, water, and gas obtained during production processes. This research work was concerned with the investigation of the suitability of gamma radiation methods to provide an economical means of clamp-on multiphase flow measurement. The reduced hardware and installation costs associated with deploying such units as multiphase flow meters, in conjunction with increasing oil prices, would enable economic justification of the industry's ultimate goal of a per well MPFM installation basis.

The objectives of the research work were:

- Conduct a literature review of multiphase flow and its measurement, gamma radiation in multiphase metering and the application of pattern recognition techniques in multiphase measurement.
- Undertake experimental data collection of a gamma-densitometer's response to a variety of vertical multiphase flow conditions.
- Analyse the gamma densitometer signal characteristics in relation to key multiphase flow parameters.
- Investigate a mechanistic approach to determining the individual phase flow fractions and phase velocities from the gamma densitometer output data.
- Investigate the suitability of the gamma densitometer data for exploitation in a pattern recognition based multiphase flow measurement system.

A review multiphase flow and its metering reiterated the need for the development of a versatile, low-cost measurement solution to meet the oil and gas industry's requirements. Employing gamma densitometry for multiphase flow analysis has been documented by a number of researchers to resolve the volume fractions multiphase flow mixtures or to identify the prevalent flow regime. The use of gamma densitometry in conjunction with pattern recognition in multiphase flow measurement has also been reported where the gamma-densitometer forms part of a sensor array for horizontal flow.

Gamma densitometers are already exploited in these capacities as part of several commercial multiphase metering systems. However, the flow in these meters is normally 'homogenised' employing a blind-tee upstream of the installation or deployment of a Venturi constriction in the measurement section, or involves other intrusive measurement components that do not lend themselves to clamp-on multiphase metering.

No information has been published in the public domain on the ability of a single gamma densitometer unit to provide both phase composition and velocity information for vertical multiphase flows. This research work has demonstrated that a single gamma densitometer unit can be exploited, in conjunction with pattern recognition analysis, to infer the superficial phase velocities and the liquid phase water cut; thus, enabling the individual component mass flow rates of the multiphase flow to be determined to a degree of accuracy comparable with several commercial available multiphase flow meters.

A high-speed sampling (250 Hz) gamma densitometer unit was installed at the top of the 10.5 m catenary riser in the Cranfield University multiphase flow test facility. Gamma-rays at two pre-defined energy levels of interest are detected and logged by the detection unit. Gamma count data was collected for a wide range of multiphase flow conditions for analysis. Investigation of the statistical properties of the gamma count signal revealed that 40 minutes of gamma count data collection are required to guarantee a statistically accurate description of the multiphase flow conditions being measured.

Signal analysis of the gamma count signal response to a variety of multiphase flow conditions was performed. Raw traces of the gamma counts signals gave a good visual indication of the gas and liquid phase distribution variations with time. Flow geometry classification was performed using the raw data signals. In general, the signal based flow regime classification corresponded well with published flow regime maps although some data points exhibiting characteristics of more than one regime were difficult to assign objectively to one particular regime.

A host of statistical parameters were extracted from the time-varying gamma count signals and their correlation with characteristic parameters of the multiphase flow composition investigated. Parameters demonstrating discrimination for different flow conditions were observed to be complex functions of the gas and liquid phase loadings and the water cut.

The geometry yielded by the signal probability mass function plots provided a good indication of the prevailing flow regime. A scatter plot of the mean hard gamma count against the coefficient of kurtosis produced a quantifiable quadratic relationship which enabled classification of the flow regimes. Nevertheless, classification was subjective when operating in the proximity of the defined flow regime boundary as traits of more than one regime were evident and discrepancies were obtained in classifications from experimental data with published flow maps and those from multiphase flow simulations.

Frequency domain analysis of the signals using FFT proved unsuccessful in decrypting the relationship between the frequency spectra densities and the dominating signal frequencies with respect to the multiphase flow parameters on both a global and flow regime specific basis. Investigation of the gas-structure frequency relationship proved more fruitful with the passage frequency of gas structures demonstrating a strong flow regime specific dependency on the gas phase loading. Correlation with the liquid phase was observed to increase with increased gas loading while the water cut was observed to exert a significant influence on the gas structure frequency at low liquid loadings.

Wavelet analysis indicated the intricate relationship between the time-frequency content of the signals was a complex function of the gas and liquid phase flow rates, and the liquid phase water cut. Discriminatory fractal properties were observed in the continuous wavelet transforms but it was not possible to determine any quantitative relationship between these fractal properties and the multiphase flow parameters.

A mechanistic approach to determine the multiphase flow individual phase volume fractions and velocities was investigated. Phase volume fraction information was interpreted from the degree of gamma attenuation induced by the multiphase flows.

Direct application of gamma attenuation equation to determine the phase fractions of the two-phase (air-water) data yielded significant errors owing to the presence of phase slip and flow geometry considerations. A linear correction model based on the superficial gas velocity facilitates determination of two-phase (air-water) data to within ±5% at a confidence level of 79%.

Employing the dual-energy attenuation equations for resolution of the multiphase data phase fraction resulted in irreconcilable errors. Modification of the two-phase linear correction model for application to the multiphase flow data facilitated determination of the gas volume phase fractions of the multiphase data to within ±10% with a confidence level of 100%. However, the modified correction model necessitated input of both superficial gas velocity and water cut information. Nevertheless, the phase fraction measurement performance was favourable in comparison with published correction correlations.

Linear correlations were obtained for the deviation between the mean hard and soft gamma counts and the liquid phase water cut at fixed gas volume fractions. However, this correlation was only valid for data points with gas volume fractions of up to 40%. At higher gas volume fractions, the correlation did not facilitate sufficient distinction of the water cut magnitude.

Quasi-periodic waveforms identified in the multiphase fluid density were analysed for their dependence on the gas and liquid superficial phase velocity parameters. Wavelet packet decomposition was exploited to separate the gamma densitometer signals into their low and high frequency components. The autocorrelation function of the filtered data facilitated determination of the gas structure pseudo-periods for each of the data points. The geometric form of the autocorrelation functions was observed to be sensitive to the data point flow regime for the large gas structures but was flow regime independent for the small gas structures.

It was determined that at constant liquid phase water cuts, the large gas structures had a strong dependence on the multiphase flow gas superficial velocity; while, the small gas structures exhibited a strong correlation with the liquid superficial velocity. Nevertheless, the underlying relationships between the gas structure pseudo-period data and the phase velocities proved to be too complex to be quantified and did not lend themselves to independent determination of the individual phase velocity parameters. The availability of data from a secondary sensor to facilitate cross-correlation determination of the phase velocity data may offer the best opportunity for further development of a mechanistic approach.

Analysis of the gamma-densitometer data in conjunction with pattern recognition techniques to correlate the properties of the quasi-periodic density waveforms with the individual phase velocities and the liquid phase water cut of the multiphase flows was undertaken.

A single MLP neural network system was determined to be insufficient to model the complex relationship between the statistical features studied and the multiphase flow parameters. Each multiphase flow parameter exhibited a preference for a different input feature configuration.

The single MLP model was outperformed in multiphase flow parameter classification by a multilayer hierarchical model comprising a Kohenon self-organising feature to classify the data points into their respective flow regimes in the first layer followed by individual MLP networks for each identified flow regime.

Employing a two-regime (bubble and slug) multilayer hierarchical model, it was shown that phase superficial velocities and liquid phase water cut can be determined to within ±10% with appropriate network set up. Liquid phase parameter classification in the slug regime MLP was significantly better than that obtained in the bubble regime MLP suggesting that features in the raw count signal in slug flow regimes have stronger correlations with the liquid phase parameters than those present in bubble regime flows. The optimal input vectors were also found to vary for each of the output parameters and for each regime.

In both models, gas phase parameters exhibited higher prediction accuracies than their liquid counterparts owing to the domination of the raw gamma count signal's properties by the passage of gas structures. However, liquid sensitivity to feature correlations was also found to be flow regime dependent. Good classification of slug regime liquid parameters was obtained in comparison to those exhibited in the bubble regime. Furthermore, the successful slug regime water cut classification contrasts with the mechanistic approach results where good correlation was obtained for bubble regime range GVFs of <40% and no distinct correlation for higher GVF data points.

Certain test points located near to the flow regime boundary were observed to exhibit flow regime duality and were classified within their target accuracy by both the slug and bubble MLPs. The presence of such points during a regime specific training sequence may hinder the MLP networks capability to develop an effective model for one specific regime. Consequently, caution should be exercised when developing flow regime specific models to build in boundary flexibility for flow regime specific correlations.

A three-regime (bubble, slug, and intermediate) multi-level hierarchical model was developed and tested. Results obtained reinforced the flow regime specificity of the feature correlations with the multiphase flow properties. Good classification was obtained for test points sharing a common flow regime with the MLP training data; while, test points from a differing flow regime were poorly classified. The overall performance of the three-regime model was not as strong as that observed for the two-regime model. However, the capacity to analyse a three-regime model was hindered by the decreased training data available to each flow regime specific MLP.

Application of wavelet transform based input vectors derived from the statistical moments of the first two levels packet decomposition were investigated. Reasonable classifications were obtained for the gas phase but liquid phase parameter classification was considerably poorer than conventional statistical feature input approach. Nevertheless, wavelet packet decomposition was observed to be a powerful analysis tool and offers a multitude of new approaches to signal analysis. It is anticipated that further investigation of wavelet functions and feature extraction should enable improved liquid phase parameter determination.

From the results presented, it was concluded that the use of gamma-densitometry, in conjugation with a flow regime based pattern recognition approach offers the best approach to multiphase flow parameter determination. It is believed that with further development work, a clamp-on gamma densitometer pattern recognition based system could offer a cost-effective multiphase metering method for the oil and gas industry.

7.2 Future Work

In order to build upon the research work described in this thesis, it is recommended that a number of elements be subject to further investigation.

- A step-wise approach to mechanistic model development is recommended as the phenomena observed during the current research work could not be attributed a particular source with confidence. The levels of complexity in the multiphase fluid should be introduced gradually. Data collection in a purely vertical pipe, with a static mixer installed upstream of the gamma densitometer measurement section, would facilitate the characterisation of the instrument's response to flow mixtures under non-slip conditions. Flow mixtures should be initially restricted to air-water combinations to determine the gas and liquid phase characteristics under non-slip conditions. The static mixer should then be removed to introduce slip and enable of the slip on the phase characteristics. Repetition of the steps described for air-oil systems would enable a detailed comparison of the effect of liquid phase physical properties on the gamma response. Finally, analysis of multiphase flow mixtures could be undertaken with a clear understanding of the underlying gamma-fluid interactions mechanisms.

- Better could have been made of the gamma count data collected in the pattern recognition analysis by chopping each of the time-series into two or three separate reduced duration time series. This would have increased the quantity of training and test data available for the pattern recognition model development and testing.

Count measurement periods of 15 – 20 minutes could be utilised with no appreciable loss of accuracy. This practise is recommended as a useful approach to mass data collection for future pattern recognition studies.

- Exploration of the discriminability abilities of new input feature groups for classification by the pattern recognition model could improve the generalisation and accuracy of the measurement system through the discovery of novel features with strong dependencies on the core multiphase flow parameters. Analysis of the LPCs over a longer timescale may prove to be more useful in extracting key flow parameter information. Furthermore, a strong emphasis should be placed on effective extraction of the discriminatory information residing in the wavelet transform coefficients. In addition, analysis of the gamma densitometer signal's time-frequency-energy distribution using the Hilbert-Huang transform could yield useful input feature parameter. The Hilbert-Huang transform derives an elementary wavelet function from the signal itself and is adaptive; thus, facilitating improved signal time-frequency resolution [**117**].

- Examining a number of new input features will, in conjunction with those analysed in this thesis, result in a vast number of potential input feature parameters. This will yield a large number of permutations for the creation of an input vector group for classification. Accordingly, optimisation of the pattern recognition system's input feature group should be undertaken so as to obtain maximal classification accuracy and processing performance. Branch and bound algorithms could be employed to achieve this as they enable efficient identification of an optimal parameter sub-sets from a large pool of potential candidates.

- In its current form, the pattern recognition based measurement model developed will only be valid for the same fluids in identical operating conditions. Application of the technique developed to other installations will require further development work. Expansion of the gamma attenuation data library should be undertaken to encompass a wider range of flow conditions. Key parameters that should be considered are oil density, oil viscosity, water salinity, operating pressure, operating temperature, pipe diameter, and pipe orientation. As well as developing the measurement envelope of the device, the data library compiled will be able to act as a look-up reference library for device calibration on new application.

- The current pattern recognition approach requires analysis of the flow's gamma count statistics over a period of 'steady-state' flow. In reality, a stable period of steady flow may not always be available to the measurement device, and the changes in flow conditions will affect the gamma count statistics. This will result in erroneous measurement predictions from the system. Accordingly, development to facilitate classification of the flow parameters in transient flow conditions is necessary to provide a more robust measurement solution. A series of transient multiphase flow experiments should be conducted to develop a real-time measurement system that takes into account historical statistical data from the flow. This could be undertaken employing a recurrent type neural network. In all cases of transient flow conditions, the measurement system should be able to quantify the degree of confidence in its results and log unseen conditions for user analysis and system development purposes.

- Sand production is common in a significant number of producing oil wells. As well as having the potential to lead to loss of production capacity, pipeline blockage, equipment failure and/or increased pipe corrosion, the presence of the sand is also likely to exert an influence on the measurement of the individual phase flow rates by a clamp-on gamma densitometer system. The effect of sand at various concentrations on the classification accuracy, and the ability to extract sand concentration and transportation velocity information from the gamma densitometer signal, should be investigated through experimental analysis on a laboratory-scale test facility. Once the effect of the sand on the densitometer derived measurements has been quantified, the development of a correction algorithm for the measurements' yielded by the gamma densitometer system in the presence of a measurable sand concentration can be examined. The functionality of the multiphase measurement system in the presence of sand would increase the robustness and marketability of the system while the provision of production sand information would offer enhanced well production optimisation.

References

1. Department of Trade and Industry (UK), 'Guidance Notes for Petroleum Measurement', Issue 7, December, 2003, pp. 8 – 9.

2. Scheers, A.M., Noordhuis, B. R., 'Multi-phase and Wet Gas Flow Measurement', 5th Annual Multi-Phase Metering Conference, Aberdeen, Scotland, 1999.

3. Mehdizadeh, P., 'Multiphase Measuring Advances Continue', Oil & Gas Journal, 9th July, 2001.

4. Mehdizadeh, P., '2006 Worldwide Multiphase and Wet Gas Metering Installations', Production Technology Report 03232007, 2007.

5. World Oil Journal, 'Producing Oil Wells Worldwide Reviews 1998 – 2000', World Oil Website, www.worldoil.com (accessed 08/10/2005).

6. Jamieson, A. W., 'Multiphase Metering – The Challenge of Implementation', 16th North Sea Flow Measurement Workshop, Gleneagles, Scotland, 1998.

7. Scheers, L., Busaidi, K., Parper, M., Halovorsen, M., and Wideroe, T., 'Multiphase Flow Metering Per Well – Can it be Justified?', 20th North Sea Flow Measurement Workshop, St. Andrews, Scotland, 2002.

8. Thorn, R., Johansen, G. A., and Hammer, E. A., 'Recent Developments in Three-Phase Flow Measurement', Measurement Science and Technology, Volume 8, 1997, pp. 691–701.

9. Kratirov, V., Jamieson, A. W., Yeung, H., and Blaney, S., 'Neftemer – A Versatile and Cost Effective Multiphase Meter', 24th North Sea Flow Measurement Workshop, St. Andrews, Scotland, 24th -27th October, 2006.

10. Jamieson, A. W., 'High Performance Multiphase Metering – A Personal Perspective', Norflow Seminar, 9th June, 1999.

11. Woldesemayat, M. A., and Ghajar, A. J., 'Comparison of Void Fraction Correlations for Different Flow Patterns in Horizontal and Upward Inclined Pipes', International Journal of Multiphase Flow, Volume 33, 2007, pp. 347 – 370.

12. Armand, A. A., 'The Resistance during the Movement of a Two-Phase System in Horizontal Pipes', Izv. Vses. Teplotekh. Inst. 1, 1946, pp. 16 – 23.

13. Chisholm, D., 'Two Phase Flow in Pipe Lines and Heat Exchangers', London:Pitman, pp. 8 – 57.

14. Smith, S. L., ‘Void Fractions in Two-Phase Flow: A Correlation Based Upon an Equal Velocity Head Model’, Proceedings Institution of Mechanical Engineers, Volume 184, Part. 1 (36), 1969, pp. 647 – 664.

15. Premoli, A., Francesco, D., and Prina, A., ‘An Empirical Correlation for Evaluating Two-Phase Mixture Density Under Adiabatic Conditions’, European Two-Phase Flow Group Meeting, Milan, Italy, 1970. Cited in Hewitt, G. F., ‘Pressure Drop and Void-Fraction’, Handbook of Multiphase Systems, McGraw-Hill, New York, 1982.

16. Stapelberg, H. H., and Mewes, D., ‘The Flow of Two Immiscible Liquids and Gas in Horizontal Pipes – Pressure Drop and Flow Regime’, European Two-Phase Flow Group Meeting, Varese, 21st-24th May, 1990.

17. Tjugum, S. A., Hjertaker, B. T., and Johansen, G. A., ‘Multiphase Flow Regime Identification by Multibeam Gamma-Ray Densitometry’, Meas. Sci. Technol., Volume 13, 2002, pp. 1319 – 1326.

18. Franca, F., Acikgoz, M., Lahey, R. T., and Clausse, A., ‘The Use of Fractal Techniques for Flow Regime Identification’, International Journal of Multiphase Flow, Volume 17, 1991, pp. 545 – 552.

19. Darwich, T., Toral, H., and Archer, J. S., ‘An Expert System for Multiphase Flow Measurement and Flow Regime Identification’, SPG Paper 19136 in SPG Petroleum Computer Conference, Lake Conroe, Texas.

20. Wu, H., Zhou, F., and Wu, Y., ‘Intelligent Identification System of Flow Regime of Oil-Gas-Water Multiphase Flows’, International Journal of Multiphase Flow, Volume 27, 2001, pp. 459 – 475.

21. Mi, Y., Ishii, M., and Tsoukalas, L. H., ‘Flow Regime Identification Methodology with Neural Networks and Two-Phase Flow’, Nuclear Engineering and Design, Volume 204, 2001, pp. 87 – 100.

22. Baker, O., ‘Simultaneous Flow of Oil and Gas’, Oil & Gas Journal, Volume 53, 1954, pp.185 – 195.

23. Nicklin, D. J., Wikes, J. C., and Davidson, J. F., ‘Two Phase Flow in Vertical Tubes’, Transactions of the Institution of Chemical Engineering, Volume 40, 1962, pp. 61 – 68.

24. Spedding, P. L., and Nguyen, V. T., ‘Regime Maps for Air-Water Two-Phase Flow’, Chemical Engineering Science, Volume 35, 1980, pp. 779 – 793.

25. Spedding, P. L., and Spence, D. R., ‘A Novel Approach to Flow Regime Prediction in Gas-Liquid Flows’, Developments in Chemical Engineering SST, Volume 14 (2), 1994, pp. 407 – 431.

26. Hewitt, G. F., 'Measurement of Two-Phase Parameters', Academic Press, London, 1978.

27. Mandhane, J. M., Gregory, G. A., and Aziz, K., 'A Flow Pattern Map for Gas-Liquid Flow in Horizontal Pipes', International Journal of Multiphase Flow, Volume 1, 1974, pp. 537 – 553.

28. Taitel, Y., Barnea, D., and Dukler A. E., 'Modelling Flow Pattern Transitions for Steady Upward Gas-Liquid Flow in Vertical Tubes', AIChE Journal 26, no. 6, 1980, pp. 345 – 354.

29. Acikgoz, M., Franca, F., and Lahey Jr., R. T., 'An Experimental Study of Three-Phase Flow Regimes', International Journal of Multiphase Flow, Volume 18(3), 1992, pp. 327 – 336.

30. Oddie, G., et al, 'Experimental Study of Two and Three Phase Flows in Large Diameter Inclined Pipes', International Journal of Multiphase Flow, Volume 29, 2003, pp. 527 – 558.

31. Brill, J. P., and Arirachakan, S. J., 'State of the Art in Multiphase Flow', Journal of Petroleum Technology, Volume 44 (5), 1992, pp. 538 – 541.

32. Spedding, P. L., Woods, G. S., Raghunathan, R. S., and Watterson, J. K., 'Flow Pattern, Holdup and Pressure Drop in Vertical and Near Vertical Two- and Three-Phase Upflow', Trans IChemE, Volume 78 (A), April, 2000, pp. 404 – 418.

33. Dykesteen, E., et al, 'Handbook of Multiphase Metering', Norwegian Society of Oil and Gas Measurement, NFOGM, Revision 2, March, 2005.

34. Mehdizadeh, P., 'Multiphase Measuring Advances Continue', Oil & Gas Journal, 9th July, 2001.

35. Hewitt, G. F., 'Multiphase Flow Metering', Proc. 2nd Int. Symp. Multiphase Flow and Heat Transfer (Xi'an, China), 1989.

36. Sanderson, M. L., 'Process Measurement Systems', MSc Module PSE 10, Cranfield University, Bedfordshire, England, 2001.

37. Abouelwafa, M. S. A., and Kendall, E. J. M., 'Analysis and Design of Helical Capacitance Sensors for Volume Fraction Determination', J. Phys. E: Rev. Sci. Instrum., Volume 50 (7), 1979, pp. 872 – 878.

38. Merilo, M., Dechene, R. L., and Cichowlas, W. M., 'Void Fraction Measurement with a Rotating Electric Field Conductance Gauge', ASME J. Heat Transfer, Volume 99, 1977, pp. 330 – 332.

39. Abouelwafa, M. S. A., and Kendall, E. J. M., 'The Measurement of Component Ratios in Multiphase Systems using γ-ray Attenuation', J. Phys. E: Sci. Instrum., Volume 13, 1980, pp. 341 – 345.

40. Nyfors, E., and Vainikainen, P., 'Industrial Microwave Sensors', Artech House, 1989.

41. Tuss, B., Perry, D., and Shoup, G., 'Field Tests of the High Gas Volume Fraction Multiphase Flow Meter', Proc. SPE Annual Technical Conf., Denver, USA, 1996.

42. Olsen, A. B., 'Framo Subsea Multiphase Flow Meter System', Proc. Sem. Multiphase Meters and their Subsea Applications, London, 1993.

43. Murdoch, J. W., 'Two-Phase Flow Measurements with Orifices', Journal of Basic Engineering, Vol. 84, 1962, pp. 419 – 433.

44. Chisholm, D., 'Flow of Incompressible Two-Phase Mixtures through Sharp-Edged Orifices', Journal of Mechanical Engineering Science, Vol. 9 (1), 1967, pp. 72 – 78.

45. Hammer, E. A., and Nordvedt, J. E., 'The Application of a Venturi Meter to Multiphase Flow Meters for Oil Well Production', Proc. 5th Conf. Sensors and Applications, London, 1991.

46. Hewitt, G. F., Harrison, P. S., Parry, S. J., and Shires, G. L., 'Development and Testing of the "Mixmeter" Multiphase Flow Meter', 13th North Sea Flow Measurement Workshop, Lillehammer, Norway, 1995.

47. Olsvik, K., Marshall, M., and Whitaker, T., 'Fluenta Multiphase Flow Meter, Tested and Marinised', 13th North Sea Flow Measurement Workshop, Lillehammer, Norway, 1995.

48. Beck, M. S., and Plaskowski, A., 'Cross Correlation Flow Meters: Their Design and Application', Adam Hilgar, Bristol, 1987.

49. Ong, K. H., and Beck, M. S., 'Slurry Flow Concentration and Particle Size Measurement using Flow Noise and Correlation Techniques', Meas. Control, Volume 8, 1975, pp. 453 – 460.

50. Brown, G., 'Evaluation of New Technology for High Accuracy Multiphase Flow Measurment: Part 2 – Neural Networks', NEL Flow Measurement Guidance Note No. 28, June, 2002.

51. Ismail, I., Gamio, J. C., Bukhari, S. F. A., and Yang, W. Q., 'Tomography for Multi-Phase Flow Measurement in the Oil Industry', Flow Measurement and Instrumentation, Volume 16, 2005, pp. 124 – 155.

52. Slijkerman, W. F. J, Jamieson, A. W, Priddy, W.J., Okland, O., and Moestue, H., 'Oil Companies' Needs in Multiphase Flow Metering', 13th North Sea Flow Measurement Workshop, Lillehammer, Norway, 1995.

53. Babelli, I. M. M., 'In Search of an Ideal Multiphase Flow Meter for the Oil Industry', Arabian Journal of Science and Engineering, Volume 27, Number 2B, October 2002, pp. 113 – 126.

54. Sprowll, R. L., and Phillips, W. A., 'Modern Physics, The Quantum Physics of Atoms, Solids and Nuclei', 3rd Edition Wiley, New York, 1980.

55. Key, M. J., 'Gas Microstructure X-ray Detectors and Tomographic Multiphase Flow Measurement', PhD Thesis, University of Surrey, 1999.

56. Franz, W., 'Zeitschrift für Physik', Volume 98, 1936, pp. 314.

57. Prepost, R., 'Interaction of Gammas', Advanced Physics Laboratory, University of Wisconsin, 27th April, 2001.

58. Spight, C. L., Wamsteker, A. J. J., and Van Vlaardingen, H. F., 'The Application of the Impedance Method of Transient Void Fraction Measurements and Comparison with the γ-Ray Attenuation Technique', Proceedings of the Symposium on In-Core Instrumentation., Oslo, Norway, 1964, pp. 15 – 20.

59. Price, W. J., 'Nuclear Radiation Detectors', 2nd Edition, McGraw-Hill, New York, 1964.

60. Mareuge, I. C., 'Analysis and Development of Multi-Energy Gamma Densitometry Systems', Multiphase Fluid Systems Programme, Imperial College of Science, Technology and Medicine, December, 2000.

61. Chan, A. M. C., and Banarjee, S., 'Design Aspects of Gamma Densitometers for Void Fraction Measurements in Small Scale Two-Phase Flows', Nuclear Instruments and Methods in Physics Research, Volume 190, 1981, pp. 135 – 148.

62. Jiang, Y., and Rezkallah, K. S., 'An Experimental Study of the Suitability of Using a Gamma Densitometer for Void Fraction Measurements in Gas-Liquid Flow in a Small Diameter Tube', Meas. Sci. Technol., Volume 4, 1993, pp. 496 – 505.

63. Li, D. H., Wu, Y. X., Li, Z. B., and Zhong, X. F., 'Volumetric Fraction Measurement in Oil-Water-Gas Multiphase Flow with Dual Energy Gamma-Ray System', J. Zhejiang Univ. SCI, Volume 6A (12), 2005, pp. 1405 – 1411.

64. Scheers, A. M., Slijkerman, W. F. J., 'Multiphase Flow Measurement Using Multiple Energy Gamma Ray Absorption (MEGRA) Composition', SPE Paper 36593-MS, October, 1996, pp. 203 – 211.

65. Åbro, E., and Johansen, G. A., 'Improved Void Fraction Determination by Means of Multibeam Gamma-Ray Attenuation Measurements', Flow Measurement and Instrumentation, Volume 10, 1999, pp. 99 – 108.

66. Tjugum, S. A., Frieling, J., Johansen, G. A., 'A Compact Low Energy Multibeam Gamma-Ray Densitometer for Pipe-Flow Measurements', Nuclear Instruments and Methods in Physics Research B, 197, 2002, pp. 301 – 309.

67. Stahl, P., and Von Rohr, P. R., 'On the Accuracy of Void Fraction Measurements by Single-Beam Gamma-Densitometry for Gas-Liquid Two-Phase Flows in Pipes', Experimental Thermal and Fluid Science, Volume 28, 2004, pp. 533 – 544.

68. Frøystein, T., Kvandal, H., and Aakre, H., 'Dual Energy Gamma Tomography System for High Pressure Multiphase Flow', Journal of Flow Measurement and Instrumentation, Volume 16, 2005, pp. 99 – 112.

69. Beg, N. A., McNulty, J. G., Sheppard, C. P., and Frith, A., 'Non-intrusive Multiphase Flow Measurement using Artificial Neural Networks', 6^{th} Multiphase Production Conference, Cannes, France, 1993.

70. Sheppard, C. P., and Russell, D., 'The Application of Artificial Neural Networks to Non-Intrusive Multi-Phase Metering', Control Engineering Practice, Volume 1 (2), 1993, pp. 299 – 304.

71. Bishop, C. M., and James, G. D., 'Analysis of Multiphase Flows Using Dual-Energy Gamma Densitometry and Neural Networks', Nuclear Instruments and Methods in Physics Research, A327, 1993, pp. 580 – 593.

72. Bishop, C. M., 'Multiphase Flow Monitoring in Oil Pipelines: Application of Neural Networks', Kluwer Academic Publishers, Netherlands, 1995, pp. 133 – 155.

73. Åbro, E., Khoryakov, V. A., Johansen, G. A., and Kocbach, L., 'Determination of Void Fraction and Flow Regime Using a Neural Network Trained on Simulated Data Based on Gamma-Ray Densitometry', Measurement Science and Technology, Volume 10, 1999, pp. 619 – 630.

74. Jackson, L. B., 'Digital Filters and Signal Processing', 3^{rd} Edition, Kluweir Academic Publishers, 1995, p. 156.

75. Bishop, C. M., 'Neural Networks for Pattern Recognition', Oxford University Press, Oxford, 1995.

76. Hagan, M. T., Demuth, H. B., and Beale, M., 'Neural Network Design', PWS Publishing Co., Boston, 1996.

77. McCulloch, W., and Pitts, W., 'A Logical Calculus and the Ideas Immanent in the Nervous Activity', Bulletin of Mathematical Biophysics, Volume 5, 1943 pp. 115 – 133.

78. Rosenblatt, F., 'The Perceptron: A Probabilistic Model for the Information Storage and Organisation in the Brain', Psychological Review, Volume 5, 1958, pp. 386 – 408.

79. Minsky, M., and Papert, S., 'Perceptrons: An introduction to Computational Geometry', MIT Press, 1969.

80. Grossberg, S., 'Grossberg, Contour Enhancement, Short-term Memory, and Constancies in Reverberating Neural Networks', Studies in Applied Mathematics, Volume 52, 1973, pp. 213 – 257.

81. Hornik, K., Stinchcombe, M., and White, H., 'Multilayer Feedforward Networks Are Universal Approximators', Neural Networks, Volume 2 (5), 1989, pp. 359 – 366.

82. Geman, S., Bienenstock, E., and Doursat, R., 'Neural Networks and the Bias/Variance Dilemma', Neural Computation, Volume 4, 1992, pp. 1 – 58.

83. Stuttgart University, 'SNNS User Manual', Version 4.2, Institute for Parallel and Distributed High Performance Systems, Report 6/95, 1995.

84. Doan, C. D., and Liong, S. Y., ' Generalization for Multilayer Neural Network Bayesian Regularization or Early Stopping', 2^{nd} Asia Pacific Association of Hydrology and Water Resources Conference, Singapore, 5^{th} – 8^{th} July, 2004.

85. MacKay, D. J. C., 'Bayesian Interpolation', Neural Computation, Volume 4 (3), 1992, pp. 415 – 447.

86. Foresee, F. D., and Hagan, M. T., 'Gauss-Newton Approximation to Bayesian Regularisation', International Joint Conference on Neural Networks, 1997, pp. 1930 – 1935.

87. Kohonen, T., 'Self-Organized Formation of Topologically Correct Feature Maps', Biological Cybernetics, Volume 43, 1982, pp. 59 – 69.

88. Kohonen, T., Oja, E., Simula, O., Visa, A., and Kangas, J., 'Engineering Applications Of the Self-Organizing Map', Proceedings of the IEEE, Volume 84 (10), 1996, pp. 1358 – 84.

89. Darwich, T., 'A Statistical Method for Two-Phase Flow Metering', PhD Thesis, Imperial College of Science, Technology and Medicine, London, 1989.

90. Toral, H., Beg, N., and Archer, J. S., ‘Multiphase Flow Metering by Software’, International Conference on Basic Principles & Industrial Applications of Multiphase Flow, London, 1990.

91. Akartuna, S. E., ‘Identification of Phase Flowrates in Oil-Gas-Water Flow from Turbulent Capacitance and Pressure Signals’, PhD Thesis, Imperial College of Science, Technology and Medicine, London, 1994.

92. Cai, S., ‘An Artificial Neural Network Method for Three-Phase Flow Measurement’, PhD Thesis, Imperial College of Science, Technology and Medicine, London, 1995.

93. Beg, N. A., ‘A Stochastic Method for Multiphase Flow Metering in Pipes’, PhD Thesis, Imperial College of Science, Technology and Medicine, London, 1998.

94. Toral, H., Cai, S., Akartuna, E., Stothard, K., and Jamieson, A. W., ‘Field Trials of the ESMER Multiphase Flow Meter’ North Sea Flow Measurement Workshop, Gleneagles, Scotland, 1998.

95. Wood, I., ‘Multiphase Measurement’, 20th North Sea Flow Measurement Workshop, Peebles, Scotland, 2002.

96. Goudinakis, G., ‘Investigation on the use of Raw Time Series and Artificial Neural Networks for Flow Pattern Identification in Pipelines’ , PhD Thesis, Cranfield University, 2004.

97. Jama, A. A, ‘Wet Gas Flow Metering with Pattern Recognition Techniques’, PhD Thesis, Cranfield University, 2004.

98. Ibrahim, A. A., ‘Intelligent Multiphase Flow Measurement’, PhD Thesis in Preparation, Cranfield University, 2007.

99. Wylie, S. R., Shaw, A., and Al-Shamma’a, A. I., ‘RF Sensor for Multiphase Flow Measurement through an Oil Pipeline’, Measurement Science and Technology, Volume 17, 2006, pp. 2141 – 2149.

100. Loh, W. L., ‘Cranfield University Three-Phase Test Facility Operating Procedures’, Version 1, March 2004.

101. Montgomery, J., ‘Severe Slugging and Unstable Flows in an S-Shaped Riser’, PhD Thesis, Cranfield University, 2004.

102. Cooley, J. W., and Tukey, O. W. ‘An Algorithm for the Machine Calculation of Complex Fourier Series’, Mathematics of Computation, Volume 19, 1965, pp. 297 – 301.

103. Zhang, Q., Aliaga-Rossel, R., and Choi, P., 'Denoising of Gamma-Ray Signals by Interval Dependent Thresholds of Wavelet Analysis', Measurement Science and Technology, Volume 17, 2006, pp. 731 – 735.

104. Misiti, M., Misiti, Y., Oppenheim, G., Poggi, J. M., 'MATLAB Wavelet Toolbox 4 User's Guide', Mathworks, 2007.

105. Abry, P., 'Ondelettes et Turbulence: Multirésolutions, Algorithmes de Décomposition, Invariance d'Echelles', Diderot Editeur, Paris, 1997.

106. Qin Qiming, Q., Wenjun, W., and Sijin, C., 'The Application of Dyadic Wavelet in the RS Building Image Edge Detection', Proceedings of the 2004 International Conference on Image Processing (ICIP), pp. 1731 – 1734.

107. Zheng-you, H. E., Xiaoqing, C., and Guoming, L., 'Wavelet Entropy Measure Definition and Its Application for Transmission Line Fault Detection and Identification (Part I: Definition and Methodology)', International Conference on Power System Technology 2006, October, 2006, pp. 1 – 6.

108. Van der Welle, R., 'Bubble Velocity and Bubble Sizes in Two Phase Flow', Int. J. Multiphase Flow, Volume 11, 1985, pp. 317 – 345.

109. DeJesus, J. M., and Kawaji, M., 'Measurement of Interfacial Area and Void Fraction in Upward, Co-current Gas-Liquid Flow', ASME Proc. Nat. Heat Transfer Conf., 1989, pp. 137 – 145.

110. Anderson, G. H., and Mantzouranis, B. G., 'Two Phase (Gas-Liquid) Flow Phenomena – I. Pressure Drop and Hold-Up for Two Phase Flow in Vertical Tubes', Chem. Eng. Sci., Volume 12, 1960, pp. 102 – 126.

111. Ueda, T., 'Studies on the Flow of Air-Water Mixtures – The Upward Flow in a Vertical Tube', Bull. JSME, Volume 1, 1958, pp. 139 – 145.

112. Yu, Z., Liu, S., and Li, X., 'A Study on Un-Fully Developed Slug Flow in a Vertical Tube', Hat Transfer – Asian Research, Volume 34 (4), 2005, pp. 235 – 241.

113. Zheng, D., and Che, D., 'Experimental Study on Hydrodynamic Characteristics of Upward Gas-Liquid Slug Flow', International Journal of Multiphase Flow, Volume 32, 2006, pp. 1191 – 1218.

114. Fokin, B. S., 'Calculation of Pulsating and Averaged Hydrodynamic Characteristics of Two-Phase Flow', Russian Journal of Engineering Thermophysics, Volume 5 (3), 1995, pp.265 – 292.

115. Nguyen, D., and Widrow, B., 'Improving the Learning Speed of 2-Layer Neural Networks by Choosing Initial Values of the Adaptive Weights', Information Systems Laboratory, Stanford University.

116. Carreño, I. R., and Vuskovic , M., 'Wavelet Transform Moments for Feature Extraction from Temporal Signals', 2nd International Conference in Control, Automation and Robotics (ICINCO 2005), Barcelona, Spain, 2005

117. Ding, H., Huang, Z., Song, Z., and Yan, Y., 'Hilbert-Huang Transform Based Signal Analysis for the Characterization of Gas-Liquid Two-Phase Flow', Flow Measurement and Instrumentation, Volume 18, 2007, pp. 37 – 46.

Appendices:

A1. Abbon AS, AFM Product Specification Sheet:
http://www.abbon.com/downloads/abbon_afm_productsheet.pdf/download
(accessed 12/09/2006).

A2. Accuflow AMMS Product Technology Information:
http://www.accuflow.com/about_the_technology.html (accessed 12/09/2006)

A3. Shen, J. J. S., and Riley, R. C., 'Field Evaluation of a Multiphase Meter in Well-Testing Operation', SPE Production & Facilities, 1998, pp. 109 – 117.

A4. Dutton, R., 'Determination of Net Oil for Well Performance Measurement', Class LM2100, Daniel, Emerson Process Management.

A5. Al-Taweel, A. B., and Barlow, S. G., 'Field Testing of Multiphase Meters', SPE Paper 56583, Annual Technical Conference and Exhibition, Houston, USA, 1999.

A6. McNulty, J. G., and Beg, N. A., 'Survey of Multi-Phase Flow Metering Systems', Caltec Report CR 6660, BHR Group, UK, 1997.

A7. Mohamed, P. G., and Al Saif, K. H., 'Field Trial of a Multiphase Flow Meter', SPE Paper 49161, Annual Technical Conference and Exhibition, New Orleans, USA, 1998.

A8. eProduction Solutions, 'REMMs Product Specification Sheet':
http://www.epsolutions.com/PDFs/eP_L/L_Red_Eye_Multiphase_Metering_System.pdf (accessed 08/04/2005).

A9. eProduction Solutions Corporate Website:
http://www.ep-solutions.com
(accessed 08/04/2005).

A10. Hall, A. R. W., 'Evaluation of the FlowSys TopFlow Multiphase Flowmeter', NEL, Project No FSY001, Report No 200/2000, October 2000.

A11. Klepsvik, I., Dahl, E., O., Baker, A. C., 'Multiphase Flow Test Report – TopFlow', Christian Michelsen Research, Report CMR-00-F10021, September 2000.

A12. Mazzoni, A., Halvorsen, M., Aspelund, A., 'Field Qualification – FlowSys TopFlow Meter', Agip Test Facility, Trecrate, Italy, April, 2001.

A13. Pipeline Magazine, News, 16/08/2005:
http://www.pipelinedubai.com/press/2005/pr_05_1208_002.htm
(accessed 08/10/2005).

A14. Theuvent, B. C., Segeral, G., Pinguet, B., 'Multiphase Flow Meters in Well Testing Applications', SPE Paper 717475, Annual Technical Conference and Exhibition, New Orleans, USA, 1998.

A15. Letton, W., Svaeren, J. A., and Conort, G., 'Topside and Subsea Experience with the Multiphase Flow Meter', SPE Paper 38783, October, 1997, pp. 345 – 355.

A16. Al-Bourni, H. A., Samizo, N., Bakhteyar, Z., and Alvi, A., 'Application of New Multiphase Flow Measurement Systems with Satellite-Based Monitoring in Offshore Khafji Field', International Petroleum Technology Conference, IPTC 10312, 2005.

A17. Haimo MFM Product Brochure:
http://www.haimotech.com/downloads/MFM%20Brochure.pdf
(accessed 12/09/2006).

A18. Haimo Technology Inc, 'Haimo Newswire', Issue 3, March 2005.

A19. Hewitt, G. F., Shires, G. L., Harrison, P. S., and Parry, S. J., 'The Mixmeter Flowmeter - Another step towards Routine Multiphase Flow Measurement?', 8th International Conference on Multiphase Production Technology '97, Cannes, France: 18th -20th June, 1997.

A20. Multi Phase Meters, 'Performance Newsletter':
http://www.mpm.biz/Portals/39/Performance%20Oct%2005.pdf
(accessed 03/11/2006).

A21. Scheers, L., and Wee, A., 'Challenges at High Accuracy Multi-Phase and Wet-Gas Measurements', Multiphase Measurement Roundtable, April, 2007.

A22. Multiphase Solutions Inc., 'New Project Notification':
http://www.multiphase.com/products/p_examples.htm
(accessed 10/09/2006).

A23. Phase Dynamics Inc., 'CCM Product Specification Sheet':
http://www.phasedynamics.com/ccm.html
(accessed 08/09/2006).

A24. Phase Dynamics Inc., 'CCM Sales Presentation 02/06':
http://www.phasedynamics.com/pdf/ccm_presentation_0206.pdf
(accessed 08/09/2006).

A25. Toral, H., Cai, S., Akartuna, E., Stothard, K., Jamieson, A., 'Field Tests of The ESMER Multiphase Flowmeter', 16th North Sea Flow Measurement Workshop, Gleneagles, Scotland, October 1998.

A26. Cai, S., Toral, H., Sinta, D., and Tajak, M., 'Experience In Field Tuning And Operation Of A Multiphase Meter Based On Neural Net Characterization Of Flow Conditions', FLOMEKO, September 2004.

A27. Leggett, R. B., Borling, D. C., Powers, B. S., and Shehata, K., 'Multiphase Meter Successfully Measures Three-Phase Flow at Extremely High Gas Volume Fraction', SPE Paper 36837, European Petroleum Conference, Milan, Italy, 1996.

A28. Dykesteen, E., 'Comparison of Experiences from Multiphase Metering in Different Operations', IBC Conf. Field Applications and New Technologies for Multiphase Metering, 1999.

A29. TEA Sistemi Spa Corporate Website, 'LYRA Product Information':
http://www.teasistemi.com/html/products_metering_lyra_01.htm
(accessed 08/09/2006).

B1. Makhoul, J., 'Linear Prediction: A Tutorial Review', Proc. IEEE, Volume 63, 1975, pp. 561 – 580.

B2. Golub, G. H., and Loan, C. F. V., 'Matrix Computation', The John Hopkins University Press, 2nd Ed., 1989.

B3. Deller, J. R., Proakis, J. G., and Hansen, J. H. L., 'Discrete-Time Processing of Speech Signals', MacMillan, 1993.

B4. Kabal, P., and Ramachandran, R. P., 'The Computation of Line Spectral Frequencies using Chebyshev Polynomials', IEEE Trans. Acoustics, Speech Signal Processing, Volume 34, 1986, pp. 1419 – 1426.

E1. Jackson, J. E., 'A User's Guide to Principal Components', John Wiley and Sons Inc., 1991.

Publications

1. Kratirov, V., Jamieson, A., Blaney, S., and Yeung, H, ‘Neftemer – A Versatile and Cost Effective Multiphase Meter’, 24th North Sea Flow Measurement Workshop, St. Andrews, Scotland, 24th – 27th October, 2006.

2. Kratirov, V., Jamieson, A., Blaney, S., and Yeung, H, ‘Neftemer – Metering Multiphase Flow from Heavy-Crude-Oil Wells’, Multiphase Measurement Roundtable, April, 2007.

3. Blaney, S. and Yeung, H., ‘Gamma Radiation Techniques for Cost Effective Multiphase Flow Metering’, 13th International Conference on Multiphase Production Technology ’07, Edinburgh, 13th – 15th June, 2007.

4. Blaney, S. and Yeung, H., ‘Investigation of the Exploitation of Fast-Sampling Gamma Densitometry to Resolve the Individual Phase Flow Rates in Vertically Upward Multiphase Flows’, Flow Measurement and Instrumentation, Volume 19 (2), 2008, pp. 57 – 66.

Appendix A – Review of Commercial MPFMs

A.1 Abbon Flow Master

The Abbon Flow Master (AFM) comes in two different versions, both based on the Abbon acoustic detector, electronics and software technology. The AFM 300C is a clamp-on instrument that uses either existing construction details (such as a choke valve) or a simple flow conditioner as a signal generator with a sensor attached to the surface. The AFM 300I is an in-line version that incorporates a flow conditioner that increases the acoustic signals, **Figure A.1** [**A1**]. It is claimed that the flow conditioner permits higher accuracy and easier calibration.

Figure A.1 – AMF In-Line Spool Piece

As the oil well's multiphase flow passes through the measurement section, acoustic energy signals are generated which correlate to the flow rates and composition of the medium. The AFM employs on-line detection, processing and interpretation using multivariate analysis of the acoustic fingerprint to infer variations in composition and flow rates. No information was available in the public domain relating to meter testing or commercial installations of the AFM multiphase meter.

A.2 Accuflow AMMS

The Accuflow Multiphase Metering System (AMMS) is a patented technology comprising a pipe separator design to separate a multiphase flow into a gas-free liquid stream and a liquid-free gas stream, **Figure A.2** [**A2**]. Conventional single-phase measurement devices are then employed to measure each of the separated streams.

Multiphase fluid from the production flow line enters the vertical pipe tangentially, creating a cyclonic action in the vertical pipe where a majority of gas is separated and flows upward. The downward inclination of the inlet pipe promotes liquid/gas stratification in the inlet pipe that enhances gas/liquid separation in the vertical separator pipe. The remaining gas, mostly in the form of small bubbles, is carried downward with the liquid stream and enters the horizontal pipe section.

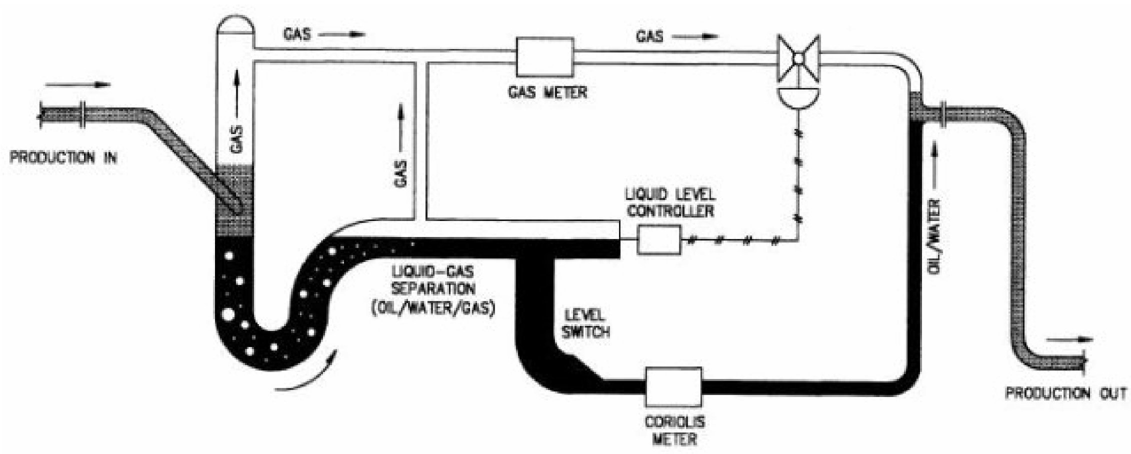

Figure A.2 – Operating Principle of the AMMS

Liquid level in the horizontal separator pipe section is controlled in the middle of the pipe using a control valve located in the gas flow line. As the liquid stream flows through the horizontal pipe, gas bubbles rise to the gas/liquid interface and are separated as the liquid stream flows toward the outlet end of the horizontal pipe. Large gas/liquid interface area, thin gas-bearing liquid layer, and quiescent flow in the horizontal pipe all contribute to efficient removal of entrained gas bubbles from the liquid stream.

Accuflow claim that their patented pipe separator design can achieve complete gas-liquid separation and can thus employ conventional proven single-phase measurement devices to measure the separated phase streams (typically vortex or ultrasonic meters for the gas and a coriolis meter for the liquid).

The AMMS has been employed by Chevron Texaco in Lost Hills and Cymric Fields in California, USA, since 1996 [**A3**]. Chevron Texaco reported AMMS volumetric liquid measurements to within 2% of those of the test separator and agreement to within 3% was obtained for the liquid phase water cut. No gas phase measurements were performed.

Accuflow Inc. claims to have installed units at 65 sites, in six countries, with similar measurement accuracies attained for flow rates of up to 30,000 bpd, and at water cuts and gas fractions up to 99% [**A4**].

A.3 Agar MPFM

Agar's MPFM-400 Series is a phase separation type meter comprising a patented Fluidic Flow Diverter (FFD) device and a gas bypass loop, **Figure A.3**. The FFD device employs the difference in flow momentum in the gas and liquid phases to divert most of the free gas in the multiphase stream into a secondary measurement loop around the core of the MPFM.

(a) (b)

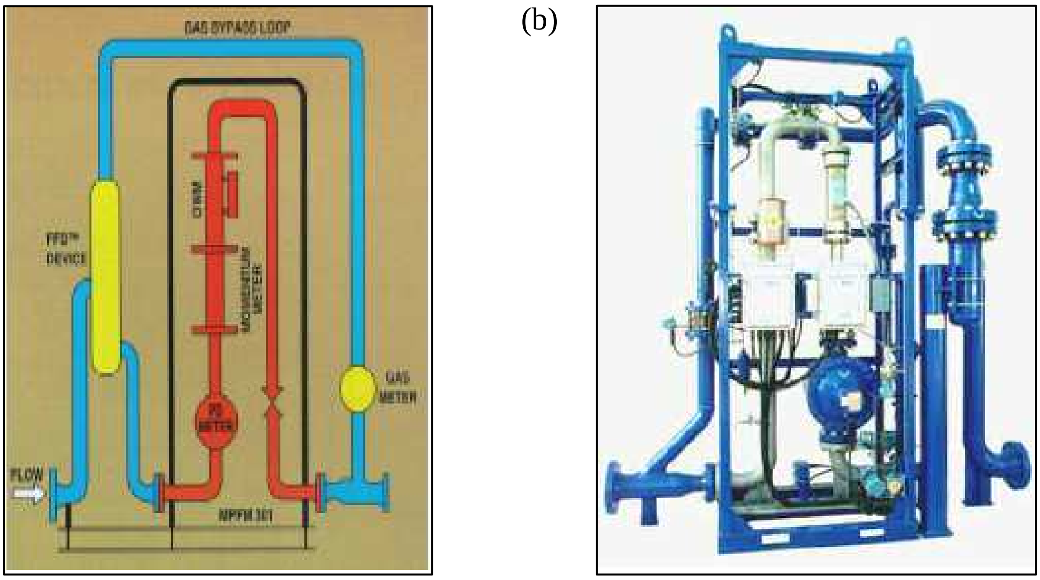

Figure A.3 – Agar MPFM 400-Series (a) Schematic and (b) Skid Mounted (mirrored)

This secondary measurement loop is essentially a wet gas metering system and consists of a Venturi and a vortex shedding flow meter in series. The primary metering loop comprises three components: a positive displacement meter to determine the total volumetric flow of the mainly liquid stream; a momentum meter (dual Venturi) which measures the gas fraction of the flow; and a microwave water-cut meter. After metering, the gas in the secondary bypass loop is recombined with the oil, water and gas measured by the core meter.

The Agar MPFM has been subjected to numerous field tests and is claimed to have performed to within its quoted specifications: ±10% for gas oil and water flow rate measurements at GVFs up to 99.9% relative to test separator measurements [**A5-A7**].

A.4 eProduction Solutions Inc. REMMS

The Red Eye Multiphase Metering System (REMMS) combines compact separation technology with conventional liquid and gas metering. The multiphase fluid enters the main body through a narrow tangential inlet into the vertical separator body. This forces the liquid and gas to accelerate through the inlet and around the vertical axis of the main body, creating a vortex, **Figure A.4** [**A8**].

Due to the large density difference between the gas and liquid phases, the gas migrates quickly to the centre while the denser liquid travels to the wall. Once separated, the individual streams

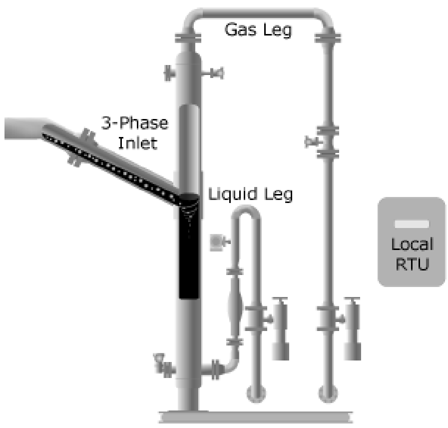

Figure A.4 – REMMS MPFM

are measured with conventional liquid and gas meters, typically coriolis and vortex meters respectively. The water cut is determined employing eProduction Solutions propriety Red Eye 2G Water Cut Meter which exploits infrared absorbance to determine the relative quantities of water and oil in the liquid phase The separated phases are then recombined or transported in separate flow lines.

In December 2004, eProduction Solutions completed installation of 18 REMMS MPFM units in Chad, Africa [**A9**]. There have been no details of the meters' performance published in the public domain.

A.5 FlowSys TopFlow

The major parts of the FlowSys TopFlow meter are the Venturi insert and the impedance electrodes incorporated inside the throat of the Venturi insert. The differential pressure is measured across the inlet of the Venturi insert while the capacitance or conductance of the mixture flowing through the Venturi insert is measured by the electrodes inside the Venturi throat. Fluid velocity is found from cross-correlation of the high-resolution time signals from pairs of electrodes within the Venturi insert.

The flow rates of the oil, water and gas are then calculated based on the measurements obtained by these sensors as illustrated in **Figure A.5**.

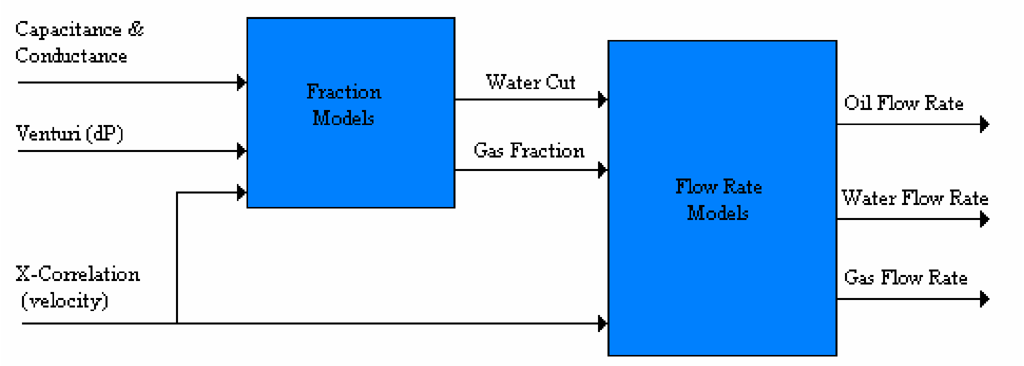

Figure A.5 – Schematic Diagram of the FlowSys TopFlow Meter

Laboratory testing of the FlowSys meter was undertaken at the National Engineering Laboratory (NEL) [**A10**]. The test matrix comprised a number of points with liquid and gas flow rates ranging between 0-60 m^3/h and 0-340 m^3/h respectively. Liquid phase and oil flow rate measurements obtained were within a relative uncertainty band of ±5%. However, for tests points with a GVF greater than 70%, or water cuts in excess of 75%, large deviations from the reference values were observed. The gas flow rate measurements were found to be within ±20% across a large proportion of the operating envelope.

Further laboratory testing of the TopFlow MPFM was carried out by Christian Michelsen Research (CMR) [**A11**]. The test matrix comprised a number of points with liquid and gas flow rates ranging between 15-40 m^3/h and 20-90 m^3/h respectively. It was reported that 99% of the liquid flow rate measurements were within a relative deviation of ±10% from reference values; 78% of oil flow rate measurements were within ±10%; and 84% of the gas flow rate measurements were within ±15%.

In 2001, FlowSys's TopFlow meter was field tested by Eni in Trecate, Italy [**A12**]. It was documented that the FlowSys meter gave phase flow rate measurements within ±10% for GVFs up to 92-93% for the gas flow rate and GVFs of up to 86-87% for the liquid flow rates. Liquid and gas flow rates ranged between 6-35 m^3/h and 35-145 m^3/h respectively. However, at GVFs in excess of 92-93% the liquid flow rate measurement accuracy deteriorated to approximately ±20%. Owing to the limitations imposed by the test wells, the water cut was only examinable between 41-51%. In this range it was reported that the meter was able to classify the majority of the test points within ±5%.

In August 2005 the Gulating Court reversed parts of this decision, concluding concluded that FlowSys had partly infringed on Roxar's technology by using the knowledge and experience that some key FlowSys personnel have from previous engagements with Fluenta (now Roxar) [**A13**]. The main conclusions reached by the Gulating Court were:

- FlowSys were prohibited from manufacturing, marketing and selling TopFlow for a 3-year period with immediate effect.
- FlowSys had to compensate Roxar approximately US$ 1.8 million for damages related to sales and costs for the appeal case to the Gulating Court.
- With respect to the rights to FlowSys unique patent, the patent ownership remains with FlowSys. The decision regarding the patent by the Stavanger City Court, which was fully in favour of FlowSys, was not appealed by Roxar to the Gulating Court.

In November 2005, the Appeal Committee of the Norwegian Supreme Court in the appeal case against Roxar decided not to accept the appeal from FlowSys for further presentation to the Supreme Court of Norway.

A.6 Framo / Schlumberger Vx MPFM

The Vx MPFM makes use of two measurement techniques: a Venturi with pressure, temperature and differential pressure sensors for mass flow measurement and dual-gamma densitometry for phase fraction determination. Following a blind tee, the multiphase flows vertically upwards through the metering area. All the measurements are made in the Venturi throat, i.e. absolute pressure, temperature, differential pressure relative to upstream conditions and phase fractions, **Figure A.6** [**A14**].

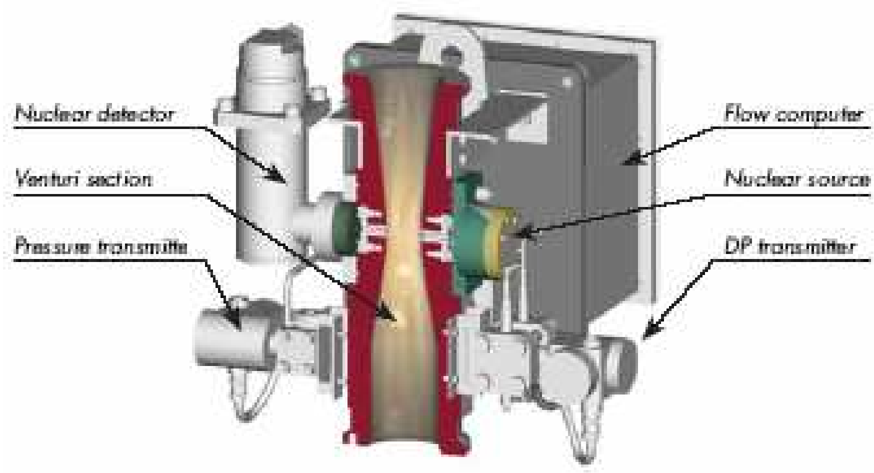

Figure A.6 – PhaseWatcher Vx MPFM

Phase fractions are measured using a dual-energy gamma densitometer employing a barium-133 radionuclide source. The source has energy levels appropriate for measurement of gas fraction and water cut (29 keV and 80 keV). The gamma densitometer is located at the narrowest part of the flow conduit, allowing the low energy levels employed by the gamma meter to be feasibly used with a low strength source.

Laboratory testing of the PhaseWater Vx meter was also undertaken at the National Engineering Laboratory (NEL) [**A15**]. The test matrix comprised a number of points with GVFs ranging from 0 to 95%. Liquid phase and oil flow rate measurements were produced within a relative uncertainty band of ±10% and water cut readings had an associated absolute error of ±6%. No quantification of the gas phase measurement performance was reported.

In 2005, Al-Khafji Joint Operations installed five PhaseWatcher Vx MPFMs in the offshore-Khafji field for satellite-based monitoring. Well tests were referenced against a test barge comprising a conventional three-phase separator set up. Measurements agreements for the PhaseWatcher Vx meters were reported to exhibit 5-10% relative error for the oil and water flow rates and in excess of 15% for the gas phase flow rate, with respect to the separator measurements [**A16**].

A.7 Haimo MPFM

The Haimo MPFM combines features of inline and partial separation type MPFMs. The phase flow rate measurements and the water cut determination are carried out independently of each other. The gas/liquid two-phase flow meter consists of a Venturi and two identical single-energy (59.5 keV) gamma sensors. The full range three-phase water cut meter comprises a dual-energy (22 and 59.5 keV) gamma sensor and a flow conditioner located upstream, **Figure A.7** [**A17**].

Both the gas and liquid flow rates are measured upstream of the flow conditioner in the two-phase flow meter: the dual-energy gamma densitometer measures the water cut of the conditioned flow mixture.

In March 2005, Haimo claimed to have completed well tests on more than 1500 wells and to have over 100 MFM meters installed in onshore and offshore applications [**A18**].

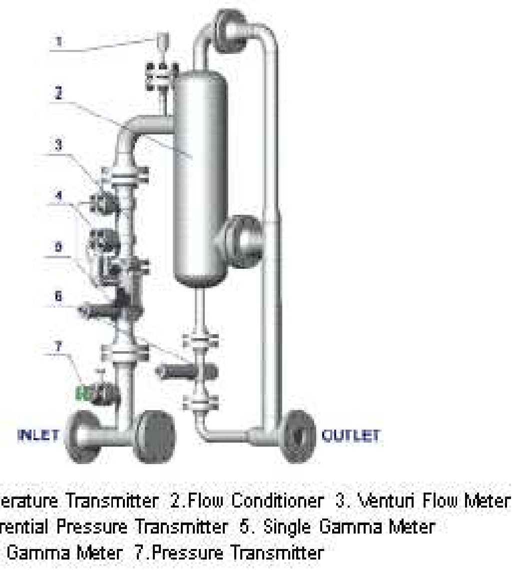

Figure A.7 – Haimo MPFM

A.8 Jiskoot Mixmeter

Jiskoot's Mixmeter utilises a patented upstream mixer to ensure a homogenous multiphase flow mixture is present in the meter's measurement section, **Figure A.8** [**A19**]. The mixer attempts to equalise the velocity of the three phases and removes the need for complex slip correction calculations. Phase fractions are determined through the employment of a dual-energy gamma densitometry system; while the phase velocities are determined through cross-correlation of sensor data. No data was found documenting the Mixmeter's performance in laboratory or field tests.

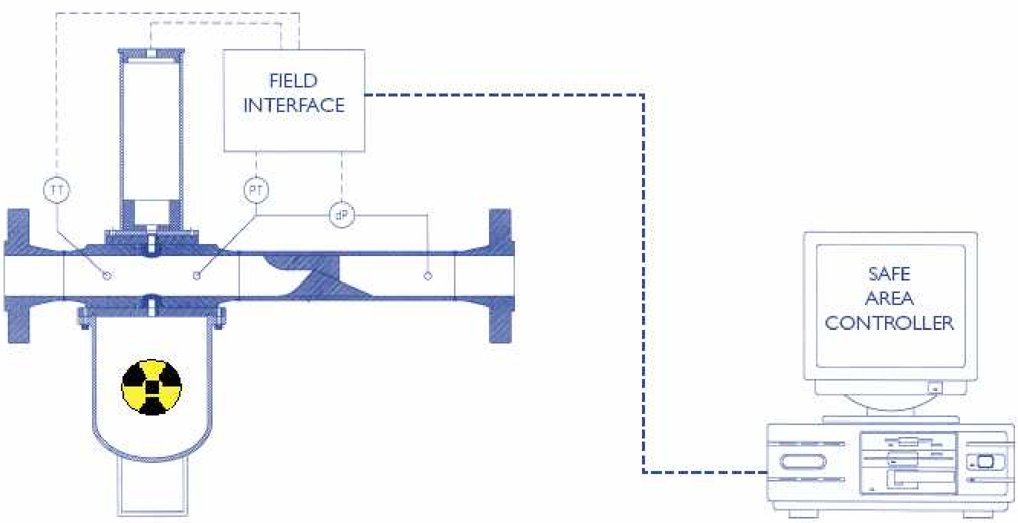

Figure A.8 – Mixmeter MPFM

A.9 Multi Phase Meters AS mpm

Multi Phase Meters AS's mpm is marketed as a high-performance meter and was developed through a JIP involving Eni, Hydro, Shell, Total, Statoil and ConocoPhillips [**A20**]. The mpm measurement system is based on patented 3DBroadband technology which measures the dielectric constant in 3-D to calculate the water density, salinity and conductivity, and the gas concentration in annular flows, **Figure A.9**. A Venturi section is employed for flow conditioning and velocity measurement, while a gamma densitometer unit is exploited for phase composition data. A subsea version of the meter has also been developed.

Figure A.9 – mpm Meter

Field validation tests were undertaken in January 2007 on the Gullfaks A field operated by Statoil and reported gas and oil flow rate measurement accuracies to within ±8% and ±3% respectively across the full range of GVFs and WLRs [**A21**].

A.10 Multiphase Solutions Inc VMS.

Multiphase Solutions Inc. take a software-based approach with their Virtual Metering System (VMS). The VMS uses measurements from existing sensors in and around the well and to infer multiphase flow rates. VMS can use several predictive models to determine flow rate. It approximates the uncertainty of each estimate and then combines these values to achieve the lowest overall uncertainty. Two installations of the Virtual Metering System have been publicised: one installation for Eni in the Gulf of Mexico and another for Shell Philippines Exploration at Malampaya [**A22**].

A.11 Phase Dynamics Inc. CCM

This Compact Cyclone Multiphase meter (CCM meter) utilises a compact gas-liquid cyclone, to separate the liquid and gas phases prior to measurement, **Figure A.10** [**A23**]. Effectively, the system is a modern version of a traditional two phase separator. Coriolis meters are used to measure the separated gas and liquid flow rates. The separated liquid phase is then routed through a Phase Dynamics full range microwave water cut meter, forming an integral part of the CCM multiphase meter.

Figure A.10 – CCM Meter

To date, Phase Dynamics have sold and installed 19 CCM meters in Alaska, Wyoming, Siberia China and Abu Dhabi. The dates of these have not published in the public domain. In 2001, Phase Dynamics reported the field testing of the CCM unit on 1152 wells in the BP operated Milne field in Alaska using a conventional separator for reference measurements. Measurement accuracies of ±5% were claimed for the gas flow rate, liquid flow rate and liquid phase water cut [**A24**].

A.12 PSL ESMER

ESMER exploits advanced signal processing techniques to determine the individual phase flow rates of a multiphase flow mixture. The ESMER system comprises two modular sub-spools: the pressure spool and the impedance spool. The pressure spool contains a differential device (orifice/Venturi/V-cone) equipped with differential pressure and absolute pressure gauges and a temperature sensor. The impedance spool comprises a capacitance sensor for oil external applications, a conductance sensor for water external applications or both for full water cut range applications. The spools are installed in a horizontal orientation.

ESMER is a pattern recognition based meter that establishes the non-linear relationships between an array of sensor measurements and the individual phase flow rates by a combination of pattern recognition and neural network training, **Figure A.11** [**A25**].

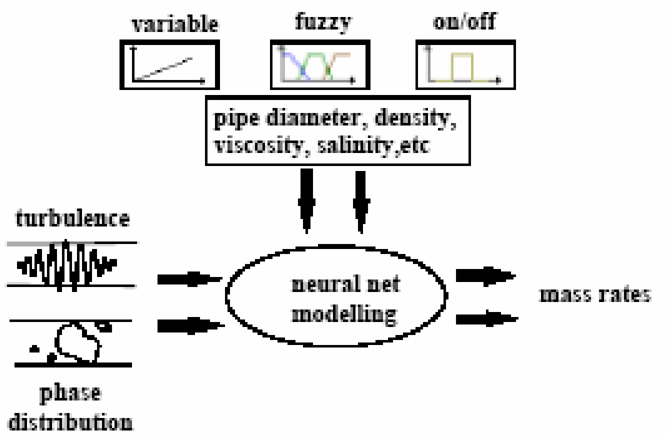

Figure A.11 – ESMER Concept Model

In 2002, ESMER was field tested by Sarawak Shell Berhad in Malaysia over a 20-month period [**A26**]. In a series of well tests, the meter's measurements were compared against those obtained from a conventional test separator. Good repeatability and trending of the meter against different production rates and flow patterns were reported and it was claimed that ESMER measurements matched the separator measurements to within ±10% for wells which were inside the operating envelope. However, it was noted that the accuracy of the meter deteriorated in well tests located at the boundary of the MPFM's operating envelope and with the passage of time.

A.13 Roxar MPFM 1900VI

The Roxar MPFM 1900VI comprises a capacitance sensor, an inductive sensor, a gamma-ray densitometer, a Venturi meter and a system computer, **Figure A.12**.

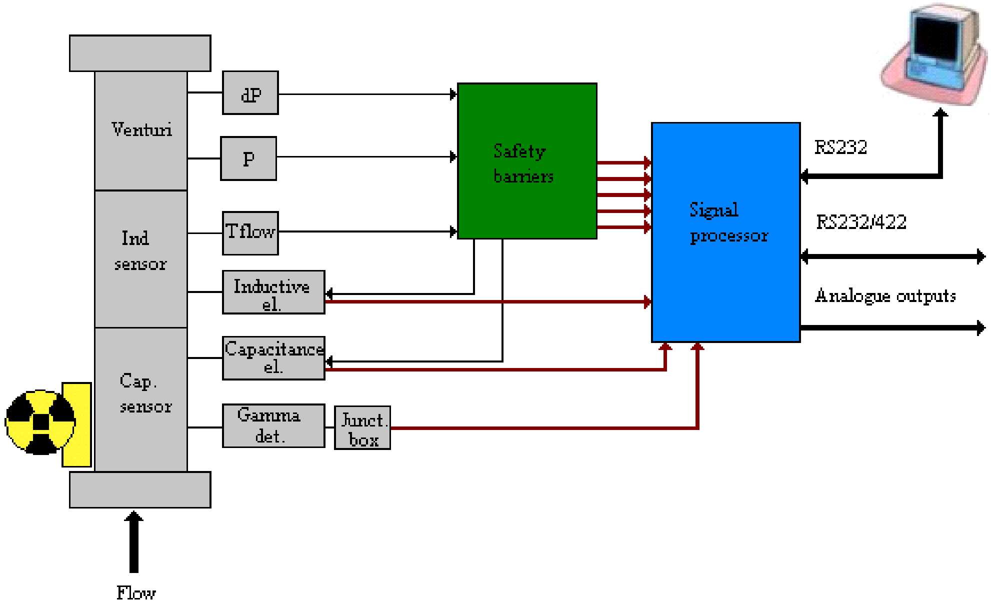

Figure A.12 – Schematic Diagram of the Roxar MPFM 1900VI Meter

Oil, gas and water fractions are determined by electrical impedance and gamma ray density measurements. A cross-correlation algorithm is used to measure individual component flow rates. The Venturi meter measures the mixture flow rate and extends the range of the MPFM 1900VI to cover single-phase liquid where the cross-correlation technique fails to operate [**A5**].

Field tests of the MPFM 1900Vi meter were undertaken by Gulf of Suez Petroleum Company (GUPCO) in Egypt on seven wells [**A27**]. During testing, the flow regime observed was noted to range from severe slugging through to annular owing to the dynamics of the gas-lift production system employed (the average GVF ranged between 93 – 98%). It was reported that gas and liquid phase flow rates were measured to within ±10%, relative to the test separator, for GVFs in the range 93 – 96%. Significant errors were reported for liquid flow rate measurements in tests where the GVF was in excess of 96%.

Saudi Aramco subjected the MPFM 1900VI meter to another series of field tests [**A28**]. The MPFM performance was examined at two different onshore gas and oil separation plants over a range of flow conditions: liquid flow rates of 1 – 15 mb/d; water cuts of 0 – 80%; and GVFs from 50% up to greater than 90%. It was reported that acceptable results were obtained by the MPFM 1900VI for wells with GVFs below 90%. Acceptable performance was defined to be ±10% for liquid flow rates; ±15% for gas flow rates and ±15% for water cut determination. At GVFs in excess of 90%, the 1900VI's performance was classified as 'poor' but was not quantified.

A.14 TEA Sistemi Spa LYRA

The TEA LYRA multiphase meter is suitable for multiphase flow measurement when the GVF is less than 90%. A differential pressure section (Venturi, nozzle or orifice, according to the fluids and process specification) is employed to determine the total mass flow rate, **Figure A.13**. The water-cut is determined using a patented impedance meter which requires input of the mean density of the gas-liquid mixture. The mean density is measured by a gamma-densitometer or, if the liquid fraction is appreciable (~30%), the pressure drop measurement is used to infer the mean density, negating the need for inclusion of a gamma-densitometer in the metering system. Interpretation of the measured data into individual phase flow rates is largely based on propriety mechanistic models and artificial neural networks trained with well testing data.

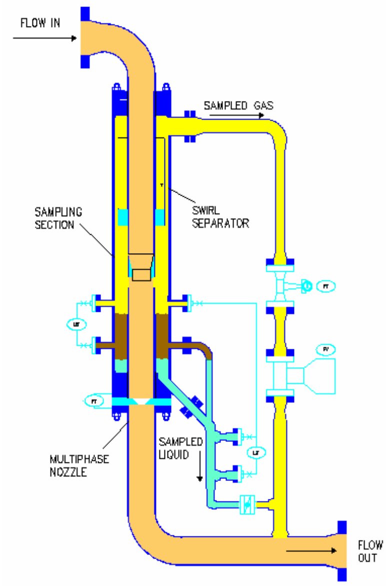

Figure A.13 – LYRA MPFM

LYRA has been marketed in Italy since 1995 and has been installed in three Agip operated oil fields, (Prezioso, Dirillo and Trecate). Although good results have been claimed, no figures pertaining to actual measurement accuracies were available [**A29**].

Appendix B – Feature Extraction Parameters

B.1 Probability Mass Function

The probability density function (PDF) defines the probability that a sampled data point will assume a particular value, within a specific range, at any instant in time. The probability density function, *P(x)*, is defined by the following expression:

$$P(x) = \lim_{\Delta x \to 0} \frac{prob[x < x(t) < x + \Delta x]}{\Delta x} \quad \text{(Eq. B.1)}$$

$$P(x) = \lim_{\Delta x \to 0} \frac{1}{\Delta x} \left(\lim_{T \to \infty} \frac{T_x}{T} \right) \quad \text{(Eq. B.2)}$$

Where *P(x)* represents the PDF of sample time history record *x(t)*, T_x is the total time, during which the signal will assume a value between *x* and *Δx*.

B.2 Mean

The mean ($\bar{x}$) is defined as the arithmetic average value of the data points. It estimates the value around which a central clustering of data points occurs. It is expressed in mathematical terms as:

$$\bar{x} = \frac{\sum_{i=1}^{N} x_i}{N} \quad \text{(Eq. B.3)}$$

Where *x* is the amplitude value of the i^{th} data point and *N* represents the total number of points in the sampled record.

B.3 Standard Deviation

The standard deviation of the data set is the root mean square of the amplitude deviations from the arithmetic mean and is effectively a measure of the spread of the data. Mathematically, the standard deviation (*SD*) can be expressed by:

$$SD = \sqrt{\frac{\sum_{i=1}^{N} (x_i - \bar{x})^2}{(N-1)}} \quad \text{(Eq. B.4)}$$

B.4 Coefficient of Variance

The coefficient of variance is a non-dimensional expression of the relative scatter in the data distribution. It is defined as the ratio of the standard distribution to the mean.

$$CV = \frac{SD}{\bar{x}} \quad \text{(Eq. B.5)}$$

B.5 Coefficient of Skewness

The coefficient of skewness characterises the degree of asymmetry exhibited by a distribution around its mean. A positive coefficient corresponds to a distribution with a greater number of large values for the parameter than one would expect if the distribution was Gaussian. Conversely, a negative value for the coefficient implies a higher occurrence of smaller values. For a Gaussian distribution, the coefficient of skewness is zero. The coefficient of skewness (*CS*) is defined by the equation shown below:

$$CS = \frac{\sum_{i=1}^{N}(x_i - \bar{x})^3}{(N-1)\cdot SD^3} \qquad \text{(Eq. B.6)}$$

B.6 Coefficient of Kurtosis

The coefficient of kurtosis characterises the degree of 'peakedness' exhibited by a distribution in comparison to that of a classical Gaussian distribution. A positive coefficient corresponds to a distribution with a greater extent of 'peakedness' than a normal distribution. On the other hand, a negative value for the coefficient implies a lesser degree of 'peakedness'. For a Gaussian distribution, the coefficient of kurtosis is zero. Mathematically, the coefficient of kurtosis (*CK*) can be expressed as:

$$CK = \left(\frac{\sum_{i=1}^{N}(x_i - \bar{x})^4}{(N-1)\cdot SD^4}\right) - 3 \qquad \text{(Eq. B.7)}$$

It should be noted that both the skewness and the kurtosis of a distribution are non-dimensional moments, unlike the mean and the standard deviation which have the same dimensions as the measured parameter.

B.7 Signal Energy

The signals' total energy is not related to the probability density function but is another useful amplitude feature that can be extracted form the signal time series. In several applications, the signals being examined are directly related to physical quantities capturing energy in a physical system.

The total energy in a discrete-time signal *x(n)* over a time interval $n_1 \le n \le N$ is defined as:

$$E_T = \frac{\sum_{n=n_1}^{N}(x_n)^2}{N} \qquad \text{(Eq. B.8)}$$

B.8 Linear Prediction Coefficients (LPCs)

Linear prediction modelling is used extensively in speech coding techniques, exploiting the redundancies of a speech signal by modelling the speech signal as a linear filter, excited by a signal referred to as the excitation (residual) signal. LPCs contain characteristic information on the spectral content of a waveform generated by a physical process. LPCs provide an efficient method of representing different signals using a small number of parameters facilitating both data compression techniques and statistical feature data [**B1**].

The linear prediction is modelled in the time domain by minimising the sum of the squared differences between the actual signal and that predicted, resulting in a residual error. In accomplishing this feat, a unique set of predictor coefficients, which were employed as the weighting coefficients in the linear combinations, are yielded.

In linear prediction, the present signal sample *x(n)* is modelled as a linear combination of the past outputs and the and the present and past inputs. In mathematical terms, this is denoted by the following expression:

$$x(n) = \sum_{k=1}^{p} a_k x(n-k) + G\sum_{l=0}^{q} b_1 u(n-1) \qquad \text{(Eq. B.9)}$$

Where b_0=1, G is a gain factor, a_k and b_1 are the filter coefficients of an unknown input u_n. The variable p denotes the number of past output samples being considered by the model which is also representative of the order of the linear prediction function. Applying a z-transform, the transfer function of the system can thus be expressed:

$$H(z) = \frac{X(z)}{U(z)} = G\frac{1+\sum_{l=1}^{q} b_1 z^{-1}}{1-\sum_{k=1}^{p} a_k z^{-k}} \qquad \text{(Eq. B.10)}$$

Where, *X(z)* denotes the z-transform of *x(n)*, *U(z)* is the z-transform of *u(n)* and *H(z)* is the transfer function of the system, which is the general pole-zero model.

Two special cases exist for the general pole-zero model. Firstly, when a_k = 0, for $1 \leq l \leq p$, *H(z)* reduces to an all pole model known as the autoregressive model. The other special case occurs when a_k = 0, for 1 ≤ k ≤ p, *H(z)* transforms to an all-zero or moving average model.

The autoregressive model is commonly employed due to its comparative simplicity and computational efficiency. To utilise the moving average model it is necessary to solve a set of non-linear equations; whereas the autoregressive model only requires a set of linear equations to be solved. The residual error, *e(n)*, is a by-product of the linear prediction techniques and is the difference between the actual input signal and the predicted signal. Accordingly, the following relationship holds:

$$e(n) = x(n) - \sum_{k=1}^{p} a_k x(n-k) \qquad \text{(Eq. B.11)}$$

A useful application for above relationship is in the selection of the optimal linear prediction order p_o. Analysing the variation in the residual error with predictor error, which is almost 'flat' for $p > p_o$, enables the optimal order to be selected. For the current gamma densitometer data set, a fifth order linear prediction model was determined to be optimal.

Autocorrelation and covariance are two widely used methods employed in the estimation of LPCs [**B2**]. Both these methods select the short-term filter coefficients in such a way as to minimise the residual error using the least-squares technique. The autocorrelation method involves the generation of a Toeplitz matrix, a matrix in which all the elements along a given diagonal are equal, which guarantees the stability of the filter. This permits the application of the Levinson-Durbin recursion algorithm to solve the set of linear equations produced by the least-squares procedure.

Correlation is a measurement of the average dependency between two random signals. The correlation between pairs of a single signal's samples is known as autocorrelation (AC). The autocorrelation function, r_{xx}, of a signal yields an average measurement of its time domain properties.

$$R_{xx}(\tau) = \lim_{T\to\infty} \frac{1}{2T} \int_{-T}^{T} x(t)x(t+\tau)dt \qquad \text{(Eq. B.12)}$$

Where, τ denotes the time shift or lag.

B.9 Line Spectral Frequencies (LSFs)

LPCs have a multitude of other representations: line spectral frequencies (LSF), reflection coefficients (RC), log area ratio (LAR), arcsine of reflection coefficients (ASRC), etc. These parameters all have a direct relationship with the LPCs and will preserve all information contained within the LPCs.

Publications have reported that LSFs are computationally efficient and have good quantisation and interpolation properties, facilitating improved system approximation. Compared to other transmission parameters, the line spectral frequencies have been found to encode speech spectral data much more efficiently [**B3**]. This enhanced efficiency is attributed to the close relationship between the LSFs and the formant frequencies. Furthermore, the line spectral frequencies naturally lend themselves to frame-to-frame interpolation, with smooth spectral changes, owing to their frequency domain interpolation.

The linear prediction analysis filter can be expressed in terms of LPCs, a_k, using the following equation:

$$A(z) = 1 - \sum_{k=1}^{p} a_k z^{-k} \qquad \text{(Eq. B.13)}$$

Where p is the order of the function *A(z)*. The $(p+1)^{th}$ order symmetric and anti-symmetric polynomials *P(z)* and *Q(z)* can be obtained from *A(z)*:

$$P(z) = A(z) + z^{-(p+1)} A(z^{-1}) \quad \text{(Eq. B.14)}$$

$$Q(z) = A(z) - z^{-(p+1)} A(z^{-1}) \quad \text{(Eq. B.15)}$$

The roots of the two polynomials lie on a unit circle and they form the LSFs. Kabal *et al* published an algorithm that enables the LSFs to be extracted from the LPCs using the Chebyshev polynomial root finding method [**B4**].

Appendix C – OLGA 2000 Input File

```
!*****************************************************
!     CASE Definition by OLGA-2000
!------------------------------------------------
CASE  AUTHOR="SB ", \
   PROJECT="Multiphase Test Modelling", \
   TITLE="AW Simulations"

!*************************************************************************
!     OPTIONS Definition
!*************************************************************************
OPTIONS  AXIALHEAT=OFF, COMPOSITIONAL=OFF, DEBUG=ON,
PHASE=TWO, POSTPROCESSOR=ON,  \
     NOSLIP=OFF, SLUGVOID=SINTEF, STEADYSTATE=ON,
TEMPERATURE=WALL, WAXDEPOSITION=OFF,  \
     DRILLING=OFF, TABLETOLERANCE=OFF

!*************************************************************************
!     FILES Definition
!*************************************************************************
FILES  PVTFILE="AWdata_1_and_2kg_waterflows.tab"

!*************************************************************************
!     INTEGRATION Definition
!*************************************************************************
INTEGRATION  CPULIMIT=1000 s, DTSTART=0.01 s, ENDTIME=3600 s,
MAXDT=0.5 s, MINDT=0.01 s,  \
        STARTTIME=0 s

!*************************************************************************
!     MATERIAL Definition
!*************************************************************************
MATERIAL  LABEL=STEEL, CAPACITY=500 J/kg-C, CONDUCTIVITY=50 W/m-
K, DENSITY=7850 kg/m3,  \
      TYPE=SOLID

!*************************************************************************
!     WALL Definition
!*************************************************************************
WALL  LABEL=WALL-1, MATERIAL=STEEL,
THICKNESS=0.0030480006766562 m


!*************************************************************************
!     GEOMETRY Definition
!*************************************************************************
GEOMETRY  LABEL=GEOMETRY-1, XSTART=0 m, YSTART=0 m
```

```
PIPE  LABEL=PIPE-1, DIAMETER=108.2 mm, NSEGMENTS=3,
ROUGHNESS=2.8e-005 m, WALL=WALL-1,  \
   XEND=10 m, YEND=-0.349 m
PIPE  LABEL=PIPE-3, DIAMETER=108.2 mm, NSEGMENTS=1,
ROUGHNESS=2.8e-005 m, WALL=WALL-1,  \
   XEND=10.98 m, YEND=-0.203 m
PIPE  LABEL=PIPE-4, DIAMETER=108.2 mm, NSEGMENTS=1,
ROUGHNESS=2.8e-005 m, WALL=WALL-1,  \
   XEND=11.965 m, YEND=0.293 m
PIPE  LABEL=PIPE-5, DIAMETER=108.2 mm, NSEGMENTS=1,
ROUGHNESS=2.8e-005 m, WALL=WALL-1,  \
   XEND=12.208 m, YEND=1.421 m
PIPE  LABEL=PIPE-6, DIAMETER=108.2 mm, NSEGMENTS=2,
ROUGHNESS=2.8e-005 m, WALL=WALL-1,  \
   XEND=13.135 m, YEND=3.769 m
PIPE  LABEL=PIPE-7, DIAMETER=108.2 mm, NSEGMENTS=1,
ROUGHNESS=2.8e-005 m, WALL=WALL-1,  \
   XEND=13.445 m, YEND=5.021 m
PIPE  LABEL=PIPE-8, DIAMETER=108.2 mm, NSEGMENTS=2,
ROUGHNESS=2.8e-005 m, WALL=WALL-1,  \
   XEND=13.7 m, YEND=7.297 m
PIPE  LABEL=PIPE-9, DIAMETER=108.2 mm, NSEGMENTS=2,
ROUGHNESS=2.8e-005 m, WALL=WALL-1,  \
   XEND=13.86 m, YEND=9.573 m
PIPE  LABEL=PIPE-11, DIAMETER=108.2 mm, NSEGMENTS=1,
ROUGHNESS=2.8e-005 m, WALL=WALL-1,  \
   XEND=13.86 m, YEND=10.122 m
PIPE  LABEL=PIPE-10, DIAMETER=108.2 mm, NSEGMENTS=5,
ROUGHNESS=2.8e-005 m, WALL=WALL-1,  \
   XEND=17.578 m, YEND=10.122 m

!*********************************************************************
!     NODE Definition
!*********************************************************************
NODE  LABEL=INLET-N, TYPE=TERMINAL
NODE  LABEL=OUTLET-N, TYPE=TERMINAL


!*********************************************************************
!     BRANCH Definition
!*********************************************************************
*********
BRANCH  LABEL=BRANCH-1, FLUID="a20w1", FROM=INLET-N,
GEOMETRY=GEOMETRY-1, TO=OUTLET-N

!*********************************************************************
!     BOUNDARY Definition
!*********************************************************************
```

```
BOUNDARY  NODE=INLET-N, TYPE=CLOSED
BOUNDARY  GASFRACTION=( -1, -1 ) -, NODE=OUTLET-N,
PRESSURE=2:2.263 bara, TEMPERATURE=2:20 C,  \
       TIME=( 0, 3600 ) s, TYPE=PRESSURE, WATERFRACTION=( 0, 0 ) -

!*********************************************************************
!     HEATTRANSFER Definition
!*********************************************************************
HEATTRANSFER  HOUTEROPTION=AIR, TAMBIENT=20 C

!*********************************************************************
!     SOURCE Definition
!*********************************************************************
SOURCE  LABEL=SOURCE-1, BRANCH=BRANCH-1, GASFRACTION=-1 %,
MASSFLOW=1.006667 kg/s,  \
     PIPE=PIPE-1, SECTION=1, TEMPERATURE=20 C, TIME=0 s,
WATERFRACTION=0 %

!*********************************************************************
!     OUTPUT Definition
!*********************************************************************
OUTPUT  BRANCH=BRANCH-1, DTOUT=1 s, PIPE=PIPE-9, SECTION=2,
VARIABLE=( UG, UL, HOL,  \
        ID )

!*********************************************************************
!     TREND Definition
!*********************************************************************
TREND  BRANCH=BRANCH-1, DTPLOT=1 s, PIPE=PIPE-9, SECTION=2,
VARIABLE=( TM, PT, HOL,  \
       ID, UG, UL )

!*********************************************************************
!     PROFILE Definition
!*********************************************************************
PROFILE  BRANCH=BRANCH-1, DTPLOT=1 s, VARIABLE=( Tm, QLT, HOL, ID,
UG, UL )

!*********************************************************************
!     PLOT Definition
!*********************************************************************
PLOT  DTPLOT=1 s, VARIABLE=( UG, UL, HOL, ID )
!
ENDCASE
```

Appendix D – Wavelet Packet Coefficient Statistics

D.1 Wavelet Packet Decomposition Notation

The original signal [0 0] was decomposed into wavelet packets up to its fourth level. For each packet, the level of decomposition is denoted by the packet's first digit and its sequence in the level is given by the second digit in its identifying label. The wavelet packet notation employed in compiling the tables of coefficient statistics (**Appendices D.2 – D.5**) is illustrated in **Figure D.1**.

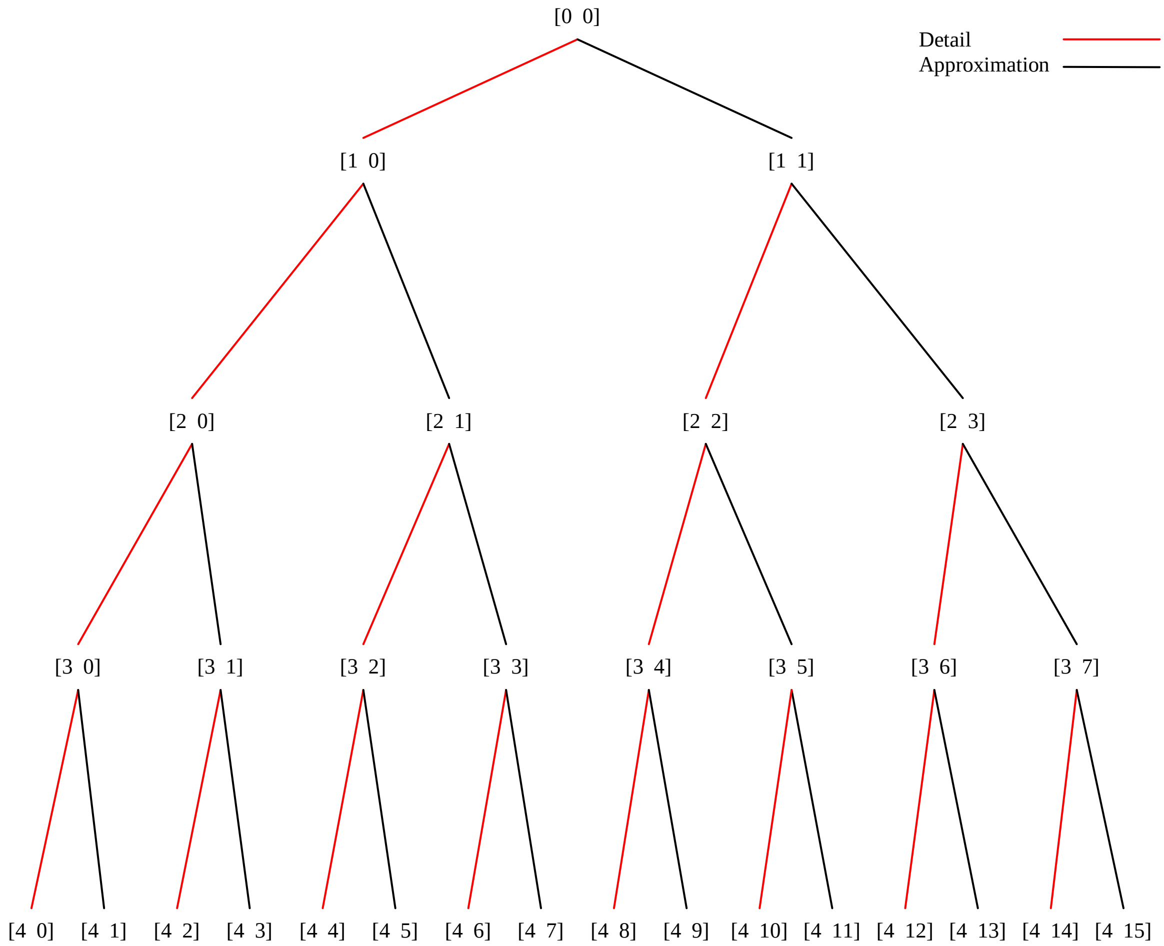

Figure D.1 – Wavelet Packet Decomposition Tree

D.2 Wavelet Packet Coefficient Statistics: Packets [1 0] – [3 1]

Packet	Experiment	1	2	3	4	5	6	7	8	9	10	11	12	13	14	15	16
	V_{sg} (m/s)	0.13	0.30	0.58	0.99	0.13	0.30	0.59	1.32	0.13	0.30	0.59	1.32	0.13	0.31	0.59	1.29
	V_{sl} (m/s)	0.12	0.12	0.12	0.12	0.24	0.24	0.24	0.24	0.37	0.37	0.37	0.37	0.49	0.49	0.49	0.49
	WC (%)	1.00	1.00	1.00	1.00	1.00	1.00	1.00	1.00	1.00	1.00	1.00	1.00	1.00	1.00	1.00	1.00
1 0	Mean	90.65	103.50	117.06	135.01	87.35	99.45	112.08	128.73	85.62	97.30	109.08	127.03	83.95	94.72	106.34	123.04
	Median	86.39	95.85	112.34	136.82	84.10	92.36	105.46	130.21	83.38	91.09	101.57	128.89	82.06	89.31	98.96	122.93
	Standard dev.	14.48	19.85	20.65	19.26	12.63	18.98	20.12	19.69	10.50	17.61	19.81	23.22	9.66	16.47	19.28	22.74
	Variance	6.3E+00	5.2E+00	5.7E+00	7.0E+00	6.9E+00	5.2E+00	5.6E+00	6.5E+00	8.2E+00	5.5E+00	5.5E+00	5.5E+00	8.7E+00	5.8E+00	5.5E+00	5.4E+00
	Skewness	1.9E+00	1.1E+00	4.7E-01	-2.3E-01	2.1E+00	1.3E+00	6.9E-01	-7.1E-02	2.2E+00	1.6E+00	9.1E-01	-4.2E-02	2.2E+00	1.7E+00	1.1E+00	1.1E-01
	Kurtosis	3.429	0.290	-0.852	-0.734	4.880	0.896	-0.605	-0.941	6.164	1.640	-0.257	-1.089	7.024	2.425	0.116	-1.123
1 1	Mean	0.000	0.000	0.000	0.000	0.000	0.000	0.000	0.000	0.000	0.000	0.000	0.000	0.000	0.000	0.000	0.000
	Median	-0.007	-0.007	-0.004	-0.021	-0.015	0.000	-0.004	-0.013	-0.022	-0.008	-0.027	-0.011	-0.007	-0.015	-0.021	-0.002
	Standard dev.	5.098	5.349	5.646	6.054	5.015	5.302	5.558	5.926	4.973	5.199	5.489	5.868	4.901	5.176	5.454	5.803
	Variance	1.0E-06	8.0E-07	-1.4E-06	7.2E-07	1.2E-06	3.0E-07	-7.2E-07	-3.6E-06	1.5E-07	-2.8E-06	8.3E-07	-4.3E-07	2.9E-07	-1.4E-07	8.2E-07	3.6E-07
	Skewness	1.3E-02	7.9E-03	1.2E-02	1.2E-02	1.5E-02	1.5E-02	1.2E-02	6.9E-03	9.5E-03	1.9E-02	1.7E-02	7.7E-03	1.0E-02	1.6E-02	7.1E-03	-1.7E-03
	Kurtosis	0.051	0.117	0.087	0.073	0.055	0.132	0.087	0.070	0.065	0.086	0.107	0.111	0.082	0.097	0.096	0.117
2 0	Mean	90.653	103.505	117.059	135.006	87.348	99.448	112.084	128.726	85.624	97.299	109.083	127.035	83.947	94.719	106.340	123.039
	Median	86.025	95.200	112.129	137.095	83.804	91.768	104.844	130.404	83.153	90.585	100.847	129.108	81.839	88.890	98.289	123.052
	Standard dev.	14.059	19.490	20.261	18.770	12.163	18.621	19.735	19.228	9.941	17.233	19.431	22.835	9.057	16.079	18.898	22.348
	Variance	6.4E+00	5.3E+00	5.8E+00	7.2E+00	7.2E+00	5.3E+00	5.7E+00	6.7E+00	8.6E+00	5.6E+00	5.6E+00	5.6E+00	9.3E+00	5.9E+00	5.6E+00	5.5E+00
	Skewness	2.0E+00	1.2E+00	4.8E-01	-2.6E-01	2.3E+00	1.4E+00	7.1E-01	-9.0E-02	2.5E+00	1.6E+00	9.4E-01	-5.7E-02	2.7E+00	1.8E+00	1.1E+00	1.1E-01
	Kurtosis	3.736	0.273	-0.934	-0.806	5.526	0.916	-0.677	-1.028	7.480	1.721	-0.304	-1.157	8.817	2.580	0.087	-1.195
2 1	Mean	0.000	0.000	0.000	0.000	0.000	0.000	0.000	0.000	0.000	0.000	0.000	0.000	0.000	0.000	0.000	0.000
	Median	-0.003	0.003	0.008	0.012	-0.006	0.004	-0.007	-0.001	0.004	0.005	0.006	0.010	0.001	0.002	0.001	-0.002
	Standard dev.	3.451	3.738	3.998	4.338	3.406	3.655	3.932	4.259	3.381	3.613	3.865	4.213	3.362	3.565	3.830	4.183
	Variance	-8.0E-07	-1.4E-06	-1.2E-06	-7.1E-08	-3.6E-06	-5.4E-07	3.6E-06	3.0E-06	-3.2E-06	1.5E-06	-1.9E-06	5.4E-06	-4.6E-07	-4.4E-06	-1.8E-06	1.0E-06
	Skewness	1.1E-03	-3.9E-04	-4.4E-03	-1.1E-03	-9.9E-04	-2.8E-03	3.8E-03	-2.3E-03	-2.3E-03	-2.5E-03	6.3E-04	3.1E-03	2.8E-03	-5.7E-04	3.6E-04	2.4E-03
	Kurtosis	0.327	0.313	0.267	0.226	0.250	0.275	0.244	0.241	0.251	0.283	0.291	0.264	0.218	0.292	0.279	0.205
2 2	Mean	0.000	0.000	0.000	0.000	0.000	0.000	0.000	0.000	0.000	0.000	0.000	0.000	0.000	0.000	0.000	0.000
	Median	-0.004	-0.008	0.008	-0.008	0.012	0.004	-0.002	0.008	0.003	0.002	0.000	-0.001	0.002	-0.002	0.002	-0.006
	Standard dev.	3.632	3.811	4.027	4.299	3.590	3.780	3.947	4.190	3.556	3.715	3.930	4.164	3.509	3.692	3.897	4.123
	Variance	-2.4E-07	3.0E-07	7.8E-07	7.9E-07	8.6E-07	-5.9E-07	4.5E-07	-3.0E-07	3.8E-07	1.1E-06	3.8E-07	-8.1E-07	-4.6E-07	1.2E-06	1.2E-06	-1.1E-06
	Skewness	8.1E-07	-9.8E-07	-2.1E-06	-4.1E-06	-3.3E-06	1.9E-06	-1.5E-06	2.1E-06	-8.9E-07	-3.3E-06	-1.1E-06	2.5E-06	1.7E-06	-4.0E-06	-3.4E-06	3.5E-06
	Kurtosis	0.062	0.100	0.098	0.064	0.049	0.073	0.056	0.032	0.073	0.077	0.113	0.093	0.064	0.098	0.070	0.077
2 3	Mean	0.000	0.000	0.000	0.000	0.000	0.000	0.000	0.000	0.000	0.000	0.000	0.000	0.000	0.000	0.000	0.000
	Median	-0.003	-0.013	-0.005	-0.001	-0.001	-0.015	-0.001	-0.002	-0.006	-0.015	-0.012	0.001	-0.018	0.005	-0.009	-0.003
	Standard dev.	3.578	3.752	3.957	4.262	3.501	3.718	3.913	4.191	3.476	3.636	3.832	4.134	3.422	3.627	3.816	4.084
	Variance	1.7E-06	8.4E-07	-2.8E-06	2.1E-07	8.7E-07	1.0E-06	-1.5E-06	-4.8E-06	-1.8E-07	-5.2E-06	8.0E-07	2.0E-07	8.8E-07	-1.4E-06	-3.6E-08	1.6E-06
	Skewness	1.6E-02	1.1E-02	2.6E-03	1.3E-02	1.1E-02	1.3E-02	9.3E-03	6.3E-03	9.6E-03	1.3E-02	3.1E-03	5.3E-03	6.6E-03	-2.5E-04	5.9E-03	-4.3E-03
	Kurtosis	0.205	0.276	0.258	0.253	0.238	0.278	0.252	0.266	0.214	0.279	0.252	0.292	0.180	0.262	0.257	0.241
3 0	Mean	90.653	103.505	117.059	135.006	87.348	99.448	112.084	128.726	85.624	97.299	109.083	127.035	83.947	94.719	106.340	123.039
	Median	85.792	94.865	111.911	137.140	83.602	91.500	104.518	130.455	82.981	90.273	100.501	129.167	81.718	88.608	97.913	123.060
	Standard dev.	13.819	19.267	19.983	18.420	11.891	18.395	19.457	18.893	9.596	17.001	19.174	22.557	8.658	15.819	18.631	22.065
	Variance	6.6E+00	5.4E+00	5.9E+00	7.3E+00	7.3E+00	5.4E+00	5.8E+00	6.8E+00	8.9E+00	5.7E+00	5.7E+00	5.6E+00	9.7E+00	6.0E+00	5.7E+00	5.6E+00
	Skewness	2.1E+00	1.2E+00	4.9E-01	-2.7E-01	2.4E+00	1.4E+00	7.3E-01	-9.4E-02	2.7E+00	1.7E+00	9.7E-01	-6.1E-02	2.9E+00	1.9E+00	1.2E+00	1.1E-01
	Kurtosis	3.932	0.260	-0.982	-0.857	5.890	0.929	-0.712	-1.083	8.284	1.785	-0.317	-1.190	9.511	2.685	0.096	-1.235
3 1	Mean	0.000	0.000	0.000	0.000	0.000	0.000	0.000	0.000	0.000	0.000	0.000	0.000	0.000	0.000	0.000	0.000
	Median	-0.004	0.006	-0.003	-0.010	0.006	0.002	0.004	-0.002	0.000	-0.001	0.002	-0.002	0.005	-0.006	-0.006	0.002
	Standard dev.	2.591	2.941	3.346	3.609	2.560	2.893	3.296	3.572	2.596	2.815	3.148	3.551	2.661	2.880	3.162	3.543
	Variance	-8.8E-06	3.7E-06	-1.9E-06	-1.8E-06	-9.0E-07	-3.7E-06	9.9E-06	-9.6E-07	1.2E-06	1.2E-05	-8.6E-07	-1.7E-05	4.7E-06	1.0E-05	4.6E-06	-5.9E-06
	Skewness	5.5E-04	3.7E-03	4.2E-03	9.1E-04	5.7E-03	-2.7E-03	1.9E-03	3.5E-04	-4.0E-03	5.1E-04	-2.4E-03	3.4E-03	-3.2E-03	-3.2E-03	-2.5E-03	-2.5E-03
	Kurtosis	0.381	0.567	0.352	0.329	0.536	0.511	0.310	0.286	0.473	0.540	0.349	0.339	0.599	0.630	0.446	0.318

Packet	Experiment	17	18	19	20	21	22	23	24	25	26	27	28	29	30	31	32
	V_{sg} (m/s)	0.15	0.30	0.59	1.32	0.15	0.31	0.59	1.33	0.15	0.30	0.59	1.32	0.15	0.30	0.59	1.00
	V_{sl} (m/s)	0.61	0.61	0.61	0.61	0.73	0.73	0.73	0.73	0.79	0.79	0.79	0.79	0.13	0.13	0.13	0.13
	WC (%)	1.00	1.00	1.00	1.00	1.00	1.00	1.00	1.00	1.00	1.00	1.00	1.00	0.80	0.80	0.80	0.80
1 0	Mean	84.10	92.76	104.29	119.99	82.65	90.65	104.23	120.54	85.19	90.58	101.33	117.43	95.96	106.25	119.94	133.59
	Median	82.02	88.11	97.18	116.41	80.76	86.50	97.38	114.62	83.35	86.52	94.88	111.24	90.53	98.19	116.37	135.52
	Standard dev.	10.15	15.14	18.77	20.01	9.71	14.36	18.58	20.49	9.85	14.19	17.83	20.00	16.47	20.86	22.78	24.15
	Variance	8.3E+00	6.1E+00	5.6E+00	6.0E+00	8.5E+00	6.3E+00	5.6E+00	5.9E+00	8.6E+00	6.4E+00	5.7E+00	5.9E+00	5.8E+00	5.1E+00	5.3E+00	5.5E+00
	Skewness	2.3E+00	1.8E+00	1.2E+00	3.5E-01	2.4E+00	2.0E+00	1.3E+00	5.1E-01	2.3E+00	2.0E+00	1.4E+00	5.7E-01	1.7E+00	1.1E+00	3.8E-01	-1.1E-01
	Kurtosis	7.009	3.044	0.536	-1.030	7.787	3.731	0.871	-0.904	7.304	3.954	1.064	-0.825	2.529	0.162	-0.949	-0.957
1 1	Mean	0.000	0.000	0.000	0.000	0.000	0.000	0.000	0.000	0.000	0.000	0.000	0.000	0.000	0.000	0.000	0.000
	Median	-0.002	-0.007	-0.006	-0.011	-0.007	0.002	-0.004	-0.011	-0.002	-0.006	-0.025	-0.011	-0.004	-0.019	-0.024	-0.001
	Standard dev.	4.887	5.108	5.399	5.746	4.862	5.059	5.370	5.751	4.952	5.064	5.336	5.719	5.186	5.443	5.715	6.013
	Variance	-4.8E-07	-8.0E-07	4.1E-06	-2.9E-07	-9.9E-07	1.9E-06	-1.7E-06	-3.5E-06	-5.1E-07	2.1E-06	2.1E-07	-1.1E-06	1.5E-06	-3.6E-06	-1.4E-06	-5.9E-07
	Skewness	8.4E-03	5.7E-03	7.0E-03	4.8E-03	1.4E-02	1.1E-02	2.4E-03	1.1E-02	1.2E-02	8.9E-03	1.2E-02	1.4E-02	5.9E-03	8.9E-03	1.3E-02	1.0E-02
	Kurtosis	0.055	0.036	0.117	0.068	0.023	0.074	0.101	0.078	0.026	0.063	0.087	0.096	0.113	0.085	0.086	0.101
2 0	Mean	84.101	92.757	104.286	119.991	82.650	90.649	104.231	120.539	85.194	90.578	101.329	117.428	95.964	106.246	119.940	133.587
	Median	81.798	87.727	96.581	116.129	80.590	86.144	96.804	113.961	83.158	86.145	94.314	110.487	90.093	97.499	116.303	135.735
	Standard dev.	9.574	14.714	18.374	19.569	9.110	13.918	18.183	20.058	9.238	13.744	17.433	19.566	16.084	20.513	22.409	23.757
	Variance	8.8E+00	6.3E+00	5.7E+00	6.1E+00	9.1E+00	6.5E+00	5.7E+00	6.0E+00	9.2E+00	6.6E+00	5.8E+00	6.0E+00	6.0E+00	5.2E+00	5.4E+00	5.6E+00
	Skewness	2.7E+00	2.0E+00	1.3E+00	3.6E-01	2.8E+00	2.1E+00	1.4E+00	5.3E-01	2.7E+00	2.2E+00	1.5E+00	5.9E-01	1.8E+00	1.1E+00	3.8E-01	-1.2E-01
	Kurtosis	8.588	3.302	0.537	-1.124	9.768	4.109	0.901	-0.987	9.182	4.371	1.111	-0.901	2.695	0.134	-1.023	-1.016
2 1	Mean	0.000	0.000	0.000	0.000	0.000	0.000	0.000	0.000	0.000	0.000	0.000	0.000	0.000	0.000	0.000	0.000
	Median	-0.001	-0.001	-0.003	0.003	0.001	-0.003	0.000	-0.003	-0.001	0.009	0.000	0.008	-0.002	0.002	0.002	0.006
	Standard dev.	3.379	3.566	3.811	4.184	3.361	3.533	3.816	4.192	3.427	3.543	3.755	4.167	3.556	3.783	4.071	4.324
	Variance	1.6E-06	1.5E-06	-5.2E-06	1.4E-06	1.9E-06	-2.4E-06	2.0E-06	5.8E-06	-1.3E-06	-2.3E-06	-1.7E-06	1.9E-06	2.1E-06	-2.7E-06	4.9E-07	2.9E-06
	Skewness	4.8E-05	-2.0E-03	-3.8E-04	-2.5E-03	1.2E-04	-1.6E-04	1.5E-04	1.4E-03	1.2E-03	-1.2E-03	5.1E-04	4.4E-03	4.0E-04	-8.8E-04	2.3E-03	2.2E-06
	Kurtosis	0.272	0.264	0.266	0.218	0.238	0.271	0.294	0.217	0.249	0.291	0.333	0.249	0.284	0.328	0.278	0.300
2 2	Mean	0.000	0.000	0.000	0.000	0.000	0.000	0.000	0.000	0.000	0.000	0.000	0.000	0.000	0.000	0.000	0.000
	Median	0.000	-0.004	0.002	0.005	-0.002	-0.001	-0.001	0.003	-0.004	0.001	0.005	-0.001	-0.002	-0.005	0.001	-0.002
	Standard dev.	3.495	3.643	3.845	4.089	3.469	3.596	3.823	4.087	3.531	3.608	3.798	4.069	3.692	3.879	4.073	4.287
	Variance	-3.2E-07	-1.2E-06	4.5E-07	5.6E-07	-1.9E-07	-9.6E-07	-3.8E-07	-1.1E-06	-6.8E-07	7.0E-07	-9.1E-07	-1.1E-06	-8.5E-07	1.6E-07	-3.1E-07	-9.5E-07
	Skewness	1.0E-06	4.4E-06	-1.2E-06	-2.0E-06	5.3E-07	3.6E-06	1.1E-06	3.8E-06	2.0E-06	-2.2E-06	3.2E-06	6.2E-06	5.0E-06	-7.5E-06	1.3E-06	3.0E-06
	Kurtosis	0.057	0.022	0.071	0.034	0.005	0.018	0.090	0.086	0.017	0.046	0.086	0.048	0.078	0.096	0.053	0.117
2 3	Mean	0.000	0.000	0.000	0.000	0.000	0.000	0.000	0.000	0.000	0.000	0.000	0.000	0.000	0.000	0.000	0.000
	Median	-0.010	0.004	-0.009	-0.002	-0.017	0.002	-0.009	0.001	-0.007	0.014	-0.011	0.004	-0.005	-0.006	-0.023	0.005
	Standard dev.	3.416	3.580	3.791	4.036	3.407	3.559	3.771	4.047	3.472	3.554	3.748	4.019	3.641	3.818	4.009	4.216
	Variance	-3.6E-07	8.7E-08	5.4E-06	-9.8E-07	-1.2E-06	3.6E-06	-2.0E-06	-3.8E-06	-3.4E-08	2.3E-06	1.2E-06	-4.5E-07	3.0E-06	-5.3E-06	-1.7E-06	1.2E-07
	Skewness	8.5E-03	-1.5E-03	1.0E-02	9.9E-03	1.5E-02	-1.1E-03	7.0E-03	8.1E-03	6.7E-03	-5.1E-04	9.1E-03	4.7E-03	1.4E-02	9.0E-03	2.1E-02	1.2E-02
	Kurtosis	0.227	0.241	0.281	0.227	0.199	0.214	0.251	0.227	0.184	0.248	0.189	0.269	0.274	0.273	0.275	0.252
3 0	Mean	84.101	92.757	104.286	119.991	82.650	90.649	104.231	120.539	85.194	90.578	101.329	117.428	95.964	106.246	119.940	133.587
	Median	81.652	87.470	96.232	115.913	80.478	85.919	96.424	113.674	83.061	85.971	93.993	110.063	89.804	97.237	116.115	135.860
	Standard dev.	9.173	14.422	18.115	19.238	8.641	13.600	17.898	19.735	8.731	13.402	17.144	19.237	15.848	20.274	22.116	23.465
	Variance	9.2E+00	6.4E+00	5.8E+00	6.2E+00	9.6E+00	6.7E+00	5.8E+00	6.1E+00	9.8E+00	6.8E+00	5.9E+00	6.1E+00	6.1E+00	5.2E+00	5.4E+00	5.7E+00
	Skewness	2.9E+00	2.0E+00	1.3E+00	3.7E-01	2.9E+00	2.2E+00	1.4E+00	5.5E-01	2.7E+00	2.2E+00	1.5E+00	6.2E-01	1.9E+00	1.1E+00	3.8E-01	-1.3E-01
	Kurtosis	9.142	3.499	0.569	-1.167	9.959	4.390	0.948	-1.019	9.091	4.622	1.173	-0.923	2.782	0.118	-1.064	-1.050
3 1	Mean	0.000	0.000	0.000	0.000	0.000	0.000	0.000	0.000	0.000	0.000	0.000	0.000	0.000	0.000	0.000	0.000
	Median	-0.005	-0.005	-0.008	-0.005	0.005	-0.001	0.000	0.001	0.006	0.003	0.002	0.004	0.006	-0.005	0.002	-0.001
	Standard dev.	2.741	2.921	3.078	3.581	2.887	2.961	3.206	3.585	3.020	3.046	3.163	3.573	2.742	3.127	3.611	3.719
	Variance	7.7E-06	-2.3E-05	9.6E-07	8.7E-06	2.8E-06	3.0E-07	-2.9E-06	-8.3E-06	-7.0E-07	5.5E-06	-4.2E-06	-1.1E-05	-5.7E-06	-2.4E-06	1.0E-05	3.9E-06
	Skewness	-8.5E-03	-8.7E-03	1.2E-03	2.7E-03	-1.0E-02	3.3E-03	2.4E-03	-2.6E-03	-3.6E-03	7.3E-04	-1.2E-02	9.5E-04	-2.9E-03	2.1E-03	-6.8E-03	1.6E-03
	Kurtosis	0.616	0.717	0.423	0.345	1.220	0.830	0.558	0.389	1.323	0.988	0.554	0.397	0.476	0.604	0.476	0.295

Packet	Experiment	33	34	35	36	37	38	39	40	41	42	43	44	45	46	47	48
	V_{sg} (m/s)	0.15	0.30	0.59	1.00	0.15	0.30	0.59	1.00	0.15	0.30	0.59	1.00	0.15	0.31	0.59	1.33
	V_{sl} (m/s)	0.13	0.13	0.13	0.13	0.14	0.14	0.14	0.14	0.14	0.14	0.14	0.14	0.25	0.25	0.25	0.25
	WC (%)	0.60	0.60	0.60	0.60	0.40	0.40	0.40	0.40	0.20	0.20	0.20	0.20	0.80	0.80	0.80	0.80
1 0	Mean	95.39	104.40	116.46	130.27	96.70	105.70	118.60	129.88	102.15	111.41	122.81	134.82	88.03	97.01	107.78	124.57
	Median	90.85	97.81	113.64	131.66	89.70	97.07	114.81	131.33	99.27	107.21	120.84	135.66	83.87	89.92	102.13	126.48
	Standard dev.	14.86	19.51	22.21	23.93	19.70	23.10	26.04	24.36	11.93	15.24	16.59	17.25	14.16	18.66	20.52	20.24
	Variance	6.4E+00	5.4E+00	5.2E+00	5.4E+00	4.9E+00	4.6E+00	4.6E+00	5.3E+00	8.6E+00	7.3E+00	7.4E+00	7.8E+00	6.2E+00	5.2E+00	5.3E+00	6.2E+00
	Skewness	1.6E+00	1.0E+00	3.9E-01	-6.5E-02	1.8E+00	1.0E+00	4.1E-01	-7.7E-02	1.6E+00	1.0E+00	3.8E-01	-7.4E-02	1.9E+00	1.3E+00	6.1E-01	-1.4E-01
	Kurtosis	2.412	0.282	-0.832	-0.893	2.856	0.143	-0.916	-0.908	3.255	0.625	-0.625	-0.725	3.691	0.691	-0.682	-0.899
1 1	Mean	0.000	0.000	0.000	0.000	0.000	0.000	0.000	0.000	0.000	0.000	0.000	0.000	0.000	0.000	0.000	0.000
	Median	-0.011	-0.007	-0.010	-0.008	-0.004	-0.014	0.000	0.003	-0.021	-0.018	-0.004	0.002	-0.009	-0.007	0.000	-0.022
	Standard dev.	5.167	5.400	5.652	5.950	5.194	5.412	5.671	5.923	5.319	5.556	5.793	6.039	5.018	5.243	5.464	5.816
	Variance	-1.8E-06	-1.5E-06	8.3E-08	2.1E-06	1.3E-06	-1.0E-06	-1.0E-06	1.4E-06	7.8E-07	8.2E-07	3.4E-07	1.2E-06	-3.8E-07	1.0E-06	2.2E-07	-1.9E-06
	Skewness	1.4E-02	1.6E-02	9.4E-03	1.1E-02	9.2E-03	1.8E-02	8.3E-03	1.5E-02	1.7E-02	1.3E-02	1.1E-02	1.4E-02	1.0E-02	6.0E-03	5.1E-03	1.0E-02
	Kurtosis	0.060	0.084	0.115	0.094	0.101	0.128	0.165	0.086	0.063	0.066	0.070	0.091	0.089	0.102	0.096	0.079
2 0	Mean	95.392	104.405	116.462	130.270	96.696	105.698	118.597	129.882	102.149	111.405	122.809	134.823	88.028	97.014	107.778	124.571
	Median	90.388	97.308	113.609	131.763	89.110	96.574	114.854	131.455	98.889	106.751	120.726	135.782	83.530	89.371	101.673	126.771
	Standard dev.	14.426	19.145	21.844	23.540	19.365	22.780	25.718	23.971	11.352	14.740	16.080	16.720	13.733	18.310	20.149	19.795
	Variance	6.6E+00	5.5E+00	5.3E+00	5.5E+00	5.0E+00	4.6E+00	4.6E+00	5.4E+00	9.0E+00	7.6E+00	7.6E+00	8.1E+00	6.4E+00	5.3E+00	5.3E+00	6.3E+00
	Skewness	1.7E+00	1.1E+00	4.0E-01	-8.0E-02	1.9E+00	1.1E+00	4.1E-01	-9.1E-02	1.9E+00	1.1E+00	3.9E-01	-9.5E-02	2.1E+00	1.3E+00	6.2E-01	-1.6E-01
	Kurtosis	2.637	0.265	-0.897	-0.947	2.993	0.119	-0.970	-0.961	3.839	0.667	-0.718	-0.814	4.040	0.697	-0.750	-0.968
2 1	Mean	0.000	0.000	0.000	0.000	0.000	0.000	0.000	0.000	0.000	0.000	0.000	0.000	0.000	0.000	0.000	0.000
	Median	0.001	-0.003	0.006	-0.005	0.004	-0.010	0.008	0.000	0.012	0.000	0.005	0.004	0.006	-0.001	0.003	0.009
	Standard dev.	3.574	3.755	4.012	4.281	3.594	3.825	4.058	4.341	3.669	3.857	4.091	4.253	3.438	3.622	3.876	4.207
	Variance	3.2E-06	-5.8E-07	-5.4E-06	-5.1E-06	-1.7E-06	5.3E-07	2.3E-06	-2.4E-06	2.0E-06	3.2E-06	1.4E-06	-2.5E-06	2.8E-06	-1.3E-06	6.6E-07	6.9E-06
	Skewness	3.2E-03	2.1E-03	1.2E-03	9.2E-04	2.9E-03	-5.1E-04	3.1E-03	2.5E-03	4.2E-03	-2.2E-03	-1.8E-03	-2.2E-03	2.2E-03	2.0E-03	3.5E-03	6.5E-03
	Kurtosis	0.217	0.315	0.293	0.260	0.326	0.378	0.303	0.279	0.223	0.202	0.222	0.195	0.243	0.298	0.294	0.209
2 2	Mean	0.000	0.000	0.000	0.000	0.000	0.000	0.000	0.000	0.000	0.000	0.000	0.000	0.000	0.000	0.000	0.000
	Median	-0.008	-0.007	-0.005	0.004	0.000	0.000	0.005	-0.006	0.006	-0.007	-0.004	0.004	-0.004	-0.001	0.000	0.003
	Standard dev.	3.680	3.845	4.025	4.239	3.711	3.857	4.030	4.217	3.808	3.971	4.123	4.300	3.587	3.734	3.895	4.128
	Variance	1.3E-06	1.2E-06	6.7E-07	-1.4E-06	-8.0E-08	5.8E-08	-6.7E-07	-7.5E-07	-6.7E-08	-6.4E-07	-1.9E-06	-9.8E-07	-3.2E-07	-8.8E-07	3.6E-07	-1.2E-06
	Skewness	-4.0E-06	-3.7E-06	-2.2E-06	6.2E-06	-4.3E-07	6.8E-07	1.7E-06	2.5E-06	-2.2E-07	2.2E-06	5.3E-06	3.1E-06	9.7E-07	5.1E-06	-8.3E-07	4.1E-06
	Kurtosis	0.057	0.085	0.097	0.088	0.104	0.181	0.142	0.067	0.036	0.050	0.020	0.084	0.057	0.082	0.046	0.058
2 3	Mean	0.000	0.000	0.000	0.000	0.000	0.000	0.000	0.000	0.000	0.000	0.000	0.000	0.000	0.000	0.000	0.000
	Median	0.014	-0.007	-0.008	0.000	-0.007	-0.004	-0.018	-0.003	-0.007	-0.016	0.005	0.011	-0.001	-0.004	-0.011	0.013
	Standard dev.	3.627	3.791	3.968	4.176	3.633	3.796	3.990	4.159	3.714	3.886	4.070	4.241	3.509	3.681	3.832	4.096
	Variance	-3.9E-06	-3.3E-06	-5.7E-07	4.4E-06	1.9E-06	-1.5E-06	-7.7E-07	2.8E-06	1.2E-06	1.8E-06	2.4E-06	2.7E-06	-2.2E-07	2.4E-06	-6.0E-08	-1.6E-06
	Skewness	7.6E-04	1.5E-02	7.6E-03	6.6E-03	1.4E-02	1.9E-02	2.0E-02	8.4E-03	7.3E-03	5.6E-03	7.9E-03	4.7E-04	6.6E-03	6.3E-03	7.7E-03	-5.6E-03
	Kurtosis	0.198	0.243	0.254	0.269	0.239	0.275	0.287	0.247	0.215	0.205	0.222	0.200	0.219	0.264	0.278	0.257
3 0	Mean	95.392	104.405	116.462	130.270	96.696	105.698	118.597	129.882	102.149	111.405	122.809	134.823	88.028	97.014	107.778	124.571
	Median	90.174	97.080	113.381	131.799	88.850	96.481	114.563	131.478	98.671	106.547	120.609	135.800	83.306	89.108	101.438	126.804
	Standard dev.	14.121	18.854	21.527	23.219	19.136	22.523	25.428	23.621	10.979	14.393	15.721	16.351	13.475	18.059	19.860	19.444
	Variance	6.8E+00	5.5E+00	5.4E+00	5.6E+00	5.1E+00	4.7E+00	4.7E+00	5.5E+00	9.3E+00	7.7E+00	7.8E+00	8.2E+00	6.5E+00	5.4E+00	5.4E+00	6.4E+00
	Skewness	1.8E+00	1.1E+00	4.0E-01	-8.1E-02	1.9E+00	1.1E+00	4.2E-01	-8.8E-02	2.0E+00	1.2E+00	4.1E-01	-9.8E-02	2.2E+00	1.3E+00	6.3E-01	-1.6E-01
	Kurtosis	2.836	0.280	-0.929	-0.979	3.119	0.127	-0.988	-0.990	4.309	0.738	-0.762	-0.876	4.273	0.724	-0.780	-1.017
3 1	Mean	0.000	0.000	0.000	0.000	0.000	0.000	0.000	0.000	0.000	0.000	0.000	0.000	0.000	0.000	0.000	0.000
	Median	0.000	0.009	-0.004	0.003	-0.001	-0.003	-0.004	0.005	0.001	-0.007	0.001	0.001	-0.005	-0.001	-0.003	0.006
	Standard dev.	2.948	3.328	3.712	3.876	2.971	3.414	3.848	4.078	2.888	3.178	3.380	3.496	2.648	3.021	3.400	3.707
	Variance	5.0E-06	4.9E-06	7.9E-06	2.1E-05	7.4E-06	-8.7E-06	3.5E-06	9.8E-07	-1.1E-05	-9.7E-06	1.1E-07	-6.7E-06	-1.8E-06	-1.8E-06	7.9E-06	-9.7E-06
	Skewness	-3.9E-04	-1.1E-02	2.2E-03	-2.9E-03	2.0E-03	-1.7E-03	3.1E-04	-2.3E-03	3.0E-04	9.3E-03	-1.1E-04	-1.3E-03	-4.1E-03	6.6E-03	1.2E-05	-3.0E-03
	Kurtosis	0.365	0.370	0.404	0.408	0.618	0.521	0.405	0.438	0.209	0.190	0.217	0.226	0.524	0.364	0.362	0.336

Packet	Experiment	49	50	51	52	53	54	55	56	57	58	59	60	61	62	63	64
	V_{sg} (m/s)	0.15	0.23	0.60	1.31	0.15	0.31	0.59	1.32	0.15	0.31	0.59	1.32	0.15	0.31	0.59	1.34
	V_{sl} (m/s)	0.27	0.27	0.27	0.27	0.28	0.28	0.28	0.28	0.29	0.29	0.29	0.29	0.38	0.38	0.38	0.38
	WC (%)	0.60	0.60	0.60	0.60	0.40	0.40	0.40	0.40	0.20	0.20	0.20	0.20	0.80	0.80	0.80	0.80
1 0	Mean	88.04	92.80	106.85	122.75	89.76	97.30	107.14	122.16	93.67	101.77	111.71	127.40	86.11	94.76	105.26	120.86
	Median	84.22	88.24	102.50	124.21	83.32	89.52	101.79	124.24	91.57	98.37	108.94	128.67	82.61	88.40	98.41	121.75
	Standard dev.	13.28	14.86	20.44	20.53	18.81	20.66	23.07	21.13	10.05	13.06	15.00	16.05	13.01	17.59	20.07	20.41
	Variance	6.6E+00	6.2E+00	5.2E+00	6.0E+00	4.8E+00	4.7E+00	4.6E+00	5.8E+00	9.3E+00	7.8E+00	7.4E+00	7.9E+00	6.6E+00	5.4E+00	5.2E+00	5.9E+00
	Skewness	1.8E+00	1.4E+00	5.3E-01	-1.3E-01	2.0E+00	1.2E+00	5.7E-01	-1.7E-01	1.8E+00	1.2E+00	5.6E-01	-1.5E-01	2.1E+00	1.4E+00	7.8E-01	7.8E-03
	Kurtosis	3.285	1.576	-0.729	-0.819	3.378	0.602	-0.712	-0.826	4.399	1.276	-0.376	-0.732	4.624	1.230	-0.429	-1.027
1 1	Mean	0.000	0.000	0.000	0.000	0.000	0.000	0.000	0.000	0.000	0.000	0.000	0.000	0.000	0.000	0.000	0.000
	Median	-0.011	-0.011	-0.004	-0.014	0.005	-0.015	-0.007	-0.025	-0.016	-0.007	0.001	-0.005	-0.003	-0.015	0.001	0.004
	Standard dev.	5.035	5.145	5.430	5.807	5.068	5.246	5.440	5.788	5.162	5.330	5.548	5.908	4.985	5.189	5.437	5.776
	Variance	1.2E-06	7.6E-07	3.1E-07	-3.8E-06	-1.0E-06	-9.0E-07	-1.9E-06	2.8E-06	1.2E-07	-1.5E-06	-1.0E-06	2.5E-06	2.3E-06	-1.4E-06	4.4E-08	2.1E-06
	Skewness	2.4E-02	9.0E-03	1.0E-02	7.5E-03	-1.2E-03	7.5E-03	1.6E-02	6.3E-03	1.7E-02	1.5E-02	8.4E-03	2.2E-03	8.5E-03	9.2E-03	7.6E-03	1.3E-02
	Kurtosis	0.082	0.078	0.120	0.087	0.134	0.136	0.131	0.108	0.045	0.042	0.067	0.095	0.051	0.095	0.135	0.109
2 0	Mean	88.043	92.802	106.847	122.748	89.761	97.303	107.140	122.163	93.673	101.774	111.708	127.400	86.114	94.761	105.257	120.861
	Median	83.804	87.782	102.269	124.350	82.764	88.962	101.604	124.416	91.284	97.904	108.659	128.887	82.301	87.857	97.862	121.958
	Standard dev.	12.827	14.429	20.069	20.092	18.478	20.330	22.729	20.700	9.411	12.535	14.474	15.497	12.554	17.215	19.701	19.981
	Variance	6.9E+00	6.4E+00	5.3E+00	6.1E+00	4.9E+00	4.8E+00	4.7E+00	5.9E+00	1.0E+01	8.1E+00	7.7E+00	8.2E+00	6.9E+00	5.5E+00	5.3E+00	6.0E+00
	Skewness	1.9E+00	1.5E+00	5.4E-01	-1.5E-01	2.1E+00	1.2E+00	5.8E-01	-1.9E-01	2.1E+00	1.3E+00	6.1E-01	-1.8E-01	2.3E+00	1.5E+00	8.0E-01	-1.3E-03
	Kurtosis	3.669	1.713	-0.794	-0.880	3.546	0.599	-0.763	-0.886	5.519	1.435	-0.442	-0.829	5.194	1.285	-0.481	-1.109
2 1	Mean	0.000	0.000	0.000	0.000	0.000	0.000	0.000	0.000	0.000	0.000	0.000	0.000	0.000	0.000	0.000	0.000
	Median	0.000	0.003	0.002	0.001	-0.006	0.003	0.006	-0.002	-0.003	0.004	-0.006	-0.006	0.000	-0.005	-0.001	0.009
	Standard dev.	3.438	3.564	3.879	4.235	3.503	3.673	3.955	4.250	3.531	3.683	3.923	4.193	3.422	3.601	3.834	4.169
	Variance	7.9E-07	1.1E-07	1.3E-06	7.4E-06	2.6E-06	2.8E-06	1.0E-06	-4.1E-06	-2.0E-06	4.8E-06	-1.1E-06	-6.9E-06	-2.8E-06	4.0E-07	4.7E-06	-7.7E-07
	Skewness	2.1E-03	5.8E-03	-1.3E-03	3.4E-04	4.4E-04	2.2E-03	5.0E-03	1.8E-03	2.9E-03	1.1E-03	-6.2E-03	-2.2E-03	-1.9E-03	2.1E-03	2.7E-03	4.2E-04
	Kurtosis	0.301	0.318	0.232	0.163	0.335	0.371	0.314	0.235	0.208	0.237	0.180	0.200	0.244	0.261	0.279	0.225
2 2	Mean	0.000	0.000	0.000	0.000	0.000	0.000	0.000	0.000	0.000	0.000	0.000	0.000	0.000	0.000	0.000	0.000
	Median	0.000	0.001	-0.003	0.004	-0.001	0.006	0.004	0.009	0.006	0.006	0.006	-0.008	-0.001	0.004	-0.002	0.001
	Standard dev.	3.599	3.665	3.874	4.134	3.615	3.751	3.859	4.093	3.688	3.810	3.939	4.198	3.570	3.721	3.866	4.110
	Variance	7.0E-07	-7.5E-08	4.9E-07	1.3E-06	1.1E-07	6.5E-07	-4.9E-07	5.8E-07	-6.7E-07	1.8E-08	-1.9E-06	7.3E-07	-3.2E-07	-2.7E-08	-8.5E-07	3.2E-09
	Skewness	-2.1E-06	2.5E-07	-1.9E-06	-8.7E-06	-2.6E-07	-2.4E-06	1.7E-06	-1.7E-06	2.4E-06	-5.9E-08	6.5E-06	-3.2E-06	9.0E-07	-1.4E-07	2.4E-06	-1.4E-07
	Kurtosis	0.085	0.070	0.111	0.035	0.062	0.124	0.111	0.053	0.033	0.028	0.049	0.072	0.027	0.059	0.090	0.096
2 3	Mean	0.000	0.000	0.000	0.000	0.000	0.000	0.000	0.000	0.000	0.000	0.000	0.000	0.000	0.000	0.000	0.000
	Median	-0.005	-0.012	0.005	-0.017	-0.006	0.003	0.003	-0.013	-0.013	-0.012	-0.007	-0.006	-0.003	-0.014	-0.012	0.002
	Standard dev.	3.521	3.611	3.805	4.078	3.552	3.667	3.834	4.092	3.612	3.727	3.908	4.156	3.479	3.617	3.823	4.058
	Variance	1.0E-06	1.2E-06	-5.1E-08	-6.8E-06	-1.6E-06	-1.9E-06	-2.2E-06	3.4E-06	8.6E-07	-2.2E-06	5.3E-07	2.9E-06	3.6E-06	-2.0E-06	9.2E-07	3.0E-06
	Skewness	1.1E-02	9.6E-03	7.0E-04	1.5E-02	-8.8E-03	-3.2E-03	1.5E-03	5.5E-03	1.2E-02	9.3E-03	7.1E-03	4.8E-03	1.1E-02	-3.1E-03	1.2E-02	8.2E-04
	Kurtosis	0.273	0.235	0.231	0.231	0.283	0.291	0.256	0.257	0.195	0.197	0.209	0.213	0.234	0.286	0.250	0.234
3 0	Mean	88.043	92.802	106.847	122.748	89.761	97.303	107.140	122.163	93.673	101.774	111.708	127.400	86.114	94.761	105.257	120.861
	Median	83.664	87.600	102.029	124.286	82.512	88.905	101.385	124.452	91.157	97.726	108.405	128.929	82.063	87.614	97.577	121.898
	Standard dev.	12.507	14.092	19.741	19.721	18.237	20.055	22.414	20.301	8.992	12.138	14.079	15.119	12.257	16.953	19.408	19.640
	Variance	7.0E+00	6.6E+00	5.4E+00	6.2E+00	4.9E+00	4.9E+00	4.8E+00	6.0E+00	1.0E+01	8.4E+00	7.9E+00	8.4E+00	7.0E+00	5.6E+00	5.4E+00	6.2E+00
	Skewness	2.0E+00	1.5E+00	5.6E-01	-1.5E-01	2.1E+00	1.3E+00	6.0E-01	-1.8E-01	2.4E+00	1.4E+00	6.5E-01	-1.8E-01	2.4E+00	1.5E+00	8.2E-01	1.9E-03
	Kurtosis	3.989	1.882	-0.819	-0.926	3.717	0.653	-0.772	-0.918	6.498	1.640	-0.451	-0.902	5.561	1.347	-0.490	-1.160
3 1	Mean	0.000	0.000	0.000	0.000	0.000	0.000	0.000	0.000	0.000	0.000	0.000	0.000	0.000	0.000	0.000	0.000
	Median	0.004	0.009	0.000	0.003	-0.002	-0.004	-0.006	0.011	-0.002	-0.008	-0.009	-0.001	-0.005	-0.007	-0.002	-0.007
	Standard dev.	2.846	3.101	3.613	3.843	2.973	3.334	3.767	4.045	2.777	3.127	3.361	3.399	2.714	2.994	3.386	3.670
	Variance	-7.4E-06	-1.2E-05	-7.2E-06	-4.0E-06	-2.2E-06	-4.1E-06	1.2E-05	-1.2E-05	-9.1E-06	-1.0E-05	-9.5E-06	5.7E-06	4.0E-07	8.8E-06	4.8E-06	6.6E-06
	Skewness	2.8E-03	4.6E-03	1.9E-03	2.9E-03	3.2E-05	-4.6E-03	5.6E-04	9.7E-04	7.8E-03	-1.7E-05	2.0E-03	-2.8E-03	-2.5E-04	5.3E-03	-3.5E-03	-4.7E-03
	Kurtosis	0.417	0.326	0.358	0.364	0.704	0.431	0.484	0.499	0.306	0.246	0.205	0.202	0.614	0.472	0.444	0.365

Packet	Experiment	65	66	67	68	69	70	71	72	73	74	75	76	77	78	79	80
	V_{sg} (m/s)	0.15	0.29	0.59	1.33	0.15	0.31	0.59	1.32	0.16	0.31	0.59	1.33	0.15	0.31	0.59	1.34
	V_{sl} (m/s)	0.40	0.40	0.40	0.40	0.41	0.41	0.41	0.41	0.43	0.43	0.43	0.43	0.51	0.51	0.51	0.51
	WC (%)	0.60	0.60	0.60	0.60	0.40	0.40	0.40	0.40	0.20	0.20	0.20	0.20	0.80	0.80	0.80	0.80
1 0	Mean	87.18	93.84	104.41	119.85	88.39	95.21	104.77	119.42	91.60	99.65	109.31	124.22	85.01	92.95	103.04	118.12
	Median	83.73	88.45	98.86	121.08	83.62	88.66	98.96	121.05	90.05	96.39	106.04	124.86	82.01	87.09	95.79	117.78
	Standard dev.	12.61	16.15	19.81	20.67	15.02	18.34	21.59	21.61	8.84	12.55	14.46	15.93	11.90	16.84	19.60	20.53
	Variance	6.9E+00	5.8E+00	5.3E+00	5.8E+00	5.9E+00	5.2E+00	4.9E+00	5.5E+00	1.0E+01	7.9E+00	7.6E+00	7.8E+00	7.1E+00	5.5E+00	5.3E+00	5.8E+00
	Skewness	1.9E+00	1.3E+00	6.9E-01	-5.8E-02	1.8E+00	1.3E+00	6.5E-01	-8.8E-02	1.9E+00	1.4E+00	7.6E-01	-2.4E-02	2.2E+00	1.6E+00	9.1E-01	1.4E-01
	Kurtosis	3.820	1.257	-0.485	-0.947	3.285	0.919	-0.615	-0.978	5.418	2.090	0.018	-0.802	5.255	1.776	-0.181	-1.057
1 1	Mean	0.000	0.000	0.000	0.000	0.000	0.000	0.000	0.000	0.000	0.000	0.000	0.000	0.000	0.000	0.000	0.000
	Median	-0.009	0.001	-0.005	0.000	-0.004	0.004	0.005	-0.009	-0.011	-0.005	0.004	0.012	-0.004	-0.011	-0.024	-0.009
	Standard dev.	4.992	5.157	5.421	5.748	5.013	5.209	5.426	5.738	5.086	5.294	5.520	5.834	4.943	5.133	5.355	5.714
	Variance	-1.1E-06	8.4E-07	-1.8E-06	-8.4E-07	-4.2E-07	-9.5E-07	-2.3E-07	2.4E-06	-1.8E-06	-4.6E-07	3.4E-07	-1.6E-06	-2.4E-06	9.3E-07	1.1E-06	2.0E-07
	Skewness	1.6E-02	4.0E-03	9.3E-03	3.6E-03	7.2E-03	4.1E-03	6.5E-03	6.5E-03	8.0E-03	1.0E-02	6.0E-03	1.0E-02	1.6E-02	1.3E-02	1.4E-02	5.9E-03
	Kurtosis	0.071	0.085	0.103	0.095	0.088	0.108	0.106	0.102	0.030	0.049	0.056	0.075	0.069	0.112	0.091	0.106
2 0	Mean	87.181	93.838	104.405	119.853	88.392	95.209	104.769	119.416	91.597	99.654	109.312	124.222	85.005	92.948	103.038	118.117
	Median	83.347	87.917	98.493	121.163	83.144	88.116	98.598	121.167	89.812	95.952	105.617	125.047	81.709	86.613	95.088	117.855
	Standard dev.	12.132	15.744	19.428	20.229	14.610	17.970	21.228	21.185	8.121	12.000	13.921	15.369	11.407	16.463	19.224	20.098
	Variance	7.2E+00	6.0E+00	5.4E+00	5.9E+00	6.1E+00	5.3E+00	4.9E+00	5.6E+00	1.1E+01	8.3E+00	7.9E+00	8.1E+00	7.5E+00	5.6E+00	5.4E+00	5.9E+00
	Skewness	2.0E+00	1.4E+00	7.1E-01	-7.2E-02	2.0E+00	1.3E+00	6.7E-01	-1.0E-01	2.3E+00	1.6E+00	8.3E-01	-4.1E-02	2.4E+00	1.7E+00	9.5E-01	1.4E-01
	Kurtosis	4.330	1.336	-0.536	-1.021	3.590	0.956	-0.664	-1.047	7.310	2.419	-0.001	-0.916	6.036	1.877	-0.224	-1.143
2 1	Mean	0.000	0.000	0.000	0.000	0.000	0.000	0.000	0.000	0.000	0.000	0.000	0.000	0.000	0.000	0.000	0.000
	Median	0.004	0.003	0.006	-0.005	-0.001	0.007	-0.006	0.011	0.002	-0.003	0.006	0.001	0.003	0.001	-0.008	0.004
	Standard dev.	3.437	3.613	3.892	4.232	3.490	3.683	3.921	4.272	3.485	3.686	3.918	4.181	3.401	3.564	3.840	4.166
	Variance	2.6E-06	4.8E-07	2.9E-06	-1.1E-06	-2.7E-06	-2.5E-06	-1.2E-07	-2.4E-06	7.6E-06	2.1E-06	-3.0E-06	3.3E-07	2.1E-06	-3.2E-06	-4.4E-06	-1.3E-08
	Skewness	3.0E-03	1.9E-03	-2.0E-03	5.3E-03	1.5E-04	-4.3E-03	1.3E-03	3.3E-03	-9.6E-04	-2.4E-03	2.0E-03	-1.7E-03	-1.1E-03	6.1E-05	2.3E-03	1.8E-03
	Kurtosis	0.281	0.249	0.233	0.242	0.244	0.295	0.295	0.203	0.215	0.240	0.248	0.204	0.248	0.312	0.266	0.225
2 2	Mean	0.000	0.000	0.000	0.000	0.000	0.000	0.000	0.000	0.000	0.000	0.000	0.000	0.000	0.000	0.000	0.000
	Median	-0.002	0.003	0.003	0.007	-0.004	-0.007	-0.001	0.000	-0.001	-0.008	0.006	-0.006	0.002	0.003	-0.002	-0.003
	Standard dev.	3.556	3.671	3.857	4.070	3.576	3.716	3.865	4.075	3.633	3.784	3.946	4.159	3.536	3.666	3.807	4.039
	Variance	9.1E-07	8.9E-08	-1.3E-07	1.7E-06	1.5E-06	6.3E-07	-1.1E-06	-1.5E-07	-1.7E-07	-1.4E-06	-6.6E-07	2.8E-07	-1.8E-06	-1.3E-06	-1.6E-06	-6.8E-07
	Skewness	-2.9E-06	-3.6E-07	1.3E-07	-6.6E-06	-5.9E-06	-2.0E-06	3.3E-06	5.1E-07	4.8E-07	3.9E-06	2.2E-06	-9.1E-07	5.3E-06	4.8E-06	4.7E-06	2.5E-06
	Kurtosis	0.025	0.046	0.093	0.038	0.043	0.069	0.103	0.042	0.008	0.041	0.023	0.071	0.043	0.068	0.062	0.057
2 3	Mean	0.000	0.000	0.000	0.000	0.000	0.000	0.000	0.000	0.000	0.000	0.000	0.000	0.000	0.000	0.000	0.000
	Median	-0.008	-0.014	-0.022	-0.008	-0.008	-0.004	0.010	-0.016	-0.005	0.003	-0.005	-0.001	0.009	0.001	-0.017	-0.004
	Standard dev.	3.504	3.622	3.809	4.059	3.513	3.651	3.809	4.039	3.560	3.702	3.859	4.091	3.455	3.593	3.765	4.041
	Variance	-2.4E-06	1.1E-06	-2.5E-06	-2.9E-06	-2.1E-06	-2.0E-06	8.2E-07	3.6E-06	-2.3E-06	7.3E-07	1.2E-06	-2.6E-06	-1.6E-06	2.7E-06	3.2E-06	9.7E-07
	Skewness	1.4E-02	1.0E-02	8.3E-03	7.4E-03	1.2E-02	6.8E-03	6.9E-03	4.6E-03	1.1E-02	3.1E-04	3.0E-03	7.6E-03	1.4E-03	2.8E-03	5.5E-03	-2.1E-04
	Kurtosis	0.229	0.190	0.258	0.247	0.244	0.237	0.276	0.264	0.201	0.218	0.201	0.234	0.210	0.233	0.290	0.272
3 0	Mean	87.181	93.838	104.405	119.853	88.392	95.209	104.769	119.416	91.597	99.654	109.312	124.222	85.005	92.948	103.038	118.117
	Median	83.220	87.760	98.256	121.111	83.026	88.077	98.316	121.006	89.702	95.828	105.369	125.034	81.558	86.365	94.908	117.843
	Standard dev.	11.769	15.410	19.090	19.860	14.281	17.624	20.872	20.784	7.641	11.580	13.491	14.973	11.088	16.182	18.921	19.761
	Variance	7.4E+00	6.1E+00	5.5E+00	6.0E+00	6.2E+00	5.4E+00	5.0E+00	5.7E+00	1.2E+01	8.6E+00	8.1E+00	8.3E+00	7.7E+00	5.7E+00	5.4E+00	6.0E+00
	Skewness	2.2E+00	1.5E+00	7.4E-01	-6.8E-02	2.1E+00	1.4E+00	6.9E-01	-9.0E-02	2.6E+00	1.7E+00	8.9E-01	-3.7E-02	2.5E+00	1.7E+00	9.8E-01	1.5E-01
	Kurtosis	4.830	1.480	-0.521	-1.064	3.904	1.077	-0.647	-1.077	8.656	2.775	0.060	-0.987	6.518	1.980	-0.211	-1.180
3 1	Mean	0.000	0.000	0.000	0.000	0.000	0.000	0.000	0.000	0.000	0.000	0.000	0.000	0.000	0.000	0.000	0.000
	Median	0.001	-0.001	-0.009	0.008	0.001	0.009	-0.002	-0.006	-0.001	0.006	0.003	0.004	0.005	0.011	-0.007	-0.005
	Standard dev.	2.943	3.229	3.610	3.844	3.082	3.509	3.871	4.107	2.750	3.149	3.433	3.468	2.680	3.032	3.394	3.667
	Variance	-6.7E-06	-2.6E-09	1.4E-05	3.8E-06	1.3E-05	-2.1E-06	1.3E-05	-1.4E-05	-9.2E-06	3.6E-06	-3.4E-07	7.2E-06	3.3E-06	-1.2E-06	6.6E-06	-3.6E-06
	Skewness	5.0E-03	3.5E-03	3.4E-03	2.9E-03	3.0E-03	-2.8E-03	-2.5E-03	8.9E-03	-6.9E-05	9.4E-04	-4.2E-03	1.6E-03	-1.1E-03	-2.4E-03	3.3E-03	1.8E-03
	Kurtosis	0.468	0.446	0.430	0.425	0.505	0.520	0.412	0.508	0.366	0.384	0.342	0.337	0.683	0.664	0.404	0.353

Packet	Experiment	81	82	83	84	85	86	87	88	89	90	91	92	93	94	95	96
	V_{sg} (m/s)	0.15	0.24	0.59	1.34	0.16	0.31	0.59	1.34	0.16	0.35	0.66	1.33	0.15	0.31	0.60	1.32
	V_{sl} (m/s)	0.53	0.53	0.53	0.53	0.55	0.55	0.55	0.55	0.57	0.57	0.57	0.57	0.64	0.64	0.64	0.64
	WC (%)	0.60	0.60	0.60	0.60	0.40	0.40	0.40	0.40	0.20	0.20	0.20	0.20	0.80	0.80	0.80	0.80
1 0	Mean	86.20	90.25	102.43	116.87	87.51	93.93	102.57	117.40	93.14	82.99	106.76	121.06	83.88	91.37	101.31	116.10
	Median	83.04	86.05	96.64	117.17	82.39	87.06	95.73	118.33	92.27	82.94	103.28	120.91	81.28	86.09	93.97	113.91
	Standard dev.	12.05	14.00	19.14	20.76	15.79	18.49	21.46	19.63	7.31	4.61	13.94	15.75	11.12	15.98	19.22	20.80
	Variance	7.2E+00	6.4E+00	5.4E+00	5.6E+00	5.5E+00	5.1E+00	4.8E+00	6.0E+00	1.3E+01	1.8E+01	7.7E+00	7.7E+00	7.5E+00	5.7E+00	5.3E+00	5.6E+00
	Skewness	1.9E+00	1.6E+00	7.8E-01	6.7E-02	2.0E+00	1.3E+00	7.4E-01	-2.0E-02	1.6E+00	4.1E-02	9.1E-01	1.1E-01	2.2E+00	1.7E+00	1.1E+00	2.7E-01
	Kurtosis	4.266	2.438	-0.294	-1.007	3.459	1.045	-0.500	-0.992	5.079	0.065	0.366	-0.823	5.899	2.336	0.115	-1.075
1 1	Mean	0.000	0.000	0.000	0.000	0.000	0.000	0.000	0.000	0.000	0.000	0.000	0.000	0.000	0.000	0.000	0.000
	Median	-0.004	-0.001	-0.007	-0.016	0.000	-0.011	-0.018	-0.011	-0.012	-0.014	-0.015	-0.017	-0.019	-0.012	-0.001	-0.009
	Standard dev.	4.979	5.072	5.375	5.715	5.012	5.143	5.379	5.709	5.162	4.897	5.466	5.793	4.902	5.119	5.325	5.679
	Variance	1.3E-06	1.5E-06	-3.8E-07	4.9E-07	2.6E-07	9.0E-07	-1.0E-06	5.6E-07	-1.5E-06	5.6E-07	-4.0E-06	1.6E-06	-1.6E-06	1.7E-07	-2.2E-06	-6.0E-07
	Skewness	4.2E-03	1.8E-02	1.0E-02	1.6E-02	5.3E-03	1.5E-02	1.6E-02	7.1E-03	1.6E-02	1.0E-02	8.3E-03	1.1E-02	2.1E-02	1.1E-02	5.7E-03	8.6E-03
	Kurtosis	0.016	0.081	0.097	0.073	0.094	0.100	0.129	0.093	0.047	0.005	0.052	0.070	0.046	0.067	0.099	0.088
2 0	Mean	86.203	90.254	102.432	116.869	87.513	93.932	102.574	117.398	93.137	82.987	106.756	121.059	83.875	91.368	101.308	116.098
	Median	82.700	85.653	96.251	117.248	81.903	86.518	95.270	118.366	92.161	82.972	102.824	121.044	81.027	85.642	93.322	113.879
	Standard dev.	11.534	13.536	18.731	20.329	15.397	18.115	21.097	19.178	6.411	3.222	13.371	15.182	10.586	15.574	18.835	20.381
	Variance	7.5E+00	6.7E+00	5.5E+00	5.7E+00	5.7E+00	5.2E+00	4.9E+00	6.1E+00	1.5E+01	2.6E+01	8.0E+00	8.0E+00	7.9E+00	5.9E+00	5.4E+00	5.7E+00
	Skewness	2.1E+00	1.7E+00	8.1E-01	6.3E-02	2.1E+00	1.4E+00	7.6E-01	-2.9E-02	2.2E+00	2.3E-02	1.0E+00	1.1E-01	2.5E+00	1.8E+00	1.1E+00	2.7E-01
	Kurtosis	4.923	2.710	-0.336	-1.083	3.732	1.093	-0.544	-1.073	8.270	0.058	0.411	-0.944	6.976	2.510	0.091	-1.161
2 1	Mean	0.000	0.000	0.000	0.000	0.000	0.000	0.000	0.000	0.000	0.000	0.000	0.000	0.000	0.000	0.000	0.000
	Median	-0.003	0.000	-0.004	0.009	-0.010	-0.004	-0.004	-0.010	0.009	0.006	-0.010	0.004	-0.001	-0.002	-0.006	0.003
	Standard dev.	3.474	3.574	3.920	4.224	3.506	3.692	3.944	4.201	3.506	3.295	3.928	4.192	3.390	3.581	3.823	4.155
	Variance	3.2E-07	-1.9E-06	-2.4E-06	3.9E-06	6.0E-07	2.2E-07	1.1E-06	-1.8E-06	4.1E-06	-2.9E-06	5.9E-06	9.1E-07	2.5E-06	2.6E-06	4.2E-06	1.9E-06
	Skewness	-2.1E-03	2.0E-03	-6.5E-05	3.2E-03	3.4E-03	-1.2E-04	9.6E-04	1.5E-03	-1.0E-03	-3.1E-04	8.3E-04	4.1E-03	-1.1E-03	3.2E-03	1.3E-03	2.5E-04
	Kurtosis	0.222	0.239	0.306	0.252	0.296	0.294	0.239	0.227	0.195	0.211	0.213	0.230	0.264	0.336	0.276	0.203
2 2	Mean	0.000	0.000	0.000	0.000	0.000	0.000	0.000	0.000	0.000	0.000	0.000	0.000	0.000	0.000	0.000	0.000
	Median	-0.001	-0.010	-0.005	0.002	-0.002	0.004	-0.004	-0.001	0.003	0.002	0.006	0.001	0.000	0.007	-0.003	0.004
	Standard dev.	3.565	3.636	3.830	4.040	3.584	3.653	3.816	4.042	3.687	3.513	3.895	4.109	3.499	3.655	3.777	4.029
	Variance	-1.2E-06	5.1E-07	1.7E-06	2.5E-07	-2.0E-06	1.2E-07	1.1E-06	9.1E-07	1.8E-06	5.8E-07	1.1E-06	-8.4E-07	-9.2E-07	8.6E-07	2.2E-08	-1.7E-06
	Skewness	3.8E-06	-1.9E-06	-7.4E-06	-7.9E-07	6.5E-06	-3.7E-07	-8.2E-06	-3.2E-06	-5.3E-06	-2.3E-06	-4.2E-06	2.6E-06	4.2E-06	-2.6E-06	-2.4E-08	4.9E-06
	Kurtosis	0.034	0.049	0.089	0.084	0.077	0.103	0.079	0.061	-0.017	-0.006	0.053	0.062	0.039	0.063	0.061	0.077
2 3	Mean	0.000	0.000	0.000	0.000	0.000	0.000	0.000	0.000	0.000	0.000	0.000	0.000	0.000	0.000	0.000	0.000
	Median	-0.012	0.002	0.000	0.009	-0.002	-0.007	0.000	-0.007	-0.013	0.006	-0.013	-0.015	-0.001	-0.011	-0.006	-0.009
	Standard dev.	3.475	3.536	3.772	4.042	3.503	3.621	3.790	4.031	3.613	3.412	3.836	4.083	3.433	3.584	3.753	4.002
	Variance	3.2E-06	1.6E-06	-2.2E-06	4.5E-07	2.4E-06	1.2E-06	-2.5E-06	-1.2E-07	-4.0E-06	2.1E-07	-6.9E-06	3.1E-06	-1.4E-06	-6.3E-07	-3.2E-06	8.6E-07
	Skewness	8.8E-03	4.5E-03	5.8E-03	3.2E-04	3.2E-03	6.9E-03	1.1E-02	1.4E-02	1.4E-02	7.3E-03	7.9E-03	5.9E-03	1.5E-02	8.6E-03	2.7E-03	8.4E-03
	Kurtosis	0.199	0.199	0.250	0.249	0.281	0.268	0.265	0.255	0.199	0.183	0.208	0.193	0.207	0.249	0.294	0.229
3 0	Mean	86.203	90.254	102.432	116.869	87.513	93.932	102.574	117.398	93.137	82.987	106.756	121.060	83.875	91.368	101.308	116.098
	Median	82.581	85.553	96.112	117.106	81.781	86.520	95.137	118.353	92.101	82.974	102.655	121.050	80.890	85.400	93.070	113.657
	Standard dev.	11.123	13.123	18.356	19.948	15.051	17.751	20.726	18.796	5.824	2.263	12.894	14.772	10.214	15.281	18.528	20.042
	Variance	7.8E+00	6.9E+00	5.6E+00	5.9E+00	5.8E+00	5.3E+00	4.9E+00	6.2E+00	1.6E+01	3.7E+01	8.3E+00	8.2E+00	8.2E+00	6.0E+00	5.5E+00	5.8E+00
	Skewness	2.3E+00	1.8E+00	8.5E-01	7.3E-02	2.1E+00	1.5E+00	8.0E-01	-2.1E-02	2.6E+00	2.4E-02	1.1E+00	1.2E-01	2.7E+00	1.9E+00	1.1E+00	2.9E-01
	Kurtosis	5.569	3.058	-0.293	-1.118	4.021	1.242	-0.503	-1.116	9.876	0.062	0.567	-1.004	7.573	2.639	0.136	-1.194
3 1	Mean	0.000	0.000	0.000	0.000	0.000	0.000	0.000	0.000	0.000	0.000	0.000	0.000	0.000	0.000	0.000	0.000
	Median	-0.002	-0.001	0.001	0.003	0.002	0.003	0.001	0.000	0.002	-0.004	0.002	0.001	-0.005	0.000	0.000	-0.007
	Standard dev.	3.053	3.317	3.730	3.915	3.246	3.612	3.939	3.810	2.681	2.293	3.540	3.506	2.782	3.007	3.388	3.701
	Variance	4.9E-06	-5.8E-06	-1.8E-06	-5.9E-06	-8.6E-06	-9.8E-06	9.2E-06	1.4E-05	2.3E-06	8.1E-06	-6.1E-06	-7.1E-06	9.3E-06	1.9E-06	2.0E-06	-6.7E-06
	Skewness	4.9E-03	7.9E-03	4.8E-03	-6.8E-03	3.6E-03	-4.6E-03	2.0E-04	-9.4E-04	-2.2E-03	-3.8E-04	6.5E-03	-5.4E-03	-1.0E-03	1.3E-03	-4.6E-04	9.7E-04
	Kurtosis	0.574	0.486	0.422	0.457	0.926	0.478	0.474	0.450	0.417	0.108	0.266	0.253	0.908	0.687	0.487	0.408

Packet	Experiment	97	98	99	100	101	102	103	104	105	106	107	108	109	110	111	112
	V_{sg} (m/s)	0.15	0.59	1.31	0.16	0.31	0.60	1.34	0.16	0.32	0.61	1.25	0.15	0.30	0.60	1.33	0.15
	V_{sl} (m/s)	0.66	0.66	0.66	0.69	0.69	0.69	0.69	0.72	0.72	0.72	0.72	0.76	0.76	0.76	0.76	0.80
	WC (%)	0.60	0.60	0.60	0.40	0.40	0.40	0.40	0.20	0.20	0.20	0.20	0.80	0.80	0.80	0.80	0.60
1 0	Mean	85.32	100.83	114.83	86.22	92.38	100.81	115.10	88.20	94.71	104.29	118.50	83.07	89.98	99.58	114.29	84.37
	Median	82.43	94.70	114.29	83.19	87.94	95.76	115.23	87.19	92.21	100.84	117.69	80.78	85.20	92.61	110.64	81.69
	Standard dev.	11.58	18.80	20.86	11.81	14.73	17.17	19.19	7.48	10.87	13.39	15.58	10.38	15.15	18.46	20.53	11.11
	Variance	7.4E+00	5.4E+00	5.5E+00	7.3E+00	6.3E+00	5.9E+00	6.0E+00	1.2E+01	8.7E+00	7.8E+00	7.6E+00	8.0E+00	5.9E+00	5.4E+00	5.6E+00	7.6E+00
	Skewness	2.0E+00	8.9E-01	1.6E-01	2.0E+00	1.5E+00	9.2E-01	8.6E-02	1.6E+00	1.7E+00	1.0E+00	2.1E-01	2.2E+00	1.8E+00	1.2E+00	3.8E-01	2.1E+00
	Kurtosis	4.911	-0.060	-1.011	4.894	2.269	0.149	-0.987	5.094	3.362	0.753	-0.795	6.293	2.911	0.447	-1.000	5.239
1 1	Mean	0.000	0.000	0.000	0.000	0.000	0.000	0.000	0.000	0.000	0.000	0.000	0.000	0.000	0.000	0.000	0.000
	Median	0.004	-0.018	0.008	-0.014	-0.008	0.001	-0.023	-0.011	-0.019	-0.010	-0.022	-0.009	-0.005	0.000	0.002	-0.016
	Standard dev.	4.928	5.300	5.649	4.971	5.125	5.322	5.688	5.038	5.167	5.402	5.731	4.891	5.050	5.289	5.625	4.968
	Variance	-1.1E-06	5.7E-07	-1.3E-06	-1.3E-06	-1.7E-06	9.6E-07	2.4E-06	2.4E-06	1.8E-06	-5.2E-06	2.3E-06	-1.4E-06	4.7E-07	4.1E-07	1.5E-06	-5.3E-07
	Skewness	1.1E-02	8.1E-03	1.1E-02	1.7E-02	2.0E-02	8.8E-03	1.2E-02	1.1E-02	1.3E-02	2.1E-02	1.5E-02	8.4E-03	1.1E-02	1.7E-02	2.6E-03	1.6E-02
	Kurtosis	0.065	0.111	0.089	0.093	0.082	0.075	0.108	0.049	0.048	0.037	0.044	0.069	0.091	0.149	0.087	0.067
2 0	Mean	85.319	100.833	114.833	86.222	92.376	100.805	115.101	88.197	94.713	104.286	118.496	83.074	89.979	99.582	114.290	84.368
	Median	82.130	94.239	114.251	82.905	87.509	95.357	115.283	87.039	91.924	100.441	117.624	80.557	84.792	92.005	110.410	81.424
	Standard dev.	11.053	18.391	20.430	11.287	14.258	16.715	18.730	6.617	10.231	12.801	15.004	9.811	14.732	18.073	20.106	10.557
	Variance	7.7E+00	5.5E+00	5.6E+00	7.6E+00	6.5E+00	6.0E+00	6.1E+00	1.3E+01	9.3E+00	8.1E+00	7.9E+00	8.5E+00	6.1E+00	5.5E+00	5.7E+00	8.0E+00
	Skewness	2.3E+00	9.4E-01	1.6E-01	2.3E+00	1.7E+00	9.8E-01	8.4E-02	2.3E+00	1.9E+00	1.2E+00	2.2E-01	2.6E+00	1.9E+00	1.2E+00	3.9E-01	2.4E+00
	Kurtosis	5.763	-0.077	-1.084	5.718	2.525	0.161	-1.070	7.914	4.154	0.883	-0.914	7.636	3.146	0.450	-1.080	6.240
2 1	Mean	0.000	0.000	0.000	0.000	0.000	0.000	0.000	0.000	0.000	0.000	0.000	0.000	0.000	0.000	0.000	0.000
	Median	0.004	-0.003	0.000	0.004	0.005	0.009	0.003	-0.007	0.002	0.007	-0.003	0.004	-0.003	-0.003	0.001	0.012
	Standard dev.	3.462	3.907	4.212	3.486	3.701	3.942	4.183	3.485	3.671	3.911	4.217	3.388	3.546	3.780	4.151	3.467
	Variance	-2.2E-06	-1.0E-06	-2.2E-06	4.0E-06	2.8E-06	-7.1E-07	-4.8E-06	-6.4E-06	-4.2E-06	6.1E-06	-1.2E-06	3.5E-06	1.4E-07	-1.5E-06	-3.3E-06	-4.4E-07
	Skewness	2.5E-03	4.6E-03	1.6E-03	3.8E-03	-5.0E-04	-3.1E-03	2.7E-03	1.9E-03	-1.2E-03	-4.6E-04	3.1E-03	-5.2E-04	-1.2E-03	1.0E-03	-1.7E-03	5.3E-03
	Kurtosis	0.264	0.273	0.215	0.231	0.270	0.234	0.225	0.186	0.213	0.207	0.185	0.233	0.306	0.251	0.240	0.275
2 2	Mean	0.000	0.000	0.000	0.000	0.000	0.000	0.000	0.000	0.000	0.000	0.000	0.000	0.000	0.000	0.000	0.000
	Median	-0.001	-0.003	-0.003	-0.002	-0.004	-0.002	-0.006	-0.003	0.002	-0.006	-0.005	0.003	0.005	0.002	0.002	0.002
	Standard dev.	3.507	3.786	4.014	3.539	3.667	3.787	4.037	3.604	3.688	3.854	4.063	3.490	3.603	3.777	3.989	3.559
	Variance	9.7E-08	-8.2E-07	8.5E-07	-2.0E-06	2.3E-07	-2.7E-07	1.3E-07	-4.2E-07	5.7E-07	1.2E-06	-9.3E-07	5.5E-07	-1.9E-06	-1.1E-06	7.8E-07	-2.6E-07
	Skewness	-3.9E-07	2.9E-06	-3.3E-06	9.9E-06	-5.7E-07	8.5E-07	-2.5E-07	1.3E-06	-1.8E-06	-4.3E-06	4.3E-06	-1.7E-06	7.7E-06	3.4E-06	-2.6E-06	1.7E-06
	Kurtosis	0.044	0.108	0.094	0.069	0.058	0.024	0.082	-0.002	0.023	0.016	0.027	0.037	0.057	0.135	0.094	0.034
2 3	Mean	0.000	0.000	0.000	0.000	0.000	0.000	0.000	0.000	0.000	0.000	0.000	0.000	0.000	0.000	0.000	0.000
	Median	0.000	-0.010	-0.024	-0.014	-0.004	0.004	-0.007	-0.004	-0.005	-0.020	-0.001	-0.007	0.008	-0.007	-0.009	0.003
	Standard dev.	3.462	3.709	3.975	3.491	3.580	3.740	4.007	3.520	3.619	3.784	4.042	3.427	3.539	3.703	3.965	3.466
	Variance	-1.6E-06	1.7E-06	-2.7E-06	2.0E-07	-2.7E-06	1.6E-06	3.2E-06	3.8E-06	1.9E-06	-8.7E-06	4.2E-06	-2.5E-06	2.6E-06	1.7E-06	1.4E-06	-4.9E-07
	Skewness	1.5E-02	1.1E-02	6.6E-03	2.2E-02	1.1E-02	5.7E-03	1.5E-02	1.3E-02	4.1E-03	2.0E-02	-9.9E-04	7.0E-03	-3.8E-03	1.2E-02	3.6E-03	2.9E-04
	Kurtosis	0.218	0.264	0.285	0.213	0.265	0.234	0.210	0.223	0.163	0.229	0.209	0.212	0.226	0.300	0.234	0.221
3 0	Mean	85.319	100.833	114.833	86.222	92.376	100.805	115.100	88.197	94.713	104.286	118.496	83.074	89.978	99.582	114.290	84.368
	Median	82.026	94.185	114.076	82.850	87.579	95.277	115.174	86.968	91.823	100.348	117.505	80.419	84.573	91.722	110.206	81.328
	Standard dev.	10.597	17.977	20.027	10.810	13.780	16.243	18.335	5.925	9.707	12.265	14.555	9.369	14.413	17.758	19.750	10.062
	Variance	8.1E+00	5.6E+00	5.7E+00	8.0E+00	6.7E+00	6.2E+00	6.3E+00	1.5E+01	9.8E+00	8.5E+00	8.1E+00	8.9E+00	6.2E+00	5.6E+00	5.8E+00	8.4E+00
	Skewness	2.4E+00	9.8E-01	1.8E-01	2.4E+00	1.8E+00	1.0E+00	9.5E-02	2.4E+00	2.1E+00	1.3E+00	2.4E-01	2.7E+00	2.0E+00	1.3E+00	4.0E-01	2.5E+00
	Kurtosis	6.463	-0.013	-1.109	6.485	2.918	0.275	-1.106	7.878	4.852	1.100	-0.964	7.747	3.357	0.512	-1.104	6.767
3 1	Mean	0.000	0.000	0.000	0.000	0.000	0.000	0.000	0.000	0.000	0.000	0.000	0.000	0.000	0.000	0.000	0.000
	Median	0.002	0.005	-0.004	0.008	0.000	-0.003	-0.007	0.006	0.002	-0.003	-0.004	-0.005	0.003	-0.007	0.006	0.003
	Standard dev.	3.143	3.878	4.039	3.247	3.662	3.944	3.831	2.945	3.233	3.664	3.642	2.909	3.049	3.362	3.765	3.196
	Variance	5.3E-06	-7.5E-07	-7.0E-06	5.3E-06	1.7E-05	-1.6E-05	4.3E-06	6.8E-06	6.5E-06	1.9E-05	-1.1E-06	-1.8E-06	6.9E-06	-1.5E-07	4.4E-06	-3.5E-06
	Skewness	2.7E-03	5.6E-03	4.8E-03	-6.2E-04	5.3E-03	6.2E-04	4.3E-03	7.7E-03	1.2E-03	8.1E-03	5.6E-04	5.6E-03	7.1E-03	2.8E-03	7.2E-03	2.7E-03
	Kurtosis	0.674	0.438	0.510	0.590	0.385	0.342	0.404	0.757	0.500	0.273	0.279	0.911	0.765	0.505	0.517	0.862

Packet	Experiment	113	114	115	116	117	118	119	120	121	122	123	124	125	126
	V_{sg} (m/s)	0.23	0.62	1.32	0.16	0.32	0.60	1.33	0.15	0.32	0.66	1.32	0.15	0.31	0.60
	V_{sl} (m/s)	0.80	0.80	0.80	0.83	0.83	0.83	0.83	0.86	0.86	0.86	0.86	0.15	0.15	0.15
	WC (%)	0.60	0.60	0.60	0.40	0.40	0.40	0.40	0.20	0.20	0.20	0.20	0.00	0.00	0.00
1 0	Mean	90.58	99.23	113.47	85.90	91.43	99.67	113.67	87.25	93.68	103.44	116.16	100.70	109.83	120.15
	Median	85.77	92.87	112.09	83.24	87.19	94.50	112.96	86.30	91.32	99.88	114.52	98.38	106.62	118.56
	Standard dev.	15.05	18.45	20.91	11.12	14.18	16.93	19.12	7.33	10.54	13.48	15.03	10.69	12.84	13.39
	Variance	6.0E+00	5.4E+00	5.4E+00	7.7E+00	6.4E+00	5.9E+00	5.9E+00	1.2E+01	8.9E+00	7.7E+00	7.7E+00	9.4E+00	8.6E+00	9.0E+00
	Skewness	1.6E+00	9.8E-01	2.3E-01	2.1E+00	1.6E+00	1.0E+00	1.8E-01	1.6E+00	1.7E+00	1.1E+00	3.6E-01	1.7E+00	1.1E+00	4.4E-01
	Kurtosis	2.258	0.121	-1.013	5.315	2.592	0.348	-0.972	5.141	3.610	0.934	-0.617	3.710	0.973	-0.372
1 1	Mean	0.000	0.000	0.000	0.000	0.000	0.000	0.000	0.000	0.000	0.000	0.000	0.000	0.000	0.000
	Median	-0.015	-0.020	-0.011	-0.015	-0.008	-0.005	-0.020	-0.010	-0.009	-0.004	-0.010	-0.010	-0.027	0.003
	Standard dev.	5.084	5.300	5.680	4.967	5.104	5.325	5.650	5.011	5.135	5.405	5.696	5.310	5.538	5.739
	Variance	1.6E-06	-8.8E-07	-5.0E-07	-5.2E-08	-1.5E-07	2.4E-06	1.8E-06	-1.8E-06	-2.9E-09	-2.3E-06	-4.5E-07	2.4E-06	-2.7E-06	5.6E-07
	Skewness	1.6E-02	2.0E-02	9.1E-03	1.5E-02	1.2E-02	1.3E-02	1.6E-02	1.1E-02	8.6E-03	1.4E-02	1.4E-02	1.9E-02	5.6E-03	8.4E-03
	Kurtosis	0.098	0.133	0.107	0.061	0.081	0.063	0.085	0.015	0.078	0.087	0.055	0.058	0.040	0.092
2 0	Mean	90.575	99.230	113.472	85.896	91.426	99.666	113.669	87.248	93.678	103.442	116.157	100.698	109.828	120.147
	Median	85.318	92.325	112.042	82.977	86.826	94.084	112.908	86.179	91.026	99.447	114.303	98.078	106.168	118.330
	Standard dev.	14.595	18.024	20.474	10.552	13.689	16.450	18.641	6.459	9.879	12.881	14.421	10.046	12.256	12.774
	Variance	6.2E+00	5.5E+00	5.5E+00	8.1E+00	6.7E+00	6.1E+00	6.1E+00	1.4E+01	9.5E+00	8.0E+00	8.1E+00	1.0E+01	9.0E+00	9.4E+00
	Skewness	1.7E+00	1.0E+00	2.4E-01	2.4E+00	1.8E+00	1.1E+00	1.9E-01	2.2E+00	2.0E+00	1.2E+00	3.9E-01	2.0E+00	1.2E+00	4.8E-01
	Kurtosis	2.494	0.127	-1.088	6.407	2.920	0.389	-1.053	8.008	4.506	1.094	-0.716	4.574	1.117	-0.464
2 1	Mean	0.000	0.000	0.000	0.000	0.000	0.000	0.000	0.000	0.000	0.000	0.000	0.000	0.000	0.000
	Median	0.012	-0.001	0.001	-0.006	-0.002	-0.001	-0.006	0.006	0.006	0.001	0.003	0.003	0.003	0.005
	Standard dev.	3.664	3.938	4.239	3.509	3.718	3.996	4.234	3.468	3.673	3.961	4.245	3.650	3.819	3.999
	Variance	-3.0E-06	4.7E-06	3.3E-06	-1.3E-06	-4.6E-07	-4.0E-06	-5.7E-06	4.2E-06	-3.9E-07	3.5E-06	5.0E-07	-4.2E-06	3.3E-06	2.6E-06
	Skewness	-1.8E-03	-3.9E-03	3.4E-05	1.6E-03	-2.8E-04	4.6E-03	-2.0E-03	6.1E-04	3.6E-03	-2.0E-03	-1.8E-03	2.0E-03	5.1E-04	-7.6E-04
	Kurtosis	0.262	0.244	0.235	0.281	0.249	0.244	0.232	0.197	0.261	0.237	0.214	0.238	0.222	0.204
2 2	Mean	0.000	0.000	0.000	0.000	0.000	0.000	0.000	0.000	0.000	0.000	0.000	0.000	0.000	0.000
	Median	0.007	0.007	0.001	0.007	0.003	0.000	0.003	0.000	0.011	0.005	-0.002	0.003	0.000	0.001
	Standard dev.	3.624	3.754	4.021	3.550	3.618	3.799	4.003	3.586	3.673	3.849	4.027	3.787	3.942	4.078
	Variance	7.7E-07	1.1E-06	-1.1E-06	-7.4E-08	-2.0E-06	3.1E-07	-1.3E-06	-9.3E-07	-9.0E-07	-4.1E-07	-9.6E-07	-7.2E-07	-6.5E-07	3.7E-07
	Skewness	-4.9E-06	-3.4E-06	3.6E-06	-2.7E-06	7.4E-06	-8.1E-07	4.7E-06	6.6E-06	3.6E-06	1.1E-06	3.5E-06	1.9E-06	2.1E-06	-1.2E-06
	Kurtosis	0.088	0.090	0.079	0.031	0.039	0.042	0.076	0.000	0.065	0.097	0.025	0.023	0.045	0.029
2 3	Mean	0.000	0.000	0.000	0.000	0.000	0.000	0.000	0.000	0.000	0.000	0.000	0.000	0.000	0.000
	Median	-0.008	-0.009	-0.002	-0.006	-0.008	-0.008	-0.013	-0.018	0.000	0.010	-0.008	0.000	-0.011	0.003
	Standard dev.	3.566	3.742	4.012	3.475	3.600	3.731	3.988	3.500	3.589	3.794	4.028	3.722	3.890	4.038
	Variance	1.6E-06	-2.4E-06	3.7E-07	9.5E-10	1.7E-06	3.1E-06	3.9E-06	-1.6E-06	9.1E-07	-2.9E-06	3.2E-07	4.2E-06	-3.1E-06	4.3E-07
	Skewness	1.4E-02	1.2E-02	-5.2E-04	5.3E-03	9.6E-03	1.8E-02	1.2E-02	1.2E-02	4.2E-03	5.1E-05	6.4E-03	9.1E-03	9.1E-03	-4.5E-03
	Kurtosis	0.249	0.250	0.240	0.255	0.245	0.244	0.248	0.165	0.216	0.234	0.213	0.190	0.182	0.210
3 0	Mean	90.575	99.230	113.472	85.896	91.426	99.666	113.669	87.248	93.678	103.442	116.157	100.698	109.828	120.147
	Median	85.267	92.309	111.985	82.950	86.907	94.060	112.822	86.146	90.930	99.399	114.198	97.884	105.976	118.093
	Standard dev.	14.130	17.581	20.061	10.033	13.178	15.934	18.222	5.693	9.333	12.328	13.934	9.677	11.882	12.359
	Variance	6.4E+00	5.6E+00	5.7E+00	8.6E+00	6.9E+00	6.3E+00	6.2E+00	1.5E+01	1.0E+01	8.4E+00	8.3E+00	1.0E+01	9.2E+00	9.7E+00
	Skewness	1.8E+00	1.1E+00	2.5E-01	2.5E+00	1.9E+00	1.1E+00	2.0E-01	2.3E+00	2.1E+00	1.4E+00	4.2E-01	2.2E+00	1.3E+00	5.2E-01
	Kurtosis	2.808	0.224	-1.103	7.127	3.409	0.563	-1.084	7.731	4.992	1.361	-0.745	5.161	1.265	-0.500
3 1	Mean	0.000	0.000	0.000	0.000	0.000	0.000	0.000	0.000	0.000	0.000	0.000	0.000	0.000	0.000
	Median	0.004	0.007	-0.009	0.002	-0.002	0.004	-0.008	0.005	0.008	-0.007	0.004	-0.003	0.004	0.005
	Standard dev.	3.655	3.969	4.092	3.268	3.705	4.088	3.930	3.051	3.236	3.733	3.717	2.700	3.007	3.227
	Variance	-4.7E-06	-2.1E-05	-9.3E-06	-5.0E-06	-3.4E-06	-4.0E-06	2.1E-06	-1.4E-05	6.7E-06	-1.7E-06	7.1E-06	-1.6E-06	3.2E-06	-3.9E-06
	Skewness	7.5E-03	2.0E-04	8.9E-03	-1.4E-03	1.3E-02	8.1E-03	3.8E-03	9.5E-03	-2.4E-03	-1.4E-03	2.7E-03	4.1E-03	-5.4E-03	2.1E-04
	Kurtosis	0.571	0.502	0.486	0.722	0.474	0.446	0.411	1.021	0.516	0.346	0.292	0.227	0.258	0.133

D.3 Wavelet Packet Coefficient Statistics: Packets [3 2] – [4 1]

Packet	Experiment	1	2	3	4	5	6	7	8	9	10	11	12	13	14	15	16
	V_{sg} (m/s)	0.13	0.30	0.58	0.99	0.13	0.30	0.59	1.32	0.13	0.30	0.59	1.32	0.13	0.31	0.59	1.29
	V_{sl} (m/s)	0.12	0.12	0.12	0.12	0.24	0.24	0.24	0.24	0.37	0.37	0.37	0.37	0.49	0.49	0.49	0.49
	WC (%)	1.00	1.00	1.00	1.00	1.00	1.00	1.00	1.00	1.00	1.00	1.00	1.00	1.00	1.00	1.00	1.00
3 2	Mean	0.000	0.000	0.000	0.000	0.000	0.000	0.000	0.000	0.000	0.000	0.000	0.000	0.000	0.000	0.000	0.000
	Median	0.000	0.000	0.001	0.000	0.002	-0.001	0.000	-0.003	0.001	-0.001	0.002	-0.002	-0.005	0.002	0.002	-0.001
	Standard dev.	2.463	2.618	2.794	3.018	2.409	2.575	2.729	2.971	2.403	2.562	2.695	2.929	2.394	2.501	2.672	2.892
	Variance	-7.7E-06	-1.6E-06	1.9E-06	1.9E-07	-5.8E-06	-1.5E-06	1.4E-07	5.3E-06	9.3E-07	4.7E-06	-2.3E-06	-2.3E-06	-3.2E-06	6.6E-07	-3.7E-06	2.2E-06
	Skewness	-3.8E-05	4.7E-06	4.3E-06	-7.3E-07	-5.9E-06	4.3E-06	-8.9E-07	9.7E-06	-7.0E-06	-1.2E-05	-5.9E-06	5.4E-06	7.3E-06	-2.1E-06	6.3E-06	-3.2E-06
	Kurtosis	0.874	0.770	0.778	0.765	0.720	0.782	0.782	0.752	0.701	0.757	0.824	0.731	0.729	0.793	0.810	0.706
3 3	Mean	0.000	0.000	0.000	0.000	0.000	0.000	0.000	0.000	0.000	0.000	0.000	0.000	0.000	0.000	0.000	0.000
	Median	0.002	0.000	0.003	0.004	0.002	0.002	0.000	-0.005	0.003	-0.002	0.003	-0.001	0.003	-0.001	0.001	0.001
	Standard dev.	2.417	2.668	2.861	3.116	2.407	2.593	2.831	3.052	2.379	2.548	2.771	3.028	2.361	2.541	2.745	3.022
	Variance	6.7E-06	-3.9E-07	-3.5E-06	-2.8E-07	7.9E-07	6.9E-07	4.9E-06	-9.1E-07	-5.5E-06	-2.5E-06	-3.7E-07	9.7E-06	2.6E-06	-6.9E-06	1.2E-06	-7.2E-07
	Skewness	6.0E-05	1.8E-06	-9.3E-05	3.6E-06	-9.6E-05	1.3E-04	1.9E-04	-7.4E-05	5.1E-05	1.0E-04	-4.8E-05	1.2E-04	8.6E-05	1.1E-04	3.7E-05	-5.1E-05
	Kurtosis	0.171	0.227	0.187	0.144	0.168	0.212	0.179	0.147	0.191	0.254	0.172	0.202	0.120	0.187	0.247	0.156
3 4	Mean	0.000	0.000	0.000	0.000	0.000	0.000	0.000	0.000	0.000	0.000	0.000	0.000	0.000	0.000	0.000	0.000
	Median	0.000	0.001	-0.003	-0.001	-0.007	0.002	-0.001	0.001	-0.001	-0.002	0.001	0.000	0.001	0.001	0.000	-0.002
	Standard dev.	2.569	2.690	2.858	3.056	2.556	2.696	2.808	2.962	2.524	2.641	2.788	2.947	2.491	2.628	2.761	2.908
	Variance	-4.3E-07	-1.6E-07	-2.7E-07	3.3E-07	5.3E-07	3.8E-07	-2.5E-07	-2.9E-07	6.6E-07	5.4E-07	-1.1E-06	-6.8E-07	4.2E-07	-1.0E-06	-4.7E-07	3.8E-07
	Skewness	1.3E-06	5.1E-07	8.3E-07	-9.9E-07	-1.6E-06	-1.2E-06	4.8E-07	8.5E-07	-1.9E-06	-1.6E-06	3.2E-06	2.1E-06	-1.3E-06	2.9E-06	1.4E-06	-1.1E-06
	Kurtosis	0.069	0.036	0.097	0.092	0.076	0.028	0.059	0.051	0.047	0.041	0.093	0.054	0.042	0.078	0.084	0.084
3 5	Iean	0.000	0.000	0.000	0.000	0.000	0.000	0.000	0.000	0.000	0.000	0.000	0.000	0.000	0.000	0.000	0.000
	Median	0.006	0.001	0.004	0.011	-0.003	0.002	-0.002	0.002	-0.004	-0.004	-0.005	-0.006	0.001	0.004	0.004	-0.006
	Standard dev.	2.568	2.700	2.837	3.023	2.521	2.650	2.774	2.963	2.505	2.613	2.770	2.943	2.472	2.592	2.749	2.922
	Variance	9.7E-08	5.8E-07	1.4E-06	8.0E-07	7.0E-07	-1.2E-06	8.9E-07	-1.4E-07	-1.2E-07	1.0E-06	1.6E-06	-4.6E-07	-1.1E-06	2.7E-06	2.1E-06	-2.0E-06
	Skewness	-1.9E-07	-1.5E-06	-3.5E-06	-7.5E-06	-3.2E-06	3.9E-06	-2.7E-06	2.2E-06	7.6E-07	-3.3E-06	-4.8E-06	8.5E-07	3.0E-06	-8.7E-06	-6.3E-06	5.7E-06
	Kurtosis	0.153	0.158	0.122	0.202	0.110	0.183	0.165	0.107	0.188	0.140	0.153	0.141	0.122	0.181	0.194	0.168
3 6	Mean	0.000	0.000	0.000	0.000	0.000	0.000	0.000	0.000	0.000	0.000	0.000	0.000	0.000	0.000	0.000	0.000
	Median	0.005	0.000	0.001	0.002	0.000	-0.006	-0.003	0.003	0.008	0.000	0.004	-0.001	0.002	0.003	0.004	-0.005
	Standard dev.	2.513	2.648	2.785	2.987	2.461	2.599	2.754	2.955	2.419	2.543	2.702	2.922	2.411	2.551	2.701	2.871
	Variance	2.5E-06	1.6E-06	-4.1E-06	-1.0E-06	2.0E-06	-1.1E-06	-1.0E-06	-7.2E-06	-7.5E-07	-6.8E-06	4.5E-06	-1.3E-06	7.1E-07	-1.2E-06	1.4E-06	7.4E-07
	Skewness	-4.2E-06	1.0E-06	1.0E-05	1.5E-05	-5.2E-06	-2.5E-05	7.1E-07	-3.8E-05	2.2E-06	1.6E-05	2.0E-05	2.0E-06	-1.4E-06	2.2E-06	-2.6E-06	-1.7E-05
	Kurtosis	0.769	0.887	0.799	0.802	0.782	0.859	0.775	0.784	0.715	0.796	0.763	0.804	0.704	0.795	0.772	0.716
3 7	Mean	0.000	0.000	0.000	0.000	0.000	0.000	0.000	0.000	0.000	0.000	0.000	0.000	0.000	0.000	0.000	0.000
	Median	-0.003	-0.003	0.000	0.009	-0.004	-0.008	-0.010	-0.009	-0.008	0.003	-0.004	0.006	-0.003	-0.001	0.002	-0.014
	Standard dev.	2.547	2.658	2.812	3.041	2.490	2.659	2.780	2.972	2.497	2.600	2.717	2.924	2.427	2.579	2.696	2.905
	Variance	-1.2E-07	-3.8E-07	1.5E-07	1.3E-06	-7.5E-07	2.5E-06	-1.1E-06	3.3E-07	4.7E-07	-5.8E-07	-3.3E-06	1.6E-06	5.4E-07	-7.5E-07	-1.4E-06	1.6E-06
	Skewness	8.8E-03	4.0E-03	-7.2E-03	2.3E-04	1.1E-02	1.4E-02	2.3E-02	7.6E-03	1.7E-02	1.5E-02	4.2E-04	7.9E-03	-4.7E-03	1.1E-02	1.5E-03	6.7E-03
	Kurtosis	0.138	0.167	0.151	0.147	0.130	0.144	0.200	0.124	0.164	0.170	0.155	0.178	0.136	0.160	0.160	0.199
4 0	Mean	90.653	103.504	117.059	135.006	87.348	99.448	112.084	128.726	85.624	97.299	109.083	127.035	83.947	94.719	106.340	123.039
	Median	85.669	94.777	111.735	137.263	83.517	91.422	104.475	130.413	82.953	90.177	100.478	129.062	81.757	88.544	97.906	122.721
	Standard dev.	13.562	18.997	19.639	18.061	11.531	18.110	19.096	18.519	8.932	16.718	18.845	22.240	7.770	15.509	18.316	21.745
	Variance	6.7E+00	5.4E+00	6.0E+00	7.5E+00	7.6E+00	5.5E+00	5.9E+00	7.0E+00	9.6E+00	5.8E+00	5.8E+00	5.7E+00	1.1E+01	6.1E+00	5.8E+00	5.7E+00
	Skewness	2.1E+00	1.2E+00	4.9E-01	-2.7E-01	2.3E+00	1.4E+00	7.4E-01	-9.4E-02	2.3E+00	1.7E+00	9.9E-01	-5.9E-02	2.3E+00	1.9E+00	1.2E+00	1.1E-01
	Kurtosis	3.995	0.250	-1.006	-0.883	5.384	0.955	-0.727	-1.119	5.874	1.903	-0.293	-1.196	5.904	2.739	0.142	-1.238
4 1	Mean	0.000	0.000	0.000	0.000	0.000	0.000	0.000	0.000	0.000	0.000	0.000	0.000	0.000	0.000	0.000	0.000
	Median	0.004	0.000	0.005	-0.004	0.008	0.006	0.010	-0.007	0.013	0.006	-0.001	0.006	0.015	0.001	-0.002	-0.005
	Standard dev.	2.650	3.217	3.695	3.615	2.905	3.226	3.733	3.739	3.507	3.090	3.538	3.767	3.817	3.115	3.414	3.745
	Variance	1.8E-06	3.2E-05	-2.2E-05	6.6E-06	3.0E-06	1.4E-05	-3.1E-05	6.5E-06	-5.3E-07	-4.2E-05	-1.4E-05	3.4E-06	-2.0E-05	4.0E-06	-6.4E-06	3.1E-06
	Skewness	-7.8E-03	-1.1E-03	-1.1E-03	2.4E-04	-2.2E-02	-8.6E-04	4.7E-03	1.8E-02	2.3E-02	3.6E-03	9.1E-03	9.8E-03	3.5E-02	-2.6E-02	-5.5E-03	1.3E-02
	Kurtosis	1.568	1.188	0.515	0.711	2.180	1.276	0.764	0.463	2.507	1.447	0.744	0.711	2.544	1.461	0.789	0.653

Packet	Experiment	17	18	19	20	21	22	23	24	25	26	27	28	29	30	31	32
	V_{sg} (m/s)	0.15	0.30	0.59	1.32	0.15	0.31	0.59	1.33	0.15	0.30	0.59	1.32	0.15	0.30	0.59	1.00
	V_{sl} (m/s)	0.61	0.61	0.61	0.61	0.73	0.73	0.73	0.73	0.79	0.79	0.79	0.79	0.13	0.13	0.13	0.13
	WC (%)	1.00	1.00	1.00	1.00	1.00	1.00	1.00	1.00	1.00	1.00	1.00	1.00	0.80	0.80	0.80	0.80
3 2	Mean	0.000	0.000	0.000	0.000	0.000	0.000	0.000	0.000	0.000	0.000	0.000	0.000	0.000	0.000	0.000	0.000
	Median	-0.001	-0.005	0.002	0.002	-0.001	0.001	-0.002	0.003	0.003	0.005	0.000	0.002	-0.002	-0.003	-0.004	0.001
	Standard dev.	2.393	2.503	2.655	2.899	2.375	2.465	2.654	2.899	2.386	2.473	2.603	2.858	2.519	2.656	2.834	3.006
	Variance	1.3E-06	2.9E-06	-9.8E-06	2.6E-06	2.3E-06	-4.1E-06	2.6E-06	6.8E-06	1.6E-06	2.6E-07	2.2E-06	6.2E-08	-1.4E-06	5.7E-06	-3.1E-07	2.8E-06
	Skewness	-1.6E-07	-7.2E-06	1.9E-05	-2.9E-06	-5.9E-06	-6.2E-06	-2.6E-07	7.8E-05	-3.5E-06	9.2E-06	-6.6E-06	3.4E-06	2.8E-06	1.6E-05	6.2E-06	-8.8E-07
	Kurtosis	0.732	0.740	0.778	0.752	0.705	0.748	0.794	0.705	0.733	0.755	0.787	0.779	0.779	0.873	0.756	0.795
3 3	Mean	0.000	0.000	0.000	0.000	0.000	0.000	0.000	0.000	0.000	0.000	0.000	0.000	0.000	0.000	0.000	0.000
	Median	-0.003	0.001	-0.001	-0.001	-0.004	0.001	-0.001	-0.007	-0.004	-0.005	0.001	-0.003	-0.004	-0.001	0.000	-0.001
	Standard dev.	2.387	2.540	2.734	3.017	2.378	2.531	2.742	3.028	2.461	2.538	2.707	3.032	2.511	2.693	2.923	3.108
	Variance	1.0E-06	-6.6E-07	2.3E-06	-5.0E-07	3.7E-07	5.6E-07	2.0E-07	1.6E-06	-3.4E-06	-3.5E-06	-4.5E-06	2.6E-06	4.4E-06	-9.4E-06	9.8E-07	1.3E-06
	Skewness	-1.8E-04	4.4E-05	1.5E-04	1.2E-04	-1.1E-04	7.1E-05	-2.7E-05	-2.5E-06	-6.9E-05	-7.8E-05	4.9E-05	-1.7E-04	2.7E-04	1.0E-05	-3.9E-05	-3.9E-05
	Kurtosis	0.160	0.246	0.248	0.170	0.160	0.244	0.201	0.222	0.176	0.229	0.225	0.223	0.179	0.216	0.241	0.252
3 4	Mean	0.000	0.000	0.000	0.000	0.000	0.000	0.000	0.000	0.000	0.000	0.000	0.000	0.000	0.000	0.000	0.000
	Median	0.001	0.002	0.000	0.000	0.002	0.000	0.001	-0.002	0.001	0.000	0.001	0.001	0.003	0.003	0.000	0.004
	Standard dev.	2.471	2.594	2.739	2.907	2.450	2.532	2.699	2.897	2.503	2.571	2.703	2.873	2.614	2.756	2.865	3.038
	Variance	-9.6E-07	6.6E-07	1.1E-06	-2.2E-07	-1.3E-06	-1.0E-06	-1.6E-07	1.8E-06	-1.2E-06	1.7E-06	1.7E-07	8.3E-07	6.6E-07	-1.4E-06	2.9E-07	-5.9E-07
	Skewness	2.8E-06	-2.0E-06	-3.3E-06	6.9E-07	3.8E-06	3.0E-06	5.1E-07	-5.3E-06	3.6E-06	-5.0E-06	-4.9E-07	-3.0E-06	-2.0E-06	3.8E-06	-7.8E-07	1.7E-06
	Kurtosis	0.062	0.020	0.053	0.054	0.016	0.081	0.043	0.052	0.033	0.079	0.077	0.071	0.090	0.080	0.057	0.066
3 5	Mean	0.000	0.000	0.000	0.000	0.000	0.000	0.000	0.000	0.000	0.000	0.000	0.000	0.000	0.000	0.000	0.000
	Median	-0.002	-0.003	-0.006	0.004	0.004	-0.001	0.007	0.003	0.004	0.002	0.001	-0.002	-0.002	-0.002	-0.001	-0.004
	Standard dev.	2.472	2.558	2.699	2.876	2.455	2.553	2.707	2.882	2.491	2.531	2.669	2.881	2.607	2.730	2.896	3.025
	Variance	5.0E-07	-2.4E-06	-5.0E-07	1.0E-06	1.0E-06	-3.5E-07	-3.7E-07	-3.3E-06	2.3E-07	-7.2E-07	-1.5E-06	-2.4E-06	-1.9E-06	1.6E-06	-7.2E-07	-7.5E-07
	Skewness	-1.4E-06	9.9E-06	1.9E-06	-5.0E-06	-3.7E-06	1.2E-06	1.2E-06	1.2E-05	-5.5E-07	2.3E-06	5.2E-06	1.1E-05	1.2E-05	-3.1E-05	2.0E-06	2.7E-06
	Kurtosis	0.124	0.102	0.177	0.072	0.141	0.091	0.164	0.179	0.106	0.105	0.100	0.185	0.192	0.201	0.173	0.201
3 6	Mean	0.000	0.000	0.000	0.000	0.000	0.000	0.000	0.000	0.000	0.000	0.000	0.000	0.000	0.000	0.000	0.000
	Median	0.002	0.004	-0.003	0.001	0.003	-0.002	-0.001	0.001	-0.001	0.003	-0.003	-0.001	0.003	0.005	0.003	-0.003
	Standard dev.	2.375	2.527	2.672	2.860	2.388	2.498	2.653	2.849	2.439	2.492	2.644	2.820	2.563	2.688	2.826	2.992
	Variance	-1.8E-06	-3.3E-06	9.1E-06	-2.6E-06	1.5E-06	4.1E-06	-4.6E-06	-8.0E-06	-8.5E-07	4.9E-06	-1.5E-06	-6.6E-07	3.1E-06	-8.3E-06	-2.4E-06	-2.6E-06
	Skewness	-2.5E-06	1.9E-06	2.3E-05	-1.2E-06	1.6E-05	-9.8E-06	-2.3E-05	-5.3E-05	3.9E-06	-9.4E-06	4.4E-06	1.9E-06	-4.0E-06	1.1E-05	-6.4E-07	3.3E-06
	Kurtosis	0.694	0.746	0.817	0.771	0.699	0.784	0.773	0.677	0.711	0.715	0.679	0.768	0.723	0.781	0.773	0.770
3 7	Mean	0.000	0.000	0.000	0.000	0.000	0.000	0.000	0.000	0.000	0.000	0.000	0.000	0.000	0.000	0.000	0.000
	Median	0.002	-0.003	0.003	-0.003	0.000	0.004	-0.001	0.001	-0.001	0.008	-0.001	0.000	0.002	-0.011	-0.010	-0.005
	Standard dev.	2.455	2.535	2.688	2.848	2.430	2.534	2.680	2.874	2.471	2.533	2.656	2.864	2.586	2.711	2.843	2.970
	Variance	1.2E-06	3.4E-06	-1.4E-06	1.2E-06	-3.1E-06	1.1E-06	1.7E-06	2.5E-06	7.9E-07	-1.6E-06	3.2E-06	8.4E-09	1.2E-06	7.6E-07	-1.9E-08	2.8E-06
	Skewness	2.9E-03	-2.0E-03	-3.9E-03	4.6E-03	8.2E-03	-9.0E-03	5.4E-03	-9.2E-03	1.0E-02	1.9E-03	3.2E-03	2.1E-02	1.0E-02	6.0E-03	1.0E-02	1.1E-02
	Kurtosis	0.139	0.166	0.192	0.174	0.080	0.143	0.235	0.150	0.133	0.126	0.109	0.173	0.170	0.195	0.181	0.207
4 0	Mean	84.100	92.757	104.286	119.991	82.650	90.649	104.231	120.539	85.194	90.578	101.329	117.428	95.964	106.246	119.941	133.587
	Median	81.701	87.417	96.118	115.875	80.537	85.944	96.381	113.797	83.189	86.001	93.924	110.095	89.757	97.435	115.722	135.784
	Standard dev.	8.256	14.030	17.795	18.864	7.543	13.036	17.560	19.351	7.606	12.744	16.781	18.860	15.569	19.912	21.710	23.072
	Variance	1.0E+01	6.6E+00	5.9E+00	6.4E+00	1.1E+01	7.0E+00	5.9E+00	6.2E+00	1.1E+01	7.1E+00	6.0E+00	6.2E+00	6.2E+00	5.3E+00	5.5E+00	5.8E+00
	Skewness	2.2E+00	2.0E+00	1.4E+00	3.8E-01	2.2E+00	2.0E+00	1.5E+00	5.7E-01	2.0E+00	1.9E+00	1.5E+00	6.4E-01	1.9E+00	1.1E+00	3.8E-01	-1.2E-01
	Kurtosis	5.346	3.123	0.653	-1.166	5.723	3.322	1.083	-1.004	5.094	3.291	1.308	-0.896	2.871	0.128	-1.082	-1.058
4 1	Mean	0.000	0.000	0.000	0.000	0.000	0.000	0.000	0.000	0.000	0.000	0.000	0.000	0.000	0.000	0.000	0.000
	Median	0.018	0.010	-0.011	0.006	0.025	-0.004	-0.006	-0.001	0.015	-0.016	0.005	0.000	0.005	0.007	0.000	-0.017
	Standard dev.	3.999	3.340	3.386	3.774	4.216	3.875	3.460	3.872	4.287	4.147	3.508	3.787	2.960	3.811	4.224	4.274
	Variance	1.2E-05	5.7E-05	1.6E-05	-4.1E-06	5.6E-07	8.0E-06	-6.6E-06	9.5E-06	-1.4E-05	-3.1E-05	2.3E-05	-5.4E-06	-4.0E-05	-2.0E-05	-2.9E-05	9.4E-06
	Skewness	3.8E-02	-2.5E-02	6.3E-03	5.8E-03	6.5E-02	-1.7E-02	-2.7E-03	1.4E-03	4.2E-02	-4.4E-03	-1.2E-02	3.8E-03	6.3E-03	-1.8E-03	-5.2E-03	6.9E-03
	Kurtosis	2.672	1.638	0.790	0.704	2.896	1.764	0.870	0.758	2.554	1.882	1.011	0.584	1.746	0.905	0.447	0.675

Packet	Experiment	33	34	35	36	37	38	39	40	41	42	43	44	45	46	47	48
	V_{sg} (m/s)	0.15	0.30	0.59	1.00	0.15	0.30	0.59	1.00	0.15	0.30	0.59	1.00	0.15	0.31	0.59	1.33
	V_{sl} (m/s)	0.13	0.13	0.13	0.13	0.14	0.14	0.14	0.14	0.14	0.14	0.14	0.14	0.25	0.25	0.25	0.25
	WC (%)	0.60	0.60	0.60	0.60	0.40	0.40	0.40	0.40	0.20	0.20	0.20	0.20	0.80	0.80	0.80	0.80
3 2	Mean	0.000	0.000	0.000	0.000	0.000	0.000	0.000	0.000	0.000	0.000	0.000	0.000	0.000	0.000	0.000	0.000
	Median	0.001	0.001	0.002	0.000	0.001	0.002	-0.003	0.008	-0.002	0.000	0.001	0.003	0.001	0.001	-0.003	0.001
	Standard dev.	2.526	2.633	2.761	2.980	2.550	2.666	2.799	2.988	2.593	2.715	2.864	2.967	2.429	2.543	2.699	2.896
	Variance	6.2E-06	6.0E-06	2.0E-06	-4.1E-06	-2.0E-06	2.0E-06	5.2E-06	-3.0E-06	5.5E-07	7.9E-07	1.1E-07	-3.2E-06	1.1E-06	-3.8E-06	-1.5E-06	3.5E-06
	Skewness	-1.1E-05	-6.9E-06	-6.9E-06	-8.7E-06	6.1E-06	1.6E-06	5.2E-05	6.8E-06	3.6E-06	-1.1E-06	3.8E-06	-1.1E-05	4.0E-07	7.6E-06	3.2E-06	-6.2E-06
	Kurtosis	0.703	0.797	0.776	0.740	0.842	0.884	0.808	0.849	0.791	0.694	0.754	0.714	0.724	0.792	0.781	0.682
3 3	Mean	0.000	0.000	0.000	0.000	0.000	0.000	0.000	0.000	0.000	0.000	0.000	0.000	0.000	0.000	0.000	0.000
	Median	-0.004	0.001	-0.005	-0.002	-0.003	-0.003	0.007	0.000	-0.002	-0.001	0.002	-0.004	-0.003	0.000	0.002	-0.008
	Standard dev.	2.529	2.677	2.911	3.073	2.533	2.742	2.939	3.149	2.597	2.740	2.922	3.047	2.433	2.579	2.782	3.052
	Variance	-1.7E-06	-6.7E-06	-9.4E-06	-3.1E-06	-3.9E-07	-1.2E-06	-1.8E-06	-5.1E-07	2.3E-06	3.7E-06	1.9E-06	-3.5E-07	2.9E-06	1.9E-06	2.3E-06	6.1E-06
	Skewness	-8.0E-05	7.2E-05	3.7E-05	1.4E-04	-1.2E-04	7.6E-05	1.8E-04	-3.2E-05	3.1E-05	2.3E-05	-7.7E-06	-1.9E-05	-1.5E-04	1.0E-04	1.3E-04	-7.0E-05
	Kurtosis	0.217	0.201	0.230	0.189	0.260	0.360	0.292	0.230	0.111	0.139	0.143	0.118	0.175	0.259	0.174	0.173
3 4	Mean	0.000	0.000	0.000	0.000	0.000	0.000	0.000	0.000	0.000	0.000	0.000	0.000	0.000	0.000	0.000	0.000
	Median	-0.003	0.003	0.001	0.004	-0.005	-0.005	0.003	0.000	-0.001	0.001	0.002	0.004	0.003	0.003	-0.003	-0.001
	Standard dev.	2.624	2.722	2.863	3.020	2.629	2.745	2.866	2.980	2.695	2.824	2.928	3.052	2.543	2.652	2.751	2.927
	Variance	1.0E-06	-7.2E-07	3.5E-07	9.4E-07	-4.8E-07	6.9E-08	-1.5E-06	-7.3E-07	-3.6E-07	-8.4E-07	-2.9E-07	-1.1E-07	1.3E-06	1.8E-06	-6.5E-07	3.3E-07
	Skewness	-2.8E-06	2.2E-06	-1.0E-06	-2.8E-06	1.5E-06	-1.3E-07	4.5E-06	2.2E-06	1.1E-06	2.6E-06	8.9E-07	3.2E-07	-4.0E-06	-4.2E-06	1.9E-06	-1.0E-06
	Kurtosis	0.006	0.048	0.118	0.079	0.076	0.185	0.149	0.065	0.009	-0.002	0.018	0.082	0.052	0.103	0.085	0.097
3 5	Mean	0.000	0.000	0.000	0.000	0.000	0.000	0.000	0.000	0.000	0.000	0.000	0.000	0.000	0.000	0.000	0.000
	Median	0.001	0.003	0.002	-0.003	-0.009	0.000	-0.007	0.001	-0.001	-0.008	-0.004	0.006	-0.002	-0.001	0.003	-0.006
	Standard dev.	2.581	2.716	2.829	2.974	2.619	2.710	2.833	2.984	2.690	2.792	2.902	3.028	2.531	2.629	2.758	2.911
	Variance	8.3E-07	2.4E-06	6.1E-07	-2.9E-06	3.7E-07	1.3E-08	5.8E-07	-3.3E-07	2.7E-07	-6.3E-08	-2.4E-06	-1.3E-06	-1.8E-06	-3.0E-06	1.2E-06	-2.0E-06
	Skewness	-3.0E-06	-6.9E-06	-4.8E-06	1.4E-05	-2.3E-06	2.8E-06	-2.1E-06	1.6E-06	-2.9E-06	8.6E-07	7.3E-06	4.5E-06	5.1E-06	1.3E-05	-3.4E-06	8.3E-06
	Kurtosis	0.136	0.205	0.166	0.159	0.169	0.208	0.205	0.202	0.145	0.164	0.143	0.166	0.124	0.148	0.143	0.126
3 6	Mean	0.000	0.000	0.000	0.000	0.000	0.000	0.000	0.000	0.000	0.000	0.000	0.000	0.000	0.000	0.000	0.000
	Median	-0.005	0.000	-0.001	0.002	0.004	-0.006	0.000	0.001	0.007	-0.002	0.001	-0.004	-0.001	0.000	-0.002	-0.003
	Standard dev.	2.541	2.664	2.817	2.932	2.553	2.665	2.810	2.936	2.615	2.725	2.858	3.000	2.458	2.577	2.707	2.887
	Variance	-5.4E-06	-4.2E-06	1.2E-06	5.3E-06	3.4E-06	-2.3E-06	-3.5E-07	2.4E-06	1.3E-06	1.5E-06	7.2E-07	4.5E-06	-3.9E-07	1.6E-06	1.4E-06	-3.5E-06
	Skewness	8.9E-06	-4.1E-06	-2.6E-06	-3.4E-06	-8.8E-06	1.3E-05	-4.2E-05	-4.3E-06	-4.9E-06	1.8E-06	3.3E-06	-9.1E-06	-2.5E-05	-1.1E-06	-3.9E-06	2.6E-06
	Kurtosis	0.674	0.787	0.719	0.783	0.693	0.746	0.857	0.741	0.759	0.733	0.708	0.700	0.715	0.800	0.807	0.832
3 7	Mean	0.000	0.000	0.000	0.000	0.000	0.000	0.000	0.000	0.000	0.000	0.000	0.000	0.000	0.000	0.000	0.000
	Median	0.001	0.000	-0.009	0.009	-0.011	-0.004	-0.024	-0.009	-0.010	-0.005	0.004	-0.002	0.006	-0.005	-0.002	0.013
	Standard dev.	2.589	2.698	2.794	2.975	2.585	2.703	2.833	2.946	2.638	2.771	2.897	2.998	2.504	2.628	2.713	2.906
	Variance	-1.3E-07	-5.9E-07	-2.0E-06	1.0E-06	-6.9E-07	1.1E-07	-7.3E-07	1.5E-06	3.8E-07	1.1E-06	2.7E-06	-6.2E-07	6.9E-08	1.8E-06	-1.5E-06	1.3E-06
	Skewness	-3.2E-03	1.4E-02	5.9E-03	3.4E-03	1.2E-02	1.0E-02	3.2E-02	5.3E-03	1.0E-02	1.6E-02	-3.9E-03	-3.6E-06	5.0E-03	3.5E-03	-1.2E-03	-5.4E-03
	Kurtosis	0.119	0.143	0.179	0.206	0.178	0.195	0.189	0.147	0.129	0.148	0.196	0.105	0.171	0.183	0.140	0.172
4 0	Mean	95.392	104.405	116.462	130.270	96.696	105.698	118.597	129.882	102.149	111.405	122.809	134.823	88.028	97.014	107.778	124.571
	Median	90.373	97.516	113.172	131.825	89.221	96.870	114.177	131.312	98.811	106.761	120.393	135.716	83.239	89.268	101.606	126.785
	Standard dev.	13.621	18.345	21.012	22.778	18.758	22.051	24.941	23.093	10.498	13.895	15.258	15.965	13.158	17.675	19.419	19.027
	Variance	7.0E+00	5.7E+00	5.5E+00	5.7E+00	5.2E+00	4.8E+00	4.8E+00	5.6E+00	9.7E+00	8.0E+00	8.0E+00	8.4E+00	6.7E+00	5.5E+00	5.5E+00	6.5E+00
	Skewness	1.8E+00	1.1E+00	4.1E-01	-7.4E-02	2.0E+00	1.1E+00	4.4E-01	-7.5E-02	2.1E+00	1.2E+00	4.4E-01	-8.9E-02	2.2E+00	1.3E+00	6.4E-01	-1.6E-01
	Kurtosis	2.921	0.334	-0.926	-0.979	3.372	0.207	-0.958	-0.975	4.680	0.895	-0.767	-0.925	4.216	0.775	-0.774	-1.051
4 1	Mean	0.000	0.000	0.000	0.000	0.000	0.000	0.000	0.000	0.000	0.000	0.000	0.000	0.000	0.000	0.000	0.000
	Median	0.005	0.012	0.001	-0.001	-0.003	0.007	0.011	0.001	0.003	0.000	0.002	0.000	0.005	0.002	-0.004	-0.010
	Standard dev.	3.724	4.351	4.679	4.503	3.784	4.584	4.952	4.967	3.214	3.753	3.786	3.530	2.908	3.707	4.158	4.008
	Variance	-5.6E-06	9.2E-06	-1.4E-05	-1.4E-05	-1.9E-05	1.0E-05	1.7E-05	-8.0E-06	-4.8E-06	2.1E-05	-7.3E-07	1.2E-05	-1.9E-06	-3.7E-06	4.3E-06	-9.9E-07
	Skewness	1.8E-03	6.3E-03	7.1E-03	-2.1E-03	8.0E-03	4.5E-03	-2.8E-03	4.4E-03	9.9E-03	-6.7E-03	-3.3E-03	-1.6E-02	-1.3E-02	3.0E-03	3.7E-03	7.5E-03
	Kurtosis	0.774	0.533	0.343	0.411	1.295	0.732	0.546	0.438	0.786	0.454	0.462	0.499	1.732	1.037	0.577	0.433

Packet	Experiment	49	50	51	52	53	54	55	56	57	58	59	60	61	62	63	64
	V_{sg} (m/s)	0.15	0.23	0.60	1.31	0.15	0.31	0.59	1.32	0.15	0.31	0.59	1.32	0.15	0.31	0.59	1.34
	V_{sl} (m/s)	0.27	0.27	0.27	0.27	0.28	0.28	0.28	0.28	0.29	0.29	0.29	0.29	0.38	0.38	0.38	0.38
	WC (%)	0.60	0.60	0.60	0.60	0.40	0.40	0.40	0.40	0.20	0.20	0.20	0.20	0.80	0.80	0.80	0.80
3 2	Mean	0.000	0.000	0.000	0.000	0.000	0.000	0.000	0.000	0.000	0.000	0.000	0.000	0.000	0.000	0.000	0.000
	Median	0.002	0.001	-0.004	0.001	0.004	-0.004	0.000	0.000	-0.002	-0.004	0.002	0.006	0.006	-0.005	0.003	0.004
	Standard dev.	2.414	2.505	2.668	2.906	2.469	2.547	2.728	2.895	2.507	2.587	2.728	2.901	2.430	2.521	2.663	2.870
	Variance	-8.3E-06	-2.4E-06	3.8E-07	4.3E-06	5.1E-06	-8.5E-07	4.8E-06	-5.8E-06	1.4E-06	6.2E-06	6.7E-06	-4.3E-06	-6.7E-06	2.8E-07	-7.3E-08	-3.5E-06
	Skewness	1.7E-05	7.1E-06	3.7E-07	2.0E-05	6.2E-08	8.5E-07	-1.3E-05	1.3E-05	4.4E-06	-1.5E-05	-3.3E-06	9.3E-06	1.3E-05	-1.8E-06	-4.3E-08	8.3E-06
	Kurtosis	0.776	0.707	0.736	0.722	0.863	0.835	0.810	0.762	0.703	0.790	0.670	0.728	0.768	0.787	0.753	0.764
3 3	Mean	0.000	0.000	0.000	0.000	0.000	0.000	0.000	0.000	0.000	0.000	0.000	0.000	0.000	0.000	0.000	0.000
	Median	0.004	0.002	0.000	0.007	-0.002	0.003	-0.002	0.002	0.004	0.002	-0.006	0.005	0.000	0.002	0.002	0.002
	Standard dev.	2.449	2.535	2.816	3.082	2.485	2.646	2.864	3.111	2.487	2.621	2.819	3.028	2.409	2.572	2.759	3.023
	Variance	9.3E-06	2.6E-06	1.5E-06	6.1E-06	-1.5E-06	4.8E-06	-3.1E-06	-2.2E-07	-4.3E-06	5.4E-07	-8.0E-06	-5.4E-06	2.8E-06	2.9E-07	6.6E-06	2.2E-06
	Skewness	-1.4E-04	8.0E-05	3.0E-05	5.3E-05	-2.0E-05	-2.9E-05	1.5E-04	5.3E-05	1.1E-04	-7.8E-05	1.1E-04	1.5E-04	-8.9E-05	2.0E-05	9.4E-06	2.0E-04
	Kurtosis	0.232	0.225	0.179	0.091	0.267	0.276	0.202	0.157	0.117	0.080	0.155	0.125	0.222	0.231	0.197	0.134
3 4	Mean	0.000	0.000	0.000	0.000	0.000	0.000	0.000	0.000	0.000	0.000	0.000	0.000	0.000	0.000	0.000	0.000
	Median	-0.002	0.003	0.002	0.000	0.002	-0.003	0.002	0.000	0.000	0.001	0.001	0.001	0.001	-0.002	0.000	0.003
	Standard dev.	2.549	2.600	2.744	2.935	2.559	2.667	2.731	2.906	2.620	2.694	2.772	2.968	2.524	2.638	2.762	2.914
	Variance	-3.5E-07	-7.8E-07	4.4E-07	-3.0E-07	4.1E-08	7.2E-07	2.9E-07	1.1E-07	4.9E-07	-4.8E-07	-1.5E-06	-1.9E-07	-8.5E-07	8.4E-07	-2.6E-07	-8.7E-08
	Skewness	9.8E-07	2.3E-06	-1.3E-06	9.4E-07	-1.1E-07	-2.4E-06	-8.6E-07	-3.3E-07	-1.5E-06	1.6E-06	5.0E-06	6.3E-07	2.4E-06	-2.6E-06	7.4E-07	1.4E-07
	Kurtosis	0.073	0.030	0.126	0.072	0.058	0.083	0.112	0.099	-0.013	0.069	0.065	-0.002	0.044	0.052	0.123	0.109
3 5	Mean	0.000	0.000	0.000	0.000	0.000	0.000	0.000	0.000	0.000	0.000	0.000	0.000	0.000	0.000	0.000	0.000
	Median	0.002	-0.003	-0.007	0.001	-0.004	-0.003	-0.004	-0.002	-0.001	-0.009	0.002	-0.004	0.003	-0.002	0.009	0.006
	Standard dev.	2.541	2.584	2.735	2.911	2.553	2.637	2.727	2.883	2.595	2.695	2.799	2.970	2.524	2.624	2.704	2.898
	Variance	1.3E-06	6.8E-07	2.5E-07	2.2E-06	1.1E-07	1.9E-07	-9.8E-07	7.2E-07	-1.4E-06	5.1E-07	-1.2E-06	1.2E-06	4.0E-07	-8.8E-07	-9.5E-07	9.2E-08
	Skewness	-4.1E-06	-2.5E-06	-1.2E-06	-1.8E-05	-3.5E-07	-1.6E-06	3.7E-06	-2.1E-06	5.1E-06	-2.4E-06	5.7E-06	-5.1E-06	-1.3E-06	3.3E-06	2.6E-06	-3.1E-07
	Kurtosis	0.130	0.143	0.186	0.151	0.174	0.209	0.221	0.131	0.151	0.141	0.134	0.172	0.100	0.181	0.180	0.218
3 6	Mean	0.000	0.000	0.000	0.000	0.000	0.000	0.000	0.000	0.000	0.000	0.000	0.000	0.000	0.000	0.000	0.000
	Median	0.002	0.000	-0.002	0.002	-0.001	0.003	0.003	0.001	-0.002	-0.002	-0.003	0.000	0.003	-0.003	-0.002	0.005
	Standard dev.	2.460	2.536	2.683	2.889	2.485	2.584	2.706	2.890	2.529	2.618	2.744	2.920	2.436	2.550	2.684	2.860
	Variance	3.5E-06	1.9E-06	-2.3E-07	-7.7E-06	-2.2E-06	-1.8E-06	-4.9E-06	6.2E-06	3.6E-07	-4.2E-06	-1.7E-06	4.8E-06	4.9E-06	-2.2E-06	2.0E-06	4.9E-06
	Skewness	-9.6E-06	1.1E-07	6.1E-07	-4.7E-05	6.4E-06	3.3E-06	5.8E-06	4.6E-06	-4.9E-07	1.2E-05	3.3E-06	-9.4E-06	-7.8E-06	-3.6E-05	-4.4E-06	-1.1E-05
	Kurtosis	0.805	0.778	0.704	0.726	0.835	0.761	0.809	0.777	0.748	0.739	0.714	0.688	0.734	0.828	0.752	0.733
3 7	Mean	0.000	0.000	0.000	0.000	0.000	0.000	0.000	0.000	0.000	0.000	0.000	0.000	0.000	0.000	0.000	0.000
	Median	-0.001	-0.007	-0.011	-0.005	0.012	-0.002	0.002	-0.002	-0.009	-0.002	0.005	0.003	-0.007	0.005	-0.012	0.011
	Standard dev.	2.518	2.571	2.699	2.879	2.539	2.603	2.717	2.897	2.579	2.653	2.782	2.957	2.485	2.565	2.722	2.879
	Variance	-2.0E-06	-2.3E-07	1.6E-07	-1.9E-06	-4.6E-08	-9.6E-07	1.8E-06	-1.4E-06	8.5E-07	1.1E-06	2.4E-06	-7.2E-07	2.6E-07	-6.2E-07	-6.6E-07	-7.1E-07
	Skewness	5.2E-03	5.5E-03	-1.2E-03	1.0E-02	-1.1E-02	1.4E-02	-3.8E-03	8.8E-03	5.7E-03	1.8E-03	2.9E-03	5.7E-03	7.0E-03	-1.9E-03	1.0E-02	-5.1E-03
	Kurtosis	0.205	0.115	0.113	0.145	0.189	0.185	0.159	0.177	0.113	0.126	0.152	0.110	0.144	0.211	0.128	0.180
4 0	Mean	88.043	92.801	106.847	122.748	89.761	97.303	107.140	122.163	93.673	101.774	111.708	127.400	86.114	94.761	105.257	120.861
	Median	83.879	88.079	102.246	124.006	82.728	89.585	101.506	124.009	91.220	98.010	108.311	128.881	82.076	87.761	97.886	121.772
	Standard dev.	11.951	13.498	19.220	19.235	17.844	19.540	21.861	19.693	8.397	11.549	13.569	14.768	11.772	16.556	18.962	19.220
	Variance	7.4E+00	6.9E+00	5.6E+00	6.4E+00	5.0E+00	5.0E+00	4.9E+00	6.2E+00	1.1E+01	8.8E+00	8.2E+00	8.6E+00	7.3E+00	5.7E+00	5.6E+00	6.3E+00
	Skewness	2.0E+00	1.6E+00	5.6E-01	-1.4E-01	2.2E+00	1.3E+00	6.2E-01	-1.7E-01	2.2E+00	1.5E+00	6.9E-01	-1.8E-01	2.2E+00	1.6E+00	8.4E-01	7.6E-03
	Kurtosis	3.942	2.089	-0.787	-0.937	4.048	0.814	-0.711	-0.903	5.756	1.969	-0.390	-0.949	4.819	1.516	-0.439	-1.188
4 1	Mean	0.000	0.000	0.000	0.000	0.000	0.000	0.000	0.000	0.000	0.000	0.000	0.000	0.000	0.000	0.000	0.000
	Median	0.005	0.007	0.006	0.000	0.004	0.007	0.015	0.009	0.005	-0.008	-0.010	-0.002	0.004	-0.001	0.000	0.005
	Standard dev.	3.687	4.048	4.505	4.354	3.767	4.515	4.948	4.933	3.217	3.736	3.754	3.242	3.414	3.644	4.138	4.042
	Variance	2.2E-05	2.3E-05	2.2E-06	-1.9E-05	2.2E-06	-2.2E-05	9.2E-06	-1.4E-05	4.6E-05	-1.0E-05	2.9E-05	9.9E-06	8.9E-06	-2.0E-05	1.5E-06	-1.2E-05
	Skewness	5.1E-03	1.7E-02	-1.2E-03	-1.2E-02	1.4E-02	7.7E-03	3.4E-03	5.4E-03	2.6E-03	1.3E-02	-1.0E-03	-2.2E-03	-3.6E-03	4.6E-03	1.2E-02	3.2E-03
	Kurtosis	0.913	0.627	0.388	0.462	1.465	0.682	0.500	0.567	1.191	0.539	0.492	0.563	1.962	1.212	0.651	0.516

Packet	Experiment	65	66	67	68	69	70	71	72	73	74	75	76	77	78	79	80
	V_{sg} (m/s)	0.15	0.29	0.59	1.33	0.15	0.31	0.59	1.32	0.16	0.31	0.59	1.33	0.15	0.31	0.59	1.34
	V_{sl} (m/s)	0.40	0.40	0.40	0.40	0.41	0.41	0.41	0.41	0.43	0.43	0.43	0.43	0.51	0.51	0.51	0.51
	WC (%)	0.60	0.60	0.60	0.60	0.40	0.40	0.40	0.40	0.20	0.20	0.20	0.20	0.80	0.80	0.80	0.80
3 2	Mean	0.000	0.000	0.000	0.000	0.000	0.000	0.000	0.000	0.000	0.000	0.000	0.000	0.000	0.000	0.000	0.000
	Median	0.001	-0.001	0.001	0.007	-0.001	-0.002	-0.002	-0.001	0.005	-0.001	0.005	-0.001	-0.002	0.002	0.000	0.002
	Standard dev.	2.413	2.530	2.698	2.899	2.439	2.546	2.688	2.912	2.468	2.595	2.712	2.902	2.394	2.480	2.656	2.864
	Variance	1.2E-06	-1.1E-06	-1.6E-06	-2.4E-06	1.6E-06	1.1E-06	-1.3E-06	-3.2E-06	7.9E-06	2.6E-06	-1.9E-06	5.0E-06	7.4E-06	-2.7E-06	-1.2E-06	-5.0E-07
	Skewness	3.3E-06	-5.8E-06	1.2E-06	-3.2E-05	7.5E-07	-2.4E-06	-4.5E-06	1.5E-06	-8.1E-06	7.4E-07	-1.7E-06	1.4E-05	2.2E-06	5.4E-06	-3.2E-05	5.3E-06
	Kurtosis	0.750	0.740	0.772	0.722	0.770	0.771	0.771	0.715	0.737	0.721	0.778	0.691	0.695	0.761	0.798	0.703
3 3	Mean	0.000	0.000	0.000	0.000	0.000	0.000	0.000	0.000	0.000	0.000	0.000	0.000	0.000	0.000	0.000	0.000
	Median	0.001	-0.003	-0.001	-0.002	0.002	0.000	0.005	0.003	-0.003	-0.001	0.000	0.003	-0.001	0.003	0.000	-0.002
	Standard dev.	2.448	2.580	2.805	3.083	2.496	2.662	2.855	3.126	2.460	2.618	2.828	3.010	2.415	2.559	2.773	3.025
	Variance	2.4E-06	1.8E-06	5.6E-06	6.8E-07	-5.3E-06	-4.4E-06	1.0E-06	-2.9E-07	2.8E-06	4.0E-07	-2.3E-06	-4.3E-06	-4.3E-06	-1.9E-06	-4.9E-06	4.6E-07
	Skewness	2.0E-05	8.5E-05	-5.7E-05	1.0E-04	-1.2E-04	-9.2E-05	-1.0E-04	8.0E-05	5.1E-05	-1.6E-04	2.8E-05	-9.5E-05	8.6E-06	1.3E-04	-7.8E-05	-6.6E-05
	Kurtosis	0.202	0.227	0.186	0.185	0.214	0.213	0.248	0.226	0.134	0.166	0.120	0.095	0.189	0.259	0.184	0.199
3 4	Mean	0.000	0.000	0.000	0.000	0.000	0.000	0.000	0.000	0.000	0.000	0.000	0.000	0.000	0.000	0.000	0.000
	Median	-0.002	-0.003	0.001	0.000	0.002	0.002	-0.001	0.000	-0.002	-0.001	-0.003	-0.002	0.001	-0.001	-0.004	-0.006
	Standard dev.	2.501	2.598	2.755	2.872	2.534	2.640	2.736	2.866	2.580	2.691	2.801	2.950	2.495	2.583	2.706	2.861
	Variance	6.2E-07	6.2E-08	3.8E-07	-1.4E-09	5.8E-08	-8.4E-07	-3.7E-07	4.6E-07	1.0E-06	-1.4E-07	9.3E-07	4.8E-07	6.3E-07	-9.6E-07	-3.7E-07	1.7E-06
	Skewness	-1.8E-06	-2.0E-07	-1.2E-06	-1.1E-08	-1.1E-07	3.0E-06	1.1E-06	-1.4E-06	-2.9E-06	4.7E-07	-2.9E-06	-1.5E-06	-2.0E-06	2.5E-06	1.1E-06	-5.3E-06
	Kurtosis	0.036	0.036	0.085	0.020	-0.002	0.067	0.100	0.087	-0.007	-0.004	-0.018	0.022	0.043	0.038	0.037	0.052
3 5	Mean	0.000	0.000	0.000	0.000	0.000	0.000	0.000	0.000	0.000	0.000	0.000	0.000	0.000	0.000	0.000	0.000
	Median	0.004	0.004	-0.005	-0.006	-0.006	-0.002	0.004	0.002	0.002	0.000	-0.003	0.001	-0.003	0.001	-0.001	0.001
	Standard dev.	2.527	2.593	2.700	2.884	2.523	2.615	2.729	2.896	2.558	2.659	2.780	2.933	2.505	2.602	2.679	2.851
	Variance	6.6E-07	6.4E-08	-5.7E-07	2.4E-06	2.0E-06	1.8E-06	-1.2E-06	-6.7E-07	-1.3E-06	-1.8E-06	-1.9E-06	-9.1E-08	-3.2E-06	-8.8E-07	-2.0E-06	-2.6E-06
	Skewness	-1.2E-06	-4.1E-07	1.5E-06	-1.2E-05	-8.7E-06	-4.1E-06	3.4E-06	2.0E-06	3.4E-06	5.1E-06	6.9E-06	4.9E-07	9.2E-06	3.3E-06	5.2E-06	7.6E-06
	Kurtosis	0.152	0.167	0.148	0.166	0.108	0.124	0.165	0.145	0.118	0.184	0.103	0.166	0.125	0.166	0.230	0.138
3 6	Mean	0.000	0.000	0.000	0.000	0.000	0.000	0.000	0.000	0.000	0.000	0.000	0.000	0.000	0.000	0.000	0.000
	Median	0.000	0.002	-0.002	0.001	-0.001	0.000	-0.002	0.000	-0.005	0.002	0.005	0.002	-0.001	0.003	-0.004	-0.001
	Standard dev.	2.458	2.539	2.691	2.862	2.463	2.562	2.674	2.859	2.503	2.617	2.714	2.873	2.421	2.517	2.652	2.864
	Variance	-1.3E-06	1.3E-06	-4.4E-06	-2.2E-06	-1.1E-06	-1.0E-06	7.2E-07	3.3E-06	-2.6E-06	9.5E-07	-9.2E-07	-4.2E-06	-5.5E-06	6.4E-07	3.1E-06	1.2E-06
	Skewness	1.7E-05	2.7E-05	5.8E-06	5.5E-06	-3.5E-06	6.1E-06	3.5E-05	-7.2E-06	4.9E-06	-1.9E-05	2.4E-06	1.1E-05	-2.7E-06	-1.5E-05	-9.5E-06	3.5E-05
	Kurtosis	0.704	0.680	0.775	0.826	0.692	0.779	0.707	0.736	0.661	0.746	0.706	0.754	0.680	0.755	0.830	0.785
3 7	Mean	0.000	0.000	0.000	0.000	0.000	0.000	0.000	0.000	0.000	0.000	0.000	0.000	0.000	0.000	0.000	0.000
	Median	0.005	-0.001	-0.006	0.000	-0.004	0.000	-0.004	-0.011	-0.008	-0.018	-0.001	-0.006	-0.003	-0.008	-0.011	-0.002
	Standard dev.	2.497	2.583	2.696	2.878	2.506	2.601	2.713	2.854	2.531	2.619	2.743	2.912	2.465	2.564	2.672	2.851
	Variance	-2.1E-06	3.2E-07	9.4E-07	-2.0E-06	-1.8E-06	-1.8E-06	4.4E-07	1.8E-06	-7.2E-07	8.6E-08	2.5E-06	5.6E-07	3.2E-06	3.1E-06	1.4E-06	1.3E-07
	Skewness	6.4E-03	8.2E-03	1.9E-04	9.1E-04	7.3E-03	-4.6E-03	5.3E-03	1.1E-02	3.2E-03	1.8E-02	-1.2E-02	1.4E-02	1.1E-02	1.2E-02	2.0E-03	-6.2E-03
	Kurtosis	0.135	0.149	0.147	0.135	0.119	0.100	0.235	0.214	0.119	0.153	0.159	0.147	0.144	0.096	0.116	0.166
4 0	Mean	87.181	93.838	104.405	119.853	88.392	95.209	104.769	119.416	91.597	99.654	109.312	124.222	85.005	92.948	103.038	118.117
	Median	83.479	88.289	98.810	120.993	83.430	88.914	98.776	120.448	89.781	96.063	105.395	124.993	81.549	86.417	95.265	117.625
	Standard dev.	11.090	14.818	18.507	19.353	13.674	16.986	20.238	20.185	6.837	10.971	12.910	14.599	10.420	15.798	18.454	19.319
	Variance	7.9E+00	6.3E+00	5.6E+00	6.2E+00	6.5E+00	5.6E+00	5.2E+00	5.9E+00	1.3E+01	9.1E+00	8.5E+00	8.5E+00	8.2E+00	5.9E+00	5.6E+00	6.1E+00
	Skewness	2.0E+00	1.5E+00	7.5E-01	-6.4E-02	2.1E+00	1.4E+00	7.2E-01	-7.6E-02	2.2E+00	1.8E+00	9.5E-01	-2.7E-02	2.2E+00	1.7E+00	1.0E+00	1.6E-01
	Kurtosis	4.314	1.678	-0.447	-1.070	4.280	1.366	-0.539	-1.050	6.312	3.011	0.210	-1.028	4.693	2.135	-0.120	-1.193
4 1	Mean	0.000	0.000	0.000	0.000	0.000	0.000	0.000	0.000	0.000	0.000	0.000	0.000	0.000	0.000	0.000	0.000
	Median	0.004	0.006	-0.017	-0.002	0.008	0.005	-0.003	0.003	0.013	0.000	0.002	-0.010	0.006	0.008	-0.009	0.012
	Standard dev.	3.940	4.229	4.681	4.458	4.121	4.698	5.104	4.952	3.412	3.706	3.917	3.326	3.790	3.503	4.179	4.157
	Variance	-5.8E-06	3.9E-06	-1.7E-05	-2.0E-05	1.1E-05	-2.1E-05	-1.3E-05	-3.3E-06	-6.9E-06	1.0E-05	-5.5E-06	-7.0E-06	-2.4E-06	2.5E-06	8.0E-06	2.2E-06
	Skewness	2.9E-03	-1.5E-04	1.7E-02	7.4E-03	1.3E-02	1.2E-02	-3.5E-03	1.9E-03	1.8E-02	6.4E-03	1.5E-02	3.1E-03	1.1E-02	-1.4E-03	1.0E-02	2.1E-03
	Kurtosis	1.045	0.720	0.584	0.454	0.946	0.647	0.374	0.555	1.719	0.715	0.483	0.435	2.051	1.120	0.788	0.573

Packet	Experiment	81	82	83	84	85	86	87	88	89	90	91	92	93	94	95	96
	V_{sg} (m/s)	0.15	0.24	0.59	1.34	0.16	0.31	0.59	1.34	0.16	0.35	0.66	1.33	0.15	0.31	0.60	1.32
	V_{sl} (m/s)	0.53	0.53	0.53	0.53	0.55	0.55	0.55	0.55	0.57	0.57	0.57	0.57	0.64	0.64	0.64	0.64
	WC (%)	0.60	0.60	0.60	0.60	0.40	0.40	0.40	0.40	0.20	0.20	0.20	0.20	0.80	0.80	0.80	0.80
3 2	Mean	0.000	0.000	0.000	0.000	0.000	0.000	0.000	0.000	0.000	0.000	0.000	0.000	0.000	0.000	0.000	0.000
	Median	-0.002	0.003	0.000	-0.002	-0.002	-0.004	0.000	0.002	-0.002	-0.002	-0.002	0.000	0.003	-0.004	-0.003	0.000
	Standard dev.	2.437	2.482	2.687	2.885	2.458	2.545	2.664	2.876	2.492	2.352	2.728	2.894	2.384	2.511	2.632	2.846
	Variance	-3.1E-06	-3.3E-06	-5.1E-07	-1.4E-07	-2.6E-06	-1.2E-06	3.9E-06	-8.6E-07	3.4E-06	-1.3E-06	9.4E-06	-3.1E-06	4.8E-06	-1.2E-06	1.6E-06	9.5E-07
	Skewness	-9.3E-07	2.4E-06	2.3E-06	-4.1E-07	7.1E-06	2.5E-06	-4.0E-06	-1.4E-05	-9.6E-06	3.4E-06	2.9E-05	-1.7E-05	-1.1E-05	3.4E-06	7.2E-06	6.9E-07
	Kurtosis	0.746	0.731	0.834	0.735	0.762	0.733	0.766	0.742	0.672	0.728	0.702	0.733	0.809	0.770	0.768	0.746
3 3	Mean	0.000	0.000	0.000	0.000	0.000	0.000	0.000	0.000	0.000	0.000	0.000	0.000	0.000	0.000	0.000	0.000
	Median	0.001	-0.004	-0.002	0.001	0.001	-0.002	-0.005	-0.001	-0.003	0.000	0.000	-0.001	-0.002	0.002	-0.004	-0.001
	Standard dev.	2.477	2.572	2.855	3.085	2.500	2.675	2.909	3.063	2.466	2.307	2.827	3.034	2.410	2.552	2.773	3.027
	Variance	3.5E-06	6.3E-07	-2.8E-06	5.5E-06	3.4E-06	1.5E-06	-2.1E-06	-1.6E-06	2.4E-06	-2.8E-06	-9.1E-07	4.2E-06	-1.2E-06	4.8E-06	4.3E-06	1.7E-06
	Skewness	-9.5E-05	-7.2E-06	-1.4E-04	7.6E-07	1.9E-04	1.5E-05	1.2E-05	-1.7E-04	3.0E-05	-2.4E-04	-6.5E-05	-1.0E-04	-1.4E-04	-1.2E-04	-8.3E-05	1.2E-05
	Kurtosis	0.182	0.165	0.220	0.197	0.258	0.249	0.234	0.200	0.104	0.138	0.151	0.141	0.135	0.277	0.212	0.137
3 4	Mean	0.000	0.000	0.000	0.000	0.000	0.000	0.000	0.000	0.000	0.000	0.000	0.000	0.000	0.000	0.000	0.000
	Median	-0.004	0.002	0.003	-0.002	0.003	0.002	0.001	0.003	-0.001	-0.001	0.003	-0.001	0.001	0.000	0.001	0.000
	Standard dev.	2.528	2.577	2.709	2.894	2.562	2.598	2.695	2.861	2.615	2.485	2.758	2.914	2.499	2.589	2.668	2.859
	Variance	-1.8E-07	-1.1E-06	-1.0E-06	6.2E-07	6.9E-07	1.2E-06	3.5E-07	-4.4E-07	1.4E-07	5.3E-07	-9.1E-07	7.4E-07	1.1E-06	-1.3E-06	7.1E-07	1.1E-06
	Skewness	5.7E-07	3.2E-06	3.1E-06	-2.0E-06	-2.1E-06	-3.9E-06	-1.2E-06	1.5E-06	-4.1E-07	-1.6E-06	2.6E-06	-2.3E-06	-3.2E-06	3.8E-06	-2.4E-06	-3.3E-06
	Kurtosis	0.066	0.015	0.086	0.133	0.031	0.138	0.076	0.056	0.021	-0.005	0.081	0.054	0.053	0.077	0.066	0.017
3 5	Mean	0.000	0.000	0.000	0.000	0.000	0.000	0.000	0.000	0.000	0.000	0.000	0.000	0.000	0.000	0.000	0.000
	Median	0.004	-0.001	0.000	-0.001	-0.003	0.007	0.003	-0.007	0.000	0.001	0.002	0.003	0.002	-0.002	0.001	0.000
	Standard dev.	2.514	2.565	2.707	2.819	2.507	2.568	2.702	2.856	2.599	2.483	2.750	2.897	2.448	2.580	2.673	2.840
	Variance	-1.6E-06	1.9E-06	3.4E-06	-2.8E-07	-3.6E-06	-1.1E-06	1.1E-06	1.7E-06	2.4E-06	2.9E-07	2.5E-06	-1.9E-06	-2.4E-06	2.5E-06	-6.8E-07	-3.5E-06
	Skewness	5.7E-06	-7.1E-06	-1.6E-05	1.4E-06	1.2E-05	4.0E-06	-9.6E-06	-5.0E-06	-6.5E-06	-2.4E-06	-9.3E-06	6.6E-06	1.2E-05	-7.3E-06	1.8E-06	9.2E-06
	Kurtosis	0.174	0.126	0.188	0.161	0.133	0.199	0.172	0.171	0.123	0.101	0.125	0.161	0.115	0.187	0.166	0.136
3 6	Mean	0.000	0.000	0.000	0.000	0.000	0.000	0.000	0.000	0.000	0.000	0.000	0.000	0.000	0.000	0.000	0.000
	Median	0.002	0.005	-0.003	0.006	-0.002	0.000	0.002	0.001	0.000	-0.007	0.003	-0.001	-0.003	-0.001	-0.007	-0.006
	Standard dev.	2.438	2.479	2.649	2.850	2.454	2.539	2.662	2.857	2.545	2.384	2.694	2.878	2.418	2.510	2.639	2.822
	Variance	1.5E-06	2.9E-06	-5.9E-07	6.3E-07	-3.1E-07	3.4E-08	-1.6E-06	1.7E-06	-4.3E-06	2.4E-06	-9.0E-06	3.0E-06	-8.0E-07	-5.0E-07	-3.4E-06	3.6E-07
	Skewness	3.1E-06	-3.8E-06	4.6E-06	-5.2E-06	8.2E-07	-3.6E-07	-1.0E-06	4.6E-06	-1.4E-05	1.1E-06	-1.9E-06	2.7E-06	-8.8E-06	-1.8E-05	-2.7E-05	-3.0E-06
	Kurtosis	0.643	0.608	0.806	0.750	0.840	0.788	0.777	0.740	0.653	0.700	0.711	0.725	0.700	0.836	0.735	0.724
3 7	Mean	0.000	0.000	0.000	0.000	0.000	0.000	0.000	0.000	0.000	0.000	0.000	0.000	0.000	0.000	0.000	0.000
	Median	-0.014	-0.006	-0.001	0.002	-0.001	-0.006	0.008	-0.009	-0.010	0.000	0.002	0.007	0.005	-0.009	-0.005	-0.002
	Standard dev.	2.477	2.521	2.685	2.867	2.500	2.581	2.698	2.844	2.566	2.442	2.730	2.897	2.437	2.558	2.668	2.838
	Variance	3.0E-06	-6.0E-07	-2.6E-06	9.8E-09	3.7E-06	1.6E-06	-1.9E-06	-1.9E-06	-1.4E-06	-2.0E-06	-7.7E-07	1.4E-06	-1.2E-06	-3.9E-07	-1.1E-06	8.5E-07
	Skewness	3.1E-02	3.7E-03	5.4E-03	-4.1E-03	3.9E-03	1.4E-02	7.1E-03	8.6E-03	2.0E-02	-1.1E-04	-7.6E-03	-5.8E-03	4.9E-03	4.8E-03	1.2E-02	8.3E-03
	Kurtosis	0.142	0.136	0.131	0.149	0.121	0.193	0.154	0.199	0.117	0.118	0.111	0.105	0.098	0.173	0.191	0.124
4 0	Mean	86.203	90.254	102.432	116.869	87.513	93.932	102.574	117.398	93.137	82.987	106.756	121.060	83.875	91.368	101.308	116.098
	Median	82.919	86.061	96.860	116.894	82.166	87.350	96.017	118.237	92.111	82.968	102.915	120.958	80.976	85.412	93.379	113.380
	Standard dev.	10.255	12.304	17.678	19.412	14.391	17.069	20.042	18.332	5.002	1.585	12.220	14.354	9.307	14.864	18.051	19.595
	Variance	8.4E+00	7.3E+00	5.8E+00	6.0E+00	6.1E+00	5.5E+00	5.1E+00	6.4E+00	1.9E+01	5.2E+01	8.7E+00	8.4E+00	9.0E+00	6.1E+00	5.6E+00	5.9E+00
	Skewness	2.0E+00	1.7E+00	8.7E-01	8.5E-02	2.1E+00	1.5E+00	8.3E-01	-1.0E-02	2.0E+00	3.4E-02	1.2E+00	1.4E-01	2.1E+00	1.8E+00	1.2E+00	3.0E-01
	Kurtosis	4.341	2.852	-0.164	-1.106	4.163	1.573	-0.342	-1.108	6.078	-0.037	0.865	-1.016	4.826	2.460	0.265	-1.179
4 1	Mean	0.000	0.000	0.000	0.000	0.000	0.000	0.000	0.000	0.000	0.000	0.000	0.000	0.000	0.000	0.000	0.000
	Median	0.013	0.010	-0.014	0.000	0.020	0.004	0.016	-0.009	0.011	-0.002	0.016	-0.002	0.022	0.014	0.009	0.004
	Standard dev.	4.307	4.566	4.942	4.596	4.409	4.872	5.283	4.152	2.983	1.615	4.115	3.490	4.208	3.546	4.176	4.206
	Variance	-1.4E-05	-6.8E-06	4.5E-06	1.5E-05	-8.9E-06	-4.0E-07	2.8E-06	-2.2E-05	-2.2E-05	-1.9E-05	-8.6E-06	-1.3E-05	1.6E-05	-8.3E-06	-1.0E-06	-5.7E-06
	Skewness	1.3E-02	1.8E-03	7.9E-03	6.8E-03	5.6E-03	1.6E-02	4.9E-03	6.3E-03	5.0E-02	8.4E-03	4.9E-03	8.4E-03	4.0E-02	-2.8E-02	1.2E-02	8.2E-04
	Kurtosis	1.139	0.788	0.527	0.527	1.364	0.617	0.441	0.491	2.578	0.122	0.377	0.513	2.078	1.551	0.852	0.797

Packet	Experiment	**97**	**98**	**99**	**100**	**101**	**102**	**103**	**104**	**105**	**106**	**107**	**108**	**109**	**110**	**111**	**112**
	V_{sg} (m/s)	0.15	0.59	1.31	0.16	0.31	0.60	1.34	0.16	0.32	0.61	1.25	0.15	0.30	0.60	1.33	0.15
Packet	V_{sl} (m/s)	0.66	0.66	0.66	0.69	0.69	0.69	0.69	0.72	0.72	0.72	0.72	0.76	0.76	0.76	0.76	0.80
	WC (%)	0.60	0.60	0.60	0.40	0.40	0.40	0.40	0.20	0.20	0.20	0.20	0.80	0.80	0.80	0.80	0.60
3 2	Mean	0.000	0.000	0.000	0.000	0.000	0.000	0.000	0.000	0.000	0.000	0.000	0.000	0.000	0.000	0.000	0.000
	Median	-0.002	0.005	0.002	0.000	0.001	0.001	0.002	0.002	0.006	0.001	0.001	-0.002	-0.002	0.000	0.002	0.002
	Standard dev.	2.413	2.647	2.837	2.438	2.527	2.670	2.849	2.464	2.546	2.690	2.871	2.365	2.482	2.608	2.828	2.417
	Variance	2.6E-06	-3.5E-06	4.4E-06	3.1E-06	7.6E-07	2.6E-06	-6.7E-06	-6.1E-06	-3.3E-06	9.3E-06	-6.3E-06	6.3E-06	2.9E-06	-1.3E-06	-5.9E-06	2.5E-07
	Skewness	-6.9E-07	-4.1E-06	3.0E-06	-8.1E-06	-1.7E-06	4.2E-06	-4.0E-05	-7.4E-05	8.7E-06	2.6E-05	-4.6E-05	2.9E-05	5.8E-07	3.7E-06	1.2E-05	-3.3E-06
	Kurtosis	0.704	0.705	0.722	0.756	0.723	0.764	0.714	0.707	0.675	0.713	0.702	0.740	0.821	0.745	0.774	0.727
3 3	Mean	0.000	0.000	0.000	0.000	0.000	0.000	0.000	0.000	0.000	0.000	0.000	0.000	0.000	0.000	0.000	0.000
	Median	0.005	-0.002	0.002	0.000	-0.003	0.003	0.005	0.003	-0.002	-0.002	-0.001	0.003	0.001	0.004	0.006	-0.002
	Standard dev.	2.483	2.873	3.114	2.491	2.704	2.900	3.063	2.464	2.644	2.840	3.089	2.426	2.532	2.736	3.039	2.486
	Variance	-5.6E-06	1.9E-06	-7.0E-06	2.6E-06	3.1E-06	-3.3E-06	-2.9E-07	-3.0E-06	-2.6E-06	-4.2E-07	4.3E-06	-1.2E-06	-2.6E-06	-9.1E-07	9.3E-07	-8.5E-07
	Skewness	1.6E-04	4.6E-06	3.0E-05	2.7E-05	1.1E-04	-1.4E-05	1.0E-04	8.7E-05	1.2E-04	9.0E-05	1.1E-04	8.1E-06	7.9E-05	5.1E-05	-5.6E-05	-5.2E-05
	Kurtosis	0.209	0.155	0.216	0.200	0.234	0.169	0.223	0.135	0.184	0.182	0.155	0.192	0.259	0.176	0.163	0.223
3 4	Mean	0.000	0.000	0.000	0.000	0.000	0.000	0.000	0.000	0.000	0.000	0.000	0.000	0.000	0.000	0.000	0.000
	Median	-0.004	0.001	-0.003	-0.003	-0.001	0.002	0.001	0.000	0.002	0.001	-0.001	0.000	0.000	-0.003	-0.002	0.002
	Standard dev.	2.487	2.692	2.848	2.521	2.584	2.666	2.849	2.551	2.622	2.725	2.871	2.493	2.550	2.700	2.843	2.533
	Variance	-4.4E-08	9.8E-07	-4.5E-07	-7.4E-07	1.6E-07	1.5E-07	1.5E-07	3.5E-07	1.2E-06	-1.2E-06	1.0E-06	-1.6E-07	-1.8E-06	3.2E-07	5.1E-07	9.8E-07
	Skewness	4.1E-08	-2.9E-06	1.3E-06	2.2E-06	-5.0E-07	-4.4E-07	-4.9E-07	-1.3E-06	-3.4E-06	3.9E-06	-3.2E-06	5.1E-07	5.3E-06	-9.1E-07	-1.5E-06	-2.9E-06
	Kurtosis	0.058	0.102	0.105	0.102	0.024	0.037	0.086	0.043	0.071	-0.003	0.087	0.056	0.019	0.142	0.095	-0.017
3 5	Mean	0.000	0.000	0.000	0.000	0.000	0.000	0.000	0.000	0.000	0.000	0.000	0.000	0.000	0.000	0.000	0.000
	Median	0.000	-0.001	0.006	-0.003	0.001	-0.001	-0.001	-0.005	0.001	0.001	-0.001	0.002	-0.002	-0.003	-0.001	0.002
	Standard dev.	2.473	2.662	2.829	2.484	2.601	2.689	2.859	2.546	2.594	2.726	2.876	2.442	2.545	2.642	2.799	2.500
	Variance	1.8E-07	-2.2E-06	1.7E-06	-2.0E-06	1.8E-07	-5.3E-07	4.1E-08	-9.5E-07	-3.6E-07	2.9E-06	-2.3E-06	9.5E-07	-8.7E-07	-1.9E-06	5.9E-07	-1.4E-06
	Skewness	-8.0E-07	7.6E-06	-7.8E-06	1.5E-05	-9.2E-08	1.6E-06	-5.1E-08	3.5E-06	3.8E-07	-7.9E-06	1.1E-05	-3.3E-06	5.3E-06	6.1E-06	-2.2E-06	9.0E-06
	Kurtosis	0.160	0.211	0.137	0.087	0.101	0.125	0.158	0.094	0.082	0.085	0.118	0.085	0.136	0.195	0.154	0.153
3 6	Mean	0.000	0.000	0.000	0.000	0.000	0.000	0.000	0.000	0.000	0.000	0.000	0.000	0.000	0.000	0.000	0.000
	Median	-0.003	0.001	0.002	-0.001	-0.004	-0.002	-0.002	-0.005	0.002	-0.002	0.002	0.001	0.003	-0.003	-0.004	0.002
	Standard dev.	2.422	2.609	2.796	2.445	2.508	2.650	2.845	2.472	2.545	2.668	2.850	2.405	2.486	2.598	2.799	2.425
	Variance	-1.7E-06	2.1E-06	-2.7E-06	-2.7E-06	-3.5E-06	2.3E-06	4.6E-06	4.2E-06	5.1E-06	-8.4E-06	4.1E-06	-3.4E-06	1.2E-06	1.9E-07	2.2E-06	-2.5E-06
	Skewness	5.1E-06	-4.1E-06	6.9E-06	6.4E-06	8.0E-06	7.3E-07	6.6E-05	1.7E-05	-1.1E-05	-6.6E-05	-9.2E-06	1.8E-06	-1.6E-07	-8.0E-06	1.4E-05	6.3E-06
	Kurtosis	0.759	0.773	0.784	0.676	0.794	0.774	0.738	0.724	0.753	0.757	0.703	0.683	0.713	0.811	0.723	0.711
3 7	Mean	0.000	0.000	0.000	0.000	0.000	0.000	0.000	0.000	0.000	0.000	0.000	0.000	0.000	0.000	0.000	0.000
	Median	-0.005	-0.004	-0.005	-0.010	-0.005	0.005	0.005	-0.001	-0.012	-0.010	-0.008	-0.004	0.004	-0.010	-0.001	0.006
	Standard dev.	2.474	2.635	2.825	2.492	2.555	2.639	2.821	2.506	2.572	2.684	2.866	2.440	2.518	2.638	2.809	2.476
	Variance	-6.2E-07	2.2E-07	-1.1E-06	2.9E-06	-3.6E-07	6.1E-08	-6.6E-08	1.2E-06	-2.3E-06	-3.9E-06	1.8E-06	-1.5E-07	2.5E-06	2.2E-06	-2.8E-07	1.7E-06
	Skewness	1.4E-02	2.7E-03	1.5E-03	1.4E-02	2.1E-02	7.9E-03	2.0E-03	-6.7E-03	1.3E-02	1.7E-02	1.3E-02	4.4E-03	-9.8E-04	1.1E-02	-1.3E-02	6.6E-03
	Kurtosis	0.114	0.199	0.171	0.143	0.180	0.179	0.147	0.139	0.095	0.134	0.122	0.115	0.174	0.187	0.152	0.147
4 0	Mean	85.319	100.833	114.833	86.221	92.376	100.805	115.101	88.197	94.713	104.286	118.496	83.074	89.979	99.582	114.290	84.368
	Median	82.357	95.121	114.045	83.260	88.169	95.663	115.187	87.085	92.155	100.653	117.415	80.539	84.655	91.869	110.380	81.656
	Standard dev.	9.600	17.219	19.476	9.812	12.930	15.488	17.853	4.818	8.725	11.535	14.085	8.265	13.850	17.307	19.295	8.889
	Variance	8.9E+00	5.9E+00	5.9E+00	8.8E+00	7.1E+00	6.5E+00	6.4E+00	1.8E+01	1.1E+01	9.0E+00	8.4E+00	1.0E+01	6.5E+00	5.8E+00	5.9E+00	9.5E+00
	Skewness	2.0E+00	1.0E+00	1.9E-01	2.1E+00	1.8E+00	1.1E+00	9.7E-02	1.7E+00	1.7E+00	1.3E+00	2.5E-01	2.0E+00	1.8E+00	1.3E+00	4.2E-01	1.9E+00
	Kurtosis	4.701	0.213	-1.072	5.244	3.237	0.573	-1.091	3.821	3.230	1.441	-0.971	4.243	2.737	0.697	-1.070	4.146
4 1	Mean	0.000	0.000	0.000	0.000	0.000	0.000	0.000	0.000	0.000	0.000	0.000	0.000	0.000	0.000	0.000	0.000
	Median	0.027	0.001	0.009	0.030	0.012	0.005	0.007	0.013	0.016	-0.001	-0.010	0.016	0.015	-0.007	0.010	0.012
	Standard dev.	4.489	5.167	4.666	4.538	4.767	4.893	4.173	3.448	4.253	4.169	3.669	4.413	3.989	3.977	4.215	4.714
	Variance	3.5E-05	8.5E-06	-1.2E-05	1.9E-05	-3.3E-05	-1.2E-06	-1.6E-05	-1.4E-05	-1.3E-05	-1.5E-05	-6.0E-08	-8.4E-06	-1.0E-05	-6.8E-07	-1.3E-05	2.2E-05
	Skewness	2.3E-02	1.6E-02	7.3E-03	2.9E-02	6.0E-03	1.8E-02	2.6E-03	5.4E-02	1.8E-02	1.1E-02	7.8E-03	3.3E-02	-2.0E-02	1.1E-02	1.5E-02	3.4E-02
	Kurtosis	1.453	0.404	0.667	1.348	0.703	0.392	0.647	2.159	0.992	0.457	0.493	2.101	1.550	0.926	0.754	1.540

Packet	Experiment	113	114	115	116	117	118	119	120	121	122	123	124	125	126
	V_{sg} (m/s)	0.23	0.62	1.32	0.16	0.32	0.60	1.33	0.15	0.32	0.66	1.32	0.15	0.31	0.60
	V_{sl} (m/s)	0.80	0.80	0.80	0.83	0.83	0.83	0.83	0.86	0.86	0.86	0.86	0.15	0.15	0.15
	WC (%)	0.60	0.60	0.60	0.40	0.40	0.40	0.40	0.20	0.20	0.20	0.20	0.00	0.00	0.00
3 2	Mean	0.000	0.000	0.000	0.000	0.000	0.000	0.000	0.000	0.000	0.000	0.000	0.000	0.000	0.000
	Median	0.002	-0.003	0.000	-0.002	0.001	0.009	0.003	0.001	-0.001	-0.002	0.000	-0.002	0.005	0.002
	Standard dev.	2.512	2.665	2.874	2.422	2.519	2.689	2.848	2.444	2.537	2.700	2.884	2.589	2.688	2.798
	Variance	-4.4E-06	2.1E-06	-6.7E-08	1.8E-06	2.2E-06	-1.6E-06	-5.1E-06	5.4E-06	-2.1E-06	7.2E-06	3.6E-07	-3.7E-06	6.1E-06	-2.8E-06
	Skewness	9.9E-06	-8.2E-07	1.7E-07	-4.3E-06	-5.5E-06	-1.1E-05	-1.5E-05	-1.4E-05	4.7E-06	1.4E-05	1.9E-07	7.5E-06	-8.7E-06	6.2E-06
	Kurtosis	0.801	0.761	0.798	0.762	0.734	0.743	0.719	0.747	0.728	0.714	0.689	0.726	0.666	0.678
3 3	Mean	0.000	0.000	0.000	0.000	0.000	0.000	0.000	0.000	0.000	0.000	0.000	0.000	0.000	0.000
	Median	-0.003	-0.001	-0.004	0.003	-0.002	0.001	-0.001	-0.003	0.002	0.003	0.004	-0.002	-0.007	0.002
	Standard dev.	2.668	2.900	3.116	2.540	2.735	2.955	3.133	2.461	2.656	2.898	3.115	2.574	2.713	2.857
	Variance	-4.8E-08	4.5E-06	4.5E-06	-3.5E-06	-2.7E-06	-4.0E-06	-3.1E-06	5.1E-07	1.5E-06	-1.9E-06	3.4E-07	-2.2E-06	-1.4E-06	6.3E-06
	Skewness	-1.7E-04	-7.5E-05	1.7E-05	3.8E-05	8.2E-05	9.2E-05	-6.6E-05	1.6E-05	8.7E-05	1.6E-05	6.0E-05	6.4E-05	-3.0E-05	6.1E-06
	Kurtosis	0.198	0.181	0.182	0.238	0.249	0.225	0.205	0.139	0.190	0.187	0.169	0.119	0.159	0.133
3 4	Mean	0.000	0.000	0.000	0.000	0.000	0.000	0.000	0.000	0.000	0.000	0.000	0.000	0.000	0.000
	Median	-0.002	0.000	-0.001	0.001	0.000	0.001	-0.001	-0.001	0.002	-0.001	0.000	0.002	-0.001	-0.002
	Standard dev.	2.564	2.668	2.846	2.521	2.561	2.694	2.829	2.540	2.607	2.726	2.858	2.686	2.797	2.882
	Variance	2.1E-07	-7.8E-07	-1.1E-06	-3.2E-07	1.8E-06	-5.7E-07	-1.8E-07	-8.9E-07	6.1E-07	1.6E-06	-3.2E-08	1.4E-06	-6.7E-07	4.2E-07
	Skewness	-7.2E-07	2.5E-06	3.3E-06	8.2E-07	-5.4E-06	1.8E-06	5.3E-07	2.8E-06	-1.7E-06	-4.9E-06	7.0E-08	-4.0E-06	2.2E-06	-1.3E-06
	Kurtosis	0.091	0.093	0.108	0.026	0.033	0.062	0.053	0.053	0.019	0.092	0.072	0.044	0.056	0.058
3 5	Mean	0.000	0.000	0.000	0.000	0.000	0.000	0.000	0.000	0.000	0.000	0.000	0.000	0.000	0.000
	Median	0.003	-0.005	0.001	-0.007	-0.003	0.007	-0.003	-0.005	-0.005	-0.005	0.000	0.004	0.006	-0.001
	Standard dev.	2.561	2.641	2.840	2.499	2.555	2.678	2.831	2.532	2.587	2.717	2.837	2.670	2.777	2.886
	Variance	8.7E-07	2.4E-06	-4.6E-07	2.2E-07	-4.6E-06	1.0E-06	-1.7E-06	-4.3E-07	-1.9E-06	-2.2E-06	-1.3E-06	-2.4E-06	-2.6E-07	1.1E-07
	Skewness	-8.3E-06	-6.6E-06	3.1E-06	-1.0E-05	1.6E-05	-2.9E-06	6.8E-06	7.0E-06	8.7E-06	6.3E-06	4.9E-06	6.1E-06	8.1E-07	-3.1E-07
	Kurtosis	0.147	0.161	0.118	0.088	0.089	0.128	0.143	0.082	0.098	0.138	0.109	0.100	0.140	0.127
3 6	Mean	0.000	0.000	0.000	0.000	0.000	0.000	0.000	0.000	0.000	0.000	0.000	0.000	0.000	0.000
	Median	-0.002	0.001	0.003	0.001	-0.007	0.000	0.001	0.001	-0.002	-0.001	0.003	-0.001	0.001	0.001
	Standard dev.	2.498	2.636	2.834	2.444	2.520	2.627	2.850	2.463	2.519	2.697	2.843	2.619	2.737	2.846
	Variance	3.0E-06	-3.6E-06	7.4E-07	-1.9E-06	2.5E-07	1.3E-06	2.7E-06	-3.5E-06	9.7E-07	-4.2E-06	-8.9E-07	4.7E-06	-5.8E-06	2.2E-06
	Skewness	2.0E-05	1.4E-05	-7.9E-06	-1.5E-05	8.6E-07	-2.8E-05	-6.9E-06	-5.6E-07	-2.4E-06	-1.5E-05	2.6E-06	-1.1E-05	-5.7E-05	-6.1E-06
	Kurtosis	0.782	0.732	0.747	0.743	0.794	0.765	0.782	0.643	0.698	0.765	0.760	0.785	0.683	0.686
3 7	Mean	0.000	0.000	0.000	0.000	0.000	0.000	0.000	0.000	0.000	0.000	0.000	0.000	0.000	0.000
	Median	-0.001	-0.005	0.005	-0.002	-0.005	0.006	-0.004	-0.009	0.001	-0.002	-0.006	-0.010	-0.016	0.001
	Standard dev.	2.545	2.656	2.839	2.471	2.572	2.649	2.790	2.486	2.557	2.668	2.854	2.645	2.765	2.864
	Variance	-7.3E-07	2.2E-07	-2.1E-07	1.9E-06	2.2E-06	3.0E-06	2.8E-06	1.2E-06	3.3E-07	8.3E-08	1.3E-06	1.2E-06	1.3E-06	-1.6E-06
	Skewness	5.3E-03	1.2E-02	-1.2E-02	9.2E-03	6.8E-03	-8.1E-04	3.7E-03	5.6E-03	4.8E-03	-9.7E-03	1.4E-03	1.4E-02	2.0E-02	3.9E-03
	Kurtosis	0.137	0.154	0.198	0.137	0.126	0.099	0.115	0.147	0.119	0.122	0.072	0.063	0.120	0.117
4 0	Mean	90.575	99.230	113.472	85.896	91.426	99.666	113.669	87.248	93.678	103.442	116.157	100.698	109.828	120.147
	Median	85.960	93.427	111.827	83.319	87.471	94.543	112.872	86.285	91.335	99.734	114.180	97.833	106.107	117.952
	Standard dev.	13.208	16.754	19.469	8.830	12.275	15.136	17.721	4.601	8.165	11.556	13.404	9.316	11.438	11.911
	Variance	6.9E+00	5.9E+00	5.8E+00	9.7E+00	7.4E+00	6.6E+00	6.4E+00	1.9E+01	1.1E+01	9.0E+00	8.7E+00	1.1E+01	9.6E+00	1.0E+01
	Skewness	1.6E+00	1.1E+00	2.7E-01	2.0E+00	1.8E+00	1.2E+00	2.0E-01	1.6E+00	1.6E+00	1.4E+00	4.4E-01	2.2E+00	1.4E+00	5.6E-01
	Kurtosis	2.543	0.530	-1.050	4.744	3.233	0.873	-1.061	3.953	2.749	1.513	-0.736	5.275	1.479	-0.474
4 1	Mean	0.000	0.000	0.000	0.000	0.000	0.000	0.000	0.000	0.000	0.000	0.000	0.000	0.000	0.000
	Median	0.018	0.024	0.012	0.019	0.026	-0.006	-0.007	0.019	0.032	0.006	0.013	0.001	0.008	-0.008
	Standard dev.	5.020	5.328	4.840	4.764	4.794	4.981	4.242	3.352	4.521	4.295	3.804	2.617	3.216	3.298
	Variance	2.5E-05	1.5E-06	-4.9E-06	1.2E-05	-2.2E-05	-9.7E-06	-7.6E-06	-2.2E-06	2.5E-06	1.2E-05	-2.7E-05	-4.9E-06	-5.9E-06	-1.6E-06
	Skewness	-3.1E-03	1.4E-02	2.9E-03	3.1E-02	2.5E-04	1.2E-02	1.1E-02	3.1E-02	3.9E-02	-1.7E-03	7.4E-03	-1.3E-02	6.1E-03	-1.1E-03
	Kurtosis	0.714	0.447	0.447	1.386	0.649	0.326	0.430	2.199	1.147	0.454	0.425	1.014	0.398	0.520

D.4 Wavelet Packet Coefficient Statistics: Packets [4 2] – [4 9]

Packet	Experiment	1	2	3	4	5	6	7	8	9	10	11	12	13	14	15	16
	V_{sg} (m/s)	0.13	0.30	0.58	0.99	0.13	0.30	0.59	1.32	0.13	0.30	0.59	1.32	0.13	0.31	0.59	1.29
	V_{sl} (m/s)	0.12	0.12	0.12	0.12	0.24	0.24	0.24	0.24	0.37	0.37	0.37	0.37	0.49	0.49	0.49	0.49
	WC (%)	1.00	1.00	1.00	1.00	1.00	1.00	1.00	1.00	1.00	1.00	1.00	1.00	1.00	1.00	1.00	1.00
4 2	Mean	0.000	0.000	0.000	0.000	0.000	0.000	0.000	0.000	0.000	0.000	0.000	0.000	0.000	0.000	0.000	0.000
	Median	0.002	-0.002	0.000	0.001	0.000	0.003	0.001	0.000	0.002	0.000	0.002	0.000	0.000	0.001	-0.001	0.002
	Standard dev.	1.771	1.946	2.199	2.368	1.724	1.917	2.150	2.344	1.736	1.868	2.071	2.306	1.737	1.890	2.051	2.298
	Variance	4.4E-06	6.1E-06	1.1E-05	-1.6E-06	-3.9E-07	3.3E-06	-4.7E-06	2.9E-06	5.6E-06	6.0E-06	5.5E-07	-3.4E-06	2.9E-06	6.5E-06	1.8E-06	1.3E-06
	Skewness	1.7E-06	-4.9E-06	-2.9E-05	3.5E-06	-1.8E-05	4.9E-07	-1.3E-05	-8.2E-07	-9.6E-06	-1.3E-05	-1.5E-06	9.5E-06	1.7E-05	-2.2E-05	-5.1E-06	-1.9E-06
	Kurtosis	0.502	0.717	0.463	0.514	0.524	0.527	0.478	0.471	0.422	0.613	0.474	0.417	0.353	0.611	0.529	0.455
4 3	Mean	0.000	0.000	0.000	0.000	0.000	0.000	0.000	0.000	0.000	0.000	0.000	0.000	0.000	0.000	0.000	0.000
	Median	0.000	0.002	0.001	0.003	0.003	0.003	0.001	0.003	0.000	0.002	0.000	0.001	0.000	0.001	-0.004	0.001
	Standard dev.	1.891	2.205	2.521	2.723	1.892	2.167	2.499	2.695	1.930	2.105	2.371	2.701	2.017	2.174	2.406	2.696
	Variance	-1.6E-05	-4.9E-07	-1.2E-05	-1.0E-06	-8.6E-07	-7.8E-06	1.7E-05	-3.8E-06	-3.4E-06	1.1E-05	-1.6E-06	-1.9E-05	3.7E-06	8.0E-06	4.6E-06	-8.8E-06
	Skewness	-2.1E-04	-1.0E-04	-1.6E-04	1.8E-04	-2.3E-05	-6.5E-05	1.8E-04	1.5E-05	1.3E-04	2.5E-04	-1.7E-04	-1.4E-04	-1.4E-04	-8.1E-05	-1.6E-04	-8.1E-06
	Kurtosis	0.625	0.541	0.329	0.344	0.600	0.502	0.350	0.240	0.654	0.632	0.413	0.453	0.813	0.733	0.460	0.302
4 4	Mean	0.000	0.000	0.000	0.000	0.000	0.000	0.000	0.000	0.000	0.000	0.000	0.000	0.000	0.000	0.000	0.000
	Median	0.000	0.002	-0.002	-0.002	-0.001	0.000	-0.001	0.000	-0.001	-0.001	0.000	0.000	0.000	0.001	0.000	-0.001
	Standard dev.	1.740	1.846	1.977	2.140	1.711	1.816	1.947	2.087	1.705	1.815	1.902	2.061	1.686	1.774	1.873	2.048
	Variance	-3.3E-06	-2.4E-06	2.0E-07	-4.8E-06	-1.5E-06	-1.3E-06	1.4E-06	7.8E-06	-8.0E-07	1.1E-05	-2.6E-06	3.1E-06	-1.2E-06	-1.1E-06	-4.1E-06	-1.8E-06
	Skewness	-3.0E-05	3.5E-06	-1.5E-06	-1.1E-04	-1.3E-05	4.0E-06	-3.6E-06	-8.3E-06	3.3E-06	6.5E-05	-5.8E-05	-9.1E-06	-2.3E-07	1.6E-06	4.2E-06	2.2E-06
	Kurtosis	2.016	2.041	1.923	1.800	1.807	1.873	2.003	1.916	1.782	1.885	2.007	1.881	1.787	2.012	1.927	1.933
4 5	Mean	0.000	0.000	0.000	0.000	0.000	0.000	0.000	0.000	0.000	0.000	0.000	0.000	0.000	0.000	0.000	0.000
	Median	-0.002	0.000	0.003	0.003	0.004	0.000	0.003	0.001	0.007	0.000	0.002	-0.001	0.001	-0.002	0.001	-0.002
	Standard dev.	1.743	1.856	1.974	2.128	1.696	1.827	1.912	2.114	1.693	1.808	1.908	2.082	1.699	1.763	1.905	2.042
	Variance	-7.6E-06	1.0E-07	2.4E-06	5.1E-06	-6.8E-06	-7.3E-07	-1.2E-06	-3.2E-07	2.1E-06	-3.9E-06	-7.3E-07	-6.3E-06	-3.3E-06	2.0E-06	-1.1E-06	4.9E-06
	Skewness	-1.5E-06	-5.0E-07	-4.3E-06	-1.0E-05	-6.3E-06	2.2E-06	-1.4E-07	-5.9E-07	-2.0E-06	-1.4E-05	2.2E-06	8.0E-06	7.1E-06	-6.0E-06	4.5E-06	-2.5E-06
	Kurtosis	0.291	0.236	0.322	0.230	0.221	0.228	0.269	0.219	0.275	0.250	0.246	0.228	0.235	0.244	0.242	0.219
4 6	Mean	0.000	0.000	0.000	0.000	0.000	0.000	0.000	0.000	0.000	0.000	0.000	0.000	0.000	0.000	0.000	0.000
	Median	-0.001	-0.002	0.001	-0.002	0.003	0.000	-0.001	0.000	0.001	0.004	0.000	0.004	0.000	0.001	0.002	0.000
	Standard dev.	1.713	1.904	2.060	2.230	1.704	1.865	2.036	2.190	1.684	1.824	1.976	2.159	1.679	1.805	1.968	2.172
	Variance	-8.8E-07	5.7E-06	-5.4E-06	2.4E-06	-3.6E-06	1.0E-06	4.1E-06	-2.4E-06	-8.0E-06	-3.1E-06	-3.2E-06	9.9E-06	-9.3E-07	-8.9E-06	-6.0E-07	3.4E-06
	Skewness	-3.3E-06	-5.4E-06	-2.1E-06	-6.2E-06	1.1E-05	-1.7E-05	-7.2E-06	1.0E-06	8.4E-06	4.9E-06	6.3E-06	-4.0E-06	2.7E-06	2.1E-05	1.8E-06	2.2E-05
	Kurtosis	0.437	0.504	0.442	0.380	0.495	0.546	0.462	0.369	0.458	0.640	0.430	0.437	0.337	0.448	0.529	0.364
4 7	Mean	0.000	0.000	0.000	0.000	0.000	0.000	0.000	0.000	0.000	0.000	0.000	0.000	0.000	0.000	0.000	0.000
	Median	0.000	-0.001	-0.001	-0.002	0.001	-0.002	-0.001	0.000	-0.002	0.001	-0.001	0.000	0.000	0.000	0.002	0.000
	Standard dev.	1.705	1.869	1.984	2.176	1.700	1.802	1.967	2.126	1.680	1.780	1.942	2.123	1.661	1.787	1.914	2.101
	Variance	1.0E-05	-6.4E-06	6.2E-07	-2.9E-06	4.7E-06	-8.6E-08	2.7E-06	1.1E-06	2.5E-07	-4.9E-07	2.7E-06	3.7E-06	4.7E-06	-8.0E-07	2.3E-06	-4.5E-06
	Skewness	7.3E-05	3.0E-05	3.2E-05	7.0E-05	-3.5E-05	3.4E-05	4.3E-05	-4.3E-05	-1.6E-05	3.8E-05	-3.9E-05	-4.9E-05	6.5E-05	-2.3E-05	4.6E-06	6.8E-05
	Kurtosis	0.184	0.195	0.222	0.103	0.105	0.183	0.128	0.110	0.041	0.160	0.157	0.109	0.149	0.160	0.187	0.148
4 8	Mean	0.000	0.000	0.000	0.000	0.000	0.000	0.000	0.000	0.000	0.000	0.000	0.000	0.000	0.000	0.000	0.000
	Median	0.001	-0.001	0.000	0.000	0.000	-0.002	-0.001	-0.002	-0.001	0.001	0.001	0.002	0.000	-0.002	0.000	0.000
	Standard dev.	1.814	1.910	2.026	2.160	1.819	1.912	1.978	2.097	1.786	1.853	1.971	2.087	1.755	1.846	1.937	2.067
	Variance	4.0E-07	-1.5E-06	-9.7E-07	-7.9E-07	1.3E-06	8.0E-07	6.3E-07	7.6E-07	-1.7E-06	8.3E-07	-1.4E-06	-6.3E-07	4.7E-07	-5.9E-07	-1.8E-07	1.8E-06
	Skewness	-1.1E-06	4.3E-06	3.0E-06	2.0E-06	-3.9E-06	-1.9E-06	-2.0E-06	-2.3E-06	4.7E-06	-2.2E-06	4.2E-06	1.8E-06	-1.4E-06	1.7E-06	6.7E-07	-4.7E-06
	Kurtosis	-0.038	0.120	0.059	0.061	0.040	-0.005	0.054	0.115	0.025	0.090	0.088	0.027	0.041	0.094	0.109	0.092
4 9	Mean	0.000	0.000	0.000	0.000	0.000	0.000	0.000	0.000	0.000	0.000	0.000	0.000	0.000	0.000	0.000	0.000
	Median	-0.003	0.001	0.002	0.000	0.001	0.000	0.000	-0.003	0.000	0.000	0.000	0.001	0.003	0.002	0.001	0.002
	Standard dev.	1.819	1.894	2.016	2.162	1.796	1.900	1.992	2.092	1.783	1.882	1.972	2.080	1.767	1.871	1.968	2.045
	Variance	-1.0E-06	1.2E-06	6.0E-07	1.2E-06	-5.8E-07	-2.6E-07	-9.8E-07	-1.2E-06	2.6E-06	-5.8E-08	-7.9E-08	-3.3E-07	1.3E-07	-8.3E-07	-4.7E-07	-1.3E-06
	Skewness	2.6E-06	-3.5E-06	-1.7E-06	-3.5E-06	1.7E-06	8.2E-07	2.6E-06	3.4E-06	-7.5E-06	4.1E-08	2.2E-07	1.0E-06	-4.2E-07	1.2E-06	1.4E-06	3.3E-06
	Kurtosis	0.133	0.111	0.196	0.132	0.156	0.239	0.149	0.105	0.140	0.113	0.081	0.143	0.074	0.191	0.171	0.132

Packet	Experiment	17	18	19	20	21	22	23	24	25	26	27	28	29	30	31	32
	V_{sg} (m/s)	0.15	0.30	0.59	1.32	0.15	0.31	0.59	1.33	0.15	0.30	0.59	1.32	0.15	0.30	0.59	1.00
	V_{sl} (m/s)	0.61	0.61	0.61	0.61	0.73	0.73	0.73	0.73	0.79	0.79	0.79	0.79	0.13	0.13	0.13	0.13
	WC (%)	1.00	1.00	1.00	1.00	1.00	1.00	1.00	1.00	1.00	1.00	1.00	1.00	0.80	0.80	0.80	0.80
4 2	Mean	0.000	0.000	0.000	0.000	0.000	0.000	0.000	0.000	0.000	0.000	0.000	0.000	0.000	0.000	0.000	0.000
	Median	-0.004	-0.001	-0.002	0.000	0.003	0.001	0.001	-0.002	-0.002	0.001	-0.003	0.003	0.001	-0.001	0.002	0.002
	Standard dev.	1.797	1.905	2.012	2.340	1.804	1.909	2.104	2.339	1.846	1.950	2.047	2.327	1.822	2.009	2.287	2.394
	Variance	6.1E-06	-9.5E-07	-3.4E-07	-5.9E-06	-2.2E-06	-3.1E-06	-3.9E-06	-2.2E-06	5.9E-06	-3.3E-06	-2.9E-06	-1.4E-06	-1.0E-05	1.8E-05	4.6E-06	-1.5E-06
	Skewness	8.6E-06	5.0E-06	6.6E-07	1.3E-05	3.3E-06	8.3E-06	8.3E-06	6.2E-06	-1.1E-05	-1.4E-05	5.7E-06	3.5E-06	1.4E-05	-1.0E-05	-1.1E-05	1.5E-07
	Kurtosis	0.472	0.485	0.452	0.486	0.525	0.615	0.570	0.440	0.692	0.664	0.513	0.385	0.554	0.592	0.447	0.455
4 3	Mean	0.000	0.000	0.000	0.000	0.000	0.000	0.000	0.000	0.000	0.000	0.000	0.000	0.000	0.000	0.000	0.000
	Median	0.002	0.000	0.001	0.000	-0.001	0.000	0.000	0.001	-0.001	0.003	-0.002	-0.001	-0.001	0.002	0.001	0.002
	Standard dev.	2.069	2.214	2.330	2.710	2.254	2.263	2.419	2.717	2.391	2.339	2.412	2.712	2.048	2.397	2.795	2.847
	Variance	4.9E-06	-3.0E-05	1.6E-06	1.7E-05	5.4E-06	3.0E-06	-4.7E-07	-9.1E-06	-5.5E-06	9.9E-06	-3.1E-06	-1.3E-05	1.7E-06	-1.8E-05	9.6E-06	6.4E-06
	Skewness	-8.2E-05	2.2E-05	-3.9E-05	-1.6E-04	3.8E-05	1.1E-04	1.9E-04	1.7E-04	2.2E-04	1.3E-04	2.5E-05	2.1E-04	1.5E-04	1.5E-04	-5.6E-05	-1.6E-05
	Kurtosis	1.009	0.847	0.480	0.393	1.663	0.858	0.570	0.397	1.583	1.089	0.671	0.497	0.575	0.653	0.602	0.341
4 4	Mean	0.000	0.000	0.000	0.000	0.000	0.000	0.000	0.000	0.000	0.000	0.000	0.000	0.000	0.000	0.000	0.000
	Median	-0.001	0.000	-0.001	0.000	0.001	-0.002	-0.001	0.000	0.002	-0.001	-0.001	-0.001	0.000	0.001	0.001	-0.001
	Standard dev.	1.696	1.770	1.873	2.039	1.683	1.727	1.879	2.038	1.686	1.755	1.849	2.005	1.786	1.892	2.011	2.130
	Variance	-8.9E-07	2.7E-06	-1.3E-05	-1.3E-06	4.4E-07	-3.3E-06	4.7E-06	8.7E-06	2.4E-06	-4.2E-06	1.6E-06	2.7E-06	-6.2E-06	9.7E-06	4.2E-06	7.2E-07
	Skewness	2.6E-06	-4.9E-06	-9.8E-05	3.0E-06	-1.6E-06	-8.4E-06	-5.0E-06	1.7E-04	3.9E-06	3.0E-07	1.1E-05	5.7E-06	1.2E-05	9.2E-06	3.7E-05	-1.8E-06
	Kurtosis	1.896	1.857	2.000	1.832	1.897	1.788	1.937	1.963	1.804	1.843	1.894	1.937	1.987	2.182	1.901	1.897
4 5	Mean	0.000	0.000	0.000	0.000	0.000	0.000	0.000	0.000	0.000	0.000	0.000	0.000	0.000	0.000	0.000	0.000
	Median	-0.005	0.002	-0.001	0.002	-0.003	0.001	0.000	0.001	0.002	0.003	0.000	-0.001	-0.004	0.004	0.005	-0.002
	Standard dev.	1.688	1.769	1.882	2.061	1.676	1.759	1.875	2.062	1.689	1.742	1.832	2.037	1.776	1.865	1.996	2.121
	Variance	2.7E-06	1.3E-06	-1.1E-06	5.0E-06	2.8E-06	-2.4E-06	-1.0E-06	9.5E-07	-9.4E-08	4.6E-06	1.6E-06	-2.5E-06	4.3E-06	-1.7E-06	-4.6E-06	3.3E-06
	Skewness	-3.9E-06	-2.8E-06	-5.5E-06	-1.3E-05	-2.7E-06	6.8E-06	-1.7E-05	-2.4E-06	-2.2E-07	-6.3E-06	1.4E-05	-2.9E-06	6.0E-06	2.1E-06	1.1E-05	-6.4E-06
	Kurtosis	0.248	0.149	0.243	0.294	0.204	0.168	0.268	0.167	0.290	0.270	0.221	0.283	0.167	0.303	0.284	0.320
4 6	Mean	0.000	0.000	0.000	0.000	0.000	0.000	0.000	0.000	0.000	0.000	0.000	0.000	0.000	0.000	0.000	0.000
	Median	0.002	0.000	-0.001	-0.004	0.001	-0.002	0.003	0.000	0.000	-0.001	0.002	0.000	0.001	-0.002	0.002	0.000
	Standard dev.	1.682	1.831	1.970	2.169	1.694	1.812	1.978	2.170	1.760	1.811	1.941	2.193	1.777	1.916	2.093	2.259
	Variance	4.8E-07	2.9E-06	-2.0E-06	1.4E-08	4.3E-06	-2.8E-07	-1.5E-06	9.6E-07	-2.8E-06	1.4E-06	-4.1E-06	1.1E-06	9.6E-06	-1.8E-05	-3.7E-06	5.2E-06
	Skewness	-1.4E-06	-7.3E-06	1.0E-05	1.1E-07	1.3E-05	7.2E-07	4.2E-06	-2.9E-06	3.5E-06	1.7E-05	-3.8E-05	3.9E-06	6.2E-05	-1.2E-04	7.5E-06	1.3E-07
	Kurtosis	0.505	0.551	0.483	0.419	0.460	0.382	0.477	0.541	0.441	0.565	0.454	0.511	0.457	0.421	0.518	0.476
4 7	Mean	0.000	0.000	0.000	0.000	0.000	0.000	0.000	0.000	0.000	0.000	0.000	0.000	0.000	0.000	0.000	0.000
	Median	0.002	0.001	0.001	0.001	0.001	0.000	0.001	-0.001	0.000	-0.002	-0.002	0.001	0.000	0.000	0.000	0.001
	Standard dev.	1.693	1.760	1.896	2.097	1.669	1.766	1.899	2.111	1.719	1.778	1.886	2.094	1.773	1.892	2.040	2.135
	Variance	9.3E-07	-3.9E-06	5.4E-06	-7.4E-07	-3.8E-06	1.1E-06	1.8E-06	1.3E-06	-1.9E-06	-6.4E-06	-2.2E-06	2.6E-06	-3.4E-06	4.4E-06	5.2E-06	-3.6E-06
	Skewness	-4.0E-06	2.0E-05	5.3E-06	-5.9E-05	1.5E-05	-9.5E-06	-2.3E-05	1.5E-05	9.9E-06	-2.3E-05	-2.6E-05	2.8E-05	1.3E-04	-2.1E-05	5.9E-05	-2.8E-05
	Kurtosis	0.089	0.145	0.209	0.099	0.107	0.279	0.217	0.077	0.116	0.114	0.202	0.146	0.168	0.175	0.226	0.204
4 8	Mean	0.000	0.000	0.000	0.000	0.000	0.000	0.000	0.000	0.000	0.000	0.000	0.000	0.000	0.000	0.000	0.000
	Median	-0.001	0.000	0.000	0.001	0.002	-0.002	-0.001	0.000	0.001	0.000	-0.001	0.000	0.001	0.001	0.000	0.001
	Standard dev.	1.743	1.832	1.929	2.043	1.724	1.784	1.907	2.030	1.771	1.816	1.912	2.037	1.846	1.958	2.031	2.150
	Variance	-4.8E-07	1.1E-06	-1.2E-06	3.9E-07	4.0E-07	6.0E-07	-1.2E-06	-1.8E-06	4.8E-08	-4.4E-07	1.5E-06	1.5E-06	-1.7E-07	1.6E-06	-2.5E-06	6.8E-07
	Skewness	1.3E-06	-3.2E-06	3.2E-06	-1.1E-06	-1.3E-06	-1.8E-06	3.7E-06	5.3E-06	-2.3E-07	1.2E-06	-4.4E-06	-3.5E-06	4.1E-07	-4.4E-06	6.5E-06	-2.1E-06
	Kurtosis	0.113	0.016	0.105	0.186	0.120	0.044	0.008	0.001	0.008	0.026	0.072	0.045	0.032	0.112	0.110	0.138
4 9	Mean	0.000	0.000	0.000	0.000	0.000	0.000	0.000	0.000	0.000	0.000	0.000	0.000	0.000	0.000	0.000	0.000
	Median	-0.001	-0.003	-0.003	-0.001	0.003	0.000	-0.001	0.002	-0.002	0.001	-0.002	0.000	-0.001	0.000	0.002	0.000
	Standard dev.	1.751	1.836	1.944	2.067	1.741	1.797	1.910	2.067	1.770	1.820	1.910	2.027	1.852	1.939	2.019	2.146
	Variance	-8.7E-07	-2.1E-07	2.7E-06	-7.0E-07	-2.2E-06	-2.0E-06	1.0E-06	4.3E-06	-1.7E-06	2.8E-06	-1.2E-06	-3.1E-07	1.1E-06	-3.5E-06	2.9E-06	-1.5E-06
	Skewness	2.7E-06	5.4E-07	-6.5E-06	2.1E-06	5.7E-06	5.5E-06	-3.2E-06	-1.1E-05	5.2E-06	-7.9E-06	3.6E-06	1.5E-06	-3.1E-06	5.8E-06	-9.5E-06	4.6E-06
	Kurtosis	0.083	0.101	0.113	0.094	0.109	0.181	0.156	0.168	0.076	0.155	0.126	0.179	0.189	0.196	0.193	0.149

Packet	Experiment	33	34	35	36	37	38	39	40	41	42	43	44	45	46	47	48
	V_{sg} (m/s)	0.15	0.30	0.59	1.00	0.15	0.30	0.59	1.00	0.15	0.30	0.59	1.00	0.15	0.31	0.59	1.33
	V_{sl} (m/s)	0.13	0.13	0.13	0.13	0.14	0.14	0.14	0.14	0.14	0.14	0.14	0.14	0.25	0.25	0.25	0.25
	WC (%)	0.60	0.60	0.60	0.60	0.40	0.40	0.40	0.40	0.20	0.20	0.20	0.20	0.80	0.80	0.80	0.80
4 2	Mean	0.000	0.000	0.000	0.000	0.000	0.000	0.000	0.000	0.000	0.000	0.000	0.000	0.000	0.000	0.000	0.000
	Median	0.001	0.002	0.001	-0.001	0.004	-0.002	-0.001	-0.001	-0.002	-0.003	-0.002	-0.001	0.001	-0.002	0.001	0.003
	Standard dev.	1.883	2.086	2.326	2.457	1.895	2.121	2.363	2.538	1.911	2.053	2.195	2.293	1.783	1.957	2.163	2.364
	Variance	-2.3E-06	1.9E-06	1.2E-05	2.4E-06	-1.6E-06	1.7E-06	-3.5E-06	-1.7E-06	-7.9E-06	-1.0E-05	-3.2E-06	3.1E-06	-1.9E-06	-1.7E-06	4.2E-06	-6.0E-06
	Skewness	2.8E-06	-7.9E-06	-2.0E-05	-5.6E-06	4.0E-06	-3.9E-06	8.2E-06	-2.2E-05	7.5E-06	1.4E-05	4.5E-06	-6.1E-06	-1.2E-06	3.4E-06	-1.1E-05	1.5E-05
	Kurtosis	0.438	0.529	0.458	0.537	0.524	0.554	0.475	0.512	0.354	0.321	0.411	0.411	0.590	0.439	0.662	0.455
4 3	Mean	0.000	0.000	0.000	0.000	0.000	0.000	0.000	0.000	0.000	0.000	0.000	0.000	0.000	0.000	0.000	0.000
	Median	0.002	-0.001	0.004	0.002	0.002	-0.002	-0.003	-0.006	-0.004	-0.001	-0.002	-0.002	0.005	0.001	-0.001	0.000
	Standard dev.	2.268	2.592	2.893	2.998	2.288	2.675	3.036	3.192	2.165	2.426	2.571	2.638	1.958	2.301	2.622	2.856
	Variance	8.4E-06	4.8E-06	7.4E-07	2.5E-05	1.1E-05	-1.3E-05	7.2E-06	2.6E-06	-7.3E-06	-4.0E-06	2.9E-06	-1.2E-05	-6.9E-07	-9.6E-07	6.8E-06	-7.6E-06
	Skewness	-1.9E-04	2.1E-05	-2.5E-04	1.0E-04	-1.1E-04	-6.5E-06	-1.2E-04	1.8E-05	-2.1E-04	8.1E-05	-4.6E-05	1.9E-05	-1.5E-04	2.8E-05	1.3E-05	-1.0E-05
	Kurtosis	0.478	0.373	0.382	0.429	1.000	0.581	0.427	0.459	0.326	0.264	0.234	0.300	0.660	0.523	0.378	0.347
4 4	Mean	0.000	0.000	0.000	0.000	0.000	0.000	0.000	0.000	0.000	0.000	0.000	0.000	0.000	0.000	0.000	0.000
	Median	0.000	0.000	-0.001	-0.001	0.001	0.000	-0.002	0.000	-0.002	0.000	0.002	0.001	0.000	0.001	0.001	-0.001
	Standard dev.	1.786	1.859	1.962	2.089	1.817	1.880	1.962	2.103	1.823	1.916	2.040	2.101	1.734	1.797	1.909	2.050
	Variance	4.4E-06	4.3E-06	-1.0E-06	-2.4E-06	-5.8E-06	3.1E-06	4.2E-08	-2.7E-06	-2.9E-06	-2.3E-06	1.5E-06	-2.7E-06	-5.0E-07	-3.8E-06	1.4E-06	5.1E-06
	Skewness	-1.1E-05	-1.0E-05	6.7E-07	1.8E-06	1.2E-05	-6.4E-06	-5.9E-06	6.2E-06	-7.1E-07	1.3E-06	-2.4E-06	-2.3E-05	1.5E-06	1.1E-05	-3.5E-06	-7.3E-07
	Kurtosis	1.876	1.986	1.894	1.915	2.029	2.084	1.982	2.003	2.072	1.782	1.902	1.802	1.859	1.953	1.930	1.808
4 5	Mean	0.000	0.000	0.000	0.000	0.000	0.000	0.000	0.000	0.000	0.000	0.000	0.000	0.000	0.000	0.000	0.000
	Median	-0.005	-0.003	0.004	0.002	0.002	-0.001	-0.001	-0.001	0.002	-0.001	0.004	0.001	-0.006	-0.002	-0.002	-0.004
	Standard dev.	1.786	1.865	1.943	2.125	1.789	1.890	1.995	2.122	1.843	1.923	2.011	2.096	1.702	1.799	1.908	2.045
	Variance	4.3E-06	4.2E-06	3.9E-06	-3.4E-06	3.0E-06	-2.8E-07	7.2E-06	-1.6E-06	3.6E-06	3.4E-06	-1.4E-06	-1.9E-06	2.0E-06	-1.5E-06	-3.5E-06	-1.6E-07
	Skewness	-9.3E-06	-7.3E-06	-6.4E-06	-2.4E-06	-5.2E-06	7.4E-06	1.7E-05	2.6E-06	3.5E-05	-6.6E-06	3.2E-05	6.1E-06	-5.6E-06	1.9E-06	-2.8E-06	8.2E-07
	Kurtosis	0.174	0.393	0.193	0.268	0.283	0.211	0.282	0.293	0.200	0.186	0.257	0.192	0.192	0.275	0.248	0.223
4 6	Mean	0.000	0.000	0.000	0.000	0.000	0.000	0.000	0.000	0.000	0.000	0.000	0.000	0.000	0.000	0.000	0.000
	Median	0.000	-0.001	-0.002	-0.004	0.000	-0.001	-0.003	-0.002	0.001	-0.003	0.001	0.003	-0.002	0.001	0.002	-0.001
	Standard dev.	1.818	1.918	2.103	2.220	1.820	1.996	2.149	2.293	1.848	1.958	2.089	2.186	1.721	1.846	1.994	2.219
	Variance	-3.5E-07	-4.6E-06	-1.2E-05	-5.0E-06	3.5E-06	-1.9E-06	1.4E-06	-4.3E-07	7.6E-06	5.5E-06	5.4E-06	-4.2E-06	7.9E-06	3.0E-08	1.4E-06	6.1E-06
	Skewness	3.6E-06	9.7E-06	-3.3E-05	1.2E-05	-1.5E-06	-4.2E-06	-3.7E-06	4.4E-06	-1.6E-05	3.0E-05	-1.2E-05	4.6E-06	-8.0E-06	9.8E-07	-2.7E-07	5.3E-05
	Kurtosis	0.482	0.472	0.543	0.417	0.513	0.671	0.525	0.574	0.355	0.395	0.355	0.400	0.402	0.570	0.511	0.480
4 7	Mean	0.000	0.000	0.000	0.000	0.000	0.000	0.000	0.000	0.000	0.000	0.000	0.000	0.000	0.000	0.000	0.000
	Median	0.000	0.000	-0.003	0.001	0.000	0.001	0.001	0.001	0.002	-0.002	0.000	0.000	-0.003	0.001	0.002	-0.004
	Standard dev.	1.758	1.868	2.013	2.125	1.761	1.881	2.005	2.159	1.824	1.917	2.043	2.122	1.719	1.801	1.941	2.095
	Variance	-2.0E-06	-4.9E-06	-6.1E-07	7.6E-07	-4.1E-06	2.5E-07	-4.1E-06	-2.8E-07	-4.4E-06	-2.9E-07	-2.8E-06	3.8E-06	-3.8E-06	2.7E-06	2.0E-06	2.5E-06
	Skewness	-2.6E-05	5.9E-05	3.2E-05	4.4E-05	1.5E-05	-2.4E-05	-4.7E-05	4.0E-05	5.0E-05	3.4E-05	6.4E-05	-1.9E-05	3.6E-05	1.6E-05	1.1E-05	5.9E-05
	Kurtosis	0.212	0.156	0.161	0.223	0.181	0.275	0.274	0.170	0.089	0.126	0.116	0.140	0.158	0.197	0.104	0.182
4 8	Mean	0.000	0.000	0.000	0.000	0.000	0.000	0.000	0.000	0.000	0.000	0.000	0.000	0.000	0.000	0.000	0.000
	Median	0.001	0.002	0.000	0.003	0.000	-0.001	0.001	0.001	0.001	0.000	0.000	0.000	0.000	-0.001	0.000	-0.002
	Standard dev.	1.859	1.929	2.023	2.150	1.866	1.959	2.029	2.108	1.912	1.993	2.079	2.158	1.798	1.886	1.966	2.074
	Variance	3.3E-08	-2.2E-07	1.2E-06	3.2E-07	-1.3E-07	8.3E-07	1.3E-06	1.3E-07	1.3E-06	-1.9E-06	1.1E-07	4.1E-07	1.5E-06	6.4E-07	6.1E-07	5.7E-07
	Skewness	-1.1E-07	6.6E-07	-3.5E-06	-1.0E-06	3.9E-07	-2.3E-06	-3.9E-06	-3.3E-07	-3.6E-06	4.8E-06	-3.4E-07	-1.3E-06	-4.5E-06	-1.9E-06	-1.8E-06	-1.7E-06
	Kurtosis	0.071	0.054	0.114	0.068	0.108	0.126	0.106	0.065	0.018	0.034	0.045	0.099	0.052	0.066	0.101	0.014
4 9	Mean	0.000	0.000	0.000	0.000	0.000	0.000	0.000	0.000	0.000	0.000	0.000	0.000	0.000	0.000	0.000	0.000
	Median	0.001	-0.001	-0.002	-0.001	-0.003	0.001	0.000	-0.002	-0.003	-0.001	0.000	-0.002	0.001	0.003	-0.002	-0.001
	Standard dev.	1.851	1.921	2.027	2.122	1.852	1.922	2.023	2.106	1.899	2.000	2.062	2.159	1.798	1.865	1.924	2.066
	Variance	1.4E-06	-8.0E-07	-6.6E-07	1.0E-06	-5.6E-07	-7.5E-07	-3.5E-06	-1.2E-06	-1.8E-06	6.7E-07	-5.2E-07	-5.7E-07	3.2E-07	1.9E-06	-1.5E-06	-9.9E-08
	Skewness	-3.6E-06	2.5E-06	1.9E-06	-3.0E-06	1.6E-06	2.2E-06	9.5E-06	3.5E-06	5.2E-06	-2.1E-06	1.6E-06	1.7E-06	-1.1E-06	-2.7E-06	4.6E-06	2.6E-07
	Kurtosis	0.179	0.177	0.171	0.092	0.166	0.236	0.247	0.161	0.093	0.128	0.127	0.113	0.087	0.188	0.188	0.151

Packet	Experiment	49	50	51	52	53	54	55	56	57	58	59	60	61	62	63	64
	V_{sg} (m/s)	0.15	0.23	0.60	1.31	0.15	0.31	0.59	1.32	0.15	0.31	0.59	1.32	0.15	0.31	0.59	1.34
	V_{sl} (m/s)	0.27	0.27	0.27	0.27	0.28	0.28	0.28	0.28	0.29	0.29	0.29	0.29	0.38	0.38	0.38	0.38
	WC (%)	0.60	0.60	0.60	0.60	0.40	0.40	0.40	0.40	0.20	0.20	0.20	0.20	0.80	0.80	0.80	0.80
4 2	Mean	0.000	0.000	0.000	0.000	0.000	0.000	0.000	0.000	0.000	0.000	0.000	0.000	0.000	0.000	0.000	0.000
	Median	0.003	-0.001	0.001	-0.003	0.000	0.001	0.000	0.001	0.001	-0.001	0.000	0.001	0.001	-0.001	-0.004	0.005
	Standard dev.	1.807	1.954	2.238	2.427	1.888	2.076	2.317	2.516	1.827	2.015	2.143	2.277	1.791	1.932	2.143	2.373
	Variance	-7.9E-06	1.9E-06	5.5E-07	-4.9E-06	-1.8E-06	-1.0E-06	6.4E-06	5.2E-08	1.6E-06	-6.0E-06	6.0E-06	4.0E-06	-8.7E-06	-2.5E-06	-6.0E-06	-2.1E-06
	Skewness	2.1E-05	-5.0E-06	3.5E-06	1.2E-05	5.1E-06	3.4E-06	-1.1E-05	-3.1E-07	-3.1E-06	8.7E-06	-1.4E-05	-1.0E-05	-1.0E-05	-2.0E-06	1.0E-05	9.1E-06
	Kurtosis	0.397	0.396	0.535	0.542	0.584	0.540	0.555	0.447	0.424	0.388	0.362	0.394	0.449	0.539	0.405	0.418
4 3	Mean	0.000	0.000	0.000	0.000	0.000	0.000	0.000	0.000	0.000	0.000	0.000	0.000	0.000	0.000	0.000	0.000
	Median	0.003	0.000	-0.001	0.008	-0.003	-0.005	-0.001	-0.005	0.000	-0.001	0.000	0.001	0.001	0.002	0.001	-0.002
	Standard dev.	2.199	2.407	2.837	2.979	2.297	2.608	2.971	3.168	2.091	2.392	2.589	2.523	2.039	2.287	2.622	2.800
	Variance	-3.0E-06	-1.7E-05	-9.6E-06	-1.2E-06	-1.4E-06	-4.5E-06	1.0E-05	-1.5E-05	-1.3E-05	-8.4E-06	-1.7E-05	4.1E-06	8.2E-06	1.4E-05	1.1E-05	1.0E-05
	Skewness	7.9E-05	-1.2E-06	-5.1E-05	2.0E-04	-1.5E-04	-1.5E-05	5.5E-05	-1.9E-04	-1.0E-04	1.2E-04	-1.5E-04	-1.6E-04	2.0E-04	-3.4E-04	-8.3E-05	-8.5E-06
	Kurtosis	0.525	0.383	0.380	0.352	0.912	0.457	0.486	0.643	0.400	0.252	0.232	0.233	0.783	0.500	0.500	0.356
4 4	Mean	0.000	0.000	0.000	0.000	0.000	0.000	0.000	0.000	0.000	0.000	0.000	0.000	0.000	0.000	0.000	0.000
	Median	-0.002	-0.001	0.000	0.000	0.001	0.000	0.001	-0.001	0.000	0.000	0.002	-0.002	0.000	0.002	0.002	-0.001
	Standard dev.	1.728	1.765	1.883	2.049	1.754	1.811	1.922	2.029	1.769	1.833	1.932	2.029	1.727	1.776	1.889	2.029
	Variance	-3.4E-06	-6.1E-07	1.6E-06	1.1E-05	3.7E-06	3.2E-06	5.8E-06	-8.5E-06	-3.1E-08	4.6E-06	3.5E-06	-7.4E-06	-6.0E-06	1.9E-06	5.9E-08	-8.3E-06
	Skewness	8.7E-06	2.3E-06	-3.4E-06	5.8E-05	1.7E-07	6.5E-06	-6.0E-06	1.5E-05	-4.5E-07	-5.7E-06	1.9E-05	8.0E-06	-2.4E-06	2.6E-05	-1.7E-07	4.2E-06
	Kurtosis	1.912	1.825	1.939	1.863	2.006	2.034	1.975	1.891	1.897	1.958	1.872	1.928	1.894	1.920	1.844	2.002
4 5	Mean	0.000	0.000	0.000	0.000	0.000	0.000	0.000	0.000	0.000	0.000	0.000	0.000	0.000	0.000	0.000	0.000
	Median	-0.004	0.005	-0.004	0.004	-0.002	-0.002	0.000	0.003	0.000	-0.006	0.005	0.001	-0.004	-0.001	0.007	-0.001
	Standard dev.	1.685	1.778	1.890	2.060	1.738	1.791	1.936	2.064	1.775	1.826	1.926	2.074	1.709	1.788	1.877	2.030
	Variance	-8.4E-06	-2.8E-06	-1.0E-06	-5.1E-06	3.5E-06	-4.4E-06	1.0E-06	2.4E-07	2.0E-06	4.1E-06	6.0E-06	1.2E-06	-3.5E-06	-1.5E-06	-1.6E-07	3.3E-06
	Skewness	1.8E-05	6.7E-06	4.0E-06	-1.5E-07	-8.8E-06	4.1E-06	-1.5E-06	-4.8E-06	7.9E-06	-8.0E-06	-1.5E-05	2.9E-07	6.7E-06	2.0E-06	-8.6E-08	-8.3E-06
	Kurtosis	0.270	0.223	0.188	0.296	0.252	0.349	0.323	0.234	0.193	0.208	0.188	0.217	0.254	0.337	0.187	0.232
4 6	Mean	0.000	0.000	0.000	0.000	0.000	0.000	0.000	0.000	0.000	0.000	0.000	0.000	0.000	0.000	0.000	0.000
	Median	0.000	0.000	0.001	-0.001	0.003	-0.001	0.004	-0.002	0.000	0.002	0.000	-0.002	-0.001	-0.002	-0.002	0.001
	Standard dev.	1.756	1.831	2.029	2.233	1.756	1.902	2.074	2.266	1.779	1.872	2.035	2.165	1.714	1.839	1.996	2.183
	Variance	5.8E-06	1.6E-06	3.5E-06	4.0E-06	1.7E-06	4.3E-07	-3.0E-06	-1.9E-06	-2.5E-06	6.4E-06	-3.5E-06	-4.3E-06	-1.8E-07	-4.4E-06	1.0E-05	4.8E-06
	Skewness	2.9E-06	-3.4E-06	-5.6E-06	-1.0E-05	-7.5E-06	3.4E-06	-3.4E-05	4.6E-06	7.8E-06	1.3E-06	-3.4E-05	-5.2E-05	-1.8E-07	-4.1E-06	1.6E-05	-1.1E-05
	Kurtosis	0.492	0.472	0.391	0.383	0.466	0.520	0.560	0.368	0.392	0.361	0.404	0.417	0.415	0.436	0.382	0.510
4 7	Mean	0.000	0.000	0.000	0.000	0.000	0.000	0.000	0.000	0.000	0.000	0.000	0.000	0.000	0.000	0.000	0.000
	Median	-0.002	0.000	0.000	0.002	-0.001	-0.001	0.001	-0.001	0.002	0.000	0.000	-0.001	-0.002	0.000	0.002	0.001
	Standard dev.	1.707	1.753	1.952	2.124	1.758	1.839	1.975	2.132	1.738	1.834	1.951	2.117	1.693	1.798	1.905	2.092
	Variance	7.4E-06	2.0E-06	-1.5E-06	4.7E-06	-3.8E-06	6.4E-06	-1.4E-06	1.7E-06	-3.6E-06	-5.8E-06	-8.0E-06	-3.4E-06	4.2E-06	5.0E-06	-9.5E-07	-1.7E-06
	Skewness	-6.3E-05	-7.2E-05	7.9E-05	5.3E-05	1.5E-05	4.7E-05	2.0E-05	-1.1E-04	-2.9E-05	-2.1E-07	-7.1E-05	3.8E-05	2.5E-05	-3.3E-06	2.1E-05	7.2E-05
	Kurtosis	0.153	0.093	0.225	0.066	0.179	0.287	0.183	0.181	0.082	0.050	0.157	0.153	0.192	0.186	0.133	0.123
4 8	Mean	0.000	0.000	0.000	0.000	0.000	0.000	0.000	0.000	0.000	0.000	0.000	0.000	0.000	0.000	0.000	0.000
	Median	-0.001	0.000	-0.002	0.000	0.001	-0.003	0.002	0.002	0.000	0.000	0.000	-0.002	0.000	-0.001	0.001	0.001
	Standard dev.	1.808	1.841	1.947	2.069	1.805	1.889	1.920	2.060	1.849	1.906	1.970	2.099	1.795	1.870	1.947	2.058
	Variance	-4.8E-07	3.5E-07	1.1E-06	-1.0E-06	-6.6E-07	-1.0E-06	4.5E-07	-3.9E-07	-3.0E-07	4.6E-07	-6.7E-07	-3.5E-07	-1.5E-07	1.3E-06	1.6E-06	1.7E-06
	Skewness	1.4E-06	-1.0E-06	-2.8E-06	2.5E-06	1.9E-06	2.9E-06	-1.4E-06	1.1E-06	8.5E-07	-1.3E-06	1.7E-06	1.0E-06	4.1E-07	-3.7E-06	-4.6E-06	-4.6E-06
	Kurtosis	0.023	0.008	0.122	0.135	0.166	0.147	0.062	0.025	0.061	0.054	0.051	-0.033	0.049	0.087	0.026	0.080
4 9	Mean	0.000	0.000	0.000	0.000	0.000	0.000	0.000	0.000	0.000	0.000	0.000	0.000	0.000	0.000	0.000	0.000
	Median	0.002	0.006	0.003	-0.001	0.001	0.000	0.000	-0.002	0.001	0.003	0.002	-0.002	-0.001	-0.002	0.000	0.002
	Standard dev.	1.797	1.835	1.933	2.082	1.815	1.883	1.942	2.049	1.855	1.904	1.949	2.098	1.776	1.861	1.959	2.063
	Variance	-1.8E-08	-1.5E-06	-5.0E-07	5.6E-07	7.1E-07	2.0E-06	-3.9E-08	5.4E-07	9.9E-07	-1.1E-06	-1.5E-06	7.7E-08	-1.0E-06	-7.1E-08	-1.9E-06	-1.8E-06
	Skewness	4.6E-08	3.6E-06	1.3E-06	-1.7E-06	-2.1E-06	-5.7E-06	1.1E-07	-1.6E-06	-3.0E-06	3.5E-06	2.6E-06	-1.2E-07	3.0E-06	1.6E-07	5.5E-06	5.7E-06
	Kurtosis	0.192	0.147	0.145	0.083	0.059	0.200	0.162	0.136	0.061	0.146	0.099	0.097	0.136	0.097	0.186	0.143

Packet	Experiment	65	66	67	68	69	70	71	72	73	74	75	76	77	78	79	80
	V_{sg} (m/s)	0.15	0.29	0.59	1.33	0.15	0.31	0.59	1.32	0.16	0.31	0.59	1.33	0.15	0.31	0.59	1.34
	V_{sl} (m/s)	0.40	0.40	0.40	0.40	0.41	0.41	0.41	0.41	0.43	0.43	0.43	0.43	0.51	0.51	0.51	0.51
	WC (%)	0.60	0.60	0.60	0.60	0.40	0.40	0.40	0.40	0.20	0.20	0.20	0.20	0.80	0.80	0.80	0.80
4 2	Mean	0.000	0.000	0.000	0.000	0.000	0.000	0.000	0.000	0.000	0.000	0.000	0.000	0.000	0.000	0.000	0.000
	Median	-0.001	0.005	-0.001	0.004	0.000	0.003	-0.003	0.000	-0.003	0.001	0.002	0.000	-0.001	-0.004	0.002	-0.001
	Standard dev.	1.863	2.001	2.257	2.455	1.906	2.149	2.334	2.549	1.811	2.039	2.200	2.295	1.758	1.946	2.142	2.341
	Variance	4.2E-06	-6.3E-06	8.9E-08	1.0E-05	6.2E-06	1.1E-05	4.3E-06	3.8E-06	-1.0E-05	-2.9E-06	6.7E-06	4.8E-06	3.2E-06	9.6E-06	5.9E-06	3.2E-06
	Skewness	-9.6E-06	1.5E-05	-1.3E-06	-2.2E-05	-1.7E-05	-2.0E-05	-1.1E-05	-3.4E-06	2.1E-05	8.2E-06	-1.8E-05	-8.4E-07	-8.1E-06	-1.8E-05	-1.5E-05	-8.5E-06
	Kurtosis	0.443	0.502	0.448	0.498	0.429	0.499	0.472	0.457	0.487	0.366	0.553	0.420	0.639	0.549	0.336	0.472
4 3	Mean	0.000	0.000	0.000	0.000	0.000	0.000	0.000	0.000	0.000	0.000	0.000	0.000	0.000	0.000	0.000	0.000
	Median	-0.002	-0.001	0.000	0.000	0.000	0.002	-0.003	0.003	0.001	-0.001	0.000	-0.001	0.003	-0.002	-0.003	0.003
	Standard dev.	2.279	2.534	2.818	2.958	2.422	2.773	3.089	3.220	2.070	2.399	2.636	2.601	2.023	2.325	2.633	2.822
	Variance	-1.2E-05	5.0E-06	1.8E-05	-3.7E-06	1.1E-05	-1.2E-05	1.2E-05	-2.0E-05	-3.5E-06	7.2E-06	-6.1E-06	5.4E-06	1.5E-06	-9.6E-06	3.7E-06	-7.4E-06
	Skewness	-1.3E-04	-1.7E-04	-2.1E-05	1.2E-05	-1.3E-04	-2.2E-04	5.0E-05	-1.7E-04	-8.3E-05	-8.7E-05	-1.6E-04	-3.6E-05	-4.2E-06	-1.3E-04	2.4E-04	7.0E-06
	Kurtosis	0.448	0.581	0.407	0.398	0.590	0.568	0.447	0.539	0.458	0.494	0.391	0.421	0.846	0.557	0.447	0.416
4 4	Mean	0.000	0.000	0.000	0.000	0.000	0.000	0.000	0.000	0.000	0.000	0.000	0.000	0.000	0.000	0.000	0.000
	Median	0.000	0.000	-0.001	0.001	0.000	0.000	0.000	0.000	0.000	0.001	0.000	0.000	-0.001	-0.001	0.001	0.002
	Standard dev.	1.719	1.773	1.911	2.031	1.726	1.800	1.888	2.035	1.748	1.841	1.927	2.046	1.693	1.761	1.871	2.010
	Variance	1.7E-06	-7.9E-07	2.9E-06	4.6E-06	1.0E-06	4.6E-06	1.8E-06	-4.6E-06	3.4E-06	7.4E-07	-1.1E-06	6.7E-06	5.6E-06	-4.0E-06	-2.9E-06	1.6E-06
	Skewness	2.9E-05	7.7E-06	-7.7E-06	1.4E-05	-2.1E-06	3.6E-07	3.0E-05	-5.8E-06	-8.7E-06	-2.1E-06	1.3E-06	2.0E-05	2.0E-05	-8.0E-06	-3.2E-06	-1.7E-06
	Kurtosis	1.959	2.015	1.884	1.931	2.002	1.943	1.985	1.886	1.764	1.808	1.849	1.831	1.825	1.871	2.051	1.859
4 5	Mean	0.000	0.000	0.000	0.000	0.000	0.000	0.000	0.000	0.000	0.000	0.000	0.000	0.000	0.000	0.000	0.000
	Median	-0.001	-0.005	-0.003	-0.003	-0.001	-0.002	-0.002	-0.004	-0.005	0.000	-0.002	0.003	-0.001	-0.002	-0.001	-0.006
	Standard dev.	1.693	1.805	1.904	2.069	1.724	1.800	1.913	2.083	1.742	1.829	1.909	2.059	1.693	1.746	1.886	2.040
	Variance	6.8E-09	-8.1E-07	-5.1E-06	-7.8E-06	1.3E-06	-3.1E-06	-3.6E-06	9.1E-08	7.8E-06	2.9E-06	-1.5E-06	3.6E-07	4.9E-06	2.4E-07	1.3E-06	-2.3E-06
	Skewness	3.9E-07	-2.1E-06	7.6E-07	1.2E-05	-4.1E-06	7.9E-06	-1.6E-06	-5.3E-07	-9.6E-06	7.0E-06	1.9E-06	-1.3E-06	-1.0E-05	-2.5E-05	-1.5E-05	3.0E-06
	Kurtosis	0.165	0.189	0.198	0.284	0.230	0.231	0.246	0.171	0.236	0.262	0.244	0.210	0.174	0.180	0.185	0.186
4 6	Mean	0.000	0.000	0.000	0.000	0.000	0.000	0.000	0.000	0.000	0.000	0.000	0.000	0.000	0.000	0.000	0.000
	Median	0.000	-0.001	-0.001	0.001	0.000	0.001	-0.001	0.001	-0.002	0.000	-0.001	-0.003	0.000	0.001	-0.001	0.004
	Standard dev.	1.746	1.866	2.044	2.253	1.790	1.920	2.091	2.289	1.764	1.875	2.045	2.170	1.713	1.837	2.000	2.187
	Variance	2.6E-06	5.4E-06	-7.3E-07	-7.4E-06	-6.4E-06	-1.1E-05	8.5E-07	-1.1E-06	9.2E-06	3.0E-06	-7.0E-06	-3.6E-06	-2.3E-06	-1.8E-06	-7.3E-06	-1.1E-07
	Skewness	-2.5E-07	3.5E-05	-2.2E-05	1.7E-05	4.5E-06	-1.2E-05	-3.6E-06	8.8E-06	7.4E-05	-8.3E-06	1.6E-05	4.2E-06	-4.3E-07	-1.2E-05	-6.9E-05	8.5E-06
	Kurtosis	0.423	0.558	0.442	0.423	0.464	0.419	0.518	0.504	0.446	0.407	0.466	0.391	0.422	0.574	0.402	0.479
4 7	Mean	0.000	0.000	0.000	0.000	0.000	0.000	0.000	0.000	0.000	0.000	0.000	0.000	0.000	0.000	0.000	0.000
	Median	0.000	0.000	-0.001	0.001	-0.001	0.000	0.000	0.001	0.000	0.000	0.002	0.001	0.002	-0.001	-0.001	0.001
	Standard dev.	1.715	1.781	1.921	2.104	1.739	1.844	1.944	2.129	1.714	1.827	1.953	2.085	1.702	1.783	1.920	2.089
	Variance	7.7E-07	-3.0E-06	8.9E-06	9.0E-06	-1.1E-06	5.0E-06	6.2E-07	7.0E-07	-5.4E-06	-2.5E-06	3.9E-06	-2.4E-06	-3.9E-06	-9.1E-07	4.5E-07	7.8E-07
	Skewness	4.4E-05	8.5E-05	6.7E-05	2.0E-04	-3.4E-05	-1.0E-05	3.1E-05	-1.7E-05	6.4E-06	-4.3E-05	-2.0E-05	5.7E-05	2.6E-05	-3.8E-05	6.4E-05	7.0E-06
	Kurtosis	0.145	0.102	0.175	0.113	0.141	0.198	0.100	0.140	0.055	0.146	0.040	0.028	0.143	0.125	0.186	0.119
4 8	Mean	0.000	0.000	0.000	0.000	0.000	0.000	0.000	0.000	0.000	0.000	0.000	0.000	0.000	0.000	0.000	0.000
	Median	-0.001	0.001	-0.001	-0.001	0.002	0.000	-0.001	0.001	0.002	0.000	-0.001	0.001	-0.002	0.001	0.001	0.000
	Standard dev.	1.772	1.841	1.945	2.034	1.803	1.857	1.926	2.026	1.828	1.894	2.002	2.083	1.759	1.825	1.920	2.013
	Variance	-9.1E-08	1.8E-06	6.7E-07	-6.5E-07	-8.0E-07	-4.6E-07	-6.2E-07	1.1E-06	-3.6E-07	-1.9E-07	1.6E-06	-1.9E-06	2.5E-07	5.3E-07	-1.5E-07	8.9E-08
	Skewness	2.9E-07	-5.0E-06	-2.0E-06	1.9E-06	2.4E-06	1.5E-06	1.8E-06	-3.3E-06	1.1E-06	5.4E-07	-4.6E-06	5.0E-06	-7.0E-07	-1.5E-06	3.7E-07	-2.1E-07
	Kurtosis	0.071	0.020	0.023	0.090	0.039	0.051	0.122	0.072	-0.011	0.018	0.051	0.035	0.020	0.040	0.066	-0.007
4 9	Mean	0.000	0.000	0.000	0.000	0.000	0.000	0.000	0.000	0.000	0.000	0.000	0.000	0.000	0.000	0.000	0.000
	Median	-0.002	0.000	0.000	0.001	0.001	-0.001	-0.002	-0.001	0.001	0.003	0.000	0.002	0.003	0.001	-0.001	-0.003
	Standard dev.	1.765	1.834	1.951	2.028	1.781	1.876	1.943	2.028	1.821	1.912	1.959	2.089	1.768	1.828	1.906	2.033
	Variance	9.7E-07	-1.7E-06	-1.3E-07	6.5E-07	8.9E-07	-7.3E-07	9.3E-08	-4.8E-07	1.8E-06	-5.0E-09	-2.6E-07	2.6E-06	6.5E-07	-1.9E-06	-3.8E-07	2.3E-06
	Skewness	-2.4E-06	4.5E-06	2.3E-07	-2.0E-06	-2.8E-06	2.8E-06	-2.9E-07	1.4E-06	-5.2E-06	2.0E-08	8.3E-07	-6.3E-06	-1.9E-06	2.8E-06	1.1E-06	-6.8E-06
	Kurtosis	0.141	0.141	0.158	0.192	0.081	0.112	0.159	0.213	0.068	0.056	0.080	0.094	0.125	0.091	0.066	0.164

Packet	Experiment	81	82	83	84	85	86	87	88	89	90	91	92	93	94	95	96
	V_{sg} (m/s)	0.15	0.24	0.59	1.34	0.16	0.31	0.59	1.34	0.16	0.35	0.66	1.33	0.15	0.31	0.60	1.32
	V_{sl} (m/s)	0.53	0.53	0.53	0.53	0.55	0.55	0.55	0.55	0.57	0.57	0.57	0.57	0.64	0.64	0.64	0.64
	WC (%)	0.60	0.60	0.60	0.60	0.40	0.40	0.40	0.40	0.20	0.20	0.20	0.20	0.80	0.80	0.80	0.80
4 2	Mean	0.000	0.000	0.000	0.000	0.000	0.000	0.000	0.000	0.000	0.000	0.000	0.000	0.000	0.000	0.000	0.000
	Median	0.002	-0.002	-0.002	-0.002	0.001	-0.001	0.002	0.000	0.000	0.000	0.000	0.003	-0.002	-0.002	0.004	0.003
	Standard dev.	1.908	2.029	2.305	2.459	1.975	2.171	2.387	2.429	1.785	1.622	2.251	2.270	1.804	1.932	2.148	2.375
	Variance	-4.1E-06	7.1E-07	1.4E-06	-5.1E-06	-2.5E-07	-3.5E-06	9.5E-06	4.2E-06	-6.2E-06	2.5E-06	-1.5E-06	-8.7E-06	7.4E-06	-4.1E-06	-9.9E-06	-5.8E-07
	Skewness	1.9E-05	-3.8E-06	-3.3E-06	1.2E-05	6.8E-07	3.5E-06	-1.1E-05	-8.6E-06	1.0E-05	-9.3E-06	4.1E-06	2.3E-05	4.2E-05	1.1E-05	-5.6E-06	2.0E-05
	Kurtosis	0.340	0.371	0.429	0.541	0.720	0.512	0.464	0.477	0.341	0.370	0.365	0.404	0.545	0.540	0.487	0.489
4 3	Mean	0.000	0.000	0.000	0.000	0.000	0.000	0.000	0.000	0.000	0.000	0.000	0.000	0.000	0.000	0.000	0.000
	Median	0.002	-0.001	-0.003	0.004	-0.002	0.002	-0.003	0.000	-0.001	-0.001	-0.002	-0.002	0.004	0.000	0.001	0.000
	Standard dev.	2.384	2.623	2.933	3.046	2.577	2.887	3.133	2.935	2.000	1.621	2.732	2.672	2.118	2.305	2.620	2.839
	Variance	9.5E-06	-7.8E-06	-3.4E-06	-3.5E-06	-1.1E-05	-9.7E-06	4.4E-06	1.4E-05	8.6E-06	8.9E-06	-6.6E-06	-2.0E-06	5.9E-06	6.0E-06	1.1E-05	-8.3E-06
	Skewness	1.6E-04	7.8E-05	-9.0E-05	-1.9E-04	-1.4E-04	1.2E-04	2.3E-05	1.5E-04	5.6E-05	-3.2E-05	-1.7E-05	-2.0E-05	-8.4E-05	-2.3E-04	-9.8E-05	2.1E-04
	Kurtosis	0.689	0.530	0.483	0.531	0.754	0.423	0.494	0.465	0.719	0.109	0.348	0.379	1.187	0.743	0.493	0.423
4 4	Mean	0.000	0.000	0.000	0.000	0.000	0.000	0.000	0.000	0.000	0.000	0.000	0.000	0.000	0.000	0.000	0.000
	Median	0.002	-0.001	0.000	0.001	0.002	0.000	0.001	0.001	0.001	-0.002	-0.003	-0.001	-0.001	0.002	-0.001	0.000
	Standard dev.	1.729	1.751	1.894	2.034	1.740	1.783	1.865	2.018	1.768	1.661	1.921	2.036	1.690	1.776	1.843	1.999
	Variance	-5.0E-06	-2.9E-06	3.3E-06	-1.0E-06	-2.4E-08	-5.6E-07	1.5E-06	4.8E-07	3.1E-06	-1.6E-06	1.2E-05	-4.4E-06	4.4E-06	-4.1E-06	6.0E-06	1.8E-06
	Skewness	-1.4E-05	6.6E-06	-4.6E-06	-4.1E-06	-1.9E-06	-2.2E-06	-4.3E-06	-5.1E-06	-7.6E-06	3.5E-06	6.0E-05	-3.1E-06	-1.2E-05	-1.7E-05	1.7E-05	3.2E-05
	Kurtosis	1.830	1.816	1.906	1.870	1.897	1.935	1.869	1.995	1.803	1.863	1.932	1.965	2.002	1.935	1.939	1.902
4 5	Mean	0.000	0.000	0.000	0.000	0.000	0.000	0.000	0.000	0.000	0.000	0.000	0.000	0.000	0.000	0.000	0.000
	Median	-0.003	0.002	0.001	-0.003	-0.001	-0.002	-0.006	-0.001	0.001	0.000	-0.003	0.006	-0.003	0.003	0.005	-0.002
	Standard dev.	1.716	1.760	1.906	2.046	1.737	1.817	1.902	2.049	1.757	1.665	1.937	2.056	1.681	1.776	1.879	2.026
	Variance	6.2E-07	-1.8E-06	-4.0E-06	8.1E-07	-3.6E-06	-1.2E-06	4.0E-06	-1.7E-06	1.6E-06	-1.3E-07	1.3E-06	7.7E-08	2.4E-06	2.4E-06	-3.6E-06	-4.2E-07
	Skewness	-1.9E-06	-7.0E-07	1.5E-05	-2.3E-06	1.0E-05	3.9E-06	-3.5E-06	4.3E-06	-2.5E-06	3.1E-07	-3.2E-06	-2.3E-06	-1.8E-08	-4.3E-06	-1.5E-06	-4.0E-06
	Kurtosis	0.237	0.187	0.251	0.208	0.315	0.261	0.194	0.223	0.233	0.177	0.262	0.168	0.202	0.222	0.212	0.246
4 6	Mean	0.000	0.000	0.000	0.000	0.000	0.000	0.000	0.000	0.000	0.000	0.000	0.000	0.000	0.000	0.000	0.000
	Median	-0.002	0.002	-0.002	0.002	0.001	-0.001	-0.001	-0.001	0.001	0.003	-0.001	0.000	-0.003	0.000	0.000	0.001
	Standard dev.	1.791	1.865	2.075	2.232	1.793	1.946	2.132	2.213	1.743	1.633	2.048	2.172	1.723	1.827	2.002	2.203
	Variance	5.1E-06	-1.8E-06	-4.4E-06	1.0E-05	3.2E-06	1.6E-06	-4.6E-07	-1.4E-07	5.2E-06	-5.2E-06	1.7E-06	6.7E-06	-2.2E-06	8.2E-06	2.8E-06	1.8E-06
	Skewness	-3.3E-06	-3.6E-07	5.6E-06	1.8E-05	-9.2E-06	2.9E-05	-6.1E-07	-1.2E-05	-1.2E-05	8.9E-06	-2.8E-06	-2.7E-06	-9.7E-06	-1.5E-05	-1.5E-06	-9.5E-06
	Kurtosis	0.475	0.354	0.453	0.509	0.462	0.496	0.625	0.434	0.355	0.395	0.430	0.389	0.408	0.471	0.475	0.354
4 7	Mean	0.000	0.000	0.000	0.000	0.000	0.000	0.000	0.000	0.000	0.000	0.000	0.000	0.000	0.000	0.000	0.000
	Median	0.000	0.001	0.001	-0.001	0.002	-0.002	0.001	-0.001	0.002	0.000	0.000	-0.002	0.000	0.000	0.000	-0.001
	Standard dev.	1.710	1.771	1.960	2.130	1.742	1.835	1.979	2.117	1.745	1.629	1.948	2.118	1.685	1.782	1.919	2.076
	Variance	-3.1E-07	2.8E-06	5.7E-07	-3.0E-06	1.5E-06	4.6E-07	-2.6E-06	-2.2E-06	-1.8E-06	1.2E-06	-3.1E-06	-8.9E-07	4.8E-07	-1.5E-06	3.3E-06	5.9E-07
	Skewness	6.1E-05	-6.4E-05	2.3E-05	4.4E-06	3.7E-05	5.1E-05	2.7E-05	-1.9E-05	-2.5E-05	-4.8E-05	-9.8E-05	-7.3E-06	-5.0E-05	-4.2E-05	-2.1E-05	1.1E-06
	Kurtosis	0.132	0.087	0.151	0.155	0.149	0.173	0.164	0.166	0.068	0.151	0.127	0.146	0.128	0.220	0.212	0.141
4 8	Mean	0.000	0.000	0.000	0.000	0.000	0.000	0.000	0.000	0.000	0.000	0.000	0.000	0.000	0.000	0.000	0.000
	Median	-0.002	0.001	0.001	0.002	-0.002	0.000	-0.001	0.000	0.000	0.001	0.002	0.000	-0.001	-0.002	0.000	-0.001
	Standard dev.	1.784	1.832	1.923	2.032	1.816	1.848	1.900	2.008	1.859	1.768	1.944	2.068	1.780	1.838	1.893	2.012
	Variance	-5.2E-07	-2.2E-06	-1.1E-06	9.4E-08	-8.1E-08	2.0E-07	-1.8E-07	-1.2E-06	-1.1E-07	-8.1E-07	6.8E-07	-1.9E-07	-1.9E-06	-2.6E-06	-5.0E-07	7.0E-07
	Skewness	1.3E-06	6.2E-06	3.3E-06	-2.6E-07	2.5E-07	-6.8E-07	6.6E-07	3.4E-06	3.1E-07	2.1E-06	-2.0E-06	6.0E-07	5.4E-06	7.2E-06	1.6E-06	-2.1E-06
	Kurtosis	0.005	-0.005	0.022	0.069	0.121	0.140	0.021	-0.034	0.013	0.014	0.044	0.020	0.055	0.086	0.014	0.001
4 9	Mean	0.000	0.000	0.000	0.000	0.000	0.000	0.000	0.000	0.000	0.000	0.000	0.000	0.000	0.000	0.000	0.000
	Median	-0.001	-0.002	0.002	-0.001	0.002	0.000	-0.001	0.000	0.001	-0.001	0.000	0.000	-0.001	0.000	0.001	-0.002
	Standard dev.	1.791	1.812	1.908	2.061	1.806	1.826	1.911	2.038	1.840	1.746	1.956	2.052	1.754	1.824	1.881	2.031
	Variance	2.6E-07	5.8E-07	-3.3E-07	7.8E-07	1.1E-06	1.6E-06	6.8E-07	5.2E-07	3.0E-07	1.6E-06	-2.0E-06	1.2E-06	3.5E-06	7.4E-07	1.5E-06	8.6E-07
	Skewness	-6.5E-07	-8.6E-07	1.1E-06	-1.9E-06	-2.9E-06	-4.8E-06	-2.1E-06	-1.4E-06	-8.2E-07	-2.8E-06	4.9E-06	-3.8E-06	-9.2E-06	-1.3E-06	-4.9E-06	-2.3E-06
	Kurtosis	0.127	0.062	0.253	0.174	0.137	0.147	0.261	0.097	0.117	0.063	0.173	0.067	0.197	0.069	0.174	0.112

Packet	Experiment	97	98	99	100	101	102	103	104	105	106	107	108	109	110	111	112
	V_{sg} (m/s)	0.15	0.59	1.31	0.16	0.31	0.60	1.34	0.16	0.32	0.61	1.25	0.15	0.30	0.60	1.33	0.15
	V_{sl} (m/s)	0.66	0.66	0.66	0.69	0.69	0.69	0.69	0.72	0.72	0.72	0.72	0.76	0.76	0.76	0.76	0.80
	WC (%)	0.60	0.60	0.60	0.40	0.40	0.40	0.40	0.20	0.20	0.20	0.20	0.80	0.80	0.80	0.80	0.60
4 2	Mean	0.000	0.000	0.000	0.000	0.000	0.000	0.000	0.000	0.000	0.000	0.000	0.000	0.000	0.000	0.000	0.000
	Median	0.001	0.002	0.003	0.000	-0.002	0.002	0.001	0.000	-0.002	-0.003	0.000	0.000	-0.002	0.001	0.001	0.000
	Standard dev.	1.945	2.339	2.532	2.015	2.163	2.411	2.424	1.837	2.079	2.291	2.356	1.805	1.943	2.131	2.399	1.974
	Variance	7.8E-06	8.6E-07	-8.1E-08	1.8E-06	-1.3E-06	-2.0E-06	2.1E-06	4.1E-06	1.5E-06	-1.2E-06	-5.8E-06	-3.2E-07	-2.9E-06	4.5E-06	-2.6E-06	-5.2E-06
	Skewness	-2.0E-05	-2.4E-06	-4.5E-05	7.4E-06	8.5E-06	1.4E-06	-3.0E-06	-1.1E-05	-5.0E-06	3.2E-06	1.5E-05	8.1E-07	-2.5E-06	-1.2E-05	5.9E-06	1.2E-05
	Kurtosis	0.514	0.455	0.434	0.392	0.328	0.422	0.581	0.467	0.435	0.380	0.391	0.510	0.559	0.484	0.450	0.523
4 3	Mean	0.000	0.000	0.000	0.000	0.000	0.000	0.000	0.000	0.000	0.000	0.000	0.000	0.000	0.000	0.000	0.000
	Median	0.001	0.004	0.008	-0.003	-0.002	0.000	0.001	-0.001	0.002	0.004	0.004	0.000	0.001	-0.002	-0.001	-0.002
	Standard dev.	2.469	3.093	3.147	2.546	2.955	3.121	2.966	2.302	2.476	2.860	2.777	2.281	2.350	2.600	2.901	2.514
	Variance	6.1E-07	-1.6E-06	-8.9E-06	5.4E-06	2.2E-05	-1.9E-05	3.8E-06	5.5E-06	7.2E-06	2.5E-05	3.5E-06	-2.0E-06	1.1E-05	-3.9E-06	7.8E-06	-4.3E-07
	Skewness	-1.4E-04	-7.0E-06	2.2E-04	-8.6E-05	1.8E-04	-1.5E-04	-2.1E-04	1.3E-04	-4.8E-05	-5.9E-05	-4.3E-05	3.1E-04	-5.4E-05	1.3E-04	-2.1E-05	-2.1E-05
	Kurtosis	0.693	0.452	0.452	0.559	0.395	0.405	0.443	0.905	0.502	0.262	0.429	1.127	0.934	0.431	0.525	0.959
4 4	Mean	0.000	0.000	0.000	0.000	0.000	0.000	0.000	0.000	0.000	0.000	0.000	0.000	0.000	0.000	0.000	0.000
	Median	0.000	-0.001	0.000	0.000	0.000	0.001	-0.003	0.000	-0.001	0.000	0.002	0.001	0.000	0.001	0.000	0.001
	Standard dev.	1.698	1.852	1.974	1.726	1.783	1.875	2.007	1.745	1.788	1.888	2.017	1.681	1.767	1.833	1.984	1.710
	Variance	3.4E-06	7.1E-08	4.1E-06	5.6E-06	1.5E-06	-1.5E-06	-5.6E-06	-6.7E-06	-7.6E-06	1.3E-05	-7.5E-06	4.3E-06	5.3E-07	-6.5E-07	-3.7E-06	-3.3E-07
	Skewness	7.2E-06	-1.6E-05	2.3E-06	4.4E-06	7.2E-06	3.5E-06	-1.1E-04	-1.1E-04	8.3E-06	1.3E-05	-9.4E-05	7.3E-06	-1.8E-06	1.1E-06	5.2E-06	7.3E-07
	Kurtosis	1.757	1.883	1.820	1.977	1.818	1.895	1.898	1.822	1.823	1.827	1.871	1.857	2.016	1.889	1.960	1.877
4 5	Mean	0.000	0.000	0.000	0.000	0.000	0.000	0.000	0.000	0.000	0.000	0.000	0.000	0.000	0.000	0.000	0.000
	Median	0.001	0.000	-0.002	-0.004	0.003	0.000	-0.001	-0.003	-0.003	-0.001	0.001	-0.001	-0.001	-0.002	0.007	-0.006
	Standard dev.	1.715	1.890	2.037	1.722	1.791	1.901	2.022	1.739	1.813	1.916	2.044	1.664	1.743	1.856	2.014	1.709
	Variance	2.4E-07	-4.9E-06	2.2E-06	-1.3E-06	-3.9E-07	5.0E-06	-3.8E-06	-1.8E-06	2.9E-06	3.5E-07	-1.5E-06	4.5E-06	3.6E-06	-1.2E-06	-4.6E-06	6.8E-07
	Skewness	-8.5E-07	1.1E-05	1.0E-05	1.1E-05	6.3E-07	1.2E-05	-1.2E-05	3.6E-06	-9.2E-06	1.0E-06	-7.2E-06	2.1E-06	3.7E-06	2.1E-06	1.1E-05	-3.5E-06
	Kurtosis	0.240	0.220	0.232	0.269	0.200	0.134	0.190	0.134	0.221	0.176	0.235	0.200	0.281	0.212	0.274	0.198
4 6	Mean	0.000	0.000	0.000	0.000	0.000	0.000	0.000	0.000	0.000	0.000	0.000	0.000	0.000	0.000	0.000	0.000
	Median	-0.002	-0.002	-0.002	0.000	-0.002	0.002	0.002	-0.002	-0.001	0.000	0.000	-0.001	-0.002	0.000	0.000	-0.001
	Standard dev.	1.787	2.107	2.283	1.791	1.979	2.127	2.246	1.760	1.907	2.068	2.231	1.733	1.825	1.977	2.190	1.790
	Variance	-5.2E-06	3.0E-08	-5.6E-06	4.5E-06	4.9E-08	1.3E-06	-3.9E-06	-4.4E-06	-4.4E-06	-4.8E-06	3.5E-06	2.3E-06	3.9E-06	-7.9E-07	-1.1E-07	-8.6E-07
	Skewness	-2.0E-05	-5.4E-06	4.8E-06	-1.1E-05	-1.6E-06	1.4E-05	-3.5E-05	-8.8E-06	7.7E-06	1.1E-05	-4.0E-06	-6.5E-06	-1.1E-05	-3.6E-06	4.1E-07	-2.8E-07
	Kurtosis	0.547	0.506	0.438	0.436	0.464	0.430	0.545	0.382	0.442	0.429	0.335	0.446	0.566	0.411	0.308	0.501
4 7	Mean	0.000	0.000	0.000	0.000	0.000	0.000	0.000	0.000	0.000	0.000	0.000	0.000	0.000	0.000	0.000	0.000
	Median	-0.002	0.001	-0.002	0.001	-0.001	0.002	0.000	-0.002	0.001	-0.001	-0.003	-0.001	-0.001	-0.001	0.001	0.001
	Standard dev.	1.723	1.954	2.118	1.732	1.842	1.971	2.083	1.725	1.832	1.946	2.136	1.698	1.755	1.892	2.107	1.724
	Variance	-2.6E-06	2.7E-06	-4.2E-06	-9.3E-07	4.5E-06	-6.3E-06	3.8E-06	1.6E-07	8.3E-07	4.4E-06	2.6E-06	-4.1E-06	-7.9E-06	-4.9E-07	1.4E-06	-3.3E-07
	Skewness	8.0E-05	-1.8E-05	2.5E-05	4.5E-05	-2.3E-05	5.4E-05	7.4E-05	4.2E-05	3.5E-05	-3.0E-05	7.0E-06	-2.2E-05	-2.7E-06	-3.0E-05	8.3E-05	-4.5E-05
	Kurtosis	0.139	0.155	0.149	0.191	0.164	0.092	0.133	0.108	0.097	0.154	0.107	0.113	0.129	0.143	0.142	0.083
4 8	Mean	0.000	0.000	0.000	0.000	0.000	0.000	0.000	0.000	0.000	0.000	0.000	0.000	0.000	0.000	0.000	0.000
	Median	0.001	0.000	0.000	0.000	-0.002	-0.001	0.000	0.000	0.001	0.001	-0.001	0.000	0.000	0.000	-0.001	-0.001
	Standard dev.	1.763	1.894	2.023	1.782	1.828	1.878	2.023	1.798	1.853	1.930	2.037	1.768	1.808	1.913	2.003	1.781
	Variance	6.9E-07	1.6E-06	3.4E-07	7.7E-07	4.6E-07	2.6E-07	1.8E-06	-1.3E-07	3.0E-07	8.5E-07	1.4E-07	-3.9E-07	1.6E-07	-5.2E-07	-9.2E-07	2.3E-07
	Skewness	-2.1E-06	-4.8E-06	-1.1E-06	-2.1E-06	-1.4E-06	-6.9E-07	-4.5E-06	4.4E-07	-9.3E-07	-1.8E-06	-4.6E-07	1.2E-06	-3.0E-07	1.7E-06	2.7E-06	-7.1E-07
	Kurtosis	0.018	0.112	0.168	0.072	0.028	-0.008	0.071	0.020	0.053	0.005	0.023	0.025	0.060	0.097	0.047	0.015
4 9	Mean	0.000	0.000	0.000	0.000	0.000	0.000	0.000	0.000	0.000	0.000	0.000	0.000	0.000	0.000	0.000	0.000
	Median	0.002	0.001	0.003	0.003	0.001	-0.001	0.002	-0.001	-0.001	-0.001	0.004	0.000	0.001	-0.001	-0.002	-0.002
	Standard dev.	1.755	1.914	2.005	1.783	1.827	1.892	2.006	1.809	1.855	1.923	2.023	1.758	1.798	1.906	2.018	1.801
	Variance	-7.5E-07	-2.4E-07	-9.8E-07	-1.8E-06	-2.4E-07	-5.3E-08	-1.6E-06	6.3E-07	1.3E-06	-2.5E-06	1.3E-06	1.7E-07	-2.8E-06	9.7E-07	1.6E-06	1.2E-06
	Skewness	2.3E-06	6.1E-07	2.8E-06	5.2E-06	7.4E-07	2.3E-07	4.8E-06	-2.3E-06	-3.4E-06	6.8E-06	-3.8E-06	-4.8E-07	7.9E-06	-3.0E-06	-5.1E-06	-3.1E-06
	Kurtosis	0.189	0.135	0.137	0.158	0.214	0.119	0.136	0.189	0.117	0.111	0.135	0.093	0.063	0.127	0.110	0.102

Packet	Experiment	113	114	115	116	117	118	119	120	121	122	123	124	125	126
	V_{sg} (m/s)	0.23	0.62	1.32	0.16	0.32	0.60	1.33	0.15	0.32	0.66	1.32	0.15	0.31	0.60
	V_{sl} (m/s)	0.80	0.80	0.80	0.83	0.83	0.83	0.83	0.86	0.86	0.86	0.86	0.15	0.15	0.15
	WC (%)	0.60	0.60	0.60	0.40	0.40	0.40	0.40	0.20	0.20	0.20	0.20	0.00	0.00	0.00
4 2	Mean	0.000	0.000	0.000	0.000	0.000	0.000	0.000	0.000	0.000	0.000	0.000	0.000	0.000	0.000
	Median	-0.001	-0.002	0.000	0.000	0.000	0.005	0.002	0.000	0.002	-0.001	0.000	0.003	0.004	-0.003
	Standard dev.	2.201	2.402	2.564	2.018	2.259	2.498	2.531	1.922	2.069	2.370	2.414	1.825	1.979	2.140
	Variance	-5.8E-07	3.4E-06	-7.0E-07	-1.9E-06	8.4E-07	2.2E-06	3.7E-06	-6.2E-06	-2.3E-06	-3.7E-06	2.8E-06	4.4E-07	1.9E-06	-1.0E-05
	Skewness	6.0E-07	2.5E-05	1.9E-06	5.6E-06	-2.3E-06	-5.0E-06	-1.0E-05	1.5E-05	3.1E-06	1.1E-05	-6.4E-06	-3.8E-06	-5.5E-06	1.9E-05
	Kurtosis	0.469	0.540	0.500	0.575	0.409	0.396	0.512	0.636	0.341	0.425	0.361	0.400	0.509	0.361
4 3	Mean	0.000	0.000	0.000	0.000	0.000	0.000	0.000	0.000	0.000	0.000	0.000	0.000	0.000	0.000
	Median	0.001	0.000	-0.002	0.001	-0.001	0.002	0.003	0.005	0.000	0.003	-0.001	0.004	-0.005	0.001
	Standard dev.	2.918	3.160	3.189	2.570	2.936	3.236	3.007	2.369	2.489	2.885	2.826	1.990	2.264	2.416
	Variance	-5.5E-06	-2.9E-05	-1.1E-05	-4.8E-06	-4.9E-06	-6.7E-06	-3.3E-07	-1.3E-05	1.1E-05	8.7E-07	7.0E-06	-2.5E-06	2.7E-06	3.7E-06
	Skewness	9.6E-05	-2.6E-04	4.3E-05	-8.0E-05	-1.2E-04	8.4E-05	2.6E-04	-1.1E-04	-1.2E-04	3.5E-04	-3.1E-04	-7.7E-05	3.1E-04	2.2E-04
	Kurtosis	0.508	0.495	0.490	0.787	0.540	0.423	0.380	1.061	0.632	0.246	0.286	0.239	0.283	0.303
4 4	Mean	0.000	0.000	0.000	0.000	0.000	0.000	0.000	0.000	0.000	0.000	0.000	0.000	0.000	0.000
	Median	-0.001	-0.001	0.001	-0.001	-0.001	0.000	0.000	0.000	-0.002	-0.001	0.002	-0.001	-0.001	0.000
	Standard dev.	1.763	1.857	2.011	1.707	1.764	1.884	1.991	1.749	1.805	1.886	2.031	1.856	1.902	1.981
	Variance	-7.0E-06	4.0E-06	1.3E-06	5.7E-07	3.5E-07	-3.4E-06	-4.9E-06	4.7E-06	-2.1E-06	4.1E-06	9.1E-07	-7.2E-06	5.4E-06	-2.3E-06
	Skewness	1.1E-05	1.1E-05	8.2E-06	-1.7E-06	3.1E-07	-1.8E-06	-6.8E-06	-2.0E-06	5.4E-06	-6.0E-06	-2.0E-06	1.1E-05	-9.3E-06	2.5E-06
	Kurtosis	1.902	1.804	2.018	1.897	1.973	1.949	1.882	1.893	1.920	1.864	1.725	1.853	1.812	1.730
4 5	Mean	0.000	0.000	0.000	0.000	0.000	0.000	0.000	0.000	0.000	0.000	0.000	0.000	0.000	0.000
	Median	0.000	-0.005	-0.002	-0.003	0.001	0.000	0.005	0.000	-0.002	-0.003	0.004	-0.002	0.003	-0.001
	Standard dev.	1.789	1.911	2.054	1.718	1.798	1.919	2.037	1.707	1.782	1.933	2.047	1.805	1.900	1.976
	Variance	7.2E-07	-9.8E-07	-1.4E-06	2.0E-06	2.8E-06	1.1E-06	-2.3E-06	2.9E-06	-8.7E-07	6.0E-06	-3.9E-07	2.1E-06	3.2E-06	-1.7E-06
	Skewness	-1.5E-06	2.9E-06	-1.6E-06	-4.1E-06	-6.3E-06	8.7E-07	3.4E-06	-9.0E-06	1.7E-06	4.8E-06	-2.1E-06	-5.4E-06	-8.2E-06	3.7E-06
	Kurtosis	0.310	0.325	0.267	0.247	0.261	0.245	0.189	0.220	0.135	0.218	0.121	0.212	0.164	0.215
4 6	Mean	0.000	0.000	0.000	0.000	0.000	0.000	0.000	0.000	0.000	0.000	0.000	0.000	0.000	0.000
	Median	0.000	-0.002	0.000	0.000	-0.001	-0.002	0.002	0.001	0.000	0.001	0.002	-0.001	0.002	-0.002
	Standard dev.	1.929	2.143	2.272	1.846	2.015	2.173	2.298	1.768	1.928	2.096	2.263	1.831	1.928	2.034
	Variance	-3.2E-07	6.8E-06	3.1E-06	-1.6E-06	-1.5E-06	-5.8E-06	-7.3E-06	5.3E-06	-1.3E-06	4.4E-07	6.6E-07	-6.3E-07	-1.7E-06	8.1E-06
	Skewness	9.2E-07	2.2E-05	1.7E-05	-1.4E-05	-1.3E-06	9.7E-06	3.3E-06	-1.2E-05	1.3E-06	-5.5E-07	2.4E-05	1.3E-06	8.8E-06	-3.8E-06
	Kurtosis	0.381	0.477	0.501	0.523	0.607	0.475	0.485	0.398	0.461	0.470	0.389	0.447	0.376	0.360
4 7	Mean	0.000	0.000	0.000	0.000	0.000	0.000	0.000	0.000	0.000	0.000	0.000	0.000	0.000	0.000
	Median	0.001	0.001	-0.002	0.001	0.001	0.000	0.000	0.000	-0.003	-0.001	0.000	-0.003	-0.003	0.001
	Standard dev.	1.843	1.953	2.131	1.744	1.849	2.002	2.129	1.711	1.827	2.001	2.141	1.809	1.909	2.006
	Variance	2.7E-07	-7.5E-07	3.3E-06	-3.5E-06	-2.3E-06	3.4E-07	3.3E-06	-4.7E-06	3.5E-06	-3.2E-06	-2.0E-07	-2.5E-06	-2.9E-07	8.3E-07
	Skewness	-1.5E-05	2.8E-05	6.9E-05	2.7E-05	4.3E-05	7.2E-05	1.7E-05	-5.7E-06	4.0E-05	1.8E-05	-2.8E-05	1.6E-05	-2.7E-05	6.9E-05
	Kurtosis	0.186	0.185	0.127	0.174	0.084	0.170	0.160	0.075	0.210	0.099	0.150	0.078	0.144	0.073
4 8	Mean	0.000	0.000	0.000	0.000	0.000	0.000	0.000	0.000	0.000	0.000	0.000	0.000	0.000	0.000
	Median	0.001	0.000	0.000	0.000	-0.001	0.002	0.000	0.000	-0.001	0.000	0.001	-0.001	0.000	0.002
	Standard dev.	1.811	1.876	2.014	1.773	1.813	1.911	2.009	1.780	1.840	1.928	2.034	1.904	1.969	2.017
	Variance	2.4E-07	4.1E-07	1.6E-06	1.8E-06	-3.2E-07	-5.1E-07	-9.6E-07	-3.5E-07	2.7E-07	1.2E-07	4.5E-07	-1.7E-06	1.2E-06	-1.3E-06
	Skewness	-8.2E-07	-1.1E-06	-4.7E-06	-4.7E-06	8.9E-07	1.6E-06	2.6E-06	9.7E-07	-7.1E-07	-3.9E-07	-1.4E-06	5.0E-06	-3.6E-06	3.6E-06
	Kurtosis	0.047	0.104	0.058	-0.027	0.008	0.109	0.116	0.153	0.036	0.047	0.031	0.041	0.005	0.023
4 9	Mean	0.000	0.000	0.000	0.000	0.000	0.000	0.000	0.000	0.000	0.000	0.000	0.000	0.000	0.000
	Median	0.002	-0.002	0.003	-0.004	0.001	-0.002	0.002	-0.002	0.000	0.000	-0.002	0.000	-0.002	-0.002
	Standard dev.	1.815	1.896	2.012	1.792	1.809	1.899	1.992	1.812	1.847	1.928	2.008	1.894	1.987	2.059
	Variance	5.3E-08	-1.5E-06	-3.1E-06	-2.2E-06	2.9E-06	-2.9E-07	7.1E-07	-8.9E-07	6.0E-07	2.1E-06	-5.0E-07	3.7E-06	-2.1E-06	1.8E-06
	Skewness	-1.9E-07	4.7E-06	9.2E-06	7.0E-06	-8.8E-06	9.6E-07	-1.9E-06	2.8E-06	-1.8E-06	-6.8E-06	1.5E-06	-8.5E-06	7.0E-06	-5.3E-06
	Kurtosis	0.118	0.199	0.099	0.109	0.105	0.193	0.100	0.093	0.097	0.168	0.128	0.097	0.131	0.160

D.5 Wavelet Packet Coefficient Statistics: Packets [4 10] – [4 15]

Packet	Experiment	1	2	3	4	5	6	7	8	9	10	11	12	13	14	15	16
	V_{sg} (m/s)	0.13	0.30	0.58	0.99	0.13	0.30	0.59	1.32	0.13	0.30	0.59	1.32	0.13	0.31	0.59	1.29
	V_{sl} (m/s)	0.12	0.12	0.12	0.12	0.24	0.24	0.24	0.24	0.37	0.37	0.37	0.37	0.49	0.49	0.49	0.49
	WC (%)	1.00	1.00	1.00	1.00	1.00	1.00	1.00	1.00	1.00	1.00	1.00	1.00	1.00	1.00	1.00	1.00
4 10	Mean	0.000	0.000	0.000	0.000	0.000	0.000	0.000	0.000	0.000	0.000	0.000	0.000	0.000	0.000	0.000	0.000
	Median	-0.001	-0.001	0.000	0.000	-0.004	0.001	0.000	-0.004	0.000	0.004	-0.002	-0.007	0.002	-0.002	-0.003	0.000
	Standard dev.	1.823	1.925	2.006	2.140	1.785	1.857	1.964	2.114	1.774	1.845	1.960	2.099	1.733	1.831	1.932	2.059
	Variance	-3.0E-07	1.2E-06	7.4E-07	2.5E-07	1.9E-06	-1.7E-06	5.5E-07	2.0E-07	2.8E-06	2.4E-06	1.6E-06	-6.0E-07	-1.9E-06	3.1E-06	1.9E-06	-1.8E-06
	Skewness	8.9E-07	-8.6E-06	-3.6E-06	-1.1E-05	-2.5E-07	5.9E-06	-1.3E-06	7.2E-07	-1.3E-05	-9.5E-06	-3.7E-06	-8.3E-09	7.4E-06	-1.4E-05	-7.3E-06	5.6E-06
	Kurtosis	0.424	0.361	0.420	0.375	0.450	0.418	0.370	0.368	0.422	0.428	0.444	0.348	0.325	0.439	0.461	0.390
4 11	Mean	0.000	0.000	0.000	0.000	0.000	0.000	0.000	0.000	0.000	0.000	0.000	0.000	0.000	0.000	0.000	0.000
	Median	-0.002	0.003	-0.001	-0.001	-0.004	-0.001	-0.002	0.001	0.000	0.000	0.002	0.000	0.002	-0.001	-0.005	0.005
	Standard dev.	1.808	1.894	2.006	2.135	1.780	1.890	1.959	2.076	1.769	1.850	1.957	2.063	1.763	1.835	1.957	2.073
	Variance	4.4E-07	-3.6E-07	1.2E-06	8.9E-07	-9.7E-07	-4.9E-08	7.2E-07	-4.0E-07	-3.0E-06	-9.5E-07	6.8E-07	-4.8E-08	3.9E-07	6.9E-07	1.2E-06	-9.6E-07
	Skewness	-1.0E-06	7.5E-07	-3.2E-06	-2.9E-06	5.0E-06	1.4E-07	-1.6E-06	1.1E-06	8.8E-06	3.0E-06	-1.7E-06	2.3E-07	-3.2E-06	-1.5E-06	-3.7E-06	3.0E-06
	Kurtosis	0.120	0.155	0.112	0.078	0.131	0.151	0.172	0.100	0.176	0.129	0.139	0.188	0.093	0.109	0.115	0.135
4 12	Mean	0.000	0.000	0.000	0.000	0.000	0.000	0.000	0.000	0.000	0.000	0.000	0.000	0.000	0.000	0.000	0.000
	Median	0.000	-0.001	-0.002	-0.001	-0.001	0.000	-0.001	0.002	0.002	-0.002	0.001	0.000	0.000	0.000	0.001	0.001
	Standard dev.	1.765	1.874	1.966	2.116	1.730	1.840	1.953	2.090	1.697	1.817	1.911	2.066	1.693	1.790	1.910	2.026
	Variance	4.2E-06	3.0E-06	-1.9E-06	2.5E-06	4.5E-06	2.5E-06	-2.0E-06	-6.1E-06	2.6E-06	-8.0E-06	1.2E-06	-2.5E-06	1.5E-06	9.3E-07	3.7E-06	1.7E-06
	Skewness	-5.3E-06	-7.1E-06	5.3E-06	9.9E-05	-7.6E-06	-5.2E-06	-7.3E-07	-3.1E-05	4.0E-06	-1.7E-05	3.8E-05	6.7E-06	-4.0E-06	-3.2E-06	-6.5E-06	5.1E-06
	Kurtosis	1.939	2.101	1.899	1.942	1.885	2.067	1.875	2.020	1.943	1.978	1.917	1.964	1.908	1.956	1.924	1.908
4 13	Mean	0.000	0.000	0.000	0.000	0.000	0.000	0.000	0.000	0.000	0.000	0.000	0.000	0.000	0.000	0.000	0.000
	Median	0.003	0.003	0.000	-0.002	0.001	-0.001	0.002	0.000	0.003	0.001	0.002	0.002	0.001	-0.002	-0.003	0.003
	Standard dev.	1.788	1.871	1.972	2.108	1.750	1.836	1.942	2.090	1.723	1.779	1.910	2.066	1.717	1.818	1.909	2.035
	Variance	-6.2E-07	-7.5E-07	-3.9E-06	-4.0E-06	-1.6E-06	-4.1E-06	6.2E-07	-4.1E-06	-3.7E-06	-1.6E-06	5.1E-06	7.0E-07	-5.2E-07	-2.6E-06	-1.7E-06	-6.5E-07
	Skewness	1.1E-06	4.7E-06	3.9E-06	6.8E-06	5.1E-07	-6.9E-05	8.5E-06	2.9E-06	-6.9E-06	4.6E-06	-1.2E-05	1.2E-05	2.2E-06	5.1E-06	4.1E-06	-1.1E-05
	Kurtosis	0.185	0.330	0.238	0.228	0.188	0.251	0.283	0.289	0.158	0.297	0.195	0.238	0.171	0.266	0.287	0.229
4 14	Mean	0.000	0.000	0.000	0.000	0.000	0.000	0.000	0.000	0.000	0.000	0.000	0.000	0.000	0.000	0.000	0.000
	Median	0.001	-0.001	-0.001	-0.001	0.002	0.000	-0.001	-0.001	0.000	-0.002	0.002	0.002	-0.001	0.000	0.000	0.000
	Standard dev.	1.798	1.895	1.993	2.152	1.753	1.886	1.974	2.086	1.778	1.851	1.919	2.066	1.718	1.825	1.896	2.057
	Variance	1.5E-06	1.7E-07	-1.9E-06	-1.4E-06	-1.5E-06	3.5E-06	-2.6E-06	2.0E-07	-1.8E-06	2.9E-07	-3.8E-07	1.0E-06	1.3E-06	-2.5E-06	-3.0E-06	2.2E-06
	Skewness	-5.7E-06	-2.7E-07	1.2E-05	9.4E-06	2.5E-05	-1.2E-05	4.4E-05	-2.4E-07	2.4E-06	-6.4E-06	3.2E-06	-4.5E-06	-4.5E-06	1.1E-05	7.1E-06	-6.6E-06
	Kurtosis	0.364	0.431	0.391	0.394	0.399	0.412	0.469	0.402	0.385	0.425	0.356	0.414	0.310	0.431	0.459	0.529
4 15	Mean	0.000	0.000	0.000	0.000	0.000	0.000	0.000	0.000	0.000	0.000	0.000	0.000	0.000	0.000	0.000	0.000
	Median	0.000	0.000	0.003	0.011	0.000	-0.003	-0.002	0.000	-0.016	-0.008	0.003	-0.005	0.002	0.004	-0.007	-0.009
	Standard dev.	1.803	1.864	1.983	2.149	1.768	1.874	1.958	2.117	1.753	1.826	1.923	2.069	1.715	1.822	1.917	2.051
	Variance	-1.7E-06	-7.1E-07	2.1E-06	3.2E-06	4.8E-07	8.9E-08	1.0E-06	2.7E-07	2.5E-06	-1.1E-06	-4.3E-06	1.2E-06	-5.2E-07	1.5E-06	9.6E-07	1.2E-08
	Skewness	1.5E-03	5.2E-03	3.1E-03	-1.2E-02	1.8E-02	1.7E-02	1.5E-02	6.6E-03	2.6E-02	1.7E-02	3.7E-04	1.9E-02	-5.7E-03	9.8E-03	1.8E-02	1.6E-02
	Kurtosis	0.115	0.166	0.158	0.143	0.097	0.150	0.304	0.116	0.159	0.149	0.204	0.139	0.180	0.116	0.183	0.103

Packet	Experiment	17	18	19	20	21	22	23	24	25	26	27	28	29	30	31	32
	V_{sg} (m/s)	0.15	0.30	0.59	1.32	0.15	0.31	0.59	1.33	0.15	0.30	0.59	1.32	0.15	0.30	0.59	1.00
	V_{sl} (m/s)	0.61	0.61	0.61	0.61	0.73	0.73	0.73	0.73	0.79	0.79	0.79	0.79	0.13	0.13	0.13	0.13
	WC (%)	1.00	1.00	1.00	1.00	1.00	1.00	1.00	1.00	1.00	1.00	1.00	1.00	0.80	0.80	0.80	0.80
4 10	Mean	0.000	0.000	0.000	0.000	0.000	0.000	0.000	0.000	0.000	0.000	0.000	0.000	0.000	0.000	0.000	0.000
	Median	0.000	0.001	-0.001	0.006	0.000	-0.005	0.002	0.005	-0.003	0.003	0.001	-0.003	0.001	0.000	0.006	0.006
	Standard dev.	1.759	1.817	1.906	2.026	1.745	1.799	1.928	2.032	1.752	1.789	1.894	2.056	1.853	1.926	2.038	2.128
	Variance	-6.1E-07	-2.1E-06	-3.4E-07	1.5E-06	-2.4E-07	-3.1E-06	-4.4E-07	-3.0E-06	-2.6E-06	3.3E-06	-1.5E-06	-1.9E-06	-1.6E-06	-1.9E-06	-3.6E-06	-2.9E-06
	Skewness	2.8E-06	8.2E-06	-2.1E-08	-5.9E-06	7.5E-07	8.9E-06	1.6E-06	1.2E-05	7.9E-06	-9.4E-06	6.4E-06	1.1E-05	1.2E-05	-1.1E-05	5.6E-06	1.9E-05
	Kurtosis	0.333	0.450	0.459	0.379	0.369	0.308	0.292	0.507	0.400	0.381	0.294	0.413	0.410	0.467	0.460	0.473
4 11	Mean	0.000	0.000	0.000	0.000	0.000	0.000	0.000	0.000	0.000	0.000	0.000	0.000	0.000	0.000	0.000	0.000
	Median	-0.002	-0.001	0.000	-0.002	0.000	-0.003	0.001	-0.003	0.000	0.002	-0.003	0.001	0.004	-0.003	0.003	0.004
	Standard dev.	1.736	1.801	1.911	2.040	1.727	1.812	1.900	2.044	1.770	1.791	1.880	2.018	1.835	1.934	2.058	2.151
	Variance	1.3E-06	-1.3E-06	-3.7E-07	-1.0E-08	1.7E-06	2.6E-06	-7.7E-08	-1.7E-06	2.9E-06	-4.3E-06	-5.4E-07	-1.5E-06	-1.0E-06	4.2E-06	2.6E-06	1.8E-06
	Skewness	-5.2E-06	4.6E-06	1.4E-06	5.4E-07	-5.4E-06	-9.5E-06	2.4E-07	5.5E-06	-7.8E-06	1.6E-05	1.8E-06	4.7E-06	3.0E-06	-2.0E-05	-6.9E-06	-6.9E-06
	Kurtosis	0.071	0.074	0.095	0.105	0.099	0.067	0.174	0.053	0.088	0.168	0.138	0.135	0.146	0.157	0.150	0.125
4 12	Mean	0.000	0.000	0.000	0.000	0.000	0.000	0.000	0.000	0.000	0.000	0.000	0.000	0.000	0.000	0.000	0.000
	Median	-0.001	-0.001	0.000	0.002	0.000	0.000	0.001	0.002	-0.001	0.000	0.001	0.000	-0.001	-0.003	0.000	0.001
	Standard dev.	1.660	1.768	1.892	2.023	1.682	1.753	1.873	1.998	1.716	1.752	1.868	2.018	1.807	1.892	2.000	2.121
	Variance	-1.5E-06	-3.7E-06	1.0E-05	8.3E-07	4.4E-07	4.2E-06	-5.7E-06	-8.7E-06	-3.1E-06	3.3E-06	-1.9E-06	-2.3E-06	2.3E-06	-9.7E-06	-5.5E-06	-1.4E-06
	Skewness	7.2E-06	8.6E-06	1.1E-04	3.1E-06	2.7E-07	-7.3E-06	-7.4E-05	-8.7E-05	2.7E-06	-6.2E-06	4.2E-06	-8.6E-07	-6.0E-06	-2.7E-06	-4.3E-05	-4.2E-06
	Kurtosis	1.794	1.986	1.930	1.869	1.800	1.901	1.968	1.859	1.792	1.802	1.868	1.987	1.876	1.955	1.936	1.909
4 13	Mean	0.000	0.000	0.000	0.000	0.000	0.000	0.000	0.000	0.000	0.000	0.000	0.000	0.000	0.000	0.000	0.000
	Median	0.003	-0.004	0.003	0.000	0.003	-0.001	-0.001	0.003	-0.002	0.002	0.001	0.002	0.000	0.000	-0.001	0.000
	Standard dev.	1.699	1.806	1.887	2.022	1.696	1.780	1.879	2.031	1.734	1.773	1.871	1.970	1.818	1.910	1.997	2.110
	Variance	-1.1E-06	-1.0E-06	2.9E-06	-4.5E-06	1.6E-06	1.6E-06	-8.4E-07	-2.6E-06	1.9E-06	3.6E-06	-2.3E-07	1.4E-06	2.1E-06	-2.1E-06	2.1E-06	-2.3E-06
	Skewness	-9.1E-06	-1.6E-05	-3.7E-06	-3.0E-06	4.1E-06	-3.6E-06	-1.2E-05	2.8E-06	-3.3E-06	7.6E-06	-3.9E-06	1.6E-06	-2.9E-06	-1.3E-05	-2.2E-05	4.8E-06
	Kurtosis	0.254	0.294	0.288	0.278	0.220	0.208	0.268	0.221	0.209	0.241	0.236	0.242	0.202	0.295	0.273	0.268
4 14	Mean	0.000	0.000	0.000	0.000	0.000	0.000	0.000	0.000	0.000	0.000	0.000	0.000	0.000	0.000	0.000	0.000
	Median	-0.001	-0.001	-0.002	0.003	-0.002	0.001	-0.002	0.001	-0.001	0.000	-0.001	0.001	-0.001	-0.001	0.000	0.001
	Standard dev.	1.739	1.803	1.915	2.024	1.724	1.798	1.894	2.032	1.761	1.809	1.881	2.028	1.833	1.909	2.011	2.124
	Variance	8.1E-07	5.8E-07	-6.5E-07	-6.3E-07	2.1E-06	9.9E-07	3.1E-07	2.4E-06	7.7E-07	-1.1E-06	1.6E-06	2.7E-06	9.0E-07	-1.8E-06	4.1E-07	4.0E-06
	Skewness	-2.0E-05	5.1E-06	2.3E-06	-8.3E-07	-6.0E-06	-9.3E-06	-3.5E-06	-2.3E-05	-3.5E-06	4.4E-06	-5.3E-06	-1.6E-05	-8.4E-07	3.4E-07	-3.1E-06	-2.7E-05
	Kurtosis	0.324	0.409	0.437	0.368	0.318	0.374	0.386	0.467	0.390	0.365	0.375	0.376	0.465	0.459	0.410	0.492
4 15	Mean	0.000	0.000	0.000	0.000	0.000	0.000	0.000	0.000	0.000	0.000	0.000	0.000	0.000	0.000	0.000	0.000
	Median	-0.005	-0.003	0.001	0.003	0.000	0.003	-0.010	0.007	-0.004	-0.003	-0.001	0.000	0.002	-0.005	0.005	-0.007
	Standard dev.	1.734	1.782	1.886	2.004	1.712	1.786	1.896	2.032	1.733	1.773	1.875	2.021	1.825	1.925	2.010	2.076
	Variance	9.2E-07	4.3E-06	-1.3E-06	2.3E-06	-6.6E-06	5.0E-07	2.1E-06	1.1E-06	3.5E-07	-1.2E-06	2.9E-06	-2.7E-06	8.0E-07	2.8E-06	-4.3E-07	-8.2E-08
	Skewness	3.0E-02	-1.2E-02	-7.8E-03	-1.1E-02	1.9E-02	-5.1E-03	1.1E-02	-1.5E-02	5.3E-03	-5.6E-03	-3.3E-03	1.8E-02	6.4E-03	1.0E-02	-1.1E-02	4.0E-03
	Kurtosis	0.216	0.141	0.215	0.164	0.072	0.136	0.239	0.161	0.149	0.172	0.067	0.204	0.127	0.171	0.127	0.165

Packet	Experiment	33	34	35	36	37	38	39	40	41	42	43	44	45	46	47	48
	V_{sg} (m/s)	0.15	0.30	0.59	1.00	0.15	0.30	0.59	1.00	0.15	0.30	0.59	1.00	0.15	0.31	0.59	1.33
	V_{sl} (m/s)	0.13	0.13	0.13	0.13	0.14	0.14	0.14	0.14	0.14	0.14	0.14	0.14	0.25	0.25	0.25	0.25
	WC (%)	0.60	0.60	0.60	0.60	0.40	0.40	0.40	0.40	0.20	0.20	0.20	0.20	0.80	0.80	0.80	0.80
4 10	Mean	0.000	0.000	0.000	0.000	0.000	0.000	0.000	0.000	0.000	0.000	0.000	0.000	0.000	0.000	0.000	0.000
	Median	-0.001	0.001	-0.002	-0.002	0.003	-0.004	-0.004	-0.001	0.001	0.002	-0.005	-0.001	0.000	0.003	0.002	-0.001
	Standard dev.	1.809	1.917	2.000	2.081	1.824	1.902	1.993	2.115	1.892	1.985	2.046	2.140	1.782	1.855	1.935	2.061
	Variance	1.5E-06	1.4E-06	4.8E-07	-2.1E-06	-1.1E-06	1.5E-06	-2.3E-06	-1.7E-06	-4.7E-07	-2.1E-06	-3.5E-06	-3.8E-06	-1.8E-06	3.0E-07	1.7E-06	-1.9E-06
	Skewness	-4.5E-06	-4.1E-06	-1.2E-06	7.1E-06	8.5E-07	-3.4E-06	4.2E-06	6.9E-06	6.1E-07	8.9E-06	7.8E-06	1.4E-05	5.3E-06	1.6E-06	-3.1E-06	7.0E-06
	Kurtosis	0.369	0.453	0.470	0.371	0.391	0.392	0.419	0.470	0.399	0.379	0.325	0.386	0.303	0.468	0.394	0.435
4 11	Mean	0.000	0.000	0.000	0.000	0.000	0.000	0.000	0.000	0.000	0.000	0.000	0.000	0.000	0.000	0.000	0.000
	Median	-0.001	0.000	0.001	0.000	-0.001	0.001	0.000	0.001	0.001	-0.001	0.001	0.001	0.001	-0.001	0.001	0.000
	Standard dev.	1.841	1.924	2.001	2.125	1.879	1.930	2.013	2.105	1.913	1.963	2.058	2.142	1.796	1.863	1.965	2.056
	Variance	-2.9E-07	2.0E-06	3.8E-07	-2.0E-06	1.5E-06	-1.4E-06	3.1E-06	1.2E-06	8.4E-07	2.1E-06	8.7E-08	1.9E-06	-6.5E-07	-4.6E-06	-1.7E-08	-9.3E-07
	Skewness	7.3E-07	-5.8E-06	-3.8E-06	8.0E-06	-4.5E-06	4.6E-06	-8.2E-06	-2.3E-06	-3.4E-06	-6.1E-06	3.7E-08	-5.7E-06	2.0E-06	1.3E-05	-8.5E-08	3.1E-06
	Kurtosis	0.140	0.149	0.083	0.143	0.090	0.226	0.230	0.205	0.075	0.229	0.169	0.126	0.116	0.134	0.081	0.107
4 12	Mean	0.000	0.000	0.000	0.000	0.000	0.000	0.000	0.000	0.000	0.000	0.000	0.000	0.000	0.000	0.000	0.000
	Median	0.000	-0.001	0.000	-0.001	0.001	0.000	0.001	0.001	-0.001	0.000	0.000	-0.001	0.000	-0.002	0.000	-0.001
	Standard dev.	1.796	1.869	1.988	2.073	1.803	1.881	1.983	2.056	1.837	1.924	2.018	2.118	1.728	1.814	1.911	2.039
	Variance	-4.8E-06	8.3E-07	3.0E-07	4.4E-06	4.9E-06	-8.1E-07	-1.8E-06	3.0E-06	2.2E-07	1.3E-06	-8.6E-07	2.8E-06	1.7E-06	3.9E-06	-2.2E-07	-3.0E-06
	Skewness	7.6E-06	-9.3E-06	9.2E-06	-6.8E-06	4.9E-06	2.8E-06	-1.5E-05	-6.8E-06	-4.5E-06	8.7E-06	2.2E-06	1.6E-06	-3.3E-06	9.9E-06	2.8E-06	8.2E-06
	Kurtosis	1.873	1.949	1.943	2.038	1.817	1.858	2.053	1.815	1.965	1.874	1.929	1.861	1.882	1.909	2.034	1.852
4 13	Mean	0.000	0.000	0.000	0.000	0.000	0.000	0.000	0.000	0.000	0.000	0.000	0.000	0.000	0.000	0.000	0.000
	Median	0.002	-0.002	-0.001	-0.002	0.000	-0.001	-0.004	-0.003	0.002	-0.003	0.001	-0.001	0.001	0.000	0.002	-0.002
	Standard dev.	1.798	1.899	1.996	2.073	1.809	1.888	1.991	2.096	1.860	1.929	2.023	2.124	1.749	1.831	1.918	2.043
	Variance	-2.8E-06	-6.6E-06	1.4E-06	3.1E-06	-9.2E-08	-2.4E-06	1.3E-06	3.7E-07	1.6E-06	8.1E-07	1.9E-06	3.5E-06	-2.2E-06	-1.6E-06	2.2E-06	-1.9E-06
	Skewness	-4.2E-06	1.2E-05	5.6E-06	-8.7E-06	2.4E-06	-1.3E-05	5.3E-06	-9.1E-07	-3.3E-06	5.8E-06	-1.7E-06	1.2E-05	-4.6E-06	4.6E-06	1.9E-07	6.8E-06
	Kurtosis	0.218	0.169	0.284	0.166	0.289	0.268	0.281	0.274	0.168	0.189	0.178	0.218	0.209	0.293	0.222	0.299
4 14	Mean	0.000	0.000	0.000	0.000	0.000	0.000	0.000	0.000	0.000	0.000	0.000	0.000	0.000	0.000	0.000	0.000
	Median	0.000	0.002	-0.002	0.005	0.000	0.002	0.002	-0.002	0.000	0.002	0.001	-0.002	-0.001	0.003	0.000	0.000
	Standard dev.	1.830	1.924	1.984	2.100	1.843	1.914	2.012	2.108	1.865	1.968	2.044	2.117	1.780	1.864	1.932	2.056
	Variance	-1.4E-06	-3.1E-06	-3.9E-07	2.1E-06	1.3E-06	3.0E-07	1.7E-06	1.4E-06	6.9E-07	1.3E-06	4.7E-06	3.3E-06	2.4E-07	2.5E-06	-6.4E-08	2.0E-06
	Skewness	-2.8E-05	9.8E-06	-3.4E-06	-6.6E-05	-2.1E-05	-1.5E-05	-3.9E-05	-4.8E-06	-4.3E-06	-5.8E-06	-5.1E-05	-1.9E-05	-1.0E-06	-1.1E-05	3.1E-06	-1.1E-05
	Kurtosis	0.445	0.396	0.431	0.411	0.445	0.419	0.486	0.417	0.363	0.381	0.481	0.312	0.446	0.462	0.343	0.409
4 15	Mean	0.000	0.000	0.000	0.000	0.000	0.000	0.000	0.000	0.000	0.000	0.000	0.000	0.000	0.000	0.000	0.000
	Median	0.002	-0.006	-0.014	0.008	0.003	-0.004	-0.015	-0.003	0.007	-0.006	-0.005	-0.012	0.002	-0.008	0.004	0.000
	Standard dev.	1.831	1.891	1.967	2.107	1.813	1.909	1.995	2.059	1.866	1.951	2.053	2.123	1.761	1.853	1.904	2.053
	Variance	1.2E-06	2.3E-06	-2.5E-06	-5.9E-07	-2.3E-06	-1.5E-07	-2.8E-06	7.6E-07	-1.5E-07	2.7E-07	-8.8E-07	-4.2E-06	-1.4E-07	4.0E-08	-2.0E-06	-1.8E-07
	Skewness	-9.6E-03	2.0E-02	3.4E-02	-5.5E-03	3.7E-03	3.4E-03	2.8E-02	1.1E-02	-5.4E-03	-8.1E-03	5.3E-03	2.0E-02	-7.0E-03	6.0E-03	-7.2E-05	1.2E-02
	Kurtosis	0.065	0.106	0.193	0.237	0.118	0.185	0.142	0.129	0.072	0.088	0.133	0.097	0.164	0.089	0.161	0.136

Packet	Experiment	49	50	51	52	53	54	55	56	57	58	59	60	61	62	63	64
	V_{sg} (m/s)	0.15	0.23	0.60	1.31	0.15	0.31	0.59	1.32	0.15	0.31	0.59	1.32	0.15	0.31	0.59	1.34
	V_{sl} (m/s)	0.27	0.27	0.27	0.27	0.28	0.28	0.28	0.28	0.29	0.29	0.29	0.29	0.38	0.38	0.38	0.38
	WC (%)	0.60	0.60	0.60	0.60	0.40	0.40	0.40	0.40	0.20	0.20	0.20	0.20	0.80	0.80	0.80	0.80
4 10	Mean	0.000	0.000	0.000	0.000	0.000	0.000	0.000	0.000	0.000	0.000	0.000	0.000	0.000	0.000	0.000	0.000
	Median	0.002	0.002	0.000	-0.005	0.000	-0.001	-0.001	-0.002	0.000	0.005	0.001	0.001	0.001	0.004	-0.001	0.003
	Standard dev.	1.790	1.820	1.932	2.051	1.807	1.864	1.923	2.031	1.828	1.895	1.984	2.114	1.771	1.847	1.897	2.042
	Variance	1.6E-07	-8.4E-07	-4.3E-07	1.7E-06	-7.1E-08	-3.4E-07	-1.2E-06	2.2E-06	-4.7E-07	6.8E-07	-2.9E-06	-2.7E-07	1.8E-06	1.5E-06	-1.8E-06	4.0E-07
	Skewness	-3.7E-07	3.1E-06	1.2E-06	-2.0E-05	4.8E-07	4.6E-07	4.6E-06	-7.6E-06	2.5E-06	-3.6E-06	1.9E-05	1.0E-06	-5.3E-06	-4.4E-06	3.3E-06	-2.5E-07
	Kurtosis	0.353	0.424	0.368	0.337	0.367	0.397	0.458	0.396	0.398	0.432	0.370	0.344	0.276	0.467	0.373	0.485
4 11	Mean	0.000	0.000	0.000	0.000	0.000	0.000	0.000	0.000	0.000	0.000	0.000	0.000	0.000	0.000	0.000	0.000
	Median	0.001	-0.002	-0.001	-0.002	0.000	0.003	0.000	0.003	0.001	0.003	0.000	0.004	-0.001	-0.001	0.000	0.002
	Standard dev.	1.804	1.835	1.936	2.065	1.803	1.866	1.934	2.047	1.842	1.916	1.973	2.087	1.798	1.864	1.927	2.057
	Variance	1.7E-06	1.8E-06	7.8E-07	1.4E-06	2.3E-07	6.1E-07	-2.2E-07	-1.1E-06	-1.6E-06	4.3E-08	1.1E-06	2.0E-06	-1.2E-06	-2.7E-06	4.4E-07	-2.6E-07
	Skewness	-4.7E-06	-6.4E-06	-2.3E-06	-4.7E-06	-6.0E-07	-2.0E-06	1.1E-06	3.3E-06	4.7E-06	4.0E-08	-3.7E-06	-6.5E-06	3.8E-06	6.8E-06	-1.3E-06	1.0E-06
	Kurtosis	0.169	0.099	0.243	0.155	0.194	0.107	0.249	0.101	0.094	0.072	0.164	0.235	0.098	0.130	0.198	0.164
4 12	Mean	0.000	0.000	0.000	0.000	0.000	0.000	0.000	0.000	0.000	0.000	0.000	0.000	0.000	0.000	0.000	0.000
	Median	0.001	-0.001	0.000	0.000	0.002	-0.001	0.001	0.001	0.000	-0.001	-0.001	-0.001	0.000	0.000	-0.004	0.000
	Standard dev.	1.736	1.785	1.899	2.035	1.749	1.825	1.896	2.052	1.786	1.853	1.931	2.065	1.708	1.789	1.895	2.023
	Variance	2.8E-06	9.8E-07	-2.9E-06	-8.9E-06	-1.1E-06	-4.7E-06	-4.9E-06	9.0E-06	1.0E-06	-5.0E-06	-4.0E-06	8.0E-06	8.0E-06	-1.1E-06	-2.6E-07	7.9E-06
	Skewness	-6.3E-06	-3.1E-06	-2.7E-06	-1.3E-04	2.9E-06	-1.6E-05	-2.1E-05	3.7E-05	-7.4E-07	8.6E-07	1.0E-05	1.2E-05	-5.8E-06	5.5E-08	7.6E-07	3.2E-06
	Kurtosis	1.942	1.903	1.845	1.885	2.115	2.008	1.942	1.974	1.889	1.918	2.020	1.778	1.859	1.994	1.913	1.837
4 13	Mean	0.000	0.000	0.000	0.000	0.000	0.000	0.000	0.000	0.000	0.000	0.000	0.000	0.000	0.000	0.000	0.000
	Median	0.001	0.003	0.000	0.001	-0.001	0.000	0.003	0.000	-0.003	0.002	0.002	-0.003	0.001	0.000	-0.001	0.001
	Standard dev.	1.744	1.802	1.895	2.051	1.765	1.829	1.930	2.035	1.791	1.849	1.950	2.065	1.737	1.817	1.901	2.021
	Variance	2.1E-06	1.7E-06	2.6E-06	-2.1E-06	-2.0E-06	2.1E-06	-2.1E-06	-2.1E-07	-5.4E-07	-9.6E-07	1.6E-06	-1.2E-06	-1.1E-06	-2.1E-06	3.1E-06	-9.2E-07
	Skewness	-1.3E-06	5.0E-06	1.2E-05	5.4E-06	4.1E-06	-4.8E-06	4.2E-06	-2.3E-06	1.6E-06	5.5E-06	7.4E-06	3.6E-06	2.5E-07	-2.7E-05	-3.5E-06	-1.1E-05
	Kurtosis	0.155	0.229	0.228	0.153	0.316	0.195	0.365	0.321	0.169	0.247	0.190	0.250	0.260	0.294	0.241	0.163
4 14	Mean	0.000	0.000	0.000	0.000	0.000	0.000	0.000	0.000	0.000	0.000	0.000	0.000	0.000	0.000	0.000	0.000
	Median	-0.002	-0.001	0.000	0.003	0.002	-0.003	-0.001	0.000	0.000	0.000	0.000	0.003	-0.001	-0.002	0.001	0.001
	Standard dev.	1.800	1.823	1.929	2.046	1.793	1.834	1.921	2.040	1.847	1.865	1.977	2.108	1.749	1.825	1.932	2.030
	Variance	-1.6E-06	2.7E-07	-1.3E-06	-1.9E-06	2.6E-07	-1.5E-06	6.2E-07	-2.6E-06	9.5E-07	-1.4E-06	2.8E-06	-1.9E-06	2.4E-06	-1.0E-07	2.5E-06	2.0E-06
	Skewness	5.4E-06	-8.9E-06	6.9E-06	3.2E-06	-1.4E-06	5.5E-06	-2.0E-06	1.8E-05	-3.9E-06	6.7E-06	-1.0E-05	5.4E-06	-1.5E-05	1.4E-06	-1.1E-05	-1.7E-05
	Kurtosis	0.401	0.392	0.373	0.393	0.459	0.483	0.393	0.426	0.368	0.387	0.371	0.389	0.395	0.407	0.313	0.430
4 15	Mean	0.000	0.000	0.000	0.000	0.000	0.000	0.000	0.000	0.000	0.000	0.000	0.000	0.000	0.000	0.000	0.000
	Median	0.007	0.002	-0.005	-0.001	-0.001	-0.007	0.000	0.000	0.004	-0.008	0.006	0.001	0.004	0.000	-0.009	-0.009
	Standard dev.	1.761	1.814	1.887	2.025	1.797	1.846	1.920	2.057	1.800	1.887	1.956	2.074	1.765	1.803	1.918	2.042
	Variance	-1.2E-06	-5.9E-07	1.6E-06	-6.9E-07	-3.3E-07	1.1E-07	2.0E-06	5.6E-07	2.4E-07	3.0E-06	5.5E-07	9.1E-07	-2.0E-06	-7.8E-07	-3.5E-06	-3.0E-06
	Skewness	-1.2E-02	-3.2E-03	1.8E-02	1.4E-02	-1.1E-02	-2.7E-03	-1.3E-02	6.0E-03	-7.6E-03	7.2E-03	-5.4E-04	2.3E-03	8.5E-03	-1.9E-02	1.4E-02	-8.9E-03
	Kurtosis	0.159	0.115	0.106	0.105	0.215	0.148	0.191	0.150	0.168	0.213	0.103	0.086	0.100	0.168	0.132	0.127

Packet	Experiment	65	66	67	68	69	70	71	72	73	74	75	76	77	78	79	80
	V_{sg} (m/s)	0.15	0.29	0.59	1.33	0.15	0.31	0.59	1.32	0.16	0.31	0.59	1.33	0.15	0.31	0.59	1.34
	V_{sl} (m/s)	0.40	0.40	0.40	0.40	0.41	0.41	0.41	0.41	0.43	0.43	0.43	0.43	0.51	0.51	0.51	0.51
	WC (%)	0.60	0.60	0.60	0.60	0.40	0.40	0.40	0.40	0.20	0.20	0.20	0.20	0.80	0.80	0.80	0.80
4 10	Mean	0.000	0.000	0.000	0.000	0.000	0.000	0.000	0.000	0.000	0.000	0.000	0.000	0.000	0.000	0.000	0.000
	Median	0.001	-0.002	0.002	-0.002	0.004	0.002	-0.001	0.006	0.004	0.003	-0.002	-0.001	-0.002	-0.002	0.001	-0.003
	Standard dev.	1.801	1.842	1.887	2.023	1.773	1.861	1.935	2.048	1.806	1.864	1.951	2.072	1.765	1.837	1.877	2.016
	Variance	3.8E-06	-2.1E-06	-1.4E-06	2.7E-06	3.4E-06	2.2E-06	-1.6E-06	-2.9E-07	8.7E-07	-3.2E-06	-1.8E-06	1.6E-06	-4.7E-06	-3.3E-06	-4.1E-06	-1.1E-06
	Skewness	-1.2E-05	8.7E-06	4.9E-06	-2.3E-05	-1.2E-05	-5.3E-06	4.6E-06	7.6E-07	-2.4E-06	8.3E-06	5.9E-06	-4.5E-06	1.0E-05	8.8E-06	9.5E-06	3.3E-06
	Kurtosis	0.365	0.472	0.350	0.350	0.344	0.386	0.472	0.416	0.359	0.312	0.382	0.487	0.481	0.401	0.438	0.364
4 11	Mean	0.000	0.000	0.000	0.000	0.000	0.000	0.000	0.000	0.000	0.000	0.000	0.000	0.000	0.000	0.000	0.000
	Median	0.000	0.003	0.004	0.000	0.002	0.000	0.003	-0.003	-0.003	-0.001	0.001	0.001	0.002	0.003	-0.003	-0.002
	Standard dev.	1.773	1.825	1.931	2.056	1.796	1.837	1.924	2.048	1.811	1.897	1.981	2.076	1.778	1.843	1.911	2.017
	Variance	-2.9E-06	2.2E-06	6.1E-07	7.4E-07	-5.1E-07	2.3E-07	-1.5E-07	-6.5E-07	-2.6E-06	6.1E-07	-8.1E-07	-1.7E-06	1.3E-07	2.1E-06	1.3E-06	-2.7E-06
	Skewness	1.1E-05	-5.8E-06	-3.1E-06	-2.5E-06	1.5E-06	-9.7E-07	8.5E-07	2.0E-06	7.6E-06	-2.3E-06	2.6E-06	1.1E-06	-1.7E-07	-5.3E-06	-3.8E-06	7.4E-06
	Kurtosis	0.124	0.109	0.128	0.110	0.073	0.168	0.174	0.091	0.066	0.191	0.168	0.156	0.077	0.110	0.198	0.150
4 12	Mean	0.000	0.000	0.000	0.000	0.000	0.000	0.000	0.000	0.000	0.000	0.000	0.000	0.000	0.000	0.000	0.000
	Median	0.000	0.002	0.001	0.000	0.000	0.001	-0.002	-0.001	-0.001	-0.002	0.000	-0.002	0.000	0.000	0.000	0.000
	Standard dev.	1.728	1.774	1.915	2.025	1.717	1.807	1.886	2.028	1.768	1.839	1.916	2.023	1.704	1.783	1.879	2.022
	Variance	-9.3E-07	1.0E-06	-5.2E-06	-4.4E-06	-2.0E-06	-5.3E-06	-5.1E-06	5.6E-06	-1.8E-06	3.2E-07	1.2E-06	-8.4E-06	-4.1E-06	2.0E-06	4.7E-06	-1.5E-06
	Skewness	-6.0E-06	6.2E-06	-1.3E-06	-6.4E-05	-1.6E-05	9.0E-06	9.8E-06	9.9E-06	5.1E-06	1.9E-07	-3.6E-06	-3.3E-05	-7.5E-06	4.9E-06	9.5E-06	-7.4E-06
	Kurtosis	1.910	1.812	1.927	1.907	1.853	1.961	1.866	1.925	1.829	1.987	1.877	1.821	1.802	1.932	2.039	2.032
4 13	Mean	0.000	0.000	0.000	0.000	0.000	0.000	0.000	0.000	0.000	0.000	0.000	0.000	0.000	0.000	0.000	0.000
	Median	-0.004	0.002	0.003	0.000	-0.004	0.000	-0.003	-0.002	-0.003	0.001	0.001	0.002	-0.001	-0.003	0.000	0.003
	Standard dev.	1.748	1.817	1.890	2.023	1.765	1.817	1.896	2.015	1.773	1.861	1.922	2.040	1.720	1.776	1.872	2.028
	Variance	-9.2E-07	7.7E-07	-1.0E-06	1.3E-06	3.4E-07	3.8E-06	6.0E-06	-1.0E-06	-1.9E-06	1.0E-06	-2.5E-06	2.3E-06	-3.7E-06	-1.0E-06	-2.9E-07	3.3E-06
	Skewness	-1.7E-05	6.0E-06	3.0E-06	-1.1E-05	-1.1E-06	2.3E-06	7.2E-05	-4.2E-05	5.7E-06	-4.9E-05	5.5E-06	8.9E-06	5.8E-06	-1.6E-05	2.8E-06	4.1E-06
	Kurtosis	0.231	0.252	0.278	0.272	0.213	0.247	0.212	0.253	0.177	0.161	0.205	0.267	0.182	0.194	0.225	0.257
4 14	Mean	0.000	0.000	0.000	0.000	0.000	0.000	0.000	0.000	0.000	0.000	0.000	0.000	0.000	0.000	0.000	0.000
	Median	-0.001	0.000	0.003	0.001	0.002	0.000	0.000	-0.001	0.001	0.000	-0.001	0.001	0.001	0.000	0.002	-0.001
	Standard dev.	1.784	1.832	1.922	2.037	1.768	1.843	1.907	2.028	1.798	1.852	1.950	2.074	1.753	1.805	1.892	2.026
	Variance	-2.5E-06	-1.7E-06	6.5E-07	-3.9E-06	-3.0E-06	-8.1E-07	2.7E-06	2.2E-06	-1.4E-06	1.8E-06	2.5E-06	-2.6E-06	3.8E-06	2.9E-06	5.6E-06	1.3E-06
	Skewness	7.0E-06	2.9E-05	-9.5E-07	6.5E-05	3.0E-05	2.3E-06	-1.8E-05	-7.0E-06	1.5E-05	1.5E-06	-7.3E-06	9.8E-06	-8.5E-05	-6.1E-06	-8.0E-05	-1.1E-05
	Kurtosis	0.377	0.505	0.439	0.400	0.393	0.398	0.493	0.391	0.348	0.363	0.418	0.366	0.381	0.396	0.308	0.448
4 15	Mean	0.000	0.000	0.000	0.000	0.000	0.000	0.000	0.000	0.000	0.000	0.000	0.000	0.000	0.000	0.000	0.000
	Median	-0.007	-0.003	-0.001	-0.001	-0.002	-0.016	-0.002	0.002	-0.001	0.006	0.005	-0.012	-0.005	-0.005	0.001	-0.008
	Standard dev.	1.747	1.820	1.890	2.032	1.776	1.835	1.929	2.008	1.781	1.852	1.930	2.045	1.732	1.822	1.887	2.006
	Variance	-5.5E-07	2.1E-06	6.9E-07	1.1E-06	3.8E-07	-1.7E-06	-2.0E-06	3.1E-07	3.5E-07	-1.6E-06	1.1E-06	3.5E-06	7.5E-07	1.4E-06	-3.6E-06	-1.1E-06
	Skewness	1.3E-02	1.8E-02	-1.3E-02	1.1E-03	-7.0E-03	8.0E-03	1.4E-02	6.0E-03	3.7E-03	-1.8E-04	-8.9E-04	1.8E-02	1.7E-02	3.6E-02	3.3E-03	1.4E-02
	Kurtosis	0.110	0.137	0.075	0.133	0.140	0.077	0.172	0.248	0.149	0.144	0.075	0.099	0.077	0.096	0.116	0.123

Packet	Experiment	**81**	**82**	**83**	**84**	**85**	**86**	**87**	**88**	**89**	**90**	**91**	**92**	**93**	**94**	**95**	**96**
	V_{sg} (m/s)	0.15	0.24	0.59	1.34	0.16	0.31	0.59	1.34	0.16	0.35	0.66	1.33	0.15	0.31	0.60	1.32
	V_{sl} (m/s)	0.53	0.53	0.53	0.53	0.55	0.55	0.55	0.55	0.57	0.57	0.57	0.57	0.64	0.64	0.64	0.64
	WC (%)	0.60	0.60	0.60	0.60	0.40	0.40	0.40	0.40	0.20	0.20	0.20	0.20	0.80	0.80	0.80	0.80
4 10	Mean	0.000	0.000	0.000	0.000	0.000	0.000	0.000	0.000	0.000	0.000	0.000	0.000	0.000	0.000	0.000	0.000
	Median	0.002	-0.001	0.000	0.001	0.004	-0.007	-0.001	-0.002	-0.004	0.001	-0.005	-0.004	-0.002	0.001	-0.001	-0.002
	Standard dev.	1.768	1.814	1.917	1.999	1.770	1.813	1.904	2.026	1.844	1.750	1.944	2.058	1.733	1.806	1.896	2.001
	Variance	-1.1E-06	1.9E-06	1.4E-06	2.0E-06	-3.0E-06	-5.3E-07	-1.2E-06	1.8E-06	5.2E-06	4.6E-07	2.0E-06	-4.2E-07	-3.8E-06	6.8E-07	1.2E-06	-4.2E-06
	Skewness	3.7E-06	-4.8E-06	-5.4E-06	-5.1E-06	1.2E-05	1.3E-06	8.4E-06	-2.3E-06	-1.2E-05	-3.0E-06	8.1E-07	1.2E-06	3.1E-05	-1.5E-06	-3.7E-06	1.2E-05
	Kurtosis	0.454	0.462	0.427	0.346	0.370	0.373	0.481	0.416	0.398	0.350	0.447	0.405	0.394	0.382	0.490	0.355
4 11	Mean	0.000	0.000	0.000	0.000	0.000	0.000	0.000	0.000	0.000	0.000	0.000	0.000	0.000	0.000	0.000	0.000
	Median	0.001	0.002	-0.001	-0.002	-0.003	0.002	0.003	0.002	0.000	-0.003	0.001	0.003	0.003	0.004	0.000	0.000
	Standard dev.	1.788	1.814	1.911	1.987	1.775	1.819	1.917	2.013	1.832	1.761	1.946	2.040	1.730	1.842	1.884	2.015
	Variance	-1.1E-06	7.2E-07	3.4E-06	-2.4E-06	-2.1E-06	-1.0E-06	2.8E-06	6.8E-07	-1.8E-06	-4.3E-08	1.5E-06	-2.3E-06	3.8E-07	2.9E-06	-2.2E-06	-8.0E-07
	Skewness	3.2E-06	-1.6E-06	-1.1E-05	7.9E-06	6.2E-06	3.0E-06	-8.5E-06	-3.1E-06	5.1E-06	3.0E-07	-1.5E-06	8.8E-06	-1.1E-06	-4.1E-06	6.3E-06	2.5E-06
	Kurtosis	0.126	0.119	0.142	0.158	0.105	0.195	0.171	0.184	0.085	0.134	0.114	0.178	0.094	0.180	0.143	0.130
4 12	Mean	0.000	0.000	0.000	0.000	0.000	0.000	0.000	0.000	0.000	0.000	0.000	0.000	0.000	0.000	0.000	0.000
	Median	-0.001	0.000	0.001	0.002	0.001	0.000	0.001	-0.001	-0.001	0.001	0.000	0.001	0.002	-0.001	0.000	-0.002
	Standard dev.	1.702	1.743	1.856	2.032	1.741	1.794	1.890	2.032	1.789	1.674	1.901	2.039	1.703	1.775	1.878	1.993
	Variance	5.9E-06	1.5E-06	-3.0E-06	4.1E-06	1.7E-06	8.7E-07	-2.0E-06	1.0E-06	-6.4E-06	-5.3E-07	-1.1E-05	3.6E-06	-1.5E-06	3.3E-06	-5.4E-06	-1.4E-06
	Skewness	7.3E-06	-4.1E-06	4.4E-06	2.6E-06	-5.1E-06	-6.2E-07	4.1E-06	-1.9E-06	1.5E-05	1.5E-06	-8.3E-05	4.6E-07	-1.6E-06	2.8E-05	-4.8E-05	-5.3E-06
	Kurtosis	1.717	1.798	1.935	2.023	1.948	1.920	1.912	1.820	1.840	1.909	1.963	1.880	1.860	1.925	2.014	1.912
4 13	Mean	0.000	0.000	0.000	0.000	0.000	0.000	0.000	0.000	0.000	0.000	0.000	0.000	0.000	0.000	0.000	0.000
	Median	0.000	0.002	-0.001	-0.001	0.002	-0.001	0.003	0.000	0.000	0.000	-0.001	-0.005	0.001	0.000	0.000	0.000
	Standard dev.	1.745	1.763	1.889	1.998	1.730	1.797	1.875	2.008	1.809	1.697	1.909	2.032	1.717	1.775	1.854	1.998
	Variance	-3.7E-06	2.6E-06	2.1E-06	-3.2E-06	-2.2E-06	-8.2E-07	-2.5E-07	1.4E-06	2.1E-07	3.9E-06	-2.0E-06	7.1E-07	4.1E-07	-4.1E-06	5.8E-07	1.9E-06
	Skewness	2.7E-06	2.5E-06	-2.6E-06	2.2E-06	6.4E-06	-1.6E-06	-8.1E-07	9.2E-06	9.3E-06	5.7E-07	3.0E-06	1.9E-05	5.9E-06	-2.0E-06	-1.5E-06	4.0E-07
	Kurtosis	0.189	0.177	0.288	0.180	0.256	0.249	0.291	0.238	0.236	0.180	0.233	0.239	0.125	0.242	0.226	0.250
4 14	Mean	0.000	0.000	0.000	0.000	0.000	0.000	0.000	0.000	0.000	0.000	0.000	0.000	0.000	0.000	0.000	0.000
	Median	0.000	0.002	0.000	0.000	0.003	0.000	0.000	-0.004	0.000	0.002	-0.003	-0.001	-0.003	0.000	-0.002	0.004
	Standard dev.	1.768	1.790	1.895	2.002	1.799	1.823	1.904	2.025	1.811	1.727	1.933	2.050	1.725	1.810	1.892	2.020
	Variance	2.2E-06	-1.6E-06	-2.7E-06	-1.9E-06	3.3E-06	5.9E-07	-1.3E-06	-5.2E-07	-3.8E-06	-3.3E-07	-3.2E-06	4.2E-07	4.4E-07	-5.8E-07	-1.3E-07	3.4E-06
	Skewness	-5.4E-05	1.4E-05	1.9E-05	1.4E-05	-6.1E-05	-3.8E-06	4.5E-06	5.4E-06	3.1E-05	1.4E-05	4.0E-05	1.6E-06	-9.0E-07	6.1E-06	4.2E-07	-1.7E-05
	Kurtosis	0.440	0.399	0.404	0.377	0.420	0.486	0.382	0.486	0.346	0.344	0.334	0.298	0.385	0.413	0.359	0.354
4 15	Mean	0.000	0.000	0.000	0.000	0.000	0.000	0.000	0.000	0.000	0.000	0.000	0.000	0.000	0.000	0.000	0.000
	Median	-0.012	0.008	0.004	0.007	-0.007	-0.005	0.011	-0.003	0.007	0.007	0.009	-0.010	0.000	-0.007	0.008	0.001
	Standard dev.	1.735	1.775	1.903	2.052	1.736	1.827	1.912	1.996	1.817	1.727	1.928	2.046	1.722	1.807	1.882	1.994
	Variance	2.1E-06	7.4E-07	-9.7E-07	1.9E-06	1.9E-06	1.7E-06	-1.4E-06	-2.1E-06	1.9E-06	-2.5E-06	2.1E-06	1.5E-06	-2.1E-06	2.8E-08	-1.4E-06	-2.2E-06
	Skewness	3.4E-02	-3.5E-03	1.2E-03	-2.9E-03	1.2E-02	8.4E-03	5.7E-04	6.8E-04	1.2E-02	4.0E-03	-1.8E-02	9.3E-03	1.5E-02	1.0E-02	8.1E-03	1.9E-02
	Kurtosis	0.092	0.103	0.138	0.135	0.105	0.161	0.193	0.121	0.088	0.100	0.146	0.130	0.101	0.138	0.172	0.158

Packet	Experiment	97	98	99	100	101	102	103	104	105	106	107	108	109	110	111	112
	V_{sg} (m/s)	0.15	0.59	1.31	0.16	0.31	0.60	1.34	0.16	0.32	0.61	1.25	0.15	0.30	0.60	1.33	0.15
	V_{sl} (m/s)	0.66	0.66	0.66	0.69	0.69	0.69	0.69	0.72	0.72	0.72	0.72	0.76	0.76	0.76	0.76	0.80
	WC (%)	0.60	0.60	0.60	0.40	0.40	0.40	0.40	0.20	0.20	0.20	0.20	0.80	0.80	0.80	0.80	0.60
4 10	Mean	0.000	0.000	0.000	0.000	0.000	0.000	0.000	0.000	0.000	0.000	0.000	0.000	0.000	0.000	0.000	0.000
	Median	0.001	-0.001	0.003	-0.004	-0.001	0.001	0.000	-0.001	0.002	-0.002	0.002	-0.005	0.002	-0.002	0.002	-0.001
	Standard dev.	1.751	1.884	1.990	1.760	1.857	1.907	2.029	1.795	1.822	1.925	2.021	1.728	1.794	1.853	1.958	1.772
	Variance	-1.8E-06	-1.8E-06	1.1E-06	-4.3E-06	1.4E-06	-9.0E-07	-4.8E-07	4.3E-07	4.1E-08	1.5E-06	1.9E-08	7.6E-07	-4.2E-06	-2.7E-06	3.9E-07	7.5E-07
	Skewness	5.4E-06	2.1E-06	-5.3E-06	2.7E-05	-6.7E-07	2.9E-06	1.3E-06	-1.7E-06	4.8E-08	-7.0E-06	5.6E-06	-1.8E-06	2.5E-05	9.3E-06	-1.5E-06	-8.4E-07
	Kurtosis	0.414	0.480	0.377	0.320	0.389	0.449	0.402	0.341	0.356	0.298	0.416	0.398	0.381	0.458	0.467	0.426
4 11	Mean	0.000	0.000	0.000	0.000	0.000	0.000	0.000	0.000	0.000	0.000	0.000	0.000	0.000	0.000	0.000	0.000
	Median	0.001	0.003	-0.001	-0.001	-0.001	-0.002	-0.003	-0.001	0.003	-0.002	-0.002	0.002	-0.003	-0.001	-0.001	-0.001
	Standard dev.	1.746	1.881	2.012	1.753	1.822	1.896	2.015	1.806	1.846	1.931	2.045	1.726	1.805	1.883	2.000	1.763
	Variance	2.1E-06	-1.3E-06	1.2E-06	1.4E-06	-1.1E-06	1.5E-07	5.5E-07	-1.8E-06	-5.4E-07	2.5E-06	-3.3E-06	5.7E-07	3.0E-06	9.1E-08	4.5E-07	-2.7E-06
	Skewness	-7.8E-06	2.6E-06	-4.3E-06	-4.3E-06	3.2E-06	-4.1E-07	-1.8E-06	4.4E-06	1.5E-06	-7.9E-06	8.9E-06	-1.5E-06	-8.4E-06	-2.5E-07	-1.7E-06	1.1E-05
	Kurtosis	0.121	0.132	0.165	0.083	0.085	0.122	0.237	0.109	0.162	0.166	0.174	0.090	0.118	0.115	0.044	0.144
4 12	Mean	0.000	0.000	0.000	0.000	0.000	0.000	0.000	0.000	0.000	0.000	0.000	0.000	0.000	0.000	0.000	0.000
	Median	-0.001	0.000	0.001	0.000	-0.001	-0.001	0.000	0.000	0.001	0.002	-0.001	-0.003	0.001	0.002	-0.001	-0.001
	Standard dev.	1.719	1.854	1.978	1.719	1.771	1.870	2.003	1.754	1.799	1.892	2.027	1.686	1.744	1.826	1.977	1.705
	Variance	-2.8E-06	2.5E-06	-4.7E-06	-3.9E-06	-2.3E-06	2.3E-06	6.1E-06	8.0E-06	5.4E-06	-1.4E-05	5.5E-06	-2.2E-06	2.2E-06	-1.8E-06	3.5E-06	2.0E-06
	Skewness	7.0E-06	5.2E-06	1.2E-05	1.1E-05	3.8E-06	-6.5E-06	9.1E-05	9.3E-05	-9.6E-07	-6.9E-05	3.1E-05	6.6E-06	-5.0E-06	5.6E-06	2.4E-06	-4.8E-06
	Kurtosis	1.852	1.826	1.996	1.805	1.890	2.014	1.816	1.887	1.865	1.892	1.854	1.871	1.896	1.938	1.812	1.860
4 13	Mean	0.000	0.000	0.000	0.000	0.000	0.000	0.000	0.000	0.000	0.000	0.000	0.000	0.000	0.000	0.000	0.000
	Median	0.001	0.002	-0.002	0.003	0.002	0.000	0.001	-0.002	0.000	-0.002	0.003	-0.001	0.000	0.002	-0.001	0.000
	Standard dev.	1.706	1.837	1.977	1.739	1.776	1.878	2.021	1.742	1.801	1.881	2.003	1.715	1.771	1.848	1.981	1.725
	Variance	3.5E-07	5.3E-07	8.3E-07	1.4E-07	-2.6E-06	8.5E-07	3.8E-07	-2.1E-06	1.8E-06	1.9E-06	2.8E-07	-2.6E-06	-5.0E-07	2.0E-06	-3.2E-07	-5.4E-06
	Skewness	-8.7E-07	-2.1E-06	-2.3E-06	1.4E-06	5.9E-07	1.2E-05	-2.1E-06	4.9E-06	2.5E-05	1.5E-05	4.4E-06	7.6E-07	-5.0E-06	1.9E-05	1.8E-06	2.3E-06
	Kurtosis	0.210	0.242	0.242	0.215	0.222	0.299	0.226	0.190	0.271	0.269	0.238	0.152	0.288	0.235	0.213	0.260
4 14	Mean	0.000	0.000	0.000	0.000	0.000	0.000	0.000	0.000	0.000	0.000	0.000	0.000	0.000	0.000	0.000	0.000
	Median	0.002	-0.001	-0.001	0.001	0.001	0.000	-0.002	-0.002	0.000	0.002	0.003	0.001	0.001	0.002	-0.001	0.000
	Standard dev.	1.752	1.879	2.001	1.779	1.806	1.863	2.001	1.776	1.828	1.908	2.041	1.736	1.786	1.882	1.983	1.757
	Variance	-1.7E-06	2.0E-06	-1.3E-06	3.0E-06	-2.1E-06	1.9E-06	-4.3E-07	1.5E-06	-3.6E-07	-3.5E-06	4.2E-07	-1.2E-06	3.8E-06	6.0E-07	-1.7E-06	-3.7E-07
	Skewness	5.8E-06	-1.6E-05	3.8E-06	-2.3E-05	7.4E-06	-8.6E-06	-4.7E-07	-4.4E-06	-3.3E-07	1.8E-05	-9.7E-07	1.1E-05	-9.3E-06	-7.6E-08	4.5E-06	-7.1E-06
	Kurtosis	0.323	0.338	0.426	0.324	0.391	0.469	0.401	0.366	0.344	0.446	0.342	0.375	0.369	0.435	0.338	0.356
4 15	Mean	0.000	0.000	0.000	0.000	0.000	0.000	0.000	0.000	0.000	0.000	0.000	0.000	0.000	0.000	0.000	0.000
	Median	-0.014	0.006	0.004	-0.016	0.002	0.008	-0.003	0.007	-0.006	-0.002	-0.004	-0.009	0.002	-0.002	-0.003	0.004
	Standard dev.	1.747	1.848	1.995	1.744	1.807	1.869	1.989	1.767	1.810	1.887	2.012	1.715	1.775	1.849	1.988	1.745
	Variance	8.5E-07	-1.7E-06	-2.3E-07	1.1E-06	1.6E-06	-1.9E-06	3.4E-07	2.4E-07	-2.9E-06	-1.9E-06	2.2E-06	1.0E-06	-3.4E-07	2.5E-06	1.3E-06	2.8E-06
	Skewness	3.7E-02	-2.3E-02	-1.8E-02	2.4E-02	8.2E-03	-6.4E-03	1.4E-02	-6.8E-03	2.3E-02	8.3E-03	1.7E-02	7.3E-03	-6.1E-03	4.6E-03	2.1E-02	5.3E-03
	Kurtosis	0.103	0.218	0.107	0.078	0.121	0.116	0.125	0.196	0.096	0.103	0.121	0.119	0.122	0.241	0.188	0.114

Packet	Experiment	113	114	115	116	117	118	119	120	121	122	123	124	125	126
	V_{sg} (m/s)	0.23	0.62	1.32	0.16	0.32	0.60	1.33	0.15	0.32	0.66	1.32	0.15	0.31	0.60
	V_{sl} (m/s)	0.80	0.80	0.80	0.83	0.83	0.83	0.83	0.86	0.86	0.86	0.86	0.15	0.15	0.15
	WC (%)	0.60	0.60	0.60	0.40	0.40	0.40	0.40	0.20	0.20	0.20	0.20	0.00	0.00	0.00
4 10	Mean	0.000	0.000	0.000	0.000	0.000	0.000	0.000	0.000	0.000	0.000	0.000	0.000	0.000	0.000
	Median	0.000	0.002	0.004	0.002	0.003	0.002	-0.001	-0.001	-0.004	-0.001	-0.002	0.002	-0.002	0.000
	Standard dev.	1.815	1.858	2.006	1.754	1.797	1.895	2.000	1.783	1.834	1.913	2.020	1.875	1.966	2.047
	Variance	1.9E-06	3.4E-06	-1.7E-06	-2.1E-06	-3.5E-06	8.7E-07	-1.4E-06	-1.1E-07	-1.4E-06	1.3E-06	-1.7E-06	-3.2E-06	-5.1E-07	1.1E-06
	Skewness	-2.5E-05	-1.0E-05	5.4E-06	3.0E-06	2.6E-06	-2.3E-06	6.8E-06	1.8E-05	4.2E-06	-5.9E-06	5.8E-06	1.1E-05	1.5E-06	-3.6E-06
	Kurtosis	0.345	0.432	0.408	0.371	0.359	0.358	0.311	0.373	0.327	0.490	0.408	0.350	0.317	0.348
4 11	Mean	0.000	0.000	0.000	0.000	0.000	0.000	0.000	0.000	0.000	0.000	0.000	0.000	0.000	0.000
	Median	-0.001	0.001	0.001	-0.002	0.003	-0.001	0.001	-0.002	0.001	-0.003	-0.001	-0.002	0.000	-0.004
	Standard dev.	1.806	1.877	2.011	1.780	1.817	1.892	2.004	1.798	1.825	1.929	1.992	1.901	1.961	2.034
	Variance	-6.4E-07	-2.4E-08	1.0E-06	2.4E-06	-3.0E-06	5.5E-07	-1.0E-06	-4.9E-07	-1.3E-06	-4.3E-06	-1.3E-07	-1.6E-07	1.5E-07	-9.7E-07
	Skewness	1.9E-06	9.0E-08	-2.0E-06	-6.9E-06	5.0E-06	-2.0E-06	3.1E-06	1.5E-06	4.1E-06	1.4E-05	4.2E-07	-5.2E-07	-3.2E-07	3.2E-06
	Kurtosis	0.125	0.161	0.090	0.030	0.118	0.122	0.134	0.121	0.168	0.011	0.073	0.110	0.162	0.095
4 12	Mean	0.000	0.000	0.000	0.000	0.000	0.000	0.000	0.000	0.000	0.000	0.000	0.000	0.000	0.000
	Median	0.001	0.000	0.002	0.000	-0.001	0.000	-0.001	-0.001	0.000	0.000	-0.004	0.000	-0.001	0.000
	Standard dev.	1.774	1.851	2.016	1.702	1.771	1.847	2.027	1.734	1.771	1.924	2.000	1.846	1.933	2.010
	Variance	8.2E-06	-3.5E-06	6.1E-07	-1.1E-06	-4.3E-06	3.3E-06	5.1E-06	-3.3E-06	5.5E-07	-4.6E-06	-2.1E-06	6.9E-06	-4.0E-06	2.3E-06
	Skewness	-1.6E-05	-4.2E-09	4.4E-06	2.3E-06	8.7E-06	-1.2E-06	-9.4E-06	5.0E-06	4.8E-06	1.1E-05	5.0E-06	8.0E-06	5.7E-06	1.5E-05
	Kurtosis	1.921	1.891	1.828	1.847	1.897	1.900	1.848	1.796	1.887	1.851	1.885	1.960	1.888	1.879
4 13	Mean	0.000	0.000	0.000	0.000	0.000	0.000	0.000	0.000	0.000	0.000	0.000	0.000	0.000	0.000
	Median	-0.001	-0.004	0.002	-0.002	0.002	-0.004	-0.003	0.000	0.000	0.001	0.002	0.000	-0.003	0.000
	Standard dev.	1.760	1.877	1.992	1.754	1.793	1.869	2.003	1.749	1.791	1.890	2.021	1.857	1.937	2.016
	Variance	-4.1E-06	-1.6E-06	4.3E-07	-1.6E-06	4.6E-06	-1.4E-06	-1.3E-06	-1.6E-06	8.1E-07	-1.3E-06	8.7E-07	-2.1E-07	-4.1E-06	8.3E-07
	Skewness	-5.1E-05	-6.8E-06	2.2E-06	-3.0E-05	4.4E-06	-5.4E-05	-8.5E-06	1.5E-06	2.1E-05	-5.5E-06	-3.0E-06	1.9E-07	-4.3E-05	-5.9E-07
	Kurtosis	0.240	0.275	0.196	0.232	0.261	0.275	0.278	0.123	0.181	0.185	0.210	0.174	0.179	0.223
4 14	Mean	0.000	0.000	0.000	0.000	0.000	0.000	0.000	0.000	0.000	0.000	0.000	0.000	0.000	0.000
	Median	0.001	0.002	0.000	0.004	-0.002	-0.001	0.002	0.005	-0.002	-0.001	0.000	0.000	0.004	0.002
	Standard dev.	1.797	1.888	2.019	1.753	1.832	1.877	1.974	1.766	1.809	1.892	2.013	1.870	1.962	2.033
	Variance	-5.7E-07	-1.8E-06	2.2E-06	-3.7E-07	3.6E-06	-1.6E-07	1.6E-06	2.5E-06	3.5E-06	2.7E-06	2.6E-06	3.1E-06	1.6E-06	3.6E-07
	Skewness	1.5E-06	1.3E-05	-1.3E-05	6.8E-06	-3.9E-05	3.6E-07	-1.0E-05	3.4E-06	-3.7E-05	-5.3E-05	-7.6E-06	-4.1E-05	-6.0E-06	-8.3E-06
	Kurtosis	0.383	0.427	0.493	0.427	0.373	0.271	0.296	0.391	0.381	0.451	0.351	0.376	0.342	0.362
4 15	Mean	0.000	0.000	0.000	0.000	0.000	0.000	0.000	0.000	0.000	0.000	0.000	0.000	0.000	0.000
	Median	-0.003	-0.007	-0.016	0.005	0.001	0.002	0.004	0.003	-0.010	0.005	-0.006	0.003	-0.009	-0.013
	Standard dev.	1.802	1.867	1.997	1.742	1.804	1.869	1.972	1.750	1.806	1.881	2.023	1.870	1.948	2.017
	Variance	-4.6E-07	2.2E-06	-2.6E-06	3.1E-06	-4.8E-07	4.5E-06	2.4E-06	-8.3E-07	-3.0E-06	-2.6E-06	-7.4E-07	-1.4E-06	1.8E-07	-2.6E-06
	Skewness	5.5E-03	1.5E-02	1.8E-02	3.1E-03	1.5E-03	2.1E-02	5.5E-03	-1.8E-02	4.2E-03	-2.7E-03	4.8E-03	9.9E-04	1.9E-02	8.0E-03
	Kurtosis	0.109	0.064	0.132	0.133	0.125	0.192	0.101	0.152	0.052	0.077	0.116	0.150	0.157	0.132

Appendix E – ANN Feature Contouring and Selection

E.1 Feature Selection and Pre-Processing

Preliminary investigation of a wide range of candidate features was undertaken employing digital signal processing techniques. Certain features failed to exhibit any appreciable discriminatory ability and were not considered worthy candidates for further analysis (maximum, minimum and range features).

Definite discriminability abilities were shown by the moments of distribution amplitude features, linear prediction coefficients, linear spectral frequencies and autocorrelation parameters. These features were selected for further analysis using feature contour mapping techniques.

Table E.1 summaries the features extracted from the different domains for further examination. Definition of these features is given in **Appendix B**.

		Information Domain			
Feature	**Symbol**	**Amplitude**	**LPC**	**LSF**	**ACF**
Mean Value	AV	✓			
Standard Deviation	SD	✓			
Coefficient of Variation	CV	✓			
Coefficient of Skewness	CS	✓			
Coefficient of Kurtosis	CK	✓			
Signal Total Energy	E_T	✓			
Linear Prediction Coefficient 2	LPC2		✓		
Linear Prediction Coefficient 3	LPC3		✓		
Linear Prediction Coefficient 4	LPC4		✓		
Linear Prediction Coefficient 5	LPC5		✓		
Linear Prediction Coefficient 6	LPC6		✓		
Linear Prediction Error	E_R		✓		
Line Spectral Frequency 1	LSF1			✓	
Line Spectral Frequency 2	LSF2			✓	
Line Spectral Frequency 3	LSF3			✓	
Line Spectral Frequency 4	LSF4			✓	
Line Spectral Frequency 5	LSF5			✓	
ACF Coefficient at Minimum	AC1				✓
ACF Lag Minimum	AC2				✓
ACF Coefficient at Pseudo Period	AC3				✓
ACF Pseudo Period	AC4				✓

Table E.1 – List of Features Extracted from Information Domains

Experience has shown pattern recognition system generalisation can be improved if certain pre-processing steps are performed on both the pattern recognition system's inputs and targets. These techniques can range from simple normalisation to feature pruning. Three commonly applied routines are described:

- Range Equalisation: input features are scaled so that they all fall within a specified range, usually -1 to 1.

- Zero-Mean and Unit Variance: input features are normalised by centring the data values and then dividing them by their standard deviation so that they will have zero mean and unity standard deviation.

- Principal Component Analysis (PCA): a procedure for performing dimensionality reduction of a feature set. This technique has three effects: orthogonalisation of the components comprising the input vectors (inputs are uncorrelated); ordering of the resulting orthogonal components (the so-called principal components) so that those with the largest variation come first; and elimination of components that contribute only a small amount to the variation in the data set [**E1**].

  The PCA routine subtracts the mean of each feature from input vector. The covariance matrix of the adjusted data set is then calculated. The eigenvector and eigenvalues of the covariance matrix are then determined. The significance of the features can be determined from the relative magnitude of their eigenvalues: the eigenvector which has the largest eigenvalue is the principle component.

Preliminary examinations of the three techniques pre-processing routines with the gamma densitometer data established that the simple normalisation routine was significantly less effective than the other methods. The marked difference between the routines' performances was attributed to the inability of the simple normalisation technique to assign an equal emphasis to each input vector. The other techniques achieve equalisation of the input vector through the application of zero-mean and unit variance normalisation.

As an extended number of features had been extracted from the raw data signals, it was considered that PCA may prove to be a valuable tool in facilitating further dimensionality reduction and it could aid in the determination of a subset of features with strong discriminatory abilities. Nevertheless, it was recognised that for some problems the key discriminatory data may exist amongst the lower order PCA vectors.

Two main comparisons were undertaken using the two remaining pre-processing routines of interest. In the first instance the PCA was employed in an orthogonalising capacity only (no features were pruned) and its performance assessed against that of the zero-mean and unit variance normalisation. The results obtained showed that the network performances were comparable with no appreciable difference in their classification accuracy.

The pre-processing routines were subjected to further analysis; however, on this occasion the PCA routine was also used to reduce the dimensions of the input feature vector: features contributing less than 0.01% to the overall variation in the data set were removed. **Figure E.1** illustrates the effect of dimensionality reduction on the classification capabilities of the neural network. It can be clearly seen that the lower the number of principal components, the poorer the network performance. The principle components identified in the hard spectrum input feature, and their relative ranking, is detailed in **Table E.2**.

Rank	Feature
1	Mean Value
2	Coefficient of Kurtosis
3	Coefficient of Variation
4	Standard Deviation
5	Coefficient of Skewness
6	LPC2
7	ACF Pseudo Period
8	ACF Coefficient at Minimum
9	LSF4

Table E.2 – List of Principle Components in Hard Spectrum Input Feature

In this instance, it was observed that the network performance varied with both the pre-processing routine used, depending on the feature input set being examined. There was no apparent trend in the routine-feature combinations that offered a satisfactory explanation for the discrepancies observed in the network performance for certain permutations.

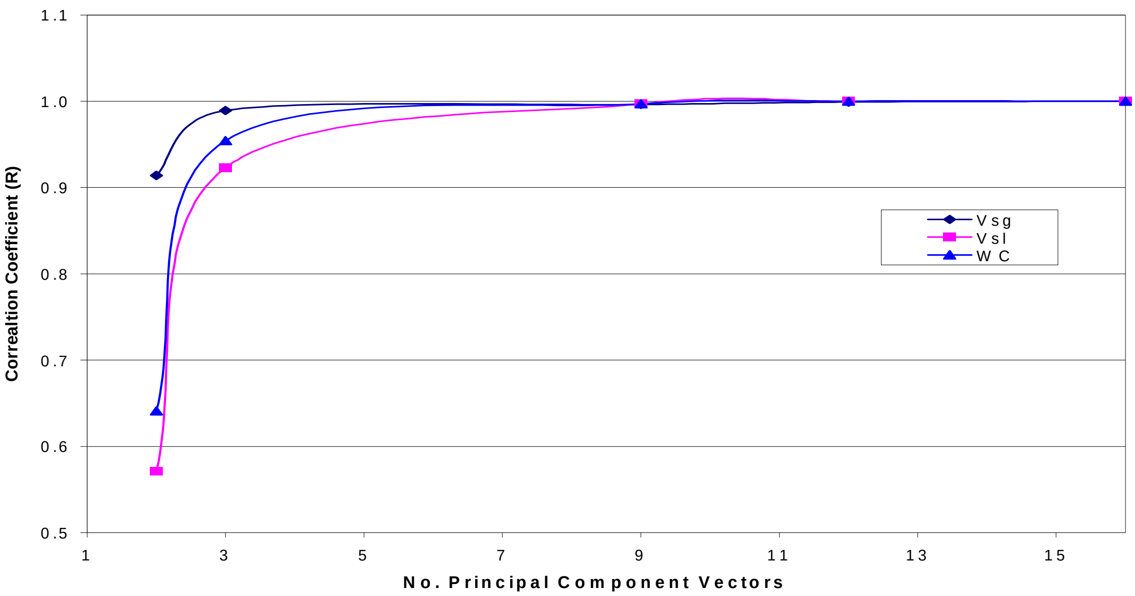

Figure E.1 – Principal Component Analysis Evaluation

Consequently, both the zero-mean and unit-variance normalisation and PCA were studied as part of the current research programme. Neural network simulations were repeated using both pre-processing routines; thus, enabling the influence of the pre-processing routine on the network's performance to be evaluated over a wider range of input feature combinations.

E.2 Feature Contour Mapping

Identified features had all shown some degree discrimination during the preliminary analysis. These features were extracted from the both the hard and soft gamma signals. As the response of the gamma photons to variations in multiphase flow is energy dependent, the hard and soft energies operate effectively as two independent sensors. A third signal was from the hard and soft spectra by subtracting the hard signal from soft signal to yield the difference between the spectra. This enables the differing spectra response to be analysed for pattern recognition traits. The features in **Table E.1** were also extracted from the 'difference' signal for use in pattern recognition analysis.

Investigation of the extracted features' responses over the range of flows examined was undertaken using feature a contour plotting technique. Contour plots facilitate the representation of three-dimensional data on a two-dimensional plot. Consequently, the feature trends could be visualised by monitoring the variations in their magnitude with alterations in gas and liquid superficial velocities (V_{sg} and V_{sl} respectively). The feature magnitude can then be plotted as a series of contours over an intersecting grid of superficial gas and liquid velocities. The test points were superimposed onto the grid to aid trend visualisation. The test point water cuts have also been identified for trending purposes.

E.2.1 Hard Energy Features

Figure E.2 (a) – (f) show normalised feature distribution maps for the amplitude features extracted from the hard energy. A zero-mean and unit-variance normalisation procedure was applied to all feature data sets to facilitate effective comparison between different features.

The mean value feature shows a definite response to both the gas and liquid superficial velocities, although with a distinct bias towards the gas. The mean value's magnitude increased with increasing gas and decreasing liquid superficial velocities. The mean feature contour reaches a peak at minimum liquid velocity and a gas velocity of 1 ms^{-1}. The maximum was located in this position as no data points for the highest gas and lowest liquid rates were obtainable during test campaign.

Examining the standard deviation feature contour, a general increase in the feature magnitude was observed with increasing gas superficial velocities. The liquid loading displays a complex relationship with the standard deviation, having little influence at the upper and lower gas velocities but dominating the feature between gas loadings of between 0.6 and 1 ms^{-1}. As a result, two regions of feature maxima are found on the standard deviation contour plot: $0.2 \leq V_{sg} \leq 0.3$ ms^{-1} and $0.6 \leq V_{sl} \leq 0.6$ ms^{-1}; and $1 \leq V_{sg} \leq 1.25$ ms^{-1} and $V_{sl} \leq 0.6$ ms^{-1}.

It would seem likely that the different contouring regions are induced by the presence of data points of different flow regimes. The dominating flow regime will have a significant influence on the feature response. It was hypothesised that the contouring features observed for superficial gas velocities less than 1 ms^{-1} would depict feature trending in the bubble flow regime while those at the higher gas velocities would be representative of feature response in the slug flow regime. The sensitivity of pattern recognitions techniques to the prevailing flow regimes will be examined later in this report.

Feature contours for the coefficient of variation show complex swirling patterns for low gas loads ($V_{sg} \leq 0.7$ ms^{-1}). Two maxima regions can be found for the variation feature in this complex swirling region. At gas superficial velocities greater than 1 ms^{-1} the liquid loading dominates the feature magnitude, increasing with decreasing liquid loads.

The magnitude of the coefficient of skewness feature exhibited an affinity for the both the gas and liquid superficial velocities. A strong dependency on the gas velocity was evident across the whole of the flow range with the coefficient of skewness feature magnitude decreasing with increasing gas velocities. The skewness showed an increased sensitivity towards the liquid loading at $V_{sg} \geq 0.4$ ms^{-1}. At low gas flow rates, the skewness is unaffected by liquid velocity variations, but as the gas velocity increases, so does the liquid velocity's influence: increasing feature magnitude with increased liquid superficial velocity.

The coefficient of kurtosis feature contour plot illustrates a strong dependence on the gas loading, with feature magnitude decreasing with increasing gas phase velocity. In a similar fashion to the coefficient of skewness feature, liquid loading exhibited little influence at low superficial gas velocities but at $V_{sg} \geq 0.4$ ms^{-1} increasing the liquid loading results in an increased coefficient of kurtosis feature magnitude.

Analysing the total signal energy, an almost identical response to that of the mean was produced: the feature magnitude increases with increasing gas and decreasing liquid superficial velocities. Accordingly, the total signal energy of the hard energy was eliminated from further analysis.

Figure E.3 (a) – (f) show normalised feature distribution maps for the linear prediction coefficients extracted from the hard energy signal.

LPC2 exhibits a strong dependence on the liquid phase superficial velocity for low gas velocities (< 0.5 ms^{-1}), increasing with decreasing liquid velocity. At the upper range of gas velocities, the feature's response was weak with variations in both gas and liquid superficial velocities.

Examining the LPC3 feature, three regions of different response were identified. At gas velocities less than 1 ms^{-1}, the feature shows a strong affinity for the liquid velocity: decreasing with increases in the magnitude of the superficial liquid velocity. For gas velocities between 1 and 2 ms^{-1}, the feature demonstrates an identical response but is more sensitive to the liquid load. Gas superficial velocities greater than 2 ms^{-1} resulted in gas velocity dominated LPC3 values, the feature magnitude decreasing as the gas velocity increases.

The LPC4 parameter displayed three distinct regions of response as seen with the LPC3 feature. At low gas loads, the LPC4 feature magnitude was observed to increase with liquid superficial velocity. Between gas velocities of 1 and 2 ms^{-1}, the liquid velocity continues to dominate the feature response, the contour height increasing with the liquid velocity. The LPC4 response at a superficial gas velocity greater than 2 ms^{-1} was dominated in a similar fashion by the liquid load.

LPC5 and LPC6 revealed similar responses across the flow range, feature magnitude increasing with liquid load except that the LPC5 was more sensitive to these variations in superficial liquid velocity.

The error associated with the LPC parameters E_R show discernable discriminatory abilities. The error was observed to increase with increasing gas loads and decreasing liquid loads. The parameters sensitivity to the liquid loading is a function of the gas velocity, with sensitivity increasing with the superficial gas velocity.

Figure E.4 (a) – (e) show normalised feature distribution maps for the linear spectral frequency features extracted from the hard energy.

LSF1 showed dependency on both the gas and liquid superficial velocities. The largest feature magnitudes were produced for low gas loads and high liquid loads. The feature's sensitivity to the liquid loading decreased significantly with increasing gas velocity.

LSF3 exhibited the same response to gas velocity variations as the LSF1 parameter but yielded an inverse response with respect to the liquid loading. The feature's sensitivity to the liquid loading was similarly a strong function of the gas superficial velocity, decreasing with increasing gas velocities.

The LSF5 feature yielded a response evocative of that observed for LSF3 aside from the sensitivity to the liquid loading. LSF5 was observed to be more sensitive to liquid load variations as seen with the increased contour spacing along the vertical axis.

The contour plots for the LSF2 and LSF4 features are quite similar. There appears to be three distinct regions exhibiting very response patterns to variations in the gas and liquid superficial velocities. At gas velocities less than 1 ms^{-1}, the liquid velocity dominates the feature magnitude which increases with liquid flow. Between 1 and 2 ms^{-1}, there is an increased sensitivity to the gas load. In this region, increasing liquid flow continues to increase the feature magnitude while increasing the gas velocity tends to reduce the feature magnitude. The features' sensitivity to the gas loading decreases as a function of increasing liquid load. At the upper range of the gas loads examined (2 – 2.7 ms^{-1}), the feature magnitude remains dominated by the liquid velocity. However, its magnitude now increases with decreasing liquid velocity.

Figure E.5 (a) – (d) show normalised feature distribution maps for the autocorrelation function parameters extracted from the hard energy.

ACF 1 and ACF 3 showed a strong dependency on the gas superficial velocity. Complex feature contours with localised maximums across the flow domain were observed for these parameters.

The magnitude of the ACF2 and ACF4 features decreased with increasing liquid flow rate and decreasing gas load. The feature response of the ACF4 feature is very weak at low gas flow rates.

(a)

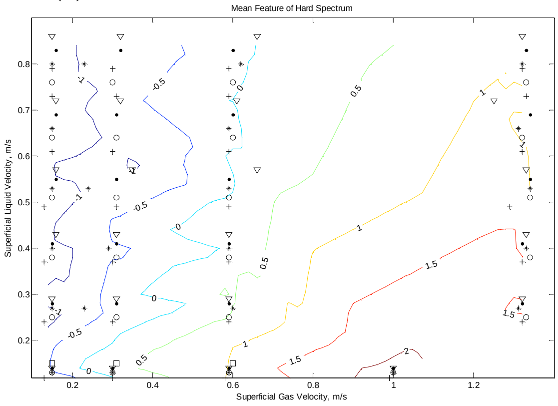

(b)

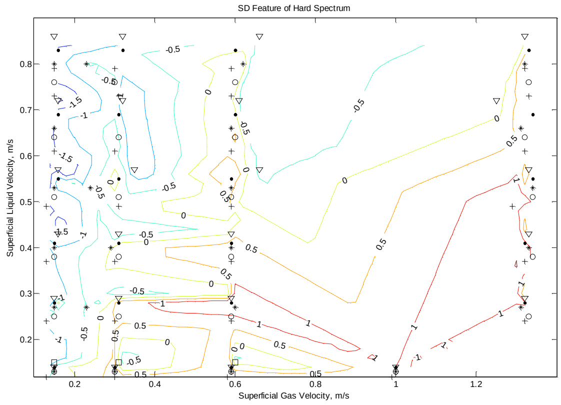

(c)

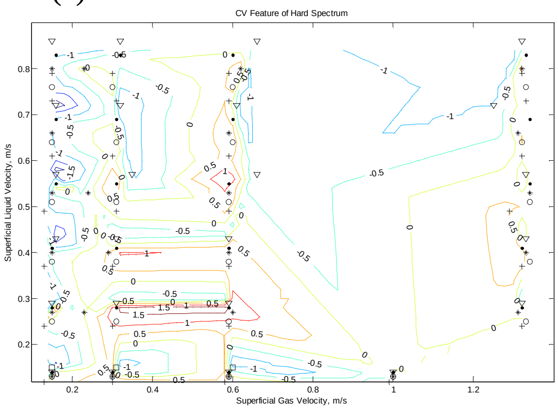

(d)

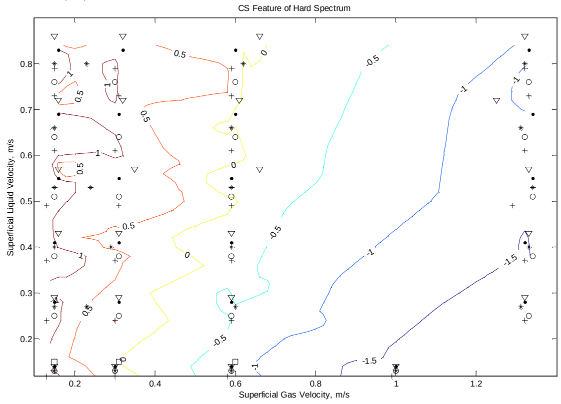

(e)

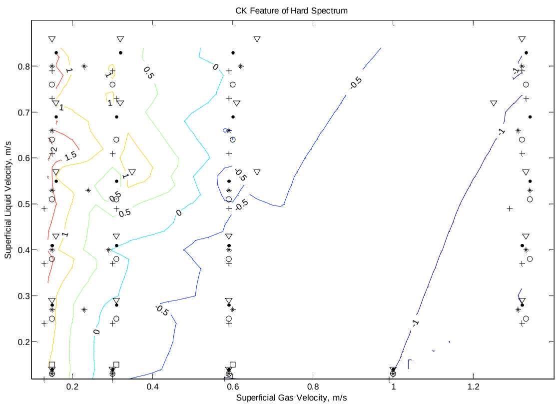

(f)

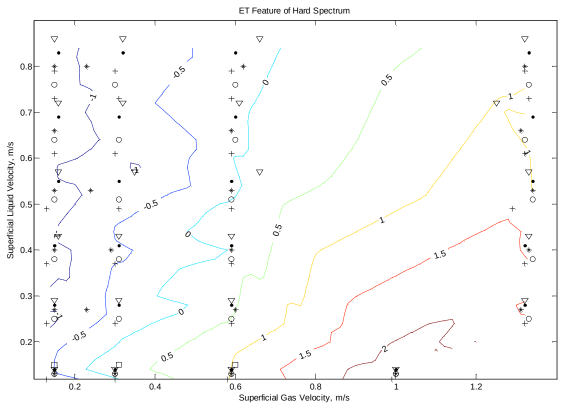

<u>Key to Test Point Water Cuts</u>

+	- 100%	•	- 40%
o	- 80%	▽	- 20%
*	- 60%	□	- 0%

Figure E.2 – Contour Plots of Hard Energy Amplitude Features

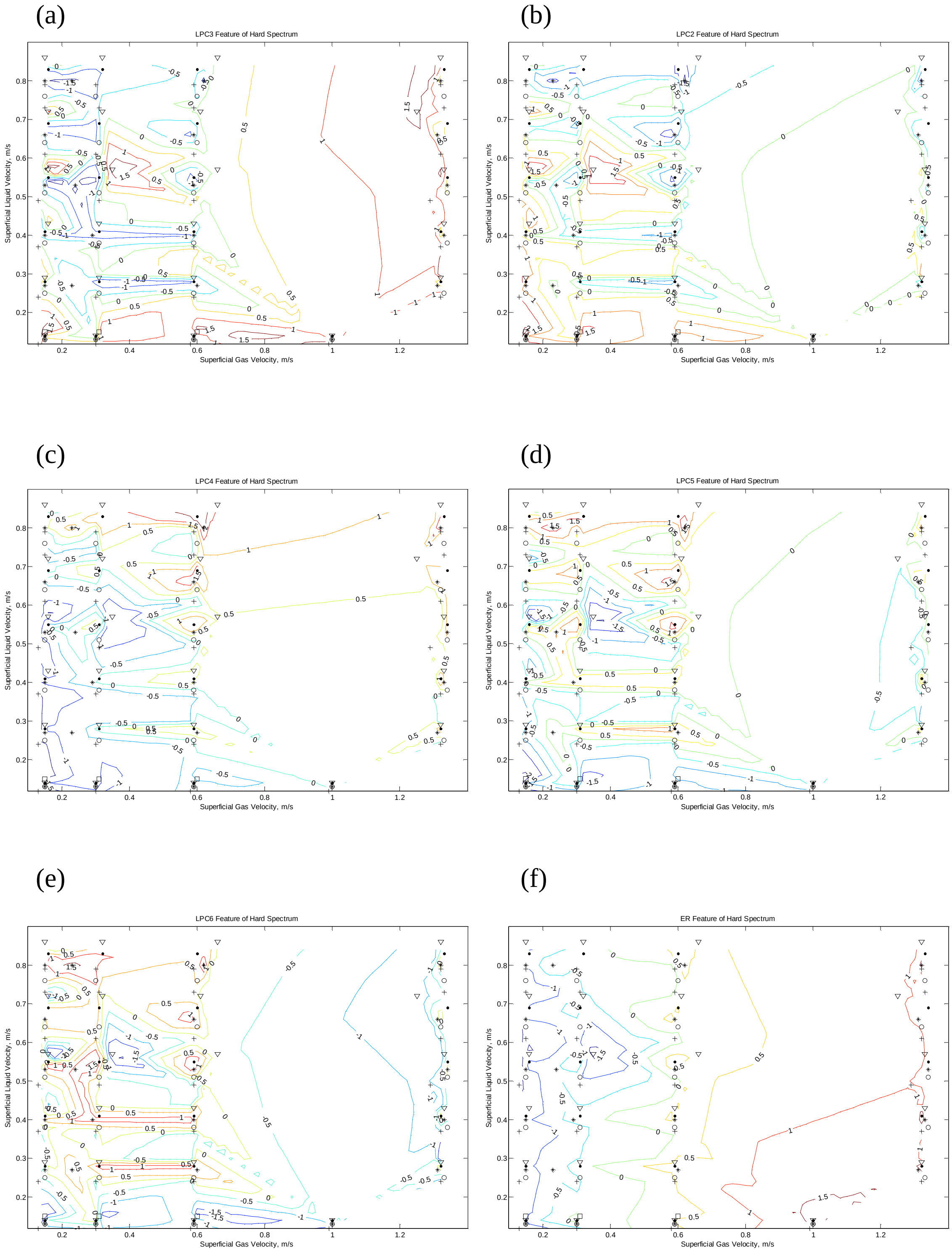

<u>Key to Test Point Water Cuts</u>

+	- 100%	•	- 40%
o	- 80%	▽	- 20%
*	- 60%	□	- 0%

Figure E.3 – Contour Plots of Hard Energy LPC Features

(a)

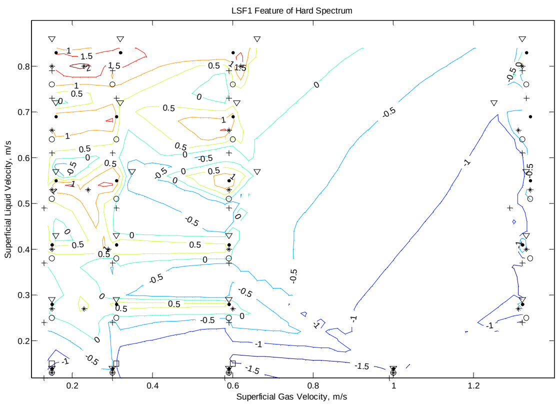

(b)

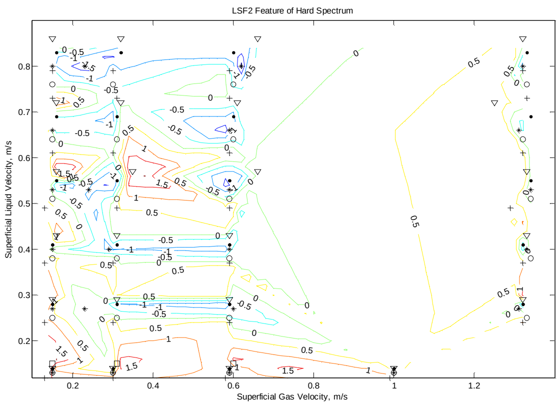

(c)

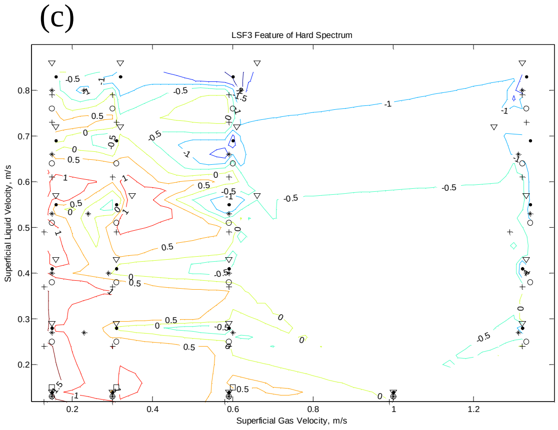

(d)

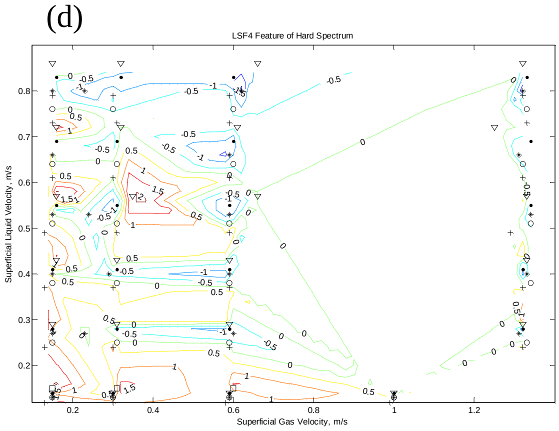

(e)

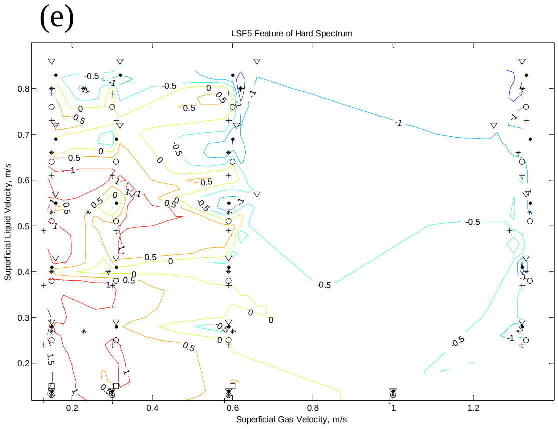

<u>Key to Test Point Water Cuts</u>

+	- 100%	•	- 40%
o	- 80%	▽	- 20%
*	- 60%	□	- 0%

Figure E.4 – Contour Plots of Hard Energy LSF Features

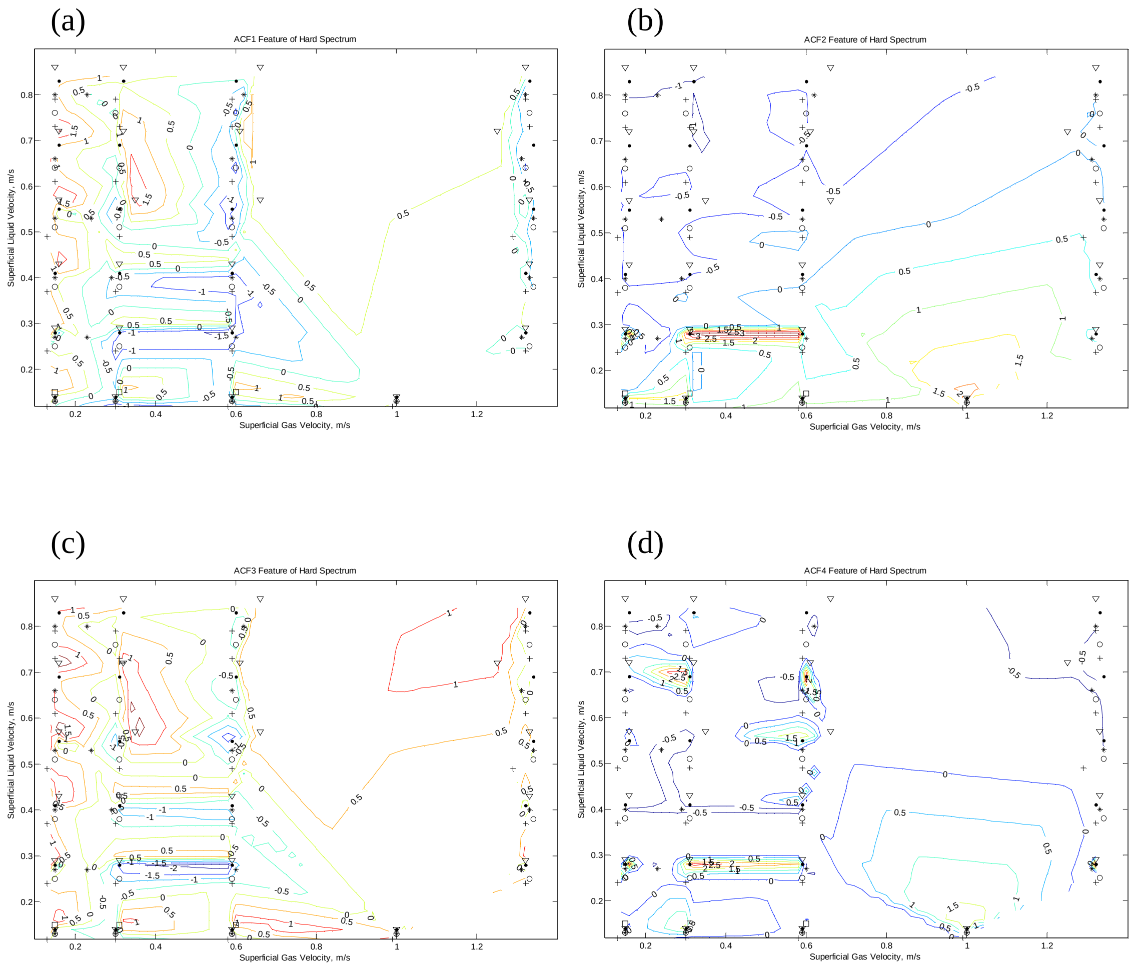

<u>Key to Test Point Water Cuts</u>

+	- 100%	•	- 40%
o	- 80%	▽	- 20%
*	- 60%	□	- 0%

Figure E.5– Contour Plots of Hard Energy ACF Features

E.2.2 Soft Energy Features

Figure E.6 (a) – (f) show normalised feature distribution maps for the amplitude features extracted from the soft energy. As one would expect, the feature maps produced were very similar to those acquired from the soft energy.

The soft energy mean feature exhibits a definite response to both the gas and liquid superficial velocities, although the liquid influence on the feature diminishes with increasing gas velocity. The hard and soft spectra mean feature maps are virtually identical.

The soft energy standard deviation was in accordance with that obtained from the hard energy with the relative feature contour magnitudes comparable with analogous variations in the phase superficial velocities.

The coefficient of variation feature exhibited minimal discrepancies between its hard and soft spectra responses. This corresponds well with the similarities observed for the hard and soft spectra mean and standard deviation feature contour plots.

Plotting the feature magnitude for the soft energy coefficient of skewness feature, one can observe a similar mapping pattern to that obtained by the hard energy. However, at superficial gas velocities greater than 1.5 ms^{-1}, the feature magnitude of the soft energy reveals a weaker dependence on the liquid superficial velocity than the hard energy coefficient of skewness.

It was observed that the coefficient of kurtosis yielded a similar response to that of its hard energy counterpart except a less sensitive dependency on the gas phase velocity was exhibited at gas superficial velocities in excess of 2 ms^{-1}.

The response of the total signal energy feature contour plot for the soft energy produced an identical response to that of the soft energy mean feature: feature magnitude increasing with increasing gas and decreasing liquid superficial velocities. Accordingly, the total signal energy of the soft energy was eliminated from further analysis.

Figure E.7 (a) – (f) show normalised feature distribution maps for the linear prediction coefficients extracted from the soft energy. It can be seen that the LPC2, LPC4 and LPC5 contour plots for the soft energy yielded essentially similar responses to their hard energy counterparts.

Analysing the contour plot for the soft energy LPC3 feature, a broadly similar response was generated to that of the hard energy. However, a reduced sensitivity to the liquid superficial velocity was identified for: gas superficial velocities less than 0.5 ms^{-1} and liquid phase superficial velocities greater than 0.65 ms^{-1} and for gas superficial velocities greater than 1 ms^{-1}.

LPC6 exhibited an increased feature magnitude dependence on the gas superficial velocity for the soft energy in comparison to the hard energy across the measurement range. Furthermore, the soft energy LPC residual error feature, E_R, demonstrated a more pronounced sensitivity to the gas phase loading than was obtained with the hard energy.

Figure E.8 (a) – (e) show normalised feature distribution maps for the linear spectral frequency features extracted from the soft energy. LSF2, LSF3 and LSF4 contour plots for the soft energy exhibited responses akin to those of the corresponding hard Energy features. The soft energy LSF1 and LSF5 features demonstrated a decreased sensitivity towards the gas loadings in comparison to their hard energy counterparts.

Figure E.9 (a) – (d) show normalised feature distribution maps for the autocorrelation function parameters extracted from the soft energy. The soft energy ACF2 and ACF4 feature contour plots (the minimum and maximum autocorrelation coefficients respectively) did not produce any significant deviations from those obtained from the hard energy. ACF 1 and ACF 3 (the autocorrelation function minimum and maximum lag respectively) showed an increased and decreased sensitivity, respectively, towards the liquid loading for gas superficial velocities greater than 2 ms^{-1}.

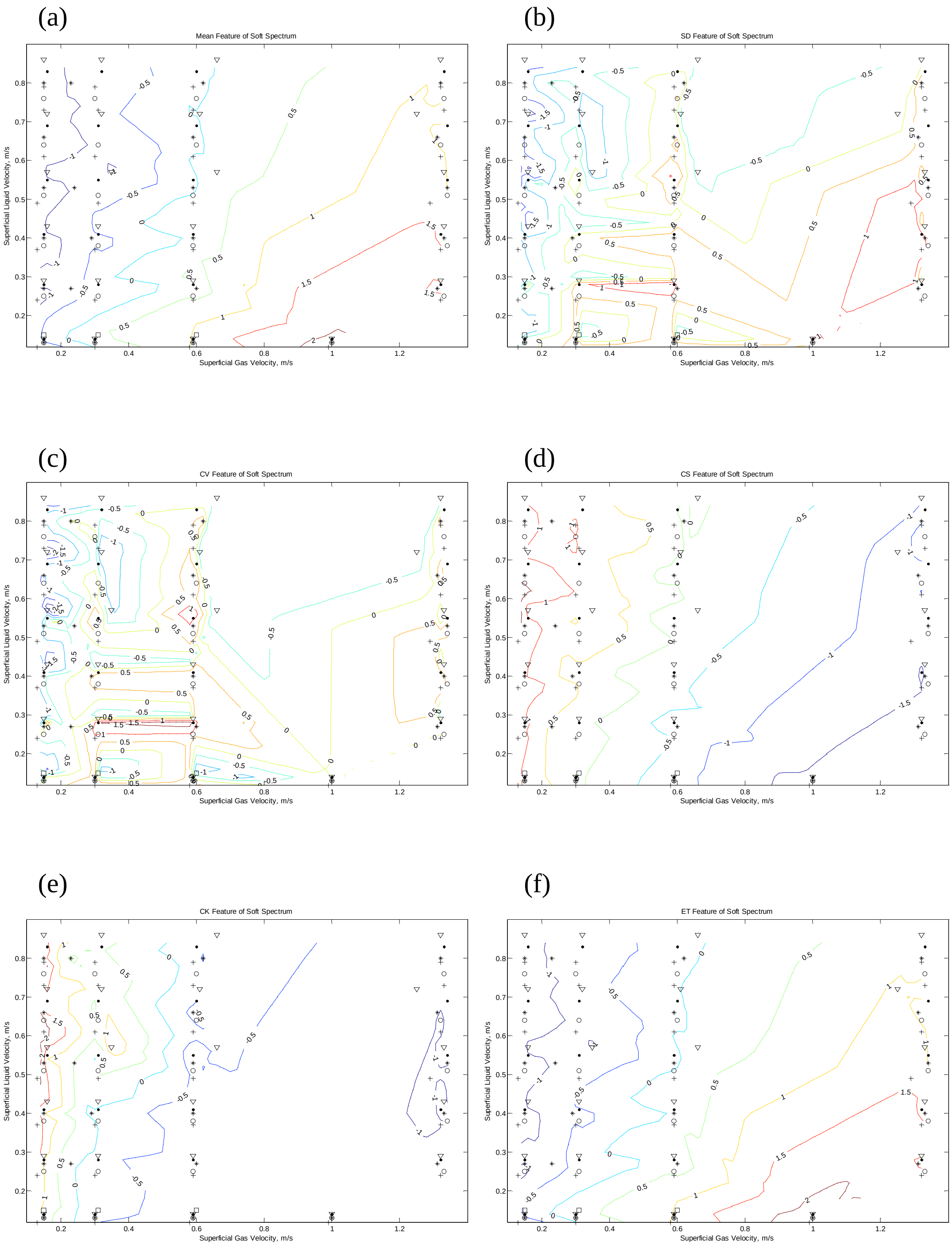

Key to Test Point Water Cuts

+	- 100%	•	- 40%
o	- 80%	▽	- 20%
*	- 60%	□	- 0%

Figure E.6 – Contour Plots of Soft Energy Amplitude Features

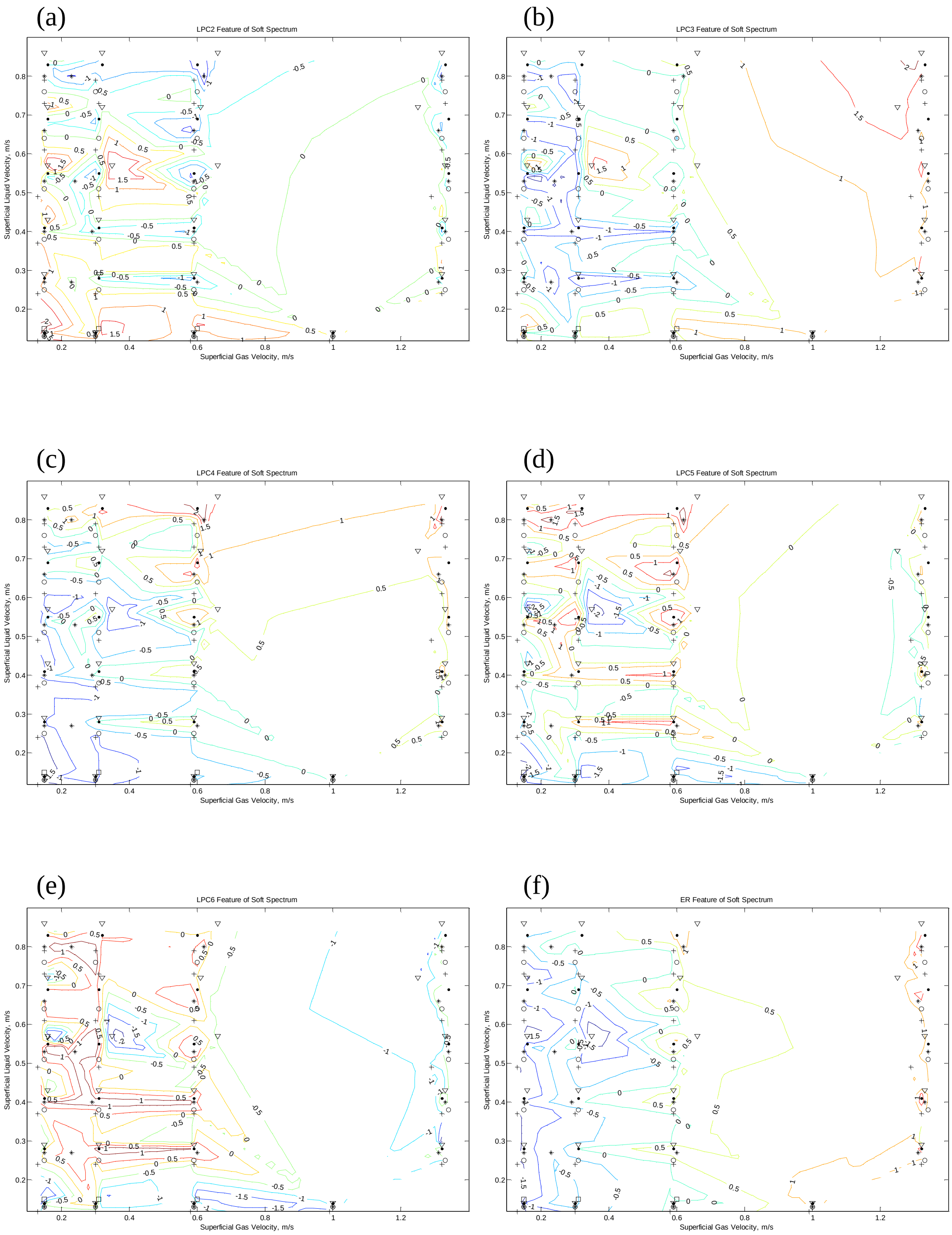

Key to Test Point Water Cuts

+	- 100%	•	- 40%
o	- 80%	▽	- 20%
*	- 60%	□	- 0%

Figure E.7 – Contour Plots of Soft Energy LPC Features

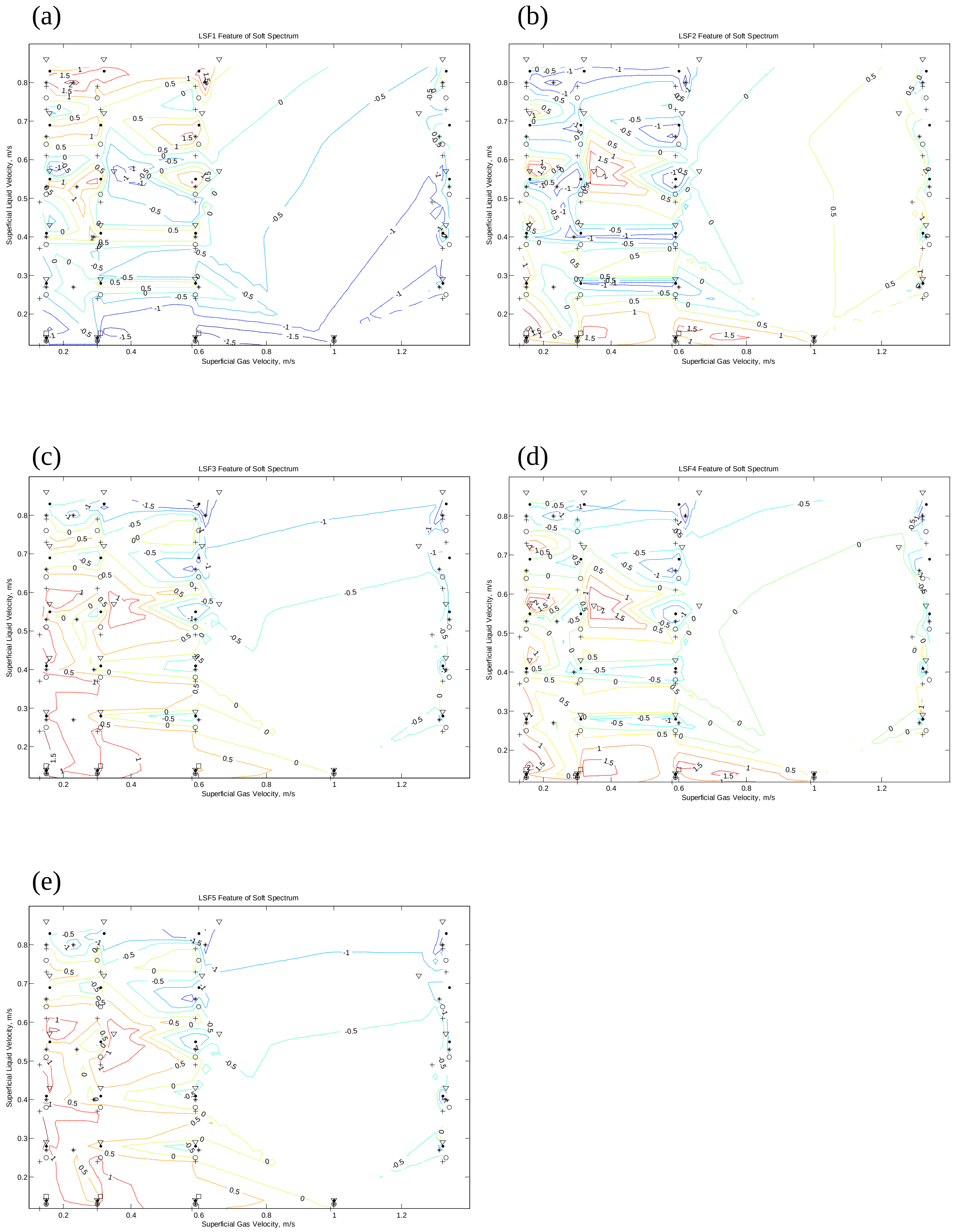

<u>Key to Test Point Water Cuts</u>

+	- 100%	•	- 40%
o	- 80%	▽	- 20%
*	- 60%	□	- 0%

Figure E.8– Contour Plots of Soft Energy LSF Features

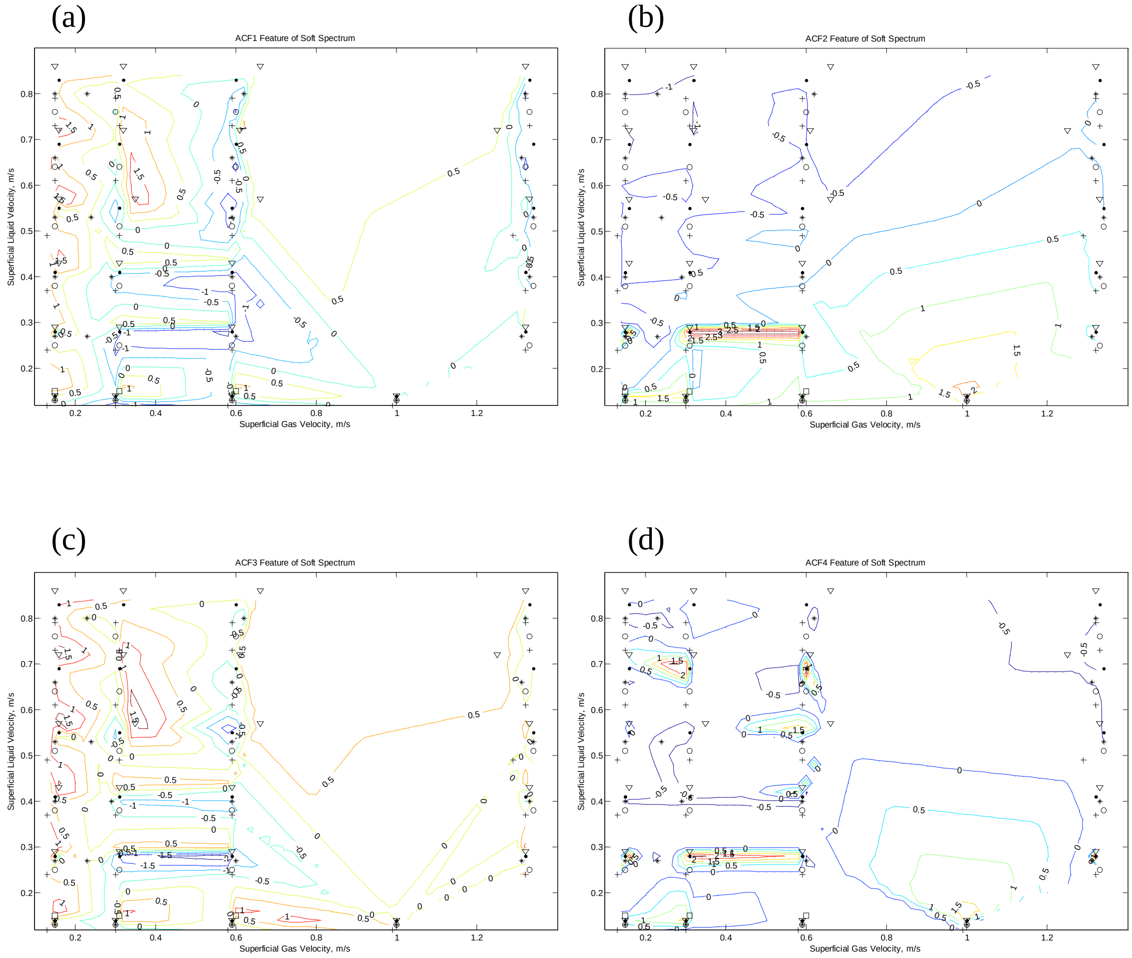

<u>Key to Test Point Water Cuts</u>

+	- 100%	•	- 40%
o	- 80%	▽	- 20%
*	- 60%	□	- 0%

Figure E.9 – Contour Plots of Soft Energy ACF Features

E.2.3 Spectra Difference Features

Figure E.10 (a) – (f) show normalised feature distribution maps for the difference between the soft and hard spectra amplitude features.

The difference between the spectra means, standard deviations and variances produced contour responses in accordance with those produced by both the hard and soft spectra.

Examining the contour plot of the difference between the spectra coefficients of skewness, an increased dependence on the liquid loading was observed for gas superficial velocities below 1 ms^{-1} and decreased dependency for gas superficial velocities greater than 1 ms^{-1}, relative to the hard and soft spectra responses.

Contrary to the hard and soft spectra responses, the difference between the coefficients of kurtosis exhibited insensitivity towards increases in the gas loading at superficial gas velocities greater 1.5 ms^{-1}.

As observed for both the hard and soft spectra signal energy features, the contour plot is identical to that obtained for the mean feature; thus, the signal energy was eliminated from further study.

Figure E.11 (a) – (f) show normalised feature distribution maps the difference between the soft and hard spectra amplitude features. The LPC 2 and LPC4 difference feature plots yielded contour geometries approximately similar to those obtained from the hard and soft spectra. However, the LPC3 and LPC5 based features demonstrated an increased and decreased sensitivity to the liquid loading respectively, at gas superficial velocities below 2 ms^{-1}. LPC6 produced a contour plot detailing the feature's reduced sensitivity towards the gas loading across the range and increased dependence on the liquid loading at gas superficial velocities below 1 ms^{-1}. The LPC residual error difference feature exhibited increased sensitivity towards both liquid and gas phase superficial velocities.

Figure E.12 (a) – (e) show normalised feature distribution maps for the difference between the soft and hard spectra amplitude features. LSF2, LSF3 and LSF4 contour plots produced similar responses to those given by the hard and soft spectra features. The spectra difference LSF1 and LSF5 features demonstrated decreased sensitivity towards both the gas and liquid loadings in comparison to both hard and soft spectra features.

Figure E.13 (a) – (d) show normalised feature distribution maps for the difference between the soft and hard spectra amplitude features. ACF1 and ACF3 produced contour plots in accordance with the hard and soft spectra feature contour plots. However, the ACF2 and ACF4 demonstrated an almost inert response to the difference between the hard and soft spectra.

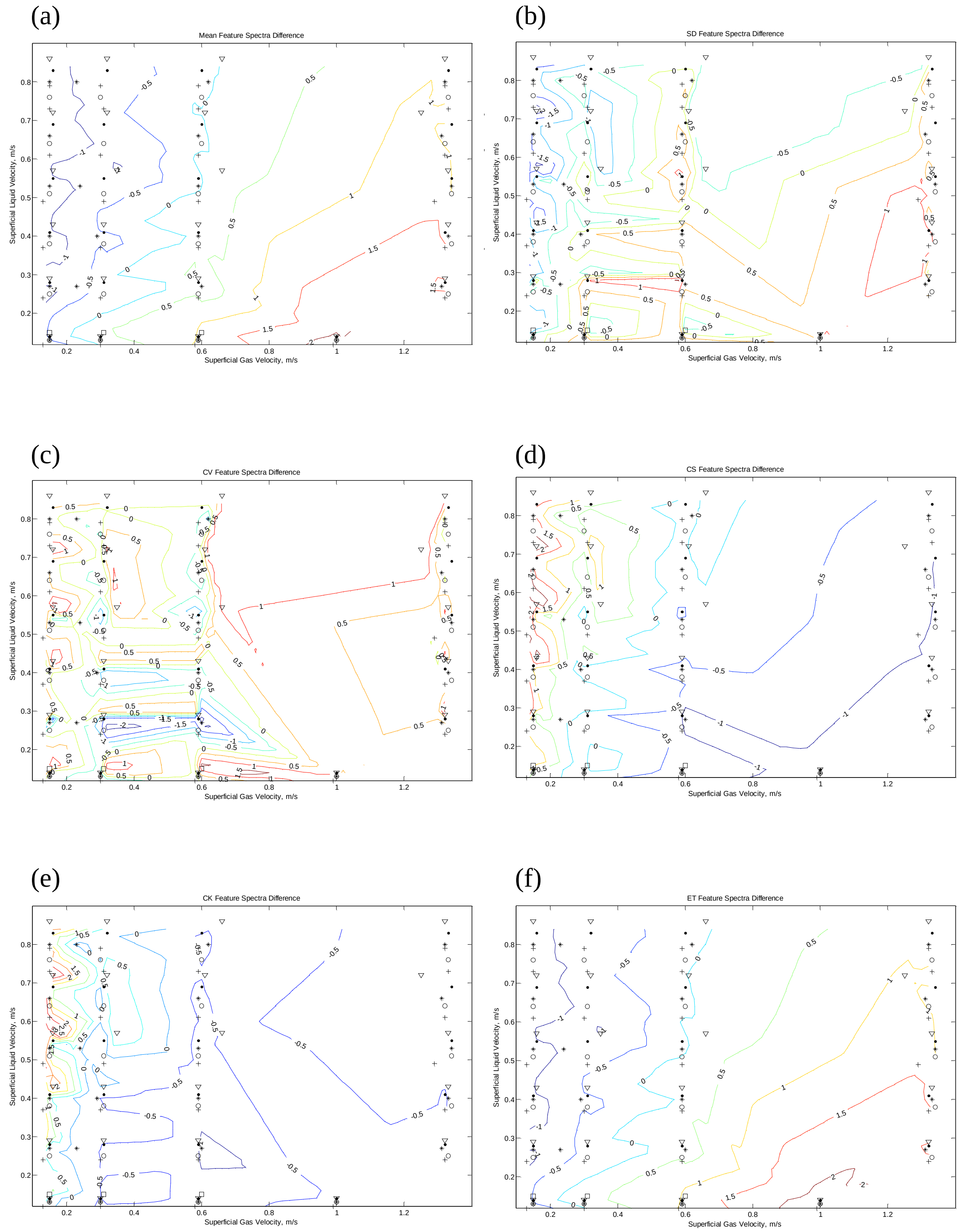

<u>Key to Test Point Water Cuts</u>

+	- 100%	•	- 40%
o	- 80%	▽	- 20%
*	- 60%	□	- 0%

Figure E.10 – Contour Plots of Spectra Difference Amplitude Features

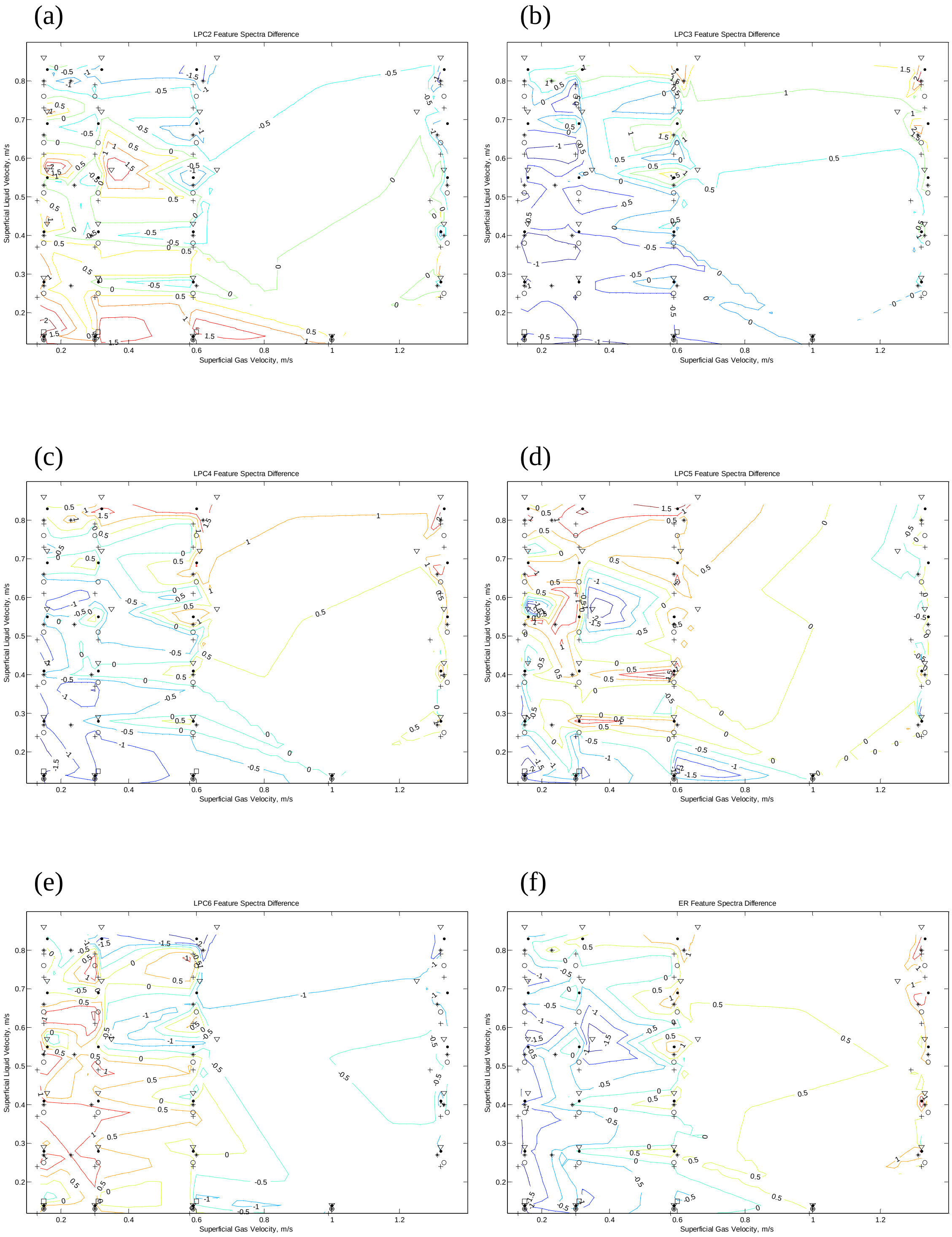

Key to Test Point Water Cuts			
+	- 100%	•	- 40%
o	- 80%	▽	- 20%
*	- 60%	□	- 0%

Figure E.11 – Contour Plots of Spectra Difference LPC Features

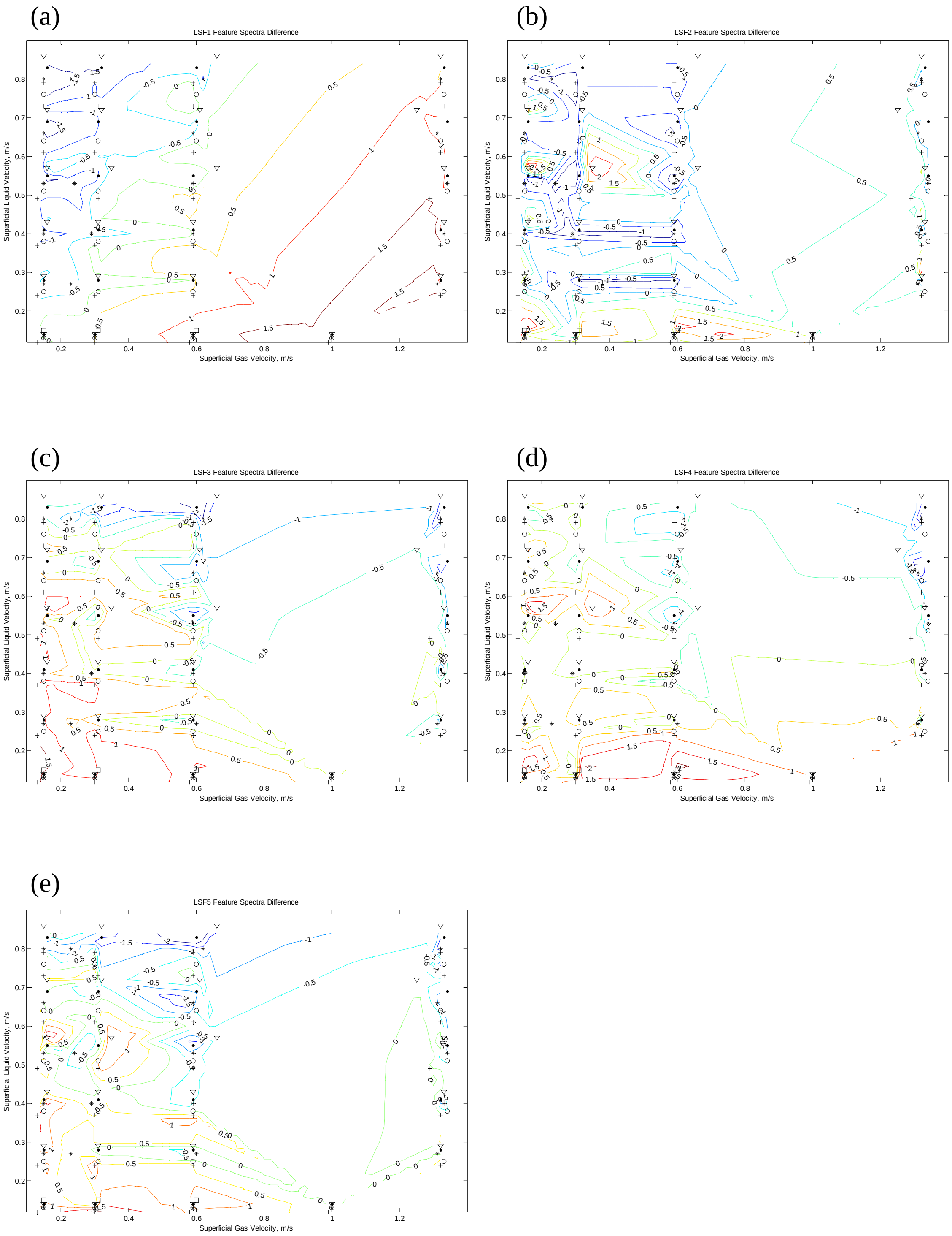

Key to Test Point Water Cuts

+	- 100%	•	- 40%
o	- 80%	▽	- 20%
*	- 60%	□	- 0%

Figure E.12 – Contour Plots of Spectra Difference LSF Features

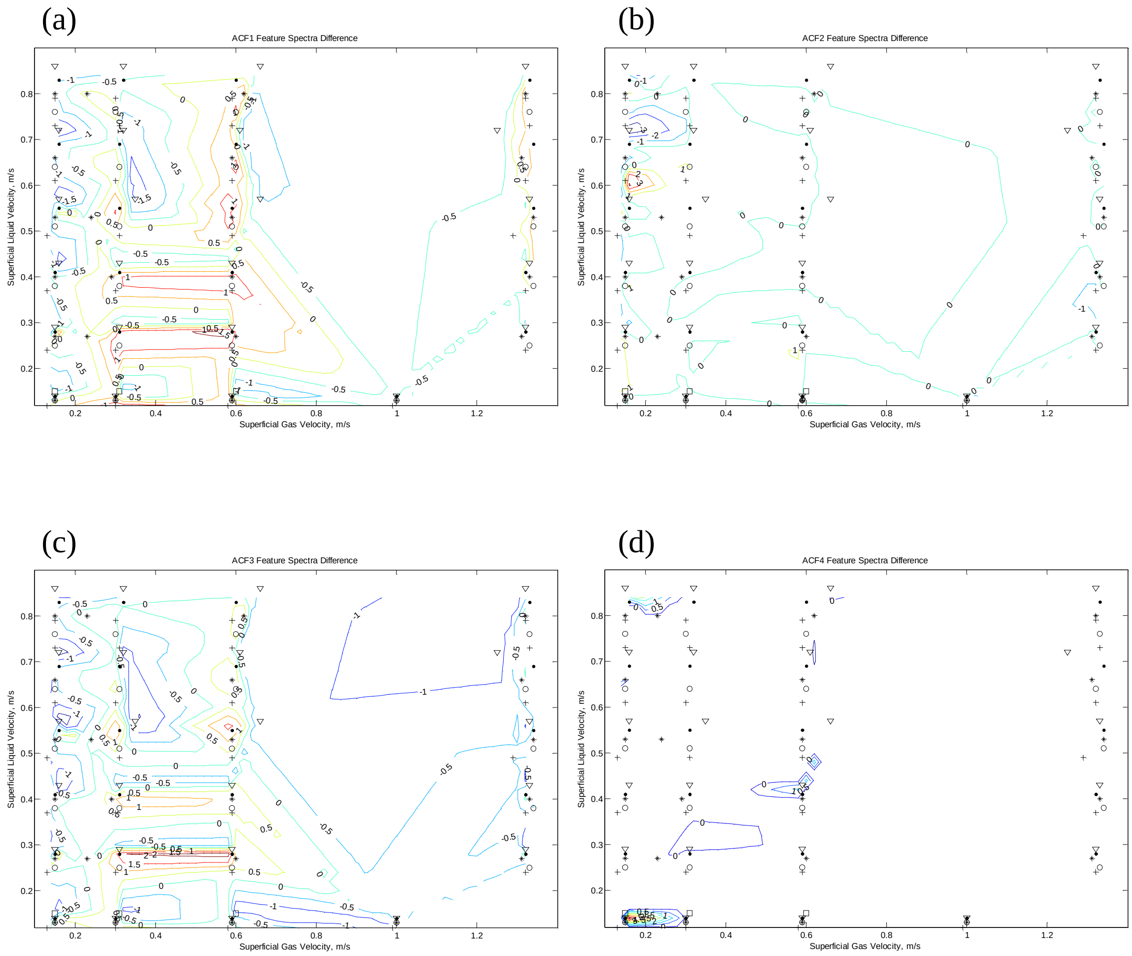

Key to Test Point Water Cuts

+	- 100%	•	- 40%
o	- 80%	▽	- 20%
*	- 60%	□	- 0%

Figure E.13 – Contour Plots of Spectra Difference ACF Features